

**MASARYK UNIVERSITY**

**FACULTY OF SCIENCE**

**DEPARTMENT OF EXPERIMENTAL  
BIOLOGY**

**PHYSIOLOGY AND BIOTECHNOLOGY OF  
ARCHAEA**

**CUMULATIVE HABILITATION THESIS**

**SIMON K.-M. R. RITTMANN**

**BRNO/WIEN 2025**

*Trpělivost růže přináší.*

## **Index**

<b>Acknowledgements</b>	<b>1</b>
<b>Abstract</b>	<b>2</b>
<b>Keywords</b>	<b>2</b>
<b>Introduction</b>	<b>3</b>
Extremophilic microorganisms	3
Anaerobic microorganisms	3
Archaea	5
Methanogenic archaea	6
Archaea Biotechnology	9
Archaeal polyhydroxyalkanoate production	12
Archaeal lipid production and utilization	13
Gaseous biofuels production and carbonic anhydrases of archaea	15
<b>Author contribution statement</b>	<b>17</b>
<b>Approbations of results and peer-reviewed publication results of this habilitation thesis</b>	<b>17</b>
<b>Methods used in the frame of this habilitation thesis</b>	<b>18</b>
Strains	18
Chemicals	18
Analysis of ammonium, amino acids, lipids and gases	18
Media and closed batch cultivation of thermophilic and hyperthermophilic methanogens	18
Media and fed-batch cultivation of <i>M. marburgensis</i>	20
<b>Chapter 1</b>	<b>20</b>
Comparative lipidomics of thermophilic and hyperthermophilic methanogens	21
Comparative amino acid excretion of thermophilic and hyperthermophilic methanogens	24
<b>Chapter 2</b>	<b>26</b>
Amino acid excretion by <i>M. marburgensis</i> grown in fed-batch cultivation mode	26
<b>Summary, conclusions and outlook</b>	<b>29</b>
<b>References</b>	<b>31</b>
<b>Annex 1</b>	<b>43</b>
<b>Annex 2</b>	<b>59</b>
<b>Annex 3</b>	<b>78</b>
<b>Annex 4</b>	<b>92</b>
<b>Annex 5</b>	<b>109</b>
<b>Annex 6</b>	<b>123</b>
<b>Annex 7</b>	<b>136</b>
<b>Annex 8</b>	<b>148</b>
<b>Annex 9</b>	<b>162</b>
<b>Annex 10</b>	<b>175</b>
<b>Annex 11</b>	<b>196</b>
<b>Annex 12</b>	<b>206</b>
<b>Curriculum vitae</b>	<b>218</b>

## **Acknowledgements**

My acknowledgment goes to the Department of Experimental Biology of the Faculty of Science at Masarykova univerzita, Brno, Czech Republic allowing and enabling me to submit this cumulative habilitation thesis. I would like to thank to Assoc. Prof. Dr. Monika Vítězová, Prof. Dr. Tomas Vítěz, and Assoc. Prof. Dr. Ivan Kushkevych for their ongoing support, help, and guidance, as well as for a fruitful, close, and highly productive scientific collaboration that has led to scientific exchange between the Masarykova univerzita, Universität Wien, and beyond. I also want to thank Dr. Nikola Hanišáková and Mgr. David Novak for working with me and for joining my lab at Universität Wien for scientific exchange projects.

I want to thank Univ.-Prof. Dr. Christa Schleper for her long-lasting support for my research and for scientific collaborations, working on and sharing many scientific breakthroughs in archaea biology, and many jointly published peer-reviewed papers. I would also like to thank Assoc. Prof. Dr. Silvia Bulgheresi for being a trusted colleague and friend.

Special thanks go to my former and current bachelors, master, PhD students and post docs at the Universität Wien and from abroad, with whom I worked over the years on many scientific and industrial basic and applied research projects, as well as on many peer-reviewed publications. Specifically, I want to mention Dr. Ruth-Sophie Taubner, Ipek Ergal, PhD, Mag. Nika Pende, PhD, MSc, Barbara Reischl, MSc, Angus Hiltz, MSc, Hayk Palabikyan, MSc, Ing. Walter Hofmann, MSc, Aquilla Ruddyard MSc, Lara Pomper, MSc, Nicolas Salas Wallach, BSc, Andrew Y. King, BSc and Selina Madlmayr, BSc.

I would like to thank my current and former long-term project collaboration partners Ao. Univ.-Prof. Dr. Werner Fuchs, Ao. Univ.-Prof. Dr. Bernhard Schuster, Dr. Günther Bochmann, DI Franziska Steger (Universität für Bodenkultur Wien, Vienna, Austria), Prof. Dr. Christian Paulik (Johannes Kepler Universität Linz), Alexander Krajete, Arne H. Seifert, Sebastien Bernacchi (Krajete GmbH) for great scientific collaborations and many successful research projects and published papers.

I also want to thank my international collaboration partners, Prof. Dr. Simonetta Gribaldo (Institute Pasteur, Paris, France), Prof. Dr. Jörn Peckmann, Dr. Monika Baumann and Dr. Daniel Birgel (Universität Hamburg, Hamburg, Germany) for fruitful collaborations, jointly achieved scientific breakthroughs, and several published peer-reviewed papers.

I would like to acknowledge my company Arkeon GmbH (Tulln a.d. Donau, Austria), specifically Dr. Günther Bochmann, Dr. Christian Fink and DI Justin Smith, for the generous support, fruitful discussions and for the possibility to jointly work on novel scientific and technological developments in the field of gas fermentation and Archaea Biotechnology as well as for publishing together.

I am indebted to my wife and my children for making my parallel academic and industrial career possible and for accepting and supporting my highly dynamic and flexible work-life balance.



## **Abstract**

Microorganisms have adapted by tailoring their cellular and metabolic constituents to thrive at the boundaries and limits of life. Especially extremophilic and anaerobic microorganisms must regularly cope with energy stress and limitation of nutrients. However, such microorganisms take advantage of the resources that are available in natural and artificial environments in an efficient way, still considering that sometimes low levels of nutrients are prevailing in their ecosystem, or that the physical and/or chemical environmental/bioprocess technological conditions are extremophilic. Yet, microorganisms were successful in diversifying regarding their physiology, metabolism, cell biology, and morphology.

Archaea are prokaryotic organisms with fascinating morphological, cell biological, and physiological characteristics and they possess an enormous ecological importance. Archaea have colonized Earth for almost 3.5 billion years. Together with bacteria they are regarded to be one the most ancient life forms that exist on our planet. Regarding metabolic and pathway engineering and in biotechnology, archaea are still massively overshadowed by bacteria and eukaryotes in terms of scientific studies, public awareness, research, and development as well as in industrial application. However, the genomic, biochemical, physiological, and cell biological properties of archaea show a vast potential for a wide range of applications that allows using or developing them as natural or into engineered microbial cell factories through synthetic biology or bioprocess development.

Today, most microbial cell factories that are utilized to produce value-added and high-value bioproducts on an industrial scale are hence, bacterial, fungal, or algae-based. However, Archaea Biotechnology is on the rise. This is since more and more are using archaea as production organisms or some of their enzymes to manufacture products for pharmaceutical, cosmetics, energy, and the food sector.

Some of the many advantages of utilizing archaeal cell factories include the ability to cultivate many of these sometimes extremophilic strains under non-sterile conditions for e.g., bioplastics production. Another advantage is that some bioprocesses use inexpensive or sometimes toxic feedstock, which reduces the cultivation costs. Finally, there are often simply no bacterial or eukaryotic cell factories available that could produce the desired products.

This cumulative habilitation thesis provides an introduction on extremophilic and anaerobic microorganisms. Then the characteristics of archaea biology are introduced, and an overview of the research and development field of Archaea Biotechnology is provided, specifically focussing on methanogenic and extreme halophilic archaea, as well as on selected topics of Archaea Biotechnology, such as artificial archaeal co-cultures and carbon dioxide converting enzymes. Moreover, the role and the potential of archaea in the future of sustainable bioprocessing and biorefining are highlighted and discussed. In addition, this habilitation thesis comprises results from lipidomic and amino acid excretion experiments of thermophilic and hyperthermophilic methanogenic archaea. Finally, 12 of my co-, last-, or corresponding authored research papers that I have published in the field of archaea physiology, cell biology, and biotechnology are compiled in this cumulative habilitation thesis.

## **Keywords**

Microbiology, biotechnology, microorganism, anaerobe, bioreactor, bioprocess, gas fermentation

## Introduction

### Extremophilic microorganisms

Earth is commonly regarded as a planet that is still vastly inhabited by plants, animals and, sometimes, microorganisms. These organisms are viewed as being able to grow under conditions that are compatible with life as it is found in most terrestrial and shallow water marine ecosystems (e.g., temperature between 0-45 °C, a pH value of around 7, atmospheric pressure at sea level of 1 bar). However, extremophilic microorganisms (extremophiles) have succeeded in inhabiting environmental niches with physico-chemical parameters very much outside the specification of the aforementioned conditions (Jebbar et al., 2020). Extreme environments are characterized by parameters at the boundaries of conditions that sustain and shape life in its various forms. Extremophilic environments, whether terrestrial, oceanic, cryospheric or deep endolithic, are widespread on our planet. Especially the deep ocean and polar regions are among the important niches of the Earth biosphere in terms of biomass volume (Jebbar et al., 2020). Extreme environments are to a large extent dominated by prokaryotic microorganisms – Bacteria and Archaea (Shu and Huang, 2021). Some extremophiles thrive under conditions that are at the limits of their physiological and energy potential, whereas others have highly adapted genetic features that result in a crucial requirement of such conditions.

When classifying microorganisms as extremophiles, the concept of a normal, above specified, environment is used as a reference. However, extreme environments are considered to have putatively predominated when the first life forms appeared on Earth. Nowadays, these environments are still colonized by highly diverse microbial communities. Depending on the physico-chemical characteristics, the extremophiles can be subdivided into different categories: hyperthermophiles ( $T_{\text{opt}} \geq 80$  °C) e.g., *Methanopyrus kandleri* (Takai et al., 2008), the archaeon with the highest recorded temperature growth record); psychrophiles ( $T_{\text{opt}} \leq 15$  °C) such as the bacterium *Psychrobacter fulvigenes* (Romanenko et al., 2009), capable of growing at temperatures as low as 5 °C; acidophiles ( $\text{pH}_{\text{opt}} \leq 3$ ) including *Picrophilus oshimae* (Schleper et al., 1995), an archaeon that is the record holder with growth at low pH values, with a  $\text{pH}_{\text{opt}}$  of for growth at 0.7; alkaliphiles ( $\text{pH}_{\text{opt}} \geq 9$ ) such as *Bacillus pseudofirmus* (Nielsen et al., 1995), capable of growing at a pH of 11, halophiles such as the archaeon *Halobacterium salinarum* (Ventosa and Oren, 1996), that is able to grow up to 5.5 mol L<sup>-1</sup> NaCl, and piezophiles e.g., *Thermococcus piezophilus*, the archaeon that holds the record for withstanding the highest hydrostatic pressure of 130 MPa (Dalmasso et al., 2016).

Extremophiles expand our understanding of physiology and biodiversity on Earth. By deducing the mechanisms that enable extremophiles to grow optimally under extremophilic conditions it could lead to interesting application possibilities in biotechnology regarding biofuels and biocommodities production. Among the extremophiles, especially anaerobic microorganisms and archaea have a yet untapped, but tremendous, biotechnological application potential.

### Anaerobic microorganisms

Anaerobic microorganisms (anaerobes) can be found in almost all environments on Earth. Anaerobes are found among the phyla Archaea, Bacteria and Eukarya. They are known inhabitants of molecular oxygen (O<sub>2</sub>)-free or O<sub>2</sub>-limited niches (Ferry, 2003; Hanišáková et al., 2022; Hungate and Macy, 1973; Kushkevych et al., 2021; Mauerhofer et al., 2019; Müller, 2019). Anaerobes were already enriched and isolated from sediments of rivers, lakes and Earth's oceans as well as from the gastrointestinal (GIT) of

animals or humans (Borrel et al., 2023, 2020). By far the largest habitat for anaerobic organisms is the deep biosphere, specifically terrestrial and marine sediments (Jebbar et al., 2020; Meister and Reyes, 2019). The energy metabolism of anaerobes is, in most cases, adapted to an O<sub>2</sub>-free anoxic environment. In such environments, substrate-limiting or oligotrophic conditions are often encountered (Hanišáková et al., 2022; Hoehler and Jørgensen, 2013; Jebbar et al., 2020; Lever et al., 2015; Mauerhofer et al., 2019; Thauer et al., 2008). However, the metabolic processes of anaerobes are known to play an important role in the global carbon cycle (Evans et al., 2019; Fuchs, 2011; Offre et al., 2013; Schuchmann and Müller, 2016; Tveit et al., 2019). To gain energy and/or carbon, some anaerobes degrade organic matter as heterotrophic organisms, such as lignocellulosic compounds, polysaccharides, proteins, lipids, organic acids and alcohols. Other anaerobes are able to gain energy through a chemolithoautotrophic metabolism, that is solely based on utilization of inorganic salts or gases or through anaerobic photosynthesis. Among the anaerobes, facultative anaerobes and strict or obligate anaerobes are distinguished.

As the awareness for anaerobes was increasing towards the end of the 19<sup>th</sup> century, the need for specific methods for their cultivation and manipulation had been realized (Hanišáková et al., 2022). For most of the commonly used anaerobic and aerotolerant microorganisms, the cultivation techniques can be performed under standard laboratory conditions. However, more well-designed and sophisticated anaerobic cultivation methods are required to successfully grow strict (obligate) anaerobic microorganisms. Hence, the methods for cultivation of aerobic and strict anaerobic microorganisms differ significantly. By circumventing that anaerobes will be exposed to O<sub>2</sub> is hence crucial for successful enrichment, isolation and cultivation attempts. The reason to avoid the exposure to O<sub>2</sub> of anaerobes is due to the fact that O<sub>2</sub> is toxic to anaerobic microorganisms to varying degrees (Hanišáková et al., 2022; Mauerhofer et al., 2019). In addition, anaerobes require a specific but low oxidation-reduction potential (ORP) for being able to grow. Maintaining an ORP of  $\leq -100$  mV for facultative anaerobes and  $< -330$  mV for strict anaerobes, such as methanogenic archaea (methanogens) is required (Mauerhofer et al., 2019). An ORP tremendously above the optimal condition is not necessary lethal to anaerobes, but their growth might be impaired (Hanišáková et al., 2022; Mauerhofer et al., 2019). An O<sub>2</sub>-free environment for propagating anaerobes can be generated by using specific cultivation methods that have initially been developed by Robert Hungate (Hungate and Macy, 1973). Later these anaerobic cultivation methods for anaerobes have been adapted to using serum bottles (Miller and Wolin, 1974). Furthermore, enrichment of anaerobes can be performed by mimicking growth conditions of the original microbial habitat (salt concentrations, temperature, pH, ORP) and applying a minimized O<sub>2</sub> exposure during inoculation (Lewis et al., 2020). By reducing the residual molecular O<sub>2</sub> that still remains in the cultivation tube for growth of anaerobes, even after the main O<sub>2</sub> removal had been completed, the addition of organism-specific reducing agents to the anaerobes' growth media declines the ORP to desired values, that are required to successfully cultivate the organism (Mauerhofer et al., 2019). The methods for managing, handling, and cultivation of anaerobic microorganisms are often considered to be rather demanding. They might be preventive to grow these organisms in common microbiological laboratories. Apart from this, there are laboratory limitations regarding setup of anaerobic cultivation equipment. That specifically means that e.g., high-throughput cultivation methods for studying the physiological or biotechnological response of an anaerobes towards a particular gas composition, gas supply rates (gassing rates), and/or applied pressure is still

not fully possible. Moreover, the toxicity and flammability of some (co-)substrates of anaerobes and microbial product gasses needs to be considered, too, which might even render cultivation of anaerobes difficult to impossible in common microbiological laboratories (Hanišáková et al., 2022). Anaerobes are fascinating organisms with regard to their eco-physiological characteristics, their metabolic features, and their biotechnological application potential. Several physiologically and biotechnologically well-investigated anaerobes belong to the phylum Archaea, such as methanogens, whose ecological importance and biotechnological application possibilities have become of utmost interest.

### Archaea

Archaea are present on Earth for almost 3.5 billion years. Together with bacteria they are regarded as one the most ancient life forms existing on our planet (Woese, 2002). Archaea were initially described as an independent phylogenetic group of organisms in 1977 (Woese and Fox, 1977). Based on archaeal rRNA gene analysis, the first two established archaeal phyla were the Euryarchaeota and the Crenarchaeota (Olsen et al., 1986). Throughout the last decades many more archaeal phyla have been discovered through cultivation and metagenome sequencing (Adam et al., 2017; Williams et al., 2017). Currently, the Archaea are grouped into the following three superphyla: Asgard, DPANN and TACK. Two of these archaeal superphyla were initially named by the phyla present in them: DPANN are Diapherotrites, Parvarchaeota, Aenigmarchaeota, Nanohaloarchaeota and Nanoarchaeota. The TACK superphylum is named after Thaumarchaeota, Aigarchaeota, Crenarchaeota and Korarchaeota. Only the the Euryarchaeota do not fall within a superphylum. Moreover, among the Archaea the Euryarchaeota contain the greatest number and diversity of cultured lineages (Baker et al., 2020). Archaea form one of the three domains of life, that is clearly distinguishable from Bacteria and Eukarya, and are regarded as critical for evolutionary studies to examine the origin of life (Liu et al., 2021). Archaea possess many genetic and biochemical similarities with Eukarya. Some of the characteristics that are shared between Archaea and Eukarya that are lacking in Bacteria include the presence of histones, complex RNA polymerases and methionine translation initiation (Baker et al., 2020). Many archaea are traditionally still viewed as extremophilic organisms. Hence, archaea are certainly found living in extreme environments e.g., acidic sulphur springs, hot springs, hydrothermal vent systems and hypersaline environments (Dalmaso et al., 2016; Offre et al., 2013; Schleper et al., 1995; Takai et al., 2008; Ventosa and Oren, 1996). The extremophilic nature of archaea has stimulated astrobiologists to focus in the search for extraterrestrial life using these intriguing organisms (Jebbar et al., 2020; Taubner et al., 2018). However, evidence has piled up that archaea also fulfil an important role in the turnover of micro- and macronutrients in moderate environments, such as soil, and marine waters, and in as well as in the GIT of vertebrates (Borrel et al., 2023, 2020). For instance, some Thaumarchaeota, that belong to the most abundant groups of archaea in oceans on Earth, belong to the ammonium-oxidizing archaea (AOA). They are able to obtain cellular energy by ammonia oxidation, but also from urea and cyanate (Offre et al., 2013; Stieglmeier et al., 2014b). Thaumarchaeota are linked to the production of the greenhouse gas nitrous oxide (N<sub>2</sub>O), which is by mass an approx. 250 times more potent greenhouse gas compared to carbon dioxide (CO<sub>2</sub>). Thaumarchaeota, together with other archaeal groups, are part of the human-associated archaeome (Borrel et al., 2020). For instance, Methanomassiliicoccales might have a beneficial impact on the health of humans (Borrel et al., 2017; Brugère et al., 2014). Other

archaea were discovered on human skin and their presence could possibly be linked to age and skin physiology (Probst et al., 2013). Finally, other human-associated archaea are recognized by the immune system and could be involved in pro-inflammatory processes (Bang et al., 2017, 2014). Most archaea possess a cell envelope that is built of a proteinaceous surface layer (S-layer) (Rodrigues-Oliveira et al., 2017). Only the sister clades, Methanobacteriales and Methanopyrales, are known to possess a cell wall consisting of archaeal peptidoglycan (Mukhopadhyay, 2024). Archaeal peptidoglycan is in its overall structure similar to bacterial peptidoglycan (Mukhopadhyay, 2024; Pende et al., 2021). However, the differences between archaeal peptidoglycan and bacterial peptidoglycan – still in the current view – regard the oligosaccharide backbone to be composed of L-N-acetylalosaminuronic acid connected by a  $\beta$ -1,3 linkage to N-acetylglucosamin and the stem peptide consists only of L-amino acids. These characteristics make archaeal peptidoglycan resistant to  $\beta$ -lactam antibiotics, most lysozymes, and proteases (Khelaifia and Drancourt, 2012). Some archaea have been recently investigated with regard to cell division, shape and the cell envelope architecture. Models for archaeal cell biology studies involved the Crenarchaea *Sulfolobus acidocaldarius* and *Sulfolobus solfataricus* as well as the Euryarchaeon *Haloferax volcanii* (Leigh et al., 2011). For cell division, the Crenarchaeota were shown to use homologues of the eukaryotic ESCRT system (Lindås et al., 2008; Samson et al., 2008). On the contrary, haloarchaea were shown to divide by a bacteria-like FtsZ-based cell division (Wang and Lutkenhaus, 1996). In conclusion archaea already possess a high diversity of cell division mechanisms. Furthermore, there might be a lack of fundamental knowledge about the cell biology in the other than the aforementioned archaeal groups.

Among the archaea, methanogens and AOA (e.g., some of the Thaumarchaeota) are key organisms in the anaerobic and marine food webs, respectively (Lyu et al., 2018; Pester et al., 2011; Thauer et al., 2008). Thereof, methanogens are a physiologically and phylogenetically diverse group of anaerobic microorganisms, that are already of high biotechnological relevance (Pfeifer et al., 2021; Rittmann et al., 2021). Methanogens produce e.g., methane ( $\text{CH}_4$ ) as an end product of their carbon and energy metabolism (Liu and Whitman, 2008; Lyu et al., 2018; Thauer et al., 2008). AOA are a metabolically diverse group of microbes found in almost every environment on Earth, ranging from marine waters and arctic soils to the human skin microbiome (Stieglmeier et al., 2014a, 2014b). Other ecologically and biotechnologically important archaea are found among the Sulfolobales, that were first cultivated from volcanic hot springs at pH values of 2 to 3 and 80 °C (Lewis et al., 2021), the halophilic archaea (“haloarchaea”), an ecological and biotechnological important group of archaea, that grow at salt solutions up to saturation (Ventosa and Oren, 1996), and the anaerobic, hyperthermophilic Thermococcales, a group of biotechnologically important anaerobic archaea, that can be cultivated under hyperthermophilic conditions (Ergal et al., 2018; S. K.-M. R. Rittmann et al., 2015).

### Methanogenic archaea

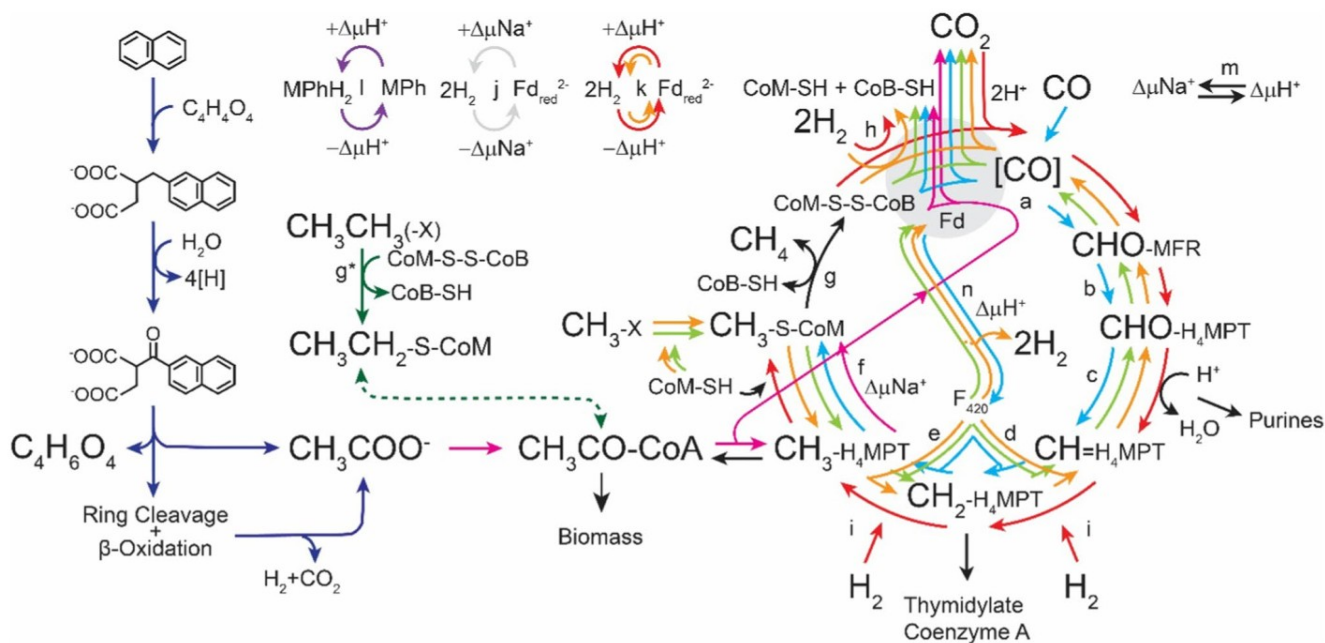
Methanogenic archaea (methanogens) are microorganisms that generate methane ( $\text{CH}_4$ ) as an end product of their energy metabolism (Ferry, 2015, 2010, 2003, 2003, 1999; Liu and Whitman, 2008; Lyu et al., 2024, 2022, 2018; Thauer, 2012, 1998, 1990; Thauer et al., 2010, 2008). The  $\text{CH}_4$  that is produced by methanogens accounts for more than one-half of all  $\text{CH}_4$  produced on Earth per year (Evans et al., 2019). Therefore, methanogens are an ecologically very important group of organisms (Borrel, 2022; Liu and Whitman, 2008; Lyu et al., 2018; Offre et al., 2013; Thauer et al., 2008; Welte,

2016). However, methanogens increasingly received attention due to research and development in the field of energy storage, especially during the last 10-15 years (Abdel Azim et al., 2017, 2018; S. Bernacchi et al., 2014; Sébastien Bernacchi et al., 2014; Krajete et al., 2014; Mauerhofer et al., 2018, 2021; Pappenreiter et al., 2019; Simon Rittmann et al., 2012; S. Rittmann et al., 2015; Rittmann et al., 2014; Rittmann, 2015; Rittmann et al., 2018; Seifert et al., 2013, 2014). Methanogens are strict anaerobic microorganisms (Hanišáková et al., 2022). The energy metabolism of methanogens, which is independent of O<sub>2</sub> might have developed early on Earth (Evans et al., 2019) is often independent of the presence of any organic molecule (Abdel Azim et al., 2017; Mauerhofer et al., 2021; Simon Rittmann et al., 2012). Methanogens act as the final consumers of volatile fatty acids, alcohols, or gases in the terminal step of the anaerobic food chain (Lyu et al., 2018; Thauer et al., 2008), and, as such, their estimated contribution to the global carbon cycle is high (approx. 1 Gt carbon yr<sup>-1</sup> (Tian et al., 2016). As the name already implies, methanogens produce CH<sub>4</sub>, which is a potent greenhouse gas (Lyu et al., 2018). The global warming potential of CH<sub>4</sub> is about 25 times higher compared to CO<sub>2</sub> by mass. They are the only archaea known on Earth capable of producing CH<sub>4</sub>, which, together with molecular hydrogen (H<sub>2</sub>), is considered a key compound that could have enabled prebiotic biosynthesis (Martin et al., 2008). Methanogens, as we know them from Earth, might also be able to produce CH<sub>4</sub> under conditions that prevail on Saturn's icy moon Enceladus (Taubner et al., 2018).

Methanogens are a phylogenetically diverse group of organisms (Adam et al., 2018; Borrel et al., 2019, 2016). Their taxonomic clustering is constantly in flux, especially in the last 10-15 years. Currently, they belong to 6 classes (Methanobacteria, Methanococci, Methanonatronarchaeia, Methanopyri, Methanomicrobia and Thermoplasmata) that are subdivided into 8 orders (Methanomassiliicoccales, Methanobacteriales, Methanococcales, Methanonatronarchaeales Methanopyrales, Methanomicrobiales, Methanocellales and Methanosarcinales). So far, cultured representatives of the methanogens were found among the Euryarchaeota, Halobacterota and Thermoplasmata. Within the Euryarchaeota, the Methanococcales, Methanopyrales and Methanobacteriales; among the Halobacterota the Methanonatronarchaeia, Methanomicrobiales, Methanocellales and Methanosarcinales; and among the Thermoplasmata, the Methanomassiliicoccales (Lyu et al., 2018). Metagenome sequencing and analysis recently indicated the presence of other yet uncharacterised putative methanogens in natural and artificial environments (Evans et al., 2019). Methanogens thrive in habitats from hot vents, such as black smokers, in the deep oceans (Ver Eecke et al., 2012), to ice cold and thawing permafrost soils (Mondav et al., 2014), in rice fields (Geymonat et al., 2011; Lyu et al., 2018), freshwater and seawater and their sediments (Borrel et al., 2012; Lyu et al., 2018), as well as in the intestine and oral cavity of vertebrates (Borrel et al., 2020). It is known since 1966 that methanogens thrive in the human GIT (Calloway et al., 1966). The first methanogen that was isolated from the human GIT was *Methanobrevibacter smithii* (Miller et al., 1982). Within the GIT, the most abundant archaea are representatives of the Methanobacteriales and the Methanomassiliicoccales. The Methanobacteriales of the GIT are mainly represented by *M. smithii* and *Methanosphaera stadtmanae*. However, despite we know methanogens to be associated to e.g., the GIT, the role of methanogens in health and disease is still poorly understood (Borrel et al., 2020; Moissl-Eichinger et al., 2018). In addition, methanogens are found in the cytoplasm of flagellates, anaerobic ciliates and amoebas, and they are also found as endo- and ectosymbionts of protists that live in termites, cockroaches, amphibians and ruminants (see references in (Borrel et al., 2020).

As the characteristics of these above-mentioned habitats and ecosystems are quite diverse, different strains of methanogens are able to grow at moderate (300 kPa) to extreme (hyperbaric) overpressure conditions (400 MPa) in natural environments and in the lab (Mauerhofer et al., 2021; Pappenreiter et al., 2019; Taubner et al., 2018, 2015; Taubner and Rittmann, 2016; Ver Eecke et al., 2013). The growth temperature range of methanogens spans from approx. -4 °C up to 122 °C (Taubner et al., 2015). However, the temperature niche of methanogens is characteristic for each of the individual strains of methanogens. In addition, methanogens may be characterized as stenophilic and euryphilic with regard to their growth temperature characteristics (Taubner et al., 2015).

Methanogens are known to metabolize different substrate classes: gases  $H_2$  and  $CO_2$ , carbon monoxide (CO), acetate, and methylated compounds (e.g., methanol) (Kurth et al., 2020; Lyu et al., 2018; Mayumi et al., 2016). However, not all methanogens can metabolise each of the mentioned substrate classes. Assimilation of  $CO_2$  by methanogens using  $H_2$  is referred to as autotrophic, hydrogenotrophic methanogenesis. Methanogens that metabolise CO are referred to as carboxydutrophic methanogens. Some methanogens, referred to as organotrophic methanogens, were shown to even metabolize primary and secondary alcohols in the absence of  $H_2$  as carbon and/or energy substrates. Other methanogens are able to grow hydrogenotrophic methylotrophic, or only methylotrophic, and aceticlastic methanogens exist, too (Kurth et al., 2020; Lyu et al., 2018; Thauer et al., 2008). An overview of the characterized substrate utilization pathways of methanogens is shown in **Figure 1**.



**Figure 1:** Overview of the pathways for methanogenesis. The Figure was taken from (Carr and Buan, 2022). The direction of arrows in Figure 1 represents the direction of reactions. The reactions that are utilized in every methanogenic pathway are shown in black. Hydrogenotrophic methanogenesis (also known as The Wolfe Cycle) (Thauer, 2012) is represented in red. Methyl oxidation is represented in orange. Methylotrophic methanogenesis is represented in green. Acetotrophic methanogenesis is represented in fuchsia. Degradation of polyaromatic hydrocarbons is represented in dark blue (Siegert et al., 2011). Ethylene and long chain alkane reduction is represented in purple (Lemaire and Wagner, 2022). Carboxydutrophic methanogenesis is represented in cyan. CoB-SH, coenzyme B thiol; CoM-SH, coenzyme M thiol; CoM-

S-S-CoB, coenzyme M-coenzyme B heterodisulfide; Fd, ferredoxin; Fd<sub>red</sub>, reduced ferredoxin; H<sub>4</sub>MPT, tetrahydromethanopterin; MFR, methanofuran; MPh, methanophenazine; MPhH<sub>2</sub>, reduced methanophenazine. Enzymes involved in methanogenesis: (a) Formyl-methanofuran dehydrogenase (Fmd), (b) Formyl-methanofuran:H<sub>4</sub>MPT formyl transferase (Ftr), (c) Methenyl-H<sub>4</sub>MPT cyclohydrolase (Mch), (d) F<sub>420</sub>-dependent Methylene-H<sub>4</sub>MPT dehydrogenase (Mtd), (e) F<sub>420</sub>-dependent Methylene-H<sub>4</sub>MPT reductase (Mer), (f) Methyl-H<sub>4</sub>MPT:coenzyme M methyltransferase (Mtr), (g) Methyl-coenzyme M reductase (Mcr), (g\*) Atypical methyl-coenzyme M reductase (Mcr) (Wang et al., 2019), (h) Electron-bifurcating hydrogenase:heterodisulfide reductase complex (Mvh:HdrABC), (i) F<sub>420</sub>-reducing hydrogenase (Frh), (j) Energy-converting sodium pumping ferredoxin hydrogenase, (k) Ferredoxin reducing hydrogenase (Eha/Ech), (l) Proton-translocating methanophenazine:heterodisulfide reductase (HdrED), (m) Sodium-proton antiporter (MrpA), (n) F<sub>420</sub> proton-pumping methanophenazine reductase (Fpo). The figure caption text of Figure 1 was taken from (Carr and Buan, 2022) and only slightly modified.

In addition, CH<sub>4</sub>-utilizing strains are also known among the anaerobic methanotrophic archaea (ANME). ANME utilize the core pathway for CH<sub>4</sub> production from H<sub>2</sub>/CO<sub>2</sub> in the reverse direction. However, to make the reaction energetically favourable, ANME depend on a bacterial partner, that might be a sulphate reducer, a denitrifier or a nitrate reducer. As recently also short-chain alkane-oxidising archaea were enriched, the marker gene set was extended in silico to cover marker genes specific to methanogenic, ANME and short-chain alkane-oxidizing archaea (Adam et al., 2018; Borrel et al., 2019), indicating that none of the previously defined methanogenesis markers are any longer unique to methanogens. However, they are rather more generally indicative of metabolisms involving methyl-coenzyme M reductase or methyl-coenzyme M reductase-like complexes, including methanogenesis, methanotrophy and short-chain alkane oxidation (Borrel et al., 2019).

Today, methanogens are applied for anaerobic wastewater treatment and for biogas production (Lyu et al., 2018). Furthermore, methanogens can be used for lipid production (Baumann et al., 2022, 2018; Taubner et al., 2023, 2019), isopren-derived compounds production (Carr and Buan, 2022), proteinogenic amino acid production (Reischl et al., 2025; Rittmann et al., 2023a, 2023b, 2023c, 2023d; Taubner et al., 2023, 2019), and for the reduction of CO<sub>2</sub> to CH<sub>4</sub> using H<sub>2</sub> by using the CO<sub>2</sub>-based biological CH<sub>4</sub> production (CO<sub>2</sub>-BMP) process, also referred to as biomethanation or biocatalytic methanation, wherein autotrophic, hydrogenotrophic methanogens are utilized (Abdel Azim et al., 2017; Mauerhofer et al., 2021, 2018; Pfeifer et al., 2021; S. Rittmann et al., 2015; Rittmann, 2015; Rittmann et al., 2021, 2018, 2014; Seifert et al., 2014, 2013). Taken together, methanogens and methanotrophs are players in the global carbon cycle on Earth. Moreover, methanogens are emerging as highly important organisms for biotechnological research and development endeavours.

### Archaea Biotechnology

The earliest forms of biotechnology date back several thousand years in time, even before the existence of microbes would have been known. Beer and wine fermentation dates back to about 6000 BC, while the pickling of foods in acetic acid (vinegar) produced through microbial acidification of wine dates back to 5000 BC (Buchholz and Collins, 2013; Pfeifer et al., 2021). In 1860, Louis Pasteur made the ground-breaking discovery of the involvement of yeast and acetogenic and lactic acid bacteria in these processes. This caused a shift in the perception of microbes. Microbes became more and more widely accepted as organisms that could be utilized as chemical reactors or nowadays speaking as microbial cell factories. Microbial cell factories are today indispensable in 21<sup>st</sup> century microbial biotechnology. Today, mainly microorganisms from Bacteria and Eukarya are involved in the production of bio-based



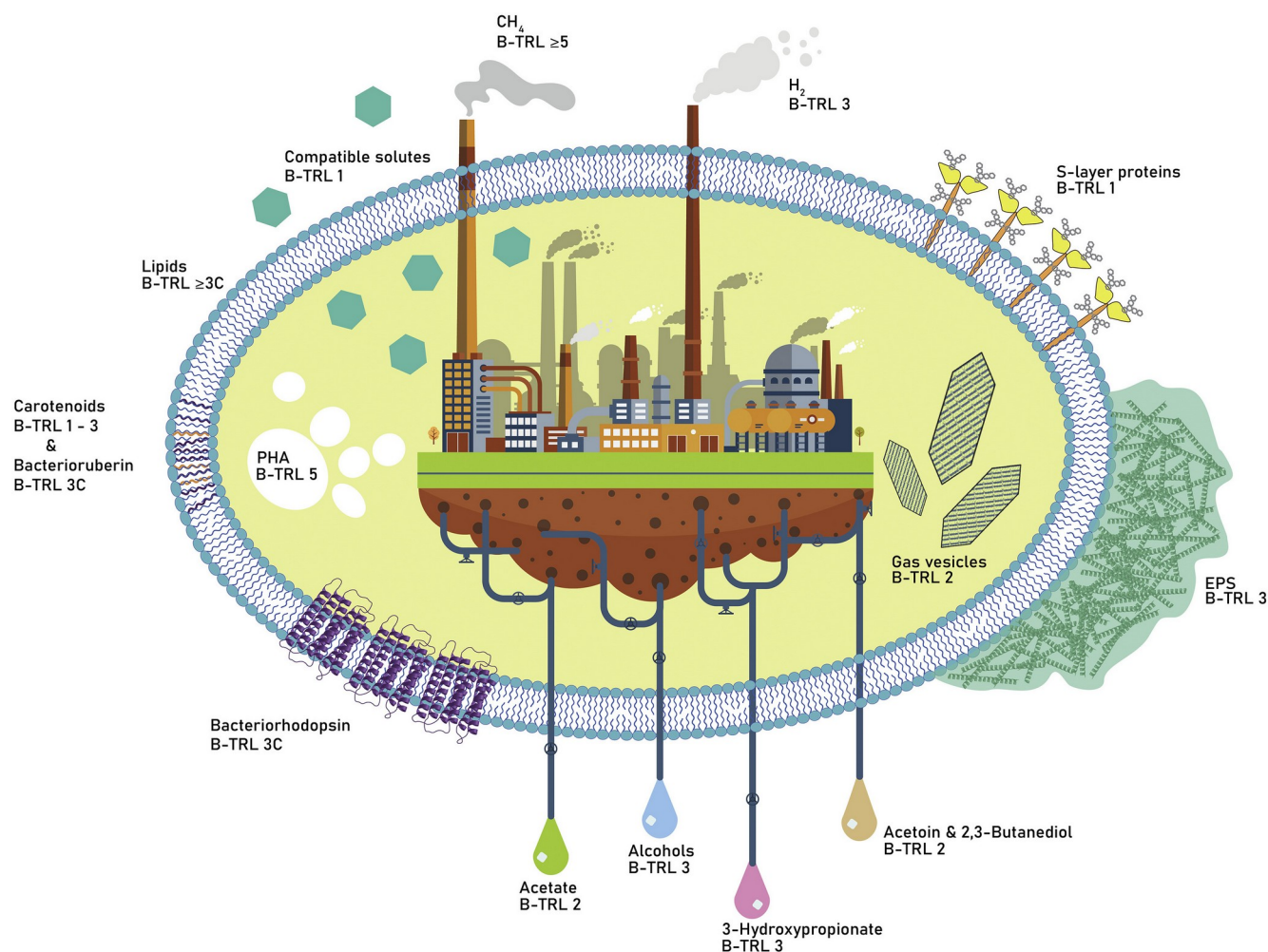
products such as bioplastics, cosmetics, food additives, high-value chemicals, biopharmaceuticals, and biogenic energy conversion. As the world aims to progress towards a sustainable and circular economy, industrial microbiology and biotechnology have become appropriate and even more powerful tools to replace petrochemistry-based technologies by biological alternatives (Harwood et al., 2018). Unfortunately, still very little is known about the fundamental aspects of archaeal physiology and cell biology compared to Bacteria and Eukarya to make Archaea become workhorses of microbial biotechnology (Pfeifer et al., 2021; Rittmann et al., 2021).

Production of bioproducts and commodity chemicals by microbial cell factories or recombinant enzymes by biotransformation, biocatalysis or fermentation advanced tremendously during the last decades. This is, as the market demand for biopharmaceuticals, fine and commodity chemicals as substitutes for various petrol-based synthetic products rises, microbial biotechnology has become ever more relevant in biological manufacturing and production. Biotechnology has been defined as follows by Pfeifer et al. 2021: “any technological application using biosystems, organisms, or derivatives thereof, to manufacture or modify bioproducts or to develop and engineer processes for specific application” (Pfeifer et al., 2021). The areas of biotechnology can be subdivided into the following categories according to Pfeifer *et al.* 2021: “white (industrial), blue (marine and fresh-water), green (plant/agricultural), red (biomedical/pharmaceutical), grey (environment/bioremediation), brown (arid land/dessert), yellow (insect biotechnology) and dark (biological weapons/biowarfare)” (Pfeifer et al., 2021). A slightly different colour codes categorization of biotechnology for archaea has also been published elsewhere (Aparici-Carratalá et al., 2023). Due to the diverse of application options, the biotechnology industry is probable to become one of the most important high-tech industries within the next few decades, with high revenues expected to exceed USD 720 billion around 2025, of which fermentation is expected to generate USD 86 billion (Pfeifer et al., 2021).

Most microbial cell factories that are utilized in industrial production processes are fungi or bacteria, with *Saccharomyces cerevisiae*, *Pichia pastoris* and *Escherichia coli* as the predominant organisms. However, the recent advances in fermentation, computational biology, synthetic biology, and precision fermentation show a vast application potential to apply, design and/or metabolically engineer Archaea to become archaeal cell factories (Pfeifer et al., 2021; Straub et al., 2018). However, in microbial biotechnology, Archaea are still overshadowed by Bacteria and Eukarya in terms of awareness among natural scientists and the public, industrial application, and studies. This underrepresentation in microbial biotechnology is unfortunately persistent, despite the biochemical, cell biological and physiological knowledge that continues to pile up for Archaea, as well as the biotechnological characteristics of archaea that showcases an enormous potential for a wide range of applications.

Archaea were utilized in defined archaea consortia for bioenergy production and have already been applied in undefined consortia together with bacteria for biomining, bioleaching, anaerobic digestion, soil remediation and wastewater remediation. Archaea are also well known for their highly stable enzymes, and there are already some industrialized applications of pure cultures of archaea (Pfeifer et al., 2021; Straub et al., 2018). Archaea may also be employed in bioremediation for the degradation of hydrocarbons, metal remediation, acid mine drainage, and dehalogenation (Krzmarzick et al., 2018). The utilization of archaea as microbial cell factories in biorefining and bioproduction will most likely become of high relevance in industrial microbiology and biotechnology (Pfeifer et al., 2021).

Archaea naturally produce or can be engineered to produce a vast range of bioproducts such as biofuels (e.g., CH<sub>4</sub>, H<sub>2</sub>, ethanol, or butanol), bioplastics such as PHAs, compatible solutes, such as betaine, components for nanobiotechnological applications S-layer proteins, lipids) and precursor molecules for the chemical industry (e.g., acetate; 2,3-butanediol) that are needed for the industrial synthesis of high value chemicals (Koller and Rittmann, 2022; Pfeifer et al., 2021; Rittmann et al., 2021; S. K.-M. R. Rittmann et al., 2015). An overview of possible applications of archaea in biotechnology is provided in **Figure 2**.



**Figure 2:** Schematic overview of products of Archaea Biotechnology and the associated Bio-Technology Readiness Levels (B-TRLs) of some archaeal cell factory products. This figure is a depiction of the cell factory producing the various products analysed through this review and shows their current B-TRLs. This image has been designed using resources from Freepik.com. The figure was taken from (Pfeifer et al., 2021) and modified regarding the B-TRL levels.

A major progress to facilitate the use of archaea in biotechnology is the continuous development of genetic manipulation techniques, which are essential for the development of archaeal production platforms. To date, there are already many archaea for which genetic tools are available (Akinyemi et al., 2021; Atomi et al., 2012; Fink et al., 2021; Gophna et al., 2017; Leigh et al., 2011; Li et al., 2022; Lyu and Whitman, 2019; Metcalf et al., 1997; Moore and Leigh, 2005; Sarmiento et al., 2011; Xu et al., 2023) and much progress in genetic methods for archaea, especially for thermophiles, was only recently made (Lewis et al., 2021; Schocke et al., 2019; Straub et al., 2018; Zeldes et al., 2015). It is

envisioned that the production of many compounds by archaea can be improved by genetic or metabolic engineering (Carr and Buan, 2022; Lyu et al., 2016; Lyu and Whitman, 2019). Nowadays, only a few companies, mostly from the *DACH* (an abbreviation for Germany, Austria, Switzerland) region, are working with archaeal cell factories, such as Arkeon GmbH, Electrochaeta GmbH, Halotek Biotechnologie GmbH, Novoarc GmbH or Krajete GmbH. Commercialization of archaeal products is still limited to few firms, but Halotek Biotechnologie GmbH produces high value products with halophilic archaea for a growing market demand for e.g., bacterioruberin and various isoprenoid-derived compounds.

#### Archaeal polyhydroxyalkanoate production

Archaeal polyhydroxyalkanoate (PHA) productivity, efficiency and scalability has been already examined for decades (Koller and Rittmann, 2022; Pfeifer et al., 2021; Rittmann et al., 2021). Among the archaea, the haloarchaea, which are moderate to extreme salt-loving archaea, have been shown to naturally produce many different PHA types. However, representatives of the Thaumarchaeota have also been shown to perform bioplastics production (Stieglmeier et al., 2014a). In general, PHAs are biopolyesters that serve the producing organism as intracellular storage compounds for carbon of the secondary metabolism. The by far best examined haloarchaeal cell factory for PHA production is *Hfx. mediterranei*, which is due to the broad substrate range and well understood genetics (Koller and Rittmann, 2022). The PHA that are produced by haloarchaea are the short chain length (scl)-PHA like poly(3-hydroxybutyrate) (PHB), poly(3-hydroxybutyrate-co-3-hydroxyvalerate) (PHBHV), and the terpolyester poly(3-hydroxybutyrate-co-3-hydroxyvalerate-co-4-hydroxybutyrate) (PHBHV4HB) when they are co-supplied during growth with  $\gamma$ -butyrolactone (GBL). Especially, PHBHV4HB together with poly(3-hydroxybutyrate-co-4-hydroxybutyrate) (PHB4HB) copolyesters are desirable for biomedical applications. The applications of PHBHV4HB and PHB4HB range from manufacturing artificial blood vessels, implants for bone regeneration, to surgical tools, dentistry purposes and to control the delivery of pharmaceutically active substances (Koller et al., 2007). PHA co-polyester compositions can be controlled by the selection of carbon sources and precursor molecules, Hence, PHAs with desired properties such as melting temperature and crystallinity can be generated (Hermann-Krauss et al., 2013; Koller, 2019; Koller et al., 2007).

A considerable advantage of using haloarchaea compared to the most widely used PHA production strain, the Gram-negative bacterium *Cupriavidus necator*, is that haloarchaea do not produce lipopolysaccharides (LPS). LPS are a group of endotoxins that are found in the cell wall of several Gram-negative bacteria (Tan et al., 2014). LPS components are typically co-extracted together with PHA during downstream processing and might pollute the product. In *in vivo* applications, LPS could cause inflammatory reactions when present in implants or other polymeric products (Zinn et al., 2001). Thus, PHA from Gram-negative bacteria must be highly purified after recovery when applications in e.g., biomedical or the pharmaceutical fields are considered. Purifying PHA from the contaminating LPS components thus increases the overall manufacturing costs (Koller, 2018). Hence, haloarchaea are clearly advantageous considering the production of PHA for biomedical applications (Koller et al., 2007). In this regard it might be interesting to note that among the archaea there are up to date no pathogens yet known (Borrel et al., 2020). Another advantage of using haloarchaea for PHA production compared to bacteria is that the PHA reserves are rather fast depolymerized by bacteria after the onset

of depletion of exogenous carbon sources (Kadouri et al., 2005). On the contrary, the most investigated haloarchaeal PHA producer *Hfx. mediterranei* degraded the intracellularly accumulated PHA very slowly under conditions that normally favour intracellular PHA degradation in bacteria, which are carbon source limitation as well as the presence of convertible nitrogen and phosphate source (Koller et al., 2015). PHA production by haloarchaea has not yet reached industrial maturity to be commercially implemented. However, PHA production under non-sterile conditions from rather inexpensive feedstock is possible using haloarchaea. A novel PHA production approach from CO<sub>2</sub> using synthetic biotechnology has recently been reported for the methanogen *Methanococcus maripaludis* (Palabikyan, 2020; Thevasundaram et al., 2022). In one of these works, *M. maripaludis* was engineered using selected and codon-optimized genes of the bacterial PHA production pathway and optimized using NADH regeneration as well as de novo improved NADH synthesis pathways in order to debottleneck the first enzyme of the PHA synthesis pathway, acetoacetyl-CoA dehydrogenase from acetyl-CoA (Thevasundaram et al., 2022). To conclude, metabolic engineering of PHA production from CO<sub>2</sub> opens avenues for PHA production from other, unconventional substrates.

### Archaeal lipid production and utilization

The cytoplasmatic membrane lipids of Archaea are considered to be among the most outstanding adaptations of life (Řezanka et al., 2023). Their unique composition is assumed to have enabled archaea to conquer the most extreme ecological niches on Earth, including those niches with high salinities, high and low temperatures and pH values, and anoxic environments (Siliakus et al., 2017; Valentine, 2007). Archaeal lipids are composed of a saturated isoprenoid that is bound to a sn-glycerol-1-phosphate backbone by ether-linkage (Benvegnu et al., 2008; Řezanka et al., 2023). In contrast to the cell membranes of Bacteria and Eukarya, which are composed of ester-bound acyl chains at the sn-1 and sn-2 position, cell membranes of Archaea are composed of isoprenoid chains that are bound to glycerol by ether bonds at the sn-2 and sn-3 position (Baumann et al., 2022, 2018; Gambacorta et al., 1995). The most abundant core lipid of archaea is archaeol (diether) and its dimer caldarchaeol (tetraether). All other core lipids are derivatives of these core lipids (Jain et al., 2014). Archaeol is ubiquitous to all examined archaea and forms a bilayer similar to that formed by phospholipids of bacteria. However, the bi-polar caldarchaeols are found in extreme thermophiles, thermoacidophiles and methanogens (Baumann et al., 2018; Taubner et al., 2019). Caldarchaeols, tetraether lipids, are de facto forming monolayers of the cytoplasmic membrane (Sprott, 2011). In this regard, the membrane-spanning tetraether lipids are of special interest to produce archaeosomes and lipid films (Jacquemet et al., 2009; Patel and Sprott, 1999). Tetraether lipids are composed of C40 alkyl chains that are connected by two glycerol backbones. Furthermore, among the tetraether-lipid-producing archaea, methanogens (Koga et al., 1993), produce high amounts of these lipids. Different methanogens produce various isoprenoidal hydrocarbons, di-, and tetraether lipids. Tetraether lipids are usually found as glycerol dialkyl glycerol tetraethers (GDGTs), glycerol monoalkyl glycerol tetraethers (GMGTs), and glycerol trialkyl glycerol tetraethers (GTGTs) (Baumann et al., 2018; Koga et al., 1993) but are also known from non-methanogens (Knappy et al., 2015).

The membrane core lipids of the methanogen *M. marburgensis* – and from other methanogens – are known (Baumann et al., 2022, 2018; Koga et al., 1993; Taubner et al., 2019). Depending on the

cultivation conditions, the core lipids comprise a range of isoprenoidal di- and tetraether lipids, partly with additional methylations in the alkyl chains (Baumann et al., 2022; Knappy et al., 2015).

Compared to bacterial phospholipids, the properties of the archaeal lipids were reported to possess higher resistances to oxidative stress, phospholipases as well as a wide range of pH-values and temperatures (Kaur et al., 2016). These features make them highly interesting as additions to, or replacements for, phospholipids in liposome-based commercial applications (Sprott, 2011). It has been reported that catheter surfaces were coated with monolayers of tetraether lipids from *Thermoplasma acidophilum* aiming to avoid the adherence of pathogens (Liefelth et al., 2018). Moreover, archaeal lipids can be used to produce artificial lipid films. These films reveal low permeability, long-term stability, and good insulating properties (Gambacorta et al., 1995; Jacquemet et al., 2009). Other potential applications are in the fields of biosensor design, nanotechnology, and biomimetics (Jacquemet et al., 2009). A complete overview of the features and application potential of archaeal lipids and isoprenoids has been presented before (Pfeifer et al., 2021). However, some intriguing examples for application possibilities are given hereafter.

Archaeal lipids can be used to produce liposomes. Liposomes are artificial lipid vesicles produced from phospholipids. Liposomes are tailored for their application in diagnostic imaging, as carriers of drugs, DNA, or peptides, and they are used as adjuvants in vaccine therapy (Akache et al., 2018; Kates et al., 1993; Kaur et al., 2016; Krishnan et al., 2003, 2000; Krishnan and Sprott, 2008; McCluskie et al., 2017; Patel and Sprott, 1999; Singh and Singh, 2017; Sprott et al., 1996; Sprott, 2011; Stark et al., 2019, 2019). Liposomes are still made from ester phospholipids harvested from eukaryotes, such as hydrogenated soy phosphatidylcholine or egg phosphatidylcholine (Patel and Sprott, 1999; Sprott et al., 1996).

Liposomes that are manufactured from archaeal lipids are also referred to as archaeosomes (Patel and Sprott, 1999; Santhosh and Genova, 2023). However, an archaeosome fulfils the same function as a liposome. Thus, the designation archaeosome is disputed among scientists. Especially tetraether-lipid-based archaeosomes, are reported to exhibit greater chemical and mechanical stability against very low and very high temperatures and pH, serum media, lipases, oxidative stress, and bile salts (Beveridge et al., 1993; Jacquemet et al., 2009; Patel and Sprott, 1999; Sprott et al., 1996). Furthermore, archaeosomes were demonstrated to possess higher stability in the GIT. Archaeosomes possess longer shelf life as they can undergo heat sterilization. Finally, archaeosomes showed no toxicity in mice (Jacquemet et al., 2009; Leriche et al., 2017; Patel and Sprott, 1999). Archaeosomes have already been produced using total polar lipid extractions from *M. smithii* (Krishnan et al., 2000). These archaeosomes were demonstrated to possess an improved immune response in comparison to the response triggered by non-archaeal phospholipids. The archaeosomes that were produced from *M. smithii* lipid extracts showed a long-lasting and robust immune response. This response could be attributed to the presence of caldarchaeol, which acted as an adjuvant. However, the issue with the production of *M. smithii*-based archaeosomes was that the batch-to-batch dependent composition of extracted total polar lipids made it impossible to reproducibly generate archaeosomes with an identical lipid composition (Stark et al., 2019). A batch-to-batch variation of core lipids produced by *M. marburgensis* was also recently observed (Baumann et al., 2022). However, it should be noted that production of archaeal lipids in these two studies was performed in closed batch cultivation mode. A

continuous production of archaeal lipids in bioreactors that are operated in chemostat culture should generate a lipid profile that is dependent on the specific growth rate ( $\mu$ ).

In summary, the generally high chemical and thermal stability of archaeal lipids could make them a valuable study object and resource for biotechnology, biomedicine, and the pharmaceutical industry. For instance, liposomes or lipid films are of interest (Patel and Sprott, 1999; Pfeifer et al., 2021). Thus, archaea have been suggested as organisms for the synthesis of a range of isoprenoids (please refer to references in: (Baumann et al., 2022, 2018; Pfeifer et al., 2021; Řezanka et al., 2023; Taubner et al., 2023, 2019)).

#### Gaseous biofuels production and carbonic anhydrases of archaea

Currently, the known archaeal  $H_2$  producers are found among the Euryarchaeota: Methanococci, Thermococci and Thermoprotei (Ergal et al., 2018; Kim et al., 2010; Lim et al., 2010; S. K.-M. R. Rittmann et al., 2015). Methanogens are not reported to be suitable producers of  $H_2$ , but the most studied and suitable archaea for  $H_2$  production are the hyperthermophilic Crenarchaeon *Desulfurococcus amylolyticus*, and the Euryarchaea *Pyrococcus furiosus*, *Thermococcus barophilus*, *Thermococcus kodakarensis*, *Thermococcus litoralis*, *Thermococcus paralvinellae*, and *Thermococcus onnurineus* (Bae et al., 2015, 2012, 2006; Kanai et al., 2005; Reischl et al., 2018a, 2018b). The highest reported volumetric  $H_2$  production rates have been achieved by *T. onnurineus* NA1 grown on formate or CO (Bae et al., 2015; Lim et al., 2012). However, *T. kodakarensis* has been systems biotechnologically examined with regard to uptake hydrogenases and production hydrogenases and might become a  $H_2$ -producing archaeal cell factory after synthetic biological improvement and dedicated bioprocess development. Finally, the highest volumetric production rates and yields of  $H_2$  from both substrates, carbohydrates and formate, have thus been reported for Thermococcales (Ergal et al., 2018; S. K.-M. R. Rittmann et al., 2015).

Among the archaea, methanogens have already become a biotechnologically very important group of organisms due to their  $CH_4$ -producing characteristics (Abdel Azim et al., 2017; Mauerhofer et al., 2021, 2018; Pappenreiter et al., 2019; Pfeifer et al., 2021; S. Rittmann et al., 2015; Rittmann, 2015; Rittmann et al., 2018, 2014; Seifert et al., 2014). With respect to their biotechnological applications, bioelectrochemical conversion of  $CO_2$  and biomethanation of  $H_2/CO_2$  are under research and development (Contreras et al., 2022; Enzmann et al., 2018). Thereof, several studies have shown that biomethanation of  $H_2/CO_2$  technology holds high potential for demand-oriented and intermittent power storage (Griese et al., 2019). Improvements in  $CH_4$  production by these and related archaea will come with improved understanding of their metabolism to inform metabolic engineering efforts. In this regard, the thermophilic methanogen, *Methanothermobacter marburgensis* is among the most promising model organisms for  $CO_2$ -BMP (Abdel Azim et al., 2017; Sébastien Bernacchi et al., 2014; Mauerhofer et al., 2021; Simon Rittmann et al., 2012; Rittmann et al., 2018; Seifert et al., 2014, 2014). During  $CO_2$ -BMP, the reduction of  $CO_2$  to  $CH_4$  by using and  $H_2$  is performed. High rates of  $CO_2$  to  $CH_4$  conversion were reported by using with *M. marburgensis* in a continuous culture set-up (Rittmann et al., 2018; Seifert et al., 2014). The thermophilic methanogen *M. marburgensis* is one of the workhorses of Archaea Biotechnology (Pfeifer et al., 2021). This is due to the fact that the biochemistry is very well known (Thauer, 2012; Thauer et al., 2010, 2008), it can be grown in bioreactors to high cell densities at a  $\mu$  up to  $0.69\ h^{-1}$  (Abdel Azim et al., 2017) and the genome is known (Liesegang et al.,

2010). Furthermore, the physiological and biotechnological features of *M. marburgensis* are well-known from closed batch (Abdel Azim et al., 2017; Mauerhofer et al., 2021; Pappenreiter et al., 2019; Taubner and Rittmann, 2016), fed-batch (Abdel Azim et al., 2017), and continuous culture (Sébastien Bernacchi et al., 2014; Rittmann et al., 2018; Seifert et al., 2014, 2013) experiments. Other methanogens, such as the hyperthermophilic methanogens *Methanocaldococcus jannaschii* or *Methanocaldococcus villosus* have been reported to suitably act as archaeal cell factories for high-pressure CH<sub>4</sub> production in closed batch mode and comprising high turnover rates and volumetric production rates (Mauerhofer et al., 2021). Finally, artificial microbial co-cultures of different methanogens and H<sub>2</sub>-producing archaea were shown to be able to convert CO-containing gasses to CH<sub>4</sub> (Zipperle et al., 2021).

Carbonic anhydrases (CAs) catalyse CO<sub>2</sub> hydration and conversion to bicarbonate. This reaction is a prerequisite for the flow of biochemical reactions within the cell (Ferry, 2015). CAs play a key role for carbonation processes and for mineralization in all three domains of life (Ferry, 2015, 1997; Kupriyanova et al., 2017; Kupriyanova and Pronina, 2011). Moreover, CAs are metalloenzymes containing zinc at its metal centre. From an evolutionary point of view, CAs are among the most ancient known enzymes. Currently, five different known classes of CAs are known, which are considered to have independently evolved. Only two CAs, one  $\beta$ -class and one  $\gamma$ -class CA, have yet been found in methanogens. Recently the CA of *Methanothermobacter thermautotrophicus* was examined regarding its hydration properties and compared to two CAs from bacteria. Regarding the biotechnological potential of the tested archaeal CA, the bacterial CAs were found to be superior with regard to turnover rates (Steger et al., 2022).

In summary, CH<sub>4</sub> production by methanogens from H<sub>2</sub>/CO<sub>2</sub> is very much advanced with several lab, pilot, and demonstration facilities in operation. However, despite the high physiological and biotechnological potential of some archaea for H<sub>2</sub> production scale-up of the H<sub>2</sub> production technology is still very much at its infancy. The same is true for CAs of methanogenic archaea, which still need to be heavily optimized to improve their conversion rates and yields.

### **Author contribution statement**

This cumulative habilitation thesis is my own work. I have compiled this cumulative habilitation thesis on my own. Some parts of the materials and methods as well as of the results that are shown in chapter 1 and in chapter 2 have been partly shown in a different form in a peer-reviewed paper in that has been published in mSystems (Taubner et al., 2023) and shall be published in another peer-reviewed paper (Reischl et al., manuscript in preparation). In both articles, I am both, the corresponding and the last author. In addition, this cumulative habilitation thesis comprises 12 published peer-reviewed research papers. My contribution to each of these peer-reviewed papers is listed in the author contribution statement of each paper and in the commentary section of this thesis. In brief, I contributed to the conceptualization of the individual studies, the design of experiments (OVAT and DoE), partially performed experiments, data analysis and data validation, (multivariate) statistical analysis, visualization of results, providing methods and equipment, supervision of research of bachelor, master, PhD students and post docs as well as drafting and writing manuscripts. Moreover, the research that is shown in this cumulative habilitation thesis and in the peer-reviewed papers was partly only possible due to acquiring third-party funding from governmental institutions and from industrial partners. In these third-party acquired projects or industrial projects, I served as the PI, Co-PI or national collaborator. Hence, I performed mentoring of students and post docs, project management, writing of interim and final project reports, project administration and management.

### **Approbations of results and peer-reviewed publication results of this habilitation thesis**

Some of the results that are shown in this cumulative habilitation thesis have been presented at national and international scientific conferences, national and international institute/department seminars, at digital conferences, and in panel discussions. All full list of my presentations, outreach activities and conference contributions are available in the curriculum vitae in this habilitation thesis. In brief, I held a keynote on “Highlights from ten years of pure culture biological CH<sub>4</sub> production from H<sub>2</sub>/CO<sub>2</sub>” at the UFZ Energy Days 2019, Leipzig, Germany, and a keynote lecture in on “Methane cell factories” in the *Webinar series on biological carbon capture and utilization* (online).



## **Methods used in the frame of this habilitation thesis**

### Strains

*Methanothermobacter marburgensis* DSM 2133, *Methanothermococcus okinawensis* DSM 14208, and *Methanocaldococcus villosus* DSM 22612 have been initially obtained from the Deutsche Sammlung von Mikroorganismen und Zellkulturen GmbH (DSMZ, Braunschweig, Germany), but all strains were stored in an in-house strain collection of the Archaea Physiology & Biotechnology Group of the University of Vienna and used whenever required.

### Chemicals

H<sub>2</sub> (99.999 Vol.-%), CO<sub>2</sub> (99.999 Vol.-%), N<sub>2</sub> (99.999 Vol.-%), H<sub>2</sub>/CO<sub>2</sub> (20 Vol.-% CO<sub>2</sub> in H<sub>2</sub>) (4:1), H<sub>2</sub>/CO<sub>2</sub>/N<sub>2</sub> (11.13 Vol.-% N<sub>2</sub> and 11.13 Vol.-% CO<sub>2</sub> in H<sub>2</sub>) (7:1:1) were used for growth of pre-cultures, for closed batch and for fed-batch experiments. For gas chromatography (GC), N<sub>2</sub>/CO<sub>2</sub> (20 Vol.-% CO<sub>2</sub> in N<sub>2</sub>), CH<sub>4</sub> (99.995 Vol.-%) and the standard test gas (Messer GmbH, Wien, Austria) (containing 0.01 Vol.-% CH<sub>4</sub>, 0.08 Vol.-% CO<sub>2</sub> in N<sub>2</sub>) were additionally used. All gases, except the standard test gas, were purchased from Air Liquide (Air Liquide GmbH, Schwechat, Austria). All other chemicals were of highest grade available.

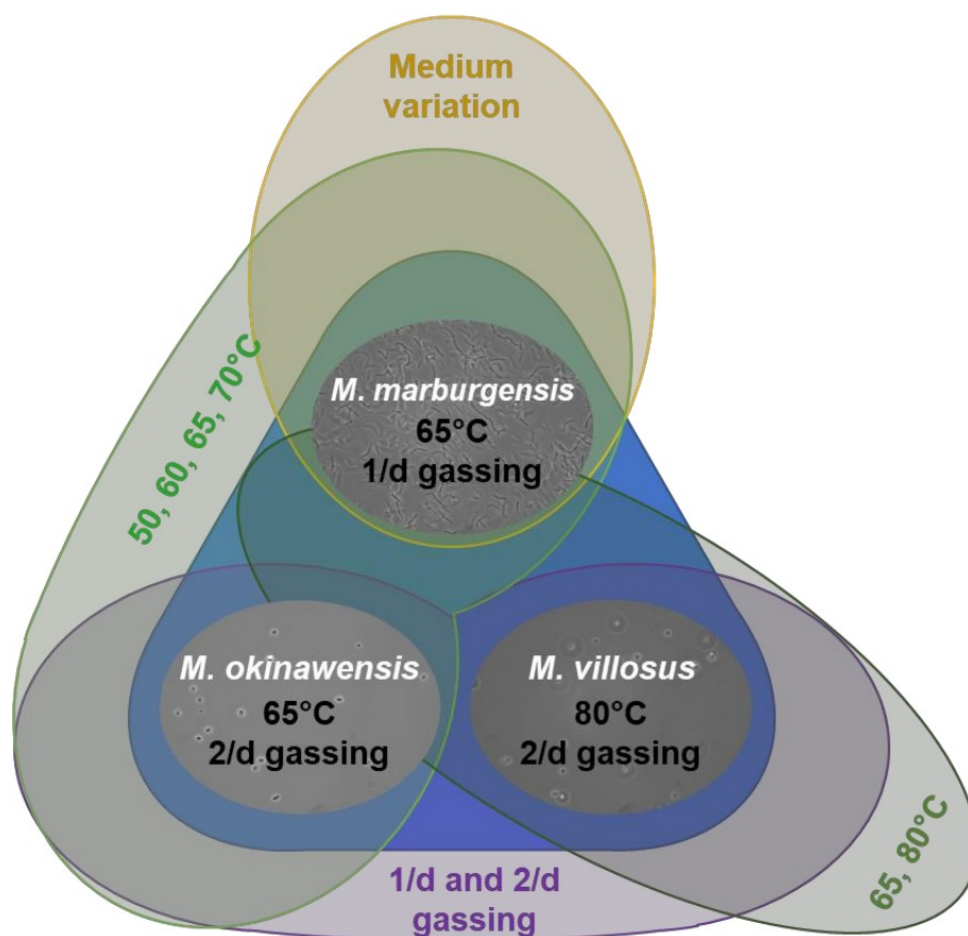
### Analysis of ammonium, amino acids, lipids and gases

NH<sub>4</sub><sup>+</sup> determination was performed as described before (Reischl et al., 2025). For analyses of proteinogenic amino acids details the method and procedure were used as it had been described before (Reischl et al., 2025; Taubner et al., 2023, 2019). Cytoplasmic lipids of methanogens were analysed as reported before (Baumann et al., 2022, 2018; Taubner et al., 2023, 2019). Gas conversion determination from closed batch cultivations was done as previously reported (Taubner and Rittmann, 2016). Off-gas sampling of fed-batch cultivations was done as described previously performed (Reischl et al., 2018a). For fed-batch experiments, the gas samples were taken after approximately 0, 13, 16, 19, 22 and 25 h. The off-gas composition analysis using gas chromatography has been performed as described before (Abdel Azim et al., 2017; Reischl et al., 2018a; Taubner and Rittmann, 2016).

### Media and closed batch cultivation of thermophilic and hyperthermophilic methanogens

Closed batch cultivations were conducted in 120 mL SB (La-Pha-Pack, Langerwehe, Germany) in chemically defined media (Baumann et al., 2022, 2018; Reischl et al., 2025; Taubner et al., 2023, 2019; Taubner and Rittmann, 2016). Depending on the experimental setup, the liquid medium volume had a volume of 25 mL, 50 mL or 75 mL. The exact procedure of media preparation, inoculation and incubation are described elsewhere (Taubner and Rittmann, 2016). The inoculum was taken from an exponentially growing pre-culture. The inoculum volume was 2% (v/v). The cultures were gassed once or twice per day with a H<sub>2</sub>/CO<sub>2</sub> test gas mixture (20 Vol.-% CO<sub>2</sub> in H<sub>2</sub>) of approximately 2 bar relative pressure (Taubner and Rittmann, 2016). The head space pressure measurements of the serum bottles were performed with a digital manometer (LEO1-Ei, -1...3 bar, Keller, Germany). For each experimental setup, two independent experiments were performed – one without (marked with “I”) and with (“II”) turbidity (optical density (OD)) measurements. The OD sampling for before each gassing event in closed batch was done according to the used method (Taubner and Rittmann, 2016). Each time approx. 0.7 mL sample was used for measurement of OD. Growth was hence

recorded via OD (at 578 nm, blanked with Milli-Q water, spectrometer: DU800, Beckman Coulter, USA). A negative control, a non-inoculated bottle that only included medium, was incubated together with the other bottles as background reference for the OD and amino acids measurements. The utilization of a background reference for the lipid measurements was not feasible due to the low amount of sampling material available after harvesting the zero controls. The incubation temperature varied between the different strains: *M. marburgensis* and *M. okinawensis* were maintained at 50 °C, 60 °C, 65 °C (optimal temperature), and 70 °C. *M. villosus* was cultured at 65 °C and 80 °C (optimal temperature). After completion of each experiment, biomass and supernatant were harvested by centrifuging each culture for 20 min at 4,500 rpm (3328 rcf) and 4 °C in 50 mL Greiner tubes (Hettich Universal 320R). Subsequently, the cell pellets and 3x1 mL of supernatant of each bottle were separately stored in sterile Eppendorf tubes at -20 °C until further analysis (Taubner et al., 2023). An overview of the experimental set-up, where the cultivation conditions are indicated, can be found in **Figure 3**.



**Figure 3:** Schematic illustration of the different cultivation environments. All experiments at 65 °C were conducted with 25 mL, 50 mL and 75 mL liquid medium. The standard growth conditions are highlighted in the blue triangle. For *M. okinawensis* and *M. marburgensis*, experiments at 50 °C, 60 °C and 70 °C were conducted only using 50 mL (no growth for *M. marburgensis* at 70 °C has been observed). In addition, experiments performed at 65 °C were conducted with *M. villosus* using 25 mL, 50 mL and 75 mL of medium. For *M. marburgensis* (65 °C), the medium (with and without carbonates) and for *M. okinawensis* and *M. villosus* the gassing ratio (once, 1/d, or twice, 2/d, per day) were additionally varied.

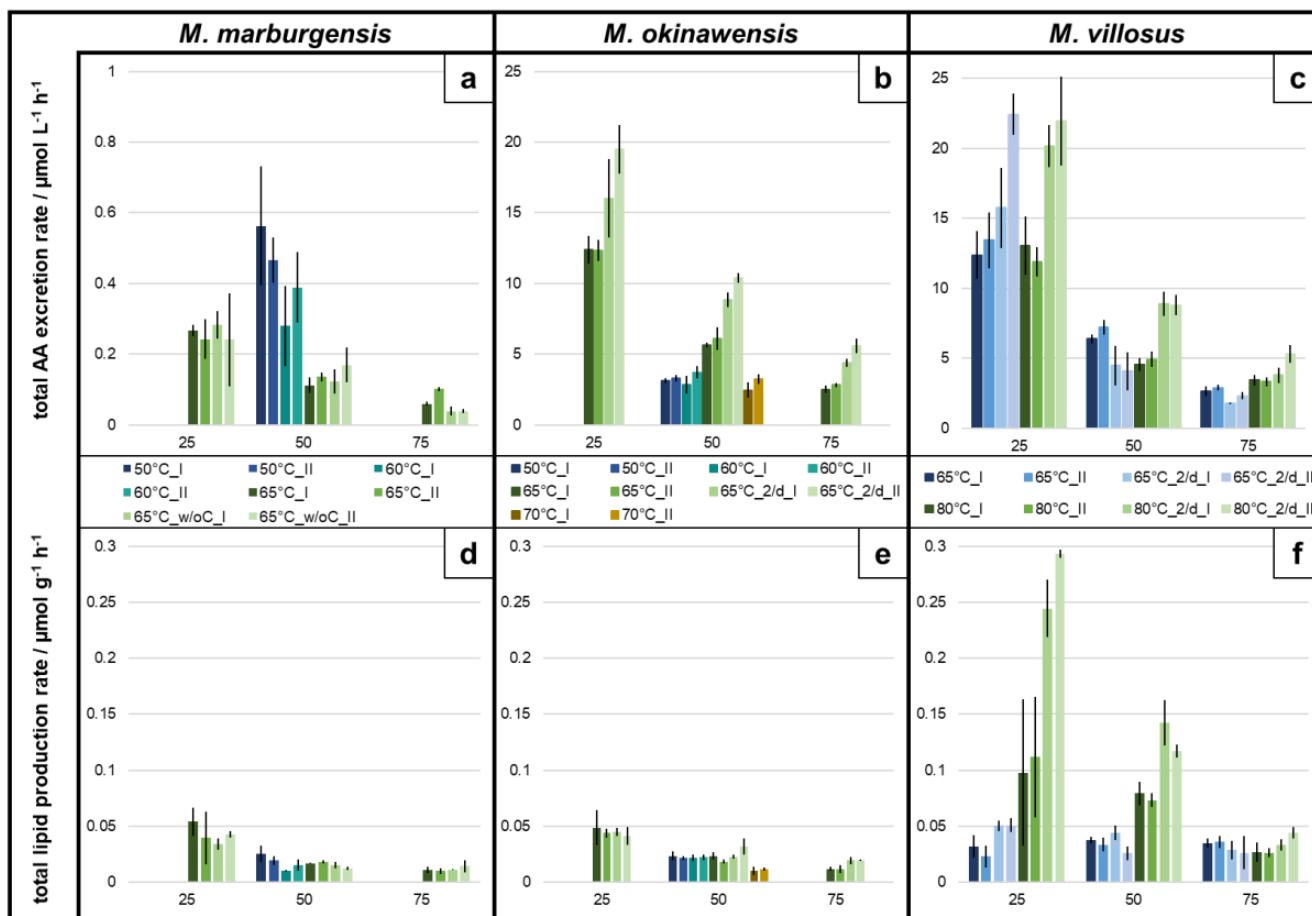
### Media and fed-batch cultivation of *M. marburgensis*

Cultures of *M. marburgensis* were grown on minimal medium (Schönheit et al., 1979) adjusted according to cultivation specific requirements (Abdel Azim et al., 2017; S. Rittmann et al., 2012). For inoculation of bioreactors, a stock culture, which was stored at 4 °C and that had been adapted to fed-batch cultivation in bioreactors was used. Fed-batch cultivation was performed at different  $\text{NH}_4^+$  concentrations (0%, 1%, 5%, 10% and 100%) in relation to original media composition of  $2.1 \text{ g L}^{-1}$  (Reischl et al., 2025). Experiments were performed with  $\text{Na}_2\text{CO}_3$  (wC) medium (S. Rittmann et al., 2012) and in medium without  $\text{Na}_2\text{CO}_3$  (carbonate-free medium) (Abdel Azim et al., 2017).  $\text{Na}_2\text{CO}_3$  in carbonate-free media was replaced by equal molarities of NaCl. All fed-batch experiments were performed with *M. marburgensis* in triplicates ( $n = 3$ ) in DASGIP® 2.2 L bioreactor system (SR1500ODLS, Eppendorf AG, Hamburg, Germany) with 1.5 L working volume of medium with  $100 \mu\text{L L}^{-1}$  of antifoam (Struktol SB2023, Schill und Seilacher, Hamburg, Germany) with  $\text{H}_2/\text{CO}_2/\text{N}_2$  (7:1:1). Optimal growth conditions for *M. marburgensis* are at a temperature of 65 °C and a pH of 7 (Abdel Azim et al., 2017; S. Rittmann et al., 2012; Rittmann et al., 2018; Seifert et al., 2014). Fed-batches with and without  $\text{Na}_2\text{CO}_3$  in the medium and fed-batches performed with  $\text{H}_2/\text{CO}_2$  (4:1) served as reference. Gassing of  $\text{N}_2$  and  $\text{CO}_2$  was controlled via the MX4/4 unit (Eppendorf AG, Hamburg, Germany).  $\text{H}_2$  gas flow was controlled via the C100L Unit (Sierra Instruments, Monterey, USA). Redox potentials and pH values were monitored by individual redox- and pH-probes (Mettler Toledo GmbH, Wien, Austria). Directly before inoculation the bioreactor was gassed with the respective gas ( $\text{H}_2/\text{N}_2/\text{CO}_2$  or  $\text{H}_2/\text{CO}_2$ ) to ensure that the conditions inside the bioreactor are anaerobic. After anaerobization, 5 mL of  $0.5 \text{ mol L}^{-1} \text{Na}_2\text{S} \cdot 9\text{H}_2\text{O}$  were added.

Immediately after inoculation of 30 mL *M. marburgensis* suspension,  $0.5 \text{ mol L}^{-1} \text{Na}_2\text{S} \cdot 9\text{H}_2\text{O}$  feeding at  $0.2 \text{ mL h}^{-1}$  of a  $0.5 \text{ mol L}^{-1} \text{Na}_2\text{S} \cdot 9\text{H}_2\text{O}$  stock solution was started, and the agitation speed was set to 1600 rpm. Gas and liquid samples were taken after approximately 0, 13, 16, 19, 22 and 25 h of cultivation. Growth was measured spectrophotometrically via OD ( $\lambda = 578 \text{ nm}$ , blanked with Milli-Q water) (Beckman Coulter, DU 800 spectrophotometer, California, USA). Liquid samples of 1 mL for amino acid analysis were taken at each timepoint and centrifuged at full speed (16,100 rcf) for 30 min (5415 R, Eppendorf AG, Hamburg, Germany). Cell pellets and supernatant were separately stored in sterile Eppendorf tubes at -20 °C until further analysis (Reischl et al., manuscript in preparation).

### **Chapter 1**

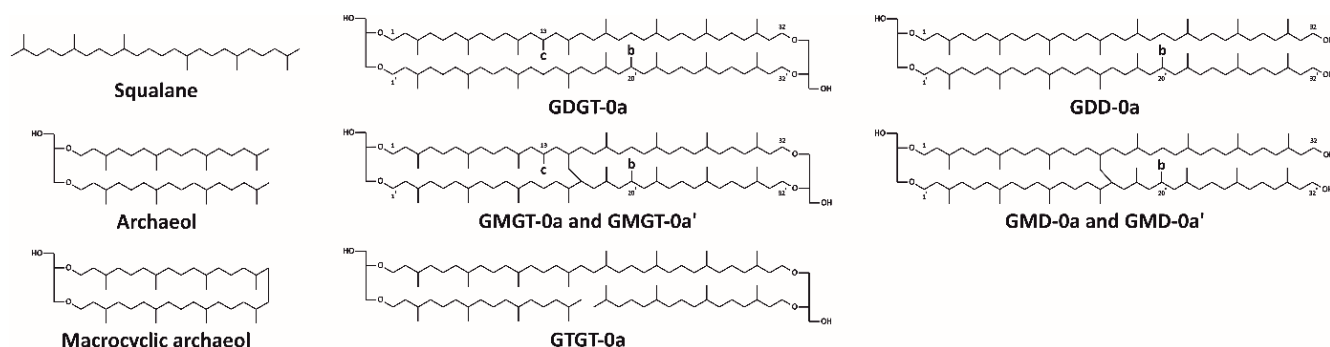
An overview of the results for the total amino acid excretion rate (AAER) /  $\mu\text{mol L}^{-1} \text{h}^{-1}$  and the total lipid production rate /  $\mu\text{mol g}^{-1} \text{h}^{-1}$  of *M. marburgensis*, *M. okinawensis* and *M. villosus* under different growth conditions in closed batch cultivation mode are shown in **Figure 4**. **Figure 4a-c** (green bars) demonstrate that an increased gaseous substrate availability was accompanied by increased amino acid excretion at optimal growth temperature for each organism. At least traces of all of the 18 tested amino acids were found in most cultures at the end of the experiments. Changes of the lipidome of three methanogens, *M. marburgensis*, *M. okinawensis* and *M. villosus*, were compared at different temperatures and substrate concentrations to reveal their lipid-specific adaptation patterns **Figure 4d-f**.



**Figure 4:** Total amino acid (AA) excretion rate /  $\mu\text{mol L}^{-1} \text{h}^{-1}$  and total lipid production rate /  $\mu\text{mol g}^{-1} \text{h}^{-1}$  for *M. marburgensis*, *M. okinawensis*, and *M. villosus*. **a, b, c:** The total amino acid excretion rate is based on endpoint measurements. **d, e, f:** The total lipid production rate is based on endpoint measurements. Each bar represents  $n = 4$ . The error bars show standard deviations. The bars were grouped regarding the volume of the liquid medium at the starting point (25 mL, 50 mL, and 75 mL). Experiments were performed at different incubation temperatures, whereby the green bars represent experiments performed at the respective optimal growth temperature. Experiments were both performed without (labelled with “I”) and with (“II”) additional optical density (OD) measurements during each gassing procedure. For *M. marburgensis*, experiments were additionally performed without carbonate addition (labelled with “w/oC”). The label “2/d” refers to two gassing procedures per day - otherwise, gassing was performed once per day. The figure and the text were adapted from Taubner et al. 2023.

### Comparative lipidomics of thermophilic and hyperthermophilic methanogens

An overview of the lipids that were detected in the three thermophilic and hyperthermophilic methanogens are shown in **Figure 5**. The lipid inventory comprised the tetraether lipids GTGT-0 (glycerol trialkyl glycerol tetraether), GDGT-0 (glycerol dialkyl glycerol tetraether), and GMGT-0 (glycerol monoalkyl glycerol tetraether), as well as the diethers archaeol and macrocyclic archaeol. For *M. marburgensis*, the degree of methylation (0, 1, 2) of the basic structure of GMGT-0 and GDGT-0 is displayed as the relative percentages of the different methylated species (a, b, c) of the sum of all di- and tetraethers, respectively (Taubner et al., 2023).

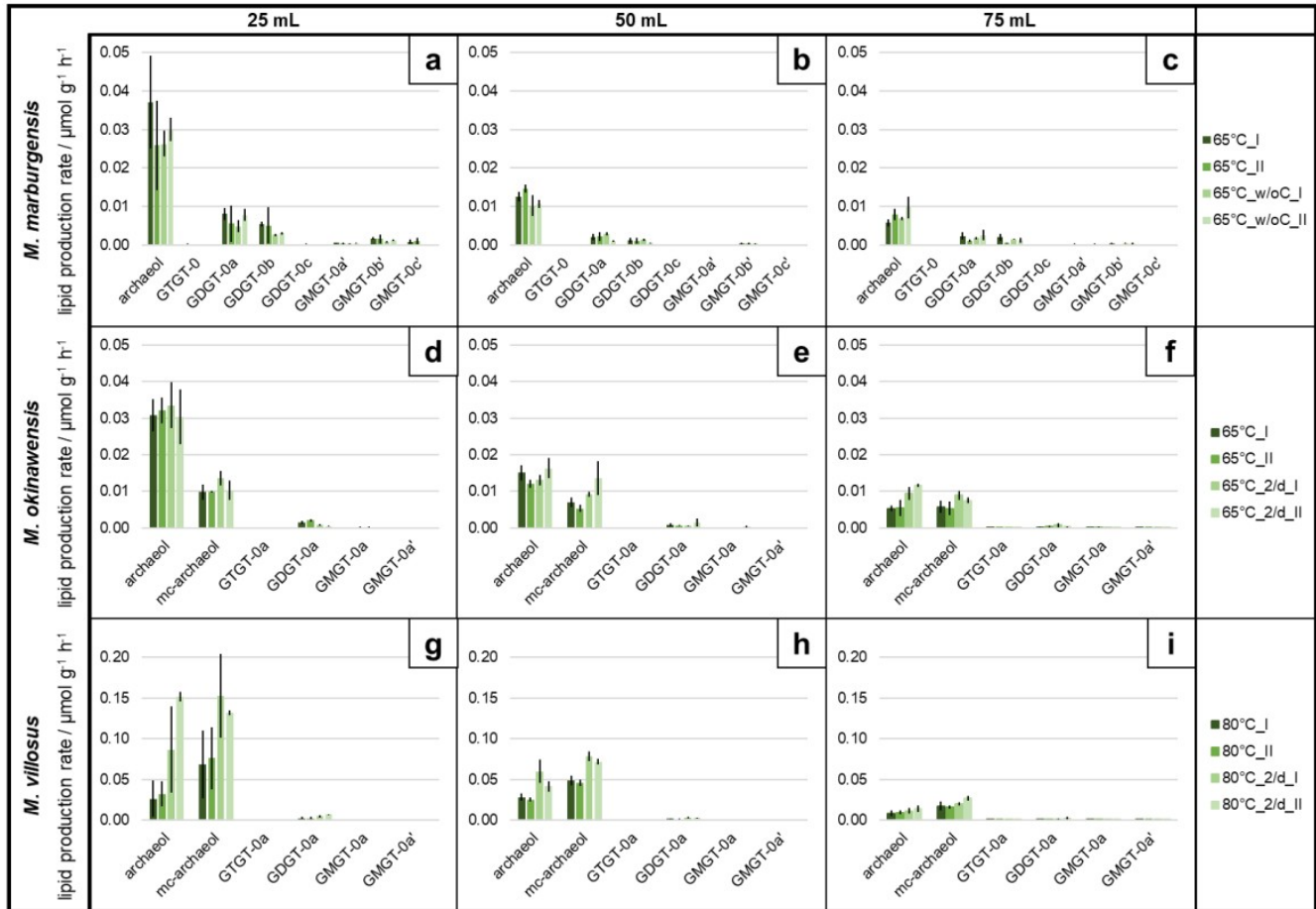


**Figure 5:** Structures of core lipids of *M. marburgensis*, *M. okinawensis*, and *M. villosus*. *M. marburgensis* produced the most diverse lipid profile, i.e. a range of diether and tetraether lipids (measured as core lipids). The major tetraether lipids produced are GDGT-0a, -0b, and -0c (glycerol dialkyl glycerol tetraether with a = zero, b = one, and c = two additional methylations), and GMGT-0a, -0a', -0b, -0b', -0c' (glycerol monoalkyl glycerol tetraether, two isomers with zero and one, and one isomer with two additional methylations), plus the tetraether lipid GTGT-0 (glycerol trialkyl glycerol tetraether). The major diether lipid synthesized by *M. marburgensis* is archaeol. It further produces minor amounts of other diethers, which are composed of two C 40 alkyl chains, GDD-0a and -0b (glycerol dialkyl diether with zero rings, without or with one additional methylation), as well as GMD-0a' (glycerol monoalkyl diether without rings and additional methylation, second structural isomer) and GMD-0b' (glycerol monoalkyl diether without rings, with one additional methylation, second structural isomer). *M. villosus* and *M. okinawensis* synthesize the diether lipids archaeol and macrocyclic archaeol, and minor amounts of GDD-0a, GMD-0a, and GMD-0a'. Their tetraether lipid inventories comprise GDGT-0a, and minor GTGT-0a, GMGT-0a, and GMGT-0a'. In contrast to *M. marburgensis*, no diether or tetraether lipids with additional methylations were found in *M. villosus* or in *M. okinawensis*. Note that the exact positions of the covalent carbon-carbon bonds between the isoprenoid chains of GMGT-0 and GMD-0 are unknown (Baumann et al., 2022, 2018; Taubner et al., 2019).

The tetraether GMGT-0 comes as two isomers, one eluting earlier, the other later (Taubner et al., 2023). For the various strains, later eluting isomers are indicated as GMGT-0a', GMGT-0b', and GMGT-0c', respectively (Taubner et al., 2023). A correlation with temperature, the presence of carbonate in the initial medium, and the volume of the medium was observed for the synthesis of GDGT-0a and -0b. The presence of carbonate in the medium influenced the distribution of methylated species of GMGT-0. The later eluting GMGT-0a' and GMGT-0c' isomer distributions were dependent on temperature, while GMGT-0a' and GMGT-0b' were correlated with the initial liquid volume (Taubner et al., 2023).

The most prominent lipids of *M. marburgensis* are archaeol, GDGT-0a, and -0b, whereas *M. okinawensis* and *M. villosus* predominantly synthesise archaeol, macrocyclic archaeol, and GDGT-0a (**Figure 6**) (Taubner et al., 2023). *M. villosus* revealed total lipid production rates up to seven times higher than production rates of *M. marburgensis* and *M. okinawensis*, respectively. Under standard growth conditions at 50 mL, *M. okinawensis* exhibited a mean total lipid production rate of  $27.6 \pm 6.9$  nmol g<sup>-1</sup> h<sup>-1</sup>, while that of *M. villosus* was  $127.7 \pm 18.5$  nmol g<sup>-1</sup> h<sup>-1</sup>. For *M. okinawensis* and *M. villosus* mainly archaeol and macrocyclic archaeol were detected. The specific lipid production rates of diethers and tetraethers of *M. okinawensis* largely depended on liquid volume. Moreover, the specific production rates of diethers were influenced by the gassing frequency. For *M. villosus*, only the ratio of diethers to tetraethers was affected by gassing frequency and by the liquid volume. A dependence on temperature was only observed in correlation with volume (and gassing). While the specific lipid production rate was similar within the experiments performed at the same liquid volume for *M.*

*marburgensis* and *M. okinawensis*, the ratio of diethers to tetraethers varied between the cultures of *M. villosus* gassed 1/d and those gassed 2/d at the optimal growth temperature of 80 °C (**Figure 6**).



**Figure 6:** Lipid production rates for *M. marburgensis*, *M. okinawensis*, and *M. villosus* at optimal growth temperature. The lipid production rates for different species in  $\mu\text{mol g}^{-1} \text{h}^{-1}$  based on endpoint measurements for **a, b, c**: *M. marburgensis*, **d, e, f**: *M. okinawensis*, and **g, h, i**: *M. villosus* at different initial liquid volumes (25 mL, 50 mL and 75 mL). Each bar represents  $n = 4$ . The error bars indicate standard deviations. Experiments were either performed without (labelled with “I”) or with (“II”) additional optical density (OD) measurements during each gassing procedure. For *M. marburgensis*, experiments were also performed without carbonate addition (labelled with “w/oC”). The label “2/d” refers to two gassing procedures per day - otherwise, gassing was performed once per day. The figure and the text were adapted from Taubner et al. 2023.

At a volume of 25 mL, gassing 2/d resulted in a higher specific lipid production rate (**Figure 6**), while at a volume of 75 mL, the gassing rate did not influence the lipidome (**Figure 6**). A variation of the cultivation temperature also affected the lipid inventory of the three methanogens. For *M. marburgensis*, the specific production rate of archaeol in 50 mL liquid medium was high at 50 °C, decreased at 60 °C and increased again at 65 °C, while the total production rate of lipids stayed almost constant at all temperatures. A similar, but slightly weaker trend than for archaeol was found for GDGT-0a and GDGT-0b. However, the specific production rate of GMGT-0 increased only at 60 °C. When comparing the 50 mL experiments at 50, 60, and 65 °C, the total specific lipid production rate stayed constant in *M. okinawensis*, but the ratio between the specific archaeol and macrocyclic archaeol production rates changed. *M. okinawensis* revealed a high specific production rate of archaeol at 50 °C

and 65 °C, while at 60 °C macrocyclic archaeol dominated. For *M. villosus* the total specific lipid production rate was found to be higher at 80 °C compared to 65 °C, and macrocyclic archaeol always dominated over archaeol in the 50 mL experiments. However, at 25 mL and 75 mL, this trend was not observed (Taubner et al., 2023).

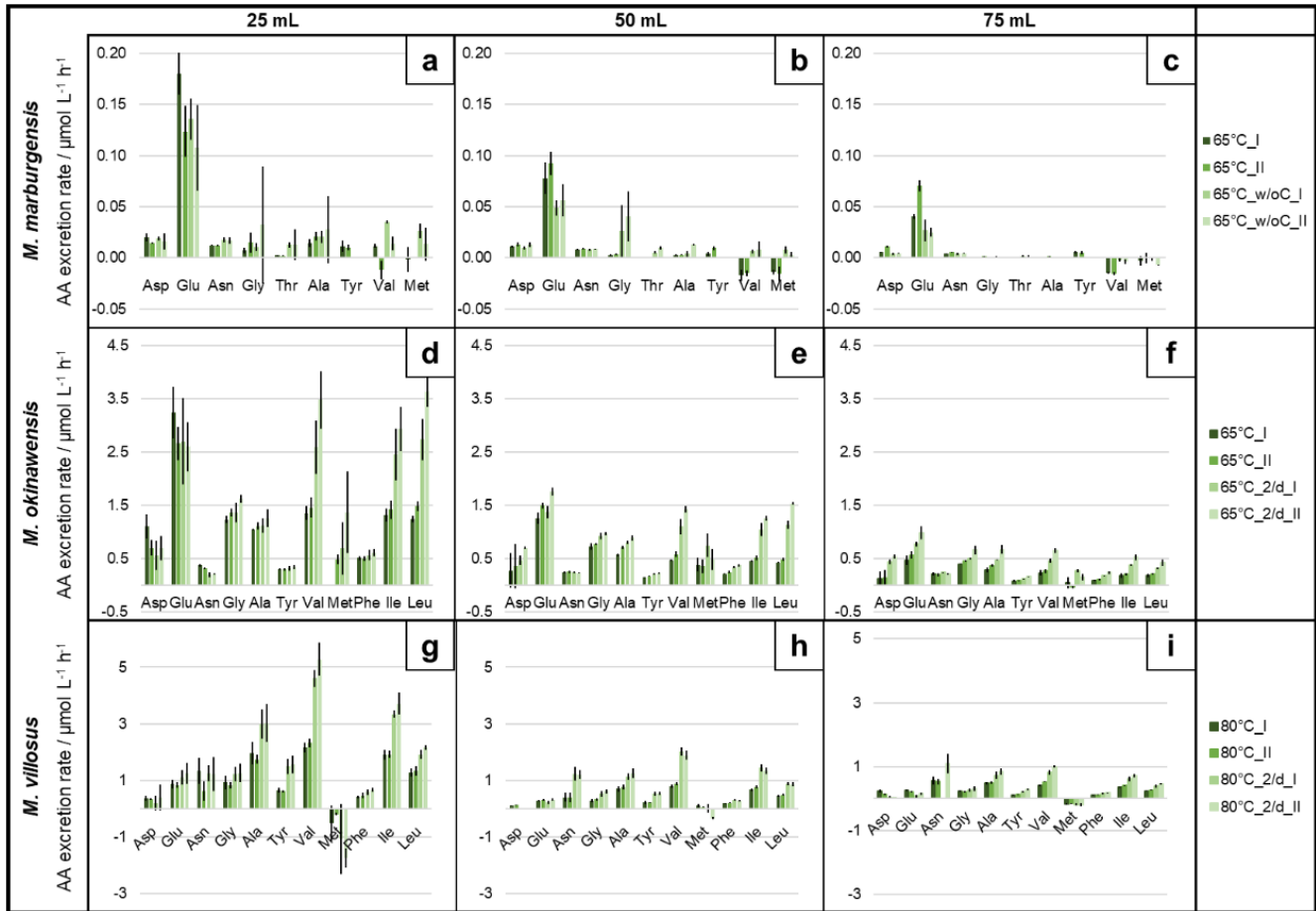
#### Comparative amino acid excretion of thermophilic and hyperthermophilic methanogens

Besides the investigation of the lipidome a quantitative determination of the proteinogenic amino acid excretion patterns of the three methanogenic strains has been performed. The amino acid excretion rates of *M. marburgensis*, *M. okinawensis* and *M. villosus* for the 18 quantifiable proteinogenic amino acids are shown in **Figure 7**. In numbers, the ratio between 25 mL, 50, mL and 75 mL (without OD) at standard growth conditions was approx. 4.5:1.9:1 for *M. marburgensis*, approx. 3.7:2.0:1 for *M. okinawensis*, and 5.3:2.3:1 for *M. villosus*. However, *M. marburgensis* excreted far less amino acids than the other two strains at the same substrate concentration and gassing interval ( $0.11 \pm 0.02 \mu\text{mol L}^{-1} \text{h}^{-1}$  compared to  $5.65 \pm 0.18$  for *M. okinawensis* and  $4.56 \pm 0.47 \mu\text{mol L}^{-1} \text{h}^{-1}$  for *M. villosus* for optimal growth temperature, 1/d gassing, without OD (**Figure 7a-c**). The most prominent excreted amino acid in all *M. marburgensis* experiments at an optimal growth temperature of 65 °C was Glu (**Figure 7a-c**). Therefore, the decrease of the AAER of *M. marburgensis* from 25 mL to higher liquid volumes is due to the decrease of Glu. Interestingly, the total AAER of *M. marburgensis* was higher at lower temperatures (50 °C and 60 °C) for a liquid volume of 50 mL (50 °C:  $0.56 \pm 0.17 \mu\text{mol L}^{-1} \text{h}^{-1}$ , 60 °C:  $0.28 \pm 0.11 \mu\text{mol L}^{-1} \text{h}^{-1}$ , 65 °C:  $0.11 \pm 0.02 \mu\text{mol L}^{-1} \text{h}^{-1}$ ), which was observed for *M. villosus* only for the 1/d gassing experiments and not at all for *M. okinawensis* (**Figure 4a-c**, blue and cyan bars). This peculiarity in *M. marburgensis* for 50 °C is due to an extreme increase in the excretion rate of Ala (from  $2.7 \pm 0.5 \mu\text{mol L}^{-1} \text{h}^{-1}$  at 65 °C to  $310 \pm 70 \mu\text{mol L}^{-1} \text{h}^{-1}$  at 50 °C), and for 60 °C of Gly (from  $2.9 \pm 0.9 \mu\text{mol L}^{-1} \text{h}^{-1}$  at 65 °C to  $206 \pm 38 \mu\text{mol L}^{-1} \text{h}^{-1}$  at 60 °C (**Figure 7**). The amount of Asp, Asn, and Tyr slightly increased with temperature, while the amount of Val and Thr decreased. The AAER for Glu was almost the same for all temperatures (Taubner et al., 2023).

*M. okinawensis* showed the highest total AAER at its optimal growth temperature (65 °C), especially when gassed twice per day ( $10.38 \pm 0.35 \mu\text{mol L}^{-1} \text{h}^{-1}$ , with OD (**Figure 4b**), which agrees with the kinetics of substrate uptake (Mauerhofer et al., 2021; Taubner et al., 2023; Taubner and Rittmann, 2016). Generally, the total AAER at 50 °C, 60 °C, and 70 °C (50 mL) were in the same range (2.5 to  $3.7 \mu\text{mol L}^{-1} \text{h}^{-1}$  (**Figure 4b**, blue, cyan, and brown bars), but the amino acid patterns varied at different temperatures (**Figure 4b**). Compared to the other temperatures tested, Val, Ile, and Leu were high at 50 °C and 65 °C, whereas Gly and Ala were excreted the most at 65 °C. Glu, Asn, Phe, and Tyr production tended to be higher at 60 °C and 65 °C. Met showed an unusual pattern, as an excretion was only observed at 65 °C. No interpretation of the Asp-pattern is possible, as it was detected only in half of the samples (Taubner et al., 2023). The total amino acid excretion rate of *M. villosus* was in the same range as that of *M. okinawensis* (**Figure 4b** and **Figure 4c**). However, the pattern of the individual amino acids was different between the two strains (**Figure 7d** to **Figure 7i**). For *M. villosus*, Val, Ile, Ala, Asn, and Leu were the most prominent excreted amino acids at the optimal growth temperature (80 °C), while for *M. okinawensis* Glu and Gly replaced Asn as additional dominant amino acids (65 °C). A different pattern was found for *M. villosus* at lower temperature (65 °C) for the 25 mL liquid volume samples, representing the only setting where Asp ( $5.14 \pm 0.22 \mu\text{mol L}^{-1} \text{h}^{-1}$ , 2/d gassing, with OD) and



Glu ( $7.37 \pm 0.49 \mu\text{mol L}^{-1} \text{h}^{-1}$ , 2/d gassing, with OD) are not only dominating, but showing the highest rate of all experiments (Taubner et al., 2023).



**Figure 7:** Amino acid excretion rates (AAERs) for *M. marburgensis*, *M. okinawensis*, and *M. villosus* at optimal temperature. AAERs for different species in  $\mu\text{mol L}^{-1} \text{h}^{-1}$  based on endpoint measurements for **a, b, c:** *M. marburgensis*, **d, e, f:** *M. okinawensis*, and **g, h, i:** *M. villosus* at different initial liquid volumes (25 mL, 50 mL and 75 mL). Each bar represents  $n = 4$ . Bars represent those amino acids, where a difference of more than  $0.5 \mu\text{mol L}^{-1}$  to the negative control was detected in most of the replicates. The error bars show standard deviations. Experiments were both performed without (labelled with “I”) and with (“II”) additional optical density (OD) measurements during each gassing procedure. For *M. marburgensis*, experiments were additionally performed without carbonate addition (labelled with “w/oC”). The label “2/d” refers to two gassing procedures per day - otherwise, gassing was performed once per day. The figure and the text were adapted from Taubner et al. 2023.

At 65 °C, gassing once per day (50 mL) (**Figure 7i**) favoured higher AAERs of *M. villosus*, especially for Glu, Gly, Ala, Val, Ile, and Leu, which was unexpected (and was not observed at 80 °C) as it has been suggested that higher gas availability leads to higher production of metabolites (Mauerhofer et al., 2021; Taubner et al., 2023; Taubner and Rittmann, 2016). At the standard growth conditions of *M. villosus* at 50 mL, 2/d gassing led to a higher excretion rate of mainly Val ( $2.02 \pm 0.16 \mu\text{mol L}^{-1} \text{h}^{-1}$ , without OD), Asn ( $1.23 \pm 0.25 \mu\text{mol L}^{-1} \text{h}^{-1}$ , without OD), Ile ( $1.45 \pm 0.13 \mu\text{mol L}^{-1} \text{h}^{-1}$ , without OD), Ala ( $1.25 \pm 0.16 \mu\text{mol L}^{-1} \text{h}^{-1}$ , with OD), Tyr ( $0.55 \pm 0.06 \mu\text{mol L}^{-1} \text{h}^{-1}$ , with OD), and Leu ( $0.88 \pm 0.06 \mu\text{mol L}^{-1} \text{h}^{-1}$ , without OD). High Met excretion rates were only observed for the cultures gassed twice per day at 65 °C (for all volumes) (Taubner et al., 2023).

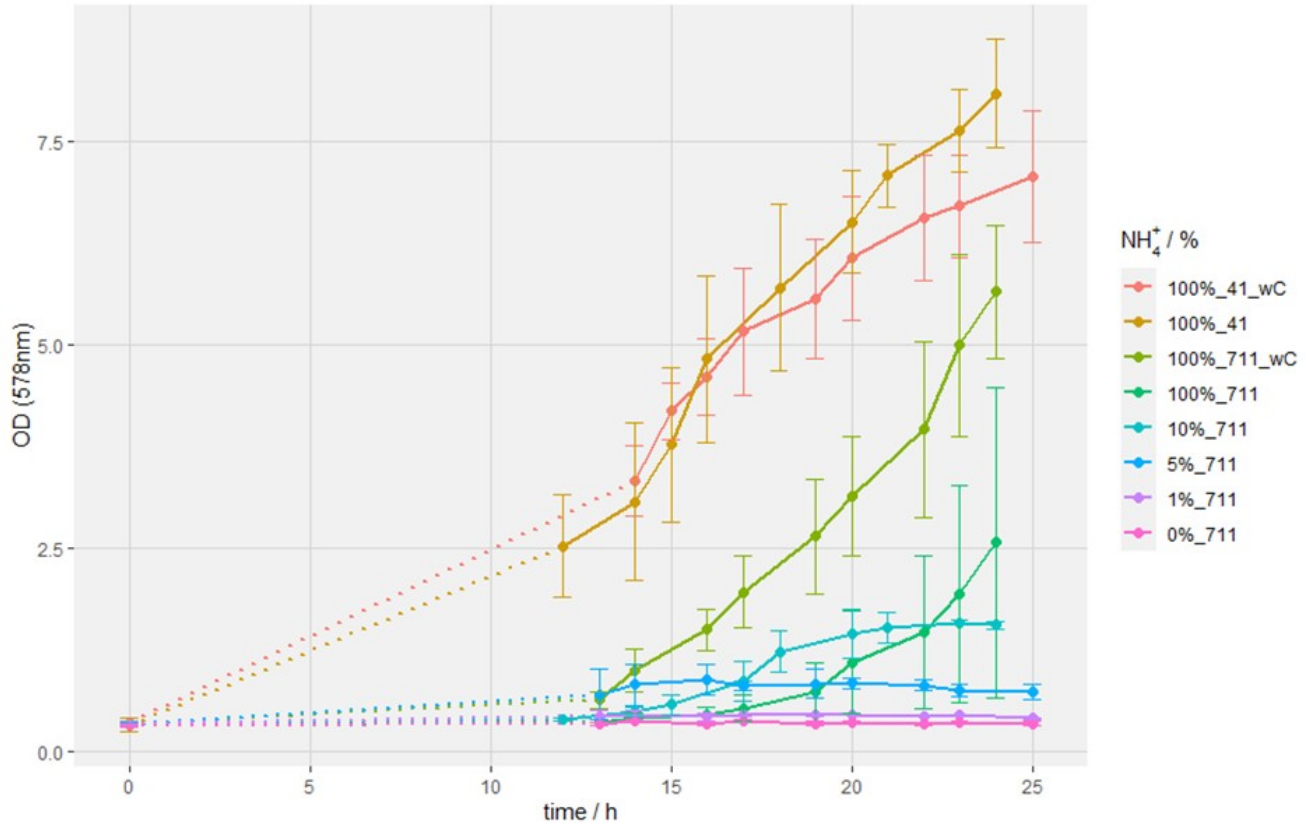


Finally, a comparison of  $\text{NH}_4^+$  uptake rates and AAERs revealed a ratio of close to 1:1 for *M. okinawensis*. For *M. marburgensis*, by far more  $\text{NH}_4^+$  was taken up than amino acids were excreted. On the contrary, the AAER of *M. villosus* was higher than the  $\text{NH}_4^+$  uptake rate (Taubner et al., 2023).

## Chapter 2

### Amino acid excretion by *M. marburgensis* grown in fed-batch cultivation mode

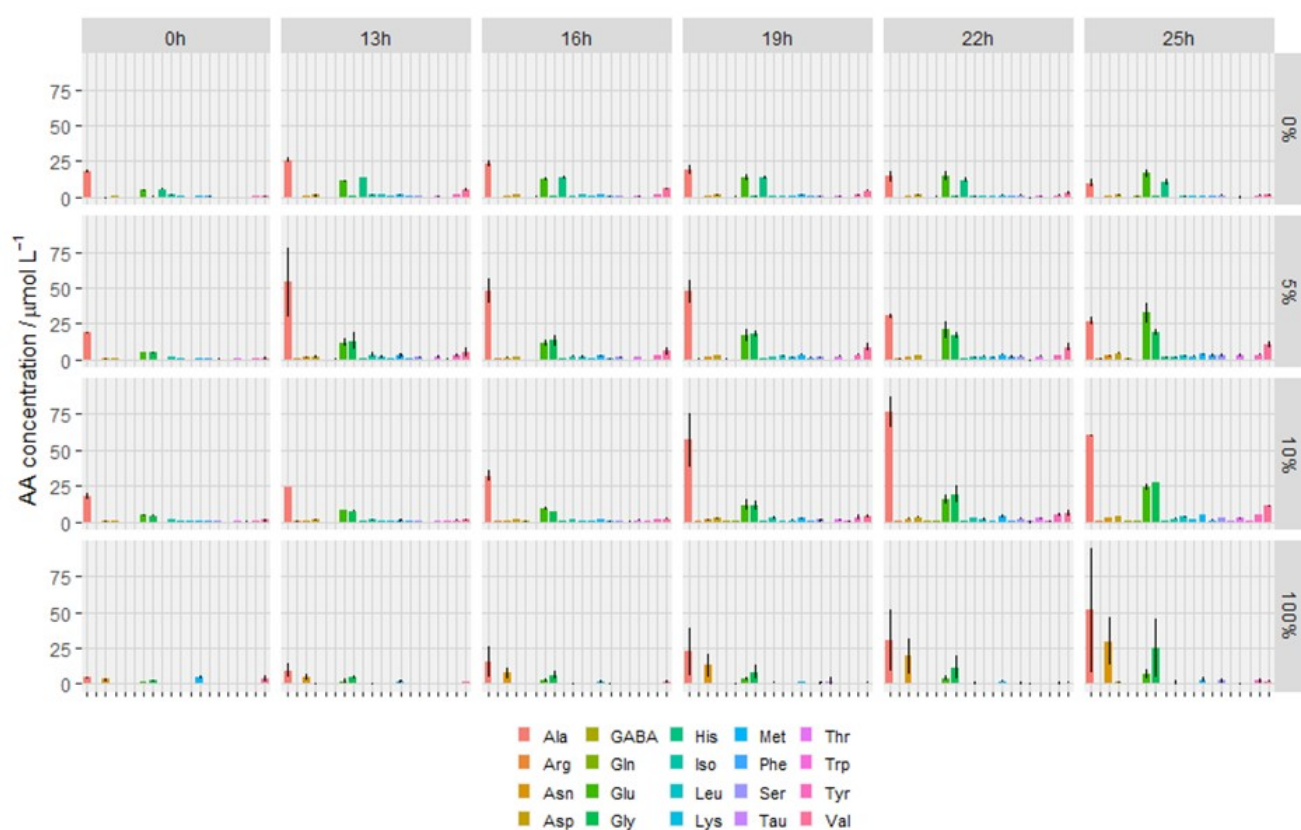
*M. marburgensis* is a suitable organism for industrial  $\text{CH}_4$  production (Krajete et al., 2014; Mauerhofer et al., 2021; Pfeifer et al., 2021; Rittmann et al., 2023a, 2023b, 2023c, 2023d, 2018, 2014; Seifert et al., 2014), for examination of proteinogenic amino acids excretion from  $\text{H}_2/\text{CO}_2$  and  $\text{H}_2\text{CO}_2/\text{N}_2$  (Reischl et al., 2025; Rittmann et al., 2023a, 2023b, 2023c, 2023d; Taubner et al., 2023) and to be cultivated in bioreactors for bioprocess development of gas fermentation processes (Abdel Azim et al., 2017; Sébastien Bernacchi et al., 2014; Mauerhofer et al., 2021; Rittmann et al., 2018; Seifert et al., 2014). Thus fed-batch experiments at  $\text{NH}_4^+$  concentrations of 0%, 1%, 5%, 10% and 100% in triplicates were performed with *M. marburgensis* (Reischl et al., manuscript in preparation). Growth curves are shown in **Figure 8**.



**Figure 8:** Growth curves of *M. marburgensis* with varying  $\text{NH}_4^+$  concentrations gassed with  $\text{H}_2/\text{CO}_2/\text{N}_2$  (7:1:1). Gassing with  $\text{H}_2/\text{CO}_2$  (4:1) (41) as well as the addition of carbon (wC) in the media served as reference growth experiments. Dashed lines represent overnight growth. In the figure legend the percentage of the  $\text{NH}_4^+$  concentration from 0%, 1%, 5%, 10% and 100% is indicated. The numbers 41 or 711 refer to the ingas flow compositions of  $\text{H}_2/\text{CO}_2$  (4:1) and  $\text{H}_2/\text{CO}_2/\text{N}_2$  (7:1:1), respectively (Reischl et al., manuscript in preparation).

Thereafter, the Ala concentration decreased during the fermentation. In gas fermentations with 10%  $\text{NH}_4^+$ , the highest Ala concentration was detected at 22 h, but also thereafter Ala was partially

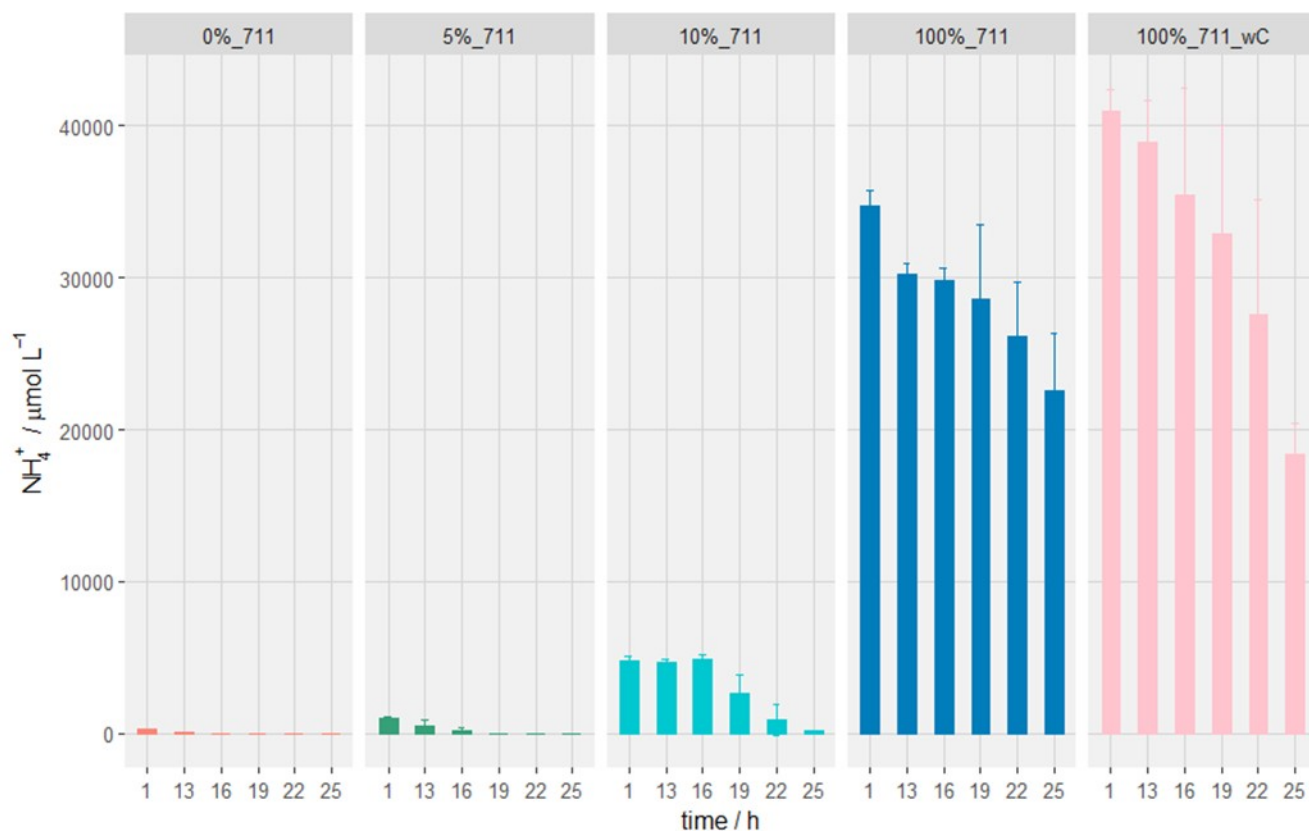
consumed. In both, the 5% and 10%  $\text{NH}_4^+$  experiments, Glu and Gly increased throughout the course of the experiment. In the 100%  $\text{NH}_4^+$  experiment Ala, Asn, Glu and Gly were the mainly excreted amino acid (Reischl et al., manuscript in preparation). Growth of *M. marburgensis* on  $\text{H}_2/\text{CO}_2$  (4:1) with carbonate and without carbonate in the medium resulted in growth up to an  $\text{OD}_{578}$  of 7.0 and 8.1, respectively, which served as reference runs to earlier findings (Abdel Azim et al., 2017). The experiments with *M. marburgensis* grown on  $\text{H}_2/\text{CO}_2/\text{N}_2$  (7:1:1) served as the actual experiments for assessment of proteinogenic amino acid excretion. The experiments with  $\text{H}_2/\text{CO}_2/\text{N}_2$  (7:1:1) and 100%  $\text{NH}_4^+$  with carbonate in the medium resulted in a 2.2-fold higher  $\text{OD}_{578}$ , compared results in medium without carbonate. At a  $\text{NH}_4^+$  concentration of 5% a stagnation of growth after 15 h to an  $\text{OD}_{578}$  of 0.9 can be seen. At a  $\text{NH}_4^+$  concentration of 10% a stagnation in growth after 20 h to a final  $\text{OD}_{578}$  of 1.6 has been found. Experiments with 0% or 1%  $\text{NH}_4^+$  concentration did not show growth (**Figure 8**) (Reischl et al., manuscript in preparation).



**Figure 9:** Amino acid (AA) concentrations of *M. marburgensis* cultivations on  $\text{H}_2/\text{CO}_2/\text{N}_2$  (7:1:1). All results are  $n = 3$  for each time point. The AA concentration is shown as individual bar charts with standard deviation. The legend on the bottom of the graph indicates the quantified amino acids. On the left-hand y-axis, the AA concentration is shown.  $\text{NH}_4^+$  concentrations of the respective time series are indicated on the right-hand y-axis from top to bottom: 0%, 5%, 10% and 100%. The sampling time is shown on the x-axis as headers from left to right. GABA serves as internal quantification standard (Reischl et al., manuscript in preparation).

For quantitative analysis of amino acid excretion and consumption by *M. marburgensis* fed-batch gas fermentations with  $\text{H}_2/\text{CO}_2/\text{N}_2$  (7:1:1) without carbonate at 0%, 5%, 10% and 100%  $\text{NH}_4^+$  in the medium were performed. The results of the analysis are shown in **Figure 9**. Almost all of the 18

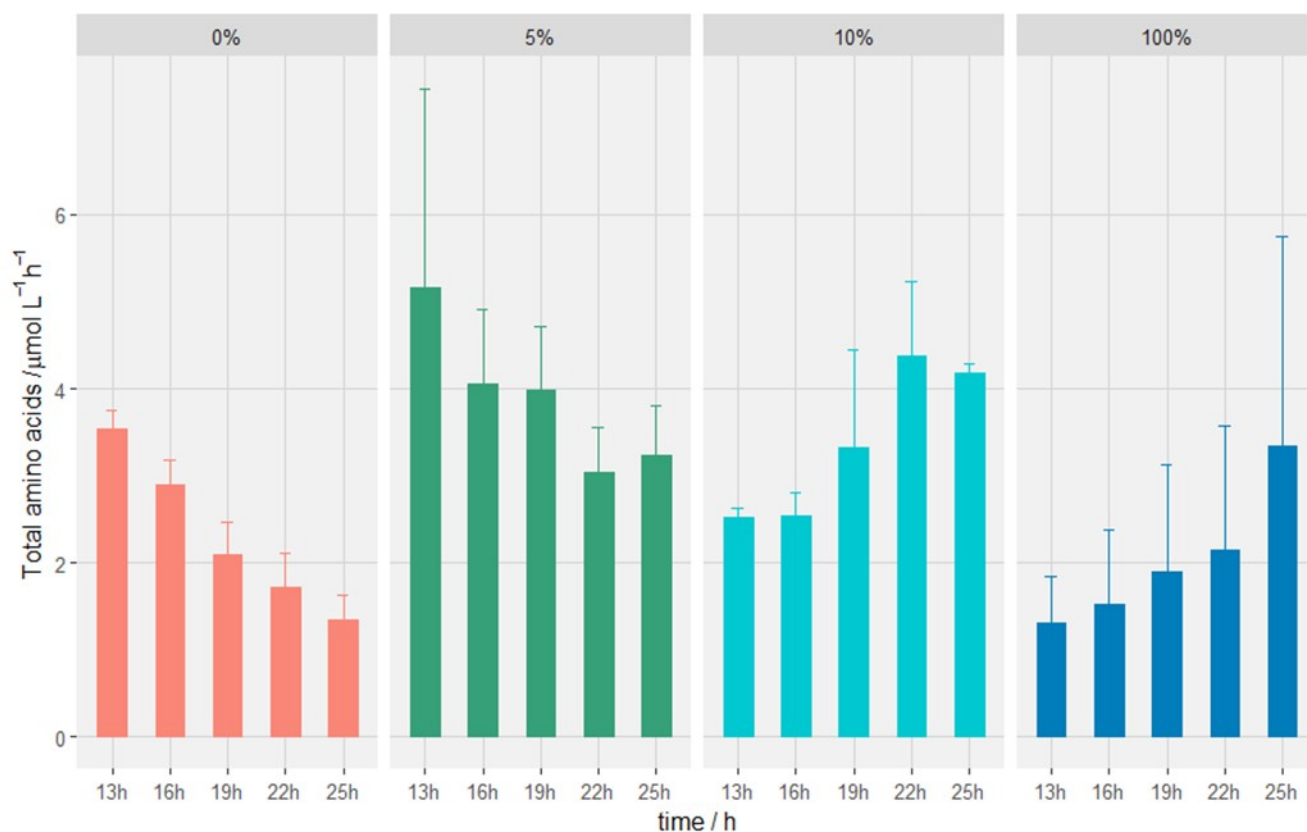
quantifiable proteinogenic amino acids were excreted by *M. marburgensis*, although, the amino acid concentration was varying throughout the experiments. The highest excreted amino acids were alanine (Ala), asparagine (Asn), glutamic acid (Glu) and glycine (Gly). In the 0%  $\text{NH}_4^+$  concentration experiment the initial amino acid concentration after inoculation is visible. At 5%  $\text{NH}_4^+$ , the highest amino acid concentration was obtained for Ala at 13 h. A decrease of the  $\text{NH}_4^+$  concentration is evident during amino acid excretion in fed-batch experiments of 5%, 10% and 100%  $\text{NH}_4^+$  (**Figure 10**). A  $\text{NH}_4^+$  limitation is observed in the 0%  $\text{NH}_4^+$  experiment directly at the beginning (**Figure 10**), which lead to a decrease of the total amino acid concentration (**Figure 11**) and growth to low  $\text{OD}_{578}$  (**Figure 8**). In the 5% and 10%  $\text{NH}_4^+$  experiments, a limitation of  $\text{NH}_4^+$  (**Figure 10**) induced consumption of Ala by *M. marburgensis* (**Figure 9**). Moreover, compared to 5% and 10%  $\text{NH}_4^+$ , 100%  $\text{NH}_4^+$  in the medium seems to serve as an inhibitor for amino acid production as less total amino acids were excreted (**Figure 11**) at higher available concentrations of  $\text{NH}_4^+$  in the medium (**Figure 10**) and at a higher ammonium uptake rate (**Figure 12**). In the experiments with 0% and 5%  $\text{NH}_4^+$  a decrease in total amino acid concentration is indicated directly with the onset of the experiment, whereas in the experiment with 10%  $\text{NH}_4^+$  a higher total amount of amino acids compared to the 100%  $\text{NH}_4^+$  experiment is visible (**Figure 11**) (Reischl et al., manuscript in preparation).



**Figure 10:**  $\text{NH}_4^+$  concentration from fed-batch experiments. All results are  $n = 3$ . Colours indicate the different concentrations of  $\text{NH}_4^+$  in the media, 0% (salmon), 5% (green), 10% (turquoise), 100% (blue), and 100% with carbonate (wC) in the media (pink). Time / h is shown on the x-axis for each fed-batch gas fermentation individually (Reischl et al., manuscript in preparation).

## Summary, conclusions and outlook

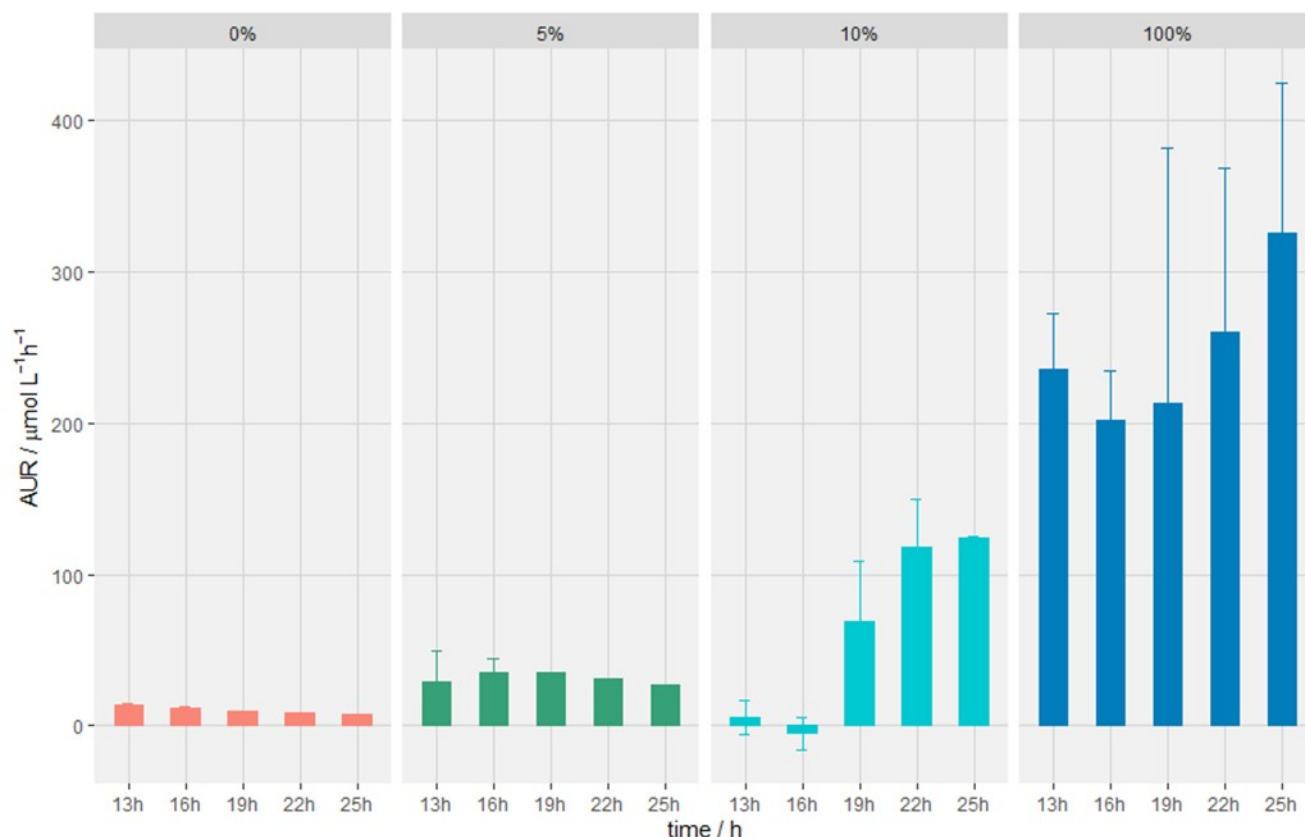
This habilitation thesis presents the background, results and discusses the physiology of archaea with regard to Archaea Biotechnology. It must be emphasized that the known nutritional requirements of archaea are neither linked to genetic or phylogenetic or taxonomic data, nor to environmental, physiological or biotechnological characteristics. This hampers the comparison and interpretation of substrate uptake, growth, and production kinetics in their natural and artificial environments. Moreover, a thorough bioinformatics analysis combined with a physiological screening with regard to the biotechnological applications of archaea was not attempted for any of the archaeal groups. Moreover, only a few studies on methanogens, extreme halophilic archaea and H<sub>2</sub>-producing archaea targeted bioprocess development and their scale-up. In this habilitaion thesis, I focus on elucidating the knowledge gaps with regard to the metabolic and physiological diversity of methanogenic archaea from mesophilic to hyperthermophilic cultivation conditions in a biotechnological context. One of the key features of my research is to examine growth, substrate uptake and production kinetics of archaea under comparable cultivation conditions from slight to high pressure conditions and to identify superior wild-type cell factories. Specifically, examples with regard to proteinogenic amino acid excretion of three thermophilic and hyperthermophilic methanogens were examined under varying substrate and temperature conditions growing on different gas compositions. Moreover, *M. marburgensis* has been selected for invetigating amino acid excretion in fed-batch cultivation mode in bioreactors.



**Figure 11:** Total amount of total excreted amino acids of fed-batch experiments. All results are  $n = 3$ . Colours indicate the different concentrations of  $\text{NH}_4^+$  in the media, 0% (salmon), 5% (green), 10% (turquoise) and 100% (blue). Time is visible on the x-axis (Reischl et al., manuscript in preparation).

The methods and the pipelines that are used in my research for targeted scale-up of product formation by archaea possess relevance for identification of regulatory mechanisms that could be addressed in subsequent systems and synthetic biology approaches to generate new metabolically engineered archaeal cell factories for amino acid production. Moreover, the peer-reviewed publications that are presented in this cumulative thesis, provide the reader with a red line on studying archaea on a quantitative physiological basis, to compare the biotechnological characteristics of organisms and to specifically develop bioprocesses with prioritized strains. In this regard, the pipeline from basis via basic applied to early B-TRL (up to 3) is a hallmark of the research and development activities of my lab.

In my future research, I intend to elucidate archaeal mono- and co-cultures grown on gaseous substrates. I want to strengthen the pipeline from meta-data analysis to identification of strains for biotechnological applications by using extensive literature paralleled by artificial intelligence studies. I hypothesise that specific patterns of growth and productivity will correspond to specific genetic signatures and that these, in turn, can be related to distinct physiologies. Moreover, patterns of growth and productivity of archaea can be linked to certain environmental/bioprocess factors.



**Figure 12:** Ammonium uptake rate (AUR) of fed-batch experiments. All experiments are  $n = 3$ . Colours indicate the different concentrations of  $\text{NH}_4^+$  in the media, 0% (salmon), 5% (green), 10% (turquoise) and 100% (blue). Time is visible on the x-axis (Reischl et al., manuscript in preparation).

In addition, I want to perform metabolic engineering in combination in a systems biotechnology approach for production of solid, liquid, and gaseous compounds in a one-step bioprocess set-up.

Furthermore, my future research shall lead to a comprehensive understanding of the functioning of archaea in natural and artificial environments – beyond the currently established (physiological) knowledge and established phylogenetic groups – by using comprehensive experimental set-ups and meta-data analysis and by combining cell biology, systems and synthetic biology/ecology, and targeted bioprocess development and scale-up.

The goal of my future research shall be to systematically link and integrate the functions and mechanisms that work in archaea in the environment to their genetic signatures, through data-driven biostatistics and bioinformatics, meta-data analysis, as well as holistic physiological, cell biological and biotechnological experiments, to unravel causal relationships in the emerging research and development field of Archaea Biotechnology.

## References

- Abdel Azim, A., Pruckner, C., Kolar, P., Taubner, R.-S., Fino, D., Saracco, G., Sousa, F.L., Rittmann, S.K.-M.R., 2017. The physiology of trace elements in biological methane production. *Bioresource Technology* 241, 775–786. <https://doi.org/10.1016/j.biortech.2017.05.211>
- Abdel Azim, A., Rittmann, S.K.-M.R., Fino, D., Bochmann, G., 2018. The physiological effect of heavy metals and volatile fatty acids on *Methanococcus maripaludis* S2. *Biotechnol Biofuels* 11, 301. <https://doi.org/10.1186/s13068-018-1302-x>
- Adam, P.S., Borrel, G., Brochier-Armanet, C., Gribaldo, S., 2017. The growing tree of Archaea: new perspectives on their diversity, evolution and ecology. *ISME J* 11, 2407–2425. <https://doi.org/10.1038/ismej.2017.122>
- Adam, P.S., Borrel, G., Gribaldo, S., 2018. Evolutionary history of carbon monoxide dehydrogenase/acetyl-CoA synthase, one of the oldest enzymatic complexes. *Proc Natl Acad Sci U S A* 115, E1166–E1173. <https://doi.org/10.1073/pnas.1716667115>
- Akache, B., Stark, F.C., Iqbal, U., Chen, W., Jia, Y., Krishnan, L., McCluskie, M.J., 2018. Safety and biodistribution of sulfated archaeal glycolipid archaeosomes as vaccine adjuvants. *Human Vaccines & Immunotherapeutics* 0, 1–14. <https://doi.org/10.1080/21645515.2017.1423154>
- Akinyemi, T.S., Shao, N., Lyu, Z., Drake, I.J., Liu, Y., Whitman, W.B., 2021. Tuning Gene Expression by Phosphate in the Methanogenic Archaeon *Methanococcus maripaludis*. *ACS Synth Biol* 10, 3028–3039. <https://doi.org/10.1021/acssynbio.1c00322>
- Aparici-Carratalá, D., Esclapez, J., Bautista, V., Bonete, M.-J., Camacho, M., 2023. Archaea: current and potential biotechnological applications. *Research in Microbiology* 174, 104080. <https://doi.org/10.1016/j.resmic.2023.104080>
- Atomi, H., Imanaka, T., Fukui, T., 2012. Overview of the genetic tools in the Archaea. *Front. Microbio* 3, 337. <https://doi.org/10.3389/fmicb.2012.00337>
- Bae, S.S., Kim, T.W., Lee, H.S., Kwon, K.K., Kim, Y.J., Kim, M.-S., Lee, J.-H., Kang, S.G., 2012. H<sub>2</sub> production from CO, formate or starch using the hyperthermophilic archaeon, *Thermococcus onnurineus*. *Biotechnol. Lett.* 34, 75–79. <https://doi.org/10.1007/s10529-011-0732-3>
- Bae, S.-S., Kim, Y.-J., Yang, S.-H., Lim, J.-K., Jeon, J.-H., Lee, H.-S., Kang, S.-G., Kim, S.-J., Lee, J.-H., 2006. *Thermococcus onnurineus* sp. nov., a Hyperthermophilic Archaeon Isolated from a Deep-Sea Hydrothermal Vent Area at the PACMANUS Field. *Journal of Microbiology and Biotechnology* 16, 1826–1831.
- Bae, S.S., Lee, H.S., Jeon, J.H., Lee, J.-H., Kang, S.G., Kim, T.W., 2015. Enhancing bio-hydrogen production from sodium formate by hyperthermophilic archaeon, *Thermococcus onnurineus* NA1. *Bioprocess Biosyst Eng* 38, 989–993. <https://doi.org/10.1007/s00449-014-1336-9>



- Baker, B.J., Anda, V.D., Seitz, K.W., Dombrowski, N., Santoro, A.E., Lloyd, K.G., 2020. Diversity, ecology and evolution of Archaea. *Nat Microbiol* 1–14. <https://doi.org/10.1038/s41564-020-0715-z>
- Bang, C., Vierbuchen, T., Gutschmann, T., Heine, H., Schmitz, R.A., 2017. Immunogenic properties of the human gut-associated archaeon *Methanomassiliicoccus luminyensis* and its susceptibility to antimicrobial peptides. *PLoS ONE* 12, e0185919. <https://doi.org/10.1371/journal.pone.0185919>
- Bang, C., Weidenbach, K., Gutschmann, T., Heine, H., Schmitz, R.A., 2014. The intestinal archaea *Methanosphaera stadtmanae* and *Methanobrevibacter smithii* activate human dendritic cells. *PLoS One* 9, e99411. <https://doi.org/10.1371/journal.pone.0099411>
- Baumann, L.M.F., Taubner, R.-S., Bauersachs, T., Steiner, M., Schleper, C., Peckmann, J., Rittmann, S.K.-M.R., Birgel, D., 2018. Intact polar lipid and core lipid inventory of the hydrothermal vent methanogens *Methanocaldococcus villosus* and *Methanothermococcus okinawensis*. *Organic Geochemistry* 126, 33–42. <https://doi.org/10.1016/j.orggeochem.2018.10.006>
- Baumann, L.M.F., Taubner, R.-S., Oláh, K., Rohrweber, A.-C., Schuster, B., Birgel, D., Rittmann, S.K.-M.R., 2022. Quantitative Analysis of Core Lipid Production in *Methanothermobacter marburgensis* at Different Scales. *Bioengineering* 9, 169. <https://doi.org/10.3390/bioengineering9040169>
- Benvegnu, T., Lemiègre, L., Cammas-Marion, S., 2008. Archaeal Lipids: Innovative Materials for Biotechnological Applications. *Eur. J. Org. Chem.* 2008, 4725–4744. <https://doi.org/10.1002/ejoc.200800452>
- Bernacchi, Sébastien, Rittmann, S., H. Seifert, A., Krajete, A., Herwig, C., 2014. Experimental methods for screening parameters influencing the growth to product yield ( $Y(x/CH_4)$ ) of a biological methane production (BMP) process performed with *Methanothermobacter marburgensis*. *AIMS Bioengineering* 1, 72–86. <https://doi.org/10.3934/bioeng.2014.2.72>
- Bernacchi, S., Weissgram, M., Wukovits, W., Herwig, C., 2014. Process efficiency simulation for key process parameters in biological methanogenesis. *AIMS Bioengineering* 1, 53–71. <https://doi.org/DOI: 10.3934/bioeng.2014.1.53>
- Beveridge, T.J., Choquet, C.G., Patel, G.B., Sprott, G.D., 1993. Freeze-fracture planes of methanogen membranes correlate with the content of tetraether lipids. *J Bacteriol* 175, 1191–1197. <https://doi.org/10.1128/jb.175.4.1191-1197.1993>
- Borrel, G., 2022. A microbe that uses crude oil to make methane. *Nature* 601, 196–197. <https://doi.org/10.1038/d41586-021-03729-3>
- Borrel, G., Adam, P.S., Gribaldo, S., 2016. Methanogenesis and the Wood–Ljungdahl Pathway: An Ancient, Versatile, and Fragile Association. *Genome Biol Evol* 8, 1706–1711. <https://doi.org/10.1093/gbe/evw114>
- Borrel, G., Adam, P.S., McKay, L.J., Chen, L.-X., Sierra-García, I.N., Sieber, C.M.K., Letourneur, Q., Ghoulane, A., Andersen, G.L., Li, W.-J., Hallam, S.J., Muyzer, G., de Oliveira, V.M., Inskeep, W.P., Banfield, J.F., Gribaldo, S., 2019. Wide diversity of methane and short-chain alkane metabolisms in uncultured archaea. *Nature Microbiology* 4, 603–613. <https://doi.org/10.1038/s41564-019-0363-3>
- Borrel, G., Brugère, J.-F., Gribaldo, S., Schmitz, R.A., Moissl-Eichinger, C., 2020. The host-associated archaeome. *Nature Reviews Microbiology* 1–15. <https://doi.org/10.1038/s41579-020-0407-y>
- Borrel, G., Fadhlou, K., Ben Hania, W., Gaci, N., Pehau-Arnaudet, G., Chaudhary, P.P., Vandekerckove, P., Ballet, N., Alric, M., O’Toole, P.W., Fardeau, M.-L., Ollivier, B., Brugère, J.-F., 2023. *Methanomethylophilus alvi* gen. nov., sp. nov., a Novel Hydrogenotrophic Methyl-Reducing Methanogenic Archaea of the Order *Methanomassiliicoccales* Isolated from the Human Gut and Proposal of the Novel Family *Methanomethylophilaceae* fam. nov. *Microorganisms* 11, 2794. <https://doi.org/10.3390/microorganisms11112794>

- Borrel, G., Joblin, K., Guedon, A., Colombet, J., Tardy, V., Lehours, A.-C., Fonty, G., 2012. *Methanobacterium lacus* sp. nov., isolated from the profundal sediment of a freshwater meromictic lake. *INTERNATIONAL JOURNAL OF SYSTEMATIC AND EVOLUTIONARY MICROBIOLOGY* 62, 1625–1629. <https://doi.org/10.1099/ijs.0.034538-0>
- Borrel, G., McCann, A., Deane, J., Neto, M.C., Lynch, D.B., Brugère, J.-F., O'Toole, P.W., 2017. Genomics and metagenomics of trimethylamine-utilizing Archaea in the human gut microbiome. *ISME J* 11, 2059–2074. <https://doi.org/10.1038/ismej.2017.72>
- Brugère, J.-F., Borrel, G., Gaci, N., Tottey, W., O'Toole, P.W., Malpuech-Brugère, C., 2014. Archaeobiotics. *Gut Microbes* 5, 5–10. <https://doi.org/10.4161/gmic.26749>
- Buchholz, K., Collins, J., 2013. The roots--a short history of industrial microbiology and biotechnology. *Appl Microbiol Biotechnol* 97, 3747–3762. <https://doi.org/10.1007/s00253-013-4768-2>
- Calloway, D.H., Colasito, D.J., Mathews, R.D., 1966. Gases produced by Human Intestinal Microflora. *Nature* 212, 1238–1239. <https://doi.org/10.1038/2121238a0>
- Carr, S., Buan, N.R., 2022. Insights into the biotechnology potential of *Methanosarcina*. *Front Microbiol* 13, 1034674. <https://doi.org/10.3389/fmicb.2022.1034674>
- Contreras, G., Thomsen, J., Pfitzer, M., Hafenbradl, D., Kostner, D., Holtmann, D., Schmitz, R.A., Rother, M., Molitor, B., 2022. New perspectives for biotechnological applications of methanogens. *Current Research in Biotechnology* 4, 468–474. <https://doi.org/10.1016/j.crbiot.2022.10.001>
- Dalmasso, C., Oger, P., Selva, G., Courtine, D., L'Haridon, S., Garlaschelli, A., Roussel, E., Miyazaki, J., Reveillaud, J., Jebbar, M., Takai, K., Maignien, L., Alain, K., 2016. *Thermococcus piezophilus* sp. nov., a novel hyperthermophilic and piezophilic archaeon with a broad pressure range for growth, isolated from a deepest hydrothermal vent at the Mid-Cayman Rise. *Systematic and Applied Microbiology* 39, 440–444. <https://doi.org/10.1016/j.syapm.2016.08.003>
- Enzmann, F., Mayer, F., Rother, M., Holtmann, D., 2018. Methanogens: biochemical background and biotechnological applications. *AMB Express* 8, 1. <https://doi.org/10.1186/s13568-017-0531-x>
- Ergal, Í., Fuchs, W., Hasibar, B., Thallinger, B., Bochmann, G., Rittmann, S.K.-M.R., 2018. The physiology and biotechnology of dark fermentative biohydrogen production. *Biotechnology Advances* 36, 2165–2186. <https://doi.org/10.1016/j.biotechadv.2018.10.005>
- Evans, P.N., Boyd, J.A., Leu, A.O., Woodcroft, B.J., Parks, D.H., Hugenholtz, P., Tyson, G.W., 2019. An evolving view of methane metabolism in the Archaea. *Nat Rev Microbiol* 17, 219–232. <https://doi.org/10.1038/s41579-018-0136-7>
- Ferry, J.G., 2015. Acetate Metabolism in Anaerobes from the Domain Archaea. *Life (Basel)* 5, 1454–1471. <https://doi.org/10.3390/life5021454>
- Ferry, J.G., 2010. How to make a living by exhaling methane. *Annu. Rev. Microbiol.* 64, 453–473. <https://doi.org/10.1146/annurev.micro.112408.134051>
- Ferry, J.G., 2003. One-Carbon Metabolism in Methanogenic Anaerobes, in: Ljungdahl, L.G., Adams, M.W., Barton, L.L., Ferry, J.G., Johnson, M.K. (Eds.), *Biochemistry and Physiology of Anaerobic Bacteria*. Springer New York, pp. 143–156.
- Ferry, J.G., 1999. Enzymology of one-carbon metabolism in methanogenic pathways. *FEMS Microbiol. Rev.* 23, 13–38.
- Ferry, J.G., 1997. Enzymology of the fermentation of acetate to methane by *Methanosarcina thermophila*. *Biofactors* 6, 25–35.
- Fink, C., Beblawy, S., Enkerlin, A.M., Mühling, L., Angenent, L.T., Molitor, B., 2021. A Shuttle-Vector System Allows Heterologous Gene Expression in the Thermophilic Methanogen *Methanothermobacter thermautotrophicus* ΔH. *mBio* 12, e0276621. <https://doi.org/10.1128/mBio.02766-21>



- Fuchs, G., 2011. Alternative pathways of carbon dioxide fixation: insights into the early evolution of life? *Annu. Rev. Microbiol.* 65, 631–658. <https://doi.org/10.1146/annurev-micro-090110-102801>
- Gambacorta, A., Gliozzi, A., Rosa, M.D., 1995. Archaeal lipids and their biotechnological applications. *World Journal of Microbiology & Biotechnology* 11, 115–131. <https://doi.org/10.1007/BF00339140>
- Geymonat, E., Ferrando, L., Tarlera, S.E., 2011. *Methylogaea oryzae* gen. nov., sp. nov., a mesophilic methanotroph isolated from a rice paddy field. *Int. J. Syst. Evol. Microbiol.* 61, 2568–2572. <https://doi.org/10.1099/ijs.0.028274-0>
- Gophna, U., Allers, T., Marchfelder, A., 2017. Finally, Archaea Get Their CRISPR-Cas Toolbox. *Trends Microbiol.* 25, 430–432. <https://doi.org/10.1016/j.tim.2017.03.009>
- Griese, M., Hoffarth, M.P., Schneider, J., Schulte, T., 2019. Hardware-in-the-Loop simulation of an optimized energy management incorporating an experimental biocatalytic methanation reactor. *Energy* 181, 77–90. <https://doi.org/10.1016/j.energy.2019.05.092>
- Hanišáková, N., Vítězová, M., Rittmann, S.K.-M.R., 2022. The Historical Development of Cultivation Techniques for Methanogens and Other Strict Anaerobes and Their Application in Modern Microbiology. *Microorganisms* 10, 412. <https://doi.org/10.3390/microorganisms10020412>
- Harwood, C.R., Park, S.H., Sauer, M., 2018. Editorial for the thematic issue on “Industrial Microbiology.” *FEMS Microbiology Letters* 365, fny275. <https://doi.org/10.1093/femsle/fny275>
- Hermann-Krauss, C., Koller, M., Muhr, A., Fasl, H., Stelzer, F., Braunegg, G., 2013. Archaeal production of polyhydroxyalkanoate (PHA) co- and terpolyesters from biodiesel industry-derived by-products. *Archaea* 2013, 129268. <https://doi.org/10.1155/2013/129268>
- Hoehler, T.M., Jørgensen, B.B., 2013. Microbial life under extreme energy limitation. *Nat Rev Micro* 11, 83–94. <https://doi.org/10.1038/nrmicro2939>
- Hungate, R.E., Macy, J., 1973. The Roll-Tube Method for Cultivation of Strict Anaerobes. *Bulletins from the Ecological Research Committee* 123–126.
- Jacquemet, A., Barbeau, J., Lemiègre, L., Benvegnu, T., 2009. Archaeal tetraether bipolar lipids: Structures, functions and applications. *Biochimie, Lipids for the future from agro-resources to human health* 91, 711–717. <https://doi.org/10.1016/j.biochi.2009.01.006>
- Jain, S., Caforio, A., Driessen, A.J.M., 2014. Biosynthesis of archaeal membrane ether lipids. *Front. Microbiol.* 5. <https://doi.org/10.3389/fmicb.2014.00641>
- Jebbar, M., Hickman-Lewis, K., Cavalazzi, B., Taubner, R.-S., Rittmann, S.K.-M.R., Antunes, A., 2020. Microbial Diversity and Biosignatures: An Icy Moons Perspective. *Space Sci Rev* 216, 10. <https://doi.org/10.1007/s11214-019-0620-z>
- Kadouri, D., Jurkevitch, E., Okon, Y., Castro-Sowinski, S., 2005. Ecological and Agricultural Significance of Bacterial Polyhydroxyalkanoates. *Critical Reviews in Microbiology* 31, 55–67. <https://doi.org/10.1080/10408410590899228>
- Kanai, T., Imanaka, H., Nakajima, A., Uwamori, K., Omori, Y., Fukui, T., Atomi, H., Imanaka, T., 2005. Continuous hydrogen production by the hyperthermophilic archaeon, *Thermococcus kodakaraensis* KOD1. *J. Biotechnol.* 116, 271–282. <https://doi.org/10.1016/j.jbiotec.2004.11.002>
- Kates, M., Moldoveanu, N., Stewart, L.C., 1993. On the revised structure of the major phospholipid of *Halobacterium salinarium*. *Biochim. Biophys. Acta* 1169, 46–53. [https://doi.org/10.1016/0005-2760\(93\)90080-s](https://doi.org/10.1016/0005-2760(93)90080-s)
- Kaur, G., Garg, T., Rath, G., Goyal, A.K., 2016. Archaeosomes: an excellent carrier for drug and cell delivery. *Drug Deliv* 23, 2497–2512. <https://doi.org/10.3109/10717544.2015.1019653>

- Khelaifia, S., Drancourt, M., 2012. Susceptibility of archaea to antimicrobial agents: applications to clinical microbiology. *Clinical Microbiology and Infection* 18, 841–848. <https://doi.org/10.1111/j.1469-0691.2012.03913.x>
- Kim, Y.J., Lee, H.S., Kim, E.S., Bae, S.S., Lim, J.K., Matsumi, R., Lebedinsky, A.V., Sokolova, T.G., Kozhevnikova, D.A., Cha, S.-S., Kim, S.-J., Kwon, K.K., Imanaka, T., Atomi, H., Bonch-Osmolovskaya, E.A., Lee, J.-H., Kang, S.G., 2010. Formate-driven growth coupled with H<sub>2</sub> production. *Nature* 467, 352–355. <https://doi.org/10.1038/nature09375>
- Knappy, C., Barillà, D., Chong, J., Hodgson, D., Morgan, H., Suleman, M., Tan, C., Yao, P., Keely, B., 2015. Mono-, di- and trimethylated homologues of isoprenoid tetraether lipid cores in archaea and environmental samples: mass spectrometric identification and significance. *J. Mass Spectrom.* 50, 1420–1432. <https://doi.org/10.1002/jms.3709>
- Koga, Y., Nishihara, M., Morii, H., Akagawa-Matsushita, M., 1993. Ether polar lipids of methanogenic bacteria: structures, comparative aspects, and biosyntheses. *Microbiol Rev* 57, 164–182.
- Koller, M., 2019. Polyhydroxyalkanoate Biosynthesis at the Edge of Water Activity-Haloarchaea as Biopolyester Factories. *Bioengineering (Basel)* 6, 34. <https://doi.org/10.3390/bioengineering6020034>
- Koller, M., 2018. Chemical and Biochemical Engineering Approaches in Manufacturing Polyhydroxyalkanoate (PHA) Biopolyesters of Tailored Structure with Focus on the Diversity of Building Blocks. *Chemical and Biochemical Engineering Quarterly* 32, 413–438. <https://doi.org/10.15255/CABEQ.2018.1385>
- Koller, M., Chiellini, E., Braunegg, G., 2015. Study on the Production and Re-use of Poly(3-hydroxybutyrate-co-3-hydroxyvalerate) and Extracellular Polysaccharide by the Archaeon *Haloferax mediterranei* Strain DSM 1411. *Chemical and Biochemical Engineering Quarterly* 29, 87–98. <https://doi.org/10.15255/CABEQ.2014.2058>
- Koller, M., Hesse, P., Bona, R., Kutschera, C., Atlić, A., Braunegg, G., 2007. Potential of Various Archae- and Eubacterial Strains as Industrial Polyhydroxyalkanoate Producers from Whey. *Macromolecular Bioscience* 7, 218–226. <https://doi.org/10.1002/mabi.200600211>
- Koller, M., Rittmann, S.K.-M.R., 2022. Haloarchaea as emerging big players in future polyhydroxyalkanoate bioproduction: Review of trends and perspectives. *Current Research in Biotechnology* 4, 377–391. <https://doi.org/10.1016/j.crbiot.2022.09.002>
- Krajete, A., Herwig, C., Rittmann, S., Seifert, A., Bernacchi, S., 2014. Method and System for Producing Methane Using Methanogenic Microorganisms and Applying Specific Nitrogen Concentrations in the Liquid Phase. WO2014128300A1.
- Krishnan, L., Dennis Sprott, G., Institute for Biological Sciences, National Research Council of Canada, 2003. Archaeosomes as self-adjuvanting delivery systems for cancer vaccines. *J Drug Target* 11, 515–524. <https://doi.org/10.1080/10611860410001670044>
- Krishnan, L., Sad, S., Patel, G.B., Sprott, G.D., 2000. Archaeosomes Induce Long-Term CD8+ Cytotoxic T Cell Response to Entrapped Soluble Protein by the Exogenous Cytosolic Pathway, in the Absence of CD4+ T Cell Help. *The Journal of Immunology* 165, 5177–5185. <https://doi.org/10.4049/jimmunol.165.9.5177>
- Krishnan, L., Sprott, G.D., 2008. Archaeosome adjuvants: immunological capabilities and mechanism(s) of action. *Vaccine* 26, 2043–2055. <https://doi.org/10.1016/j.vaccine.2008.02.026>
- Krzmarzick, M.J., Taylor, D.K., Fu, X., McCutchan, A.L., 2018. Diversity and Niche of Archaea in Bioremediation. *Archaea* 2018, Article ID 3194108. <https://doi.org/10.1155/2018/3194108>
- Kupriyanova, E., Pronina, N., Los, D., 2017. Carbonic anhydrase — a universal enzyme of the carbon-based life. *Photosynthetica* 55, 3–19. <https://doi.org/10.1007/s11099-017-0685-4>
- Kupriyanova, E.V., Pronina, N.A., 2011. Carbonic anhydrase: Enzyme that has transformed the biosphere. *Russ J Plant Physiol* 58, 197–209. <https://doi.org/10.1134/S1021443711020099>

- Kurth, J.M., Op den Camp, H.J.M., Welte, C.U., 2020. Several ways one goal—methanogenesis from unconventional substrates. *Appl Microbiol Biotechnol* 104, 6839–6854. <https://doi.org/10.1007/s00253-020-10724-7>
- Kushkevych, I., Procházka, J., Gajdács, M., Rittmann, S.K.-M.R., Vítězová, M., 2021. Molecular Physiology of Anaerobic Phototrophic Purple and Green Sulfur Bacteria. *International Journal of Molecular Sciences* 22, 6398. <https://doi.org/10.3390/ijms22126398>
- Leigh, J.A., Albers, S.-V., Atomi, H., Allers, T., 2011. Model organisms for genetics in the domain Archaea: methanogens, halophiles, Thermococcales and Sulfolobales. *FEMS Microbiology Reviews* 35, 577–608. <https://doi.org/10.1111/j.1574-6976.2011.00265.x>
- Lemaire, O.N., Wagner, T., 2022. A Structural View of Alkyl-Coenzyme M Reductases, the First Step of Alkane Anaerobic Oxidation Catalyzed by Archaea. *Biochemistry* 61, 805–821. <https://doi.org/10.1021/acs.biochem.2c00135>
- Leriche, G., Cifelli, J.L., Sibucão, K.C., Patterson, J.P., Koyanagi, T., Gianneschi, N.C., Yang, J., 2017. Characterization of drug encapsulation and retention in archaea-inspired tetraether liposomes. *Org. Biomol. Chem.* 15, 2157–2162. <https://doi.org/10.1039/C6OB02832B>
- Lever, M.A., Rogers, K.L., Lloyd, K.G., Overmann, J., Schink, B., Thauer, R.K., Hoehler, T.M., Jørgensen, B.B., 2015. Life under extreme energy limitation: a synthesis of laboratory- and field-based investigations. *FEMS Microbiol. Rev.* 39, 688–728. <https://doi.org/10.1093/femsre/fuv020>
- Lewis, A.M., Recalde, A., Bräsen, C., Counts, J.A., Nussbaum, P., Bost, J., Schocke, L., Shen, L., Willard, D.J., Quax, T.E.F., Peeters, E., Siebers, B., Albers, S.-V., Kelly, R.M., 2021. The biology of thermoacidophilic archaea from the order Sulfolobales. *FEMS Microbiol Rev* 45, fuaa063. <https://doi.org/10.1093/femsre/fuua063>
- Lewis, W.H., Tahon, G., Geesink, P., Sousa, D.Z., Ettema, T.J.G., 2020. Innovations to culturing the uncultured microbial majority. *Nature Reviews Microbiology* 1–16. <https://doi.org/10.1038/s41579-020-00458-8>
- Li, J., Zhang, L., Xu, Q., Zhang, W., Li, Z., Chen, L., Dong, X., 2022. CRISPR-Cas9 Toolkit for Genome Editing in an Autotrophic CO<sub>2</sub>-Fixing Methanogenic Archaeon. *Microbiology Spectrum* 10, e01165-22. <https://doi.org/10.1128/spectrum.01165-22>
- Liefeith, K., Frant, M., Müller, U., Stenstad, P., Johnsen, H., Schmid, R., 2018. Archaeal tetraether lipid coatings-A strategy for the development of membrane analog spacer systems for the site-specific functionalization of medical surfaces. *Biointerphases* 13, 011004. <https://doi.org/10.1116/1.5008816>
- Liesegang, H., Kaster, A.-K., Wiezer, A., Goenrich, M., Wollherr, A., Seedorf, H., Gottschalk, G., Thauer, R.K., 2010. Complete genome sequence of *Methanothermobacter marburgensis*, a methanoarchaeon model organism. *J. Bacteriol.* 192, 5850–5851. <https://doi.org/10.1128/JB.00844-10>
- Lim, J.K., Bae, S.S., Kim, T.W., Lee, J.-H., Lee, H.S., Kang, S.G., 2012. Thermodynamics of formate-oxidizing metabolism and implications for H<sub>2</sub> production. *Appl. Environ. Microbiol.* 78, 7393–7397. <https://doi.org/10.1128/AEM.01316-12>
- Lim, J.K., Kang, S.G., Lebedinsky, A.V., Lee, J.-H., Lee, H.S., 2010. Identification of a Novel Class of Membrane-Bound [NiFe]-Hydrogenases in *Thermococcus onnurineus* NA1 by In Silico Analysis. *Appl. Environ. Microbiol.* 76, 6286–6289. <https://doi.org/10.1128/AEM.00123-10>
- Lindås, A.-C., Karlsson, E.A., Lindgren, M.T., Ettema, T.J.G., Bernander, R., 2008. A unique cell division machinery in the Archaea. *PNAS* 105, 18942–18946. <https://doi.org/10.1073/pnas.0809467105>
- Liu, Y., Makarova, K.S., Huang, W.-C., Wolf, Y.I., Nikolskaya, A.N., Zhang, X., Cai, M., Zhang, C.-J., Xu, W., Luo, Z., Cheng, L., Koonin, E.V., Li, M., 2021. Expanded diversity of Asgard archaea

- and their relationships with eukaryotes. *Nature* 1–5. <https://doi.org/10.1038/s41586-021-03494-3>
- Liu, Y., Whitman, W.B., 2008. Metabolic, phylogenetic, and ecological diversity of the methanogenic archaea. *Ann. N. Y. Acad. Sci.* 1125, 171–189. <https://doi.org/10.1196/annals.1419.019>
- Lyu, Z., Jain, R., Smith, P., Fetchko, T., Yan, Y., Whitman, W.B., 2016. Engineering the Autotroph *Methanococcus maripaludis* for Geraniol Production. *ACS Synth. Biol.* 5, 577–581. <https://doi.org/10.1021/acssynbio.5b00267>
- Lyu, Z., Rotaru, A.-E., Pimentel, M., Zhang, C.-J., Rittmann, S.K.-M.R., 2022. Editorial: The methane moment - Cross-boundary significance of methanogens: Preface. *Frontiers in Microbiology* 13. <https://doi.org/10.3389/fmicb.2022.1055494>
- Lyu, Z., Rotaru, A.-E., Pimentel, M., Zhang, C.-J., Rittmann, S.K.-M.R., Ferry, J.G., 2024. Editorial: Cross-boundary significance of methanogens - the methane moment and beyond. *Front. Microbiol.* 15. <https://doi.org/10.3389/fmicb.2024.1434586>
- Lyu, Z., Shao, N., Akinyemi, T., Whitman, W.B., 2018. Methanogenesis. *Current Biology* 28, R727–R732. <https://doi.org/10.1016/j.cub.2018.05.021>
- Lyu, Z., Whitman, W.B., 2019. Transplanting the pathway engineering toolbox to methanogens. *Curr. Opin. Biotechnol.* 59, 46–54. <https://doi.org/10.1016/j.copbio.2019.02.009>
- Martin, W., Baross, J., Kelley, D., Russell, M.J., 2008. Hydrothermal vents and the origin of life. *Nat Rev Micro* 6, 805–814. <https://doi.org/10.1038/nrmicro1991>
- Mauerhofer, L.-M., Pappenreiter, P., Paulik, C., Seifert, A.H., Bernacchi, S., Rittmann, S.K.-M.R., 2019. Methods for quantification of growth and productivity in anaerobic microbiology and biotechnology. *Folia Microbiol* 64, 321–360. <https://doi.org/10.1007/s12223-018-0658-4>
- Mauerhofer, L.-M., Reischl, B., Schmider, T., Schupp, B., Nagy, K., Pappenreiter, P., Zwirtmayr, S., Schuster, B., Bernacchi, S., Seifert, A.H., Paulik, C., Rittmann, S.K.-M.R., 2018. Physiology and methane productivity of *Methanobacterium thermaggregans*. *Appl Microbiol Biotechnol* 102, 7643–7656. <https://doi.org/10.1007/s00253-018-9183-2>
- Mauerhofer, L.-M., Zwirtmayr, S., Pappenreiter, P., Bernacchi, S., Seifert, A.H., Reischl, B., Schmider, T., Taubner, R.-S., Paulik, C., Rittmann, S.K.-M.R., 2021. Hyperthermophilic methanogenic archaea act as high-pressure CH<sub>4</sub> cell factories. *Communications Biology* 4, 289. <https://doi.org/10.1038/s42003-021-01828-5>
- Mayumi, D., Mochimaru, H., Tamaki, H., Yamamoto, K., Yoshioka, H., Suzuki, Y., Kamagata, Y., Sakata, S., 2016. Methane production from coal by a single methanogen. *Science* 354, 222–225. <https://doi.org/10.1126/science.aaf8821>
- McCluskie, M.J., Deschatelets, L., Krishnan, L., 2017. Sulfated archaeal glycolipid archaeosomes as a safe and effective vaccine adjuvant for induction of cell-mediated immunity. *Hum Vaccin Immunother* 13, 2772–2779. <https://doi.org/10.1080/21645515.2017.1316912>
- Meister, P., Reyes, C., 2019. The Carbon-Isotope Record of the Sub-Seafloor Biosphere. *Geosciences* 9, 507. <https://doi.org/10.3390/geosciences9120507>
- Metcalf, W.W., Zhang, J.K., Apolinario, E., Sowers, K.R., Wolfe, R.S., 1997. A genetic system for Archaea of the genus *Methanosarcina*: Liposome-mediated transformation and construction of shuttle vectors. *PNAS* 94, 2626–2631.
- Miller, T.L., Wolin, M.J., 1974. A Serum Bottle Modification of the Hungate Technique for Cultivating Obligate Anaerobes. *Appl Microbiol* 27, 985–987.
- Miller, T.L., Wolin, M.J., de Macario, E.C., Macario, A.J., 1982. Isolation of *Methanobrevibacter smithii* from human feces. *Applied and Environmental Microbiology* 43, 227–232. <https://doi.org/10.1128/aem.43.1.227-232.1982>
- Moissl-Eichinger, C., Pausan, M., Taffner, J., Berg, G., Bang, C., Schmitz, R.A., 2018. Archaea Are Interactive Components of Complex Microbiomes. *Trends in Microbiology* 26, 70–85. <https://doi.org/10.1016/j.tim.2017.07.004>

- Mondav, R., Woodcroft, B.J., Kim, E.-H., McCalley, C.K., Hodgkins, S.B., Crill, P.M., Chanton, J., Hurst, G.B., VerBerkmoes, N.C., Saleska, S.R., Hugenholtz, P., Rich, V.I., Tyson, G.W., 2014. Discovery of a novel methanogen prevalent in thawing permafrost. *Nat Commun* 5, 1–7. <https://doi.org/10.1038/ncomms4212>
- Moore, B.C., Leigh, J.A., 2005. Markerless Mutagenesis in *Methanococcus maripaludis* Demonstrates Roles for Alanine Dehydrogenase, Alanine Racemase, and Alanine Permease. *Journal of Bacteriology* 187, 972–979. <https://doi.org/10.1128/JB.187.3.972-979.2005>
- Mukhopadhyay, B., 2024. A reminder—peptidoglycan cell walls indeed occur in the archaeal domain, specifically in the members of *Methanobacteria* and *Methanopyri* classes. *Front. Microbiol.* 15. <https://doi.org/10.3389/fmicb.2024.1329047>
- Müller, V., 2019. New horizons in acetogenic conversion of one-carbon substrates and biological hydrogen storage. *Trends in Biotechnology* 37, 1344–1354. <https://doi.org/10.1016/j.tibtech.2019.05.008>
- Nielsen, P., Fritze, D., Priest, F.G., 1995. Phenetic diversity of alkaliphilic *Bacillus* strains: proposal for nine new species. *Microbiology* 141, 1745–1761. <https://doi.org/10.1099/13500872-141-7-1745>
- Offre, P., Spang, A., Schleper, C., 2013. Archaea in Biogeochemical Cycles. *Annual Review of Microbiology* 67, 437–457. <https://doi.org/10.1146/annurev-micro-092412-155614>
- Olsen, G.J., Lane, D.J., Giovannoni, S.J., Pace, N.R., Stahl, D.A., 1986. Microbial Ecology and Evolution: A Ribosomal RNA Approach. *Annual Review of Microbiology* 40, 337–365. <https://doi.org/10.1146/annurev.mi.40.100186.002005>
- Palabikyan, H., 2020. Heterologous expression of genes encoding for the carbon storage metabolism of *Nitrososphaera viennensis* in *Methanococcus maripaludis* (Master thesis). University of Vienna, Vienna, Austria.
- Pappenreiter, P.A., Zwirtmayr, S., Mauerhofer, L.-M., Rittmann, S.K.-M.R., Paulik, C., 2019. Development of a simultaneous bioreactor system for characterization of gas production kinetics of methanogenic archaea at high pressure. *Engineering in Life Sciences* 19, 537–544. <https://doi.org/10.1002/elsc.201900035>
- Patel, G.B., Sprott, G.D., 1999. Archaeobacterial Ether Lipid Liposomes (Archaeosomes) as Novel Vaccine and Drug Delivery Systems. *Critical Reviews in Biotechnology* 19, 317–357. <https://doi.org/10.1080/0738-859991229170>
- Pende, N., Sogues, A., Megrian, D., Sartori-Rupp, A., England, P., Palabikyan, H., Rittmann, S.K.-M.R., Graña, M., Wehenkel, A.M., Alzari, P.M., Gribaldo, S., 2021. SepF is the FtsZ anchor in archaea, with features of an ancestral cell division system. *Nat Commun* 12, 3214. <https://doi.org/10.1038/s41467-021-23099-8>
- Pester, M., Schleper, C., Wagner, M., 2011. The Thaumarchaeota: an emerging view of their phylogeny and ecophysiology. *Current Opinion in Microbiology, Ecology and industrial microbiology / Special section: Archaea* 14, 300–306. <https://doi.org/10.1016/j.mib.2011.04.007>
- Pfeifer, K., Ergal, I., Koller, M., Basen, M., Schuster, B., Rittmann, S.K.-M.R., 2021. Archaea Biotechnology. *Biotechnology Advances* 47, 107668. <https://doi.org/10.1016/j.biotechadv.2020.107668>
- Probst, A.J., Auerbach, A.K., Moissl-Eichinger, C., 2013. Archaea on Human Skin. *PLoS One* 8, e65388. <https://doi.org/10.1371/journal.pone.0065388>
- Reischl, B., Ergal, I., Rittmann, S.K.-M.R., 2018a. Biohydrogen production characteristics of *Desulfurococcus amylolyticus* DSM 16532. *International Journal of Hydrogen Energy* 43, 8747–8753. <https://doi.org/10.1016/j.ijhydene.2018.03.121>
- Reischl, B., Ergal, I., Rittmann, S.K.-M.R., 2018b. Metabolic reconstruction and experimental verification of glucose utilization in *Desulfurococcus amylolyticus* DSM 16532. *Folia Microbiol* 1–11. <https://doi.org/10.1007/s12223-018-0612-5>

- Reischl, B., Schupp, B., Palabikyan, H., Steger-Mähnert, B., Fink, C., Rittmann, S.K.-M.R., 2025. Quantitative analysis of amino acid excretion by *Methanothermobacter marburgensis* under N<sub>2</sub>-fixing conditions. *Sci Rep* 15, 1–13. <https://doi.org/10.1038/s41598-025-87686-1>
- Řezanka, T., Kyselová, L., Murphy, D.J., 2023. Archaeal lipids. *Progress in Lipid Research* 91, 101237. <https://doi.org/10.1016/j.plipres.2023.101237>
- Rittmann, S., Seifert, A., Herwig, C., 2015. Essential prerequisites for successful bioprocess development of biological CH<sub>4</sub> production from CO<sub>2</sub> and H<sub>2</sub>. *Crit. Rev. Biotechnol.* 35, 141–151. <https://doi.org/10.3109/07388551.2013.820685>
- Rittmann, Simon, Seifert, A., Herwig, C., 2012. Quantitative analysis of media dilution rate effects on *Methanothermobacter marburgensis* grown in continuous culture on H<sub>2</sub> and CO<sub>2</sub>. *Biomass and Bioenergy* 36, 293–301. <https://doi.org/10.1016/j.biombioe.2011.10.038>
- Rittmann, S., Seifert, A., Herwig, C., 2012. Quantitative analysis of media dilution rate effects on *Methanothermobacter marburgensis* grown in continuous culture on H<sub>2</sub> and CO<sub>2</sub>. *Biomass Bioenerg* 36, 293–301. <https://doi.org/10.1016/j.biombioe.2011.10.038>
- Rittmann, S.K.-M.R., 2015. A Critical Assessment of Microbiological Biogas to Biomethane Upgrading Systems. *Adv Biochem Eng Biotechnol* 151, 117–135. [https://doi.org/10.1007/978-3-319-21993-6\\_5](https://doi.org/10.1007/978-3-319-21993-6_5)
- Rittmann, S.K.-M.R., Lee, H.S., Lim, J.K., Kim, T.W., Lee, J.-H., Kang, S.G., 2015. One-carbon substrate-based biohydrogen production: Microbes, mechanism, and productivity. *Biotechnology Advances* 33, 165–177. <https://doi.org/10.1016/j.biotechadv.2014.11.004>
- Rittmann, S.K.-M.R., Pfeifer, K., Palabikyan, H., Ergal, I., Schuster, B., 2021. Archaea in der Biotechnologie. *Biospektrum* 27, 96–98. <https://doi.org/10.1007/s12268-021-1514-8>
- Rittmann, S.K.-M.R., Schupp, B., Reischl, B., Taubner, R.-S., Palabikyan, H., Fink, C., Ergal, I., Fennessy, R., 2023a. Method for Fermentatively Producing Norvaline. WO2023247743A1.
- Rittmann, S.K.-M.R., Schupp, B., Reischl, B., Taubner, R.-S., Palabikyan, H., Fink, C., Ergal, I., Fennessy, R., 2023b. Method for Producing Amino Acids in a Bioreactor. WO2023247742A1.
- Rittmann, S.K.-M.R., Schupp, B., Reischl, B., Taubner, R.-S., Palabikyan, H., Fink, C., Ergal, I., Fennessy, R., 2023c. Method for Producing Amino Acids in a Bioreactor with Methanogenic Microorganisms. WO2023247741A1.
- Rittmann, S.K.-M.R., Schupp, B., Reischl, B., Taubner, R.-S., Palabikyan, H., Fink, C., Ergal, I., Fennessy, R., 2023d. Method for Producing Amino Acids with Methanogenic Microorganisms in a Bioreactor. WO2023247740A1.
- Rittmann, S.K.-M.R., Seifert, A.H., Bernacchi, S., 2018. Kinetics, multivariate statistical modelling, and physiology of CO<sub>2</sub>-based biological methane production. *Applied Energy* 216, 751–760. <https://doi.org/10.1016/j.apenergy.2018.01.075>
- Rittmann, S.K.-M.R., Seifert, A.H., Krajete, A., 2014. Biomethanisierung — ein Prozess zur Ermöglichung der Energiewende? *Biospektrum* 20, 816–817. <https://doi.org/10.1007/s12268-014-0521-3>
- Rodrigues-Oliveira, T., Belmok, A., Vasconcellos, D., Schuster, B., Kyaw, C.M., 2017. Archaeal S-Layers: Overview and Current State of the Art. *Front. Microbiol.* 8. <https://doi.org/10.3389/fmicb.2017.02597>
- Romanenko, L.A., Tanaka, N., Frolova, G.M., Mikhailov, V., 2009. *Psychrobacter fulvigenes* sp. nov., isolated from a marine crustacean from the Sea of Japan. *International Journal of Systematic and Evolutionary Microbiology* 59, 1480–1486. <https://doi.org/10.1099/ijls.0.007195-0>
- Samson, R.Y., Obita, T., Freund, S.M., Williams, R.L., Bell, S.D., 2008. A Role for the ESCRT System in Cell Division in Archaea. *Science* 322, 1710–1713. <https://doi.org/10.1126/science.1165322>
- Santhosh, P.B., Genova, J., 2023. Archaeosomes: New Generation of Liposomes Based on Archaeal Lipids for Drug Delivery and Biomedical Applications. *ACS Omega* 8, 1–9. <https://doi.org/10.1021/acsomega.2c06034>

- Sarmiento, F.B., Leigh, J.A., Whitman, W.B., 2011. Genetic systems for hydrogenotrophic methanogens. *Meth. Enzymol.* 494, 43–73. <https://doi.org/10.1016/B978-0-12-385112-3.00003-2>
- Schleper, C., Puehler, G., Holz, I., Gambacorta, A., Janekovic, D., Santarius, U., Klenk, H.P., Zillig, W., 1995. *Picrophilus* gen. nov., fam. nov.: a novel aerobic, heterotrophic, thermoacidophilic genus and family comprising archaea capable of growth around pH 0. *J Bacteriol* 177, 7050–7059.
- Schocke, L., Bräsen, C., Siebers, B., 2019. Thermoacidophilic *Sulfolobus* species as source for extremozymes and as novel archaeal platform organisms. *Current Opinion in Biotechnology, Tissue, Cell and Pathway Engineering* 59, 71–77. <https://doi.org/10.1016/j.copbio.2019.02.012>
- Schönheit, P., Moll, J., Thauer, R.K., 1979. Nickel, cobalt, and molybdenum requirement for growth of *Methanobacterium thermoautotrophicum*. *Arch. Microbiol.* 123, 105–107. <https://doi.org/10.1007/BF00403508>
- Schuchmann, K., Müller, V., 2016. Energetics and Application of Heterotrophy in Acetogenic Bacteria. *Appl. Environ. Microbiol.* 82, 4056–4069. <https://doi.org/10.1128/AEM.00882-16>
- Seifert, A.H., Rittmann, S., Bernacchi, S., Herwig, C., 2013. Method for assessing the impact of emission gasses on physiology and productivity in biological methanogenesis. *Bioresource Technology* 136, 747–751. <https://doi.org/10.1016/j.biortech.2013.03.119>
- Seifert, A.H., Rittmann, S., Herwig, C., 2014. Analysis of process related factors to increase volumetric productivity and quality of biomethane with *Methanothermobacter marburgensis*. *Applied Energy* 132, 155–162. <https://doi.org/10.1016/j.apenergy.2014.07.002>
- Shu, W.-S., Huang, L.-N., 2021. Microbial diversity in extreme environments. *Nat Rev Microbiol* 1–17. <https://doi.org/10.1038/s41579-021-00648-y>
- Siebert, M., Cichocka, D., Herrmann, S., Gründger, F., Feisthauer, S., Richnow, H.-H., Springael, D., Krüger, M., 2011. Accelerated methanogenesis from aliphatic and aromatic hydrocarbons under iron- and sulfate-reducing conditions. *FEMS Microbiology Letters* 315, 6–16. <https://doi.org/10.1111/j.1574-6968.2010.02165.x>
- Siliakus, M.F., van der Oost, J., Kengen, S.W.M., 2017. Adaptations of archaeal and bacterial membranes to variations in temperature, pH and pressure. *Extremophiles* 21, 651–670. <https://doi.org/10.1007/s00792-017-0939-x>
- Singh, A., Singh, A.K., 2017. Haloarchaea: worth exploring for their biotechnological potential. *Biotechnol. Lett.* 39, 1793–1800. <https://doi.org/10.1007/s10529-017-2434-y>
- Sprott, G., Dicaire, C., Fleming, L., Patel, G., 1996. Stability of Liposomes Prepared from Archaeobacterial Lipids and Phosphatidylcholine Mixtures. *Cells and Materials* 6.
- Sprott, G.D., 2011. Archaeal Membrane Lipids and Applications, in: eLS. John Wiley & Sons, Ltd. <https://doi.org/10.1002/9780470015902.a0000385.pub3>
- Stark, F.C., Agbayani, G., Sandhu, J.K., Akache, B., McPherson, C., Deschatelets, L., Dudani, R., Hewitt, M., Jia, Y., Krishnan, L., McCluskie, M.J., 2019. Simplified Admix Archaeal Glycolipid Adjuvanted Vaccine and Checkpoint Inhibitor Therapy Combination Enhances Protection from Murine Melanoma. *Biomedicines* 7, 91. <https://doi.org/10.3390/biomedicines7040091>
- Steger, F., Reich, J., Fuchs, W., Rittmann, S.K.-M.R., Gübitz, G.M., Ribitsch, D., Bochmann, G., 2022. Comparison of Carbonic Anhydrases for CO<sub>2</sub> Sequestration. *International Journal of Molecular Sciences* 23, 957. <https://doi.org/10.3390/ijms23020957>
- Stieglmeier, M., Alves, R.J.E., Schleper, C., 2014a. The Phylum Thaumarchaeota, in: Rosenberg, E., DeLong, E.F., Lory, S., Stackebrandt, E., Thompson, F. (Eds.), *The Prokaryotes*. Springer Berlin Heidelberg, pp. 347–362.
- Stieglmeier, M., Klingl, A., Alves, R.J.E., Rittmann, S.K.-M.R., Melcher, M., Leisch, N., Schleper, C., 2014b. *Nitrososphaera viennensis* sp. nov., an aerobic and mesophilic ammonia-oxidizing archaeon from soil and member of the archaeal phylum Thaumarchaeota. *Int. J. Syst. Evol. Microbiol.* 64, 2738–52. <https://doi.org/10.1099/ijs.0.063172-0>

- Straub, C.T., Counts, J.A., Nguyen, D.M.N., Wu, C.-H., Zeldes, B.M., Crosby, J.R., Conway, J.M., Otten, J.K., Lipscomb, G.L., Schut, G.J., Adams, M.W.W., Kelly, R.M., 2018. Biotechnology of extremely thermophilic archaea. *FEMS Microbiol Rev* 42, 543–578. <https://doi.org/10.1093/femsre/fuy012>
- Takai, K., Nakamura, K., Toki, T., Tsunogai, U., Miyazaki, M., Miyazaki, J., Hirayama, H., Nakagawa, S., Nunoura, T., Horikoshi, K., 2008. Cell proliferation at 122°C and isotopically heavy CH<sub>4</sub> production by a hyperthermophilic methanogen under high-pressure cultivation. *Proceedings of the National Academy of Sciences* 105, 10949–10954. <https://doi.org/10.1073/pnas.0712334105>
- Tan, G.-Y.A., Chen, C.-L., Li, L., Ge, L., Wang, L., Razaad, I.M.N., Li, Y., Zhao, L., Mo, Y., Wang, J.-Y., 2014. Start a Research on Biopolymer Polyhydroxyalkanoate (PHA): A Review. *Polymers* 6, 706–754. <https://doi.org/10.3390/polym6030706>
- Taubner, R.-S., Baumann, L.M.F., Bauersachs, T., Clifford, E.L., Mähnert, B., Reischl, B., Seifert, R., Peckmann, J., Rittmann, S.K.-M.R., Birgel, D., 2019. Membrane Lipid Composition and Amino Acid Excretion Patterns of *Methanothermococcus okinawensis* Grown in the Presence of Inhibitors Detected in the Enceladian Plume. *Life* 9, 85. <https://doi.org/10.3390/life9040085>
- Taubner, R.-S., Baumann, L.M.F., Steiner, M., Pfeifer, K., Reischl, B., Korynt, K., Bauersachs, T., Mähnert, B., Clifford, E.L., Peckmann, J., Schuster, B., Birgel, D., Rittmann, S.K.-M.R., 2023. Lipidomics and Comparative Metabolite Excretion Analysis of Methanogenic Archaea Reveal Organism-Specific Adaptations to Varying Temperatures and Substrate Concentrations. *mSystems* 8, e01159-22. <https://doi.org/10.1128/msystems.01159-22>
- Taubner, R.-S., Pappenreiter, P., Zwicker, J., Smrzka, D., Pruckner, C., Kolar, P., Bernacchi, S., Seifert, A.H., Krajete, A., Bach, W., Peckmann, J., Paulik, C., Firneis, M.G., Schleper, C., Rittmann, S.K.-M.R., 2018. Biological methane production under putative Enceladus-like conditions. *Nature Communications* 9, 748. <https://doi.org/10.1038/s41467-018-02876-y>
- Taubner, R.-S., Rittmann, S.K.-M.R., 2016. Method for Indirect Quantification of CH<sub>4</sub> Production via H<sub>2</sub>O Production Using Hydrogenotrophic Methanogens. *Front. Microbiol* 7, 532. <https://doi.org/10.3389/fmicb.2016.00532>
- Taubner, R.-S., Schleper, C., Firneis, M.G., Rittmann, S.K.-M.R., 2015. Assessing the Ecophysiology of Methanogens in the Context of Recent Astrobiological and Planetological Studies. *Life* 5, 1652–1686. <https://doi.org/10.3390/life5041652>
- Thauer, R.K., 2012. The Wolfe cycle comes full circle. *PNAS* 109, 15084–15085. <https://doi.org/10.1073/pnas.1213193109>
- Thauer, R.K., 1998. Biochemistry of methanogenesis: a tribute to Marjory Stephenson. *Microbiology* 144, 2377–2406. <https://doi.org/10.1099/00221287-144-9-2377>
- Thauer, R.K., 1990. Energy metabolism of methanogenic bacteria. *Biochimica et Biophysica Acta (BBA) - Bioenergetics* 1018, 256–259. [https://doi.org/10.1016/0005-2728\(90\)90261-2](https://doi.org/10.1016/0005-2728(90)90261-2)
- Thauer, R.K., Kaster, A.-K., Goenrich, M., Schick, M., Hiromoto, T., Shima, S., 2010. Hydrogenases from methanogenic archaea, nickel, a novel cofactor, and H<sub>2</sub> storage. *Annu. Rev. Biochem.* 79, 507–536. <https://doi.org/10.1146/annurev.biochem.030508.152103>
- Thauer, R.K., Kaster, A.-K., Seedorf, H., Buckel, W., Hedderich, R., 2008. Methanogenic archaea: ecologically relevant differences in energy conservation. *Nat Rev Micro* 6, 579–591. <https://doi.org/10.1038/nrmicro1931>
- Thevasundaram, K., Gallagher, J.J., Chong, F., Chang, M.C.Y., 2022. Engineering nonphotosynthetic carbon fixation for production of bioplastics by methanogenic archaea. *Proceedings of the National Academy of Sciences* 119, e2118638119. <https://doi.org/10.1073/pnas.2118638119>
- Tian, H., Lu, C., Ciais, P., Michalak, A.M., Canadell, J.G., Saikawa, E., Huntzinger, D.N., Gurney, K.R., Sitch, S., Zhang, B., Yang, J., Bousquet, P., Bruhwiler, L., Chen, G., Dlugokencky, E., Friedlingstein, P., Melillo, J., Pan, S., Poulter, B., Prinn, R., Saunio, M., Schwalm, C.R.,



- Wofsy, S.C., 2016. The terrestrial biosphere as a net source of greenhouse gases to the atmosphere. *Nature* 531, 225–228. <https://doi.org/10.1038/nature16946>
- Tveit, A.T., Hestnes, A.G., Robinson, S.L., Schintlmeister, A., Dedysh, S.N., Jehmlich, N., Bergen, M. von, Herbold, C., Wagner, M., Richter, A., Svenning, M.M., 2019. Widespread soil bacterium that oxidizes atmospheric methane. *PNAS* 201817812. <https://doi.org/10.1073/pnas.1817812116>
- Valentine, D.L., 2007. Adaptations to energy stress dictate the ecology and evolution of the Archaea. *Nature Reviews Microbiology* 5, 316–323. <https://doi.org/10.1038/nrmicro1619>
- Ventosa, A., Oren, A., 1996. *Halobacterium salinarum* nom. corrig., a Name To Replace *Halobacterium salinarum* (Elazari-Volcani) and To Include *Halobacterium halobium* and *Halobacterium cutirubrum*. *International Journal of Systematic and Evolutionary Microbiology* 46, 347–347. <https://doi.org/10.1099/00207713-46-1-347>
- Ver Eecke, H.C., Akerman, N.H., Huber, J.A., Butterfield, D.A., Holden, J.F., 2013. Growth kinetics and energetics of a deep-sea hyperthermophilic methanogen under varying environmental conditions. *Environmental Microbiology Reports* 5, 665–671. <https://doi.org/10.1111/1758-2229.12065>
- Ver Eecke, H.C.V., Butterfield, D.A., Huber, J.A., Lilley, M.D., Olson, E.J., Roe, K.K., Evans, L.J., Merkel, A.Y., Cantin, H.V., Holden, J.F., 2012. Hydrogen-limited growth of hyperthermophilic methanogens at deep-sea hydrothermal vents. *PNAS* 109, 13674–13679. <https://doi.org/10.1073/pnas.1206632109>
- Wang, X., Lutkenhaus, J., 1996. FtsZ ring: the eubacterial division apparatus conserved in archaeobacteria. *Molecular Microbiology* 21, 313–320. <https://doi.org/10.1046/j.1365-2958.1996.6421360.x>
- Wang, Y., Wegener, G., Hou, J., Wang, F., Xiao, X., 2019. Expanding anaerobic alkane metabolism in the domain of Archaea. *Nat Microbiol* 4, 595–602. <https://doi.org/10.1038/s41564-019-0364-2>
- Welte, C.U., 2016. A microbial route from coal to gas. *Science* 354, 184–184. <https://doi.org/10.1126/science.aai8101>
- Williams, T.A., Szöllősi, G.J., Spang, A., Foster, P.G., Heaps, S.E., Boussau, B., Ettema, T.J.G., Embley, T.M., 2017. Integrative modeling of gene and genome evolution roots the archaeal tree of life. *PNAS* 201618463. <https://doi.org/10.1073/pnas.1618463114>
- Woese, C.R., 2002. On the evolution of cells. *Proc Natl Acad Sci U S A* 99, 8742–8747. <https://doi.org/10.1073/pnas.132266999>
- Woese, C.R., Fox, G.E., 1977. Phylogenetic structure of the prokaryotic domain: the primary kingdoms. *Proc. Natl. Acad. Sci. U.S.A.* 74, 5088–5090. <https://doi.org/10.1073/pnas.74.11.5088>
- Xu, Q., Du, Q., Gao, J., Chen, L., Dong, X., Li, J., 2023. A robust genetic toolbox for fine-tuning gene expression in the CO<sub>2</sub>-Fixing methanogenic archaeon *Methanococcus maripaludis*. *Metabolic Engineering* 79, 130–145. <https://doi.org/10.1016/j.ymben.2023.07.007>
- Zeldes, B.M., Keller, M.W., Loder, A.J., Straub, C.T., Adams, M.W.W., Kelly, R.M., 2015. Extremely thermophilic microorganisms as metabolic engineering platforms for production of fuels and industrial chemicals. *Frontiers in Microbiology* 6.
- Zinn, M., Witholt, B., Egli, T., 2001. Occurrence, synthesis and medical application of bacterial polyhydroxyalkanoate. *Advanced Drug Delivery Reviews, Polymeric Materials for Advanced Drug Delivery* 53, 5–21. [https://doi.org/10.1016/S0169-409X\(01\)00218-6](https://doi.org/10.1016/S0169-409X(01)00218-6)
- Zipperle, A., Reischl, B., Schmider, T., Stadlbauer, M., Kushkevych, I., Pruckner, C., Vítězová, M., Rittmann, S.K.-M.R., 2021. Biomethanation of Carbon Monoxide by Hyperthermophilic Artificial Archaeal Co-Cultures. *Fermentation* 7, 276. <https://doi.org/10.3390/fermentation7040276>

# ANNEX 1

Pages 44 to 58

---

Palabikyan H., Ruddyard A., Pomper L., Novak D., Reischl B., Rittmann S.K.-M.R.

**Scale-up of biomass production by *Methanococcus maripaludis***

Frontiers in Microbiology (2022) 13

10.3389/fmicb.2022.1031131

---



## OPEN ACCESS

## EDITED BY

Barry Whitman,  
University of Georgia,  
United States

## REVIEWED BY

Kylie Allen,  
Virginia Tech,  
United States  
Nicole Buan,  
University of Nebraska-Lincoln,  
United States

## \*CORRESPONDENCE

Simon K.-M. R. Rittmann  
simon.rittmann@univie.ac.at

<sup>†</sup>These authors have contributed equally to this work

## SPECIALTY SECTION

This article was submitted to Biology of Archaea, a section of the journal Frontiers in Microbiology

RECEIVED 29 August 2022

ACCEPTED 13 October 2022

PUBLISHED 23 November 2022

## CITATION

Palabikyan H, Ruddyard A, Pomper L, Novak D, Reischl B and Rittmann SK-MR (2022) Scale-up of biomass production by *Methanococcus maripaludis*. *Front. Microbiol.* 13:1031131. doi: 10.3389/fmicb.2022.1031131

## COPYRIGHT

© 2022 Palabikyan, Ruddyard, Pomper, Novak, Reischl and Rittmann. This is an open-access article distributed under the terms of the [Creative Commons Attribution License \(CC BY\)](#). The use, distribution or reproduction in other forums is permitted, provided the original author(s) and the copyright owner(s) are credited and that the original publication in this journal is cited, in accordance with accepted academic practice. No use, distribution or reproduction is permitted which does not comply with these terms.

# Scale-up of biomass production by *Methanococcus maripaludis*

Hayk Palabikyan<sup>1†</sup>, Aquilla Ruddyard<sup>1,2†</sup>, Lara Pomper<sup>1†</sup>, David Novak<sup>3</sup>, Barbara Reischl<sup>1,2</sup> and Simon K.-M. R. Rittmann<sup>1,2\*</sup>

<sup>1</sup>Archaea Physiology & Biotechnology Group, Department of Functional and Evolutionary Ecology, Universität Wien, Vienna, Austria, <sup>2</sup>Arkeon GmbH, Tulln a.d. Donau, Austria, <sup>3</sup>Department of Biochemistry, Faculty of Science, Masaryk University, Brno, Czechia

The development of a sustainable energy economy is one of the great challenges in the current times of climate crisis and growing energy demands. Industrial production of the fifth-generation biofuel methane by microorganisms has the potential to become a crucial biotechnological milestone of the post fossil fuel era. Therefore, reproducible cultivation and scale-up of methanogenic archaea (methanogens) is essential for enabling biomass generation for fundamental studies and for defining peak performance conditions for bioprocess development. This study provides a comprehensive revision of established and optimization of novel methods for the cultivation of the model organism *Methanococcus maripaludis* S0001. In closed batch mode, 0.05 L serum bottles cultures were gradually replaced by 0.4 L Schott bottle cultures for regular biomass generation, and the time for reaching peak optical density (OD<sub>578</sub>) values was reduced in half. In 1.5 L reactor cultures, various agitation, harvesting and transfer methods were compared resulting in a specific growth rate of 0.16 h<sup>-1</sup> and the highest recorded OD<sub>578</sub> of 3.4. Finally, a 300-fold scale-up from serum bottles was achieved by growing *M. maripaludis* for the first time in a 22 L stainless steel bioreactor with 15 L working volume. Altogether, the experimental approaches described in this study contribute to establishing methanogens as essential organisms in large-scale biotechnology applications, a crucial stage of an urgently needed industrial evolution toward sustainable biosynthesis of energy and high value products.

## KEYWORDS

archaea biotechnology, bioreactor, bioprocess, fed-batch, anaerobe, methanogen

## Introduction

The global impact of a constantly expanding human civilization could be addressed by a proportionally accelerated transformation of the technological progress. Biotechnological advances utilizing natural and recombinant microorganisms, like methanogenic archaea (methanogens), can provide various solutions for decentralized sustainable energy manufacturing, such as biomethanation processes, which utilize methanogens with industrially relevant growth characteristics and high volumetric methane (CH<sub>4</sub>) biosynthesis (Seifert et al., 2014; Azim et al., 2017; Mauerhofer et al., 2018; Rittmann et al., 2018). Biological CH<sub>4</sub> production from carbon dioxide (CO<sub>2</sub>)

(CO<sub>2</sub>-BMP) can be applied to establish CH<sub>4</sub> as a CO<sub>2</sub>-neutral biofuel (Porqueras et al., 2012) of the post-fossil fuel era, as CH<sub>4</sub> can be incorporated into existing storage and transportation infrastructures for natural gas (Mauerhofer et al., 2018). In fact, methanogens have already been utilized in large scale anaerobic digestion for biogas production (Guebitz et al., 2015) and for conversion and storage of energy from renewable sources into CH<sub>4</sub> (Götz et al., 2016).

Methanogens are a remarkable group of organisms within the domain Archaea (Cavicchioli, 2011; Borrel et al., 2013). Methanogenesis might have emerged billions of years ago under primordial conditions in hydrothermal vents as one of the most ancient metabolisms (Ueno et al., 2006; Martin et al., 2008). Today, methanogens have been found in almost every anoxic environment on the planet and are responsible for the final stage of biomass mineralization by producing CH<sub>4</sub> under anaerobic conditions (Liu and Whitman, 2008; Thauer et al., 2008; Jabłoński et al., 2015). By biosynthesizing roughly 1 Gt of the potent greenhouse gas CH<sub>4</sub> annually (Howarth et al., 2011; IPCC, 2013), methanogens have become a crucial subject of studies, due to their essential role in the global carbon cycle and their ecological significance.

*Methanococcus maripaludis* is an autotrophic, hydrogenotrophic, methanogenic mesophile which grows in mineral medium at 37°C (Jones et al., 1983; Keswani et al., 1996). *M. maripaludis* requires solely CO<sub>2</sub> as a carbon source (Zellner and Winter, 1987) but it can additionally utilize acetate for biomass synthesis (Shieh and Whitman, 1987; Azim et al., 2018). For energy production, molecular hydrogen (H<sub>2</sub>) or formate are used as an electron source (Shieh and Whitman, 1988; Costa et al., 2013; Rother and Whitman, 2019). A thin S-layer has been described for *M. maripaludis* (Jarrell and Koval, 1989; Jarrell et al., 2010), which implies that *M. maripaludis* is presumably a rather fragile organism when it is exposed to low osmolarity buffers (Jones et al., 1985) or to detergents (Jones et al., 1983). Nevertheless, the cellular structure of *M. maripaludis* allows straightforward manipulation by classical molecular biology techniques.

Today, *M. maripaludis* is one of the mostly studied model organisms among obligate hydrogenotrophic methanogens (Goyal et al., 2016; Richards et al., 2016). It can be transformed (Tumbula et al., 1994) with various shuttle vectors (Argyle et al., 1996; Sarmiento et al., 2011; Walters et al., 2011), and its genome can be edited by integrative plasmids (Stathopoulos et al., 2001; Lie and Leigh, 2007) or by a markerless mutagenesis procedure (Moore and Leigh, 2005). Furthermore, two distinct CRISPR-mediated genome editing systems have been successfully established in *M. maripaludis* (Bao et al., 2022; Li et al., 2022). The extensive molecular toolbox has been used for diverse studies of the physiology of methanogens, such as the molecular architecture of the methyl coenzyme M reductase (Lyu et al., 2018). Furthermore, *M. maripaludis* S0001 has been metabolically engineered as a cell factory for the production of high value products, such as geraniol (Lyu et al., 2016) and the bioplastic polymer polyhydroxybutyrate (Thevasundaram et al., 2022).

Nevertheless, there is much space for methodological advances which would allow *M. maripaludis* to be further established as model organism with a recognizable impact on the global biotechnology sector.

A reproducible pipeline for scaling up the cultivation of *M. maripaludis* has been a missing link that has restricted this promising species to a laboratory-scale subject of studies. Even though various techniques have been used for the cultivation of *M. maripaludis* in closed batch mode (Balch et al., 1979; Sarmiento et al., 2011; Goyal et al., 2015), they are all limiting culture volumes in milliliter ranges and alter physiological footprints due to a discontinuous substrate supplementation. Nevertheless, a flexible and cost-efficient formate-based 1.5 L system in closed batch mode has been developed for formate utilizing methanogens, which allows sufficient biomass generation for analytical studies and eliminates common challenges of H<sub>2</sub>/CO<sub>2</sub>-supplied methods (Long et al., 2017).

In contrast, a fed-batch mode of cultivation allows continuous addition of feed for growth, larger culture volumes and more sophisticated control of conditions. Nevertheless, only handful of notable studies have applied chemostat-like systems (Haydock et al., 2004; Hendrickson et al., 2007, 2008; Costa et al., 2013; Müller et al., 2021) or carried out scale-up of pure cultures (Walters and Chong, 2017) for biomass generation by of *M. maripaludis*. All of them have been focused on other fundamental questions and have not developed a detailed pipeline for continuous transfer and scale-up of *M. maripaludis* cultures. Even though larger cultivation volumes of 10 L have been developed decades ago (Shieh and Whitman, 1988), no follow up studies have optimized peak performance conditions for the cultivation of *M. maripaludis* in industrially relevant scales.

Building up from established techniques for the anaerobic cultivation of methanogens (Azim et al., 2017, 2018; Taubner and Rittmann, 2016) this study initiates the completion of a missing chapter in the study of *M. maripaludis* by designing an experimental approach for rapid biomass production by various cultivation methods.

## Materials and methods

### Microorganisms and media

*Methanococcus maripaludis* S0001 was used in all experiments. The organism was provided by William Barney Whitman, University of Georgia, United States. For all experiments and cultivation modes a reduced liquid 141 medium (DSMZ 141a) with the following composition was used: (L<sup>-1</sup>): 0.14 g CaCl<sub>2</sub>·2H<sub>2</sub>O, 0.34 g KCl, 4 g MgCl<sub>2</sub>·6H<sub>2</sub>O, 0.25 g NH<sub>4</sub>Cl, 18.09 NaCl, 0.14 g K<sub>2</sub>HPO<sub>4</sub>, 3.45 g MgSO<sub>4</sub>·7H<sub>2</sub>O, 10 mL Modified Wolin's mineral solution (100×), 2 mL (0.1% w/v) Fe(NH<sub>4</sub>)<sub>2</sub>(SO<sub>4</sub>)<sub>2</sub>·6H<sub>2</sub>O (0.1% w/v). The 100× Modified Wolin's mineral solution was prepared by dissolving 1.5 g Nitrilotriacetic acid in ddH<sub>2</sub>O and adjusting pH to 6.5 with KOH. Then the following reagents were added (L<sup>-1</sup>):

3 g  $\text{MgSO}_4 \cdot 7\text{H}_2\text{O}$ , 0.585 g  $\text{MnCl}_2 \cdot 4\text{H}_2\text{O}$ , 1 g  $\text{NaCl}$ , 0.18 g  $\text{CoSO}_4 \cdot 7\text{H}_2\text{O}$ , 0.1 g  $\text{FeSO}_4 \cdot 7\text{H}_2\text{O}$ , 0.1 g  $\text{CaCl}_2 \cdot 2\text{H}_2\text{O}$ , 0.18 g  $\text{ZnSO}_4 \cdot 7\text{H}_2\text{O}$ , 0.02 g  $\text{KAl}(\text{SO}_4)_2 \cdot 12\text{H}_2\text{O}$ , 0.006 g  $\text{CuSO}_4$ , 0.01 g  $\text{H}_3\text{BO}_3$ , 0.01 g  $\text{Na}_2\text{MoO}_4 \cdot 2\text{H}_2\text{O}$ , 0.0003 g  $\text{Na}_2\text{SeO}_3 \cdot 5\text{H}_2\text{O}$ , 0.03 g  $\text{NiCl}_2 \cdot 6\text{H}_2\text{O}$ , 0.0004 g  $\text{NaWO}_4 \cdot 2\text{H}_2\text{O}$ . Finally, the pH was adjusted to 7.0 with KOH. The  $\text{Fe}(\text{NH}_4)_2(\text{SO}_4)_2 \cdot 6\text{H}_2\text{O}$  solution had the following composition ( $\text{L}^{-1}$ ): 0.00709 g  $\text{FeSO}_4 \cdot 7\text{H}_2\text{O}$  and 0.00337 g  $(\text{NH}_4)_2\text{SO}_4$ . After of the medium was made anaerobic and sterilized, it was supplemented with 20  $\text{mL L}^{-1}$  of sodium acetate (0.61  $\text{mol L}^{-1}$ ) and 4  $\text{mL L}^{-1}$  of  $\text{Na}_2\text{S} \cdot 9\text{H}_2\text{O}$  (0.5  $\text{mol L}^{-1}$ ) prior to inoculation. The following gasses were purchased from Air Liquide (Air Liquide GmbH, Schwechat, Austria) and used for cultivations:  $\text{H}_2/\text{CO}_2$  (4:1 mix),  $\text{H}_2$  ( $\geq 99.999$  Vol.-%) and  $\text{CO}_2$  ( $\geq 99.995$  Vol.-%). Due to the combustible properties of those gasses, all experiments within this study were carried out in designated anaerobic facilities, equipped with sensors and gas alarm systems where the use of open fire is forbidden.

## Closed batch

### 0.05 L serum bottle cultures

Serum bottles (SB) have total and culture volumes of 120 mL and 50 mL, respectively, and are hereafter referred as 0.05 L SB cultures. They were filled with 141 medium (48 mL) and sealed with butyl rubber stoppers (20 mm; CLS-3409-14; Chemglass Life Sciences, Vineland, NJ, United States) and aluminium crimp caps (20 mm; Ochs Laborbedarf, Bovenden, Germany). Bottles were made anaerobic by drawing vacuum (4 $\times$ ) and pressurizing (5 $\times$  1.0 bar) with  $\text{H}_2/\text{CO}_2$  gas mixture (4:1). SB were sterilized by autoclaving, and each replicate was complemented with 1 mL sodium acetate (0.61  $\text{mol L}^{-1}$ ) and 0.2 mL  $\text{Na}_2\text{S} \cdot 9\text{H}_2\text{O}$  (0.5  $\text{mol L}^{-1}$ ) to a final volume of 49.2 mL prior to inoculation. Inoculation was carried out with 0.8 mL of pre-culture (1.6% (v/v)) in an anaerobic glove box (Coy Laboratory Products, Grass Lake, United States).

### 0.4 L Schott bottle cultures

Schott bottles (SCB, DURAN® pressure plus GL-45; DWK Life Sciences, Mainz, Germany) have total and working volumes of 1,000 mL and 416.67 mL, respectively, and are hereafter referred as 0.4 L SCB cultures. They were filled with 141 medium (400 mL) and sealed with butyl rubber stoppers (40 mm; 444704, Glasgerätebau Ochs, Bovenden, Germany) and PBT screw caps (54 mm; DWK Life Sciences, Mainz, Germany). After they were made anaerobic and sterilized, each replicate was complemented with 8.33 mL sodium acetate (0.61  $\text{mol L}^{-1}$ ) and 1.67 mL  $\text{Na}_2\text{S} \cdot 9\text{H}_2\text{O}$  (0.5  $\text{mol L}^{-1}$ ) to a final volume of 410 mL prior to inoculation. Inoculation was carried out with 6.67 mL of pre-culture [1.6% (v/v)] in an anaerobic glove box (Coy Laboratory Products, Grass Lake, United States).

## Cultivation and analysis

For inoculation, sampling and gassing of anaerobic cultures of *M. maripaludis* the following sterile equipment was utilized: 1 mL, 5 mL and 10 mL gas-tight syringes (Injekt®-F, Omnifix®-F,

Omnifix®; B. Braun, Melsungen, Germany); hypodermic needles (Gr 14, 0.60  $\times$  30 mm, 23 G  $\times$  1 1/4"; B. Braun, Melsungen, Germany) and cellulose acetate filters with pore size 0.20  $\mu\text{m}$  (LLG Labware, Meckenheim, Germany). A gassing manifold (Taubner and Rittmann, 2016) was used for feeding cultures. A digital manometer (LEO1-Ei, -1...3 bar rel, Keller, Germany) was used for pressure measurements. Serum bottles were shaken or stirred with a magnetic stir bar at 37°C at various rotations per minute (rpm). Assessment of culture growth was carried out by optical density measurements utilizing a spectrophotometer Specord 200 Plus (Analytic Jena, Jena, Germany) at 578 nm ( $\text{OD}_{578}$ ).

## Experimental groups: Shaking vs. stirring

Two distinct methods for agitation of both SB and SCB were compared – shaking and stirring. Shaken closed batch cultures were agitated up to 180 rpm by two devices: an air incubator (ZWYR-2102C; Labwit Scientific, Ashwood, Australia) or an orbital shaker (No. 3019; Gesellschaft für Labortechnik GmbH, Burgwedel, Germany) which was placed in a 37°C climate chamber (TER, CMESS, University of Vienna). Stirred SB and SCB were agitated up to 1,400 rpm by a 25  $\times$  6 mm or a 40  $\times$  8 mm magnetic stir bars, respectively (BRAND GMBH + CO.KG, Wertheim, Germany). Stir bars were added to 141 media prior to sealing and sterilization of anaerobic media containing bottles, which were incubated on stirrer heating plates (2581001; IKA®-Werke GmbH & Co. KG, Staufen, Germany) that were placed either in an air incubator or in a climate chamber (mentioned above) at 37°C.

Both SB and SCB were tested under distinct conditions (shaking or stirring at various rpm) in quadruplicates with a uninoculated control, which was handled identical to the rest of the replicates. Shaken cultures were subjected to agitation rates of 100, 150 and 180 rpm, whereas stirred cultures were agitated at 100, 500, 800, 1,100, 1,400 rpm. Pressure and  $\text{OD}_{578}$  were measured in regular intervals once a day prior to feeding and further incubation at 37°C. Best experimental groups were reproduced, as a second timepoint for measurements and feed was introduced. For the optimization within each stage (SB or SCB), an inoculum from the stationary phase of the previous experimental group was used. When new series of experiments was started, the first inoculum was acquired from a pre-culture inoculated from cryogenic stocks.

## Revival of cryogenic stocks

Cryogenic backups were regularly produced from both serum and SCB cultures. For SB, 800  $\mu\text{L}$  of culture and 600  $\mu\text{L}$  of anaerobic 50% (v/v) glycerol in 141 medium were mixed in anaerobic glove box, snap frozen in liquid molecular nitrogen and stored at -70°C. For SCB, 6.67 mL of culture and 5 mL of anaerobic 50% (v/v) glycerol in 141 medium were mixed and handled as mentioned above. Upon revival, backups were slowly thawed on ice, spun down at 2,000 g, supernatant was discarded and pelleted biomass was suspended in 0.8 mL or 6.67 mL freshly prepared 141 medium and inoculated in complemented 141 medium containing SB or SCB, respectively. The first revived



generations were not subjected to experiments and were cultivated *via* shaking at 150 rpm as pre-cultures.

## Bioreactors

### 2.2 L bioreactor setup

*Methanococcus maripaludis* was cultivated with the Eppendorf commercial system DASGIP® Bioblock (76DGTBLOCK) equipped with 4× 2.2 L Bioblock stirrer reactors (Eppendorf AG, Hamburg, Germany) with a working volume of 1.5 L (reactor culture). Temperature was constantly maintained at 37°C. Cooling water was supplied to the off-gas condenser. Sensors for pH and redox potential (59903232 and 105053336, Mettler Toledo, Columbus, OH, United States) were connected to the DASGIP® module and were monitored *via* the company software. Feed solutions of sodium acetate (0.61 mol L<sup>-1</sup>) and Na<sub>2</sub>S·9H<sub>2</sub>O (0.5 mol L<sup>-1</sup>) were prepared in SCB, made anaerobic and maintained anaerobic by connecting them to gas bags filled with a gas mix of H<sub>2</sub>/CO<sub>2</sub> (4:1). The solutions were supplemented to the reactor vessels through a PTFE tubing (0.8 mm) by the DASGIP® MP4 and MP8 pumps. Gassing flow rate was usually maintained at 0.3 volume gas per volume liquid per minute (vvm) but alternative vvm were also tested for individual experiments (0.15 to 0.6 vvm). CO<sub>2</sub> was supplemented *via* the DASGIP® MX4/4 mixing module (76DGMX44, Eppendorf AG, Hamburg, Germany) and H<sub>2</sub> was managed externally *via* the mass flow controller SmartTrak® (C100L; Sierra Instruments, Monterey, CA, United States). The two distinct gas circuits were merged by a three-way junction into a single tubing which directed the gas mix of H<sub>2</sub>/CO<sub>2</sub> (4:1) through a Millex®-FG filter (SLFG05010; MilliporeSigma, Burlington, MA, United States) into the inflow sparger of the bioreactor vessels. For sampling of cultures, the in-built 370 mm pipe of stainless steel (outer diameter 4 mm, inner diameter 2 mm) was used. Silicon tubing (M0740-2445; Eppendorf AG, Hamburg, Germany) was used for completing and connecting various reactor gas circuits, tubes and ports. Off-gas tubings were directed through a 500 mL SCB (for collection of condensate) and further toward a dedicated opening of a centralized exhaust gas absorption system.

### 1.5 L reactor cultures: Cultivation and analysis

First, pH and redox probes were calibrated using distinct buffers (pH 7.0/4.1; 10000642/10545151; Fisher Scientific, Hampton, NH, United States) and an ORP solution (240 mV; HI7021L; Hanna Instruments, Woonsocket, RI, United States), respectively. Probes were then plugged into the stirrer reactors filled with 1.434 L of 141 medium without acetate supplementation and the complete reactor setup was sterilized by autoclaving. Then the vessels were positioned into the Bioblock and all circuits were connected and managed through the company software. Temperature was set at 37°C, stirring at 600 rpm and the media was made anaerobic at 0.3 vvm with a flow rate of 20 standard liter per hour (sL h<sup>-1</sup>) H<sub>2</sub> and 5 sL h<sup>-1</sup> CO<sub>2</sub>. The medium was

supplemented with 30 mL of sodium acetate (0.61 mol L<sup>-1</sup>) *via* injection through a silicone rubber septum and with 6 mL of Na<sub>2</sub>S·9H<sub>2</sub>O (0.5 mol L<sup>-1</sup>) *via* the MP4 pumps. Finally, as a last preparation step before inoculation, the pH was adjusted to 7.00 (± 0.05) with NaOH (10 mol L<sup>-1</sup>) *via* injection through the septum and was not automatically titrated later. Samples for OD<sub>578</sub> were harvested before and directly after inoculation and at regular intervals during culture growth. After inoculation, feeds of sodium acetate (0.61 mol L<sup>-1</sup>) and Na<sub>2</sub>S·9H<sub>2</sub>O (0.5 mol L<sup>-1</sup>) were supplemented at rates of 0.5 mL h<sup>-1</sup> and 0.1 mL h<sup>-1</sup>, respectively, and were manually increased upon stable growth. Biomass harvesting was carried out by connecting a needle to the silicon tubing of the sampling pipe and punctuating the butyl rubber of an empty anaerobic SCB with a negative pressure. Biomass from the reactor vessel was directed through the sampling silicon tubing and the needle into the SCB bottle, due to the negative pressure. The collected biomass was then handled in the anaerobic glove box for various purposes: calculations, inoculum preparation, pelleting for storage.

Inoculum preparation for transfer from closed batch to fed-batch cultures was a central subject of this study and various procedures were tested and are discussed later. Here, only the established reproducible methods are described. Biomass (400 mL) from both exponential and stationary phase of SCB or 1.5 L reactor cultures was concentrated by centrifuging at between 2,500 and 4,000 g, mostly at 3,000 g for 15 min at room temperature (RT) using 750 mL bottles and a LH 4000 swing-out rotor (75006475) of a Heraeus 4KR multifuge (75004461, Thermo Fisher Scientific, Waltham, MA, United States). Pelleted biomass from 400 mL starter cultures was then suspended in 30 mL of fresh 141 medium without supplemented acetate and collected into a 50 mL syringe described above and finally injected into reactors.

### 1.5 L reactor cultures agitation ramps and experimental groups

Bioreactor cultures of *M. maripaludis* were subjected to four distinct agitation ramp profiles: “conservative” and “progressive” variations of both stepwise and continuous increase of rpm. The continuous approaches were defined by a constant increase of rpm starting from the inoculation timepoint and differed in their acceleration rate: the conservative and progressive variations reached 600/1,200 rpm after 72 h and 1,200/1,600 rpm after 108 h, respectively. In contrast, the stepwise ramp profiles additionally introduced short steady states when the agitation was maintained at a constant rate. The conservative variation was maintained at 100 rpm 18 h post inoculation and reached 1,200 rpm after 69 h, whereas the progressive was set at 100 only for 6 h and reached the final steady state of 1,500 rpm after 74 h. Additional variations of the above-mentioned ramps have been tested but are not reported here due to lacking positive impact on culture growth.

To organize experiments within this study, a three-digit ID (x.y.z) was assigned to each bioreactor replicate. The digit x defines the phase, which describes bioreactor experiments, starting from an “adaptation” round (first inoculation from SCB into 1.5 L

reactor cultures), going through further transfer from stagnating reactor cultures into new reactor cultures until final biomass harvesting. The second digit y describes the consecutive bioreactor run from the beginning of bioreactor experiments within this study and the third digit describes the reactor replicate number on the Eppendorf Bioblock.

## 22 L bioreactor setup

*Methanococcus maripaludis* was cultivated in a customized 22 L Biostat® C15-3 reactor system (bbi-biotech GmbH, Sautorius Group, Berlin, Germany) with a working volume of 15 L (reactor culture). Rushton turbines were installed at 25, 50 and 80 cm from the bottom of the central agitation shaft. Temperature was constantly maintained at 37°C *via* thermometer and cooling water was supplied to the off-gas condenser. A sensor for pH (104054479, Mettler Toledo, Columbus, OH, United States) was connected to the control unit, and a sensor for redox potential (59904198, Mettler Toledo, Columbus, OH, United States) was operated externally by a multi-parameter transmitter (M300, Mettler Toledo, Columbus, OH, United States). Feed solutions of sodium acetate (0.61 mol L<sup>-1</sup>) and Na<sub>2</sub>S·9H<sub>2</sub>O (0.5 mol L<sup>-1</sup>) were prepared in SCB, made and maintained anaerobic by connecting them to gas bags filled with a gas mix of H<sub>2</sub>/CO<sub>2</sub> (4:1). The solutions were supplemented to the reactor vessels through a PTFE tubing (0.8 mm) by external pumps (0106141DA0, Watson Marlow Pumps, Falmouth, Cornwall, United Kingdom). Gas flow rate was maintained at 0.3 vvm, as both CO<sub>2</sub> and H<sub>2</sub> were managed externally *via* mass flow controllers SmartTrak®. The two distinct gas circuits were merged by a three-way junction into a single tubing which directed the gas mix of H<sub>2</sub>/CO<sub>2</sub> (4:1) through a filter into the inflow sparger of the bioreactor vessels. For sampling of cultures, a silicone tubing attached to the sampling valve SV-25 was used.

## 15 L reactor cultures: Cultivation and analysis

First, pH and redox probes were calibrated, as described above. Probes were plugged into their ports and the vessel was filled with 14.490 L of uncomplemented 141 medium and a sterilization cycle was carried out. Additionally, a steam generator Veit 2365/2 (Veit GmbH, Landsberg am Lech, Germany) was used for sterilization of sampling and harvesting valves and of the double mechanical seal. Temperature was set at 37°C, stirring at 600 rpm and the media was made anaerobic at 0.3 vvm with a flow rate of 20 sL h<sup>-1</sup> H<sub>2</sub> and 5 sL h<sup>-1</sup> CO<sub>2</sub> until pH and redox values remained stable (around 15–20 min). The medium was complemented with 300 mL of sodium acetate (0.61 mol L<sup>-1</sup>) and with 60 mL of Na<sub>2</sub>S·9H<sub>2</sub>O (0.5 mol L<sup>-1</sup>) *via* injection through a silicone rubber septum. Finally, as a last preparation step before inoculation, the pH was adjusted to 7.00 (± 0.05) with NaOH (10 mol L<sup>-1</sup>) *via* injection through the septum and was not automatically titrated later. Biomass (3×400 mL) from stationary phase of 1.5 L reactor cultures was centrifuged at 3,000 g for 15 min at room temperature (RT) using 750 mL bottles and a LH

4000 swing-out rotor (75006475) of a Heraeus 4KR multifuge (75004461, Thermo Fisher Scientific, Waltham, MA, United States). Pelleted biomass was then suspended in 30 mL of fresh uncomplemented 141 medium and collected into 50 mL syringes (3×50 mL) described above and finally injected into reactors. Samples for OD<sub>578</sub> were harvested before and directly after inoculation and at regular intervals during culture growth. After inoculation, feeds of sodium acetate (0.61 mol L<sup>-1</sup>) and Na<sub>2</sub>S·9H<sub>2</sub>O (0.5 mol L<sup>-1</sup>) were supplemented at rates 5 mL h<sup>-1</sup> and 1.2 mL h<sup>-1</sup>, respectively, and were manually increased upon stable growth. Biomass harvesting was carried out *via* the harvest and drain valve.

## Best pipeline

The best pipeline combined the most successful experimental groups from each cultivation mode for a continuous scale-up of *M. maripaludis* cultivations by transfers of actively growing culture. Unlike the optimization within each cultivation mode where the inoculum was generated from a stagnating culture, for the complete pipeline inoculum was prepared from cultures in their exponential phase. The only exception was the transfer from a 1.5 L reactor culture into the 15 L reactor cultures, where the inoculum was also in stationary phase.

## Calculations

Formula 1 utilizes a linear model (Taubner et al., 2018; Maurerhofer et al., 2021) for calculating the specific growth rate ( $\mu_L$ ) of *M. maripaludis* in closed batch mode, since exponential growth was only documented in 1.5 L reactor cultures, where an exponential formulation ( $\mu$ ) was applied for fed batch experiments (Formula 2). Subsequently, linear and exponential generation times (GT<sub>L</sub>/GT) were calculated from the linear  $\mu_L$  and exponential  $\mu$ , according to Formulas 3 and 4, respectively. Furthermore, substrate (H<sub>2</sub>/CO<sub>2</sub>) consumption was determined *via* pressure measurements of SB and SCB (Taubner and Rittmann, 2016).

$$\mu_L = \frac{OD_{578}(X)}{OD_{578}(X-1) \Delta t} \quad (1)$$

$$\mu = \frac{\ln \frac{OD_{578}(X)}{OD_{578}(X-1)}}{\Delta t} \quad (2)$$

$$GT_L = \frac{2}{\mu_L} \quad (3)$$

$$GT = \frac{\ln(2)}{\mu} \quad (4)$$

## Results

Within this study *M. maripaludis* was cultivated for 4,000 h in 0.05 L serum and 0.4 L SCB cultures, for 3,000 h in 1.5 L reactor cultures and for the first time in a volume of 15 L in a stainless-steel reactor system. Here, an extensive comparison of (linear and exponential)  $\mu$ , GT and substrate consumption for various agitation and feeding techniques in closed batch mode is presented. Furthermore, reproducible transfer and optimized biomass generation in a fed-batch reactor system is discussed in detail and applied into scale-up pipelines.

### 0.05 L SB cultures

SB were subjected to agitation by shaking or by stirring with a magnetic stir bar. Shaking at 100 rpm (100/sha, Figure 1) resulted in the lowest growth (Figure 1A) and substrate consumption (Figure 1B) from all tested groups. Transferring this culture further (100/sha.2) and cultivation under the same conditions showed adaptation and improved GT<sub>L</sub> (shaker.2, Table 1). Agitating at 100 rpm by stirring (100/str) was more efficient than shaking at the same speed. Stirring at 500 rpm (500/str) displayed a similar growth to adapted 100/sha.2 cultures but reached the highest substrate consumption (Figure 1B) of all tested groups. The best growth in SB was observed upon agitation at 500 rpm by stirring and feeding two times a day (500/str/2x) where the highest maximum OD<sub>578</sub> of 1.29 (Table 1) was reached around 6 days earlier than all other experimental groups.

### 0.4 L SCB cultures

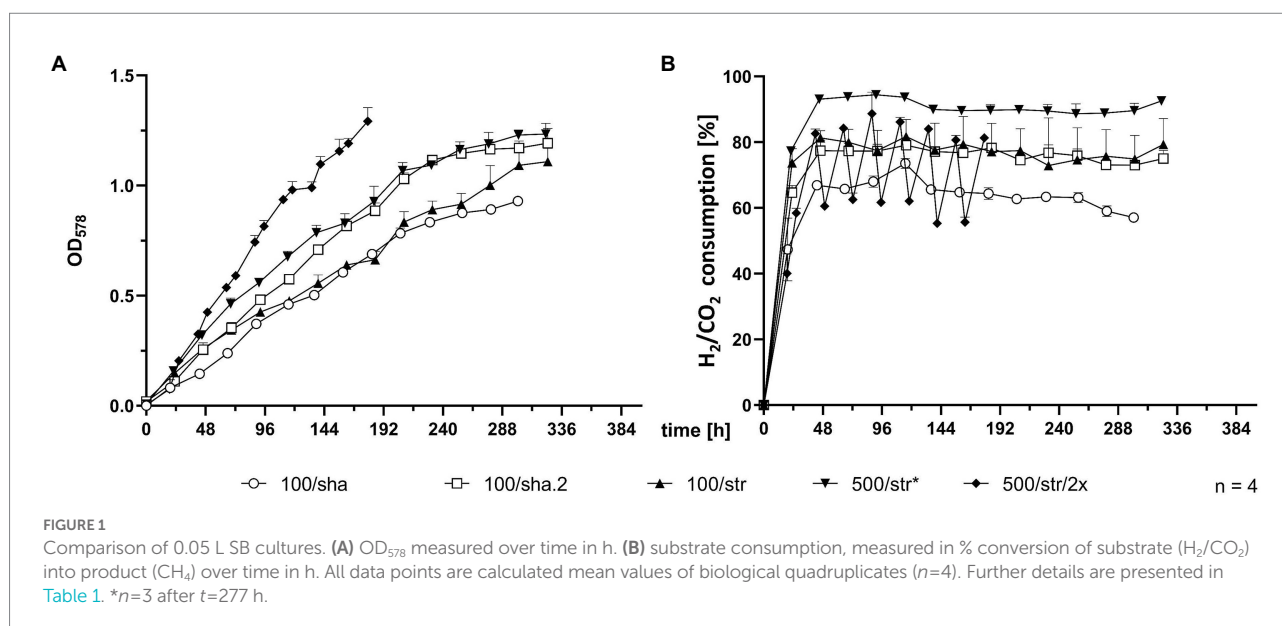
SCB were agitated either by stirring with a magnetic stir bar or by shaking. Stirred cultures generally delivered the slowest

growth curves, as the experimental groups stirred at 100 (100/str), 500 (500/str) and 1,100 rpm (1,100/str) remained at the bottom of the graph for OD<sub>578</sub> comparison (Figure 2A). However, cultures which were stirred at 800 rpm (800/str) showed strong improvement of growth and were the second-best experimental group. They also delivered their maximum OD<sub>578</sub> in the shortest measured time of 158 h (Table 1). Additionally, stirring at maximum possible 1,400 rpm was tested. Quadruplicate cultures reached a mean maximum OD<sub>578</sub> of 0.169 after 96 h (Table 1). Possible explanations for the inefficient growth at higher agitation intensities are discussed later.

Shaken cultures at 100 (100/sha) and 180 (180/sha) rpm outperformed most of the stirred groups, as the 100/sha group reached the highest OD<sub>578</sub>, and the 180/sha group delivered the lowest GT<sub>L</sub> of 3.06 h (Table 1). Subjecting 100/sha cultures to double feeding (100/sha/2x) substantially improved growth and reduced the time for reaching maximum culture growth by a day and decreased the GT<sub>L</sub> more than double (Table 1). The substrate consumption of SCB (Figure 2B) displayed very heterogenous patterns (Figure 2B) and no clear separation between stirred and shaken cultures was observed. Groups 100/str and 100/sha/2x clustered below 50%, 100/sha and 500/str around 60% and 180/sha and 800/str a bit below 90%. Samples from the group 1,100/str showed varying low substrate consumption during the first half of culture growth but reached reproducibly high values during late exponential growth.

### 1.5 L reactor cultures

Phase 1 tested various transfer procedures for inoculation of *M. maripaludis* from closed batch cultures into bioreactor vessels. Initial unsuccessful attempts relied on direct injection of 50 mL culture inoculant from SB (at first unwashed, later also spun down and resuspended in fresh 141 medium), which was





often grown to low optical densities at low  $H_2/CO_2$  pressures, due to the wrong assumption that headspace pressure was an essential adaptation factor. A first successful growth was achieved with the 9<sup>th</sup> attempt (Figure 3E), where stirring was adjusted manually in response to culture growth. The biomass from this single reactor was continuously transferred in stationary phase of growth and 4 further successful experiments (Figure 3, blue graphs in A–D) were carried out for defining 4

TABLE 1 Comparison of culture growth parameters from closed batch experiments.\*

Closed batch	Agitation		OD <sub>578</sub>		$\mu_L$ [h <sup>-1</sup> ]	GT <sub>L</sub> [h]
	Method	[rpm]	Max	time [h]		
SB	Shaker	100	0.9292	301	0.07	26.93
	Shaker.2	100	1.1929	325	0.25	7.87
	Stirrer	100	1.1089	325	0.29	6.8
	Stirrer	500	1.2339	323	0.95	2.11
	Stirrer/2x	500	1.2924	179	0.94	2.12
SCB	Shaker	100	1.0819	325	0.21	9.65
	Shaker	180	1.0530	209	0.65	3.06
	Shaker/2x	100	1.0561	291	0.48	4.19
	Stirrer	100	0.4766	326	0.12	16.63
	Stirrer	500	0.9322	321	0.27	7.37
	Stirrer	800	0.9318	158	0.24	8.48
	Stirrer	1,100	0.6804	209	0.15	13.74
	Stirrer	1,400	0.1691	96	–	–

\*Closed batch SB and SCB experimental groups are listed with their respective agitation method and intensity (rpm). Maximum (max) measured OD<sub>578</sub> and the respective needed time are compared. Highest recorded  $\mu_L$  and GT<sub>L</sub> were calculated according to Formulas 1 and 3. shaker.2, an experimental group, subjected to the same cultivation conditions after inoculation transfer to a new culture; /2x, double  $H_2/CO_2$  feeding timepoints.

distinct agitation profiles – conservative and progressive variations of continuous and stepwise increase of rpm. At the end of phase 1 several unsuccessful attempts for revival of stored reactor biomass were carried out (data not presented).

Phase 2 adopted a gentler centrifugation at 4,000 g (Table 2) during concentration of biomass upon culture transfer, which resulted in improved survival during the adaptation round, where 3 out of 4 replicates (Figure 3E) exited the lag phase around 48 h earlier than during phase 1. Additionally, those replicates were subjected to a pre-programmed agitation ramp profile (red dotted line, Figure 3E). The biomass was then further transferred in stationary phase for reproducing the stepwise ramp profiles (Figures 3C,D). At this stage the stepwise conservative ramp profile was recognized as the most promising, as all 3 replicates from phases 1 and 2 aligned perfectly and delivered high OD<sub>578</sub> peaks over 2.5 (Figure 3D).

During phase 3 for the first time a SCB inoculum in exponential growth (Table 2) was used during the adaptation round. Four reactors were subjected to the agitation ramp from phase 2 (Figure 3E) and grew perfectly aligned almost reaching a true exponential geometry of growth curves and almost matching the best runs from phase 2. This run was in fact the last stage of the proposed best pipeline from this study discussed below. Additionally, *M. maripaludis* was transferred as a stationary inoculum to further reproduce the continuous agitation ramps (Figures 3A,B), which in both cases sustained better growth than the single replicates from phase 1.

The main goal of phases 4–7 was to optimize growth of *M. maripaludis* upon agitation under the stepwise conservative ramp. Adaptation rounds were carried out unsupervised over the weekend (not shown here) according to the set-up of the adaptation round from phase 3 (Figure 3E). The resulting biomass was used to inoculate single runs ( $N=1$ ), with either 1 or 2

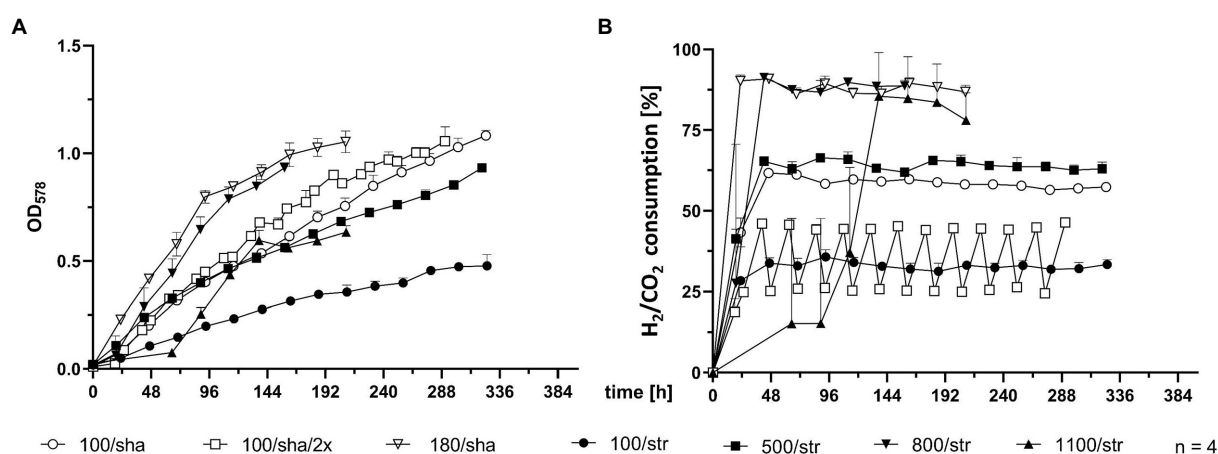


FIGURE 2 Comparison of 0.4 L SCB cultures. (A) OD<sub>578</sub> measured over time in h. (B) substrate consumption, measured in % conversion of substrate ( $H_2/CO_2$ ) into product ( $CH_4$ ) over time in h. All data points are calculated mean values of biological quadruplicates ( $n=4$ ). Further details are presented in Table 1.

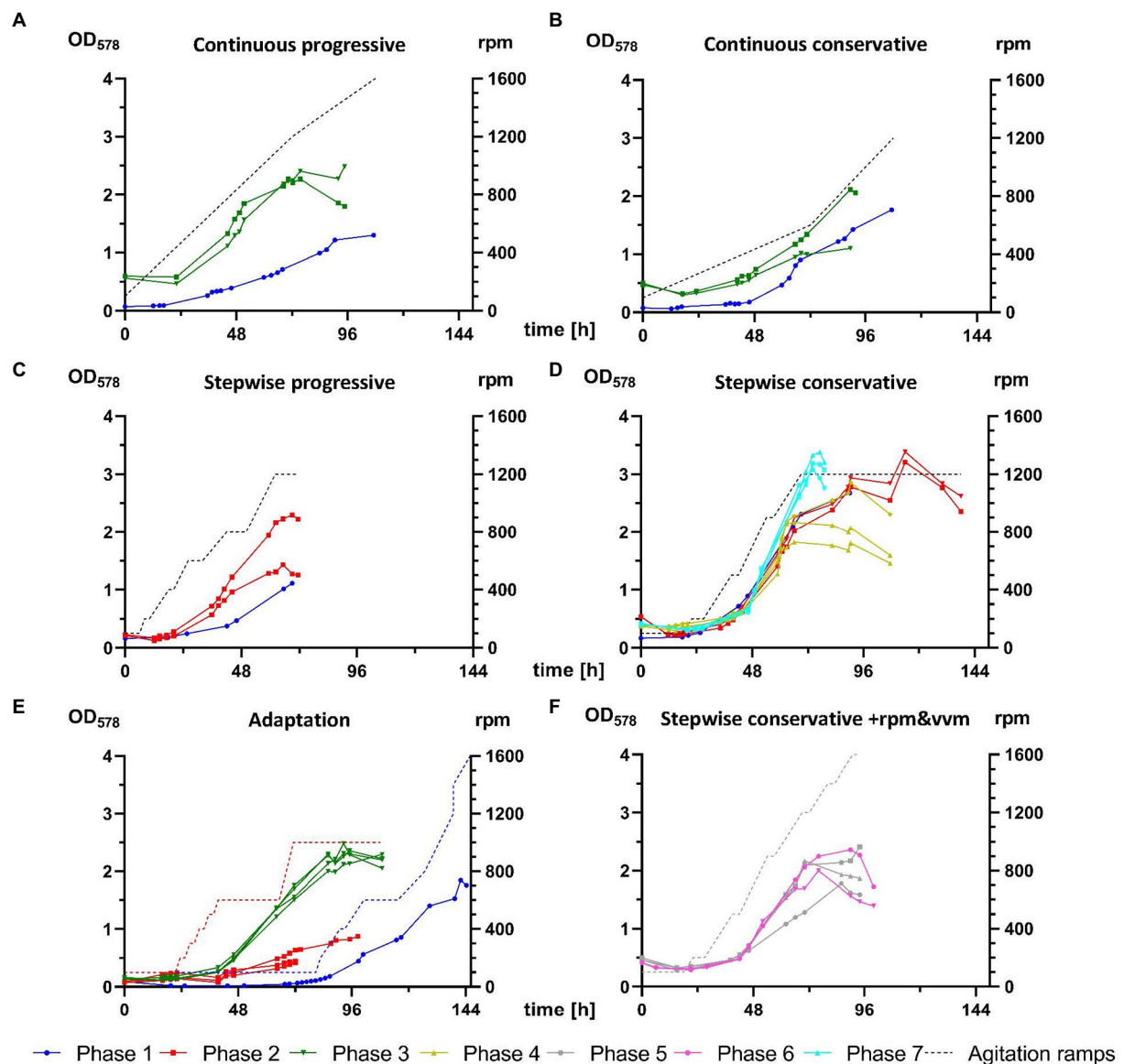


FIGURE 3

Comparison of *M. maripaludis* growth in 1.5 L reactor cultures. OD<sub>578</sub> (left Y-axis) measured over time in h for replicates subjected to the following agitation profiles (rpm on right Y-axis): (A) continuous progressive (Phases 1 and 3), (B) continuous conservative (Phases 1 and 3), (C) stepwise progressive (Phases 1 and 2), (D) stepwise conservative (Phases 1, 2, 4, and 7), (E) growth of reactors cultures from Phases 1–3 subjected to adaptation rounds, (F) optimization of stepwise conservative ramps by increase of agitation and supply of gaseous substrate (+rpm and vvm) or by increase of agitation and supply of gaseous substrate and decrease of OD<sub>578</sub> of inoculum (+rpm and vvm-OD) from Phases 5 and 6, respectively. Further details are presented in Table 2.

biological replicates ( $n \leq 2$ ), which reproduced the stepwise conservative ramp. Phase 4 had an identical setup to the respective experimental groups from phase 1 and 2. During phase 5 the agitation ramp was increased to maximum levels of 1,600 rpm and H<sub>2</sub>/CO<sub>2</sub> mix was supplied at increasing rates from 0.3 to 2.4 vvm. Phase 6 had the same experimental setup and additionally an inoculum from exponential phase (OD<sub>578</sub> = 1.3) was used. However, phases 5 and 6 (Figure 3F) were not able to sustain a better growth of *M. maripaludis* than during phases 1, 2, and 4.

Finally, the best run in this study was generated during phase 7 (Figure 3D) when the setup of phases 1, 2, and 4 was reproduced in combination with an inoculum from exponential growth, which resulted in the highest recorded OD<sub>578</sub> value for *M. maripaludis* of 3.38 (Table 3). This value was also reached under the same cultivation conditions during phase 1 (Figure 3D) but around 48 h later. Under the stepwise conservative agitation ramps (reactor IDs 2.21.3/2.21.4, 4.27.2/4.27.3/4.27.4) also the highest recorded values for  $\mu$  and GT of  $\sim 0.16 \text{ h}^{-1}$  and  $\sim 4.3 \text{ h}$ , respectively, were measured (Table 3).

TABLE 2 Distinct experimental groups of 1.5 L reactor cultures (Figure 3). \*\*

Phase	Runs [N]	n	Inoculum		Main goal	Successful/total	
			OD <sub>578</sub>	g		Runs	Time [h]
1	5	5	Stat.	10,000	Define distinct agitation ramps	6/18	612/1552
2	3	7	Stat.	4,000	Reproduce ramps	3/4	308/399
3	3	8	Exp.*	3,000	Reproduce ramps and test pipeline	3/3	303/303
4	1	3	Late exp. (2.1)		Reproduce best ramp	2/2	107/107
5	1	3	Late exp. (1.8)		Reproduce best ramp + rpm and vvm	2/2	94/94
6	1	2	Exp. (1.3)		Reproduce best ramp + rpm and vvm - OD	2/2	100/100
7	1	3	Exp. (1.5)		Reproduce best ramp -OD	2/2	79/79

\*\*Overview of experimental setup of 1.5 L reactor cultures from Figures 3A–F: Phases; number of runs (N); bioreactor replicates (n); inoculum stage of growth (stat., stationary; exp., exponential), optical density (OD<sub>578</sub>), centrifuge forces (g); main goals of each phase; number of successful/total runs and cultivation time in h. +rpm and vvm: increase of agitation and supply of gaseous substrate; +rpm and vvm-OD: increase of agitation and supply of gaseous substrate and decrease of OD<sub>578</sub> of inoculum; \*exponential only in Figure 3E, not in Figures 3A,B.

## Scale-up pipeline

*Methanococcus maripaludis* was inoculated in 0.05 L SB cultures, transferred to 0.4 L SCB cultures and finally into 1.5 L reactor cultures (Figure 4). Each stage of the scale-up pipeline utilized some of the best experimental groups, which were cultivated until reaching exponential phase and then further transferred. SB cultures were agitated by stirring at 500 rpm and were supplemented with gaseous substrate (H<sub>2</sub>/CO<sub>2</sub>) once a day at 2 bars. Quadruplicates reached a mean OD<sub>578</sub> of 0.6524 after 90 h and were transferred into 0.4 L cultures. The SCB were shaken at 180 rpm and fed twice a day at 1 bar with H<sub>2</sub>/CO<sub>2</sub>. After 69 h (159 h timepoint) they reached OD<sub>578</sub> of 0.6 but were transferred to 1.5 L cultures after 78 h (168 h timepoint). The growth curve of quadruplicate bioreactor cultures represents the adaptation round of Phase 3 (Figure 3E) and was among the most successful runs at that stage of this study. Exponential growth at OD<sub>578</sub> of 0.6 was reached after around 48 h (216 h timepoint) and a peak OD<sub>578</sub> of 2.3 was reached after 92 h (260 h timepoint).

## 15 L reactor culture

For the first time *M. maripaludis* was cultivated in a working volume of 15 L in a 22 L stainless steel bioreactor (Figure 5B). For this scale-up experiment, first a 0.4 L pre-culture was prepared in SCB, which was agitated by stirring at 800 rpm and fed twice a day with 1 bar H<sub>2</sub>/CO<sub>2</sub> (Figure 5). OD<sub>578</sub> of 0.6 was reached after 49 h (Figure 5A). After biomass harvesting and concentration, a single 1.5 L reactor culture was inoculated and subjected to adaptation round settings. This culture reached exponential growth at OD<sub>578</sub> of 0.6 after around 44 h (93 h timepoint), peak OD<sub>578</sub> of 2.4 after 64 h (113 h timepoint) and was further cultivated until stationary phase. After 75 h (124 h timepoint) at an OD<sub>578</sub> of 2.1, *M. maripaludis* was harvested and inoculated into a 15 L reactor culture. There, exponential growth with an OD<sub>578</sub> of 0.6 was reached after around 25 h (149 h timepoint), maximum growth was recorded at OD<sub>578</sub> of 1.7 after 61 h (185 h timepoint) and the

complete pipeline was completed after 188 h at OD<sub>578</sub> of 1.66. The 15 L reactor culture produced  $5.57 \pm 0.39$  g L<sup>-1</sup> wet biomass.

## Discussion and conclusion

Established large scale processes within the microbial biotechnology sector, which are essential for medicine, nutrition and research, are dominated by heterotrophic bacterial and eukaryotic cell factories, which have high carbon footprints, electricity demands and impact on valuable resources (Patel et al., 2020). In contrast, wild type and bioengineered archaea have been strongly neglected and up to date only halophiles have been used for the biosynthesis of commercial products (Pfeifer et al., 2021). However, the demand for high value bioproducts and the urgent need to stop the tremendous exploitation and destruction of natural resources require an immediate biotransformation of the global industry. Harvesting the metabolic potential of genetically tractable autotrophic, hydrogenotrophic, and methanogenic archaea (Lyu and Whitman, 2019) might be a good start.

## Relevance of methanogenic archaea for bioprocess development

Among the archaea, methanogens continue receiving attention due to their biotechnological potential for the production of CH<sub>4</sub> and other valuable bioproducts (Pfeifer et al., 2021). The documented physiological features of some methanogens, such as high  $\mu$  (Rittmann et al., 2015; Azim et al., 2017), tolerance to high gas and hydrostatic pressures (ver Eecke et al., 2013; Taubner et al., 2018; Pappenreiter et al., 2019) and resistance to shear forces (Seifert et al., 2014; Azim et al., 2017) clearly make them attractive candidates for cell factories with biotechnological applications. For the development of CH<sub>4</sub> production bioprocesses from H<sub>2</sub>/CO<sub>2</sub>, volumetric or specific CH<sub>4</sub> productivity and conversion efficiency have been defined as crucial parameters (Mauerhofer et al., 2018; Rittmann et al., 2018).

TABLE 3 Comparison of growth parameters from experiments with 1.5 L reactor cultures.\*\*\*

Replicate ID [Phase.run. replicate]	Ramp	OD <sub>578</sub>		$\mu$ [h <sup>-1</sup> ]	GT [h]	Wet biomass [g L <sup>-1</sup> ]
		Max	Time [h]			
1.9.3	Ad/man	1.8452	142	0.11	6.08	5.17
1.10.2	Cont-cons	1.7652	107	0.12	5.78	7.72
1.10.4	Cont-prog	1.3007		0.10	6.72	4.28
1.12.1	Step-cons	2.6770	90	0.06	11.24	–
1.12.2	Step-prog	1.1111	69	0.06	12.58	–
2.19.2	Ad/step-man	0.4430	72	0.06	11.43	–
2.19.3		0.4180		0.04	16.82	–
2.19.4		0.8757	99	0.10	7.04	–
2.20.1	Step-prog	1.4310	65	0.09	7.02	–
2.20.2		2.2980	69	0.08	8.86	–
2.21.3	Step-cons	3.3884	114	0.06	11.20	3.52
2.21.4		3.2096		0.09	7.86	–
3.23.1	Ad/step-man	2.2960	116	0.10	7.10	–
3.23.2		2.4864	109	0.08	8.78	4.09
3.23.3		2.3598		0.08	8.62	5.96
3.23.4		2.3122		0.10	7.12	6.27
3.24.2	Cont-cons	2.1163	90	0.06	12.58	–
3.24.4		1.1018		0.05	13.82	–
3.25.1	Cont-prog	2.2690	76	0.06	12.36	3.39
3.25.3		2.4040		0.07	9.84	5.39
4.27.2	Step-cons	2.1700	66	0.11	6.34	–
4.27.3		2.8588	91	0.13	5.53	–
4.27.4		1.8230	66	0.16	4.30	–
5.29.1	Step-cons +rpm and vvm	2.1670	70	0.07	10.20	–
5.29.2		2.4113	94	0.06	12.54	–
5.29.4		1.7824	86	0.04	17.78	–
6.31.1	Step-cons +rpm and vvm -OD	2.0025	76	0.09	8.02	–
6.31.2		2.3625	90	0.09	7.30	–
7.33.1	Step-cons. -OD	3.086	74	0.16	4.44	–
7.33.2		3.1852	74	0.14	4.91	–
7.33.3		3.3818	77	0.14	4.89	–

\*\*\*Individual reactor replicates are listed with their respective ID ([phase.run.replicate] numbers) and tested agitation ramp (ad: adaptation, man; manual, cont-cons: continuous conservative, cont-prog: continuous progressive, step-cons: stepwise conservative, step-prog: stepwise progressive), +rpm and vvm: increase of agitation and gaseous substrate supply, -OD: decrease of OD of inoculum. For each run a highest recorded (max) OD<sub>578</sub> and the corresponding time are listed. Specific growth rate ( $\mu$ ) and generation time (GT) were calculated according to Formulas 2 and 4 and compared. If biomass was harvested, the measured weight in grams (g) of wet pellets is presented in the last column on the right. IDs and noteworthy values are matching the color code of respective growth curves from Figure 3.

However, not all methanogens, that are available as pure cultures, can easily be grown in bioreactors. This and previous studies on the scale-up of methanogens (Mauerhofer et al., 2018) have shown that bioprocess development should focus on examining the type of cultivation method (e.g., closed batch, fed-batch, and continuous culture) and the type of bioreactor (e.g., stirred tank reactor, bubble column, and trickle-bed) that are envisioned for the final production process. Furthermore, identification and optimization of the scaling criteria, the medium, the feed source, quality and quantity, the inoculum storage and preparation, and the type of downstream processing operation are of major importance. For instance, some methanogens grow in inexpensive minimal medium (Taubner and Rittmann, 2016;

Mauerhofer et al., 2018) and can be cultivated in standard stirred tank bioreactors (Seifert et al., 2014; Azim et al., 2017; Rittmann et al., 2018).

Methanogens that have been applied for scale-up of CH<sub>4</sub> or biomass production in bioreactors are *Methanothermobacter marburgensis* and *M. maripaludis*, respectively. For *M. marburgensis*, successful scale-up to B-TRL  $\geq 5$  (Pfeifer et al., 2021) and growth and CH<sub>4</sub> production in fed-batch, as well as in continuous culture, have been thoroughly examined (Seifert et al., 2014; Azim et al., 2017; Rittmann et al., 2018). However, a pipeline for rapidly producing high biomass concentrations of *M. maripaludis* in fed-batch cultivation mode has up to now been missing.

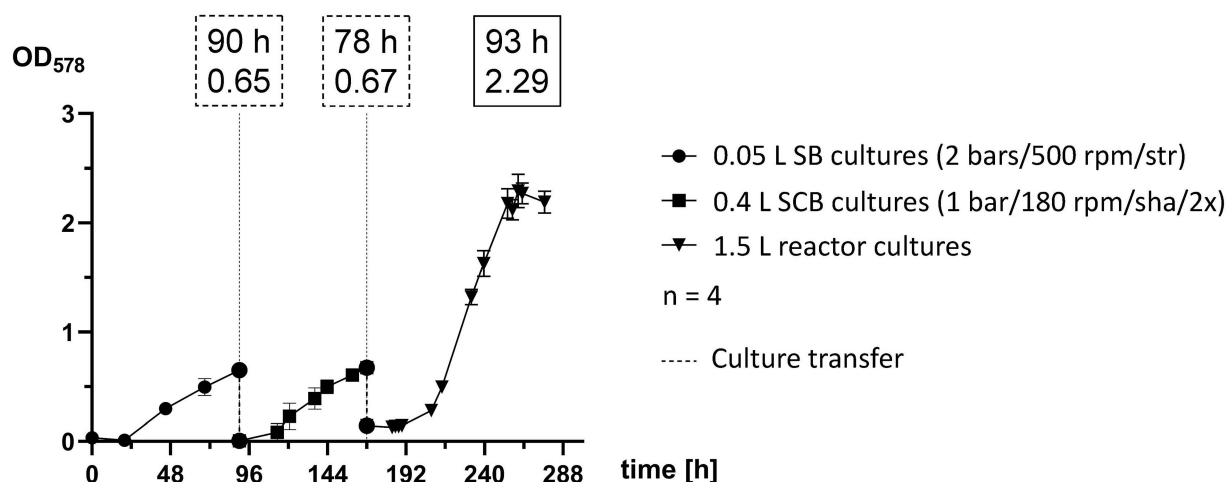
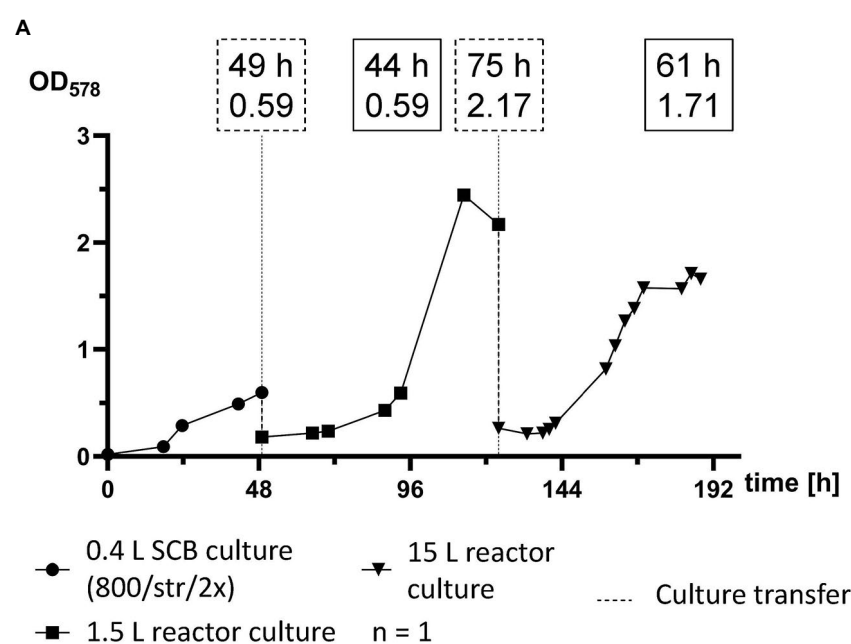


FIGURE 4

Scale-up pipeline of *M. maripaludis*. OD<sub>578</sub> (left Y axis) measured over time in h for replicates subjected to the following cultivation methods: 0.05 L SB cultures cultivated at 2 bars H<sub>2</sub>/CO<sub>2</sub> and agitated by stirring at 500 rpm (0–90 h); SCB cultivated at 1 bar H<sub>2</sub>/CO<sub>2</sub> twice (2x) a day and agitated by shaking at 180 rpm (90–168 h); 1.5 L reactor cultures subjected to adaptation round setup (168–277 h). Dotted line for culture transfer designates harvesting and inoculation procedures between the distinct groups. All data points are calculated mean values of biological quadruplicates (n=4). Dotted text boxes designate time (h) and OD of cultures during transfers. The solid text box designates time (h) of peak OD.



B



FIGURE 5

Scale-up of *M. maripaludis* toward a 15 L reactor culture. (A) OD<sub>578</sub> (left Y axis) measured over time in h for a single replicate subjected to the following cultivation methods: SCB cultivated at 1 bar H<sub>2</sub>/CO<sub>2</sub> twice (2x) a day and agitated by stirring at 800 rpm (0–49 h); 1.5 L reactor culture subjected to adaptation round setup (49–124 h); a 15 L reactor culture (124–188 h). Dotted line for culture transfer designates harvesting and inoculation procedures between the distinct groups. Dotted text boxes designate time (h) and OD of cultures during transfers. Solid text boxes designate time (h) and OD of crucial stages of culture growth. (B) Harvested biomass with the used Sautorius Biostat C 15–3.

## Expanding opportunities for the cultivation of *Methanococcus maripaludis*

This study provides a comprehensive comparison of various cultivation techniques for *M. maripaludis*. By the optimization of

established anaerobic methods, an extensive laboratory-scale manual for experimental approach toward rapid biomass generation has been developed. Everyday cultivation of *M. maripaludis* has mainly relied on closed batch bottles for decades, as the highest culture volume has increased from 0.2 L to 0.23 L for 36 years (Balch et al., 1979; Goyal et al., 2015). Here,



regular growth in 0.4 L SCB cultures supplemented by gaseous  $H_2/CO_2$  substrates is being reported, which is equally accessible, reliable and reproducible. Combined with an alternative agitation method by a magnetic stirrer, SCB cultures allow faster and cost-efficient biomass generation which is sufficient for molecular analysis without the need for sophisticated cultivation equipment. This approach was inspired by flexible closed batch systems, developed for formate-utilizing methanogens in culture volumes of 1.5 L (Long et al., 2017). However, here the cultivation of *M. maripaludis* in liter ranges relies on gaseous  $H_2/CO_2$  substrate supplementation and more sophisticated fed-batch equipment.

In chemostat vessels, *M. maripaludis* has been grown in volumes of 1.3 L reaching peak  $OD_{660}$  of around 1.7 and the highest reported  $\mu$  of  $0.24\text{ h}^{-1}$  (Haydock et al., 2004), which have almost been reproduced recently (Müller et al., 2021). This system has been established for studies of nutrient limitations (Hendrickson et al., 2007, 2008; Costa et al., 2013), where distinct *M. maripaludis* strains (S2, S52) have been cultivated at low optical density in various media (mineral McN, with or without acetate supplementation, but also defined complex McCa and McCas) and their OD has been measured at distinct wavelengths (600 or 660), hence complicating straightforward comparison, due to the Lambert–Beer’s law. The application of the chemostat cultivation procedure in a 3 L reactor with 2 L cultures of strain S2, grown in modified rich McCas medium, supplemented with casamino acids, has delivered highest reported  $OD_{600}$  of around 2.7 and doubling times of 3 to 4 h (Walters and Chong, 2017). Here, doubling time of 4 to 5 h and the highest  $OD_{578}$  of 3.4 have been reached with strain S0001, grown on gaseous  $H_2/CO_2$  substrate in reduced 141 medium, supplemented with acetate. Additionally, the first ever reported cultivation of *M. maripaludis* in a 22 L stainless steel bioreactor in 15 L working volume introduces novel opportunities for applying wild type and recombinant methanogenic cell factories in biotechnological advances of industry relevant scales.

## 0.05 L SB cultures

At a laboratory scale, closed batch mode of cultivation is usually the everyday method of choice, as it is robust, easy to handle and allows the simultaneous analysis of distinct experimental groups. *M. maripaludis* was therefore cultivated only in SB in the authors’ group before the launch of this study. Nevertheless, the generated biomass is rarely sufficient for analytical measurements of physiological processes or for scaling up toward bioprocess development. Here, 0.05 L SB cultures of *M. maripaludis* were utilized as a stable platform for testing and comparing different agitation techniques. Instead of two directional shaking in a water bath, SB were either shaken on an orbital shaker or stirred by a magnetic stir in air incubators and in climate chambers. Generally, shaking is the more accessible method, since occupying 4 (or 5 with zero control) magnetic stirrer plates for prolonged period might be problematic. However,

considering the geometry of a surface area displacement during highest possible shaking intensities ( $\sim 180$  rpm, here tested only for SCB), this mode of cultivation might have reached the limit of efficiency for transfer of the carbon-containing gaseous phase into the liquid phase within the experiments, carried out in this study.

In contrast, agitating a magnetic stir bar by a digital stirrer plate allows better resolution (1 rpm) and wider range (0–1,400), hence allowing a further increase of vortex surface area to headspace gaseous substrate. Therefore, stirring became the more favorable method for agitation already prior to scaling up to 0.4 L SCB cultures. Interestingly, an adaptation to respective conditions was observed, since subjecting the 100/sha group to the same conditions (100/sha.2) resulted in improved growth, which outperformed 100/str and grouped with the 500/str samples (Figure 1). This might be explained by the positive impact of prolonged exposure to regular feeding, cultivation and sampling intervals. Stirred SB cultures of *M. maripaludis* (500/str/2 $\times$ ) delivered highest measured  $OD_{578}$  of 1.29 only after being subjected to double feeding timepoints per day (Table 1). However, it remains unclear, whether greater shaking (180 rpm) or stirring (800–900 rpm) would be more favorable for SB cultures of *M. maripaludis* in combination with double or more gassing intervals.

## 0.4 L SCB cultures

SCB cultures of *M. maripaludis* gradually became the most favorable closed batch technique for cultivation during the progress of this study, since they proved to be as reproducible as SB and additionally, they generated sufficient biomass for culture transfer to fed-batch reactors. Furthermore, reproducible revival of scaled-up cryogenic stocks proved to be efficient for inoculation of pre-cultures, which displayed growth already after 24 h upon cultivation at 150 rpm by shaking (data not shown). Still, SCB cultures have two disadvantages. While SB can be pressurized to up to 5 bar relative pressure (6 bar absolute), SCB can only withstand 1.5 bar relative (2.5 bar absolute) pressure. Therefore, further optimization of SCB cultures must include double or triple feeding timepoints or in the best case rely on automated pressure measurement and feeding system.

The second drawback concerns technical security issues. The weight of a single SCB culture is around 1 kg. Placing 4 (or 5 including a zero control) on a shaker at maximum agitation levels around 180 rpm might damage instruments and even personnel in case of unstable holder installation. Therefore, despite the fact that *M. maripaludis* grew best upon agitation at 180 rpm by shaking (Figure 2), during later stages of this study, stirring (at 500 and 800 rpm; Figures 4, 5) was the method of choice, as cultures stirred at 800 rpm performed just slightly worse than shaking at 180 rpm (Figure 2). Identical to SB cultures, increasing the feed to twice a day, improved the growth and reduced  $GT_L$  two times for SCB cultures shaken at 100 rpm (100/sha and 100/sha/2 $\times$ ; Table 1).

Subjecting *M. maripaludis* to stirring at 1,100 and 1,400 rpm led to strongly retarded growth. Nevertheless, extreme  $\mu$  under similar conditions might be possible in combination with pre-adaptation and continuous transfer to increasing agitations. In this context, it was intriguing to observe that the growth curve of SCB cultures, stirred at 1,100 rpm (1,100/str), could only match the growth efficiency of SCB stirred at 500 rpm (500/str) around 113 h post inoculation (Figure 2A) but in terms of substrate consumption (Figure 2B), 1,100/str replicates matched the results of the most successfully growing groups 180/sha and 800/str. Therefore, despite the need for preadaptation and the apparent lower rate of biomass generation of unadapted cultures, stirring at higher rpm obviously allows better transfer of gaseous substrate into the media and higher rate of methanogenesis by less dense cultures.

## 1.5 L reactor cultures

The optimization of closed batch conditions was mainly motivated by the need to generate sufficient biomass for inoculation into bioreactor vessels, since initial bioreactor inoculations unsuccessfully attempted to utilize 0.05 L SB culture biomass (not shown in results). Stirred 0.4 L SCB cultures were later established as the most promising pre-culture due to magnetic stir bars mimicking the mechanical pressure of the Rushton impellers in bioreactor vessels. However, inoculum from SCB cultures shaken at 150 rpm was also regularly grown successfully in bioreactor cultures during unsupervised adaptations rounds from phases 4–7 (data not shown).

During crucial stages of this project, softer harvesting procedure proved to be the most important aspect for reproducible growth in a fed-batch mode. In phase 1, inoculum harvesting was carried out at 10,000 g (Table 2), leading to prolonged lag phase and slow linear growth in all tested ramps (Figures 3A–E). Reducing the g force to 4,000 (phase 2) and further to 3,000 (from phase 3 on) and reproducing the experiments from phase 1, substantially improved culture growth, which is visible by the higher starting OD<sub>578</sub>, due to enhanced cell survival, and by improved growth curves and higher peak maxima (Figures 3A,B,D).

The growth of *M. maripaludis* in 1.5 L reactor cultures was further improved as an inoculum in exponential phase was used for the first time in the adaptation round of phase 3 (Figure 3E). The same impact was observed in the case of the most successful stepwise conservative ramp profile (Figure 3D), which was reproduced several times (phases 1, 2, 4, and 7) where the best growth was recorded during phase 7 when for the first time an exponential inoculum was used. However, subjecting biomass in late and early exponential phase of growth to alternative stepwise conservative ramp profiles during phases 5 and 6, respectively (Figure 3F), did not compensate the increase of rpm above 1,200 rpm. The increase of rpm to highest possible levels aims at better solubility of gaseous H<sub>2</sub>/CO<sub>2</sub> substrate into the liquid phase but obviously there is an upper limit for *M. maripaludis*, which is

supported by reports of its rather fragile cellular structure. In combination with SCB data, results of this study suggest a value around 900 rpm ( $\pm 100$ ). Nevertheless, the use of inoculum in exponential growth has the potential to improve culture performance of *M. maripaludis* upon exposure to continuous and stepwise progressive ramp profiles, as those conditions were only tested with an inoculum in stationary phase. The reason for that is, that all 1.5 L reactor culture experiments of this project were carried out on a single reactor unit with 4 replicate vessels, meaning that inoculum could be generated only after completion of the previous cultivation round.

Despite the fact that cultivation time for closed batch has been massively reduced and fed-batch cultures of *M. maripaludis* have surpassed highest reported OD<sub>578</sub> values, much can be further improved. Regarding a best agitation ramp profile for 1.5 L reactor cultures, it seems that a continuous progressive increase supports the quickest exit of the lag phase after 24 h and sustains exponential growth until 48 h, where the increase of rpm above 800 becomes too stressful for *M. maripaludis* and marks the beginning of the stationary phase (Figure 3A). Therefore, subjecting exponential inoculum to a continuous progressive ramp ending at 800–1,000 rpm might be more favorable than a stepwise conservative ramping. A second-generation batch culture, which has been adapted to higher agitations, might even withstand a transfer into a culture with a constant agitation at 600–800 or alternatively into a culture with starting agitation at 400–600 (for 24 h), followed by continuous increase (over 12–24 h) to 800–1,000 rpm.

## Scale-up pipelines

The proposed scale-up pipeline of *M. maripaludis* does not necessarily include the best performing experimental groups for each stage but rather a flexible combination of cultivation methods. As discussed earlier, agitation at great intensities ( $\geq 500$  rpm) in closed batch mode might require pre-adaptation for peak performance of *M. maripaludis*, which would be the case for applied projects, aiming at high productivity of an archaeal cell factory. On the other hand, biomass generation for fundamental studies can easily adopt the experimental setup, presented here (Figure 4). Depending on the availability of equipment, fellow researchers may recombine cultivation techniques in closed batch mode and agitation ramps upon prolonged continuous transfer in fed-batch mode.

Furthermore, the first ever reported 15 L reactor culture of *M. maripaludis* would support scaling up of biomethanation processes toward industry relevant dimensions. Next steps would require using an inoculum in exponential growth and comparison of distinct agitation ramp profiles.

In summary, this study provides a comprehensive manual of diverse techniques for the cultivation of the autotrophic, hydrogenotrophic methanogen *M. maripaludis*. The optimization of established methods and the development of novel strategies

can be also adapted for other autotrophic organisms. In terms of closed batch mode, increasing the number of feeding timepoints and testing agitation at moderate high intensities (800–1,000 rpm) would easily define conditions for peak performance. Single stage fed-batch cultivation of *M. maripaludis* would require additional experiments for defining best cultivation conditions and can be further advanced toward a continuous culture. Developing reproducible growth in a 15 L reactor culture would generally follow the experimental approach for 1.5 L reactor cultures by testing most favorable agitation ramp profiles and applying inoculum in exponential growth.

## Data availability statement

The raw data supporting the conclusions of this article will be made available by the authors, without undue reservation.

## Author contributions

HP and SK-MRR conceived and designed the study, and wrote the manuscript. HP, AR, LP, and DN performed the research. HP,

AR, and LP analyzed the data. HP, BR, and SK-MRR contributed new methods or models. All authors contributed to the article and approved the submitted version.

## Conflict of interest

AR, BR, and SK-MRR declare to have competing commercial and financial interests due to their employment in the Arkeon GmbH.

The remaining authors declare that the research was conducted in the absence of any commercial or financial relationships that could be construed as a potential conflict of interest.

## Publisher's note

All claims expressed in this article are solely those of the authors and do not necessarily represent those of their affiliated organizations, or those of the publisher, the editors and the reviewers. Any product that may be evaluated in this article, or claim that may be made by its manufacturer, is not guaranteed or endorsed by the publisher.

## Bibliography

- Azim, A., Annalisa, C. P., Kolar, P., Taubner, R. S., Fino, D., Saracco, G., et al. (2017). The physiology of trace elements in biological methane production. *Bioresour. Technol.* 241, 775–786. doi: 10.1016/j.biortech.2017.05.211
- Azim, A., Annalisa, S. K. M. R., Rittmann, D. F., and Bochmann, G. (2018). The physiological effect of heavy metals and volatile fatty acids on *Methanococcus maripaludis* S2. *Biotechnol. Biofuels* 11, 1–16. doi: 10.1186/s13068-018-1302-x
- Argyle, J. L., Tumbula, D. L., and Leigh, J. A. (1996). Neomycin resistance as a selectable marker in *Methanococcus maripaludis*. *Appl. Environ. Microbiol.* 62, 4233–4237. doi: 10.1128/aem.62.11.4233-4237.1996
- Balch, W. E., Fox, G. E., Magrum, L. J., Woese, C. R., and Wolfe, R. S. (1979). Methanogens: reevaluation of a unique biological group. *Microbiol. Rev.* 43:519.
- Bao, J., de Dios Mateos, E., and Silvan Scheller, M. (2022). Efficient CRISPR/Cas12a-based genome-editing toolbox for metabolic engineering in *Methanococcus maripaludis*. *ACS Synthet. Biol.* 11, 2496–2503. doi: 10.1021/acssynbio.2c00137
- Borrel, G., O'Toole, P. W., Harris, H. M. B., Peyret, P., Brugère, J. F., and Gribaldo, S. (2013). Phylogenomic data support a seventh order of Methylophilic methanogens and provide insights into the evolution of Methanogenesis. *Genome Biol. Evol.* 5, 1769–1780. doi: 10.1093/gbe/evt128
- Cavicchioli, R. (2011). Archaea – timeline of the third domain. *Nat. Rev. Microbiol.* 9, 51–61. doi: 10.1038/nrmicro2482
- Costa, K. C., Yoon, S. H., Pan, M., Burn, J. A., Baliga, N. S., and Leigh, J. A. (2013). Effects of H<sub>2</sub> and Formate on growth yield and regulation of Methanogenesis in *Methanococcus maripaludis*. *J. Bacteriol.* 195, 1456–1462. doi: 10.1128/JB.02141-12
- Götz, M., Lefebvre, J., Mörs, F., Koch, A. M. D., Graf, F., Bajohr, S., et al. (2016). Renewable power-to-gas: a technological and economic review. *Renew. Energy* 85, 1371–1390. doi: 10.1016/j.renene.2015.07.066
- Goyal, N., Padhiary, M., Karimi, I. A., and Zhou, Z. (2015). Flux measurements and maintenance energy for carbon dioxide utilization by *Methanococcus maripaludis*. *Microb. Cell Factories* 14:146. doi: 10.1186/s12934-015-0336-z
- Goyal, N., Zhou, Z., and Karimi, I. A. (2016). Metabolic processes of *Methanococcus maripaludis* and potential applications. *Microb. Cell Factories* 15, 1–19. doi: 10.1186/s12934-016-0500-0
- Guebitz, G., Bauer, A., Bochmann, G., Gronauer, A., and Weiss, S. (2015). *Biogas Science and Technology. Bd. 151. Advances in Biochemical Engineering/Biotechnology.* Cham: Springer International Publishing.
- Haydock, A. K., Porat, I., Whitman, W. B., and Leigh, J. A. (2004). Continuous culture of *Methanococcus maripaludis* under defined nutrient conditions. *FEMS Microbiol. Lett.* 238, 85–91. doi: 10.1016/j.femsle.2004.07.021
- Hendrickson, E. L., Haydock, A. K., Moore, B. C., Whitman, W. B., and Leigh, J. A. (2007). Functionally distinct genes regulated by hydrogen limitation and growth rate in methanogenic Archaea. *Proc. Natl. Acad. Sci. USA.* 104, 8930–8934. doi: 10.1073/pnas.0701157104
- Hendrickson, E. L., Liu, Y., Rosas-Sandoval, G., Porat, I., Söll, D., Whitman, W. B., et al. (2008). Global responses of *Methanococcus maripaludis* to specific nutrient limitations and growth rate. *J. Bacteriol.* 190, 2198–2205. doi: 10.1128/JB.01805-07
- Howarth, R. W., Santoro, R., and Ingraffea, A. (2011). Methane and the greenhouse-gas footprint of natural gas from shale formations. *Clim. Chang.* 106, 679–690. doi: 10.1007/s10584-011-0061-5
- IPCC (2013). “Climate Change 2013: The Physical Science Basis,” in *Contribution of Working Group I to the Fifth Assessment Report of the Intergovernmental Panel on Climate Change*. eds. T. F. Stocker, D. Qin, G.-K. Plattner, M. Tignor, S. K. Allen, J. Boschung, et al (Cambridge, United Kingdom and New York, NY, USA: Cambridge University Press), 1535.
- Jabłoński, S., Rodowicz, P., and Łukaszewicz, M. (2015). Methanogenic archaea database containing physiological and biochemical characteristics. *Int. J. Syst. Evol. Microbiol.* 65, 1360–1368. doi: 10.1099/ijls.0.000065
- Jarrell, K. F., Jones, G. M., Kandiba, L., Nair, D. B., and Eichler, J. (2010). S-layer glycoproteins and Flagellins: reporters of Archaeal posttranslational modifications. *Archaea* 2010, 1–13. doi: 10.1155/2010/612948
- Jarrell, K. F., and Koval, S. F. (1989). Ultrastructure and biochemistry of *Methanococcus voltae*. *Crit. Rev. Microbiol.* 17, 53–87. doi: 10.3109/10408418909105722
- Jones, W. J., Donnelly, M. I., and Wolfe, R. S. (1985). Evidence of a common pathway of carbon dioxide reduction to methane in methanogens. *J. Bacteriol.* 163, 126–131. doi: 10.1128/jb.163.1.126-131.1985
- Jones, W., Jack, M. J. B., and Paynter, R. Gupta., (1983). Characterization of *Methanococcus maripaludis* Sp. Nov., a new methanogen isolated from salt marsh sediment. *Arch. Microbiol.* 135, 91–97. doi: 10.1007/BF00408015
- Keswani, J., Orkand, S., Premachandran, U., Mandelco, L., Franklin, M. J., and Whitman, W. B. (1996). Phylogeny and taxonomy of Mesophilic *Methanococcus* Spp. and comparison of rRNA, DNA hybridization, and phenotypic methods. *Int. J. Syst. Bacteriol.* 46, 727–735. doi: 10.1099/00207713-46-3-727



- Li, J., Zhang, L., Xu, Q., Zhang, W., Li, Z., Chen, L., et al. (2022). CRISPR-Cas9 toolkit for genome editing in an autotrophic CO<sub>2</sub>-fixing Methanogenic Archaeon. *Microbiol. Spectr.* doi: 10.1128/spectrum.01165-22
- Lie, T. J., and Leigh, J. A. (2007). Genetic screen for regulatory mutations in *Methanococcus maripaludis* and its use in identification of induction-deficient mutants of the Euryarchaeal repressor NrpR. *Appl. Environ. Microbiol.* 73, 6595–6600. doi: 10.1128/AEM.01324-07
- Liu, Y., and Whitman, W. B. (2008). Metabolic, phylogenetic, and ecological diversity of the methanogenic archaea. *Ann. N. Y. Acad. Sci.* 1125, 171–189. doi: 10.1196/annals.1419.019
- Long, F., Wang, L., Lupa, B., and Whitman, W. B. (2017). A flexible system for cultivation of Methanococcus and other Formate-utilizing methanogens. *Archaea* 2017, 1–12. doi: 10.1155/2017/7046026
- Lyu, Z., Chou, C.-W., Shi, H., Wang, L., Ghebrea, R., Phillips, D., et al. (2018). Assembly of methyl coenzyme M Reductase in the Methanogenic Archaeon *Methanococcus maripaludis*. *J. Bacteriol.* 200, 1–12. doi: 10.1128/JB.00746-17
- Lyu, Z., Jain, R., Smith, P., Fetchko, T., Yan, Y., and Whitman, W. B. (2016). Engineering the autotroph *Methanococcus maripaludis* for Geraniol production. *ACS Synth. Biol.* 5, 577–581. doi: 10.1021/acssynbio.5b00267
- Lyu, Z., and Whitman, W. B. (2019). Transplanting the pathway engineering toolbox to methanogens. *Curr. Opin. Biotechnol.* 59, 46–54. doi: 10.1016/j.copbio.2019.02.009
- Martin, W., Baross, J., Kelley, D., and Russell, M. J. (2008). Hydrothermal vents and the origin of life. *Nat. Rev. Microbiol.* 6, 805–814. doi: 10.1038/nrmicro1991
- Mauerhofer, L. M., Reischl, B., Schmider, T., Schupp, B., Nagy, K., Pappenreiter, P., et al. (2018). Physiology and methane productivity of Methanobacterium Thermaggregans. *Appl. Microbiol. Biotechnol.* 102, 7643–7656. doi: 10.1007/s00253-018-9183-2
- Mauerhofer, L. M., Zwirtmayr, S., Pappenreiter, P., Bernacchi, S., Seifert, A. H., Reischl, B., et al. (2021). Hyperthermophilic methanogenic archaea act as high-pressure CH<sub>4</sub> cell factories. *Commun. Biol.* 4:289. doi: 10.1038/s42003-021-01828-5
- Moore, B. C., and Leigh, J. A. (2005). Markerless mutagenesis in *Methanococcus maripaludis* demonstrates roles for alanine dehydrogenase, alanine Racemase, and alanine Permease. *J. Bacteriol.* 187, 972–979. doi: 10.1128/JB.187.3.972-979.2005
- Müller, A. L., Wenyu, G., Patsalo, V., Deutzmann, J. S., Williamson, J. R., and Spormann, A. M. (2021). An alternative resource allocation strategy in the Chemolithoautotrophic Archaeon *Methanococcus maripaludis*. *PNAS* 118, 1–8. doi: 10.1073/pnas.2025854118
- Pappenreiter, P. A., Zwirtmayr, S., Mauerhofer, L. M., Rittmann, S. K. M. R., and Paulik, C. (2019). Development of a simultaneous bioreactor system for characterization of gas production kinetics of methanogenic archaea at high pressure. *Eng. Life Sci.* 19, 537–544. doi: 10.1002/elsc.201900035
- Patel, A. K., Choi, Y. Y., and Sim, S. J. (2020). “Emerging prospects of mixotrophic microalgae: way forward to sustainable bioprocess for environmental remediation and cost-effective biofuels,” in *Bioresource Technology*. (Elsevier). Vol 300, 122741.
- Pfeifer, K., Ergal, I., Koller, M., Basen, M., Schuster, B., Simon, K. M. R., et al. (2021). Archaea Biotechnology. *Biotechnol. Adv.* 47:107668. doi: 10.1016/j.biotechadv.2020.107668
- Porcheras, E. M., Rittmann, S., and Herwig, C. (2012). Biofuels and CO<sub>2</sub> neutrality: an opportunity. *Biofuels* 3, 413–426. doi: 10.4155/bfs.12.25
- Richards, M. A., Lie, T. J., Zhang, J., Ragsdale, S. W., Leigh, J. A., and Price, N. D. (2016). Exploring hydrogenotrophic methanogenesis: a genome scale metabolic reconstruction of *Methanococcus maripaludis*. *J. Bacteriol.* 198, 3379–3390. doi: 10.1128/JB.00571-16
- Rittmann, S., Seifert, A., and Herwig, C. (2015). Essential prerequisites for successful bioprocess development of biological CH<sub>4</sub> production from CO<sub>2</sub> and H<sub>2</sub>. *Crit. Rev. Biotechnol.* 35, 141–151. doi: 10.3109/07388551.2013.820685
- Rittmann, S. K. M. R., Seifert, A. H., and Bernacchi, S. (2018). Kinetics, multivariate statistical modelling, and physiology of CO<sub>2</sub>-based biological methane production. *Appl. Energy* 216, 751–760. doi: 10.1016/j.apenergy.2018.01.075
- Rother, M., and Whitman, W. B. (2019). “Methanococcus,” in *Bergey's Manual of Systematics of Archaea and Bacteria* (John Wiley & Sons, Inc., in association with Bergey's Manual Trust).
- Sarmiento, F. B., Leigh, J. A., and Whitman, W. B. (2011). “Genetic systems for hydrogenotrophic methanogens,” in *Methods in Enzymology*. eds. A. C. Rosenzweig and S. W. Ragsdale (Burlington: Academic Press), 43–73.
- Seifert, A. H., Rittmann, S., and Herwig, C. (2014). Analysis of process related factors to increase volumetric productivity and quality of biomethane with *Methanothermobacter Marburgensis*. *Appl. Energy* 132, 155–162. doi: 10.1016/j.apenergy.2014.07.002
- Shieh, J., and Whitman, W. B. (1987). Pathway of acetate assimilation in autotrophic and heterotrophic Methanococci. *J. Bacteriol.* 169, 5327–5329. doi: 10.1128/jb.169.11.5327-5329.1987
- Shieh, J., and Whitman, W. B. (1988). Autotrophic acetyl coenzyme A biosynthesis in *Methanococcus maripaludis*. *J. Bacteriol.* 170, 3072–3079. doi: 10.1128/jb.170.7.3072-3079.1988
- Stathopoulos, C., Kim, W., Li, T., Anderson, I., Deutsch, B., Palioura, S., et al. (2001). Cysteineyl-TRNA Synthetase is not essential for viability of the Archaeon *Methanococcus maripaludis*. *Proc. Natl. Acad. Sci. U. S. A.* 98, 14292–14297. doi: 10.1073/pnas.201540498
- Taubner, R. S., and Rittmann, S. K. M. R. (2016). Method for indirect quantification of CH<sub>4</sub> production via H<sub>2</sub>O production using hydrogenotrophic methanogens. *Front. Microbiol.* 7:532. doi: 10.3389/fmicb.2016.00532
- Taubner, R. S., Pappenreiter, P., Zwicker, J., Smrzka, D., Pruckner, C., Kolar, P., et al. (2018). Biological methane production under putative Enceladus-like conditions. *Nat. Commun.* 9, 748–711. doi: 10.1038/s41467-018-02876-y
- Thauer, R. K., Kaster, A. K., Seedorf, H., Buckel, W., and Hedderich, R. (2008). Methanogenic archaea: ecologically relevant differences in energy conservation. *Nat. Rev. Microbiol.* 6, 579–591. doi: 10.1038/nrmicro1931
- Thevasundaram, K., Gallagher, J. J., Cherno, F., and Chang, M. C. Y. (2022). Engineering nonphotosynthetic carbon fixation for production of bioplastics by methanogenic archaea. *Proc. Natl. Acad. Sci. USA*. 119:e2118638119. doi: 10.1073/pnas.2118638119
- Tumbula, D. L., Makula, R. A., and Whitman, W. B. (1994). Transformation of *Methanococcus maripaludis* and identification of a Pst I-like restriction system. *FEMS Microbiol. Lett.* 121, 309–314. doi: 10.1111/j.1574-6968.1994.tb07118.x
- Ueno, Y., Yamada, K., Yoshida, N., Maruyama, S., and Isozaki, Y. (2006). Evidence from fluid inclusions for microbial methanogenesis in the early Archaean era. *Nature* 440, 516–519. doi: 10.1038/nature04584
- Ver Eecke, H. C., Akerman, N. H., Huber, J. A., Butterfield, D. A., and Holden, J. E. (2013). Growth kinetics and energetics of a deep-sea hyperthermophilic methanogen under varying environmental conditions. *Environ. Microbiol. Rep.* 5, 665–671. doi: 10.1111/1758-2229.12065
- Walters, A. D., and Chong, J. P. J. (2017). Non-essential MCM-related proteins mediate a response to DNA damage in the Archaeon *Methanococcus maripaludis*. *Microbiology* 163, 745–753. doi: 10.1099/mic.0.000460
- Walters, A. D., Smith, S. E., and Chong, J. P. J. (2011). Shuttle vector system for *Methanococcus maripaludis* with improved transformation efficiency. *Appl. Environ. Microbiol.* 77, 2549–2551. doi: 10.1128/AEM.02919-10
- Zellner, G., and Winter, J. (1987). Secondary alcohols as hydrogen donors for CO<sub>2</sub> reduction by methanogens. *FEMS Microbiol. Lett.* 44, 323–328. doi: 10.1111/j.1574-6968.1987.tb02309.x

# ANNEX 2

Pages 60 to 77

---

Taubner R.-S., Baumann L.M.F., Steiner M., Pfeifer K., Reischl B., Korynt K., Bauersachs T.,  
Mähnert B., Clifford E.L., Peckmann J., Schuster B., Birgel D., Rittmann S.K.-M.R.

**Lipidomics and comparative metabolite excretion analysis of methanogenic archaea  
reveal organism-specific adaptations to varying temperature and substrate  
concentration**

mSystems (2023) 8(2):e01159-22

10.1128/msystems.01159-22

---



# Lipidomics and Comparative Metabolite Excretion Analysis of Methanogenic Archaea Reveal Organism-Specific Adaptations to Varying Temperatures and Substrate Concentrations

Ruth-Sophie Taubner,<sup>a,b,c,d</sup> Lydia M. F. Baumann,<sup>e</sup> Michael Steiner,<sup>a</sup> Kevin Pfeifer,<sup>a,b</sup> Barbara Reischl,<sup>a,f</sup> Kordian Korynt,<sup>e</sup> Thorsten Bauersachs,<sup>g</sup> Barbara Mähner,<sup>h</sup> Elisabeth L. Clifford,<sup>h</sup> Jörn Peckmann,<sup>e</sup> Bernhard Schuster,<sup>b</sup> Daniel Birgel,<sup>e</sup>  Simon K.-M. R. Rittmann<sup>a,f</sup>

<sup>a</sup>Archaea Physiology & Biotechnology Group, Department of Functional and Evolutionary Ecology, Universität Wien, Vienna, Austria

<sup>b</sup>Institute for Synthetic Bioarchitectures, Department of Bionanosciences, University of Natural Resources and Life Sciences, Vienna, Austria

<sup>c</sup>Institute for Chemical Technology of Organic Materials, Johannes Kepler Universität Linz, Linz, Upper Austria, Austria

<sup>d</sup>Space Research Institute, Austrian Academy of Sciences, Graz, Styria, Austria

<sup>e</sup>Institute for Geology, Center for Earth System Research and Sustainability, Universität Hamburg, Hamburg, Germany

<sup>f</sup>Arkeon GmbH, Tulln an der Donau, Austria

<sup>g</sup>Institute of Geosciences, Department of Organic Geochemistry, Christian Albrechts Universität, Kiel, Schleswig-Holstein, Germany

<sup>h</sup>Marine Biology/Microbial Oceanography, Department of Functional and Evolutionary Ecology, Universität Wien, Vienna, Austria

Ruth-Sophie Taubner and Lydia M. F. Baumann contributed equally to this work. Author order was determined by contribution.

**ABSTRACT** Methanogenic archaea possess diverse metabolic characteristics and are an ecologically and biotechnologically important group of anaerobic microorganisms. Although the scientific and biotechnological value of methanogens is evident with regard to their methane-producing physiology, little is known about their amino acid excretion, and virtually nothing is known about the lipidome at different substrate concentrations and temperatures on a quantitative comparative basis. Here, we present the lipidome and a comprehensive quantitative analysis of proteinogenic amino acid excretion as well as methane, water, and biomass production of the three autotrophic, hydrogenotrophic methanogens *Methanothermobacter marburgensis*, *Methanothermococcus okinawensis*, and *Methanocaldococcus villosus* under varying temperatures and nutrient supplies. The patterns and rates of production of excreted amino acids and the lipidome are unique for each tested methanogen and can be modulated by varying the incubation temperature and substrate concentration, respectively. Furthermore, the temperature had a significant influence on the lipidomes of the different archaea. The water production rate was much higher, as anticipated from the rate of methane production for all studied methanogens. Our results demonstrate the need for quantitative comparative physiological studies connecting intracellular and extracellular constraints of organisms to holistically investigate microbial responses to environmental conditions.

**IMPORTANCE** Biological methane production by methanogenic archaea has been well studied for biotechnological purposes. This study reveals that methanogenic archaea actively modulate their lipid inventory and proteinogenic amino acid excretion pattern in response to environmental changes and the possible utilization of methanogenic archaea as microbial cell factories for the targeted production of lipids and amino acids.

**KEYWORDS** anaerobes, microbial physiology, amino acids, isoprenoids, lipids, methane, *Archaea*, biotechnology, ecophysiology, methanogenesis

Methanogenic archaea (methanogens) are a phylogenetically and physiologically diverse group of anaerobic microorganisms (1–3). The main metabolic end product of their carbon and energy metabolism is methane (CH<sub>4</sub>), a major greenhouse gas

**Editor** Julie A. Huber, Woods Hole Oceanographic Institution

**Copyright** © 2023 Taubner et al. This is an open-access article distributed under the terms of the [Creative Commons Attribution 4.0 International license](#).

Address correspondence to Simon K.-M. R. Rittmann, [simon.rittmann@univie.ac.at](mailto:simon.rittmann@univie.ac.at).

The authors declare a conflict of interest. Barbara Reischl and Simon K.-M. R. Rittmann declare to have competing financial interests due to their employment in the Arkeon GmbH.

**Received** 24 November 2022

**Accepted** 16 January 2023

**Published** 7 March 2023

and an important energy carrier. Methanogens are ecologically versatile in anoxic environments, consuming gaseous compounds and small organic molecules, thereby accelerating the breakdown of biomass. Due to their phylogenetic, evolutionary, ecological, and environmental importance, methanogens are model organisms for ecophysiological (2, 3), geobiological (4), astrobiological (3, 5, 6), and biotechnological (7–9) studies.

Although the scientific and biotechnological value of methanogens is evident with regard to their CH<sub>4</sub>-producing physiology (9–11), little is known about their amino acid excretion pattern, and virtually nothing is known about the lipidome at varying substrate concentrations and temperatures on a quantitative comparative basis. Both amino acids and isoprenoid-containing membrane core lipids are biotechnological products with increasing global demand (12, 13). In pure culture, methanogens are currently employed as CH<sub>4</sub> cell factories (9, 11, 14–16). With regard to isoprenoids and amino acids, however, methanogens could become cell factories for the production of additional valuable bioproducts in combined gas, liquid, and solid production bioprocesses.

Proteinogenic amino acids are widely used in food and nutritional sciences, and especially, the fermentative production of amino acids is a well-established branch of biotechnology. To date, only specifically developed mutants or genetically engineered bacteria such as *Corynebacterium glutamicum* and *Escherichia coli* are used for that purpose (12). Although the uptake of amino acids in methanogens and their pathways for amino acid synthesis were investigated previously (17, 18), the ecophysiology of proteinogenic amino acid excretion has not yet been examined. Moreover, amino acid excretion by methanogens is still new ground in microbial ecophysiology. Amino acid excretion is relevant for the functioning of microbial ecosystems as, e.g., methanogens were recently implicated in providing amino acids as the substrate for subsequent fermentation by a syntrophic archaeal partner (19).

Various microorganisms are currently utilized for the biotechnological production of lipids, but these comprise mainly representatives of *Bacteria* and *Eukarya* (20–22). Although the lipid inventory of *Archaea* (including methanogens) and its potential application for biotechnology have been studied over the past decades (23–25), only a few biotechnological inventions, like archaeosomes (26), liposomes made from isoprenoidal lipids, are established. These are utilized, e.g., as durable lipid coatings with excellent biocompatibility (27).

Little information about changes in the lipid inventory of thermophilic methanogens in various environments is available to date (28, 29). A few lipid culture experiments have addressed such issues, e.g., for *Methanocaldococcus jannaschii*, a hyperthermophilic methanogen with an optimal growth temperature of ca. 85°C (30). *M. jannaschii* was cultured in a temperature range from 47°C to 78°C and showed a decrease in archaeol and concomitant increases in macrocyclic archaeol and GDGT-0 (glycerol dialkyl glycerol tetraether) with increasing temperatures (28). *M. jannaschii* was also grown under changing pressure and revealed an increase in macrocyclic archaeol and decreases in archaeol and GDGT-0 with increasing growth pressures (29). *Methanothermobacter thermautotrophicus* was grown under varying nutrient supplies, namely, varying molecular hydrogen (H<sub>2</sub>) levels and micronutrient availabilities (limitation of potassium and phosphate) (31).

Our study represents a comprehensive physiological analysis of three isolates of methanogens: *Methanothermobacter marburgensis* (order *Methanobacteriales*), a methanogen utilized for renewable energy production (9, 11) that was isolated from sewage sludge (32); *Methanothermococcus okinawensis* (*Methanococcales*), an organism with importance to biotechnology (11) and astrobiology (6, 33); and *Methanocaldococcus villosus* (*Methanococcales*), a hyperthermophilic and methanogenic model organism (6, 10). The latter two organisms were isolated from hydrothermal systems (34, 35).

The aim of this study was to perform a quantitative analysis of the lipidome and metabolite excretion patterns of these three methanogens in response to changing environmental conditions. Specifically, our experimental approach enabled us to compare and quantitatively link archaeal amino acid excretion patterns and lipid inventories to

CH<sub>4</sub>, water (H<sub>2</sub>O), and biomass production as well as substrate and ammonium (NH<sub>4</sub><sup>+</sup>) uptake rates in relation to different temperatures and substrate concentrations.

## RESULTS

The lipidome; amino acid excretion patterns; as well as CH<sub>4</sub>, H<sub>2</sub>O, and biomass production characteristics were investigated under varying environmental conditions, i.e., varying temperatures, gas-to-liquid ratios, gassing periods, and medium compositions, respectively. An overview of the different tested conditions is given in Fig. 1 to 3.

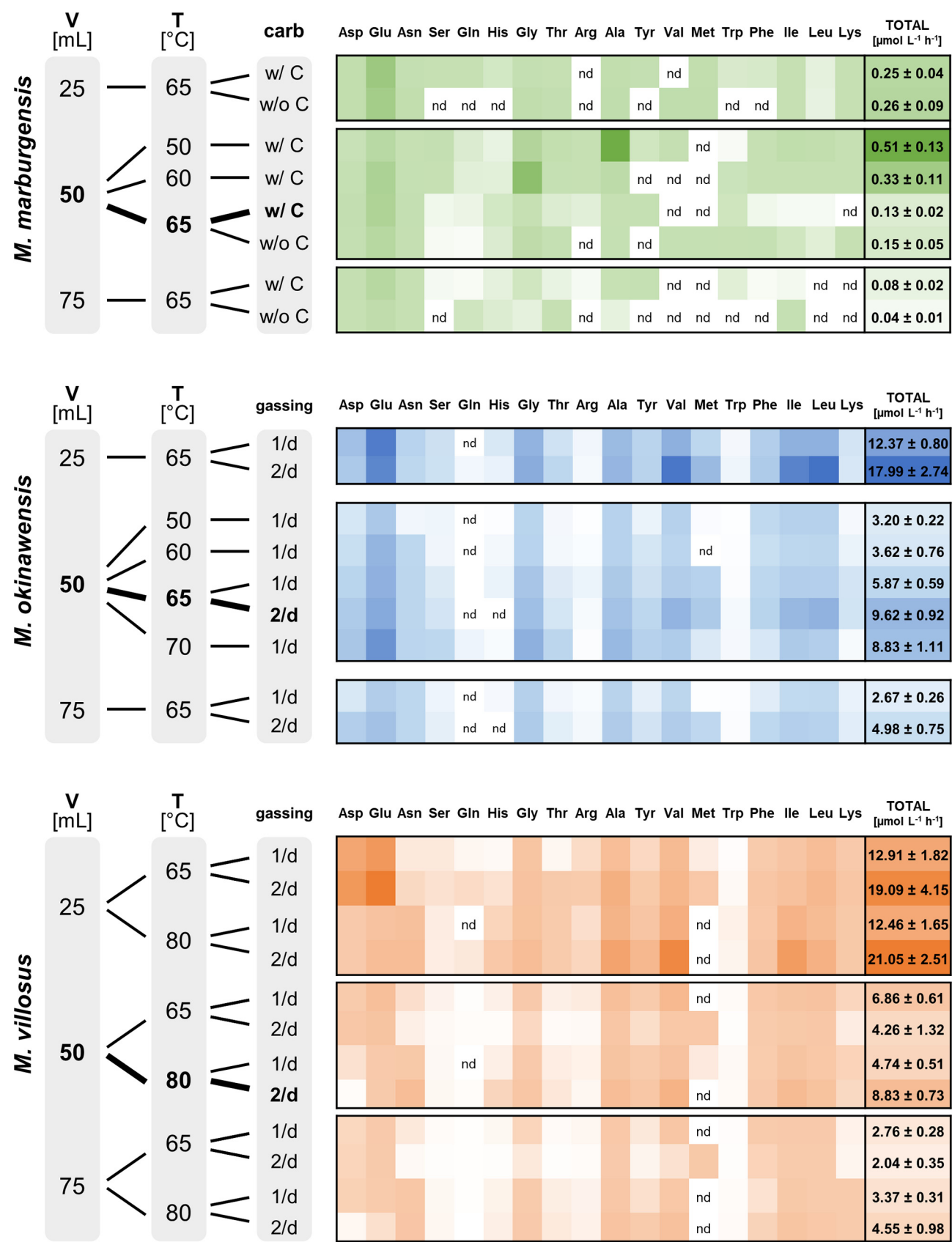
**Observed patterns under standard growth conditions.** For comparing the various strains with each other, the above-mentioned characteristics were first analyzed under standard growth conditions in a liquid volume of 50 mL (Fig. 1 to 3, left, marked in boldface type). Standard growth conditions are defined as growth at 65°C and a medium with carbonates for *M. marburgensis*, growth at 65°C and gassing two times per day for *M. okinawensis*, and growth at 80°C and gassing two times per day for *M. villosus*, all in a 50-mL volume (Fig. 1 to 3, marked boldface type, and Table 1).

Even though *M. marburgensis* showed the highest optical density measured over the total incubation time (OD<sub>end</sub>), the mean methane evolution rate (MER<sub>mean</sub>), the mean water evolution rate (WER<sub>mean</sub>), the total amino acid excretion rate (AAER) (given in micromoles per liter per hour), and the total lipid production rate (given in nanomoles per gram per hour) of this strain were lower than those of the other two strains (Table 1 and Fig. 1 to 3). While Glu (0.086 ± 0.014 μmol L<sup>-1</sup> h<sup>-1</sup>) is the dominating amino acid in *M. marburgensis* (almost 70% of the total amino acids), *M. okinawensis* shows the highest rates of production of Glu (1.567 ± 0.222 μmol L<sup>-1</sup> h<sup>-1</sup>), Val (1.265 ± 0.202 μmol L<sup>-1</sup> h<sup>-1</sup>), Ile (1.152 ± 0.139 μmol L<sup>-1</sup> h<sup>-1</sup>), and Leu (1.337 ± 0.216 μmol L<sup>-1</sup> h<sup>-1</sup>), and *M. villosus* shows the highest rates of production of Asn (1.211 ± 0.179 μmol L<sup>-1</sup> h<sup>-1</sup>), Ala (1.203 ± 0.141 μmol L<sup>-1</sup> h<sup>-1</sup>), Val (1.945 ± 0.157 μmol L<sup>-1</sup> h<sup>-1</sup>), and Ile (1.382 ± 0.123 μmol L<sup>-1</sup> h<sup>-1</sup>) (Fig. 1). The low lipid production rate is caused mainly by the longer total incubation time (division by a higher value). The archaeol production rates are high in all three strains (0.014 ± 0.001 μmol g<sup>-1</sup> h<sup>-1</sup> in *M. marburgensis*, i.e., 7% of the total lipids; 0.015 ± 0.003 μmol g<sup>-1</sup> h<sup>-1</sup> in *M. okinawensis*, i.e., 54% of the total lipids; and 0.049 ± 0.014 μmol g<sup>-1</sup> h<sup>-1</sup> in *M. villosus*, i.e., 39% of the total lipids), and in *M. okinawensis* and *M. villosus*, the rates of macrocyclic archaeol production are equal or even higher (0.014 ± 0.005 μmol g<sup>-1</sup> h<sup>-1</sup> in *M. okinawensis*, i.e., 41% of the total lipids, and 0.072 ± 0.004 μmol g<sup>-1</sup> h<sup>-1</sup> in *M. villosus*, i.e., 58% of the total lipids) (Fig. 2).

**Methanogens vary in their CH<sub>4</sub>/H<sub>2</sub>O product ratios.** H<sub>2</sub>O, as a basic requirement for life, is produced during hydrogenotrophic methanogenesis from H<sub>2</sub> and CO<sub>2</sub> according to the stoichiometry 4H<sub>2</sub> + CO<sub>2</sub> → CH<sub>4</sub> + 2H<sub>2</sub>O (2). However, there is an enigma with regard to H<sub>2</sub>O production in methanogens, where a shift to higher rates of H<sub>2</sub>O than of CH<sub>4</sub> production was detected in chemostat cultures of *M. marburgensis* (36). This prompted us to quantitatively investigate the H<sub>2</sub>O/CH<sub>4</sub> product ratio, i.e., the ratio of WER/MER, of the three strains with respect to varying substrate concentrations and temperatures.

The MERs for each experimental setup are shown in Fig. 3. The MER was higher for those experiments with a larger headspace volume, i.e., a smaller liquid volume ("25 mL"). In numbers, the ratios of 25/50/75 mL (without optical density [OD] measurements) under standard growth conditions were approximately 4.3:2.2:1 for *M. marburgensis*, approximately 5.1:2.5:1 for *M. okinawensis*, and 6.3:2.4:1 for *M. villosus*. Minor MER variations were observed for *M. marburgensis* for experiments performed with or without carbonate in the medium. The highest MERs for *M. okinawensis* and *M. villosus* were observed at their optimal growth temperatures (65°C and 80°C, respectively) at 25 mL with twice-per-day gassing (6.24 ± 0.55 mmol L<sup>-1</sup> h<sup>-1</sup> for *M. okinawensis* and 10.23 ± 0.79 mmol L<sup>-1</sup> h<sup>-1</sup> for *M. villosus*). The same pattern was observed for the WER determined via mass increases (see reference 10 for detailed information) in an isobaric setting (Fig. 3).

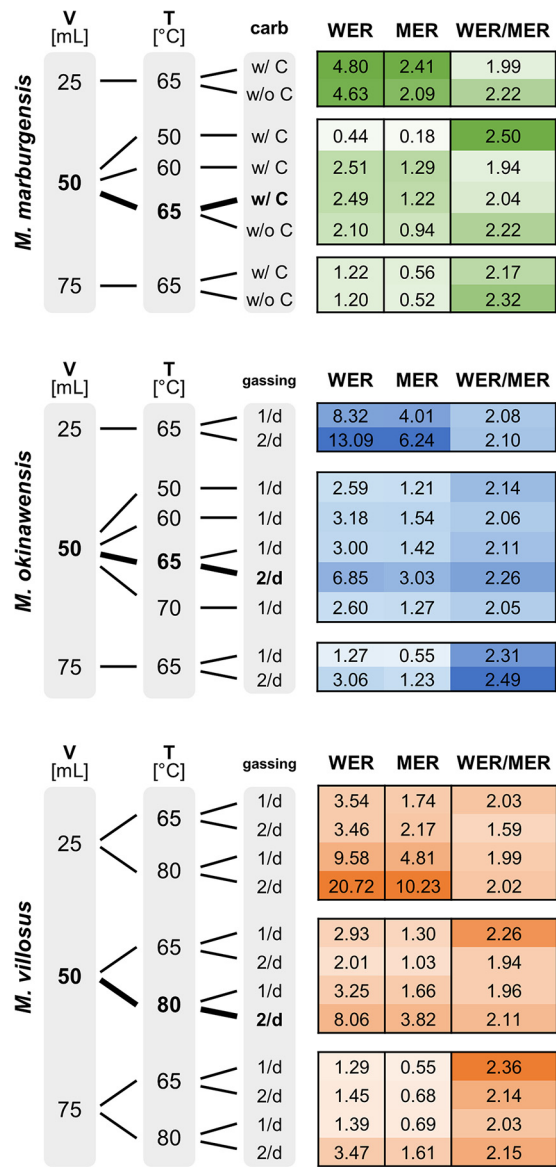
Theoretically, H<sub>2</sub>O-CH<sub>4</sub> (and, consequently, the WER and MER) should correspond to a 2:1 ratio. However, a shift toward a WER/MER ratio of >2 was observed for the majority of cultures in a closed batch mass balance setting (Fig. 3). A trend toward a ratio of <2



**FIG 1** Mean amino acid excretion rates (AAERs) for *M. marburgensis* (green), *M. okinawensis* (blue), and *M. villosus* (orange). Shown are AAERs for (Continued on next page)







**FIG 3** Mean  $\text{CH}_4$  evolution rate (MER) (millimoles per liter per hour), mean  $\text{H}_2\text{O}$  evolution rate (WER) (millimoles per liter per hour), and WER/MER ratio for *M. marburgensis* (green), *M. okinawensis* (blue), and *M. villosus* (orange). The standard growth conditions are highlighted in boldface type. A darker color represents a higher number. The medium for *M. marburgensis* (65°C) (with and without carbonates) and the gassing ratio for *M. okinawensis* (65°C) and *M. villosus* (65°C and 80°C) (once per day [1/d] and twice per day [2/d]) were varied. The liquid volume varied between 25, 50, and 75 mL in a 120-mL serum bottle. *M. marburgensis* was always gassed once per day, and there were no changes in the compositions of the *M. okinawensis* and *M. villosus* media in this study.

strains. To demonstrate that amino acids were actively excreted and not associated with cell lysis, an experiment was designed where once-per-day OD measurements were combined with daily amino acid and fluorescence-activated cell sorting (FACS) measurements (see Fig. S1 and S2 in the supplemental material). These experiments were performed by using an initial liquid volume of 50 mL under the respective standard growth conditions of the three strains (once-per-day gassing for *M. okinawensis*). As *M. villosus* showed the highest rate of cell lysis of the three methanogens, we additionally determined the level of amino acids released due to cell lysis by continuing the incubation of the culture in stationary phase without the addition of gaseous substrates. After approximately 113 h of incubation without additional gassing, the total biomass had decreased from 0.30 g L<sup>-1</sup> to 0.06 g L<sup>-1</sup> (i.e., a decrease of 82%; viable biomass, 0.29 g L<sup>-1</sup> to 0.01 g L<sup>-1</sup>) (Fig. S2c), an



**TABLE 1** Growth, production, and excretion parameters for *M. marburgensis*, *M. okinawensis*, and *M. villosus* under standard growth conditions<sup>a</sup>

Parameter	Value for organism		
	<i>M. marburgensis</i>	<i>M. okinawensis</i>	<i>M. villosus</i>
$t_{inc}$ (h)	229.3	78.6	36.9
Mean OD <sub>end</sub> (at 578 nm) $\pm$ SD	1.041 $\pm$ 0.057	0.660 $\pm$ 0.040	0.700 $\pm$ 0.012
MER <sub>mean</sub> (mmol L <sup>-1</sup> h <sup>-1</sup> ) $\pm$ SD	1.219 $\pm$ 0.076	3.030 $\pm$ 0.113	3.875 $\pm$ 0.237
WER <sub>mean</sub> (mmol L <sup>-1</sup> h <sup>-1</sup> ) $\pm$ SD	2.485 $\pm$ 0.142	6.852 $\pm$ 0.180	8.056 $\pm$ 0.419
WER/MER ratio	2.038	2.262	2.115
Mean total AAER ( $\mu$ mol L <sup>-1</sup> h <sup>-1</sup> ) $\pm$ SD	0.125 $\pm$ 0.019	9.617 $\pm$ 0.916	8.831 $\pm$ 0.734
Mean total lipid production rate ( $\mu$ mol g <sup>-1</sup> h <sup>-1</sup> ) $\pm$ SD	0.018 $\pm$ 0.001	0.027 $\pm$ 0.007	0.128 $\pm$ 0.018

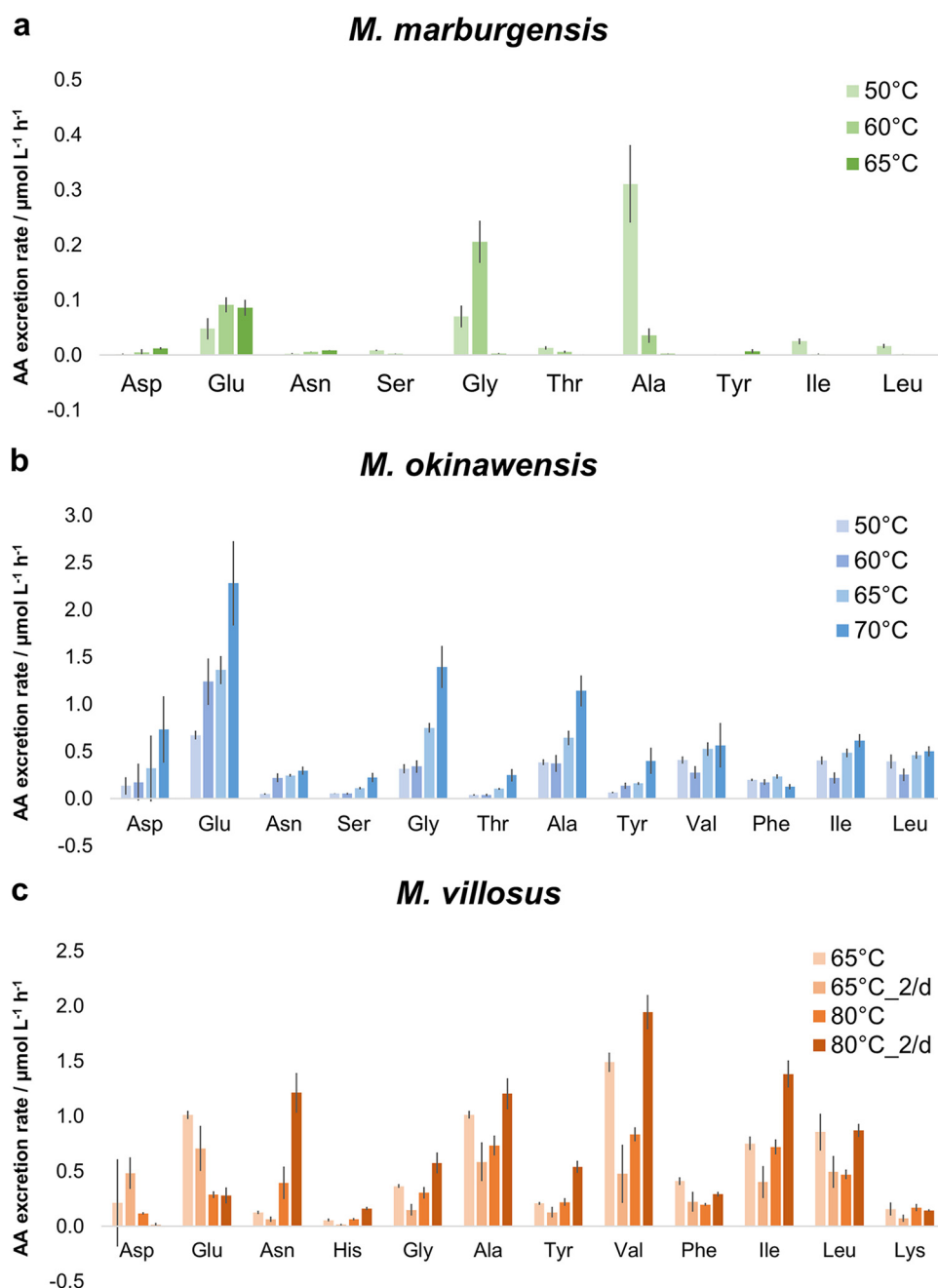
<sup>a</sup> $t_{inc}$ , total incubation time; OD<sub>end</sub>, maximal optical density (at 578 nm) measured over the total incubation time (available for only half of the samples); MER<sub>mean</sub>, mean methane evolution rate; WER<sub>mean</sub>, mean water evolution rate; AAER, amino acid excretion rate. Except for  $t_{inc}$  and the WER/MER ratio, the data presented are mean values and standard deviations ( $n = 4$ ).

indication of cell death and lysis. While the total amino acid content increased by only 25% in that period, an increase of 440% during exponential cell growth within the first 64 h of the experiment was observed (Fig. S2). These findings confirm our hypothesis that amino acids are actively excreted at a higher rate during exponential growth than during cell lysis.

Interestingly, the amino acid excretion patterns varied over time. While the total number of amino acids steadily increased over time for the other two strains, *M. marburgensis* showed a peak at the 48.1-h time point (Fig. S2a). After a decrease for the next ca. 40 h, the total number of amino acids increased again until the end of the experiment. Within the first 48 h, Ser, Gly, Arg, Ala, Val, Met, Leu, and Ile reached their highest values. While Val, Met, and Ala dominated the amino acid pool until the 48.1-h time point, Glu was predominant thereafter. Changes in production were also observed for Glu in *M. okinawensis* (highest values at 90.3 h) and for Glu, Tyr, Met, and Trp in *M. villosus*.

At least traces of all of the 18 tested amino acids were found in most cultures at the end of the experiments. Figure 1 demonstrates that increased gaseous substrate availability was accompanied by increased amino acid excretion at the optimal growth temperature for each organism. In numbers, the ratios of 25/50/75 mL (without OD measurements) under standard growth conditions were approximately 3.2:1.6:1 for *M. marburgensis*, approximately 3.6:1.9:1 for *M. okinawensis*, and 4.6:1.9:1 for *M. villosus*. However, *M. marburgensis* excreted far fewer amino acids than the other two strains at the same substrate concentration and gassing interval ( $0.13 \pm 0.02 \mu\text{mol L}^{-1} \text{h}^{-1}$  compared to  $5.87 \pm 0.59 \mu\text{mol L}^{-1} \text{h}^{-1}$  for *M. okinawensis* and  $4.74 \pm 0.51 \mu\text{mol L}^{-1} \text{h}^{-1}$  for *M. villosus* at the optimal growth temperature, with once-per-day gassing) (Fig. 1). The most prominent excreted amino acid in most *M. marburgensis* cultures at the optimal growth temperature (65°C) was Glu (up to 84% of the total measured amino acids in some cultures). Therefore, the observed decrease in the AAER in *M. marburgensis* from 25 mL to higher liquid volumes is caused mainly by the reduced production of Glu. Interestingly, the total AAER of *M. marburgensis* was higher at lower temperatures (50°C and 60°C) in a liquid volume of 50 mL (50°C,  $0.51 \pm 0.13 \mu\text{mol L}^{-1} \text{h}^{-1}$ ; 60°C,  $0.33 \pm 0.11 \mu\text{mol L}^{-1} \text{h}^{-1}$ ; 65°C,  $0.13 \pm 0.02 \mu\text{mol L}^{-1} \text{h}^{-1}$ ), which was also observed for *M. villosus* for the once-per-day gassing experiments in 25 and 50 mL and for *M. okinawensis* for the experiments performed at 70°C (Fig. 1 and 4). This characteristic of *M. marburgensis* at 50°C is due to an extreme increase in the rates of excretion of Ala (from  $2.7 \pm 0.5 \text{ nmol L}^{-1} \text{h}^{-1}$  at 65°C to  $311 \pm 70 \text{ nmol L}^{-1} \text{h}^{-1}$  at 50°C) and Gly (from  $2.9 \pm 0.9 \text{ nmol L}^{-1} \text{h}^{-1}$  at 65°C to  $206 \pm 38 \text{ nmol L}^{-1} \text{h}^{-1}$  at 60°C) (Fig. 4). The high AAER of *M. okinawensis* at 70°C is caused mainly by increases in Glu, Gly, and Ala (Fig. 4).

*M. okinawensis* showed the highest total AAER under its standard growth conditions ( $9.62 \pm 0.92 \mu\text{mol L}^{-1} \text{h}^{-1}$ ), which agrees with the kinetics of substrate uptake (10). However, the total AAER at 70°C was almost as high as that under the standard growth conditions, caused by extreme increases in the rates of production of Glu, Gly, and Ala (Fig. 4). In general, amino acid patterns varied at different growth temperatures (Fig. 4).



**FIG 4** Amino acid (AA) excretion rates (AAERs) for *M. marburgensis*, *M. okinawensis*, and *M. villosus* at different temperatures (in a 50-mL initial liquid volume). Shown are AAERs for selected species in micromoles per liter per hour based on endpoint measurements for *M. marburgensis* (50°C, 60°C, and 65°C, with carbonates) (a), *M. okinawensis* (50°C, 60°C, 65°C, and 70°C, with once-per-day gassing) (b), and *M. villosus* (65°C and 80°C) (c). Each bar represents a set of octuplicate. The error bars indicate standard deviations. Experiments were performed at different incubation temperatures. “2/d” refers to two gassing procedures per day; otherwise, gassing was performed once per day.

No interpretation of the Asp pattern is possible as it was detected in only approximately one-half of the replicates (resulting in high error bars) (Fig. 4).

The total AAER of *M. villosus* was in the same range as that of *M. okinawensis* (Fig. 1). However, the patterns of the individual amino acids were different between the two strains (Fig. 1 and 4). For *M. villosus*, Val, Ile, Ala, Asn, and Leu were the most prominent amino acids under standard growth conditions, while for *M. okinawensis*, Glu and Gly replaced Asn as the dominant amino acids. A different pattern was found for *M. villosus*

at a lower temperature (65°C) for the 25-mL samples, representing the only setting where Asp ( $3.82 \pm 1.32 \mu\text{mol L}^{-1} \text{h}^{-1}$ , with twice-per-day gassing) and Glu ( $5.66 \pm 1.92 \mu\text{mol L}^{-1} \text{h}^{-1}$ , with twice-per-day gassing) not only dominated but also showed the highest rates in all experiments performed in this study (Fig. 1). At 65°C, gassing once per day (50 mL) (Fig. 1 and 4) promoted higher AAERs of *M. villosus* than the in twice-per-day gassing experiments, which was unexpected (and was not observed at 80°C) as it has been suggested that higher substrate (gas) availability leads to the higher-level production of metabolites (10). At 80°C with a 50-mL volume, twice-per-day gassing led to higher rates of excretion of mainly Val ( $1.94 \pm 0.16 \mu\text{mol L}^{-1} \text{h}^{-1}$ ), Asn ( $1.21 \pm 0.18 \mu\text{mol L}^{-1} \text{h}^{-1}$ ), Ile ( $1.38 \pm 0.12 \mu\text{mol L}^{-1} \text{h}^{-1}$ ), Ala ( $1.20 \pm 0.14 \mu\text{mol L}^{-1} \text{h}^{-1}$ ), and Leu ( $0.87 \pm 0.06 \mu\text{mol L}^{-1} \text{h}^{-1}$ ) in *M. villosus* (Fig. 4). Noteworthy, Met excretion rates were observed only for cultures gassed twice per day at 65°C (for all volumes).

A comparison of the  $\text{NH}_4^+$  uptake rate and the AAER (both in micromoles per liter per hour) revealed a ratio close to 1:1 in *M. okinawensis*. For *M. marburgensis*, substantially more  $\text{NH}_4^+$  was taken up than amino acids were excreted (Fig. S3). In the course of the lysis experiments, it was shown that the extreme  $\text{NH}_4^+$  uptake by *M. marburgensis* mainly took place immediately before the strain entered the stationary growth phase (Fig. S2a, blue line). On the contrary, the AAER in *M. villosus* was higher than the  $\text{NH}_4^+$  uptake rate (Fig. S3).

#### Lipidomes are affected by varying substrate concentrations and temperatures.

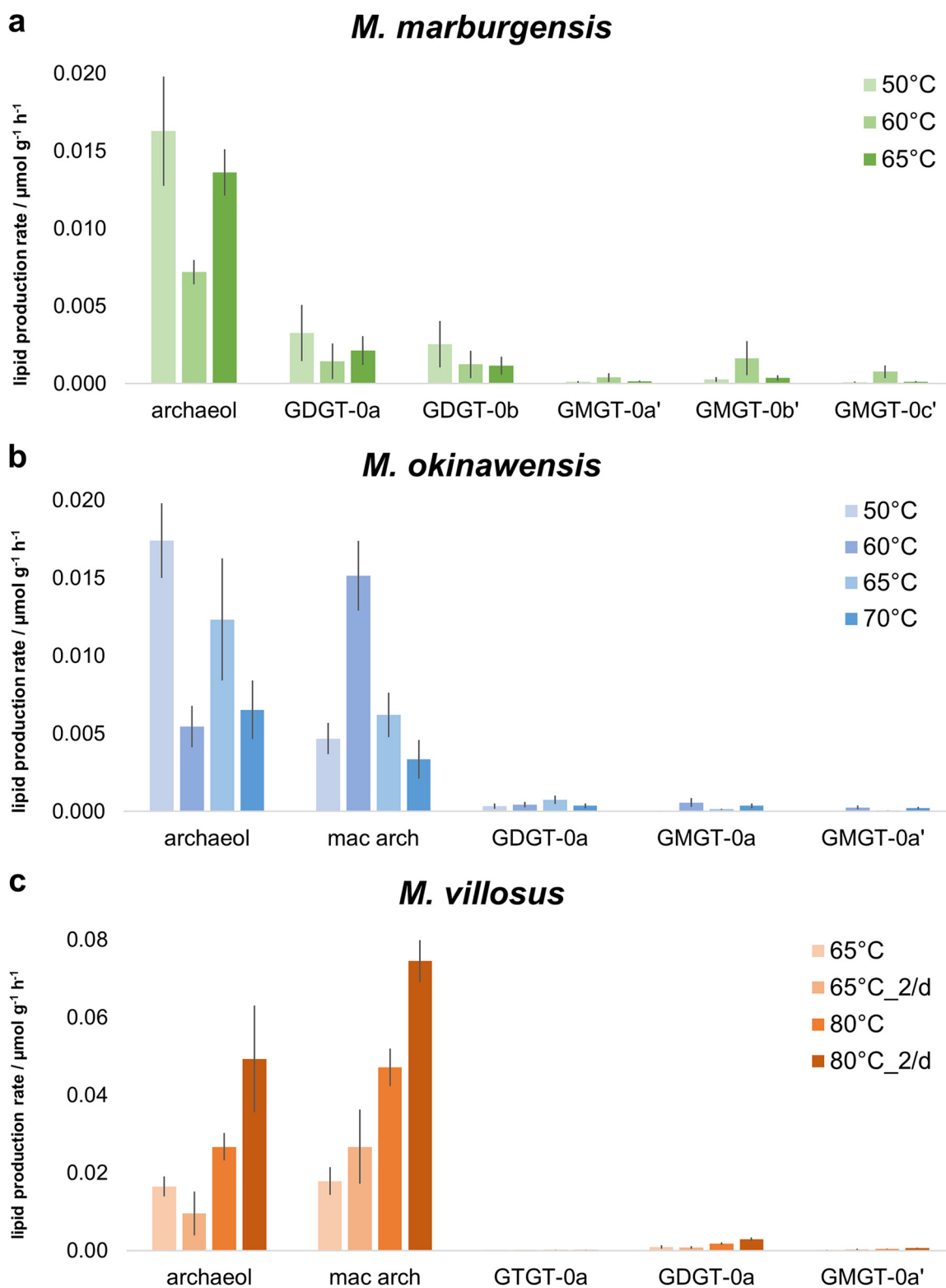
We compared the changes in the lipidomes of the three methanogens at different temperatures and substrate concentrations to reveal their lipid-specific adaptation patterns. The lipid inventory comprised the tetraether lipids GTGT-0 (glycerol trialkyl glycerol tetraether), GDGT-0 (glycerol dialkyl glycerol tetraether), and GMGT-0 (glycerol monoalkyl glycerol tetraether) as well as the diethers archaeol and macrocyclic archaeol (for chromatograms, see reference 37). For *M. marburgensis*, the degrees of methylation (0, 1, or 2) of the basic structures of GMGT-0 and GDGT-0 are displayed as the relative percentages of the different methylated species (a, b, or c) of the sum of all di- and tetraethers, respectively. The tetraether GMGT-0 comes as two isomers, one eluting earlier and the other eluting later. For the various strains, later-eluting isomers are indicated as GMGT-0a', GMGT-0b', and GMGT-0c', respectively.

The most prominent lipids of *M. marburgensis* are archaeol, GDGT-0a, and GDGT-0b, whereas *M. okinawensis* and *M. villosus* predominantly synthesize archaeol, macrocyclic archaeol, and GDGT-0a (Fig. 2). A positive correlation between the level of gaseous substrates and the lipid production rate was observed (Fig. 2). Under standard growth conditions, the total lipid production rate for *M. marburgensis* added up to approximately  $17.7 \pm 1.2 \text{ nmol g}^{-1} \text{h}^{-1}$ , of which diether lipids (archaeol) made up more than 75%.

Under standard growth conditions, *M. villosus* revealed total lipid production rates up to seven times higher than the production rates of *M. marburgensis* and *M. okinawensis* (Fig. 2). While twice-per-day gassing resulted in higher rates of lipid production by *M. villosus* at the optimal growth temperature, no clear impact of the gassing rate on the lipid production rate in *M. okinawensis* was observed. Under standard growth conditions, *M. okinawensis* exhibited a mean total lipid production rate of  $27.4 \pm 7.0 \text{ nmol g}^{-1} \text{h}^{-1}$ , while that of *M. villosus* was  $127.7 \pm 18.5 \text{ nmol g}^{-1} \text{h}^{-1}$ . For both strains, mainly archaeol and macrocyclic archaeol were detected in these experimental settings (more than 95% of the total lipids).

With a volume of 25 mL, gassing twice per day resulted in a higher lipid production rate, while with a volume of 75 mL, the gassing rate showed no clear impact on the lipidome of *M. villosus* (Fig. 2).

Variations in the temperature affected the lipid inventories of the three methanogens (Fig. 2 and 5). For *M. marburgensis*, the specific archaeol production rate in 50 mL liquid medium was high at 50°C ( $16.3 \pm 3.5 \text{ nmol g}^{-1} \text{h}^{-1}$ ), decreased at 60°C ( $7.2 \pm 0.8 \text{ nmol g}^{-1} \text{h}^{-1}$ ), and increased again at 65°C ( $13.6 \pm 1.5 \text{ nmol g}^{-1} \text{h}^{-1}$ ), while the total lipid production rate stayed almost constant at all temperatures (Fig. 2). A similar, but slightly weaker, trend was found for GDGT-0a and GDGT-0b compared to



**FIG 5** Lipid production rates for *M. marburgensis*, *M. okinawensis*, and *M. villosus* at different temperatures (in a 50-mL initial liquid volume). Shown are lipid production rates for selected species in micromoles per gram per hour based on endpoint measurements for *M. marburgensis* (50°C, 60°C, and 65°C, with carbonates) (a), *M. okinawensis* (50°C, 60°C, 65°C, and 70°C, with once-per-day gassing) (b), and *M. villosus* (65°C and 80°C) (c). Each bar represents a set of octuplicates. The error bars indicate standard deviations. Experiments were performed at different incubation temperatures. “2/d” refers to two gassing procedures per day; otherwise, gassing was performed once per day. mac arch, macrocyclic archaeol.

archaeol (Fig. 5). However, the specific GMGT-0b' production rate increased only at 60°C (Fig. 5). When comparing the results of 50-mL experiments at 50°C, 60°C, and 65°C, the total specific lipid production rate stayed constant in *M. okinawensis* (Fig. 2), but the ratio between the specific archaeol and macrocyclic archaeol production rates changed (Fig. 5). *M. okinawensis* revealed a high specific archaeol production rate at 50°C and 65°C, while at 60°C, macrocyclic archaeol dominated. A decrease in the specific total lipid production rate was observed at 70°C for *M. okinawensis* at 50 mL (Fig. 2 and Fig. 5b). For *M. villosus*, the total specific lipid production rate was higher at 80°C than at 65°C (Fig. 2), and macrocyclic archaeol always dominated over archaeol in the 50-mL experiments (Fig. 5). At 25 and 75 mL, this trend was not observed.

## DISCUSSION

The aim of this study was to gain comprehensive insights into the lipidomes and metabolite excretion patterns of three methanogens and to report the environmental conditions under which these organisms actively modulate the CH<sub>4</sub>/H<sub>2</sub>O product ratio, amino acid excretion, and their lipidome as a function of substrate availability and temperature. Examining the changes in these interdependent variables presents an unprecedented attempt to holistically understand how the three strains physiologically respond to environmental alterations at the levels of gases and excreted liquid-phase compounds and by modulating their cytoplasmatic membrane components.

**Amino acid excretion by methanogens strongly depends on temperature and other variables.** To date, studies dealing with amino acids in methanogens are limited to the uptake of amino acids from the environment and the biochemistry of amino acid production pathways (38–40). For example, amino acid uptake, amino acid catabolism, and the pathway for Ile biosynthesis were studied in *Methanococcus voltae* (41). This methanogen incorporated different amino acids from the growth medium into its protein structures. In *Methanothermobacter thermautotrophicus* (42, 43) and *M. marburgensis* (44), amino acids are early fixation products of CO<sub>2</sub> and NH<sub>4</sub><sup>+</sup> assimilation. Moreover, the effect of H<sub>2</sub>, Leu, or phosphate limitation on the free intracellular amino acid pools (and growth rates) of a Leu auxotroph mutant of *Methanococcus maripaludis* S2 was investigated. H<sub>2</sub> limitation resulted in a decrease in the free intracellular amino acid levels, with Gly being an exception, increasing 2-fold during H<sub>2</sub> limitation (45). We found that during H<sub>2</sub> limitation (75 mL compared to 25 mL and 50 mL), the AAERs of Gly and all other amino acids are lower in all three tested strains (Fig. 1). To the best of our knowledge, the only study reporting the excretion of amino acids by methanogens used U-<sup>14</sup>C labeling to quantify the contribution of the endogenous synthesis of Leu and Ile compared to Leu and Ile uptake in *M. voltae*. Increases in the Leu and Ile concentrations in the supernatant were detected, which demonstrated that excess amino acids were excreted during growth (46).

By varying the growth temperature (at a constant volume), we were able to identify conclusive shifts in the amino acid patterns. These variations might be adaptations to environmental stressors or might reflect intercellular communication signals between different species. The latter was observed in a study where “*Candidatus Prometheoarchaeum syntrophicum*” strain MK-D1 was enriched together with a *Methanogenium* archaeon (19). “*Ca. Prometheoarchaeum syntrophicum*” degraded 10 different amino acids, providing H<sub>2</sub> and/or formate to the *Methanogenium* archaeon in return, and received amino acids for its catabolism. That study and our study show that the ecophysiological interactions of microbes in enrichment cultures and natural environments, as well as their metabolic capabilities, are poorly understood on a qualitative and quantitative basis. To determine the syntrophic benefit of amino acid excretion for methanogens, further studies coupling *in vitro* and *in silico* physiologies will be of special interest to microbial ecophysiology, biotechnology, astrobiology, and beyond.

A key finding of our study is the higher AAER in *M. villosus* at 50 mL for cultures gassed once per day at 65°C than for those gassed twice per day. We hypothesize that under these specific growth conditions, *M. villosus* benefits from a longer, undisturbed incubation period. Furthermore, the AAERs of Asp and Glu in *M. villosus* at 25 mL at

65°C were higher than those in all other settings, and *M. okinawensis* showed extreme increases in the AAERs of Glu, Gly, and Ala for the experiments performed at 70°C, i.e., 5°C above the optimal growth temperature, in comparison to the experiments performed at lower temperatures (Fig. 4). These surprising findings should motivate future comprehensive studies to determine the optimal conditions for high AAERs for the different amino acids.

**The lipidome is less dependent on taxonomy than on environmental conditions.** Numerous studies have examined the lipid biomarker inventory of methanogens and other, nonmethanogenic organisms under changing temperatures, pressures, and pH (28, 47, 48). A general outcome of these studies was, among others, that diether lipid production seems to be a membrane lipid adaption to lower temperatures and higher pressures, with regard to the optimal growth conditions, and vice versa for the production of tetraether membrane lipids. It has to be noted that most experimental results are available for thermophiles, such as the archaea chosen for this study. A recent study on the piezo-hyperthermophilic archaeon *Thermococcus barophilus* already confirmed that tetraether lipids were increased with low pressure and high temperatures, whereas archaeol was produced at low temperatures and high pressure (49). In *M. villosus* and *M. okinawensis*, we additionally monitored the production of macrocyclic archaeol, which is a unique and only rarely described membrane lipid, most likely enabling the higher stability of the membrane (50). Although the general pattern described previously for other strains was also found in our samples, the influence of a changing nutrient supply on the modulation of the membrane lipid composition has been investigated in only a few studies so far (31). In the current study, temperatures and changing nutrient supplies were examined concurrently. One significant finding is that *M. villosus* revealed a higher total lipid production rate than *M. marburgensis* and *M. okinawensis* under standard growth conditions ( $127.7 \pm 18.5 \text{ nmol g}^{-1} \text{ h}^{-1}$  [*M. villosus*] compared to  $27.4 \pm 7.0 \text{ nmol g}^{-1} \text{ h}^{-1}$  [*M. okinawensis*] and  $17.7 \pm 1.2 \text{ nmol g}^{-1} \text{ h}^{-1}$  [*M. marburgensis*]) (Fig. 2). It thus appears that lipidome compositions are less dependent on taxonomy than on environmental conditions.

Among the three strains, *M. okinawensis* revealed the strongest changes in the relative lipid production rates and compositions of lipids at varying incubation temperatures (Fig. 5). Especially, the relative proportions of archaeol versus macrocyclic archaeol were highly dependent on environmental conditions. According to experiments with vesicles and tubules made from synthetic archaeon-type phosphatidylcholines (which resemble archaeol and macrocyclic archaeol), macrocyclization leads to decreased water permeability and increased stability of the vesicles (50). It was suggested that the C-C bond at the methyl ends of the phytanyl chains prevents independent motion and ultimately leads to a more closely packed assembly in the liquid-crystalline state (50). In combination with the results of other lipid culture experiments (28), the assumption was put forward that the incorporation of macrocyclic archaeol could increase overall membrane stability and rigidity and reduce membrane fluidity. Consequently, higher proportions of archaeol than of macrocyclic archaeol would be expected at the lowest temperature, similar to an overall increase in diether lipids over tetraether lipids. However, this does not explain the observation that the rates of production of macrocyclic archaeol are highest at 60°C, the lower boundary of the temperature optimum of *M. okinawensis*.

In *M. villosus*, having its temperature optimum at 80°C, macrocyclic archaeol is produced at a higher rate than archaeol under almost all tested conditions (Fig. 5). Kaneshiro and Clark made a similar observation for *Methanocaldococcus jannaschii*, a close relative of *M. villosus*, where at higher pressures, more macrocyclic archaeol than archaeol was synthesized (29). So, even though we found macrocyclic archaeol in two strains, there is no general pattern when macrocyclic archaeol is predominating, so we cannot confirm that the macrocyclic archaeol production rate is highest at low temperatures and high pressure.

*M. marburgensis* produced GDGTs and GMGTs, with additional methylations in the alkyl chains, but no macrocyclic archaeol. GDGT and GMGT proportions varied with changing temperatures. The highest degree of methylation was found at 60°C for both GDGTs and GMGTs (see reference 37). This result is in contrast to those of another



study (51), where a higher percentage of methylated lipids at 45°C than at 60°C and 70°C for GDGTs and GMGTs was reported for *M. thermautotrophicus*, a close relative of *M. marburgensis*. The authors of that study further observed distinctly higher contents of nonmethylated GDGT-0a and GMGT-0a than those with one (GDGT-0b and GMGT-0b) and two (GDGT-0c and GMGT-0c) extra methylations, whereas in the present study, almost equal amounts of GDGT-0a and GDGT-0b and a predominance of GMGT-0b' over GMGT-0a' and GMGT-0c' at all temperatures were observed.

In contrast, our results confirm the findings of the above-mentioned study (51), where a higher proportion of methylated homologs prevailed among the GMGTs than among the GDGTs at all three chosen temperatures. Another study showed a predominance of GDGT-0b, -c, and -d compared to the nonmethylated GDGT-0a in *M. thermautotrophicus* grown at 65°C (31). When comparing the results of these three studies, it has to be considered that in all experiments different growth temperatures were chosen. It is thus still an open question what triggers the expression of varying lipid patterns at different temperatures in *M. marburgensis*.

**Methanogens produce lipids and amino acids of biotechnological interest.** As the world strives for a cleaner and more sustainable future, biotechnology- and microbe-based processes will become increasingly important. Today, microbes are already a fundamental component of the industry, where they are used to produce a wide range of high-value compounds such as pharmaceuticals, alcohols, fuels, and vital precursors for industrial processes (13). Although most established production processes for amino acids are based on bacteria or yeasts, archaea are of great interest for such applications due to their unique physiologies (3, 9) and enzymes (52). Here, we demonstrate that the biotechnological potential of *M. marburgensis*, *M. villosus*, and *M. okinawensis* goes beyond CH<sub>4</sub> production. By controlling the environmental conditions, archaeal production of high-value compounds such as isoprenoid lipids and proteinogenic amino acids becomes feasible, which would allow the implementation of these revenue streams in addition to biomethanation. Moreover, the shift in the CH<sub>4</sub>/H<sub>2</sub>O product ratio might also be of biotechnological relevance as it would allow the detection of temperature deviations, and substrate limitations could then be adjusted to decrease H<sub>2</sub>O production. As shown for *M. marburgensis* and *M. okinawensis*, the average WER/MER ratio is approximately 5% lower at 60°C than at 65°C, but the growth characteristics are almost identical. For *M. okinawensis*, 60°C and 65°C are the lower and upper boundaries of its optimal growth temperature range (34). This finding has implications for both pure-culture and industrial-scale H<sub>2</sub>/CO<sub>2</sub> biomethanation (9, 11). Therefore, lowering the growth temperature, which also lowers the required (thermal) energy and, consequently, the costs, would have the potential to decrease H<sub>2</sub>O production rates during pure-culture biomethanation. Even if such a small temperature difference does not have an impact on growth, it clearly affects the AAER (Fig. 4) and the lipidome (Fig. 5).

To summarize, this study demonstrates that the levels of excreted amino acids vary between different strains, as the amino acid excretion rate was more than a magnitude lower in *M. marburgensis* than in *M. villosus* and *M. okinawensis*. Furthermore, each species excreted a specific pattern of amino acids. Regarding the lipidome, *M. villosus* showed a higher specific lipid production rate than *M. marburgensis* and *M. okinawensis*, with a particularly strong influence of the incubation temperature. Therefore, bioprocesses using one of the tested strains can now be optimized with regard to CH<sub>4</sub>, amino acid, and lipid production. By varying the temperature, the increased excretion and production of specific amino acids or lipids can be achieved. Furthermore, our study shows that a high gas-to-liquid-volume ratio favors the AAER and the lipid production rate.

Further studies are required in which changing substrate availabilities combined with different temperatures, pH, and pressures will yield more detailed insights into the physiological and biotechnological potentials of methanogens. Studies where the AAER and the lipid production rate are continuously monitored combined with studies on the metabolic pathways will help us to understand the causes of the observed variations and, furthermore, to implement these findings in biotechnological applications.

Eventually, the ability to scale up these processes utilizing a low-cost feed ( $\text{H}_2/\text{CO}_2$ ) as the substrate will bring the use of methanogens closer to industrial commercialization.

## MATERIALS AND METHODS

**Experimental setup.** *Methanothermobacter marburgensis* DSM 2133, *Methanothermococcus okina-wensis* DSM 14208, and *Methanocaldococcus villosus* DSM 22612 were obtained from the Deutsche Sammlung von Mikroorganismen und Zellkulturen GmbH (DSMZ) (Braunschweig, Germany). Cultivation was conducted in 120-mL serum bottles (La-Pha-Pack, Langerwehe, Germany) in chemically defined medium (6, 10). The cultivation medium for *M. marburgensis* contained 2.1 g  $\text{NH}_4\text{Cl}$ , 6.8 g  $\text{KH}_2\text{PO}_4$ , 3.6 g  $\text{Na}_2\text{CO}_3$ , and 5 mL of a 200 $\times$  trace element solution and was filled up to 1 L with double-distilled water ( $\text{ddH}_2\text{O}$ ). For *M. villosus* and *M. okinawensis*, DSMZ medium 282 (year 2014) was used, with the following modifications: 0.14 g  $\text{K}_2\text{HPO}_4$  was replaced with 0.183 g  $\text{K}_2\text{HPO}_4 \cdot 3\text{H}_2\text{O}$ , and 0.01 g  $\text{Fe}(\text{NH}_4)_2(\text{SO}_4)_2 \cdot 6\text{H}_2\text{O}$  was replaced with 7 mg  $\text{FeSO}_4 \cdot 7\text{H}_2\text{O}$ , without the usage of resazurin. The exact procedures for medium preparation and inoculation and the method used were described previously (10). The injected inoculum was taken from the respective precultures in exponential phase and made up 2% of the respective total liquid volumes. The cultures were flushed for approximately 3 s and then gassed once or twice per day with an  $\text{H}_2/\text{CO}_2$  test gas mixture (20 vol%  $\text{CO}_2$  in  $\text{H}_2$ ) at a relative pressure of approximately  $2 \times 10^5$  Pa (10). Headspace pressure measurements of the serum bottles were performed using a digital manometer (LEO1-Ei,  $-1 \dots 3$  bar; Keller, Germany). For each experimental setup, two independent experiments were performed: one set of quadruplicates without (marked with “I”) and one with (“II”) sampling for OD measurements before each gassing event (according to the method used [10], each time with  $\sim 0.7$  mL of the sample for OD measurements). Growth was recorded via the OD (wavelength [ $\lambda$ ] of 578 nm, blanked with MilliQ water, with a DU800 spectrometer [Beckman Coulter, USA]). No obvious variations in the  $\text{H}_2\text{O}$  evolution rate (WER) (in millimoles per liter per hour) and the mean  $\text{CH}_4$  evolution rate (MER) (in millimoles per liter per hour) were observed in the two different experimental setups. Also, no general variations in the amino acid excretion pattern and lipidome related to the slowly increasing volume of the gaseous substrates caused by the OD sampling were detected. As we have not observed a large difference in the experiments performed with and those without OD measurements, the data presented are pooled data from the two data sets. However, for completeness, the figures in the supplemental material show the two settings separately.

A negative control, i.e., a bottle that included only medium but was not inoculated, was incubated together with the other bottles as the background reference for the OD and amino acid measurements. Definition of a background reference for the lipid measurements was not feasible due to the small amount of material available after harvesting the zero controls. No eukaryotic or bacterial lipids were detected.

After the completion of each experiment, the biomass and supernatant were harvested by the centrifugation of each culture for 20 min at 4,500 rpm (3,328 relative centrifugal force [rcf]) at 4°C in 50-mL Greiner tubes (Universal 320R; Hettich). Subsequently, cell pellets and three 1-mL samples from the supernatant in each bottle were separately stored in sterile Eppendorf tubes at  $-20^\circ\text{C}$  until further analysis.

A major part of the experiments was performed at the respective optimal growth temperatures ( $65^\circ\text{C}$  for *M. marburgensis* and *M. okinawensis* and  $80^\circ\text{C}$  for *M. villosus*) and using three liquid volumes, 25, 50, and 75 mL. Furthermore, we performed several complementing experiments depending on the physiology pertaining to these organisms. To examine the influence of the incubation temperature on the lipidome and the amino acid excretion pattern, *M. marburgensis* and *M. okinawensis* were additionally grown at  $50^\circ\text{C}$ ,  $60^\circ\text{C}$ , and  $70^\circ\text{C}$  in 50 mL. No growth of *M. marburgensis* was observed at  $70^\circ\text{C}$ . For comparison, the hyperthermophilic archaeon *M. villosus* was additionally grown at  $65^\circ\text{C}$ , and the volume of the liquid medium (25, 50, and 75 mL) varied. In addition, *M. marburgensis* was grown with a carbonate-free medium, as it was of physiological and biotechnological interest to examine the changes in the lipidome and metabolite patterns in these media. *M. okinawensis* and *M. villosus* are fast-growing organisms (16), which resulted in the gas-limited growth of these strains in our closed batch experimental setting. Therefore, we examined the physiological changes of these organisms under two different gassing regimes: gassing once per day (i.e., approximately every 18 to 25 h) versus twice per day (i.e., every 5 to 15 h) with  $\text{H}_2/\text{CO}_2$  (carbon dioxide) (4:1, vol/vol). An overview of the experimental setup is given in Fig. 1.

**Amino acid and lipid analyses.** Detailed descriptions of the methods and instruments were reported previously (33, 37). All  $\text{NH}_4^+$  uptake, lipid, and amino acid excretion rates were calculated via endpoint measurements (after harvesting). The only exceptions are the amino acid values from the lysis experiment.

Prior to analysis by gas chromatography (GC)-mass spectrometry (MS) and high-performance liquid chromatography (HPLC)-MS, internal preparation standards were added to 0.1 to 15 mg of freeze-dried biomass. The internal standards used for lipid extraction and analysis were 5- $\alpha$ -cholestane (CAS no. 566 481-21-0) and 1,2-Di-O-octadecyl-rac-glycerol (DAGE)  $\text{C}_{18:18}$  (CAS no. 6076-38-6), both at concentrations of 100 mg/L. The concentration of the internal standard added was adjusted depending on the amount of biomass used for extraction. After the addition of the internal standards, the aliquot was subjected to acid hydrolysis with HCl (10%) at  $110^\circ\text{C}$  for 2 h. Subsequently, lipids were extracted four times with *n*-hexane-Dichloromethane (DCM) (4:1, vol/vol) in an ultrasonic bath to obtain the total lipid extract (TLE). An aliquot of the TLE was derivatized with acetic anhydride and pyridine (1:1, vol/vol) at  $60^\circ\text{C}$  for 1 h, after which the TLE was stored overnight at room temperature (ca.  $20^\circ\text{C}$ ) before GC-MS and GC-flame ionization detection (FID) analyses, to derivatize the compounds completely.

A Thermo Scientific Trace Ultra gas chromatograph coupled to a Thermo Scientific DSQ II mass spectrometer was used for compound identification. The GC-FID instruments used were Fisons Instruments



GC 8000 series and Fisons Instruments HRGC Mega 2 series instruments. Both instruments were used for the quantification of diether lipids as a control for the HPLC-atmospheric pressure chemical ionization (APCI)-MS measurements (compare the data in references 33 and 37). A detailed description of the GC methods was reported previously (37). In brief, the measurements on the GC-MS instrument were done on a Thermo Scientific Trace GC Ultra gas chromatograph coupled to a Thermo Scientific DSQ II mass spectrometer for identification, whereas the contents were measured with a Fisons Instruments GC 8000 series instrument equipped with a flame ionization detector. The column used for both GC systems was an Agilent HP-5 MS UI fused silica column (length, 30 m; inner diameter [ID], 0.25 mm; film thickness, 0.25  $\mu\text{m}$ ). The GC temperature program for both GC-MS and GC-FID was as follows: 50°C for 3 min, 25°C  $\text{min}^{-1}$  to 230°C with a hold for 2 min, and 6°C for 7 min to 325°C with a final hold for 25 min at 325°C. The response factor between 5- $\alpha$ -cholestane and DAGE  $\text{C}_{18:18}$  was 1.6:1 on both GC-FID instruments.

Apart from this, archaeal di- and tetraether lipids were determined using a Varian MS Workstation 6.91 HPLC system coupled to a Varian 1200L triple-quadrupole mass spectrometer with an APCI interface operated in positive-ion mode. Separation was achieved on a Grace Prevail Cyano column (150 mm by 2.1 mm, 3- $\mu\text{m}$  particle size) and a guard column of the same material, both held at a temperature of 30°C. The column was used at 30°C. The gradient program used was a linear change from 97.5% *n*-hexane and 2.5% *n*-hexane-2-propanol (90:10, vol/vol) to 75% *n*-hexane and 25% *n*-hexane-2-propanol (90:10, vol/vol) from 0 to 35 min, then linearly to 100% *n*-hexane-2-propanol (90:10, vol/vol) in 5 min with a hold for 8 min, and finally back to 97.5% *n*-hexane and 2.5% *n*-hexane-2-propanol (90:10, vol/vol) for reequilibration of column for 12 min. The solvent flow rate was constant at 0.3  $\text{mL min}^{-1}$ .  $\text{C}_{46}$ -GDGT (CAS no. 138456-87-8) was added as an internal standard to unfiltered and underivatized dry aliquots of the TLE prior to injection. For HPLC measurements, between 5 and 20% of the total lipid extracts were used for injections. The  $\text{C}_{46}$  GDGT standard (CAS no. 138456-87-8) (53) was injected at a concentration of 12  $\text{mg L}^{-1}$ , which is in the same range as the concentrations of the internal standards in the injection vials and those added prior to hydrolysis (see reference 37 for details). The response factors between archaeal di- and tetraether lipids were constantly monitored using a standard mixture, which was injected after every 4 to 5 samples. The standard mixture was prepared from synthetic archaeol (1,2-di-O-phytanyl-*sn*-glycerol) (CAS no. 99341-19-2), DAGE  $\text{C}_{18:18}$ , DAGE  $\text{C}_{18:18}$ -4ene (1,3-dilinoleoyl-*rac*-glycerol) (CAS no. 15818-46-9), and  $\text{C}_{46}$  GDGT. The response factor between DAGE  $\text{C}_{18:18}$  and  $\text{C}_{46}$  GDGT was usually between 1.5:1 and 2:1. The response factor between synthetic archaeol and  $\text{C}_{46}$  GDGT was usually around 1.5:1. The response factor between the diester DAGE  $\text{C}_{18:18}$ -4ene and  $\text{C}_{46}$  GDGT was not used for this study. The response factors between  $\text{C}_{46}$  GDGT and the glycerol dialkyl diethers GDD-0 and GMD-0 could not be determined since there was no standard available. Due to the similar structures, a response factor similar to the one for the tetraether lipids was assumed. Hence, the concentrations of GDD-0 and GMD-0 may include errors and must be taken with caution.

Structural identification of archaeal di- and tetraether lipids was conducted using HPLC-APCI-tandem MS (MS/MS) (37). Aliquots of the TLEs were dissolved in *n*-hexane-2-propanol (99:1, vol/vol) to a concentration of 1  $\text{mg mL}^{-1}$  and filtered through a 0.45- $\mu\text{m}$  polytetrafluoroethylene (PTFE) filter prior to analysis. Normal-phase HPLC was conducted using a Waters Alliance 2690 HPLC system fitted with a Grace Prevail Cyano column (150- by 2.1-mm ID, 3- $\mu\text{m}$  particle size) and a security guard column cartridge of the same material. MS/MS experiments were done using a Micromass Quattro LC triple-quadrupole mass spectrometer equipped with an APCI interface operated in positive-ion mode. Structural identification of archaeal lipids was done by comparison with published mass spectra (51, 54–56). Chromatograms showing the distribution of the archaeal lipids are provided in Fig. S4 in the supplemental material (see also references 37 and 51).

As the incubation time varied from one experiment to the other, the amino acid and lipid concentrations were normalized by dividing by the respective total incubation times. The obtained values are described as AAERs and (specific) lipid production rates, respectively. The values for the amino acids cysteine, selenocysteine, pyrrolysine, and proline were below the detection limit.

For half of the experiments with *M. villosus*, i.e., all with combinations of 65°C with twice-per-day gassing and 80°C with once-per-day gassing, the concentrations were determined using 5- $\alpha$ -cholestane and  $\text{C}_{46}$  GDGT instead of DAGE  $\text{C}_{18:18}$  and  $\text{C}_{46}$  GDGT. Quantification with 5- $\alpha$ -cholestane led to 20%-higher specific lipid production rates than by quantification with DAGE  $\text{C}_{18:18}$ . This was corrected by applying a compensation factor of 0.8.

**Dry weight determination.** All organisms were grown to a minimal optical density at 578 nm ( $\text{OD}_{578}$ ) of 0.3 in serum flasks. Ten milliliters of undiluted and diluted (1:2, 1:3, 1:4, 1:5, 1:7, 1:8, and 1:10) samples in quadruplicates ( $n = 4$ ) was pipetted onto a 0.22- $\mu\text{m}$  Durapore membrane filter (Merck Millipore, MA, USA) connected to and vacuumed on a glass filtering apparatus (Duran, Wertheim, Germany). Filters were dried overnight at 75°C and weighed before and after the addition of biomass. The biomass (milligrams) was plotted against the  $\text{OD}_{578}$  values. The resulting *k*-value was used as the factor to calculate biomass (in grams per liter) (10). The *k*-values were 0.36 for *M. marburgensis*, 0.49 for *M. okinawensis*, and 0.31 for *M. villosus*. The *k*-values in combination with the  $\text{OD}_{578}$  values were used for the calculation of the viable and unviable biomasses (in grams per liter) in the course of the lysis and fluorescence-activated cell sorting (FACS) experiments (see Fig. S2 in the supplemental material).

**Fluorescence-activated cell sorting measurement.** For cell viability analysis, FACS measurement was applied. Briefly, 20  $\mu\text{L}$  of an actively growing culture was diluted with 400  $\mu\text{L}$  of the respective minimal media, stained with Syto9 and propidium iodide (PI) (Live/Dead BacLight bacterial viability kit; Invitrogen), and analyzed (FACSCanto II; BD) (Syto9, fluorescein isothiocyanate [FITC]; PI, peridinin chlorophyll protein [PerCP]-Cy5-5H). Fluorescence compensation was performed using BD FACSDiva software. For each measurement, 10,000 events were recorded and gated (Fig. S1). Cell counts were performed as previously described (57). Total amino acid contents and dead/live biomass contents of *M. marburgensis*, *M. okinawensis*, and *M. villosus* are given in Fig. S2.

**NH<sub>4</sub><sup>+</sup> uptake determination.** NH<sub>4</sub><sup>+</sup> uptake determination was performed using a modified procedure described previously (58). The oxidation solution, the color reagent, and the NH<sub>4</sub>Cl stock solution were prepared freshly before measurements. As standards, nine different concentrations ranging from 100  $\mu\text{mol L}^{-1}$  to 1,000  $\mu\text{mol L}^{-1}$  of NH<sub>4</sub>Cl were prepared. Samples were diluted with MilliQ water to a final concentration between the standard ranges. Before measurements, 300  $\mu\text{L}$  of color reagent and 120  $\mu\text{L}$  of oxidation solution were added immediately to the standards and samples, which were then mixed briefly. After 30 min in the dark, standards and samples were measured at 660 nm on a 96-well plate (Microtest plate 96 well, F; Sarstedt AG & Co., Nümbrecht, Germany) with a plate photometer (Sunrise plate reader; Tecan Group AG, Männedorf, Switzerland). The regression curve always had an  $R^2$  value of  $>0.999$ . Results are presented in Fig. S2 and S3. Here, the value of the zero control was always subtracted to receive the actual NH<sub>4</sub><sup>+</sup> uptake (rate).

**Statistical analysis.** Outliers in the data set were identified and excluded when the respective values showed a deviation of more than 100% relative to the mean value of the other replicates from the same experimental set. When two (or more) values showed this characteristic, none were excluded. Furthermore, for some single amino acids or lipids, a value was not determinable. Some of the single values were negative. Negative values indicate that the concentration measured in the negative control was higher than that in the respective replicate (bottle). These negative values were neglected when calculating the total number. The total values presented in the figures were calculated as the mean values for the total amino acids or lipids from every single replicate (bottle) of the respective experiment.

**Data availability.** The comprehensive collection of the raw data has been deposited in the Phaidra online repository (<https://doi.org/10.25365/phaidra.380>) (59).

## SUPPLEMENTAL MATERIAL

Supplemental material is available online only.

**FIG S1**, PDF file, 0.1 MB.

**FIG S2**, PDF file, 0.1 MB.

**FIG S3**, PDF file, 0.2 MB.

**FIG S4**, PDF file, 0.1 MB.

## ACKNOWLEDGMENTS

We greatly acknowledge the Österreichische Forschungsförderungsgesellschaft (FFG) for funding the projects BioHyMe (grant 853615) and NitroFix (grant 859293) and funding from the Austrian Science Fund (FWF), project P29399-B22. Furthermore, we acknowledge financial support through the LIT Energy Lab, which is funded by the Johannes Kepler University Linz and the Federal Province of Upper Austria. The funders had no role in study design, data collection and interpretation, or the decision to submit the work for publication. R.-S.T. was partly financed by a fellowship from L'Oréal Österreich. Open-access funding is provided by the FWF.

We thank the anonymous reviewers who helped to improve the manuscript.

B.R. and S.K.-M.R.R. declare competing financial interests due to their employment at Arkeon GmbH.

## REFERENCES

- Garcia J-L, Patel BKC, Ollivier B. 2000. Taxonomic, phylogenetic, and ecological diversity of methanogenic archaea. *Anaerobe* 6:205–226. <https://doi.org/10.1006/anae.2000.0345>.
- Liu Y, Whitman WB. 2008. Metabolic, phylogenetic, and ecological diversity of the methanogenic archaea. *Ann N Y Acad Sci* 1125:171–189. <https://doi.org/10.1196/annals.1419.019>.
- Taubner R-S, Schleper C, Firneis MG, Rittmann SK-MR. 2015. Assessing the ecophysiology of methanogens in the context of recent astrobiological and planetological studies. *Life (Basel)* 5:1652–1686. <https://doi.org/10.3390/life5041652>.
- Zwicker J, Birgel D, Bach W, Richoz S, Smrzka D, Grasmann B, Gier S, Schleper C, Rittmann SK-MR, Koşun E, Peckmann J. 2018. Evidence for archaeal methanogenesis within veins at the onshore serpentinite-hosted Chimaera seeps, Turkey. *Chem Geol* 483:567–580. <https://doi.org/10.1016/j.chemgeo.2018.03.027>.
- McKay CP, Porco CC, Altheide T, Davis WL, Kral TA. 2008. The possible origin and persistence of life on Enceladus and detection of biomarkers in the plume. *Astrobiology* 8:909–919. <https://doi.org/10.1089/ast.2008.0265>.
- Taubner R-S, Pappenreiter P, Zwicker J, Smrzka D, Pruckner C, Kolar P, Bernacchi S, Seifert AH, Krajete A, Bach W, Peckmann J, Paulik C, Firneis MG, Schleper C, Rittmann SK-MR. 2018. Biological methane production under putative Enceladus-like conditions. *Nat Commun* 9:748. <https://doi.org/10.1038/s41467-018-02876-y>.
- Offre P, Spang A, Schleper C. 2013. Archaea in biogeochemical cycles. *Annu Rev Microbiol* 67:437–457. <https://doi.org/10.1146/annurev-micro-092412-155614>.
- Patel GB, Sprott GD. 1999. Archaeobacterial ether lipid liposomes (archaeosomes) as novel vaccine and drug delivery systems. *Crit Rev Biotechnol* 19:317–357. <https://doi.org/10.1080/0738-859991229170>.
- Rittmann SK-MR, Seifert AH, Bernacchi S. 2018. Kinetics, multivariate statistical modelling, and physiology of CO<sub>2</sub>-based biological methane production. *Appl Energy* 216:751–760. <https://doi.org/10.1016/j.apenergy.2018.01.075>.
- Taubner R-S, Rittmann SK-MR. 2016. Method for indirect quantification of CH<sub>4</sub> production via H<sub>2</sub>O production using hydrogenotrophic methanogens. *Front Microbiol* 7:532. <https://doi.org/10.3389/fmicb.2016.00532>.
- Abdel Azim A, Pruckner C, Kolar P, Taubner R-S, Fino D, Saracco G, Sousa FL, Rittmann SK-MR. 2017. The physiology of trace elements in biological methane production. *Bioresour Technol* 241:775–786. <https://doi.org/10.1016/j.biortech.2017.05.211>.
- D'Este M, Alvarado-Morales M, Angelidaki I. 2018. Amino acids production focusing on fermentation technologies—a review. *Biotechnol Adv* 36:14–25. <https://doi.org/10.1016/j.biotechadv.2017.09.001>.

13. Pfeifer K, Ergal I, Koller M, Basen M, Schuster B, Rittmann SK-MR. 2021. Archaea biotechnology. *Biotechnol Adv* 47:107668. <https://doi.org/10.1016/j.biotechadv.2020.107668>.
14. Abdel Azim A, Rittmann SK-MR, Fino D, Bochmann G. 2018. The physiological effect of heavy metals and volatile fatty acids on *Methanococcus maripaludis* S2. *Biotechnol Biofuels* 11:301. <https://doi.org/10.1186/s13068-018-1302-x>.
15. Mauerhofer L-M, Reischl B, Schmider T, Schupp B, Nagy K, Pappenreiter P, Zwirtmayr S, Schuster B, Bernacchi S, Seifert AH, Paulik C, Rittmann SK-MR. 2018. Physiology and methane productivity of *Methanobacterium thermaggregans*. *Appl Microbiol Biotechnol* 102:7643–7656. <https://doi.org/10.1007/s00253-018-9183-2>.
16. Mauerhofer L-M, Zwirtmayr S, Pappenreiter P, Bernacchi S, Seifert AH, Reischl B, Schmider T, Taubner R-S, Paulik C, Rittmann SK-MR. 2021. Hyperthermophilic methanogenic archaea are high-pressure CH<sub>4</sub> cell factories. *Commun Biol* 4:289. <https://doi.org/10.1038/s42003-021-01828-5>.
17. Whitman WB, Ankwarda E, Wolfe RS. 1982. Nutrition and carbon metabolism of *Methanococcus voltae*. *J Bacteriol* 149:852–863. <https://doi.org/10.1128/jb.149.3.852-863.1982>.
18. Grochowski LL, White RH. 2008. Promiscuous anaerobes: new and unconventional metabolism in methanogenic archaea. *Ann N Y Acad Sci* 1125:190–214. <https://doi.org/10.1196/annals.1419.001>.
19. Imachi H, Nobu MK, Nakahara N, Morono Y, Ogawara M, Takaki Y, Takano Y, Uematsu K, Ikuta T, Ito M, Matsui Y, Miyazaki M, Murata K, Saito Y, Sakai S, Song C, Tasumi E, Yamanaka Y, Yamaguchi T, Kamagata Y, Tamaki H, Takai K. 2020. Isolation of an archaeon at the prokaryote-eukaryote interface. *Nature* 577:519–525. <https://doi.org/10.1038/s41586-019-1916-6>.
20. Ratledge C. 1991. Microorganisms for lipids. *Acta Biotechnol* 11:429–438. <https://doi.org/10.1002/abio.370110506>.
21. Muralitharan G, Gayathri M, Shunmugam S. 2019. Qualitative and quantitative estimation of bacterial lipid production. *Methods Mol Biol* 1995:91–101. [https://doi.org/10.1007/978-1-4939-9484-7\\_4](https://doi.org/10.1007/978-1-4939-9484-7_4).
22. Ji X-J, Ledesma-Amaro R. 2020. Microbial lipid biotechnology to produce polyunsaturated fatty acids. *Trends Biotechnol* 38:832–834. <https://doi.org/10.1016/j.tibtech.2020.02.003>.
23. De Rosa M, Gambacorta A. 1988. The lipids of archaeobacteria. *Prog Lipid Res* 27:153–175. [https://doi.org/10.1016/0163-7827\(88\)90011-2](https://doi.org/10.1016/0163-7827(88)90011-2).
24. Benvegnu T, Lemiègre L, Cammas-Marion S. 2008. Archaeal lipids: innovative materials for biotechnological applications. *Eur J Org Chem* 2008:4725–4744. <https://doi.org/10.1002/ejoc.200800452>.
25. Straub CT, Counts JA, Nguyen DMN, Wu C-H, Zeldes BM, Crosby JR, Conway JM, Otten JK, Lipscomb GL, Schut GJ, Adams MWW, Kelly RM. 2018. Biotechnology of extremely thermophilic archaea. *FEMS Microbiol Rev* 42:543–578. <https://doi.org/10.1093/femsre/fuy012>.
26. Kaur G, Garg T, Rath G, Goyal AK. 2016. Archaeosomes: an excellent carrier for drug and cell delivery. *Drug Deliv* 23:2497–2512. <https://doi.org/10.3109/10717544.2015.1019653>.
27. Liefelth K, Frant M, Müller U, Stenstad P, Johnsen H, Schmid R. 2018. Archaeal tetraether lipid coatings—a strategy for the development of membrane analog spacer systems for the site-specific functionalization of medical surfaces. *Biointerphases* 13:011004. <https://doi.org/10.1116/1.5008816>.
28. Sprott GD, Meloche M, Richards JC. 1991. Proportions of diether, macrocyclic diether, and tetraether lipids in *Methanococcus jannaschii* grown at different temperatures. *J Bacteriol* 173:3907–3910. <https://doi.org/10.1128/jb.173.12.3907-3910.1991>.
29. Kaneshiro SM, Clark DS. 1995. Pressure effects on the composition and thermal behavior of lipids from the deep-sea thermophile *Methanococcus jannaschii*. *J Bacteriol* 177:3668–3672. <https://doi.org/10.1128/jb.177.13.3668-3672.1995>.
30. Jones WJ, Leigh JA, Mayer F, Woese CR, Wolfe RS. 1983. *Methanococcus jannaschii* sp. nov., an extremely thermophilic methanogen from a submarine hydrothermal vent. *Arch Microbiol* 136:254–261. <https://doi.org/10.1007/BF00425213>.
31. Yoshinaga MY, Gagen EJ, Wörmer L, Broda NK, Meador TB, Wendt J, Thomm M, Hinrichs K-U. 2015. Methanothermobacter thermotrophicus modulates its membrane lipids in response to hydrogen and nutrient availability. *Front Microbiol* 6:5. <https://doi.org/10.3389/fmicb.2015.00005>.
32. Wasserfallen A, Nölling J, Pfister P, Reeve J, Conway de Macario E. 2000. Phylogenetic analysis of 18 thermophilic *Methanobacterium* isolates supports the proposals to create a new genus, *Methanothermobacter* gen. nov., and to reclassify several isolates in three species, *Methanothermobacter thermotrophicus* comb. nov., *Methanothermobacter wolfeii* comb. nov., and *Methanothermobacter marburgensis* sp. nov. *Int J Syst Evol Microbiol* 50:43–53. <https://doi.org/10.1099/00207713-50-1-43>.
33. Taubner R-S, Baumann LMF, Bauersachs T, Clifford EL, Mähnert B, Reischl B, Seifert R, Peckmann J, Rittmann SK-MR, Birgel D. 2019. Membrane lipid composition and amino acid excretion patterns of *Methanothermobacter okinawensis* grown in the presence of inhibitors detected in the Enceladian plume. *Life (Basel)* 9:85. <https://doi.org/10.3390/life9040085>.
34. Takai K, Inoue A, Horikoshi K. 2002. *Methanothermobacter okinawensis* sp. nov., a thermophilic, methane-producing archaeon isolated from a Western Pacific deep-sea hydrothermal vent system. *Int J Syst Evol Microbiol* 52:1089–1095. <https://doi.org/10.1099/00207713-52-4-1089>.
35. Bellack A, Huber H, Rachel R, Wanner G, Wirth R. 2011. *Methanocaldococcus villosus* sp. nov., a heavily flagellated archaeon that adheres to surfaces and forms cell-cell contacts. *Int J Syst Evol Microbiol* 61:1239–1245. <https://doi.org/10.1099/ijs.0.023663-0>.
36. Rittmann S, Seifert A, Herwig C. 2012. Quantitative analysis of media dilution rate effects on *Methanothermobacter marburgensis* grown in continuous culture on H<sub>2</sub> and CO<sub>2</sub>. *Biomass Bioenergy* 36:293–301. <https://doi.org/10.1016/j.biombioe.2011.10.038>.
37. Baumann LMF, Taubner R-S, Bauersachs T, Steiner M, Schleper C, Peckmann J, Rittmann SK-MR, Birgel D. 2018. Intact polar lipid and core lipid inventory of the hydrothermal vent methanogens *Methanocaldococcus villosus* and *Methanothermobacter okinawensis*. *Org Geochem* 126:33–42. <https://doi.org/10.1016/j.orggeochem.2018.10.006>.
38. Jarrell KF, Bird SE, Sprott GD. 1984. Sodium-dependent isoleucine transport in the methanogenic archaeobacterium *Methanococcus voltae*. *FEBS Lett* 166:357–361. [https://doi.org/10.1016/0014-5793\(84\)80112-X](https://doi.org/10.1016/0014-5793(84)80112-X).
39. Cohen-Kupiec R, Marx CJ, Leigh JA. 1999. Function and regulation of gltA in the methanogenic archaeon *Methanococcus maripaludis*. *J Bacteriol* 181:256–261. <https://doi.org/10.1128/JB.181.1.256-261.1999>.
40. Whitman WB, Sohn S, Kuk S, Xing R. 1987. Role of amino acids and vitamins in nutrition of mesophilic *Methanococcus* spp. *Appl Environ Microbiol* 53:2373–2378. <https://doi.org/10.1128/aem.53.10.2373-2378.1987>.
41. Ekiel I, Jarrell KF, Sprott GD. 1985. Amino acid biosynthesis and sodium-dependent transport in *Methanococcus voltae*, as revealed by <sup>13</sup>C NMR. *Eur J Biochem* 149:437–444. <https://doi.org/10.1111/j.1432-1033.1985.tb08944.x>.
42. Bhatnagar L, Jain MK, Aubert J-P, Zeikus JG. 1984. Comparison of assimilatory organic nitrogen, sulfur, and carbon sources for growth of *Methanobacterium* species. *Appl Environ Microbiol* 48:785–790. <https://doi.org/10.1128/aem.48.4.785-790.1984>.
43. Daniels L, Zeikus JG. 1978. One-carbon metabolism in methanogenic bacteria: analysis of short-term fixation products of <sup>14</sup>C CO<sub>2</sub> and <sup>14</sup>CH<sub>3</sub>OH incorporated into whole cells. *J Bacteriol* 136:75–84. <https://doi.org/10.1128/jb.136.1.75-84.1978>.
44. Fuchs G, Stupperich E, Thauer RK. 1978. Acetate assimilation and the synthesis of alanine, aspartate and glutamate in *Methanobacterium thermoautotrophicum*. *Arch Microbiol* 117:61–66. <https://doi.org/10.1007/BF00689352>.
45. Hendrickson EL, Liu Y, Rosas-Sandoval G, Porat I, Söll D, Whitman WB, Leigh JA. 2008. Global responses of *Methanococcus maripaludis* to specific nutrient limitations and growth rate. *J Bacteriol* 190:2198–2205. <https://doi.org/10.1128/JB.01805-07>.
46. Shieh J, Mesbah M, Whitman WB. 1988. Pseudoauxotrophy of *Methanococcus voltae* for acetate, leucine, and isoleucine. *J Bacteriol* 170:4091–4096. <https://doi.org/10.1128/jb.170.9.4091-4096.1988>.
47. Koga Y. 2012. Thermal adaptation of the archaeal and bacterial lipid membranes. *Archaea* 2012:789652. <https://doi.org/10.1155/2012/789652>.
48. Siliakus MF, van der Oost J, Kengen SWM. 2017. Adaptations of archaeal and bacterial membranes to variations in temperature, pH and pressure. *Extremophiles* 21:651–670. <https://doi.org/10.1007/s00792-017-0939-x>.
49. Cario A, Grossi V, Schaeffer P, Oger PM. 2015. Membrane homeoviscous adaptation in the piezo-hyperthermophilic archaeon *Thermococcus barophilus*. *Front Microbiol* 6:1152. <https://doi.org/10.3389/fmicb.2015.01152>.
50. Dannenmüller O, Arakawa K, Eguchi T, Kakinuma K, Blanc S, Albrecht A-M, Schmutz M, Nakatani Y, Ourisson G. 2000. Membrane properties of archaeal macrocyclic diether phospholipids. *Chemistry* 6:645–654. [https://doi.org/10.1002/\(SICI\)1521-3765\(20000218\)6:4<645::AID-CHEM645>3.0.CO;2-A](https://doi.org/10.1002/(SICI)1521-3765(20000218)6:4<645::AID-CHEM645>3.0.CO;2-A).
51. Knappy C, Barillà D, Chong J, Hodgson D, Morgan H, Suleman M, Tan C, Yao P, Keely B. 2015. Mono-, di- and trimethylated homologues of isoprenoid tetraether lipid cores in archaea and environmental samples: mass spectrometric identification and significance. *J Mass Spectrom* 50:1420–1432. <https://doi.org/10.1002/jms.3709>.
52. Littlechild JA. 2015. Archaeal enzymes and applications in industrial biocatalysts. *Archaea* 2015:147671. <https://doi.org/10.1155/2015/147671>.
53. Huguet C, Hopmans EC, Febo-Ayala W, Thompson DH, Sinninghe Damsté JS, Schouten S. 2006. An improved method to determine the absolute

- abundance of glycerol dibiphytanyl glycerol tetraether lipids. *Org Geochem* 37:1036–1041. <https://doi.org/10.1016/j.orggeochem.2006.05.008>.
54. Knappy CS, Chong JPJ, Keely BJ. 2009. Rapid discrimination of archaeal tetraether lipid cores by liquid chromatography-tandem mass spectrometry. *J Am Soc Mass Spectrom* 20:51–59. <https://doi.org/10.1016/j.jasms.2008.09.015>.
55. Liu X-L, Lipp JS, Simpson JH, Lin Y-S, Summons RE, Hinrichs K-U. 2012. Mono- and dihydroxyl glycerol dibiphytanyl glycerol tetraethers in marine sediments: identification of both core and intact polar lipid forms. *Geochim Cosmochim Acta* 89:102–115. <https://doi.org/10.1016/j.gca.2012.04.053>.
56. Bauersachs T, Schwark L. 2016. Glycerol monoalkanediole diethers: a novel series of archaeal lipids detected in hydrothermal environments. *Rapid Commun Mass Spectrom* 30:54–60. <https://doi.org/10.1002/rcm.7417>.
57. Zink IA, Pfeifer K, Wimmer E, Sleytr UB, Schuster B, Schleper C. 2019. CRISPR-mediated gene silencing reveals involvement of the archaeal S-layer in cell division and virus infection. *Nat Commun* 10:4797. <https://doi.org/10.1038/s41467-019-12745-x>.
58. Kandeler E, Gerber H. 1988. Short-term assay of soil urease activity using colorimetric determination of ammonium. *Biol Fertil Soils* 6:68–72.
59. Taubner R-S, Rittmann SK-MR. 2023. Lipidomics and comparative metabolite excretion analysis of methanogenic archaea reveal organism-specific adaptations to varying temperature and substrate concentration: data Phaidra. <https://doi.org/10.25365/phaidra.380>.

# ANNEX 3

Pages 79 to 91

---

Pfeifer K., Ehmoser E.-K., Rittmann S.K.-M.R., Schleper C., Pum D., Sleytr U.B., Schuster B.

**Isolation and characterization of cell envelope fragments comprising archaeal S-layer proteins**

Nanomaterials (2022) 12(14):2502

10.3390/nano12142502

---



## Article

# Isolation and Characterization of Cell Envelope Fragments Comprising Archaeal S-Layer Proteins

Kevin Pfeifer <sup>1</sup>, Eva-Kathrin Ehmoser <sup>1</sup> , Simon K.-M. R. Rittmann <sup>2,3</sup> , Christa Schleper <sup>4</sup>, Dietmar Pum <sup>5</sup> , Uwe B. Sleytr <sup>1</sup> and Bernhard Schuster <sup>1,\*</sup>

<sup>1</sup> Institute of Synthetic Bioarchitectures, University of Natural Resources and Life Sciences, 1190 Vienna, Austria; kevinpfeifer@boku.ac.at (K.P.); eva.ehmoser@boku.ac.at (E.-K.E.); uwe.sleytr@boku.ac.at (U.B.S.)

<sup>2</sup> Archaea Physiology & Biotechnology Group, Department of Functional and Evolutionary Ecology, University of Vienna, 1030 Vienna, Austria; simon.rittmann@univie.ac.at

<sup>3</sup> Arkeon GmbH, 3430 Tulln an der Donau, Austria

<sup>4</sup> Archaea Biology and Ecogenomics Division, Department of Functional and Evolutionary Ecology, University of Vienna, 1030 Vienna, Austria; christa.schleper@univie.ac.at

<sup>5</sup> Institute of Biophysics, University of Natural Resources and Life Sciences, 1190 Vienna, Austria; dietmar.pum@boku.ac.at

\* Correspondence: bernhard.schuster@boku.ac.at; Tel.: +43-1-47654-80436

**Abstract:** The outermost component of cell envelopes of most bacteria and almost all archaea comprise a protein lattice, which is termed Surface (S)-layer. The S-layer lattice constitutes a highly porous structure with regularly arranged pores in the nm-range. Some archaea thrive in extreme milieus, thus producing highly stable S-layer protein lattices that aid in protecting the organisms. In the present study, fragments of the cell envelope from the hyperthermophilic acidophilic archaeon *Saccharolobus solfataricus* P2 (SSO) have been isolated by two different methods and characterized. The organization of the fragments and the molecular sieving properties have been elucidated by transmission electron microscopy and by determining the retention efficiency of proteins varying in size, respectively. The porosity of the archaeal S-layer fragments was determined to be 45%. S-layer fragments of SSO showed a retention efficiency of up to 100% for proteins having a molecular mass of  $\geq 66$  kDa. Moreover, the extraction costs for SSO fragments have been reduced by more than 80% compared to conventional methods, which makes the use of these archaeal S-layer material economically attractive.

**Keywords:** archaea; S-layer protein; Archaea Biotechnology; molecular sieving; extraction method; biomimetics



**Citation:** Pfeifer, K.; Ehmoser, E.-K.; Rittmann, S.K.-M.R.; Schleper, C.; Pum, D.; Sleytr, U.B.; Schuster, B. Isolation and Characterization of Cell Envelope Fragments Comprising Archaeal S-Layer Proteins. *Nanomaterials* **2022**, *12*, 2502. <https://doi.org/10.3390/nano12142502>

Academic Editor: Bryant C. Nelson

Received: 10 June 2022

Accepted: 19 July 2022

Published: 21 July 2022

**Publisher's Note:** MDPI stays neutral with regard to jurisdictional claims in published maps and institutional affiliations.



**Copyright:** © 2022 by the authors. Licensee MDPI, Basel, Switzerland. This article is an open access article distributed under the terms and conditions of the Creative Commons Attribution (CC BY) license (<https://creativecommons.org/licenses/by/4.0/>).

## 1. Introduction

A proteinaceous array in bacterial cell envelope fragments was first suggested in the 1950s [1,2] and, approx. 15 years later, evidence could be provided that a protein layer is located as the outermost structure on the cell envelope surface of intact bacteria [3,4]. This so-called Surface(S)-layer can be found in most bacteria and almost all archaea [5–7]. S-layer proteins and glycoproteins (SLPs) form a crystalline and isoporous lattice, which covers the entirety of the cell surface [8,9]. The functions of the S-layer lattice are still not fully elucidated. *Deinococcus radiodurans*, a radiation-resistant bacterium, is one of the most studied model organisms for understanding the S-layers' architecture and its function [10–13]. Functional characterization of the S-layer of *D. radiodurans* confirmed its transport properties; the nonselective permeation of ions [12,14] showed activity with different types of amino acids, behaving as a sieve barrier able to protect while allowing exchange and communication with the environment [13]. Further studies on various organisms propose that the S-layer may act as an ion trap, molecular sieve, cell-shape determining component, and it has been shown to be involved in cell surface recognition



and cell division [6,15–18]. Because SLPs as the outermost cell envelope component are in direct contact with the environment, it has been proposed that the SLPs have evolved to contribute to the protection of the cells from the natural environments. This function is most conceivable for hyperthermophilic, acidophilic, and halophilic microorganisms [15,16,19]. Studies on SLPs across bacterial and archaeal kingdoms have shown that, although the protein sequences as well as tertiary and quaternary structures differ vastly among all studied samples, the lattices formed by the proteins always showed one of three basic symmetries, which are oblique (p1, p2), square (p4) or hexagonal (p3, p6). The unit cell dimensions of these geometries range from 3 to 30 nm with uniform pores in the range of 2 to 8 nm creating a structure with a porosity between 30 and 70% [6,20,21]. It has been shown that, under the proper conditions, purified bacterial SLPs can spontaneously reassemble into their native lattice geometry in solution, on solid supports, and on interphases like lipid films [6,22–24]. These properties highlight the vast potential of SLPs as building blocks in biobased materials with various applications such as biosensors, nanocarriers for drug/gene delivery, immobilization matrices, adjuvants, matrices for controlled biomineralization and as ultrafiltration membranes [6,25–28].

The present study focused on the S-layer large protein (SlaA) from *Saccharolobus solfataricus* P2 (SSO). SSO has its optimum growth conditions at 78 °C and pH 2.5. The cytoplasmic membrane is composed of (di)ether and (tetra)ether lipids, which allow archaea to adapt to harsh conditions [29,30]. The structure of the SSO S-layer has recently been studied at a 16 Å resolution and is composed of two SLPs: the surface exposed SlaA and transmembrane S-layer small protein SlaB [31]. SlaA and SlaB protein occur in a ratio of 2:1, with each unit cell containing three SlaA dimers and three SlaB monomers [7,26,31]. The SlaB stalk anchors the SlaA proteins to the cell surface creating a pseudo-periplasmic space of 25 nm in height, while the SlaA proteins organize into a lattice with a p3 symmetry featuring circular pores of ~4.5 and ~8 nm in diameter [31]. The high glycosylation of both SlaA and SlaB adds a layer of protective sugar coating, which may modulate the antifouling characteristics of the outermost cell envelope structure [32]. The native stability of these proteins against both extreme heat and acidic conditions, as well as the ease of cultivation of the strain, make SSO SLPs interesting building blocks for biotechnological applications.

SLPs from most organisms can be extracted by chemical or physical lysing of the cells and removing the released cytosolic components. The composition of the extracted cell envelope (type of underlying polymer (if any), Gram-positive or Gram-negative envelope structure, interaction with cytoplasmic membrane, chemistry of lipids, etc.), and thus the steps needed to purify the SLPs depend strongly on the respective organism. Most often hydrogen-bond breaking agents such as guanidine hydrochloride and urea or chelating agents such as EDTA are used to disassemble the extracted S-layer lattices and purify the SLPs. Once purified, it has been shown that the bacterial SLPs can spontaneously reassemble into their native lattice structure under proper conditions [6,22–24].

In the case of SSO, the extraction protocols found in recent publications are based on protocols developed for *Sulfolobus acidocaldarius* by Grogan and Michael et al. in the 1980s [33,34]. These protocols use detergents to chemically lyse the SSO cells and consequently remove the cytosolic fraction leaving behind a ghost cell, which is an empty shell of ether lipids and membrane associated proteins. In the case of SSO and other Sulfolobales, the SLPs are highly stable against various detergents; therefore, SLPs can be enriched from the ghosts by repeatedly washing them with detergents resulting in SlaA-enriched sacculi in the native cell shape (Figure S1 of Supplementary Materials) [34–36]. Although recent improvements have been proposed for the handling of the samples during the extraction process, the protocols have not been evaluated nor optimized for industrial applications.

## 2. Materials and Methods

### 2.1. Cultivation

*Saccharolobus solfataricus* P2 (SSO) was cultivated in 100 mL (50 mL *wt/vol*) or 1 L (500 mL *wt/vol*) flasks under shaking conditions at 78 °C, pH 3, in 50 mL Brock T/S medium



supplemented with 0.1% (*wt/vol*) tryptone (T) and 0.2% (*wt/vol*) (+)D-Sucrose (S). Table S1 of Supplementary Materials specifies the cost for the cultivation of SSO.

## 2.2. Extraction of SSO Ghosts and Production of SSO Sacculi and Fragments

SSO ghosts were isolated by the extraction method described by Gambelli et al. [31] using DNase (DNase-based Extraction of Ghosts; DEG) and by a modified extraction method as described below (Sonication-based Extraction of Ghosts; SEG). The sequential steps and terminologies throughout the SLP extraction process is shown in Figure S1 of Supplementary Materials. Cells were harvested from a 50 mL exponential growing culture by centrifugation at  $2000\times g$  for 30 min. The cells were resuspended in 10 mL Buffer A ( $10\text{ mmol L}^{-1}$  NaCl, 0.5% sodium lauroylsarcosine) and incubated at  $37\text{ }^{\circ}\text{C}$  and 80 rpm for 1 h. This buffer used in SEG differs from the DEG protocol in that no phenylmethylsulfonyl fluoride (PMSF;  $1\text{ mmol L}^{-1}$ ) was added, and DNase I ( $10\text{ }\mu\text{g mL}^{-1}$ ) digestion of DNA was omitted. Instead, the suspension was sonicated for 30 s with 10 A (Thermo Fischer Q700, Thermo Fisher Scientific Inc., Eindhoven, The Netherlands) to shear the DNA. Subsequently, the SSO ghosts were pelleted by centrifugation at  $20,000\times g$  for 30 min. The resultant pellet was resuspended in 10 mL buffer B ( $10\text{ mmol L}^{-1}$  NaCl,  $0.5\text{ mmol L}^{-1}$   $\text{MgSO}_4$ , 0.5% sodium dodecylsulfate (SDS)), incubated at  $40\text{ }^{\circ}\text{C}$  for 1 h and then pelleted by centrifugation at  $20,000\times g$  for 30 min. This process was repeated 3 times to completely remove lipids and SlaB. Subsequently, the obtained SSO sacculi comprising SlaA (UniProt KB entry: Q980C7) were washed twice with Milli-Q water (MQ). Protein concentration of the SSO sacculi was determined by spectrophotometric measurements (280 nm;  $\epsilon(\times 1000)$ : 177.6;  $M_r$  131 kDa). The sacculi produced by the SEG method have been used for all further experiments. An aliquot of SSO sacculi equating to 300  $\mu\text{g}$  protein was diluted to 2 mL with MQ and sonicated with 10 A for 15 s to gently break up the SSO sacculi to form large SSO fragments (Figure S1 of Supplementary Materials).

## 2.3. SDS Polyacrylamide Gel Electrophoresis (PAGE)

For all protein gels shown, samples were denatured in Laemmli Buffer at  $98\text{ }^{\circ}\text{C}$  for 20 min and run on a 4–12% Bis-Tris Gel (Invitrogen, NuPAGE Bis-Tris, Carlsbad, CA, USA) in MOPS buffer at 140 V until the smallest marker had reached the bottom of the gel. The gels were stained in a methanol free Coomassie-G250 solution by microwaving the stain covered gel for 45 s and subsequent shaking of the gel for 30 min. The gel was de-stained in MQ, imaged (Samsung, SM-G950F, Vienna, Austria), and processed in Photoshop.

## 2.4. Electron Microscopy

For transmission electron microscopy (TEM), 10  $\mu\text{L}$  samples were incubated on a glow discharged grid (CF100H-Cu, EMS) for 2 min and stained with 2% uranyl acetate for 30 s. All samples were analyzed using a Libra 120 microscope (Zeiss, Wetzlar, Germany). Fourier domain processing was used to enhance the signal-to-noise ratio in the TEM images. The image processing routines were developed in-house as plugins for the open-source software ImageJ [37]. The central part of the Fourier spectrum of a TEM image of an SSO fragment is shown in Figure S2 of Supplementary Materials.

Samples were characterized by a scanning electron microscope (SEM) with a Thermo Fisher Scientific Apreo VS SEM (Thermo Fisher Scientific Inc., Eindhoven, The Netherlands). For this purpose, the filter membranes were cut into approx.  $7\times 7\text{ mm}$  sized pieces and fixed with a conductive double sticky tape on standard 0.5" aluminum stubs. The SEM was operated at 5.0 kV with a beam current of 0.1 nA in standard mode. Images were recorded in high vacuum with the standard electron detector.

## 2.5. Deposition of SSO Fragments on Microfilters

The 2 mL SSO fragment suspension containing 300  $\mu\text{g}$  protein (this equals 60  $\mu\text{g}$  protein per  $\text{cm}^2$  microfilter area) was filled up to 12 mL MQ. An Amicon<sup>®</sup> cell equipped with magnet stirrer and a volume of 12 mL was assembled with a microfilter clamped by

an O-ring to the bottom the cell. Two different microfilters that were 2.5 cm in diameter and having a pore size 0.2 µm were used: a track-etched hydrophilic polycarbonate filter (MF1; Millipore, Darmstadt, Germany, GTTP02500) and a foam-like cellulose acetate filter (MF2; Sartorius AG, Göttingen, Germany, 11107-25-N) (see Figure S3 of Supplementary Materials) [38]. The microfilters were washed with MQ prior to use. The suspended SSO fragments were transferred into the Amicon® cell. In all washing steps and filtration experiments, a pressure of 2 bar was applied to the Amicon® cell and the stirring speed was 200 rpm at room temperature (22 °C). The SSO fragments collected on MF1 or MF2 were chemically cross-linked with 5 mL 2.5% glutaraldehyde for 20 min. The cross-linked SSO fragments on MF1 or MF2, further referred to as SSOMF1 and SSOMF2, respectively were washed twice by running 10 mL MQ through the composite structure. The integrity of SSOMF1 and SSOMF2 was checked by filtration of a solution of ferritin (Sigma, Darmstadt, Germany: F4503; 0.7 g L<sup>-1</sup>) as described previously through spectrophotometry [38]. Ferritin, a large globular protein with a molecular mass of 474 kDa and a size of 12 nm, exceeds the size of the pores in the S-layer lattice at least by a factor of 1.5. Therefore, ferritin must be completely rejected by an intact layer of SSO fragments on the microfilters.

### 2.6. Investigation of Retention Efficiency against Proteins by SSO Fragments

To test the filter characteristics of the pores within the SSO fragments, 4 mL of 0.7 g L<sup>-1</sup> myoglobin (Sigma Aldrich, Darmstadt, Germany: M1882), carbonic anhydrase (Sigma Aldrich: C2624), horseradish peroxidase (Sigma Aldrich: 77332), bovine serum albumin (Sigma Aldrich: A2153), amyloglucosidase (Sigma Aldrich: 10115), and γ-globulin (Sigma Aldrich: G7516) were run through the SSO fragments in different order, i.e., from low molecular mass (M<sub>r</sub>) to high M<sub>r</sub> and *vice versa*. The retention efficiency of the deposited and cross-linked SSO fragments was determined by collecting the permeate after discarding the first milliliter. The measurements were performed in the Amicon® cell at 2 bar and a stirring speed of 200 rpm. The protein concentration of the feed (initial concentration) and permeate were measured using a Nanodrop spectrophotometer (ND-1000, PEQLAB Biotechnologie GmbH, Erlangen, Germany). The retention efficiency was calculated by:

$$\text{Retention efficiency [\%]} = \left( 1 - \frac{\text{Protein Concentration Permeate}}{\text{Protein Concentration Feed}} \right) \times 100$$

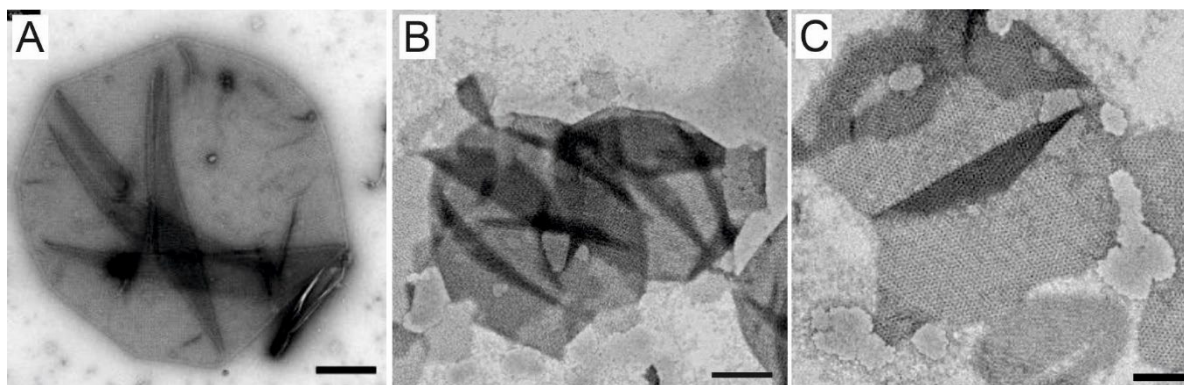
Between the runs, SSOMF1 and SSOMF2 were washed in the same orientation; then, filtration was performed with 10 mL MQ. Integrity and level of obstruction were inferred from the change in flux by measuring the time that it took to run 5 mL MQ through SSOMF1 and SSOMF2 with an active filtration area of 4.5 cm<sup>2</sup>. The concentration of all protein solutions used for filtration experiments was determined through spectrophotometry at 280 nm before (feed) and after (permeate) filtration.

## 3. Results and Discussion

### 3.1. A Modified and Cost-Effective Extraction Method for SSO Ghosts and Production of SSO Sacculi Comprising SlaA

Two different protocols to prepare SSO sacculi comprising SlaA from extracted SSO ghosts were conducted and evaluated for their effectiveness and costs. The established DEG method by Gambelli et al. [31] relies on DNase I for the digestion of the DNA, which is released during the chemical lysis of the cells. When calculating the extraction costs for SSO ghosts and subsequent sacculi production, it turned out that DNase I accounts for 58% of the material costs (Table S2 of Supplementary Materials). To reduce the extraction costs, DNase I was eliminated from the extraction protocol, and the DNA released during cell lysis was instead sheared through sonication. Furthermore, costs and handling efforts were reduced by removing the protease inhibitor PMSF from the extraction buffer and reducing the extraction volume from 40 mL to 10 mL per 50 mL culture. TEM images of the prepared ghosts showed that those resulting from the DEG method were largely intact and the S-layer appeared to retain the cell shape (Figure 1A). The ghosts prepared through

the SEG method, on the other hand, appeared slightly fragmented. The SEG method was refined to minimize damage to the ghosts, while sufficiently shearing the DNA to allow for processing (Figure 1B,C).

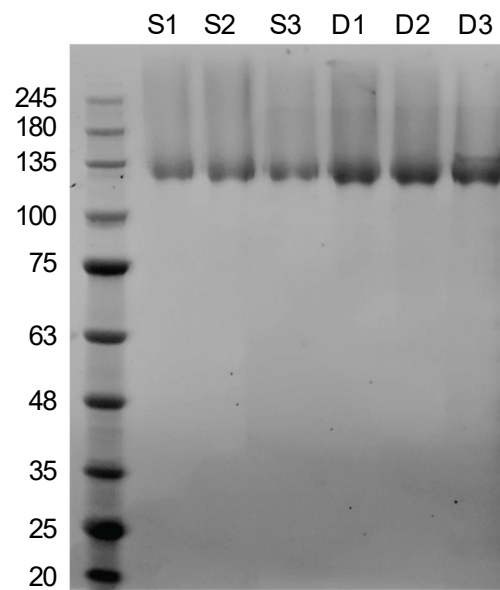


**Figure 1.** (A) *Saccharolobus solfataricus* P2 (SSO) ghost prepared using the extraction with DNase I (DEG). (B,C) SSO ghosts prepared using the extraction method with sonication (SEG). Scale Bars: A = 100 nm; B = 500 nm; C = 250 nm.

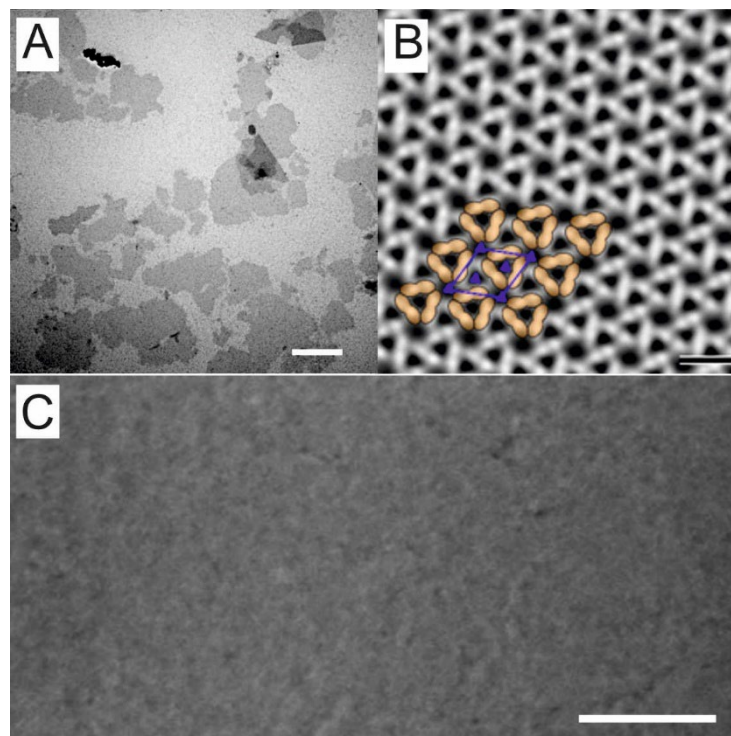
To compare the efficiency of the SEG to the DEG method, ghosts were prepared from three 50 mL cultures in the exponential growth phase with each extraction method. SDS-PAGE analysis of the extracts showed that both methods were successful in extracting ghosts and subsequent production of sacculi comprising SlaA by removing the intracellular components, lipids, and the membrane-hooked SlaB. While SEG samples showed reduced protein concentration compared to DEG samples, both extraction methods produced sacculi highly enriched in SlaA, which showed no noticeable impurities when analyzed using SDS-PAGE (Figure 2). The protein concentration of the purified SlaA proteins was determined spectrophotometrically resulting in a 21% decrease in protein concentration in the SEG samples ( $0.96 \text{ mg} \pm 0.06 \text{ mg}$ ) compared to the DEG samples ( $1.21 \text{ mg} \pm 0.08 \text{ mg}$ ). Although the yield of the SEG extraction method was lower, the costs per mg of SlaA extracted by sonication ( $0.17 \pm 0.01 \text{ € mg}^{-1}$ ;  $n = 3$ ) were 81% lower than those calculated for the DEG extraction method ( $0.84 \pm 0.05 \text{ € mg}^{-1}$ ;  $n = 3$ ) (Table S2 of Supplementary Materials). Furthermore, SEG with identical parameters was applied for the extraction of ghosts from 500 mL of culture, yielding ~10 mg enriched SlaA after processing. Therefore, the SEG method is a promising and scalable alternative to the established extraction methods and, by bringing down production costs, advances the biotechnological potential of archaeal S-layers.

### 3.2. Characterization of SSO Fragments on Microfilters

Having established a cost-efficient extraction method, the SSO fragments produced by the SEG method were investigated for their physicochemical parameters, filtration properties and thus potential biotechnological applications. For the construction of SSOMF1 and SSOMF2, ghosts comprising SlaA were extracted and purified from a 500 mL exponentially growing SSO culture with a yield of 10 mg. After sonication, TEM images revealed broken up SSO sacculi fragments ranging from 200 to >3000 nm in size (Figure 3A). The sonication step had to be optimized to obtain large fragments because both intact or partly fragmented sacculi and too small SSO fragments did not form a closed and coherent layer on the microfilters. Nevertheless, TEM investigations confirmed for large SSO fragments the two types of pores as previously described (Figure 3B) [31] and showed for the first time that the hexagonal p3 lattice of the SSO fragments exhibits a porosity of up to 45% (Figure S4 of Supplementary Materials). Moreover, it could be confirmed that the SSO fragment constitutes a crystalline patch formed by SlaA (Figure 3B).



**Figure 2.** SDS-PAGE (4–20% Bis-Tris, MES) S1–S3: 20  $\mu$ L of *Saccharolobus solfataricus* P2 (SSO) sacculi using the extraction method with sonication (SEG). D1–D3: 20  $\mu$ L of SSO sacculi using the established extraction method with DNase I (DEG). The first lane corresponds to molecular mass standard with ladder units in kDa.



**Figure 3.** (A) Transmission electron micrograph of *Saccharolobus solfataricus* P2 (SSO) fragments after sonication. Bar, 1000 nm; (B) computer image reconstruction (2D projection) of the p3-ordered hexagonal S-layer lattice from SSO. Shown are a unit cell and the corresponding three-fold axis of rotation (symmetry operators) in blue. The protein is light, the pores are dark. In addition, a possible configuration of proteins belonging to a unit cell is shown by strokes drawn by hand in orange. Bar, 20 nm; (C) scanning electron micrograph of SSO fragments deposited on microfilter 1 (100,000 $\times$  magnification). Bar, 500 nm.



This suspension of large SSO fragments was diluted, transferred onto M1 and M2 (Figure S3 of Supplementary Materials), forced to sediment by applying pressure, and finally chemically cross-linked. SEM images of SSOMF1 at a magnification of  $100,000\times$  showed that MF1 was completely covered by SSO fragments (Figure 3C). The integrity of SSOMF1 and SSOMF2 was checked by filtration of a ferritin solution. The retention efficiency of SSOMF2 was determined to be 100%, indicating that the SSO fragments could form a dense layer on MF2 due to its foam-like structure (Figure S3 of Supplementary Materials). For SSOMF1, however, not the entire ferritin could be rejected, indicating that the structure of MF1 did not allow the SSO fragments to be pushed into the microfilter structure and to form a totally dense filtration layer. With bacterial S-layer material, both types of microfilter could be tightly covered [25,38–41], but, for biotechnological utilization of these filter membranes, it turned out that open-celled foam-like microfilter membranes like MF2 gave better and more reproducible filtration membranes [38,41].

Plain MF1 and MF2 (Figure S3 of Supplementary Materials) evinced a water (MQ) flux of  $8800\text{ L h}^{-1}\text{ m}^{-2}$  and  $12,100\text{ L h}^{-1}\text{ m}^{-2}$ , respectively. The water flux of SSOMF1 and SSOMF2 was determined to be  $32\text{ L h}^{-1}\text{ m}^{-2}$  and  $60\text{ L h}^{-1}\text{ m}^{-2}$ , respectively. In comparison, a higher flux was determined for bacterial S-layer material (i.e., cell wall fragments and/or peptidoglycan-containing sacculi) deposited on microfilters. In place, the flux ranged from  $150\text{ L h}^{-1}\text{ m}^{-2}$  to  $250\text{ L h}^{-1}\text{ m}^{-2}$ , when measured at a pressure of 2 bar with MQ through a  $0.22\text{ }\mu\text{m}$  microfilter membrane. In general, the water flux strongly depends on the amount of S-layer protein deposited per membrane unit area as a noticeable flux decline is observed with increasing amounts of S-layer material. Interestingly, the latter showed no influencing effect on the rejection characteristics [38]. In turn, the S-layer material required for the formation of defects free filtration layer is determined by porosity, the pore size, and the pore size distribution of the supporting microfilter membrane [38,39,42]. The microfilters used with the bacterial S-layer material and archaeal ones are different and hence allow *per se* no conclusive comparison of the flux. The latter strongly depends on the nature of the supporting membrane as well as on the amount of S-layer material deposited [38]. A linear relationship between the flux and amount of S-layer material used per membrane unit area has been observed [25,40]. In the present study,  $60\text{ }\mu\text{g SLP per cm}^2$  microfilter area was used, whereas, in the bacterial system, in most cases, only half the amount of S-layer material was applied. This issue might be optimized so that a lower amount of archaeal S-layer material will be sufficient to obtain a dense and defect free filtration layer. However, this was not in the scope of the present study as the change of flux is not associated with alterations in retention efficiency of the SLP fragments. Another reason why the flux in the bacterial system is higher might be the fact that, in most cases, peptidoglycan-containing sacculi were deposited on microfilters, where peptidoglycan showed a much higher “pore” size and acted somehow as a spacer. In contrast, archaeal SSO fragments is comprised almost exclusively of the protein SlaA and thus may form a denser layer on microfilters.

To investigate the molecular sieving characteristics of the pores in SSO fragments, proteins varying in size were passed through the pores of the SSO fragments with pressure as a driving force (Table 1). SSOMF1 and SSOMF2 that remained intact after filtration were rinsed with MQ and reused for the next protein. To ensure that the retention efficiency of sequentially tested proteins was not affected, MQ flux was measured after rinsing, and protein solutions were passed through in various consecutive sequences. As shown in Table 1, Figures 4 and 5, and Figure S5 of Supplementary Materials, both SSOMF1 and SSOMF2 showed an increased retention efficiency for proteins with increasing  $M_r$ . This trend was observed no matter in which consecutive sequence the proteins (from small to large  $M_r$  or from large to small  $M_r$ ) were passed through the SSOMF filtration layer and when a mixture of proteins was filtered (Figure 4B; Figure S5 of Supplementary Materials).

**Table 1.** Molecular mass ( $M_r$ ), molecular size, and retention efficiency of *Saccharolobus solfataricus* P2 fragments deposited on microfilter 1 (SSOMF1) and 2 (SSOMF2), respectively, for selected proteins.

Protein	Molec. Mass $M_r$ (kDa)	Molecular Size (nm)	Retention Efficiency SSOMF1	Retention Efficiency SSOMF2
Myoglobin	17	$4.4 \times 4.4 \times 2.5$	$9\% \pm 4\%$ ; $n = 9$	$12\% \pm 7\%$ ; $n = 4$
Carbonic anhydrase	31	$4.1 \times 4.1 \times 4.7$	$66\% \pm 10\%$ ; $n = 9$	$63\% \pm 3\%$ ; $n = 4$
Horseradish peroxidase	44	$4.0 \times 6.7 \times 11.7$	$80\% \pm 12\%$ ; $n = 6$	$70\% \pm 5\%$ ; $n = 5$
Bovine serum albumin	66	$4.0 \times 4.0 \times 14.0$	$84\% \pm 9\%$ ; $n = 7$	$97\% \pm 3\%$ ; $n = 4$
Amylo-glucosidase	97	$5.7 \times 7.3 \times 10.7$	$88\% \pm 11\%$ ; $n = 9$	$98\% \pm 2\%$ ; $n = 4$
$\gamma$ -globulin	125	$4.5 \times 8.4 \times 14.5$	$84\% \pm 8\%$ ; $n = 6$	

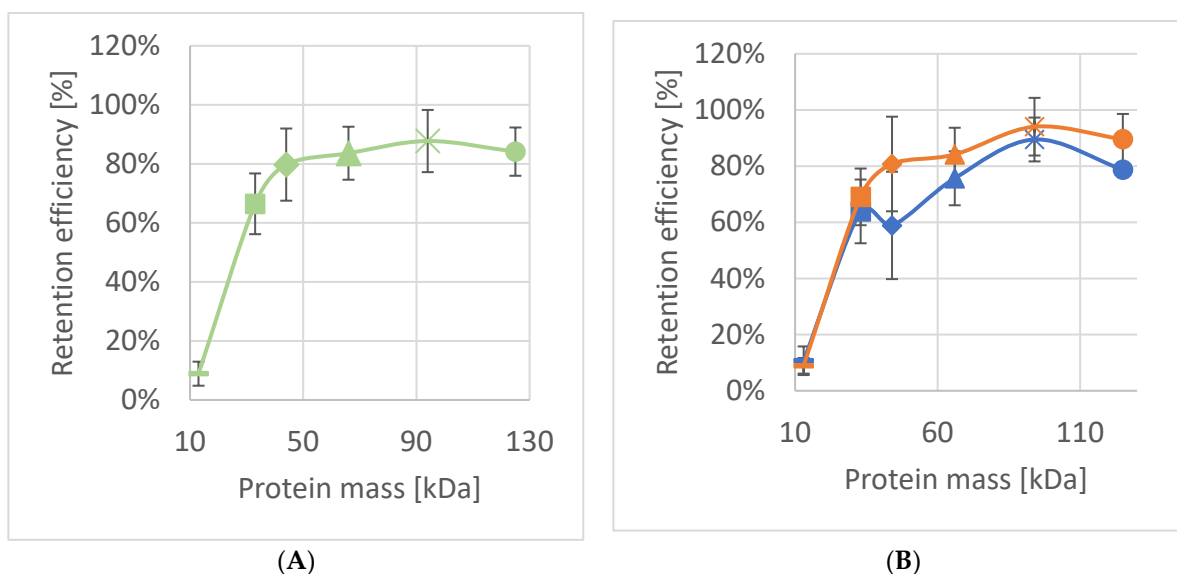
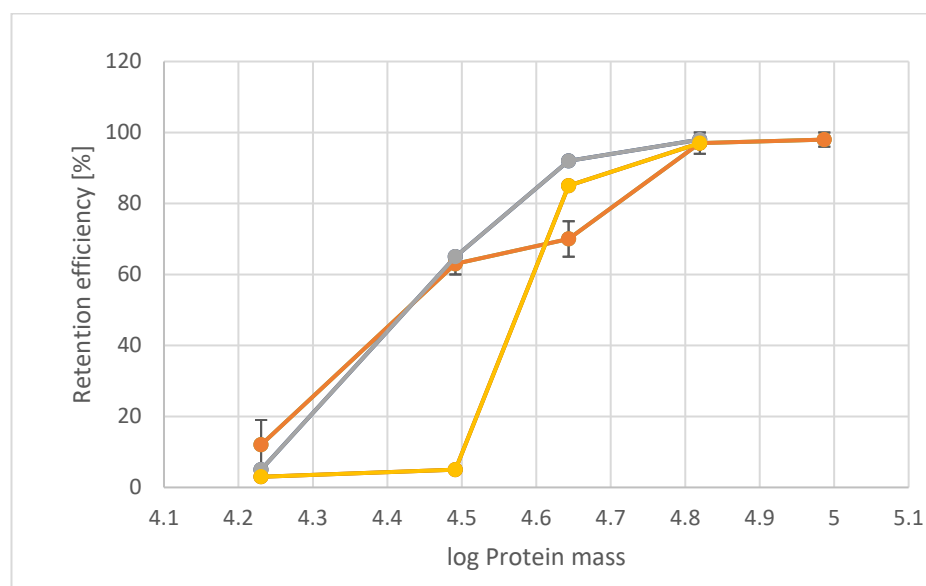
**Figure 4.** (A) Average efficiency of *Saccharolobus solfataricus* P2 fragments deposited on microfilter 1 (SSOMF1) across all experiments ( $n \geq 6$ ); (B) retention efficiency of SSOMF1 where Orange = filtration sequence largest to smallest protein ( $n \geq 3$ ) and Blue = filtration sequence smallest to largest protein ( $n \geq 3$ ); Legend for A and B: — = myoglobin (17 kDa); ■ = carbonic anhydrase (31 kDa); ◆ = horseradish peroxidase (44 kDa); ▲ = bovine serum albumin (66 kDa); x = amyloglucosidase (97 kDa) and ● =  $\gamma$ -globulin (125 kDa).

Figure 4B shows the results of filtration experiments, where the proteins listed in Table 1 were passed through the same SSOMF1 in consecutive order either from smallest to largest or vice versa with the SSOMF1 being washed with MQ between each measurement. Starting with proteins from small to large  $M_r$  resulted at first sight in a higher retention efficiency compared to the passage of the proteins in reverse order (from large to small), but only for the proteins having a  $M_r \geq 44$  kDa (Figure 4B). However, the data points of both consecutive sequences for protein passage are in between the standard deviation of each other. For myoglobin and carbonic anhydrase, almost identical data have been observed (Figure 4B). Thus, the triplicate data show that there is no significant difference in retention efficiency no matter in which order the proteins were passed through the pores of the SSOMF1 membrane (Figure 4). This allows for the conclusion that the proteins retained on the SSOMF1 were removed from the surface and pores of the latter by the washing step. Interestingly, studies on the S-layer lattice of various bacterial organisms showed diminished or even eliminated unspecific adsorption events and thus provided an efficient antifouling coating [32,43]. Hence, one may conjecture that the deposited SSO fragments may provide an antifouling coating as well.



**Figure 5.** Retention efficiency of *Saccharolobus solfataricus* P2 fragments deposited on microfilter 2 (SSOMF2) (orange); *B. stearothermophilus* pV72 (yellow) and *C. thermohydrosulfuricum* L111-69 (gray). The proteins with increasing molecular mass are myoglobin (17 kDa), carbonic anhydrase (31 kDa), ovalbumin (43 kDa; for bacterial SLP material), horseradish peroxidase (44 kDa; for SSOMF2), bovine serum albumin (66 kDa), and amyloglucosidase (97 kDa) ( $n \geq 4$ ). Data for the retention curve of *B. stearothermophilus* pV72 and *C. thermohydrosulfuricum* L111-69 are taken from Ref. [25].

A comparison of the data obtained for SSOMF2 with those from so-called S-layer ultrafiltration membranes (SUMs) comprising bacterial S-layer material revealed differences in terms of retention efficiency. The limiting pore diameter of *Bacillus stearothermophilus* strains and of *Clostridium thermohydrosulfuricum* L111-69 was reported to be 4.5 nm and 4–5 nm, respectively [42,44]. This pore diameter is in the same dimension as the smaller pore of ~4.5 nm in the S-layer lattice of SSO [31]. The retention efficiency differs from that of *B. stearothermophilus* based SUMs, which showed a low retention efficiency for carbonic anhydrase ( $M_r$  of 31 kDa) of only up to 5%. In contrast, SUMs composed of the S-layer lattice from *C. thermohydrosulfuricum*, but also of the presently used SSO fragments on MF2 revealed a retention efficiency between 60% and 66% (Figure 5) [25,39]. The divergence between the retention efficiency for the protein having a  $M_r$  of about 44 kDa may be attributed to the use of horseradish peroxidase (44 kDa) in the present study and ovalbumin (43 kDa) in the studies on the bacterial S-layer material [25,39].

The shape of the retention curve is similar for SUMs made from *C. thermohydrosulfuricum* and SSO fragments. SSO fragments, however, show two distinct types of pores (Figure 3B): a smaller one, which appears triangular shaped with a size of approximately 4.5 nm, and a larger pore with an almost circular shape with approximately 8 nm in diameter. From Figure 3B, one can estimate the distribution of the pores of two small to one large pore. One may assume that these larger pores may cause a lower retention efficiency of SSO fragments for horseradish peroxidase, bovine serum albumin and amyloglucosidase, because these proteins show a smaller molecular size (Table 1) and thus can theoretically pass the large pores. We did not find such a behavior indicating that the larger pores of the SSO fragments are not accessible to a large extent. A possible reason might be that the SSO fragments are deposited in a way that a predominant number of large pores are not accessible due to superposition of fragments. Finally, no sharp exclusion limit as it has been shown for *B. stearothermophilus* SLP based SUMs can be reported for SSO fragments. However, the pore of the S-layer lattice of *B. stearothermophilus* has a very similar pore size as those of *C. thermohydrosulfuricum*, but the retention efficiency was completely different for carbonic anhydrase, a protein with small molecular mass (31 kDa; Figure 5). This pro-



vided evidence that other factors like net charges and hydrophilic or hydrophobic surface properties may play a significant role for the sieving characteristics [45] and thus, influence the physiological functions of the S-layer lattice.

#### 4. Conclusions and Outlook

This study showed the ability of the SEG method to reduce the cost for SLP extraction from *S. solfataricus* as isolated SSO fragments by approx. 80% when compared to the established extraction method (DEG). The characterization of SSO fragments by TEM revealed an SSO S-layer lattice geometry with two types of pores (4.5 nm and 8 nm in diameter), a unit cell size of the p3 lattice of 21.3 nm, and a porosity of the lattice was calculated to 45%.

To characterize the pores of the SSO lattice, SSO fragments were deposited on different microfilters and finally cross-linked. The type of structure of the microfilter has crucial influence regarding whether a closed coherent SSO filter layer can be formed or not. An open-foam-like structure was compared to the structure of the radiation-track microfilter more appropriate as the SSO fragments could better be pushed into the microfilter structure and thus formed a totally dense filtration layer. The second important parameter is the size of the SSO fragments. Only large fragments gave a closed SSO layer on the MF2, whereas SSO sacculi and small SSO fragments formed leaky layers on both microfilters.

The molecular sieving characteristics of the pores in SSO fragments as determined by passing proteins varying in mass and thus size through the pores of the SSO fragments revealed a higher retention efficiency with increasing molecular mass of the proteins (Table 1). A comparison of the retention efficiency of SSO fragments bacterial S-layer material from *C. thermohydrosulfuricum* deposited in a dense layer on microfilters showed similar sieving properties. This result cannot be explained by the pore size because the SSO fragments have two pores (4.5 nm and 8 nm in diameter) and those of *C. thermohydrosulfuricum* have only one pore with a diameter of 4–5 nm.

Studying the molecular sieving characteristics of SSO fragments may help to advance the fundamental understanding of archaeal SLP biochemistry and biophysics and would simultaneously expand their biotechnological relevance. Lastly, established genetic systems for SSO may allow for the modification of S-layer pore properties and the construction of recombinant SLPs to produce SSOMFs with tailored functions, particularly in the pore region. Moreover, the effect of the glycosylation on the filter function of the SSO lattice could be investigated in detail by comparing wild-type and recombinant SSO SLPs.

While all application-driven S-layer publications to date have focused on bacterial S-layer proteins [24,46], a recent review on the biotechnical potential of archaea showed that the production of archaeal SLP-based applications is currently at Bio-Technology Readiness Level 2 [26]. This indicates that archaeal SLPs could be an interesting extension to the arsenal of building blocks for synthetic bioarchitectures. One expected advantage when using archaeal SLPs is the increased stability of the latter against elevated temperature, strong acidic environment, or higher ion concentration as the SLPs as outermost cell envelope structure of archaea retain by nature their structure in contact with these extreme environmental conditions. Therefore, SSO fragments and other archaeal SLP material might have application potential analogous to the bacterial ones as immobilization matrix for bioactive molecules [47] and as support for functionalized lipid membranes [48]. In summary, we have also provided evidence for the potential of archaeal SSO fragments as filtration matrix and thus expanded the field of Archaea Biotechnology.

**Supplementary Materials:** The following supporting information can be downloaded at: <https://www.mdpi.com/article/10.3390/nano12142502/s1>, Figure S1: Sequential steps and terminologies throughout the S-layer protein extraction process; Figure S2: Fourier spectrum of a TEM image of an *Saccharolobus solfataricus* P2 fragment, Figure S3: Types of microfiltration membranes and attachment of S-layer fragments; Figure S4: SDS-PAGE of a protein mixture filtered through *Saccharolobus solfataricus* P2 fragments; Table S1: Cultivation cost calculation; Table S2: Extraction cost calculation.

**Author Contributions:** Conceptualization, U.B.S., E.-K.E., B.S. and K.P.; methodology, U.B.S.; software, D.P.; validation, B.S.; investigation, K.P., B.S.; resources, S.K.-M.R.R., C.S. and B.S.; data curation, K.P., S.K.-M.R.R., C.S., D.P., U.B.S. and B.S.; writing—original draft preparation, K.P. and B.S.; writing—review and editing, K.P., S.K.-M.R.R., C.S., E.-K.E., U.B.S. and B.S.; visualization, K.P. and B.S.; supervision, B.S.; project administration, B.S.; funding acquisition, B.S. All authors have read and agreed to the published version of the manuscript.

**Funding:** This research was funded by the Austrian Science Fund (FWF), project P 29399-B22 (to B.S.). Open Access Funding by the Austrian Science Fund (FWF), project P 29399-B22 (to B.S.), is also gratefully acknowledged.

**Institutional Review Board Statement:** Not applicable.

**Informed Consent Statement:** Not applicable.

**Data Availability Statement:** The data presented in this study are available on request from the corresponding author.

**Conflicts of Interest:** S.K.-M.R.R. declares to have competing financial interests due to his employment in the Arkeon GmbH. All other authors declare no conflict of interest.

## Abbreviations

Abbreviation	Meaning
DEG	DNase-based extraction of ghosts
MF1	microfilter 1
MF2	microfilter 2
SDS	sodium dodecylsulfate
SDS-PAGE	sodium dodecylsulfate polyacrylamide gel electrophoresis
SEG	sonication-based extraction of ghosts
SEM	scanning electron microscopy
SlaA	surface layer large protein from <i>Saccharolobus solfataricus</i> P2
SlaB	surface layer small protein from <i>Saccharolobus solfataricus</i> P2
S-layer	surface-layer
SLP	surface layer protein and glycoprotein
SSO	<i>Saccharolobus solfataricus</i> P2
SSOMF1	cross-linked SSO fragments on microfilter 1
SSOMF2	cross-linked SSO fragments on microfilter 2
SUM	S-layer ultrafiltration membranes
TEM	transmission electron microscopy

## References

- Houwink, A.L. A macromolecular monolayer in the cell wall of *Spirillum* spec. *Biochim. Biophys. Acta* **1953**, *10*, 360–366. [\[CrossRef\]](#)
- Salton, M.R.J.; Horne, R.W. Studies of the bacterial cell wall I. Electron microscopical observation on heated bacteria. *Biochim. Biophys. Acta* **1951**, *7*, 19–42. [\[CrossRef\]](#)
- Remsen, C.C.; Watson, S.W.; Waterbury, J.B.; Trüper, H.G. Fine structure of *Ectothiorhodospira mobilis* Pelsh. *J. Bacteriol.* **1968**, *95*, 2374–2392. [\[CrossRef\]](#) [\[PubMed\]](#)
- Sleytr, U.B.; Adam, H.; Klaushofer, H. Die Feinstruktur der Zellwandoberfläche von zwei thermophilen Clostridienarten, dargestellt mit Hilfe der Gefrierätztechnik. *Mikroskopie* **1968**, *23*, 1–10.
- Sleytr, U.B.; Messner, P.; Pum, D.; Sara, M. *Crystalline Bacterial Cell Surface Layers*; Springer: Berlin/Heidelberg, Germany, 1988; pp. 13–31. [\[CrossRef\]](#)
- Sleytr, U.B.; Schuster, B.; Egelseer, E.M.; Pum, D. S-layers: Principles and applications. *FEMS Microbiol. Rev.* **2014**, *38*, 823–864. [\[CrossRef\]](#)
- Albers, S.V.; Meyer, B.H. The archaeal cell envelope. *Nat. Rev. Microbiol.* **2011**, *9*, 414–426. [\[CrossRef\]](#)
- Lanzoni-Mangutchi, P.; Banerji, O.; Wilson, J.; Barwinska-Sendra, A.; Kirk, J.A.; Vaz, F.; O’Beirne, S.; Baslé, A.; El Omari, K.; Wagner, A.; et al. Structure and assembly of the S-layer in *C. difficile*. *Nat. Commun.* **2022**, *13*, 970. [\[CrossRef\]](#)
- Madhurantakam, C.; Howorka, S.; Remaut, H. S-layer Structure in Bacteria and Archaea. In *Nanomicrobiology*; Barton, L., Bazylnski, D., Xu, H., Eds.; Springer: New York, NY, USA, 2014; pp. 11–37. [\[CrossRef\]](#)
- Baumeister, W.; Barth, M.; Hegerl, R.; Guckenberger, R.; Hahn, M.; Saxton, W.O. Three-dimensional structure of the regular surface layer (HPI layer) of *Deinococcus radiodurans*. *J. Mol. Biol.* **1986**, *187*, 241–250. [\[CrossRef\]](#)

11. Lister, T.E.; Pinhero, P.J. In vivo atomic force microscopy of surface proteins on *Deinococcus radiodurans*. *Langmuir* **2001**, *17*, 2624–2628. [\[CrossRef\]](#)
12. Farci, D.; Kereiche, S.; Pangeni, S.; Haniewicz, P.; Bodrenko, I.V.; Ceccarelli, M.; Winterhalter, M.; Piano, D. Structural analysis of the architecture and in situ localization of the main S-layer complex in *Deinococcus radiodurans*. *Structure* **2021**, *29*, 1279–1285.e3. [\[CrossRef\]](#)
13. Farci, D.; Haniewicz, P.; de Sanctis, D.; Iesu, L.; Kereiche, S.; Winterhalter, M.; Piano, D. The cryo-EM structure of the S-layer deinoxanthin-binding complex of *Deinococcus radiodurans* informs properties of its environmental interactions. *J. Biol. Chem.* **2022**, *298*, 102031. [\[CrossRef\]](#) [\[PubMed\]](#)
14. Farci, D.; Aksoyoglu, M.A.; Farci, S.F.; Bafna, J.A.; Bodrenko, I.; Ceccarelli, M.; Kirkpatrick, J.; Winterhalter, M.; Kereiche, S.; Piano, D. Structural insights into the main S-layer unit of *Deinococcus radiodurans* reveal a massive protein complex with porin-like features. *J. Biol. Chem.* **2020**, *295*, 4224–4236. [\[CrossRef\]](#) [\[PubMed\]](#)
15. Fagan, R.P.; Fairweather, N.F. Biogenesis and functions of bacterial S-layers. *Nat. Rev. Microbiol.* **2014**, *12*, 211–222. [\[CrossRef\]](#) [\[PubMed\]](#)
16. Rodrigues-Oliveira, T.; Belmok, A.; Vasconcellos, D.; Schuster, B.; Kyaw, C.M. Archaeal S-Layers: Overview and Current State of the Art. *Front. Microbiol.* **2017**, *8*, 2597. [\[CrossRef\]](#)
17. Zhang, C.; Wipfler, R.L.; Li, Y.; Wang, Z.; Hallett, E.N.; Whitaker, R.J. Cell Structure Changes in the Hyperthermophilic Crenarchaeon *Sulfolobus islandicus* Lacking the S-Layer. *mBio* **2019**, *10*, e01589-19. [\[CrossRef\]](#)
18. Zink, I.A.; Pfeifer, K.; Wimmer, E.; Sleytr, U.B.; Schuster, B.; Schleper, C. CRISPR-mediated gene silencing reveals involvement of the archaeal S-layer in cell division and virus infection. *Nat. Commun.* **2019**, *10*, 2540. [\[CrossRef\]](#)
19. Valentine, D.L. Adaptations to energy stress dictate the ecology and evolution of the Archaea. *Nat. Rev. Microbiol.* **2007**, *5*, 316–323. [\[CrossRef\]](#)
20. Sara, M.; Sleytr, U.B. S-layer proteins. *J. Bacteriol.* **2000**, *182*, 859–868. [\[CrossRef\]](#)
21. Schuster, B.; Sleytr, U.B. S-Layer Ultrafiltration Membranes. *Membranes* **2021**, *11*, 275. [\[CrossRef\]](#)
22. Pum, D.; Sleytr, U.B. Reassembly of S-layer proteins. *Nanotechnology* **2014**, *25*, 312001. [\[CrossRef\]](#)
23. Pum, D.; Toca-Herrera, J.L.; Sleytr, U.B. S-layer protein self-assembly. *Int. J. Mol. Sci.* **2013**, *14*, 2484–2501. [\[CrossRef\]](#)
24. Sleytr, U.B.; Huber, C.; Ilk, N.; Pum, D.; Schuster, B.; Egelseer, E.M. S-layers as a tool kit for nanobiotechnological applications. *FEMS Microbiol. Lett.* **2007**, *267*, 131–144. [\[CrossRef\]](#)
25. Sleytr, U.B.; Sára, M. Ultrafiltration membranes with uniform pores from crystalline bacterial cell envelope layers. *Appl. Microbiol. Biotechnol.* **1986**, *25*, 83–90. [\[CrossRef\]](#)
26. Pfeifer, K.; Ergal, I.; Koller, M.; Basen, M.; Schuster, B.; Rittmann, S.K.-M.R. Archaea Biotechnology. *Biotechnol. Adv.* **2021**, *47*, 107668. [\[CrossRef\]](#)
27. Ücisik, M.H.; Küpcü, S.; Debreczeny, M.; Schuster, B.; Sleytr, U.B. S-layer coated emulsomes as potential nanocarriers. *Small* **2013**, *9*, 2895–2904. [\[CrossRef\]](#)
28. Damiani, S.; Schuster, B. Electrochemical Biosensors Based on S-Layer Proteins. *Sensors* **2020**, *20*, 1721. [\[CrossRef\]](#)
29. Tornabene, T.G.; Langworthy, T.A.; Holzer, G.; Oró, J. Squalenes, Phytanes and Other Isoprenoids as Major Neutral Lipids of Methanogenic and Thermoacidophilic “Archaeobacteria”. *J. Mol. Evol.* **1979**, *13*, 73–83. [\[CrossRef\]](#)
30. Rastädter, K.; Wurm, D.J.; Spadiut, O.; Quehenberger, J. The Cell Membrane of *Sulfolobus* spp.—Homeoviscous Adaption and Biotechnological Applications. *Int. J. Mol. Sci.* **2020**, *21*, 3935. [\[CrossRef\]](#)
31. Gambelli, L.; Meyer, B.H.; McLaren, M.; Sanders, K.; Quax, T.E.F.; Gold, V.A.M.; Albers, S.-V.; Daum, B. Architecture and modular assembly of *Sulfolobus* S-layers revealed by electron cryotomography. *Proc. Nat. Acad. Sci. USA* **2019**, *116*, 25278–25286. [\[CrossRef\]](#)
32. Schuster, B.; Sleytr, U.B. Relevance of glycosylation of S-layer proteins for cell surface properties. *Acta Biomater.* **2015**, *19*, 149–157. [\[CrossRef\]](#)
33. Grogan, D.W. Phenotypic characterization of the archaeobacterial genus *Sulfolobus*: Comparison of five wild-type strains. *J. Bacteriol.* **1989**, *171*, 6710–6719. [\[CrossRef\]](#)
34. Michel, H.; Neugebauer, D.-C.; Oesterhelt, D. The 2-D Crystalline Cell Wall of *Sulfolobus acidocaldarius*: Structure, Solubilization, and Reassembly. In *Electron Microscopy at Molecular Dimensions, Proceedings in Life Sciences*; Baumeister, W., Vogel, W., Eds.; Springer: Berlin/Heidelberg, Germany, 1980; pp. 27–35. [\[CrossRef\]](#)
35. Grogan, D.W. Isolation and fractionation of cell envelope from the extreme thermo-acidophile *Sulfolobus acidocaldarius*. *J. Microbiol. Methods* **1996**, *26*, 35–43. [\[CrossRef\]](#)
36. Veith, A.; Klingl, A.; Zolghadr, B.; Lauber, K.; Mentele, R.; Lottspeich, F.; Rachel, R.; Albers, S.-V.; Kletzin, A. Acidianus, *Sulfolobus* and *Metallosphaera* surface layers: Structure, composition, and gene expression. *Mol. Microbiol.* **2009**, *73*, 58–72. [\[CrossRef\]](#)
37. Schneider, C.A.; Rasband, W.S.; Eliceiri, K.W. NIH Image to ImageJ: 25 years of image analysis. *Nat. Methods* **2012**, *9*, 671–675. [\[CrossRef\]](#)
38. Sára, M.; Sleytr, U.B. Production and characteristics of ultrafiltration membranes with uniform pores from two-dimensional arrays of proteins. *J. Membr. Sci.* **1987**, *33*, 27–49. [\[CrossRef\]](#)
39. Sára, M.; Manigley, C.; Wolf, G.; Sleytr, U.B. Isoporous ultrafiltration membranes from bacterial cell envelope layers. *J. Membr. Sci.* **1988**, *36*, 179–186. [\[CrossRef\]](#)

40. Sára, M.; Küpcü, S.; Sleytr, U.B. Crystalline bacterial cell surface layers used as ultrafiltration membranes and immobilization matrix. *Gen. Eng. Biotechnol.* **1990**, *10*, 10–13.
41. Weigert, S.; Sára, M. Surface modification of an ultrafiltration membrane with crystalline structure and studies on interactions with selected protein molecules. *J. Membr. Sci.* **1995**, *106*, 147–159. [[CrossRef](#)]
42. Sára, M.; Sleytr, U.B. Molecular sieving through S-layers of *Bacillus stearothermophilus* strains. *J. Bacteriol.* **1987**, *169*, 4092–4098. [[CrossRef](#)]
43. Picher, M.M.; Küpcü, S.; Dostalek, J.; Pum, D.; Sleytr, U.B.; Ertl, P. Nanobiotechnology advanced antifouling surfaces for the continuous electrochemical monitoring of glucose in whole blood using a lab-on-a-chip. *Lab Chip* **2013**, *13*, 1780–1789. [[CrossRef](#)]
44. Weiner, C.; Sára, M.; Sleytr, U.B. Novel protein A affinity matrix prepared from two-dimensional protein crystals. *Biotechnol. Bioeng.* **1994**, *43*, 321–330. [[CrossRef](#)]
45. Küpcü, S.; Sára, M.; Sleytr, U.B. Influence of covalent attachment of low molecular weight substances on the rejection and adsorption properties of crystalline proteinaceous ultrafiltration membranes. *Desalination* **1993**, *90*, 65–76. [[CrossRef](#)]
46. Egelseer, E.M.; Ilk, N.; Pum, D.; Messner, P.; Schäffer, C.; Schuster, B.; Sleytr, U.B. S-Layers, Microbial, Biotechnological Applications. In *Encyclopedia of Industrial Biotechnology: Bioprocess, Bioseparation, and Cell Technology*; Flickinger, M.C., Ed.; Wiley-VCH Verlag: Weinheim, Germany, 2010; pp. 4424–4448.
47. Breitwieser, A.; Küpcü, S.; Howorka, S.; Weigert, S.; Langer, C.; Hoffmann-Sommergruber, K.; Scheiner, O.; Sleytr, U.B.; Sára, M. 2-D Protein Crystals as an Immobilization Matrix for Producing Reaction Zones in Dipstick-Style Immunoassays. *BioTechniques* **1996**, *21*, 918–925. [[CrossRef](#)]
48. Schuster, B.; Pum, D.; Sára, M.; Braha, O.; Bayley, H.; Sleytr, U.B. S-layer ultrafiltration membranes: A new support for stabilizing functionalized lipid membranes. *Langmuir* **2001**, *17*, 499–503. [[CrossRef](#)]

# ANNEX 4

Pages 93 to 108

---

Baumann L.M.F., Taubner R.-S., Oláh K., Rohrweber A.-C., Schuster B., Birgel D.,  
Rittmann S.K.-M.R.

**Quantitative analysis of core lipid production in *Methanothermobacter marburgensis* at  
different scales**




Bioengineering (2022) 9(4):169

10.3390/bioengineering9040169

---

## Article

# Quantitative Analysis of Core Lipid Production in *Methanothermobacter marburgensis* at Different Scales

Lydia M. F. Baumann <sup>1,†</sup>, Ruth-Sophie Taubner <sup>2,3,4,†</sup> , Kinga Oláh <sup>3</sup>, Ann-Cathrin Rohrweber <sup>1</sup>, Bernhard Schuster <sup>3</sup> , Daniel Birgel <sup>1</sup> and Simon K.-M. R. Rittmann <sup>2,5,\*</sup> 

- <sup>1</sup> Institute for Geology, Center for Earth System Research and Sustainability, Universität Hamburg, Bundesstraße 55, 20146 Hamburg, Germany; lydia.feli.baumann@gmail.com (L.M.F.B.); geo@rohrweber.com (A.-C.R.); daniel.birgel@uni-hamburg.de (D.B.)
- <sup>2</sup> Archaea Physiology & Biotechnology Group, Department of Functional and Evolutionary Ecology, Universität Wien, Djerassiplatz 1, 1030 Wien, Austria; ruth-sophie.taubner@univie.ac.at
- <sup>3</sup> Institute for Synthetic Bioarchitectures, Department of Nanobiotechnology, University of Natural Resources and Life Sciences, Muthgasse 11, 1190 Vienna, Austria; nagykinga012@gmail.com (K.O.); bernhard.schuster@boku.ac.at (B.S.)
- <sup>4</sup> Institute for Chemical Technology of Organic Materials, Johannes Kepler Universität Linz, Altenbergerstraße 69, 4040 Linz, Austria
- <sup>5</sup> Arkeon GmbH, Technopark 1, 3430 Tulln an der Donau, Austria
- \* Correspondence: simon.rittmann@univie.ac.at; Tel.: +43-1-4277-76513
- † These authors contributed equally to this work.



**Citation:** Baumann, L.M.F.;

Taubner, R.-S.; Oláh, K.;

Rohrweber, A.-C.; Schuster, B.;

Birgel, D.; Rittmann, S.K.-M.R.

Quantitative Analysis of Core Lipid Production in *Methanothermobacter marburgensis* at Different Scales.

*Bioengineering* **2022**, *9*, 169.

<https://doi.org/10.3390/bioengineering9040169>

Academic Editor: Sabine Kleinstüber

Received: 24 March 2022

Accepted: 6 April 2022

Published: 10 April 2022

**Publisher's Note:** MDPI stays neutral with regard to jurisdictional claims in published maps and institutional affiliations.



**Copyright:** © 2022 by the authors. Licensee MDPI, Basel, Switzerland. This article is an open access article distributed under the terms and conditions of the Creative Commons Attribution (CC BY) license (<https://creativecommons.org/licenses/by/4.0/>).

**Abstract:** Archaeal lipids have a high biotechnological potential, caused by their high resistance to oxidative stress, extreme pH values and temperatures, as well as their ability to withstand phospholipases. Further, methanogens, a specific group of archaea, are already well-established in the field of biotechnology because of their ability to use carbon dioxide and molecular hydrogen or organic substrates. In this study, we show the potential of the model organism *Methanothermobacter marburgensis* to act both as a carbon dioxide based biological methane producer and as a potential supplier of archaeal lipids. Different cultivation settings were tested to gain an insight into the optimal conditions to produce specific core lipids. The study shows that up-scaling at a constant particle number ( $n/n = \text{const.}$ ) seems to be a promising approach. Further optimizations regarding the length and number of the incubation periods and the ratio of the interaction area to the total liquid volume are necessary for scaling these settings for industrial purposes.

**Keywords:** archaea biotechnology; microbial physiology; anaerobe; isoprenoids; ether lipids; methanogens

## 1. Introduction

The membrane lipids of archaea can be considered the most outstanding adaptations of life. Their unique lipid composition enabled archaea to conquer not only the mesophilic realm, but also the most extreme ecological niches on Earth, including those with high and low temperatures and pH values, high salinities, and anoxic environments (e.g., [1–3]). In contrast to the cell membranes of Bacteria and Eukarya, which are composed of ester-bound acyl chains at the *sn*-1 and *sn*-2 position, archaeal cell membranes are made of isoprenoid chains bound to glycerol by ether bonds at the *sn*-2 and *sn*-3 position (e.g., [4,5]). The generally high thermal and chemical stability of ether-bound, isoprenoidal archaeal membrane lipids, and the maintenance of their function at a wide range of chemical and physical conditions, make them a valuable study object and resource for biotechnology, biomedicine, and the pharmaceutical industry as, for example, liposomes or lipid films (e.g., [6,7]).

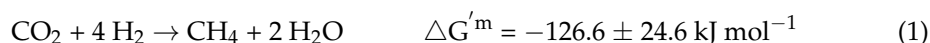
The membrane-spanning tetraether lipids, with their  $C_{40}$  alkyl chains connecting the two glycerol backbones, are of particular interest for the production of archaeosomes and lipid films (e.g., [6–8]). Among tetraether-lipid-producing archaea, methanogenic



archaea, also referred to as methanogens (e.g., [9]), produce high amounts of these membrane lipids. Different methanogens produce various isoprenoidal hydrocarbons, di-, and tetraether lipids. Tetraether lipids are usually found as GDGTs (glycerol dialkyl glycerol tetraethers), GMGTs (glycerol monoalkyl glycerol tetraethers), and GTGTs (glycerol trialkyl glycerol tetraethers) (e.g., [4,9,10]), but are also known from non-methanogenic archaea (e.g., [11–13]). However, so far, only one methanogen has produced GDGTs and GMGTs with additional methyl groups [14], which makes them unique producers of these lipids.

Methanogens represent a group of archaea that require strict anaerobic conditions for optimal growth but are nevertheless widespread and occur, for example, in marine and lacustrine sediments; at hydrothermal vents, swamps, rice paddies, and soils; and in the gastrointestinal tracts of various animals, including humans (e.g., [15,16]). They are known to be able to metabolize a variety of gaseous substrates, e.g., carbon dioxide (CO<sub>2</sub>) and molecular hydrogen (H<sub>2</sub>) (e.g., [17]). Methanogens are widely used for anaerobic wastewater treatment and biogas production, whereas anaerobic digestors produce less sewage sludge—a costly by-product—than aerobic digestors (e.g., [18]). Besides the applications regarding their lipid inventory and wastewater treatment, currently, a considerable interest has emerged to employ methanogens for the conversion of CO<sub>2</sub> to methane (CH<sub>4</sub>) using H<sub>2</sub> (e.g., [19]). This would be a way to store carbon and sustainably produce and/or convert energy. One example concerns the CO<sub>2</sub>-based biological CH<sub>4</sub> production (CO<sub>2</sub>-BMP) process, wherein autotrophic, hydrogenotrophic methanogens are utilized [19–22].

Specifically, one thermophilic methanogen, *Methanothermobacter marburgensis* [23–25], is currently the most promising model organism for CO<sub>2</sub>-BMP biotechnology. High rates of CO<sub>2</sub> to CH<sub>4</sub> conversion were obtained in a continuous culture with *M. marburgensis* [26]. During CO<sub>2</sub>-BMP, the conversion of CO<sub>2</sub> and H<sub>2</sub> to CH<sub>4</sub> is performed according to the following stoichiometry:



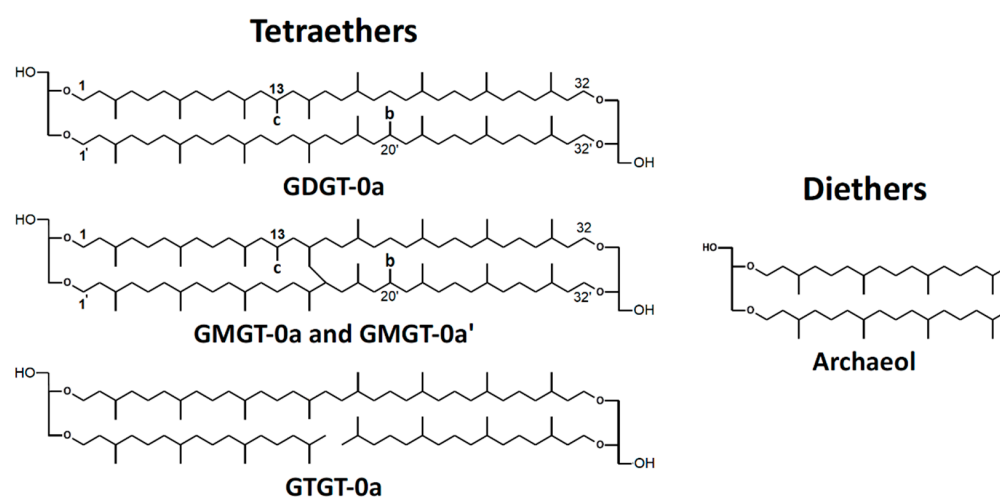
Other characteristics of *M. marburgensis* make the strain even more intriguing for further physiological and biotechnological studies. The biochemistry of *M. marburgensis* is very well known [27]; it can be grown at very high specific growth rates up to 0.69 h<sup>−1</sup> in minimal medium to high cell densities in bioreactors [21]; and the genome was sequenced [28]. Further, the physiological characteristics of the organism are well-known from closed batch [29], fed-batch [21], and continuous culture [22,23,26,30,31] experiments. *M. marburgensis* was chosen for this study, as it is one of the key organisms of Archaea Biotechnology [7,32].

The membrane core lipids of *M. marburgensis* have been described before [33] and comprise a range of isoprenoidal di- and tetraether lipids, partly with additional methylations in the alkyl chains (Figure 1). In contrast to intact polar lipids, the studied lipids do not contain the polar headgroups. None of the core lipids contain cyclopentane or cyclohexane moieties in the chains. This is indicated by a “0” after the name of the lipid. In this study, the nomenclature of Knappy *et al.* is used, which was originally introduced for a close relative of *M. marburgensis*, *Methanothermobacter thermautotrophicus* [14].

In general, archaeal lipids feature a higher resistance to oxidative stress and phospholipases, as well as a wide range of pH values and temperatures, compared to bacterial phospholipids [34,35]. Archaeal lipids can be used to manufacture artificial lipid films. Films made from archaeal lipids reveal low permeability, good insulating properties, and long-term stability [6,36]. Potential applications are in the fields of nanotechnology, biosensor design, and biomimetics [6]. Recently, catheter surfaces were coated with monolayers of tetraether lipids from the archaeon *Thermoplasma acidophilum* to avoid the adherence of pathogens [37]. Another application of archaeal lipids includes the production of liposomes. Liposomes are artificial lipid vesicles produced from phospholipids. They are tailored for their use in imaging diagnostics, as carriers of drugs, DNA, or peptides, and as adjuvants in vaccine therapy [8,38–43]. To date, liposomes were mostly made from ester phospholipids harvested from eukaryotes, such as egg phosphatidylcholine or hy-



drogenated soy phosphatidylcholine (e.g., [8,38–40,43]). Liposomes manufactured from archaeal lipids are referred to as archaeosomes (e.g., [8]). Compared to liposomes made from ester lipids, archaeosomes, especially tetraether-lipid-based archaeosomes, exhibit greater chemical and mechanical stability against very low and very high temperatures and pH, oxidative stress, lipases, bile salts, and serum media [6,8,38–40,44,45]. Archaeosomes were shown to have a higher stability in the gastrointestinal tract and to possess a longer shelf life (even in the presence of air or molecular oxygen); they can undergo heat sterilization and they showed no toxicity in mice [6,8,38,39,43]. Among other sources, archaeosomes can be produced using total polar lipid extractions from methanogens, e.g., from *Methanobrevibacter smithii* [7,46,47]. These archaeosomes showed an improved immune response in comparison to the response triggered by non-archaeal phospholipids. It could furthermore be shown that the long-lasting and robust immune response could be attributed to caldarchaeol, which acted as an adjuvant. The issue with these archaeosomes was that the batch-to-batch dependent composition of extracted *M. smithii* total polar lipids made it impossible to reproducibly generate archaeosomes with an identical lipid composition [7,48].



**Figure 1.** Structures of polar headgroups and core lipids found in *M. marburgensis*. Abbreviations of core lipids are: GDGT (glycerol dialkyl glycerol tetraether), GMGT (glycerol monoalkyl glycerol tetraether), and GTGT (glycerol trialkyl glycerol tetraether). “0”: zero rings in the alkyl chains; “a”, “b”, and “c”: no, one, or two additional methyl groups, as indicated in the structures [14]. Note that the exact positions of the additional methyl groups and the covalent carbon–carbon bonds between the isoprenoid chains of GMGT-0 are unknown.

The aim of this study was to investigate how the growth conditions alter the quality and quantity of the membrane core lipids produced by *M. marburgensis*. The emphasis in the experiments was to investigate whether *M. marburgensis* varies the specific lipid production rate, product-to-product yield, and the quality of the core lipid composition under different environmental conditions. These conditions are potentially growth-limiting ratios of gas/liquid substrates (different volume ratios tested) and either a constant volume ( $V/V = \text{const.}$ , at the starting point of the experiment) or a constant particle number ( $n/n = \text{const.}$ , at the starting point of the experiment) of the gaseous substrate. Additionally, several experiments were conducted at a higher scale for comparison. The focus was to examine whether (a) the total amount of gaseous substrates or (b) the volume ratio of gas-to-liquid phase was the basis for the production of a particular type of core lipid. The experimental approach presented here allows insights into the physiological adaptability of the membrane lipids of *M. marburgensis* and the growth parameters crucial for their adaptations, and it provides a base for approaches to scale lipid production with this strain.






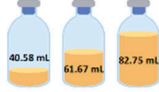


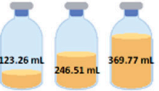
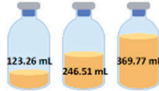
## 2. Materials and Methods

### 2.1. Archaeal Strain and Culture Set-Up

The thermophilic, hydrogenotrophic methanogen *Methanothermobacter marburgensis* DSM 2133<sup>T</sup> was originally isolated from mesophilic sewage sludge [24]. The *M. marburgensis* culture used in this study was taken from our in-house methanogen strain collection (Archaea Physiology & Biotechnology Group, Department of Functional and Evolutionary Ecology, Universität Wien, Wien, Austria). *M. marburgensis* was originally obtained from the Deutsche Sammlung für Mikroorganismen und Zellkulturen GmbH (Braunschweig, Germany).

Cultures were grown either in 120 mL glass serum bottles (La-Pha-Pack, Langerwehe, Germany) or in 500 mL glass laboratory bottles (pressure plus+, narrow neck, with thread GL 45, DURAN®, DWK Life Sciences, Wertheim, Germany) with caps (screw cap with hole, PBT, red GL 45, Lactan, Graz, Austria). The 120 mL bottles have an empirically determined volumetric capacity of approximately 117 mL with inserted blue rubber stoppers (20 mm, butyl rubber, CLS-3409-14, Chemglass Life Sciences LCC, Vineland, NJ, USA). The larger glass bottles are marketed as 500 mL bottles. However, the actual volumetric capacity, which was determined empirically, and which was also used for calculations, is approximately 570 mL with inserted rubber stopper (black butyl rubber for GL45 bottles, Glasgerätebau Ochs, Bovenden/Lengler, Germany).

The preparation, cultivation medium, inoculation, incubation, and harvesting described below were identical in the 117 mL and in the 570 mL bottles, except that the 570 mL bottles had shorter incubation intervals caused by the longer cooling down periods (see Section 2.4). For a better comparability of the experimental settings, the volumes were scaled up from the 117 mL experiments, with the final volume illustrated in Figure 2 (for the exact amount of media and inoculum, see Table S1).

Volumes	P (bar)	V/V = constant	P (bar)	n/n = constant
120 mL	1.1		1.1	
	1.5		1.5	
	2.0		2.0	
500 mL	1.1		1.1	
	1.5		1.5	

**Figure 2.** Schematic overview of the experimental set-up in 117 mL serum bottles. Pressure is given in bar relative to atmospheric pressure. Experiments in the 117 mL bottles were performed in quadruplicates ( $n = 4$ ), and samples obtained after two different incubation intervals and repeated twice ( $N = 2$ ). The final media and inoculum volumes for each experiment can be found in Table S1.

Quadruplicates of each volume and pressure variant were applied with an additional zero control to each experimental set for the 117 mL experiments. Due to logistic reasons, the experiments performed with the 570 mL flasks were performed in triplicates without zero controls. Inoculation was done in an anaerobic chamber (Coy Laboratory Products, Grass Lake, MI, USA) from a cultivated inoculum in defined media (Section 2.2). The residual  $\text{CH}_4$  was interchanged with a  $\text{H}_2/\text{CO}_2$  (4:1 ratio, 99.995% purity (Air Liquide, Schwechat, Austria)) gas mixture twice per day with different pressure values adjusted to 1.1, 1.5, or 2 bar. The pressure is given as bar relative to atmospheric pressure throughout this study. The experimental conditions and settings are detailed in Figure 2 (and Table S1), which shows an overview of the gas phase pressure values and the volumetric (V/V) and molar (n/n) constant alternatives. For the experiments termed as  $V/V = \text{const.}$ , the initial liquid volume was constant with varying pressure (1.1, 1.5, 2.0 bar) within the 117 mL (25.3, 50.6, 75.9 mL) and 570 mL (123.3, 246.5, and 369.8 mL) settings, respectively. Note that the volumetric ratios between the liquid and gaseous phase in the 117 mL and 570 mL bottles are the same for the  $V/V = \text{const.}$  setting. In contrast, for the  $n/n = \text{const.}$  settings, the aim was to have the same initial number of moles of the gas phase in three different pressure settings (treated as ideal gas at room temperature, 22 °C). These three settings were defined by the number of moles at 1.5 bar in the 117 mL bottles, at 25.3, 50.6, and 75.9 mL initial volumes. The different starting volumes of the experiments performed at different pressure values were then calculated according to the ideal gas law. For better readability, we refer in further text to the small, medium, and large volumes in the 117 mL or 570 mL bottles at the conditions  $V/V = \text{const.}$  or  $n/n = \text{const.}$  The experiments in the 117 mL setting were conducted twice at two different incubation intervals and total times.

## 2.2. Cultivation Medium

The exact procedure for the medium preparation and the medium composition were as previously described [29]. The medium was aliquoted with regard to the proper volumes (Figure 2 and Table S1) into 117 mL and 570 mL bottles and sealed with blue and black rubber stoppers, respectively, which were boiled ten times for 30 min in fresh ddH<sub>2</sub>O as a pretreatment. The 117 mL serum bottles were sealed with 20 mm aluminum crimp caps (Glasgerätebau Ochs, Bovenden/Lengler, Germany). Anaerobization was ensured by gassing with a  $\text{H}_2/\text{CO}_2$  (4:1 ratio) gas mixture (approximately 0.8 bar) five times and drawing vacuum four times. Afterwards, the bottles were autoclaved. In a final step, sterile  $0.5 \text{ mol L}^{-1} \text{ Na}_2\text{S} \cdot 9\text{H}_2\text{O}$  was added to the bottles in the anaerobic chamber (0.1 mL per 50 mL).

## 2.3. Inoculation

The inoculation was done using pre-cultures in an exponential growth phase. The exact ratios between medium and inoculum volume can be found in Table S1, and the final total volume in Figure 2. The final steps of the preparation of the flasks were the inoculation performed in the anaerobic chamber and the final pressurization to approximately 1.1, 1.5, and 2.0 bar ( $\pm 0.2$  bar), respectively, with a  $\text{H}_2/\text{CO}_2$  (4:1 ratio) gas mixture. The bottles were incubated in the dark in a shaking water bath at  $65 \pm 1$  °C.

## 2.4. Pressure Measurement and Gassing

The 117 mL serum bottles were taken out and cooled down to room temperature before each pressure measurement (30 to 45 min). For the 570 mL bottles, the interval of the cooling-down stage increased due to the higher volume of the bottles, meaning on average 2.5 h; therefore, the incubation intervals resulted in a shorter period. After reaching room temperature, the bottle headspace pressure was measured using a digital manometer (LEO1-Ei,  $-1 \dots 3$  bar rel, Keller, Germany) with filters (sterile syringe filters, w/0.2  $\mu\text{m}$  cellulose, 514-0061, VWR International, Wien, Austria), and cannulas (Gr 14,  $0.60 \times 30$  mm, 23 G  $\times 1 \frac{1}{4}$ ", RX129.1, Braun, Maria Enzersdorf, Austria). The gas phase of all bottles was exchanged with the  $\text{H}_2/\text{CO}_2$  gas mixture detailed beforehand. The abovementioned

routine took place twice per day (including the zero control bottles), and the bottles were incubated again in a water bath at  $65 \pm 1$  °C (for details, see [29]). From the difference of the bottle headspace pressure before and after the incubation, the methane evolution rate (MER) was calculated (see Tables S2 and S3).

### 2.5. End Point OD Measurement and Harvesting

Subsequent to the last cooling-down stage and following the final pressure measurement with the digital manometer, a homogenous 0.7 mL sample was taken of each flask (117 and 570 mL) for end point optical density measurements (OD,  $\lambda = 578$  nm, ddH<sub>2</sub>O serving as blank; used spectrophotometer: DU800, Beckman Coulter, Fullerton, CA, USA). Centrifugation was done in a pre-cooled centrifuge (4 °C, Heraeus Multifuge 4KR Centrifuge, Thermo Fisher Scientific, Osterode, Germany) at 4400 rpm for 20 min. The biomass (cell pellets) was transferred to 1.5 mL Eppendorf tubes. These Eppendorf tubes were further centrifuged at 4 °C for 15 min at 16,100 rpm (4 °C, Cooled Centrifuge 5424 R, Eppendorf AG, Hamburg, Germany), and the cell pellets were then stored at  $-20$  °C until further analysis.

### 2.6. Lipid Extraction

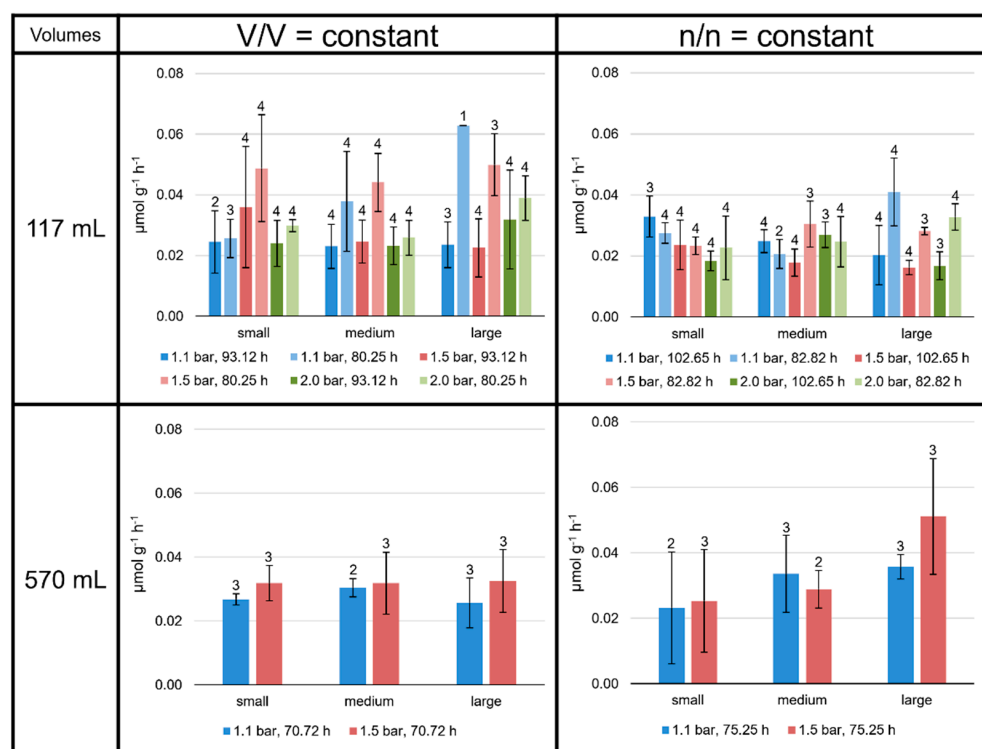
The lyophilization was accomplished at  $-81$  °C for 72 h (Alpha 2-4 LMC, Martin Christ Gefriertrocknungsanlagen GmbH, Osterode am Harz, Germany). The freeze-dried samples were aliquoted (1–20 mg) and homogenized with acetone-cleaned spatulas in glass centrifuge tubes (Präparatengläser Duran,  $16 \times 100$  mm, PTFE-filled caps, Glasgerätebau Ochs, Bovenden/Lengler, Germany). Then, 5 µg 5- $\alpha$ -cholestane (diluted from 10 mg mL<sup>-1</sup> in chloroform, SUPELCO) and 5 µg DAGE C<sub>18:18</sub> (dialkyl glycerol diether, 1,2-Di-O-octadecyl-rac-glycerol, Cayman Chemical, Biomol GmbH, Hamburg, Germany) were added as preparation standards. The samples subsequently underwent acid hydrolysis (2 mL of 10% (V/V) hydrochloric acid in methanol per sample) at 110 °C for 2 h. After that, core lipids were extracted four times with a mixture of n-hexane and dichloromethane (80:20) to obtain the total lipid extract (TLE). To an unfiltered, underivatized aliquot of each TLE, C<sub>46</sub> GDGT [49] was added as an internal standard prior to injection into a Varian MS Workstation 6.91 High Performance Liquid Chromatography (HPLC) system coupled to a Varian 1200 L triple quadrupole mass spectrometer. The Atmospheric Pressure Chemical ionization (APCI) interface was operated in positive ion mode. Response factors varied and were carefully monitored (measurement of standard mixture after four sample measurements). Details about the measurements, temperature, and solvent program can be found elsewhere [10]. Acetylated aliquots of all TLEs were additionally measured using a GC-FID system (Fisons Instruments GC 8000 series (Fisons Instruments, Ipswich, United Kingdom), Fisons Instruments HRGC MEGA 2 series (Fisons Instruments, Ipswich, United Kingdom), and Thermo Scientific Trace 1300 Series (Thermo Fisher Scientific, Waltham, MA, USA) to monitor the performance of the HPLC-APCI-MS system [10]. The response factor between the 5- $\alpha$ -cholestane and the DAGE C<sub>18:18</sub> standard was 1.6:1 on the GC-FID. Specific lipid production rates and product-to-product yields were determined using the DAGE C<sub>18:18</sub> and C<sub>46</sub> GDGT. However, due to an application error of the DAGE C<sub>18:18</sub> in some samples, the 5- $\alpha$ -cholestane and C<sub>46</sub> GDGT were used instead in these cases. The response factor between the 5- $\alpha$ -cholestane and DAGE C<sub>18:18</sub> was considered in the calculations. Tables S4–S9 indicate which samples were quantified with the 5- $\alpha$ -cholestane.

## 3. Results

### 3.1. Specific Total Lipid Production Rates Depend on Culture Conditions

Specific production rates (µmol g<sup>-1</sup> h<sup>-1</sup>) were determined for each lipid separately and for total lipids at all culture conditions (Tables S4–S9). For all the experiments performed, the mean values of the total lipid production rates lay between 0.015 and 0.070 µmol g<sup>-1</sup> h<sup>-1</sup>, depending on the experimental setting (Figure 3). Mean values were

calculated for each of the 48 experimental settings (including different incubation times): 36 in the 117 mL, and 12 different experimental settings in the 570 mL bottles.



**Figure 3.** Specific total lipid production rates in *M. marburgensis* cultures. Pressure is given in bar relative to atmospheric pressure. Production rates are given in  $\mu\text{mol g}^{-1} \text{h}^{-1}$ . Errors are standard deviations. Numbers above bars indicate number of samples. Samples quantified with 5- $\alpha$ -cholestane standard are indicated in Tables S4–S9.

Even though the environmental conditions for the 117 mL serum bottles were the same for two sets of four replicates each, the slightly different total incubation time and the varying incubation periods had an obvious influence on the  $\text{CH}_4$  production (MER; see Tables S2 and S3) and lipid production rates of *M. marburgensis*. Moreover, the MER was higher at higher atmospheric pressures and at lower liquid volumes, and the total lipid production rate tended to be higher at shorter incubation times for the  $V/V = \text{const.}$  settings. No clear trend was observed for the  $n/n = \text{const.}$  settings (Figure 3), except the significantly higher MER values for the experiments performed with small liquid volumes (see Table S3).

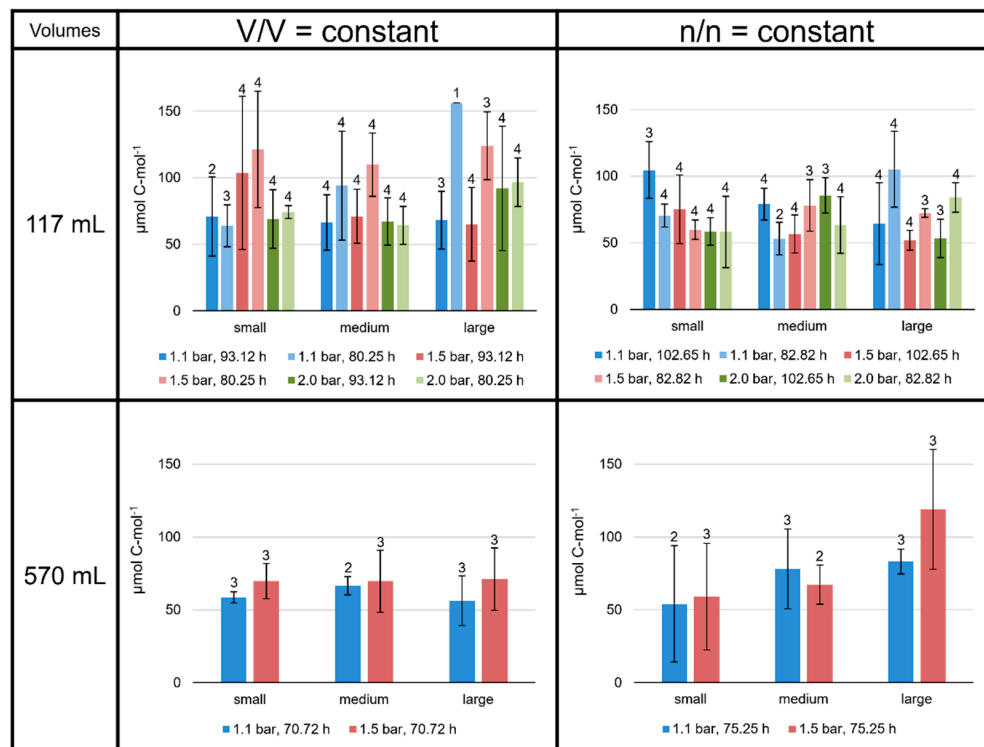
On average, the specific total lipid production rates were higher at  $V/V = \text{const.}$  than at  $n/n = \text{const.}$  Apart from these observations, there were no consistent patterns observed in the 117 mL bottles. Neither headspace pressure nor varying the volume of liquid medium clearly increased or decreased the specific total lipid production rates.

### 3.2. Product-to-Product Yield Followed the Trends of Specific Lipid Production Rates

The product-to-product yield is given as  $\mu\text{mol lipid C-mol}^{-1}$  biomass for each lipid separately and for total lipids at all culture conditions ( $\text{C-mol}^{-1}$  depicts per mole of carbon). On average, the total lipid yield lay between 50 and 160  $\mu\text{mol C-mol}^{-1}$  (Figure 4). Overall, the lipid yields followed the same patterns as the specific lipid production rates. Especially, different incubation times significantly changed the total lipid yield. The total lipid yields at  $V/V = \text{const.}$  in the 117 mL bottles tended to be high at 1.5 bar/80.25 h, exceeding 110  $\mu\text{mol C-mol}^{-1}$ . In contrast, in the  $n/n = \text{const.}$  experiments, the average total lipid yields in the 117 mL bottles were always below 110  $\mu\text{mol C-mol}^{-1}$ . In the 570 mL bottle  $V/V = \text{const.}$  experiments, all samples showed values around 60  $\mu\text{mol C-mol}^{-1}$ .



However, like the specific lipid production rates, experiments at  $n/n = \text{const.}$  in the 570 mL bottles showed an increase in total lipid yield from smaller to larger volumes ( $59 \pm 37 \mu\text{mol C}\cdot\text{mol}^{-1}$  at smaller volumes to  $118 \pm 41 \mu\text{mol C}\cdot\text{mol}^{-1}$  at larger volumes at 1.5 bar; Figure 4).

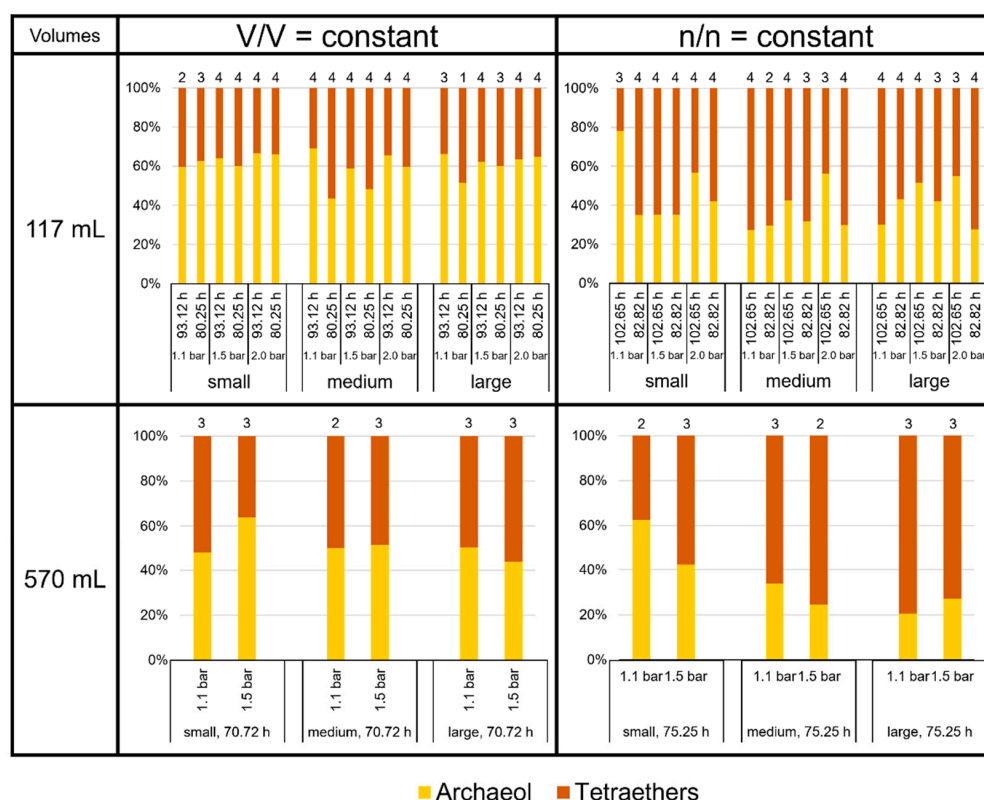


**Figure 4.** Product-to-product yields of total lipids in *M. marburgensis* cultures. Pressure is given in bar relative to atmospheric pressure. Yields are given in  $\mu\text{mol C}\cdot\text{mol}^{-1}$ . Errors are standard deviations. Numbers above bars indicate number of samples. Samples quantified with 5- $\alpha$ -cholestane standard are indicated in Tables S4–S9.

The total lipid production rates and yields at  $V/V = \text{const.}/1.1$  bar were very similar in the 117 mL bottles grown for 93.12 h to those grown in 570 mL bottles for 70.72 h (dark blue bars at  $V/V = \text{const.}$  in Figures 3 and 4). The experiments conducted at 1.5 bar did not result in such similar outcomes.

### 3.3. High Variability of Lipid Ratios Challenges Maintenance of Constant Lipid Quality

The focus of this study was to investigate the quality and product ratio of the produced core lipids. We found that archaeol and the tetraether lipids together made up more than 99% of total lipids in *M. marburgensis*. The proportion of the GDDs in this study was, in general, below 0.2%, but it reached about 0.5% of total lipids at large volumes at  $V/V = \text{const.}/1.5$  bar/80.25 h and about 0.3% at large volumes at  $n/n = \text{const.}/2.0$  bar/102.65 h in the 117 mL bottles. The relative amount of archaeol varied between 20% (570 mL bottles, large volumes at  $n/n = \text{const.}/1.1$  bar/75.25 h) and almost 80% (117 mL bottles, small volumes at  $n/n = \text{const.}/1.1$  bar/102.65 h). On average, *M. marburgensis* produced about 50% tetraether lipids, depending on the culture conditions (Figure 5). At  $V/V = \text{const.}$ , tetraether lipids comprised  $39 \pm 4\%$ , whereas at  $n/n = \text{const.}$ , they made up  $59 \pm 8\%$  in the 117 mL bottles. In the 570 mL bottles, they constituted 49% at  $V/V = \text{const.}$  and even 65% at  $n/n = \text{const.}$ . Thus, the condition  $n/n = \text{const.}$  overall led to a higher proportion of tetraethers vs. archaeol compared to  $V/V = \text{const.}$ , where archaeol was the most abundant membrane lipid. However, this ratio relied on pressure and incubation time as well, as the high proportions of archaeol in the smaller volumes at  $n/n = \text{const.}/1.1$  bar clearly demonstrate (Figure 5).

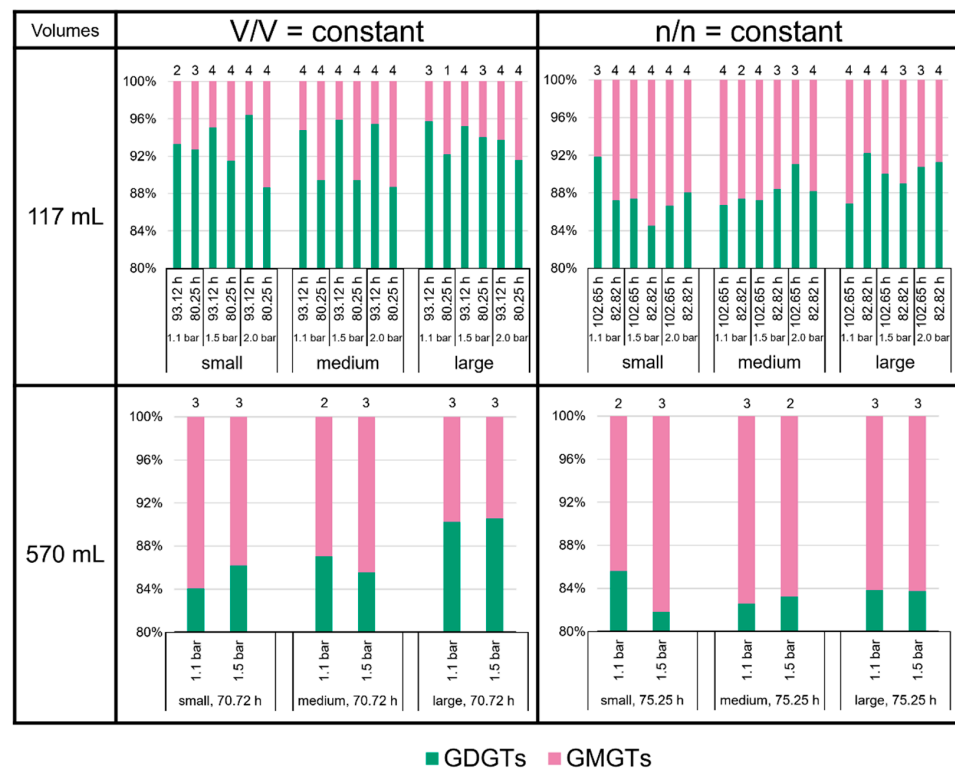


**Figure 5.** Lipid ratios of archaeol to tetraethers in *M. marburgensis* cultures in %. Pressure is given in bar relative to atmospheric pressure. Numbers above bars indicate number of samples. Samples quantified with 5- $\alpha$ -cholestane standard are indicated in Tables S4–S9.

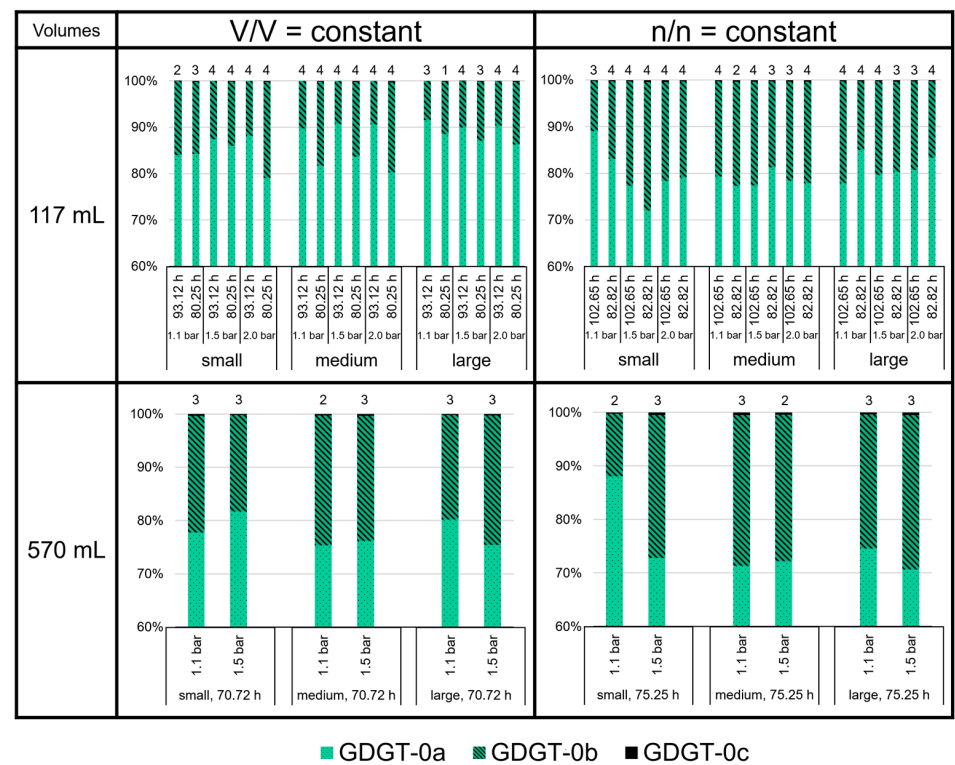
The proportions of the different groups of tetraethers—GDGTs, GMGTs, and GTGT-0a—did not vary largely (Figure 6). The GDGTs were the most abundant tetraethers at all culture conditions, accounting for about 80 to 95% of total tetraether lipids. The GMGTs were the second most abundant group of tetraethers, with an average 4 to 18% of total tetraethers. The relative amount of GTGT-0a lay well below 1% of total tetraethers at most culture conditions. It approached the 1% limit in all samples cultured at V/V = const./93.12 h in the 117 mL bottles, and it even reached more than 2% in some of the smaller volume replicates at n/n = const./1.1 bar in the 117 mL bottles at 102.65 h and in the 570 mL bottles at 75.25 h. However, the standard deviations for GTGT-0a in all cases are very high; therefore, the fluctuations of GTGT-0a are not robust, and the results should be treated with care.

Compared to GDGT-0a and -0b, the relative amounts of GDGT-0c are negligible (below 1% of total GDGTs; Figure 7). With an average 70 to 90%, GDGT-0a shows the highest relative amount among the GDGTs. The highest average proportion of GDGT-0a (91.5%) was measured at large volumes for V/V = const./1.1 bar/93.12 h in the 117 mL bottles. In contrast, the lowest average proportion of GDGT-0a (70.6%) was measured at large volumes for n/n = const./1.5 bar/75.25 h in the 570 mL bottles. The proportion of GDGT-0b and -0c relative to GDGT-0a (degree of methylation) in the 117 mL bottles at V/V = const. (especially those at 93.12 h) was, on average, lower than in the 117 mL bottles at n/n = const., and in all the experiments in the 570 mL bottles.



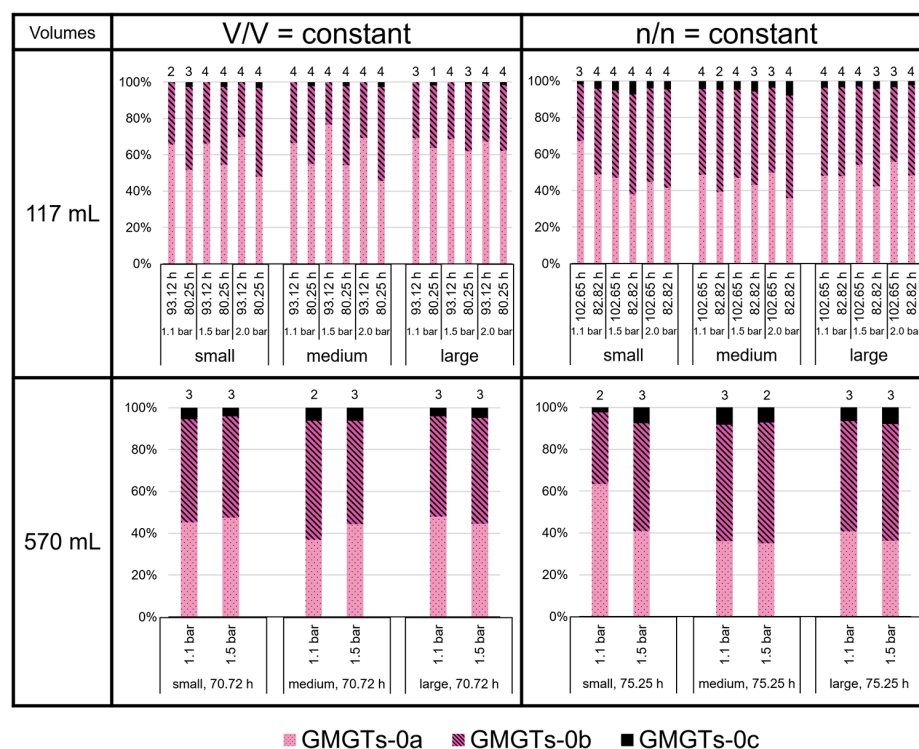


**Figure 6.** Tetraether lipid (GDGTs and GMGTs) ratios in *M. marburgensis* cultures in %. Pressure is given in bar relative to atmospheric pressure. Numbers above bars indicate number of samples. Samples quantified with 5- $\alpha$ -cholestane standard are indicated in Tables S4–S9.



**Figure 7.** GDGT lipid (GDGT-0a, GDGT-0b, and GDGT-0c) ratios in *M. marburgensis* cultures. Pressure is given in bar relative to atmospheric pressure. Numbers above bars indicate number of samples. Samples quantified with 5- $\alpha$ -cholestane standard are indicated in Tables S4–S9.

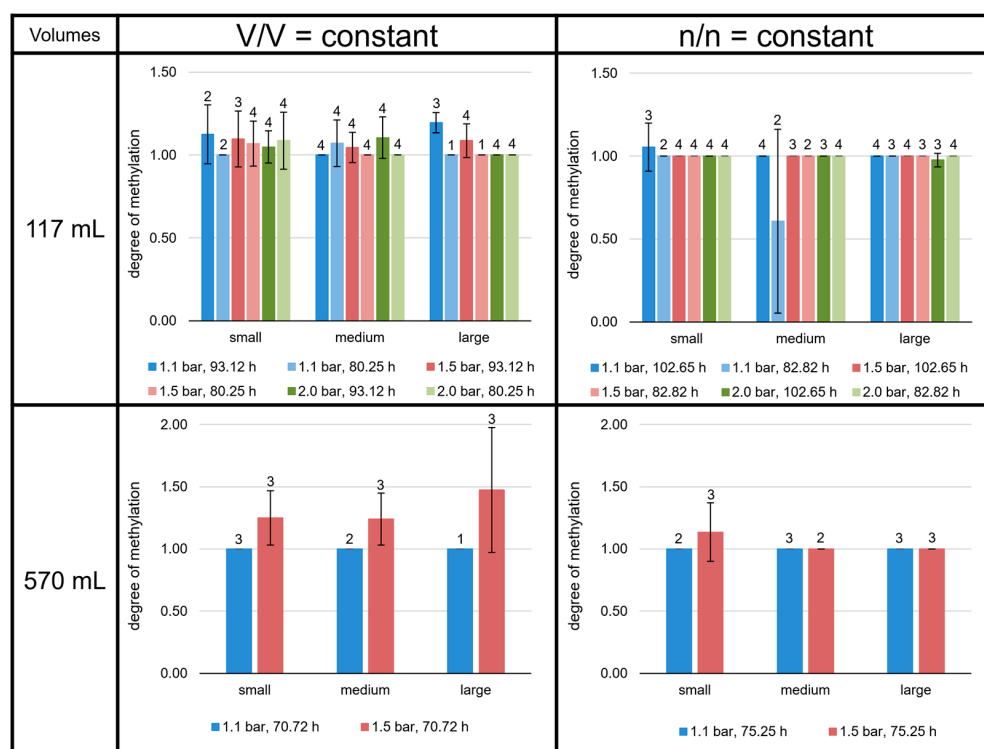
The GMGTs did not show a predominance of the 0a isomers, as shown for the GDGTs (Figure 8). In contrast to GDGT-0c, GMGTs-0c made up between 1 and 7% of total GMGTs at most growth conditions. However, in the 117 mL bottles at V/V = const./93.12 h, GMGTs-0c accounted for less than 1% of total GMGTs, which did not occur in any of the other sets of culture conditions. The relative proportion of GMGTs-0c was highest in the 117 mL bottles at n/n = const./82.82 h in the medium volume at 2.0 bar and in the 570 mL bottles at n/n = const. (except the small volume at 1.1 bar). There, it even reached 8% of total GMGTs. Depending on the culture condition, either GMGTs-0a or GMGTs-0b were predominating, whereas GMGTs-0a were dominant more often. The relative proportion of GMGTs-0b varied between 20% and almost 60% of total GMGTs. The ratio  $(1 \times \text{GMGT-0b} + 2 \times \text{GMGT-0c}) / (\text{GMGT-0a} + \text{GMGT-0b} + \text{GMGT-0c})$ , indicating the degree of methylation, tended to be higher at conditions with V/V = const., but only in the 117 mL bottles. For the 570 mL bottles, a higher degree of methylation was only observed for the cultures at V/V = const./1.5 bar (Figure 9).



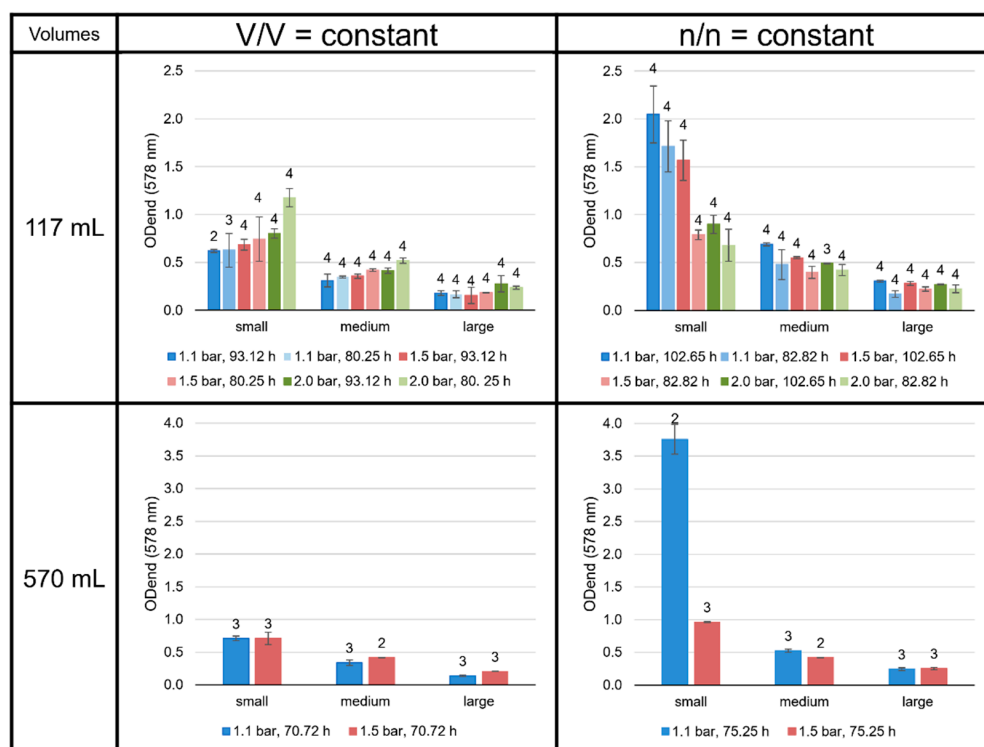
**Figure 8.** GMGT lipid ratios (two isomers each of GMGT-0a, GMGT-0b, and GMGT-0c) in *M. marburgensis* cultures. Pressure is given in bar relative to atmospheric pressure. Numbers above bars indicate number of samples. Samples quantified with 5- $\alpha$ -cholestane standard are indicated in Tables S4–S9.

### 3.4. Impact of Interaction-Area-to-Volume Ratio on Growth

As expected, the experiments performed with a small liquid volume, i.e., a high gaseous volume and, therefore, a high number of gaseous substrates, showed the highest end point optical density ( $\text{OD}_{\text{end}}$ , Figure 10). While for experiments with n/n = const. a longer incubation time led to a higher  $\text{OD}_{\text{end}}$ , this was not observed for the V/V = const. settings. Further, at V/V = const., a higher pressure resulted in a higher  $\text{OD}_{\text{end}}$ , while for n/n = const., the  $\text{OD}_{\text{end}}$  decreased with increasing pressure. However, this trend for n/n = const. could be reversed when dealing with larger volumes, as the 82.82 h pressure series at large volumes may imply. A very remarkable result was the extremely high  $\text{OD}_{\text{end}}$  value accomplished for the n/n = const. experiments at small volumes and 1.1 bar.



**Figure 9.** Degree of methylation of the *M. marburgensis* cultures. Pressure is given in bar relative to atmospheric pressure. Errors are standard deviations. Numbers above bars indicate number of samples.



**Figure 10.** OD<sub>end</sub> (578 nm) of the *M. marburgensis* cultures. Pressure is given in bar relative to atmospheric pressure. Errors are standard deviations. Numbers above bars indicate number of samples.

#### 4. Discussion

In this study, *M. marburgensis* was cultivated under different cultivation conditions and different scales. One of the most remarkable findings was the strong influence of the total incubation times and gassing intervals, not only on the specific lipid production rates and product-to-product yields, but also on the lipid ratios. For instance, in the 117 mL bottles in the small volumes at  $n/n = \text{const.}/1.1$  bar, archaeol production rates were much higher at a total incubation time of 102.65 h compared to a total incubation time of 82.82 h (Figure 5). We cannot explain this discrepancy yet; however, the pressure data showed a strikingly different growth pattern between these two settings within the first 40 h of incubation. Nevertheless, this is only the most extreme example of a series of cases within this study, where incubation times and intervals made the difference. Another important observation of this study was that the total lipid production rates and product-to-product yields in the 117 mL bottles were higher at  $V/V = \text{const.}$  than at  $n/n = \text{const.}$ , on average. The reason for that pattern is yet unknown. However, it is noteworthy that the lipid production rates and yields are, in general, more similar between the 117 mL and 570 mL bottles in the case of  $n/n = \text{const.}$  compared to  $V/V = \text{const.}$  (with some exceptions). Our data clearly stress that the incubation times and intervals need to be strictly equal when attempting to scale lipid production with *M. marburgensis*. From the current data, up-scaling at  $n/n = \text{const.}$  seems more promising, not only based on quantitative considerations. Various lipid ratios at  $V/V = \text{const.}$  in the 117 mL bottles varied in other experimental settings. Generally, lipids that are considered as more specific to *M. marburgensis*, such as GMGTs, extra-methylated GDGTs, and GMGTs [14], were less abundant at  $V/V = \text{const.}$  in the 117 mL bottles, respectively. In contrast, more prominent membrane lipids, such as archaeol and GDGT-0a (e.g., [4,50]), were more abundant at the other conditions. This observation supports a scale-up at  $n/n = \text{const.}$ , especially when a greater variety and higher yield of the minor lipids could be harvested.

An unexpected, yet intriguing, finding was the extraordinarily high growth (and  $\text{OD}_{\text{end}}$ ) in the smaller volumes at  $n/n = \text{const.}$  at 1.1 bar, when the liquid volume-to-headspace-ratio was by far the smallest applied (Figure 9). The explanation for this finding could be the very high ratio of interaction area vs. total liquid volume, in which the organisms can grow. This finding indicates that the scale-up conditions must be well-defined to consider the specific gas transfer coefficient ( $k_L a$  value) or the gas transfer rate to be able to align the specific growth rate and/or cell concentration. Moreover, it would be interesting to test even higher ratios of interaction area vs. liquid volume in future studies. If the optimal ratio is found, it could then be used for further scale-up settings for industrial purposes. The settings showing the highest  $\text{OD}_{\text{end}}$  are  $n/n = \text{const.}$  at small volumes and 1.1 bar at 117 mL (102.65 h) and 570 mL (75.25 h). These settings also reveal a relatively high amount of GDGT-0a and GMGTs-0a compared to the other experiments in the  $n/n = \text{const.}$  settings.

The results shown here indicate the need to examine the lipid production rates and yields and the composition of the lipid inventory under different cultivation conditions in closed batch cultures with the goal of identifying the scaling parameters for a reproducible archaeal-lipid-production pipeline. This is necessary because now the drawbacks and issues are known to successfully start the scale-up of archaea lipid production for the mass utilization of methanogens in Archaea Biotechnology. However, it must be noted that the closed batch growth of methanogens differs from the fed-batch or continuous culture growth of methanogens. Such differences in the cultivation set-up could induce even another lipid production characteristic. Other advantages of employing methanogens for archaeal lipid production are the ability to excrete proteinogenic amino acids into the growth medium [51] and to produce  $\text{CH}_4$  [19] in addition to ether-based lipids [10]. This makes it worthwhile to strongly consider *Methanothermobacter* spp. and other methanogens as chassis to produce various value-added products in biotechnology alongside their use as  $\text{CH}_4$  cell factories. Once such an integrated biotechnological production platform is established, hydrogenotrophic, autotrophic methanogens could replace the

synthetic production of ether lipids, which is based on non-renewable resources. Hence, a methanogen-based lipid-production bioprocess could make use of the  $H_2$  generated from excess renewable energy production, such as wind or solar power, or from biohydrogen production, and the  $CO_2$  from renewable sources, e.g., from bioethanol production. A utilization of methanogens as archaeal cell factories in biotechnology and in biorefinery concepts seems already reasonable.

## 5. Conclusions

Varying the environmental conditions and the incubation periods has a significant impact on the growth, the MER, and the lipid production rate of *M. marburgensis*. This study shows that keeping the particle number constant ( $n/n = \text{const.}$ ) at different pressure settings leads to a higher variability in the lipid pattern than keeping a constant ratio between the liquid and gaseous volumes ( $V/V = \text{const.}$ ). Besides this new insight, the study shows the significant influence of different incubation periods for the same environmental setting. For biotechnological and industrial purposes, the most important outcome of this study is the potential for optimizing the process by finding the right ratio between the interaction area and the total liquid volume. Here, future studies must be performed to optimize current approaches.

**Supplementary Materials:** The following supporting information can be downloaded at <https://www.mdpi.com/article/10.3390/bioengineering9040169/s1>: Table S1: Overview about final media and inoculum volumes for each experiment (in mL) in the 117 and 570 mL bottles; Table S2: Methane evolution rate (MER; in  $\text{mmol L}^{-1}_{\text{liq}} \text{h}^{-1}$ ) for the experiments with  $V/V = \text{const.}$  (117 mL flasks); Table S3: Methane evolution rate (MER; in  $\text{mmol L}^{-1}_{\text{liq}} \text{h}^{-1}$ ) for the experiments with  $n/n = \text{const.}$  (117 mL flasks); Table S4: Specific production rate ( $\mu\text{mol g}^{-1} \text{h}^{-1}$ ) and Product-to-product yield ( $\mu\text{mol C-mol}^{-1}$ ) of the single replicates of each experiment (117 mL flasks,  $V/V = \text{const.}$ ,  $t = 93.12 \text{ h}$ ; end point measurement); Table S5: Specific production rate ( $\mu\text{mol g}^{-1} \text{h}^{-1}$ ) and Product-to-product yield ( $\mu\text{mol C-mol}^{-1}$ ) of the single replicates of each experiment (117 mL flasks,  $V/V = \text{const.}$ ,  $t = 80.25 \text{ h}$ ; end point measurement); Table S6: Specific production rate ( $\mu\text{mol g}^{-1} \text{h}^{-1}$ ) and Product-to-product yield ( $\mu\text{mol C-mol}^{-1}$ ) of the single replicates of each experiment (117 mL flasks,  $n/n = \text{const.}$ ,  $t = 102.65 \text{ h}$ ; end point measurement); Table S7: Specific production rate ( $\mu\text{mol g}^{-1} \text{h}^{-1}$ ) and Product-to-product yield ( $\mu\text{mol C-mol}^{-1}$ ) of the single replicates of each experiment (117 mL flasks,  $n/n = \text{const.}$ ,  $t = 82.82 \text{ h}$ ; end point measurement); Table S8: Specific production rate ( $\mu\text{mol g}^{-1} \text{h}^{-1}$ ) and Product-to-product yield ( $\mu\text{mol C-mol}^{-1}$ ) of the single replicates of each experiment (570 mL flasks,  $V/V = \text{const.}$ ,  $t = 70.72 \text{ h}$ ; end point measurement); Table S9: Specific production rate ( $\mu\text{mol g}^{-1} \text{h}^{-1}$ ) and Product-to-product yield ( $\mu\text{mol C-mol}^{-1}$ ) of the single replicates of each experiment (570 mL flasks,  $n/n = \text{const.}$ ,  $t = 75.25 \text{ h}$ ; end point measurement).

**Author Contributions:** Conceptualization, S.K.-M.R.R.; methodology, D.B. and S.K.-M.R.R.; validation, L.M.F.B., R.-S.T., D.B. and S.K.-M.R.R.; formal analysis, D.B. and S.K.-M.R.R.; investigation, L.M.F.B., R.-S.T., K.O. and A.-C.R.; resources, D.B. and S.K.-M.R.R.; data curation, L.M.F.B. and R.-S.T.; writing—original draft preparation, L.M.F.B., R.-S.T., D.B. and S.K.-M.R.R.; writing—review and editing, L.M.F.B., R.-S.T., B.S., D.B. and S.K.-M.R.R.; visualization, L.M.F.B. and R.-S.T.; supervision, B.S., D.B. and S.K.-M.R.R.; project administration, B.S. and S.K.-M.R.R.; funding acquisition, B.S. and S.K.-M.R.R. All authors have read and agreed to the published version of the manuscript.

**Funding:** This research was funded by the Austrian Research Promotion Agency (Forschungsförderungsgesellschaft (FFG)), grant number 859293, and by the Austrian Science Fund (FWF), grant number P 29399-B22. Open Access Funding by the Austrian Science Fund (FWF).

**Institutional Review Board Statement:** Not applicable.

**Informed Consent Statement:** Not applicable.

**Data Availability Statement:** The datasets used and/or analyzed during the current study are available from the corresponding author on reasonable request.

**Acknowledgments:** We would like to thank Kevin Pfeifer for his assistance in creating the illustration for Figure 2.



**Conflicts of Interest:** S.K.-M.R.R. declares competing interests due to his employment in the Arkeon GmbH. All other authors declare no competing interests.

## References

1. Siliakus, M.F.; van der Oost, J.; Kengen, S.W.M. Adaptations of archaeal and bacterial membranes to variations in temperature, pH and pressure. *Extremophiles* **2017**, *21*, 651–670. [\[CrossRef\]](#) [\[PubMed\]](#)
2. Valentine, D.L. Adaptations to energy stress dictate the ecology and evolution of the Archaea. *Nat. Rev. Microbiol.* **2007**, *5*, 316–323. [\[CrossRef\]](#) [\[PubMed\]](#)
3. Adam, P.S.; Borrel, G.; Brochier-Armanet, C.; Gribaldo, S. The growing tree of Archaea: New perspectives on their diversity, evolution and ecology. *ISME J.* **2017**, *11*, 2407–2425. [\[CrossRef\]](#) [\[PubMed\]](#)
4. De Rosa, M.; Gambacorta, A. The lipids of archaebacteria. *Prog. Lipid Res.* **1988**, *27*, 153–175. [\[CrossRef\]](#)
5. Tornabene, T.G.; Langworthy, T.A.; Holzer, G.; Oró, J. Squalenes, phytanes and other isoprenoids as major neutral lipids of methanogenic and thermoacidophilic “archaebacteria”. *J. Mol. Evol.* **1979**, *13*, 73–83. [\[CrossRef\]](#) [\[PubMed\]](#)
6. Jacquemet, A.; Barbeau, J.; Lemiègre, L.; Benvegnu, T. Archaeal tetraether bipolar lipids: Structures, functions and applications. *Biochimie* **2009**, *91*, 711–717. [\[CrossRef\]](#)
7. Pfeifer, K.; Ergal, I.; Koller, M.; Basen, M.; Schuster, B.; Rittmann, S.K.-M.R. Archaea Biotechnology. *Biotechnol. Adv.* **2021**, *47*, 107668. [\[CrossRef\]](#)
8. Patel, G.B.; Sprott, G.D. Archaeobacterial Ether Lipid Liposomes (Archaeosomes) as Novel Vaccine and Drug Delivery Systems. *Crit. Rev. Biotechnol.* **1999**, *19*, 317–357. [\[CrossRef\]](#)
9. Koga, Y.; Nishihara, M.; Morii, H.; Akagawa-Matsushita, M. Ether polar lipids of methanogenic bacteria: Structures, comparative aspects, and biosyntheses. *Microbiol. Mol. Biol. Rev.* **1993**, *57*, 164–182. [\[CrossRef\]](#)
10. Baumann, L.M.F.; Taubner, R.-S.; Bauersachs, T.; Steiner, M.; Schleper, C.; Peckmann, J.; Rittmann, S.K.-M.R.; Birgel, D. Intact polar lipid and core lipid inventory of the hydrothermal vent methanogens *Methanocaldococcus villosus* and *Methanothermococcus okinawensis*. *Org. Geochem.* **2018**, *126*, 33–42. [\[CrossRef\]](#)
11. Knappy, C.S.; Nunn, C.E.M.; Morgan, H.W.; Keely, B.J. The major lipid cores of the archaeon *Ignisphaera aggregans*: Implications for the phylogeny and biosynthesis of glycerol monoalkyl glycerol tetraether isoprenoid lipids. *Extremophiles* **2011**, *15*, 517–528. [\[CrossRef\]](#) [\[PubMed\]](#)
12. Golyshina, O.V.; Lünsdorf, H.; Kublanov, I.V.; Goldenstein, N.I.; Hinrichs, K.-U.; Golyshin, P.N. The novel extremely acidophilic, cell-wall-deficient archaeon *Cuniculiplasma divulgatum* gen. nov., sp. nov. represents a new family, *Cuniculiplasmataceae* fam. nov., of the order *Thermoplasmatales*. *Int. J. Syst. Evol. Microbiol.* **2016**, *66*, 332–340. [\[CrossRef\]](#) [\[PubMed\]](#)
13. Tourte, M.; Kuentz, V.; Schaeffer, P.; Grossi, V.; Cario, A.; Oger, P.M. Novel Intact Polar and Core Lipid Compositions in the *Pyrococcus* Model Species, *P. furiosus* and *P. yayanosii*, Reveal the Largest Lipid Diversity Amongst Thermococcales. *Biomolecules* **2020**, *10*, 830. [\[CrossRef\]](#) [\[PubMed\]](#)
14. Knappy, C.; Barillà, D.; Chong, J.; Hodgson, D.; Morgan, H.; Suleman, M.; Tan, C.; Yao, P.; Keely, B. Mono-, di- and trimethylated homologues of isoprenoid tetraether lipid cores in archaea and environmental samples: Mass spectrometric identification and significance. *J. Mass Spectrom.* **2015**, *50*, 1420–1432. [\[CrossRef\]](#)
15. Borrel, G.; Brugère, J.-F.; Gribaldo, S.; Schmitz, R.A.; Moissl-Eichinger, C. The host-associated archaeome. *Nat. Rev. Microbiol.* **2020**, *18*, 622–636. [\[CrossRef\]](#)
16. Taubner, R.-S.; Schleper, C.; Firneis, M.G.; Rittmann, S.K.-M.R. Assessing the Ecophysiology of Methanogens in the Context of Recent Astrobiological and Planetological Studies. *Life* **2015**, *5*, 1652–1686. [\[CrossRef\]](#)
17. Lyu, Z.; Shao, N.; Akinyemi, T.; Whitman, W.B. Methanogenesis. *Curr. Biol.* **2018**, *28*, R727–R732. [\[CrossRef\]](#)
18. Liu, Y.; Whitman, W.B. Metabolic, phylogenetic, and ecological diversity of the methanogenic archaea. *Ann. N. Y. Acad. Sci.* **2008**, *1125*, 171–189. [\[CrossRef\]](#)
19. Mauerhofer, L.M.; Zwirtmayr, S.; Pappenreiter, P.; Bernacchi, S.; Seifert, A.H.; Reischl, B.; Schmider, T.; Taubner, R.S.; Paulik, C.; Rittmann, S.K.-M.R. Hyperthermophilic methanogenic archaea act as high-pressure CH<sub>4</sub> cell factories. *Commun. Biol.* **2021**, *4*, 289. [\[CrossRef\]](#)
20. Mauerhofer, L.-M.; Reischl, B.; Schmider, T.; Schupp, B.; Nagy, K.; Pappenreiter, P.; Zwirtmayr, S.; Schuster, B.; Bernacchi, S.; Seifert, A.H.; et al. Physiology and methane productivity of *Methanobacterium thermaggregans*. *Appl. Microbiol. Biotechnol.* **2018**, *102*, 7643–7656. [\[CrossRef\]](#)
21. Abdel Azim, A.; Pruckner, C.; Kolar, P.; Taubner, R.S.; Fino, D.; Saracco, G.; Sousa, F.L.; Rittmann, S.K.M.R. The physiology of trace elements in biological methane production. *Bioresour. Technol.* **2017**, *241*, 775–786. [\[CrossRef\]](#) [\[PubMed\]](#)
22. Rittmann, S.K.-M.R.; Seifert, A.H.; Bernacchi, S. Kinetics, multivariate statistical modelling, and physiology of CO<sub>2</sub>-based biological methane production. *Appl. Energy* **2018**, *216*, 751–760. [\[CrossRef\]](#)
23. Schönheit, P.; Moll, J.; Thauer, R.K. Nickel, cobalt, and molybdenum requirement for growth of *Methanobacterium thermoautotrophicum*. *Arch. Microbiol.* **1979**, *123*, 105–107. [\[CrossRef\]](#) [\[PubMed\]](#)
24. Wasserfallen, A.; Nöbling, J.; Pfister, P.; Reeve, J.; De Macario, E.C. Phylogenetic analysis of 18 thermophilic *Methanobacterium* isolates supports the proposals to create a new genus, *Methanothermobacter* gen. nov., and to reclassify several isolates in three species, *Methanothermobacter thermotrophicus* comb. nov., *Methano. Int. J. Syst. Evol. Microbiol.* **2000**, *50*, 43–53. [\[CrossRef\]](#)



25. Zeikus, J.G.; Wolfe, R.S. *Methanobacterium thermoautotrophicus* sp. n., an anaerobic, autotrophic, extreme thermophile. *J. Bacteriol.* **1972**, *109*, 707–715. [\[CrossRef\]](#)
26. Seifert, A.H.; Rittmann, S.; Herwig, C. Analysis of process related factors to increase volumetric productivity and quality of biomethane with *Methanothermobacter marburgensis*. *Appl. Energy* **2014**, *132*, 155–162. [\[CrossRef\]](#)
27. Kaster, A.-K.; Moll, J.; Parey, K.; Thauer, R.K. Coupling of ferredoxin and heterodisulfide reduction via electron bifurcation in hydrogenotrophic methanogenic archaea. *Proc. Natl. Acad. Sci. USA* **2011**, *108*, 2981–2986. [\[CrossRef\]](#)
28. Heiko, L.; Anne-Kristin, K.; Arnim, W.; Meike, G.; Antje, W.; Henning, S.; Gerhard, G.; Rudolf, K.T. Complete Genome Sequence of *Methanothermobacter marburgensis*, a Methanoarchaeon Model Organism. *J. Bacteriol.* **2010**, *192*, 5850–5851.
29. Taubner, R.-S.; Rittmann, S.K.-M.R. Method for Indirect Quantification of CH<sub>4</sub> Production via H<sub>2</sub>O Production Using Hydrogenotrophic Methanogens. *Front. Microbiol.* **2016**, *7*, 532. [\[CrossRef\]](#)
30. Bernacchi, S.; Rittmann, S.; Seifert, H.A.; Krajete, A.; Herwig, C. Experimental methods for screening parameters influencing the growth to product yield (Y(x/CH<sub>4</sub>)) of a biological methane production (BMP) process performed with *Methanothermobacter marburgensis*. *AIMS Bioeng.* **2014**, *1*, 72–86. [\[CrossRef\]](#)
31. Rittmann, S.; Seifert, A.; Herwig, C. Quantitative analysis of media dilution rate effects on *Methanothermobacter marburgensis* grown in continuous culture on H<sub>2</sub> and CO<sub>2</sub>. *Biomass Bioenergy* **2012**, *36*, 293–301. [\[CrossRef\]](#)
32. Rittmann, S.K.-M.R.; Pfeifer, K.; Palabikyan, H.; Ergal, I.; Schuster, B. Archaea in der Biotechnologie. *BIOspektrum* **2021**, *27*, 96–98. [\[CrossRef\]](#)
33. Gräther, O.W. *Zur Struktur und Biosynthese der Tetraetherlipide der Archaea*; ETH Zürich: Zürich, Switzerland, 1994.
34. Paltauf, F. Ether lipids in biomembranes. *Chem. Phys. Lipids* **1994**, *74*, 101–139. [\[CrossRef\]](#)
35. Kaur, G.; Garg, T.; Rath, G.; Goyal, A.K. Archaeosomes: An excellent carrier for drug and cell delivery. *Drug Deliv.* **2016**, *23*, 2497–2512. [\[CrossRef\]](#)
36. Gambacorta, A.; Gliozzi, A.; De Rosa, M. Archaeal lipids and their biotechnological applications. *World J. Microbiol. Biotechnol.* **1995**, *11*, 115–131. [\[CrossRef\]](#)
37. Liefelth, K.; Frant, M.; Müller, U.; Stenstad, P.; Johnsen, H.; Schmid, R. Archaeal tetraether lipid coatings—A strategy for the development of membrane analog spacer systems for the site-specific functionalization of medical surfaces. *Biointerphases* **2018**, *13*, 011004. [\[CrossRef\]](#)
38. Choquet, C.G.; Patel, G.B.; Sprott, G.D.; Beveridge, T.J. Stability of pressure-extruded liposomes made from archaeobacterial ether lipids. *Appl. Microbiol. Biotechnol.* **1994**, *42*, 375–384. [\[CrossRef\]](#)
39. Choquet, C.G.; Patel, G.B.; Sprott, G.D. Heat sterilization of archaeal liposomes. *Can. J. Microbiol.* **1996**, *42*, 183–186. [\[CrossRef\]](#)
40. Sprott, G.D.; Dicaire, C.J.; Fleming, L.P.; Patel, G.B. Stability of liposomes prepared from archaeobacterial lipids and phosphatidylcholine mixtures. *Cells Mater.* **1996**, *6*, 143–155.
41. Metcalf, W.W.; Zhang, J.K.; Apolinario, E.; Sowers, K.R.; Wolfe, R.S. A genetic system for Archaea of the genus *Methanosarcina*: Liposome-mediated transformation and construction of shuttle vectors. *Proc. Natl. Acad. Sci. USA* **1997**, *94*, 2626–2631. [\[CrossRef\]](#)
42. Benvegnu, T.; Lemiegre, L.; Cammas-Marion, S. New Generation of Liposomes Called Archaeosomes Based on Natural or Synthetic Archaeal Lipids as Innovative Formulations for Drug Delivery. *Recent Pat. Drug Deliv. Formul.* **2009**, *3*, 206–220. [\[CrossRef\]](#) [\[PubMed\]](#)
43. Leriche, G.; Cifelli, J.L.; Sibucio, K.C.; Patterson, J.P.; Koyanagi, T.; Gianneschi, N.C.; Yang, J. Characterization of drug encapsulation and retention in archaea-inspired tetraether liposomes. *Org. Biomol. Chem.* **2017**, *15*, 2157–2162. [\[CrossRef\]](#) [\[PubMed\]](#)
44. Beveridge, T.J.; Choquet, C.G.; Patel, G.B.; Sprott, G.D. Freeze-fracture planes of methanogen membranes correlate with the content of tetraether lipids. *J. Bacteriol.* **1993**, *175*, 1191–1197. [\[CrossRef\]](#) [\[PubMed\]](#)
45. Elferink, M.G.L.; de Wit, J.G.; Driessen, A.J.M.; Konings, W.N. Stability and proton-permeability of liposomes composed of archaeal tetraether lipids. *Biochim. Biophys. Acta Biomembr.* **1994**, *1193*, 247–254. [\[CrossRef\]](#)
46. Krishnan, L.; Dennis Sprott, G. Archaeosomes as Self-Adjuvanting Delivery Systems for Cancer Vaccines\*. *J. Drug Target.* **2003**, *11*, 515–524. [\[CrossRef\]](#)
47. Krishnan, L.; Sad, S.; Patel, G.B.; Sprott, G.D. Archaeosomes Induce Long-Term CD8 + Cytotoxic T Cell Response to Entrapped Soluble Protein by the Exogenous Cytosolic Pathway, in the Absence of CD4 + T Cell Help. *J. Immunol.* **2000**, *165*, 5177–5185. [\[CrossRef\]](#)
48. Stark, F.C.; Agbayani, G.; Sandhu, J.K.; Akache, B.; McPherson, C.; Deschatelets, L.; Dudani, R.; Hewitt, M.; Jia, Y.; Krishnan, L.; et al. Simplified Admix Archaeal Glycolipid Adjuvanted Vaccine and Checkpoint Inhibitor Therapy Combination Enhances Protection from Murine Melanoma. *Biomedicine* **2019**, *7*, 91. [\[CrossRef\]](#)
49. Huguet, C.; Hopmans, E.C.; Febo-Ayala, W.; Thompson, D.H.; Sinninghe Damsté, J.S.; Schouten, S. An improved method to determine the absolute abundance of glycerol dibiphytanyl glycerol tetraether lipids. *Org. Geochem.* **2006**, *37*, 1036–1041. [\[CrossRef\]](#)
50. Schouten, S.; Hopmans, E.C.; Sinninghe Damsté, J.S. The organic geochemistry of glycerol dialkyl glycerol tetraether lipids: A review. *Org. Geochem.* **2013**, *54*, 19–61. [\[CrossRef\]](#)
51. Taubner, R.-S.; Baumann, L.M.F.; Bauersachs, T.; Clifford, E.L.; Mähner, B.; Reischl, B.; Seifert, R.; Peckmann, J.; Rittmann, S.K.-M.R.; Birgel, D. Membrane Lipid Composition and Amino Acid Excretion Patterns of *Methanothermococcus okinawensis* Grown in the Presence of Inhibitors Detected in the Enceladian Plume. *Life* **2019**, *9*, 85. [\[CrossRef\]](#)

# ANNEX 5

Pages 110 to 122

---

Steger F., Reich J., Fuchs W., Rittmann S.K.-M.R., Gübitz G.M., Ribitsch D., Bochner G.

**Comparison of carbonic anhydrases for CO<sub>2</sub> sequestration**

International Journal of Molecular Sciences (2022) 23(2):957

10.3390/ijms23020957

---



Article

# Comparison of Carbonic Anhydrases for CO<sub>2</sub> Sequestration

Franziska Steger <sup>1</sup>, Johanna Reich <sup>1,2</sup>, Werner Fuchs <sup>1</sup>, Simon K.-M. R. Rittmann <sup>3</sup>, Georg M. Gübitz <sup>1</sup>, Doris Ribitsch <sup>2,\*</sup> and Günther Bochmann <sup>1</sup>

- <sup>1</sup> Institute of Environmental Biotechnology, Department for Agrobiotechnology, University of Natural Resources and Life Sciences Vienna, Konrad Lorenz Str. 20, A-3430 Tulln, Austria; franziska.steger@boku.ac.at (F.S.); johanna.reich@boku.ac.at (J.R.); werner.fuchs@boku.ac.at (W.F.); guebitz@boku.ac.at (G.M.G.); guenther.bochmann@boku.ac.at (G.B.)
- <sup>2</sup> ACIB—Austrian Centre of Industrial Biotechnology, Krenngasse 37, 8010 Graz, Austria
- <sup>3</sup> Archaea Physiology & Biotechnology Group, Department of Functional and Evolutionary Ecology, University of Vienna, Djerassiplatz 1, 1030 Vienna, Austria; simon.rittmann@univie.ac.at
- \* Correspondence: doris.ribitsch@boku.ac.at

**Abstract:** Strategies for depleting carbon dioxide (CO<sub>2</sub>) from flue gases are urgently needed and carbonic anhydrases (CAs) can contribute to solving this problem. They catalyze the hydration of CO<sub>2</sub> in aqueous solutions and therefore capture the CO<sub>2</sub>. However, the harsh conditions due to varying process temperatures are limiting factors for the application of enzymes. The current study aims to examine four recombinantly produced CAs from different organisms, namely CAs from *Acetobacterium woodii* (AwCA or CynT), *Persephonella marina* (PmCA), *Methanobacterium thermoautotrophicum* (MtaCA or Cab) and *Sulphurihydrogenibium yellowstonense* (SspCA). The highest expression yields and activities were found for AwCA (1814 WAU mg<sup>−1</sup> AwCA) and PmCA (1748 WAU mg<sup>−1</sup> PmCA). AwCA was highly stable in a mesophilic temperature range, whereas PmCA proved to be exceptionally thermostable. Our results indicate the potential to utilize CAs from anaerobic microorganisms to develop CO<sub>2</sub> sequestration applications.



**Citation:** Steger, F.; Reich, J.; Fuchs, W.; Rittmann, S.K.-M.R.; Gübitz, G.M.; Ribitsch, D.; Bochmann, G. Comparison of Carbonic Anhydrases for CO<sub>2</sub> Sequestration. *Int. J. Mol. Sci.* **2022**, *23*, 957. <https://doi.org/10.3390/ijms23020957>

Academic Editor:  
Maria Giulia Lionetto

Received: 19 November 2021

Accepted: 13 January 2022

Published: 16 January 2022

**Publisher's Note:** MDPI stays neutral with regard to jurisdictional claims in published maps and institutional affiliations.



**Copyright:** © 2022 by the authors. Licensee MDPI, Basel, Switzerland. This article is an open access article distributed under the terms and conditions of the Creative Commons Attribution (CC BY) license (<https://creativecommons.org/licenses/by/4.0/>).

**Keywords:** carbonic anhydrase; CO<sub>2</sub> sequestration; thermostability; activity assay; recombinant expression

## 1. Introduction

Due to the rapid growth of the world economy, there is a continual escalation in its carbon intensity. Carbon dioxide (CO<sub>2</sub>) emissions are rapidly increasing, making CO<sub>2</sub> the most abundant greenhouse gas emitted by human activities [1–3]. Reducing the CO<sub>2</sub> content in the atmosphere is imperative in meeting the UNFCCC climate goal of limiting the global temperature increase below 2 °C above pre-industrial levels [4]. Strategies for capturing CO<sub>2</sub> from flue gasses are essential, until the ultimate goal of transition from non-renewable energy sources, such as natural gas and coal, to renewable energy sources is reached. Currently, there are various technologies and advances for capturing CO<sub>2</sub> from flue gas, including chemical absorption of CO<sub>2</sub> by solvents [5–7]. Through this method, a great fraction of CO<sub>2</sub> can be depleted from the flue gas by passing it through a solvent, such as monoethanolamine (MEA), where CO<sub>2</sub> molecules are extracted [8]. In the second step, the solvent is regenerated, and pure CO<sub>2</sub> is released. A significant detrimental effect when utilizing MEA is the side generation of toxic wastes and aerosols [8,9]. Another disadvantage is the high amount of energy required for the release of CO<sub>2</sub> from the solvent at high temperatures up to 120 °C [10], leaving CO<sub>2</sub> capture with MEA unfavorable from an economic and sustainable standpoint [11].

An alternative is the “biomimetic” approach to capture CO<sub>2</sub>. Enzymes, such as carbonic anhydrases (CAs), accelerate the hydration of CO<sub>2</sub>, consequently facilitating the application of energy-efficient but kinetically-limited aqueous solvents, such as salt solutions (e.g., CaCl<sub>2</sub>, KOH) [8,12]. Biomimetic CO<sub>2</sub> capture has previously been described,

studied and implemented as a more sustainable and more economic option [12–14]. The temperature needed to release pure CO<sub>2</sub> from aqueous salt solutions can be significantly reduced to 80 °C or less in biomimetic applications due to the decreased binding of CO<sub>2</sub> compared to MEA solutions [15,16]. An existing critical challenge is to maintain the stability of the enzymes during varying temperatures from 30 °C to 80 °C in the process [15,17].

CAs are mainly zinc-containing metalloenzymes [18] and hydrate CO<sub>2</sub> to hydrogen carbonate (HCO<sub>3</sub><sup>−</sup>) according to the following two-step mechanism [19,20]:



CAs are ubiquitously found in prokaryotes as well as in eukaryotes. There are eight distinct classes of carbonic anhydrases ( $\alpha$ ,  $\beta$ ,  $\gamma$ ,  $\delta$ ,  $\zeta$ ,  $\eta$ ,  $\theta$ ,  $\iota$ ), which vary in their roles in different crucial physiological processes, amino acid sequences and 3-D tertiary structures [18,21]. CAs from extremophiles, existing at high temperatures, are a specific focus of interest, because they have been proven to be particularly active and thermostable [12,22]. The following three CAs from thermophilic organisms were selected based on literature research: PmCA originates from the bacterium *Persephonella marina* EX-H1, which exists in the deep-sea in an environment with excessive temperatures up to 133 °C and high pressures. Under laboratory conditions, *P. marina* grows in temperatures up to 80 °C [23]. SspCA is an enzyme from the bacterial strain *Sulphurihydrogenibium yellowstonense* YO3AOP1, which occurs in hot springs with a growth optimum at 70 °C and can grow autotrophically with CO<sub>2</sub>. PmCA and SspCA are  $\alpha$ -type CAs and have been studied intensely with existing patents that have been published for their uses in biomimetic CO<sub>2</sub> capture applications [24–28]. Both enzymes have been demonstrated to have high hydratase activities and to be exceptionally thermostable [24,29,30]. MtaCA, also referred to as Cab in the literature, was selected to extend the study with a  $\beta$ -type, thermostable CA [31], originating from the extreme thermophilic archaeon *Methanobacterium thermoautotrophicum*, which grows at up to 75 °C and metabolizes CO<sub>2</sub> to methane [32]. The fourth CA selected for this study was AwCA, also referred to as CynT in the literature. It originates from the bacterium *Acetobacterium woodii* DSM 1030 with a growth optimum at 30 °C [33]. According to the NCBI's Conserved Domain Database (CDD), AwCA belongs to the  $\beta$ -type class [34]. Despite AwCA originating from a mesophilic organism, it was selected due to its stated exceptional activity [35].

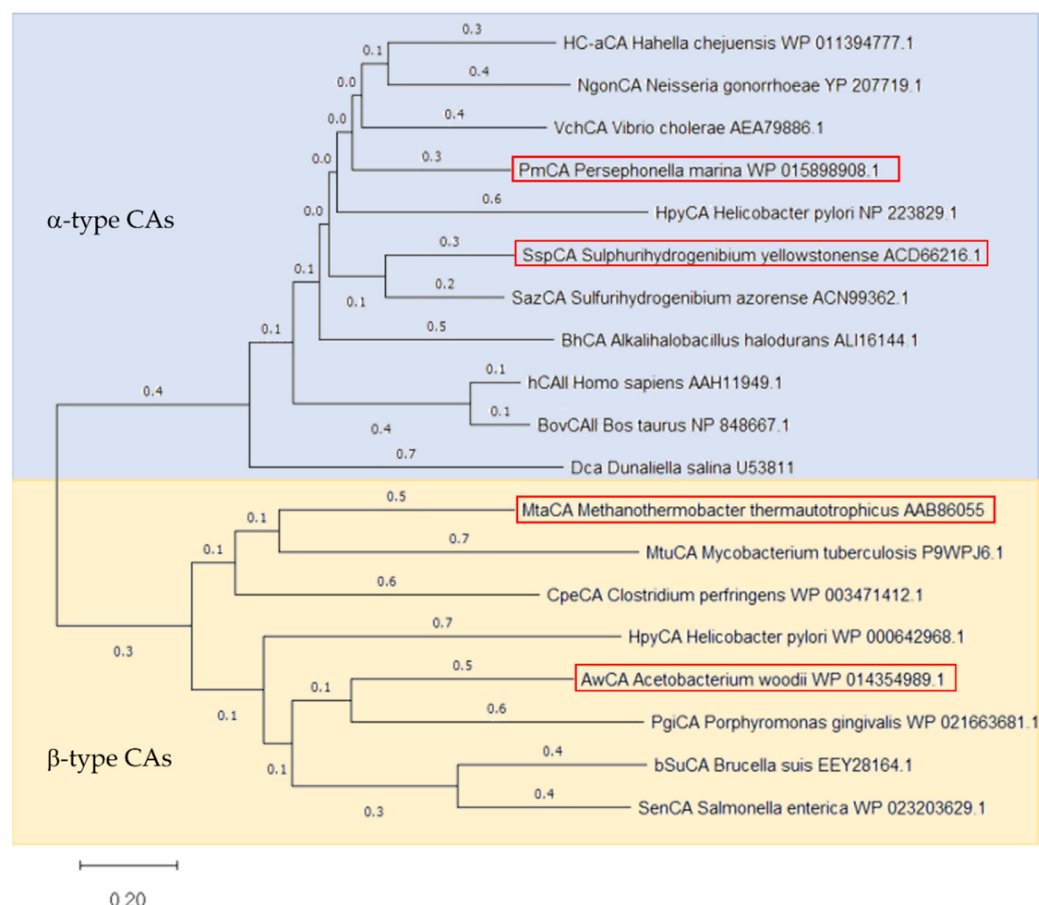
The recombinant expression of genes was the pivotal breakthrough allowing for the mass production of enzymes paving the way towards the industrial implementation of enzymes [36]. The current study aimed to examine these four recombinantly produced CAs from different organisms for biomimetic CO<sub>2</sub> sequestration. Firstly, expression yields were determined using a single expression strategy in *Escherichia coli*. The effect of the CA addition on CO<sub>2</sub> hydration at different temperatures was explored by applying the three CAs with the highest expression yields. A novel straightforward assay for the determination of CA activity was applied in this study, where measurement occurs close to industrial process conditions and temperatures [37]. The new assay allowed the characterization of CAs at temperatures exceeding 0 °C, which is unique concerning the commonly used Wilbur Anderson assay [38]. In the end, the thermostability of the two best performing CAs was compared, under the given conditions.

## 2. Results

### 2.1. Selection, Expression and Purification

Four CAs were selected for comparison regarding their ability to convert CO<sub>2</sub> into HCO<sub>3</sub><sup>−</sup>, namely CAs from *Acetobacterium woodii* (AwCA), *Persephonella marina* (PmCA), *Methanobacterium thermoautotrophicum* (MtaCA) and *Sulphurihydrogenibium yellowstonense* (SspCA). The selected CAs belong to different types of CAs and share only low homologies among each other, as shown in the phylogenetic tree built on published CA protein

sequences (Figure 1). PmCA and SspCA have been identified as  $\alpha$ -type CAs originating from Gram-negative organisms. The two CAs share 45% homology and thus the highest similarity among the selected protein sequences. AwCA and MtaCA, however, are  $\beta$ -type CAs derived from Gram-positive organisms or archaea, respectively, and share only 20% homology among each other. Homologies between  $\alpha$ -CAs and  $\beta$ -CAs are below 15%.



**Figure 1.** Phylogenetic tree of  $\alpha$ -type and  $\beta$ -type CAs. Phylogenetic tree was constructed by MEGA11 software employing the Neighbor-joining Method [39] based on the protein sequences of CAs used in this study (highlighted by a red frame) as well as CAs described in literature. The blue background indicated  $\alpha$ -type CAs, the yellow one the  $\beta$ -type CAs. The protein sequences are named by their Cryptonym followed by the microorganism's name and the NCBI accession number. The bar at the bottom provides the scale of the branch lengths.

Both  $\alpha$ - and  $\beta$ -CAs are metalloenzymes, which use Zn(II) ions for chemical catalysis. Despite their shared CO<sub>2</sub> hydratase activity, the two classes demonstrate major structural differences, which are also seen in alignments of CAs investigated in this study (Supplementary Materials Section S3). The Zinc ion, for instance, is tetrahedrally coordinated by three histidines in  $\alpha$ -CAs but by one histidine and two cysteines in  $\beta$ -CAs. A water molecule or hydroxide ion acts as a fourth ligand and nucleophile in the catalytic reaction in both CA classes. Similarly to all other  $\alpha$ -CAs described in literature, the three histidines are present in PmCA (His89, His90, His108) and SspCA (His99, His101 and His118), which are relatively close to each other in the protein sequence. Additionally, a highly conserved histidine (His74 in PmCA and His64 in SspCA) is presently proposed to act as the proton shuttle. AwCA and MtaCA, however, are displaying the Zn(II) coordinating histidine (His110 and His87, respectively) and cysteines (Cys57 and Cys113 in AwCA, Cys32 and Cys90 in MtaCA) in their protein sequences, as expected for  $\beta$ -CAs. Besides, AwCA displays the highly conserved DSRV motif (residues 59–62) and Gln48, which are



proposed to be involved in the catalytic reaction. Interestingly, Val62 is exchanged for Leu36 in this motif in MtaCA (residues 33–36) and also, Gln is not present at the corresponding amino acid position.

The protein sequences of PmCA and SspCA exhibit natural N-terminal signal peptides, comprising amino acids 1–19 in PmCA and 1–20 in SspCA, which were removed for the production of recombinant proteins in *E. coli*. Removal of the signal peptides of PmCA and SspCA was previously described as a tool to enhance expression yields [25,29,30]. The influence of the removal on hydratase activity was not evaluated during this study. Unlike the CAs mentioned above, AwCA and MtaCA do not reveal natural signal sequences. According to the analysis of the protein sequences, evidence for transmembrane domains or membrane anchors was not found in either of the applied CAs. According to Capasso and Supuran (2015), bacterial  $\alpha$ -CAs are localized in the periplasmic compartment of Gram-negative bacteria. Contrastingly, bacterial  $\beta$ -CAs are mainly localized in the cytoplasm [40]. The alignment of sequences without signal peptides but fused to the StrepTag, as expressed in this study, can be found in the Supplementary Materials Section S3.

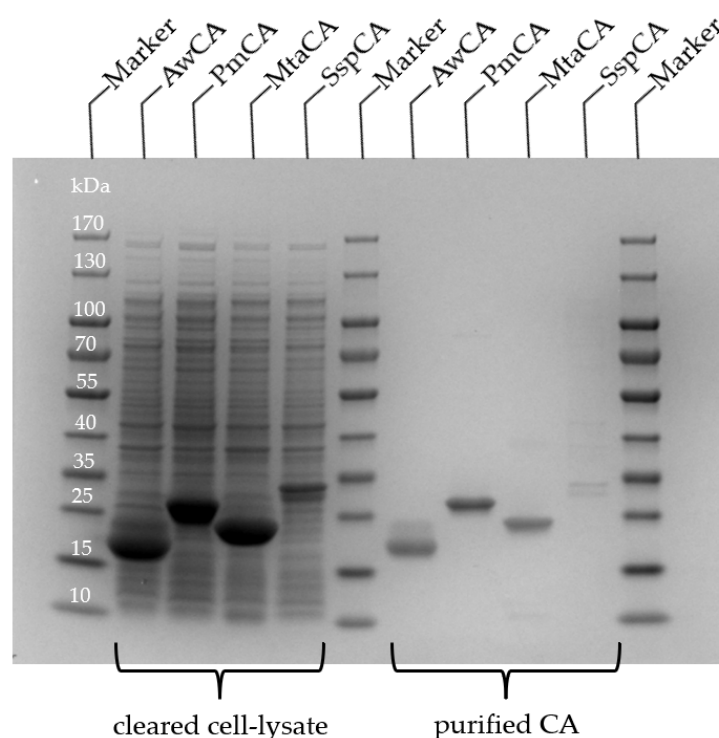
All CA encoding genes (Supplementary Materials Section S4) were codon optimized for expression in *E. coli* and fused to a C-terminal StrepTag, except for SspCA, which carried an N-terminal StrepTag. The synthetic genes were cloned into pET-vectors and expressed in *E. coli* BL21-Gold (DE3) at 37 °C. An SDS-PAGE analysis of samples withdrawn from *E. coli* liquid cultures at several time points (Supplementary Materials Figures S2, S5, S8 and S11) revealed high production levels of soluble protein at the expected molecular masses for AwCA (22.0 kDa), MtaCA (19.9 kDa) and PmCA (26.9 kDa), but only low production of SspCA (27.5 kDa). All CAs formed inclusion bodies, as determined by the SDS-PAGE analysis of insoluble cell fractions.

Purification of CAs from cleared *E. coli* cell lysates was achieved by a single step affinity chromatography through the StrepTag. Fractions containing the CAs were pooled and analyzed by SDS-PAGE (Figure 2). For SspCA, a double protein band on the SDS PAGE of cleared cell lysate and purified enzyme indicated a proteolysis on the N-terminal end during expression. The second protein band of cleared cell lysate and purified enzyme of AwCA in Figure 2 is attributed to the unspecific binding of *E. coli* proteins, whereas the second protein band in Supplementary Materials Figure S4 (elution fraction, line 7) is attributed to the formation of dimers of AwCA, which were not separated due to overloading of the SDS gel. AwCA belongs to the  $\beta$ -class, which is known to form dimers, tetramers and octamers [41], while  $\alpha$ -CAs are usually monomers [40].

Typically, 25 mg AwCA, 15 mg PmCA, 18 mg MtaCA and 0.6 mg SspCA were obtained from 100 mL *E. coli* liquid culture according to the calculation based on purified enzymes. The yields are thus significantly higher than those from the literature, based on 100 mL liquid culture, which are 4.8 mg for AwCA when produced in *A. woodii* [35], and 0.129 mg or 0.93 mg of PmCA after production with and without signal peptide, respectively, in *E. coli* [29]. Around 10 mg MtaCA were obtained from diluted *E. coli* cell paste in 20 mL buffer [31]. In the study of Capasso et al. (2012), 12 mg SspCA were produced from an unknown volume of *E. coli* liquid culture using the expression vector pET15-b. Hence, the production of SspCA may be optimized in future studies.

SspCA was excluded from the following experiments after a change of an initial C-terminal StrepTag (not shown) to the N-terminal StrepTag resulted in similarly low expression yields. A further investigation to find the optimal expression system for SspCA was not conducted due to the fact that three out of four CAs demonstrated high expression yields under the chosen conditions. An optimization of the expression and vector system for SspCA may be conducted in future studies to assess the expression yields of SspCA.





**Figure 2.** SDS-PAGE of CAs produced in *E. coli*. Samples of cleared cell lysate and after purification by affinity chromatography. Expected molecular masses are 22.0 kDa (AwCA), 26.9 kDa (PmCA), 19.9 kDa (MtCA) and 27.5 kDa (SspCA).

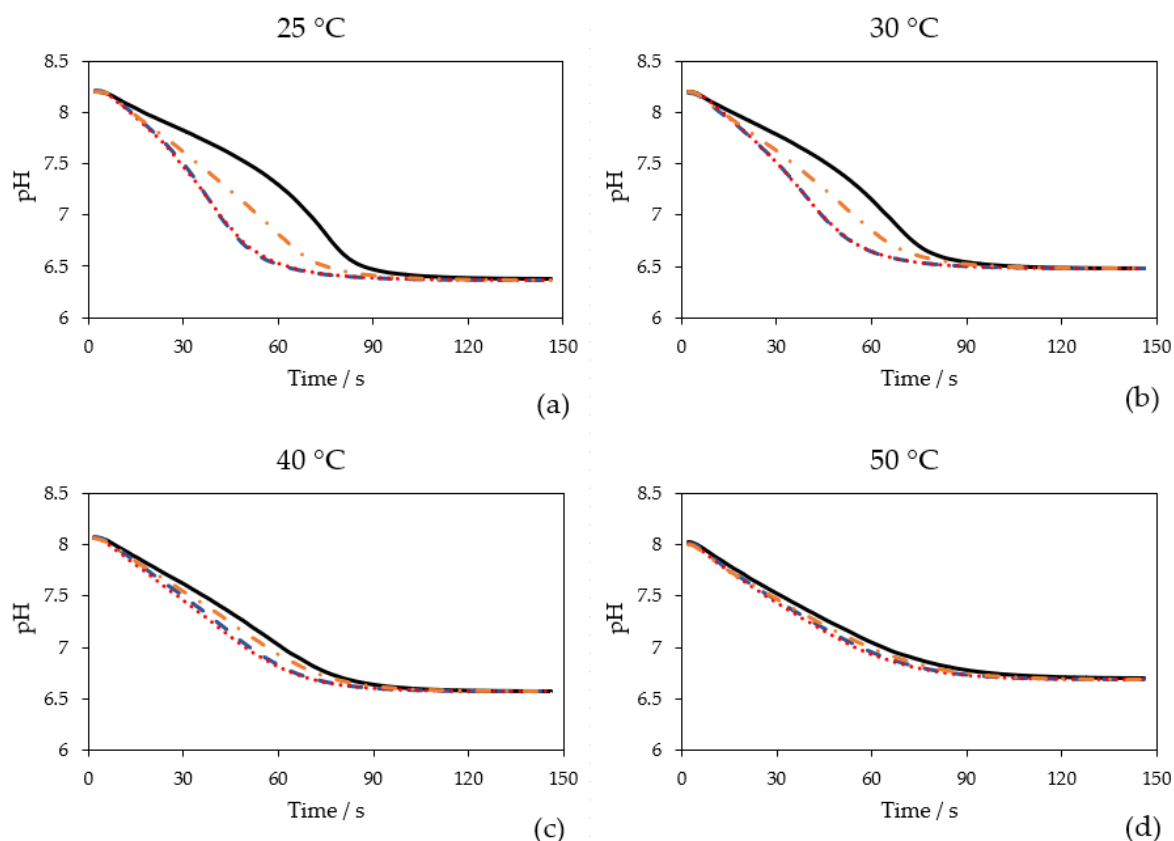
## 2.2. Effect of CAs on CO<sub>2</sub> Hydration at Different Temperatures

The effect on CO<sub>2</sub> hydration at different temperatures (25 °C, 30 °C, 40 °C and 50 °C) was investigated for AwCA, PmCA and MtaCA. Figure 3 displays the pH courses over time when 0.1 mol L<sup>−1</sup> Tris-sulfate buffer was sparged with CO<sub>2</sub> at different temperatures. At each temperature, the blank without CA showed the slowest decrease in pH compared to the measurements where CAs were added. When CO<sub>2</sub> is introduced into aqueous solutions it partly forms carbonic acid, which almost completely deprotonates into HCO<sub>3</sub><sup>−</sup> + H<sup>+</sup>, which causes a pH drop. CAs catalyze the direct conversion of CO<sub>2</sub> to HCO<sub>3</sub><sup>−</sup> + H<sup>+</sup> and vice versa [18]. Therefore, at a surplus of CO<sub>2</sub>, the more active the CA is, the faster the pH drops. The difference between the blank and CAs was most obvious at 25 °C to 40 °C, demonstrating that all enzymes had an accelerating effect on CO<sub>2</sub> hydration in this temperature range. However, it is noticeable that the effect of MtaCA was constantly minor compared to PmCA and AwCA.

The advantage of the method used in this study is that the measurement is conducted at relevant temperatures of industrial processes (25–50 °C), in contrast to the widely used Wilbur Anderson assay, which is conducted solely at 0 °C [38]. Hence, the effect of CAs at temperatures close to process conditions can be investigated. Comparing the four diagrams (Figure 3), it is visible that with temperature elevation the equilibrium pH is rising because the solubility of CO<sub>2</sub> is decreasing [42]. The starting pH at 40 °C and 50 °C was also lower being close to 8.0. The buffer stock solution (500 mL) was only preheated at the respective temperature before pH adjustment. For future measurements, it is recommended to keep the buffer stock solution in a temperature-controlled vessel during pH adjustment to avoid temperature-dependent pH shifts.

As illustrated in Figure 3, at higher temperatures the course of the blank becomes steeper and more similar to the curves in which CAs were added. At higher temperatures, the uncatalyzed formation of HCO<sub>3</sub><sup>−</sup> + H<sup>+</sup> is faster than at lower temperatures. Whereas in total, less CO<sub>2</sub> is solubilized, leading to a lower substrate concentration. At 50 °C, only a minor difference between the measurements with and without CAs can be observed. Another

potential reason might be that the CAs are eventually less active at elevated temperatures. In this publication, the activity was calculated at 25 °C (Section 2.3). Calculation of activities at 30 °C, 40 °C and 50 °C was not performed. However, it might be unlikely that CAs that originate from thermophilic organisms (PmCA and MtaCA) lose their activity at 50 °C. As visualized in Figure 3, the effect of CA addition to CO<sub>2</sub> capture at higher temperatures (>40 °C) is marginal and therefore not advisable. Fradette et al. (2017) reported that the absorption of CO<sub>2</sub> takes place at 30–40 °C, while the desorption is conducted at 80 °C [15]. Hence, when CAs are recirculated together with the solvent, the thermostability of CAs is of higher interest than their activity at temperatures exceeding 40 °C.



**Figure 3.** Time-dependent course of pH when 0.1 mol L<sup>−1</sup> Tris-sulfate buffer was sparged with 100% CO<sub>2</sub> (200 mL min<sup>−1</sup>) at different measurement temperatures: (a) 25 °C; (b) 30 °C; (c) 40 °C; (d) 50 °C. Without enzyme (black, solid line), with 0.25 mg L<sup>−1</sup> AwCA (blue, dashed line), with 0.25 mg L<sup>−1</sup> PmCA (red, dotted line), with 0.25 mg L<sup>−1</sup> MtaCA (orange, dashed-dotted line). *n* = 3.

The results for PmCA and MtaCA are in accordance with the literature where both enzymes are described to be thermophilic [29,31]. In prior studies, however, hydratase activity was only investigated at 0 °C (PmCA) [24,29,43] or room temperature (MtaCA) [31] utilizing the Wilbur Anderson assay [38] or an undescribed modification thereof [44], respectively. AwCA has not yet been described to be active at high temperatures. In contrast to PmCA and MtaCA [23,32], AwCA originates from a mesophilic organism [35], leading to the assumption that AwCA is only active at moderate temperatures around 30 °C. The results shown in Figure 3, however, indicate that AwCA has an accelerating effect on CO<sub>2</sub> hydration at temperatures up to at least 40 °C. Notably, the enzymes were kept on ice before the measurements, so the effect at different temperatures cannot prove the thermostability of the enzymes for more than a few minutes; incidentally, this was the time one measurement required. The thermostability over a longer period was determined in the following experiments, which will be described in Section 2.4.

### 2.3. Calculated Hydratase Activities at 25 °C

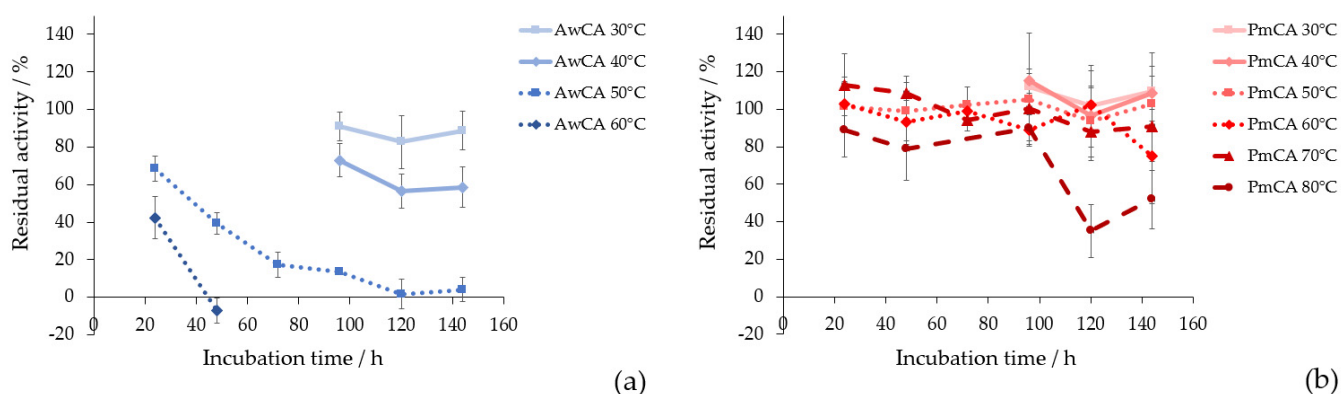
To evaluate the different hydratase activities at 25 °C in commonly used units, turnover rate per mg enzyme and WAU per mg enzyme were calculated for AwCA, MtaCA and PmCA (Table 1). When comparing WAU per mg enzyme, it becomes visible that AwCA (1814 WAU mg<sup>−1</sup>) and PmCA (1748 WAU mg<sup>−1</sup>) were about three times more active than MtaCA (580 WAU mg<sup>−1</sup>). High hydratase activities are essential for the success of CO<sub>2</sub> capturing applications. MtaCA was excluded from further investigations because of its lower measured and reported hydratase activities compared to AwCA and PmCA [31].

**Table 1.** Calculated hydratase activities at 25 °C for AwCA, MtaCA and PmCA in turnover rate per mg enzyme and WAU per mg enzyme.

Enzyme	Total Turnover Rate in $\mu\text{mol s}^{-1} \text{L}^{-1}$	Turnover Rate Minus Blank in $\mu\text{mol s}^{-1} \text{L}^{-1}$	Turnover Rate per mg Enzyme in $\mu\text{mol s}^{-1} \text{mg}^{-1}$	WAU per mg Enzyme
Blank	793 ± 16	0	n. a.	n. a.
AwCA	1502 ± 45	710 ± 48	2839 ± 97	1814 ± 228
MtaCA	1204 ± 32	411 ± 36	1646 ± 73	580 ± 102
PmCA	1490 ± 13	698 ± 21	2790 ± 42	1748 ± 63

### 2.4. Thermostability of AwCA and PmCA

Thermostability is a crucial factor for the implementation of CAs in CO<sub>2</sub> capture applications [15,17]. In Figure 4, residual hydratase activities after incubation at different temperatures over 24 h to 144 h are shown. The corresponding calculated activities can be found in Supplementary Materials Table S1. The Figure 4a shows the results for AwCA and the Figure 4b shows the results for PmCA. When AwCA was incubated at 30 °C for 144 h, 89 ± 10% of residual activity was retained. Incubation at 40 °C decreased residual activity to 59 ± 11% within 144 h. At 50 °C and 60 °C, residual activity drastically decreased to 4 ± 6% and −7 ± 7% after 144 h and 48 h of incubation, respectively. However, it is notable that AwCA retained 42 ± 11% residual after incubation at 60 °C for 24 h. Incubation at higher temperatures was not performed for AwCA due to the low stability at 60 °C compared to 30 °C and 40 °C (Figure 4). In contrast, PmCA turned out to be exceptionally thermostable, retaining 91 ± 19% residual activity after incubation at 70 °C for 144 h and 90 ± 14% residual activity after 96 h at 80 °C. When incubation time at 80 °C was prolonged to 144 h, PmCA still retained 52 ± 19% residual activity.



**Figure 4.** Residual hydratase activity over incubation time at different temperatures compared to unincubated enzyme for (a) AwCA at 30 °C, 40 °C and 50 °C; (b) PmCA at 50 °C, 60 °C, 70 °C, 80 °C. *n* = 3.

The thermostability of AwCA was tested in this study for the first time and therefore cannot be compared to the data in the literature. Regarding PmCA, the literature confirmed that this type of CA is fully active after incubation at 80 °C for 2 h [24]. Jo et al., 2014, tested the long-term stability of PmCA at 40 °C and 60 °C for 60 days, where PmCA retained 57% and 27% residual activity, respectively [43]. The current study further elucidates the insights on thermostability of PmCA, illustrating that significant amounts of activity were retained at 30 °C to 80 °C for up to 6 days (144 h). In summary, AwCA was stable long-term in a mesophilic temperature range and only short-term at temperatures exceeding 40 °C. In contrast, PmCA proved to be stable long-term at temperatures up to 80 °C.

### 3. Discussion

Thus far,  $\alpha$ - and  $\beta$ -class CAs have been purified from various species [40,45]. Functional prokaryotic CAs have the advantage of being easily produced in *E. coli*, as in the cases of, e.g.,  $\beta$ -class Caut-bCA from *Clostridium autoethanogenum* [46] and  $\alpha$ -class HC-aCA from *Hahella chejuensis*. For the latter, expression yields (24.5 mg per 100 mL liquid culture) were similarly high as in the current study [47]. Contrastingly, bacterial  $\alpha$ -class BhCA and  $\beta$ -class BCA were obtained from cell extracts of *Bacillus halodurans* and *Bacillus subtilis* SA3 cultures, respectively [48,49].  $\alpha$ -CA (Dca) from the green algae *Dunaliella salina* was functionally expressed in *E. coli* to a total amount of 15 mg. The culture volume was not given, but 1 g of wet *E. coli* cell pellet was reported to yield 1 mg of CA [50]. Marine species, such as mussels, diatoms and sea urchin exhibit functional CAs, which were mainly designated to the  $\alpha$ -class [51–54]. In the literature, primarily their esterase activity rather than their hydratase activity was determined. CA of the marine diatom *Thalassiosira pseudonana* was successfully expressed in *E. coli* [53]. Expression yields were not reported. CAs from higher plants were mainly expressed in the original species for characterization, and hydratase activities were not reported [55,56]. For CO<sub>2</sub> capture, prominent  $\alpha$ -CAs from other eukaryotes were human hCAII, which was produced using bacterial vectors [13], and BovCAII, which was simply purified from bovine erythrocytes [57].

$\alpha$ - and  $\beta$ -class CAs differ in their structures, also demonstrated by the low homologies between the selected  $\alpha$ - and  $\beta$ -CAs. Generally, the catalytic site of  $\alpha$ -CAs was reported to be larger compared to  $\beta$ -CAs, thus resulting in higher hydratase activities [40]. When comparing the  $\alpha$ - and  $\beta$ -CAs mentioned above, reported hydratase activities of  $\alpha$ -class BhCA (3425 WAU mg<sup>−1</sup>) [48] and BovCAII (1749 WAU mg<sup>−1</sup>) [57] were higher compared to  $\beta$ -class BCA (1140 WAU mg<sup>−1</sup>) [49]. Accordingly, hydratase activities of  $\alpha$ -class SspCA and hCAII were described to be amongst the highest with 7254 WAU mg<sup>−1</sup> and 8000 WAU mg<sup>−1</sup>, respectively, in the literature [30,58]. However, there are exceptions, such as  $\alpha$ -class HC-aCA (478 WAU mg<sup>−1</sup>) [47], Dca (400 WAU mg<sup>−1</sup>) [50] and CA from *T. pseudonana* (266 ± 49 WAU mg<sup>−1</sup>) [53], which exhibit comparably low hydratase activities. Although exhibiting very high hydratase activities (e.g., hCAII), the major drawback of eukaryotic  $\alpha$ -CAs is that they are typically not thermostable [26].

In the current study,  $\beta$ -class AwCA (1814 WAU mg<sup>−1</sup>) demonstrated similarly high hydratase activity as the  $\alpha$ -class PmCA (1748 WAU mg<sup>−1</sup>), whereas hydratase activity of the  $\beta$ -class MtaCA (580 WAU mg<sup>−1</sup>) was significantly lower. When comparing the protein structures, AwCA exhibited the typical features of  $\beta$ -CAs, whereas MtaCA varied by an exchanged Val62 for Leu36 in the highly conserved DSRV motif and missed Gln48. Both original amino acids are proposed to be involved in the catalytic reaction, potentially explaining the lower hydratase activity of MtaCA compared to AwCA. The highly conserved regions of  $\alpha$ -CAs were found both in PmCA and SspCA. The lower hydratase activity of MtaCA compared to AwCA and PmCA during this study was in accordance with literature [31].

Kim et al. (2019) proposed that the enhanced thermostability of PmCA likely derives from the compactly folded homodimeric structure of  $\alpha$ -CAs, which is stabilized by hydrophobic interactions, intramolecular disulfide bonds and interfacial networks of hydrogen bonds [59]. The current results confirm the exceptional thermostability of  $\alpha$ -class

PmCA compared to the mesophilic  $\beta$ -class AwCA. An exception might be the  $\beta$ -class MtaCA, which originates from a thermophilic organism and has been described to be stable after incubation for 15 min at up to 75 °C [31]; this is potentially explained by the closer relation to  $\alpha$ -CAs in the phylogenetic tree (Figure 1). In the literature, SspCA was described as  $\alpha$ -CA with one of the highest long-term thermostabilities while retaining its CO<sub>2</sub> hydration activity after incubation at 100 °C for 3 h and 10% residual activity after incubation at 70 °C for 28 days [26,60]. However, due to the significantly lower expression yield of SspCA at the chosen conditions, the thermostability of SspCA was not evaluated in this study.

Consistently, CAs from thermophilic prokaryotes were already presented as the favorable candidates for biotechnological applications due to their enhanced thermostability in the literature, whereas CAs from other species are yet to be improved by protein engineering [12]. Immobilization may be an option to improve the thermostability of AwCA in future studies [61]. Production of SspCA may be increased significantly by using other expression vectors, as reported by Capasso et al. (2012) [30].

#### 4. Materials and Methods

##### 4.1. Chemicals and Reagents

All chemicals used in this work were of analytical grade. IPTG, ZnSO<sub>4</sub>, kanamycin, biotin and the buffer components were purchased from Sigma–Aldrich (USA). Ampicillin and Nutrient Agar were purchased from Merck Millipore (Germany). SDS buffer and the SDS-PAGE gels were purchased from Bio-Rad (USA). LB media was purchased from Carl Roth (Germany) and the protein marker for SDS PAGE from VWR International (USA). Bottled CO<sub>2</sub> (purity 99.5%) was derived from Messer (Austria).

##### 4.2. Cloning, Expression and Purification

Genes coding for AwCA (accession number WP\_014354989), PmCA (WP\_015898908), MtaCA (AAB86055) and SspCA (ACD66216.1) were codon optimized and cloned over NdeI and HindIII restriction sites fused to a StrepTag for rapid purification by affinity chromatography. In the case of SspCA and MtaCA, the natural signal peptides were removed before cloning. Synthesis of genes and cloning into the expression vectors were provided by a commercial service (GenScript Biotech, Leiden, The Netherlands). Genes encoding AwCA, PmCA and MtaCA were cloned into vector pET26b(+) carrying a C-terminal StrepTag and the gene coding for SspCA into vector pET16b(+) providing a N-terminal StrepTag. The plasmids were transformed into *E. coli* BL21-Gold (DE3) (Agilent Technologies, USA). Freshly transformed *E. coli* cells were used to inoculate 20 mL LB-medium supplemented with 0.5 mmol L<sup>−1</sup> ZnSO<sub>4</sub> and 40 mg mL<sup>−1</sup> Kanamycin for pET26b(+) or 100 µg mL<sup>−1</sup> Ampicillin for pET16b(+) and cultivated overnight at 37 °C and 150 rpm. The overnight culture was used to inoculate 200 mL of the same medium in a 500 mL shake flask to an OD<sub>600</sub> = 0.1. The culture was incubated at 37 °C and 150 rpm until an OD<sub>600</sub> = 0.8 was reached. At this point, cells were induced by addition of IPTG to a final concentration of 0.1 mmol L<sup>−1</sup> and incubated at 20 °C for 20 h (AwCA and PmCA) or 22 h (MtaCA and SspCA). Cultures were harvested by centrifugation at 4000 rpm and 4 °C for 30 min.

Enzymes were purified by affinity chromatography according to the manufacturer's protocol (IBA GmbH, Goettingen, Germany). The elution fractions were collected, pooled and concentrated by vivaspin 20 columns (Sartorius, Germany). The buffer was exchanged by PD-10 desalting columns (GE Healthcare, UK) with 0.1 mol L<sup>−1</sup> Tris-HCl at a pH of 7. Enzymes were aliquoted to 500 µL and frozen at 20 °C until further usage.

##### 4.3. CO<sub>2</sub> Hydration Assay at Different Temperatures

Investigation of the effect of the CA addition on CO<sub>2</sub> hydration at different temperatures was made by monitoring the pH change in buffered solution due to the formation of carbonic acid using the method as described by Fuchs et al., 2021 [37]. The reactions were conducted in a temperature-controlled vessel and the temperature was varied between



25–50 °C. Frozen enzyme stock solutions were thawed, diluted to 0.1 mg mL<sup>−1</sup> with 0.1 mol L<sup>−1</sup> Tris-HCl (pH 7) and kept on ice until the measurement. The reaction mix contained 40 mL reaction buffer (0.1 mol L<sup>−1</sup> Tris-sulfate, pH 8.2) and 0.1 mL of the respective enzyme stock solution. The purified enzyme concentration in the reaction mix was 0.25 mg L<sup>−1</sup>, as determined by NanoPhotometer® (NP80, IMPLLEN, USA). For blank measurements, only the reaction buffer was measured. The pH of the reaction buffer was set to 8.2 at the respective measurement temperature before the experiments. CO<sub>2</sub> gassing was started and the decline of pH during the experiment due to CO<sub>2</sub> entry was recorded (Methrom Titrino, pH electrode: LL-Viscotrode and Software TiNet 2.5). Each measurement with or without CA was performed as a triplicate, and in the figures the mean values are shown.

#### 4.4. Calculation of Hydratase Activities at 25 °C

Hydratase activities at 25 °C were calculated using the logged pH data. HCO<sub>3</sub><sup>−</sup> (mol L<sup>−1</sup>) was calculated according to the formula provided by Fuchs et al., 2021 [37]. Subsequently, HCO<sub>3</sub><sup>−</sup> was converted to μmol L<sup>−1</sup> and depicted against time in a diagram. The slope of the graph between 7–18 s was taken as μmol CO<sub>2</sub> converted to μmol HCO<sub>3</sub><sup>−</sup> L<sup>−1</sup> s<sup>−1</sup>. The total turnover rate (μmol HCO<sub>3</sub><sup>−</sup> L<sup>−1</sup> s<sup>−1</sup>) of the blank measurement was subtracted from the measurements with CAs before the calculation of the turnover rate per mg enzyme (μmol HCO<sub>3</sub><sup>−</sup> s<sup>−1</sup> mg<sup>−1</sup>). To give the values in generally used units, a calibration curve with a standard enzyme (CA from bovine erythrocytes, Sigma–Aldrich, Germany) was used for conversion to Wilbur Anderson Units (WAU), as in Fuchs et al., 2021 [37].

#### 4.5. Determination of Thermostability

Determination of thermostability was conducted using the same set-up as in Section 4.3. The measuring temperature was 25 °C. CA stock solutions were diluted to 0.1 mg mL<sup>−1</sup> with 0.1 mol L<sup>−1</sup> Tris-HCl at a pH of 7. Prior to the tests, aliquots of 1 mL were incubated at 30 °C, 40 °C, 50 °C, 60 °C, 70 °C or 80 °C in a heating block (Thermomixer comfort, Eppendorf, Germany) for up to 144 h. Prior to the CO<sub>2</sub> hydration assay, the samples were cooled down to RT. For the calculation of the residual activity, the turnover rate per mg enzyme (μmol s<sup>−1</sup> mg<sup>−1</sup>) was used.

### 5. Summary and Conclusions

Four CAs from different organisms were recombinantly produced in *E. coli*. Considering a later industrial application, the production and purification of the CAs were easy to perform and provided high yields using standard procedures. Under the chosen conditions, the expression yields of AwCA, PmCA and MtaCA were at least 25 times higher than for SspCA. Hence, SspCA was excluded from further experiments during this study. Nevertheless, a variation of the expression strategy for SspCA can potentially maximize the expression yield and should be part of future studies, as SspCA was reported to be one of the most active and thermostable CAs characterized so far in the literature.

A comparison of the effect on CO<sub>2</sub> hydration at different temperatures, similar to industrial conditions, was performed for AwCA, PmCA and MtaCA using a novel assay. An accelerating effect on CO<sub>2</sub> hydration was observed at 25 °C, 30 °C, 40 °C and up to 50 °C when enzymes were added to the buffer. However, there was only a minor difference between the CAs and the blank measurement at 50 °C, leading to the conclusion that the CA addition to CO<sub>2</sub> capture at temperatures exceeding 40 °C is inapplicable. At 25 °C, hydratase activities were calculated for evaluation in general units. AwCA (1814 WAU mg<sup>−1</sup>) and PmCA (1748 WAU mg<sup>−1</sup>) were about three times more active than MtaCA (580 WAU mg<sup>−1</sup>), which led to the exclusion of MtaCA for the following thermostability experiments. AwCA was highly stable in a mesophilic temperature range with residual activities of 89 ± 10% and 59 ± 11% after incubation at 30 °C and 40 °C, respectively, for 144 h. PmCA was discovered to be exceptionally thermostable with residual activities of 91 ± 19% and 90 ± 14% after incubation at 70 °C for 144 h and at



80 °C for 96 h, respectively. The results of this study indicate that AwCA and PmCA might be suitable candidates for biomimetic CO<sub>2</sub> sequestration at either mesophilic (AwCA and PmCA) or thermophilic (PmCA) temperature ranges. Further investigation of CAs from other species, especially those from thermophilic, anaerobic prokaryotes, is endorsed for broadening the range of possible candidates for CO<sub>2</sub> sequestration.

**Supplementary Materials:** The following are available online at <https://www.mdpi.com/article/10.3390/ijms23020957/s1>.

**Author Contributions:** Conceptualization, W.F., S.K.-M.R.R., D.R. and G.B.; formal analysis, F.S.; funding acquisition, G.B.; investigation, F.S. and J.R.; supervision, G.M.G., D.R. and G.B.; writing—original draft preparation, F.S., J.R. and D.R. All authors have read and agreed to the published version of the manuscript.

**Funding:** The presented study was developed in the course of two research projects. We kindly thank the Austrian Research Promotion Agency (FFG) for the funding of CarbonATE (FFG project no. 869728) and PTLiquid (FFG project no. 865091). The COMET center: acib: Next Generation Bioproduction was funded by the BMVIT, BMDW, SFG, Standortagentur Tirol, Government of Lower Austria, and Vienna Business Agency in the framework of COMET—Competence Centers for Excellent Technologies. The COMET-Funding Program is managed by the Austrian Research Promotion Agency FFG.

**Institutional Review Board Statement:** Not applicable.

**Informed Consent Statement:** Not applicable.

**Data Availability Statement:** The original data presented in this study are available in the Supplementary Materials and on request from the corresponding author.

**Conflicts of Interest:** The authors declare no conflict of interest and the funders had no role in the design of the study; in the collection, analyses or interpretation of data; in the writing of the manuscript or in the decision to publish the results.

## References

1. Canadell, J.G.; Le Quéré, C.; Raupach, M.R.; Field, C.B.; Buitenhuis, E.T.; Ciais, P.; Conway, T.J.; Gillett, N.P.; Houghton, R.A.; Marland, G. Contributions to accelerating atmospheric CO<sub>2</sub> growth from economic activity, carbon intensity, and efficiency of natural sinks. *Proc. Natl. Acad. Sci. USA* **2007**, *104*, 18866–18870. [CrossRef] [PubMed]
2. Total Greenhouse Gas Emission Trends and Projections in Europe. Available online: <https://www.eea.europa.eu/data-and-maps/indicators/greenhouse-gas-emission-trends-7/assessment> (accessed on 21 December 2020).
3. Greenhouse Gas Emissions. Available online: <https://www.epa.gov/ghgemissions/overview-greenhouse-gases> (accessed on 21 December 2020).
4. The Paris Agreement. Available online: <https://unfccc.int/process-and-meetings/the-paris-agreement/what-is-the-paris-agreement> (accessed on 8 November 2020).
5. Benson, S.M.; Surles, T. Carbon dioxide capture and storage: An overview with emphasis on capture and storage in deep geological formations. *Proc. IEEE* **2006**, *94*, 1795–1804. [CrossRef]
6. Kanniche, M.; Gros-Bonnivard, R.; Jaud, P.; Valle-Marcos, J.; Amann, J.-M.; Bouallou, C. Pre-combustion, post-combustion and oxy-combustion in thermal power plant for CO<sub>2</sub> capture. *Appl. Therm. Eng.* **2010**, *30*, 53–62. [CrossRef]
7. Zhang, Z.; Wang, T.; Blunt, M.J.; Anthony, E.J.; Park, A.-H.A.; Hughes, R.W.; Webley, P.A.; Yan, J. Advances in carbon capture, utilization and storage. *Appl. Energy* **2020**, *278*, 115627. [CrossRef]
8. Grant, T.; Anderson, C.; Hooper, B. Comparative life cycle assessment of potassium carbonate and monoethanolamine solvents for CO<sub>2</sub> capture from post combustion flue gases. *Int. J. Greenh. Gas Control* **2014**, *28*, 35–44. [CrossRef]
9. Mazari, S.A.; Si Ali, B.; Jan, B.M.; Saeed, I.M.; Nizamuddin, S. An overview of solvent management and emissions of amine-based CO<sub>2</sub> capture technology. *Int. J. Greenh. Gas Control* **2015**, *34*, 129–140. [CrossRef]
10. Kwak, N.-S.; Lee, J.H.; Lee, I.Y.; Jang, K.R.; Shim, J.-G. A study of the CO<sub>2</sub> capture pilot plant by amine absorption. *Energy* **2012**, *47*, 41–46. [CrossRef]
11. Bhowan, A.S.; Alto, P. Direction of CO<sub>2</sub> capture R&D. In Proceedings of the NETL CO<sub>2</sub> Capture Technology Meeting, Pittsburgh, PA, USA, 29 July–1 August 2014; pp. 10–12.
12. Di Fiore, A.; Alterio, V.; Monti, S.M.; De Simone, G.; D’Ambrosio, K. Thermostable carbonic anhydrases in biotechnological applications. *Int. J. Mol. Sci.* **2015**, *16*, 15456–15480. [CrossRef]
13. Bond, G.M.; Stringer, J.; Brandvold, D.K.; Simsek, F.A.; Medina, M.-G.; Egeland, G. Development of integrated system for biomimetic CO<sub>2</sub> sequestration using the enzyme carbonic anhydrase. *Energy Fuels* **2001**, *15*, 309–316. [CrossRef]

14. González, J.M.; Fisher, S.Z. Carbonic anhydrases in industrial applications. In *Carbonic Anhydrase: Mechanism, Regulation, Links to Disease, and Industrial Applications*, 1st ed.; Frost, S.C., McKenna, R., Eds.; Springer: Dordrecht, The Netherlands, 2014; pp. 405–426. [\[CrossRef\]](#)
15. Fradette, L.; Lefebvre, S.; Carley, J. Demonstration results of enzyme-accelerated CO<sub>2</sub> capture. *Energy Procedia* **2017**, *114*, 1100–1109. [\[CrossRef\]](#)
16. Savile, C.K.; Lalonde, J.J. Biotechnology for the acceleration of carbon dioxide capture and sequestration. *Curr. Opin. Biotechnol.* **2011**, *22*, 818–823. [\[CrossRef\]](#)
17. Alterio, V.; Monti, S.M.; De Simone, G. Thermal-stable carbonic anhydrases: A structural overview. In *Carbonic Anhydrase: Mechanism, Regulation, Links to Disease, and Industrial Applications*, 1st ed.; Frost, S.C., McKenna, R., Eds.; Springer: Dordrecht, The Netherlands, 2014; pp. 387–404. [\[CrossRef\]](#)
18. Ozensoy Guler, O.; Capasso, C.; Supuran, C.T. A magnificent enzyme superfamily: Carbonic anhydrases, their purification and characterization. *J. Enzyme Inhib. Med. Chem.* **2016**, *31*, 689–694. [\[CrossRef\]](#)
19. Boone, C.D.; Pinard, M.; McKenna, R.; Silverman, D. Catalytic mechanism of  $\alpha$ -class carbonic anhydrases: CO<sub>2</sub> hydration and proton transfer. In *Carbonic Anhydrase: Mechanism, Regulation, Links to Disease, and Industrial Applications*; Frost, S.C., McKenna, R., Eds.; Springer: Dordrecht, The Netherlands, 2014; pp. 31–52. [\[CrossRef\]](#)
20. Lindskog, S. Structure and mechanism of Carbonic Anhydrase. *Pharmacol. Ther.* **1997**, *74*, 1–20. [\[CrossRef\]](#)
21. Supuran, C.T. Structure and function of carbonic anhydrases. *Biochem. J.* **2016**, *473*, 2023–2032. [\[CrossRef\]](#)
22. Littlechild, J.A. Enzymes from extreme environments and their industrial applications. *Front. Bioeng. Biotechnol.* **2015**, *3*, 1–9. [\[CrossRef\]](#) [\[PubMed\]](#)
23. Götz, D.; Banta, A.; Beveridge, T.J.; Rushdi, A.I.; Simoneit, B.R.T.; Reysenbach, A.-L. *Persephonella marina* gen. nov., sp. nov. and *Persephonella guaymasensis* sp. nov., two novel, thermophilic, hydrogen-oxidizing microaerophiles from deep-sea hydrothermal vents. *Int. J. Syst. Evol. Microbiol.* **2002**, *52*, 1349–1359. [\[CrossRef\]](#) [\[PubMed\]](#)
24. Borchert, M.S. Heat-Stable Persephonella Carbonic Anhydrases and Their Use. U.S. Patent 9909115, 6 March 2018.
25. Daigle, R.; Madore, É.; Fradette, S. Techniques for CO<sub>2</sub> Capture Using Sulfurihydrogenibium Sp. Carbonic Anhydrase. U.S. Patent 9968885, 15 May 2018.
26. Di Fiore, A.; Capasso, C.; De Luca, V.; Monti, S.M.; Carginale, V.; Supuran, C.T.; Scozzafava, A.; Pedone, C.; Rossi, M.; De Simone, G. X-ray structure of the first ‘extremo- $\alpha$ -carbonic anhydrase’, a dimeric enzyme from the thermophilic bacterium *Sulfurihydrogenibium yellowstonense* YO3AOP1. *Acta Crystallogr. Sect. D Biol. Crystallogr.* **2013**, *69*, 1150–1159. [\[CrossRef\]](#)
27. Rossi, M. A New Heat-Stable Carbonic Anhydrase and Uses. Thereof. Patent WO 2013064195, 10 May 2013.
28. Vullo, D.; De Luca, V.; Scozzafava, A.; Carginale, V.; Rossi, M.; Supuran, C.T.; Capasso, C. The first activation study of a bacterial carbonic anhydrase (CA). The thermostable  $\alpha$ -CA from *Sulfurihydrogenibium yellowstonense* YO3AOP1 is highly activated by amino acids and amines. *Bioorgan. Med. Chem. Lett.* **2012**, *22*, 6324–6327. [\[CrossRef\]](#) [\[PubMed\]](#)
29. Kanth, B.K.; Jun, S.-Y.; Kumari, S.; Pack, S.P. Highly thermostable carbonic anhydrase from *Persephonella marina* EX-H1: Its expression and characterization for CO<sub>2</sub>-sequestration applications. *Process Biochem.* **2014**, *49*, 2114–2121. [\[CrossRef\]](#)
30. Capasso, C.; De Luca, V.; Carginale, V.; Cannio, R.; Rossi, M. Biochemical properties of a novel and highly thermostable bacterial  $\alpha$ -carbonic anhydrase from *Sulfurihydrogenibium yellowstonense* YO3AOP1. *J. Enzyme Inhib. Med. Chem.* **2012**, *27*, 892–897. [\[CrossRef\]](#)
31. Smith, K.S.; Ferry, J.G. A plant-type ( $\beta$ -class) carbonic anhydrase in the thermophilic methanoarchaeon *Methanobacterium thermoautotrophicum*. *J. Bacteriol.* **1999**, *181*, 6247–6253. [\[CrossRef\]](#)
32. Zeikus, J.G.; Wolfe, R.S. *Methanobacterium thermoautotrophicus* sp. n., an anaerobic, autotrophic, extreme thermophile. *J. Bacteriol.* **1972**, *109*, 707–713. [\[CrossRef\]](#)
33. Balch, W.E.; Schoberth, S.; Tanner, R.S.; Wolfe, R.S. *Acetobacterium*, a new genus of hydrogen-oxidizing, carbon dioxide-reducing, anaerobic bacteria. *Int. Assoc. Microbiol. Soc.* **1977**, *27*, 355–361. [\[CrossRef\]](#)
34. Marchler-Bauer, A.; Bo, Y.; Han, L.; He, J.; Lanczycki, C.J.; Lu, S.; Chitsaz, F.; Derbyshire, M.K.; Geer, R.C.; Gonzales, N.R.; et al. CDD/SPARCLE: Functional classification of proteins via subfamily domain architectures. *Nucleic Acids Res.* **2017**, *45*, D200–D203. [\[CrossRef\]](#) [\[PubMed\]](#)
35. Braus-Stromeier, S.A.; Schnappauf, G.; Braus, G.H.; Gößner, A.S.; Drake, H.L. Carbonic anhydrase in *Acetobacterium woodii* and other acetogenic bacteria. *J. Bacteriol.* **1997**, *179*, 7197–7200. [\[CrossRef\]](#) [\[PubMed\]](#)
36. Kirk, O.; Borchert, T.V.; Fuglsang, C.C. Industrial enzyme applications. *Curr. Opin. Biotechnol.* **2002**, *13*, 345–351. [\[CrossRef\]](#)
37. Fuchs, W.; Steger, F.; Reich, J.; Ribitsch, D.; Rittmann, S.K.M.; Bochmann, G. A simple and straightforward method for activity measurement of carbonic anhydrases. *Catalysts* **2021**, *11*, 819. [\[CrossRef\]](#)
38. Wilbur, K.M.; Anderson, N.G. Electrometric and colorimetric determination of carbonic anhydrase. *J. Biol. Chem.* **1948**, *176*, 147–154. [\[CrossRef\]](#)
39. Tamura, K.; Stecher, G.; Kumar, S. MEGA11: Molecular Evolutionary Genetics Analysis Version 11. *Mol. Biol. Evol.* **2021**, *38*, 3022–3027. [\[CrossRef\]](#)
40. Capasso, C.; Supuran, C.T. An overview of the alpha-, beta- and gamma-carbonic anhydrases from bacteria: Can bacterial carbonic anhydrases shed new light on evolution of bacteria? *J. Enzyme Inhib. Med. Chem.* **2015**, *30*, 325–332. [\[CrossRef\]](#) [\[PubMed\]](#)

41. Rowlett, R.S. Structure and catalytic mechanism of  $\beta$ -carbonic anhydrases. In *Carbonic Anhydrase: Mechanism, Regulation, Links to Disease, and Industrial Applications*; Frost, S.C., McKenna, R., Eds.; Springer: Dordrecht, The Netherlands, 2014; pp. 53–76. [\[CrossRef\]](#)
42. Dodds, W.S.; Stutzman, L.F.; Sollami, B.J. Carbon dioxide solubility in water. *Ind. Eng. Chem. Chem. Eng. Data Ser.* **1956**, *1*, 92–95. [\[CrossRef\]](#)
43. Jo, B.H.; Seo, J.H.; Cha, H.J. Bacterial extremophilic  $\alpha$ -carbonic anhydrases from deep-sea hydrothermal vents as potential biocatalysts for CO<sub>2</sub> sequestration. *J. Mol. Catal. B Enzym.* **2014**, *109*, 31–39. [\[CrossRef\]](#)
44. Smith, K.S.; Jakubczak, C.; Whittam, T.S.; Ferry, J.G. Carbonic anhydrase is an ancient enzyme widespread in prokaryotes. *Proc. Natl. Acad. Sci. USA* **1999**, *96*, 15184–15189. [\[CrossRef\]](#) [\[PubMed\]](#)
45. Supuran, C.T. Carbonic anhydrases—An overview. *Curr. Pharm. Des.* **2008**, *14*, 603–614. [\[CrossRef\]](#) [\[PubMed\]](#)
46. Pander, B.; Harris, G.; Scott, D.J.; Winzer, K.; Köpke, M.; Simpson, S.D.; Minton, N.P.; Henstra, A.M. The carbonic anhydrase of *Clostridium autoethanogenum* represents a new subclass of  $\beta$ -carbonic anhydrases. *Appl. Microbiol. Biotechnol.* **2019**, *103*, 7275–7286. [\[CrossRef\]](#)
47. Ki, M.R.; Min, K.; Kanth, B.K.; Lee, J.; Pack, S.P. Expression, reconstruction and characterization of codon-optimized carbonic anhydrase from *Hahella chejuensis* for CO<sub>2</sub> sequestration application. *Bioprocess Biosyst. Eng.* **2013**, *36*, 375–381. [\[CrossRef\]](#)
48. Faridi, S.; Satyanarayana, T. Novel alkalistable  $\alpha$ -carbonic anhydrase from the polyextremophilic bacterium *Bacillus halodurans*: Characteristics and applicability in flue gas CO<sub>2</sub> sequestration. *Environ. Sci. Pollut. Res.* **2016**, *23*, 15236–15249. [\[CrossRef\]](#)
49. Ramanan, R.; Kannan, K.; Vinayagamorthy, N.; Ramkumar, K.M.; Sivanesan, S.D.; Chakrabarti, T. Purification and characterization of a novel plant-type carbonic anhydrase from *Bacillus subtilis*. *Biotechnol. Bioprocess Eng.* **2009**, *14*, 32–37. [\[CrossRef\]](#)
50. Premkumar, L.; Bageshwar, U.K.; Gokhman, I.; Zamir, A.; Sussman, J.L. An unusual halotolerant  $\alpha$ -type carbonic anhydrase from the alga *Dunaliella salina* functionally expressed in *Escherichia coli*. *Protein Expr. Purif.* **2003**, *28*, 151–157. [\[CrossRef\]](#)
51. Pavičić-Hamer, D.; Baričević, A.; Gerdol, M.; Hamer, B. *Mytilus galloprovincialis* carbonic anhydrase II: Activity and cDNA sequence analysis. *Key Eng. Mater.* **2015**, *672*, 137–150. [\[CrossRef\]](#)
52. Cardoso, J.C.R.; Ferreira, V.; Zhang, X.; Anjos, L.; Félix, R.C.; Batista, F.M.; Power, D.M. Evolution and diversity of alpha-carbonic anhydrases in the mantle of the Mediterranean mussel (*Mytilus galloprovincialis*). *Sci. Rep.* **2019**, *9*, 1–14. [\[CrossRef\]](#)
53. Jensen, E.L.; Clement, R.; Kosta, A.; Maberly, S.C.; Gontero, B. A new widespread subclass of carbonic anhydrase in marine phytoplankton. *ISME J.* **2019**, *13*, 2094–2106. [\[CrossRef\]](#)
54. Karakostis, K.; Costa, C.; Zito, F.; Brümmer, F.; Matranga, V. Characterization of an alpha type carbonic anhydrase from *Paracentrotus lividus* sea urchin embryos. *Mar. Biotechnol.* **2016**, *18*, 384–395. [\[CrossRef\]](#)
55. Wang, L.; Liang, J.; Zhou, Y.; Tian, T.; Zhang, B.; Duanmu, D. Molecular characterization of carbonic anhydrase genes in *Lotus japonicus* and their potential roles in symbiotic nitrogen fixation. *Int. J. Mol. Sci.* **2021**, *22*, 7766. [\[CrossRef\]](#)
56. Chatterjee, J.; Coe, R.A.; Acebron, K.; Thakur, V.; Yennamalli, R.M.; Danila, F.; Lin, H.-C.; Balahadia, C.P.; Bagunu, E.; Padhma, P.P.O.S.; et al. A low CO<sub>2</sub>-responsive mutant of *Setaria viridis* reveals that reduced carbonic anhydrase limits C<sub>4</sub> photosynthesis. *J. Exp. Bot.* **2021**, *72*, 3122–3136. [\[CrossRef\]](#)
57. Da Costa Ores, J.; Sala, L.; Cerveira, G.P.; Kalil, S.J. Purification of carbonic anhydrase from bovine erythrocytes and its application in the enzymic capture of carbon dioxide. *Chemosphere* **2012**, *88*, 255–259. [\[CrossRef\]](#)
58. Ekin, D.; Beydemir, Ş.; Alim, Z. Some drugs inhibit in vitro hydratase and esterase activities of human carbonic anhydrase-I and II. *Pharmacol. Reports* **2007**, *59*, 580–587.
59. Kim, S.; Sung, J.; Yeon, J.; Choi, S.H.; Jin, M.S. Crystal structure of a highly thermostable  $\alpha$ -carbonic anhydrase from *Persephonella marina* EX-H1. *Mol. Cells* **2019**, *42*, 460–469. [\[CrossRef\]](#) [\[PubMed\]](#)
60. Russo, M.E.; Olivieri, G.; Capasso, C.; De Luca, V.; Marzocchella, A.; Salatino, P.; Rossi, M. Kinetic study of a novel thermo-stable  $\alpha$ -carbonic anhydrase for biomimetic CO<sub>2</sub> capture. *Enzyme Microb. Technol.* **2013**, *53*, 271–277. [\[CrossRef\]](#)
61. Sharma, A.; Bhattacharya, A.; Shrivastava, A. Biomimetic CO<sub>2</sub> sequestration using purified carbonic anhydrase from indigenous bacterial strains immobilized on biopolymeric materials. *Enzyme Microb. Technol.* **2011**, *48*, 416–426. [\[CrossRef\]](#) [\[PubMed\]](#)

# ANNEX 6

Pages 124 to 135

---

Zipperle A., Reischl B., Schmider T., Stadlbauer M., Kushkevych I., Pruckner C.,  
Vítězová M., Rittmann S.K.-M.R.

**Biomethanation of carbon monoxide by artificial archaeal co-cultures**

Fermentation (2021) 7(4):276

10.3390/fermentation7040276

---

## Article

# Biomethanation of Carbon Monoxide by Hyperthermophilic Artificial Archaeal Co-Cultures

Aaron Zipperle <sup>1,†</sup> , Barbara Reischl <sup>1,2,†</sup>, Tilman Schmider <sup>1</sup>, Michael Stadlbauer <sup>1</sup>, Ivan Kushkevych <sup>3</sup> , Christian Pruckner <sup>1</sup>, Monika Vítězová <sup>3</sup>  and Simon K.-M. Rittmann <sup>1,2,\*</sup> 

<sup>1</sup> Archaea Physiology & Biotechnology Group, Department of Functional and Evolutionary Ecology, Universität Wien, 1030 Wien, Austria; aaronzipperle@gmail.com (A.Z.); barbara.reischl@univie.ac.at (B.R.); tilman.schmider@univie.ac.at (T.S.); a01005948@univie.ac.at (M.S.); greeese@gmail.com (C.P.)

<sup>2</sup> Arkeon GmbH, 3430 Tulln an der Donau, Austria

<sup>3</sup> Department of Experimental Biology, Faculty of Science, Masaryk University, 60200 Brno, Czech Republic; kushkevych@mail.muni.cz (I.K.); vitezova@sci.muni.cz (M.V.)

\* Correspondence: simon.rittmann@univie.ac.at; Tel.: +43-4277-76513; Fax: +43-4277-876513

† These authors contributed equally to this work.

**Abstract:** Climate neutral and sustainable energy sources will play a key role in future energy production. Biomethanation by gas to gas conversion of flue gases is one option with regard to renewable energy production. Here, we performed the conversion of synthetic carbon monoxide (CO)-containing flue gases to methane (CH<sub>4</sub>) by artificial hyperthermophilic archaeal co-cultures, consisting of *Thermococcus onnurineus* and *Methanocaldococcus jannaschii*, *Methanocaldococcus vulcanius*, or *Methanocaldococcus villosus*. Experiments using both chemically defined and complex media were performed in closed batch setups. Up to 10 mol% CH<sub>4</sub> was produced by converting pure CO or synthetic CO-containing industrial waste gases at a high rate using a co-culture of *T. onnurineus* and *M. villosus*. These findings are a proof of principle and advance the fields of Archaea Biotechnology, artificial microbial ecosystem design and engineering, industrial waste-gas recycling, and biomethanation.

**Keywords:** Archaea Biotechnology; anaerobic microbiology; methanogenesis; biohydrogen; biological gas conversion



**Citation:** Zipperle, A.; Reischl, B.; Schmider, T.; Stadlbauer, M.; Kushkevych, I.; Pruckner, C.; Vítězová, M.; Rittmann, S.K.-M.R. Biomethanation of Carbon Monoxide by Hyperthermophilic Artificial Archaeal Co-Cultures. *Fermentation* **2021**, *7*, 276. <https://doi.org/10.3390/fermentation7040276>

Academic Editor: Christian Kennes

Received: 18 October 2021

Accepted: 22 November 2021

Published: 25 November 2021

**Publisher's Note:** MDPI stays neutral with regard to jurisdictional claims in published maps and institutional affiliations.



**Copyright:** © 2021 by the authors. Licensee MDPI, Basel, Switzerland. This article is an open access article distributed under the terms and conditions of the Creative Commons Attribution (CC BY) license (<https://creativecommons.org/licenses/by/4.0/>).

## 1. Introduction

In the European Union, around 70% of primary energy is generated by the combustion of fossil fuels, contributing about 78% (3367 Tg-CO<sub>2</sub> equ.) of the total emitted greenhouse gases [1,2]. A transition to a carbon dioxide (CO<sub>2</sub>)-neutral and sustainable energy production system is urgently needed. One of the possibilities is to utilize the power-to-gas process [3–5]. Within this process, biomethanation of CO<sub>2</sub> to methane (CH<sub>4</sub>) offers a sustainable opportunity to enable the transition from fossil fuels, as it is an autocatalytic process. Therefore, it is envisioned that biomethanation will become an essential part of future energy production systems, as CH<sub>4</sub> could be produced at a stable pace and stored in vast amounts in the natural gas grid network [6]. Pure cultures of methanogenic archaea (methanogens) [7–12] and enrichment cultures containing methanogens [13–17] can be utilized for in situ or ex situ biomethanation [18–20].

Carbon monoxide (CO)-containing rich waste gases are a by-product of industrial processes such as steelmaking [21]. CO-containing gases can also be obtained by gasification of carbon-rich materials, such as domestic organic waste or lignocellulose conversion to syngas [22]. The fact that biofuel production directly from lignocellulose is still costly and biotechnologically challenging makes microbial gas to gas conversion from CO a promising alternative bioprocess [7,23]. Developments in the transformation of gaseous waste products to energetically valuable compounds emphasize the potential for syngas as a substrate [24–27]. CO has a high potential for donating electrons, making it a favourable



substrate for lithotrophic microorganisms [28,29]. Besides CO, waste and syngas mainly consist of molecular hydrogen (H<sub>2</sub>), CO<sub>2</sub>, and CH<sub>4</sub>. As early as 1990, it was demonstrated that methanogens can metabolize some components from syngas [30].

The direct conversion of pure CO to CH<sub>4</sub> was performed by hydrogenotrophic methanogens and subsequently analysed [31–34]. Furthermore, growth adaption to CO did not change the CH<sub>4</sub> production rates significantly in the case of *Methanothermobacter marburgensis*, and the specific growth rate ( $\mu$ ) of *Methanothermobacter thermautotrophicus* on pure CO was only a hundredth of the growth rate achieved using H<sub>2</sub>:CO<sub>2</sub> as a substrate [31]. This led to the assumption that an artificial co-culture, where CO is converted to CH<sub>4</sub> in a successive bioprocess, would lead to higher efficiency, as microorganisms specifically adapted to the task of converting CO and producing CH<sub>4</sub> can be selected. Studies showed that the independent performance of the water gas shift reaction (WGSR) and biomethanation by two different organisms in the same vessel resulted in a more than 20-fold faster conversion than direct conversion by a single organism [34]. Therefore, we hypothesized that an artificial co-culture of a carboxydophilic, hydrogenogenic microbe with a hydrogenotrophic, autotrophic organism would drive favourable thermodynamic conditions for the WGSR. These conditions are created by direct removal of the gaseous metabolic end products of the WGSR, that is H<sub>2</sub>:CO<sub>2</sub>, by the methanogen. The conversions that are successively performed by the two organisms can be summarized with the following equation:



Overall, studies using a co-culture approach showed promising results for biomethane production rates [34,35]. Based on a previous study where a bacterial/archaeal co-culture was utilized [36], we wanted to investigate the potential of artificial archaeal co-cultures consisting of a carboxydophilic, hydrogenogenic archaeon, and different hydrogenotrophic, autotrophic, and methanogenic archaea for biomethanation. We selected *Thermococcus onnurineus* for performing the catalysis of the WGSR, as it was shown that  $\mu$  and H<sub>2</sub> productivity on CO was substantially higher compared to other carboxydophilic and hydrogenogenic microbes [37–40]. To catalyse the second part of the reaction, *Methanocaldococcus jannaschii*, *Methanocaldococcus vulcanius*, and *Methanocaldococcus villosus* were selected, because of their similar cultivation requirements to *T. onnurineus* with respect to temperature, salt concentration, and pH optimum. All four organisms were isolated from deep-sea hydrothermal vents and belong to the Euryarchaeota. They are able to grow in a temperature range of 63 to 86 °C, a salt concentration of 1 to 5%, and a pH of 5.5 to 7.0. *T. onnurineus* is a heterotroph, while the methanogens are chemolithoautotrophs [41–44]. Moreover, hyperthermophilic organisms are more advantageous over mesophiles, since at higher temperatures, a faster conversion of CO by the carboxydophilic microorganism occurs, and a three times faster removal of H<sub>2</sub> is obtained by the methanogen [34,45]. Therefore, the properties of a hyperthermophilic environment positively affects growth and conversion rates and is, thus, advantageous over mesophilic conditions. Here, we analysed whether *T. onnurineus* together with one of the three methanogens can be grown as a powerful artificial archaeal co-culture to efficiently generate biological CH<sub>4</sub> from synthetic waste gases.

## 2. Materials and Methods

### 2.1. Chemicals

CO (99.999 Vol.-%), H<sub>2</sub>:CO (60 Vol.-% in CO), H<sub>2</sub>:CO<sub>2</sub> (80 Vol.-% in CO<sub>2</sub>), and an artificial CO-containing syngas (CO<sub>2</sub> 16.7 Vol.-%, H<sub>2</sub> Vol.-% 16.8%, CH<sub>4</sub> Vol.-%14.7, N<sub>2</sub> Vol.-% 14.5%, and CO 37.3 Vol.-%) were used for closed batch experiments. For gas chromatography (GC), H<sub>2</sub> (99.999 Vol.-%), CO<sub>2</sub> (99.999 Vol.-%), CO (99.999 Vol.-%), H<sub>2</sub>/CO<sub>2</sub> (80 Vol.-% in CO<sub>2</sub>), H<sub>2</sub>/N<sub>2</sub> (4.5 Vol.-% H<sub>2</sub> in N<sub>2</sub>), CH<sub>4</sub> (99.995 Vol.-%), and the standard test gas (Messer GmbH, Wien, Austria) (containing 0.01 Vol.-% CH<sub>4</sub>, 0.08 Vol.-% CO<sub>2</sub> in N<sub>2</sub>) were used in addition to the gases mentioned above. All gases, except the standard



test gas, were purchased from Air Liquide (Air Liquide GmbH, Schwechat, Austria). All other chemicals were of the highest grade available.

## 2.2. Media

Medium A is a modified version of the Deutsche Sammlung von Mikroorganismen und Zellkulturen (DSMZ) medium 282. The exact composition of medium A and medium B can be found in Supplementary Materials, Tables S1 and S2. Balch's vitamin solution was used [46]. For *M. marburgensis* and *M. thermotrophicus*, a phosphate-buffered medium was used [47].

## 2.3. Strains and Cultivation Conditions

The strains *M. jannaschii* JAL-1, *M. villosus* KIN24-T80, *M. vulcanius* M7, *M. marburgensis* DSM 2133 (Marburg), and *M. thermotrophicus* DSM 1053 (delta H) were purchased from the DSMZ. *T. onnurineus* NA1 was provided by Prof. Dr. Sung Gyun Kang (Korea Institute of Ocean Science and Technology (KIOST), Ansan, Korea).

Every cultivation was performed in closed batch mode [48]. Experiments were conducted in 120 mL serum bottles (Ochs Glasgeraetebau, Langerwehe, Germany), sealed with a 20 mm butyl rubber stopper and an aluminium crimp cap (Chemglass Life Science LLC, Vineland, NJ, USA). Serum bottles were filled with the corresponding medium and sealed. Anaerobic conditions were created by evacuating and re-pressurizing with H<sub>2</sub>:CO<sub>2</sub> (4:1) to 0.5 barg five times. The bottles were autoclaved and stored at 4 °C until further use. Unless otherwise stated, the medium was augmented with the following sterile filtered stock solutions before inoculation: NaHCO<sub>3</sub>, L-Cysteine-HCL, and Balch's Vitamin solution [46] (see Supplementary Materials, Tables S1 and S2). Afterwards, the bottles were flushed with H<sub>2</sub>:CO<sub>2</sub> (4:1) to 0.5 barg, before the addition of autoclaved Na<sub>2</sub>S·9H<sub>2</sub>O.

The inoculum, 1 mL (2% v/v) of an actively grown culture, was added anaerobically. The final liquid phase in each serum bottle added up to 50 mL. Depending on the experiment, the headspace gas phase was exchanged with the corresponding gas. Bottles were incubated at 80 °C in either a double-layer shaking incubator at 100 rpm (LABWIT ZWYR-2102C, Labwit Scientific Pty Ltd., Burwood East, Australia) or in a water bath at ~100 lateral shakes per minute (GFL 1083, LAUDA-GFL, Burgwedel, Germany).

## 2.4. Pure-Culture Closed Batch Experiments

The methanogens *M. villosus*, *M. vulcanius*, and *M. jannaschii* were grown under 2 barg H<sub>2</sub>:CO<sub>2</sub> in either medium A or B. A reduced version of them without vitamins, yeast extract, trace elements, or a combination of the three was also tested. The incubation rhythm consisted of 13 and 7 h incubation periods, with 2 h of sampling in between every period. The same rhythm was applied for cultivation of *T. onnurineus*. It was grown in the same medium, but under 1 barg CO. These incubation periods did not apply for *M. marburgensis* and *M. thermotrophicus*, because of their slow growth. Furthermore, they were grown in a phosphate-buffered *M. marburgensis* medium with either 1.7 barg CO, 1.7 barg H<sub>2</sub>:CO (4:1), or 1.7 H<sub>2</sub>:CO<sub>2</sub> (4:1).

## 2.5. Co-Culture Closed Batch Experiments

The co-cultures consisted of *T. onnurineus* and either *M. villosus*, *M. vulcanius*, or *M. jannaschii*. The experiments were conducted according to two general schemes. In the first setup, the experiment started by growing the respective *Methanocaldococcus* strain under 2 barg H<sub>2</sub>:CO<sub>2</sub> first. After 13 h in the incubator, *T. onnurineus* was added. The bottles were then pressurized with CO, H<sub>2</sub>:CO, or artificial syngas to 1 barg. In the second setup, *T. onnurineus* grew 13 h under pure CO, H<sub>2</sub>:CO, or artificial syngas before one of the *Methanocaldococcus* strains was added. From this point onward, both schemes followed the same incubation rhythm, as described in the pure-culture experiments, and ended after a maximum of 80 h of cumulative incubation time. Every experiment was performed in hexuplicates (n = 6) on media A and B, as well as on reduced versions of them.

## 2.6. Sampling

The routinely performed sampling consisted of removing the cultures from the incubator and measuring the pressure as soon as the bottles cooled down to room temperature (~60 min). To analyse growth, 0.7 mL of the cultures were withdrawn for optical density (OD) measurements ( $\lambda = 578$  nm). Lastly, the bottles were flushed and re-pressurized with the corresponding gas.

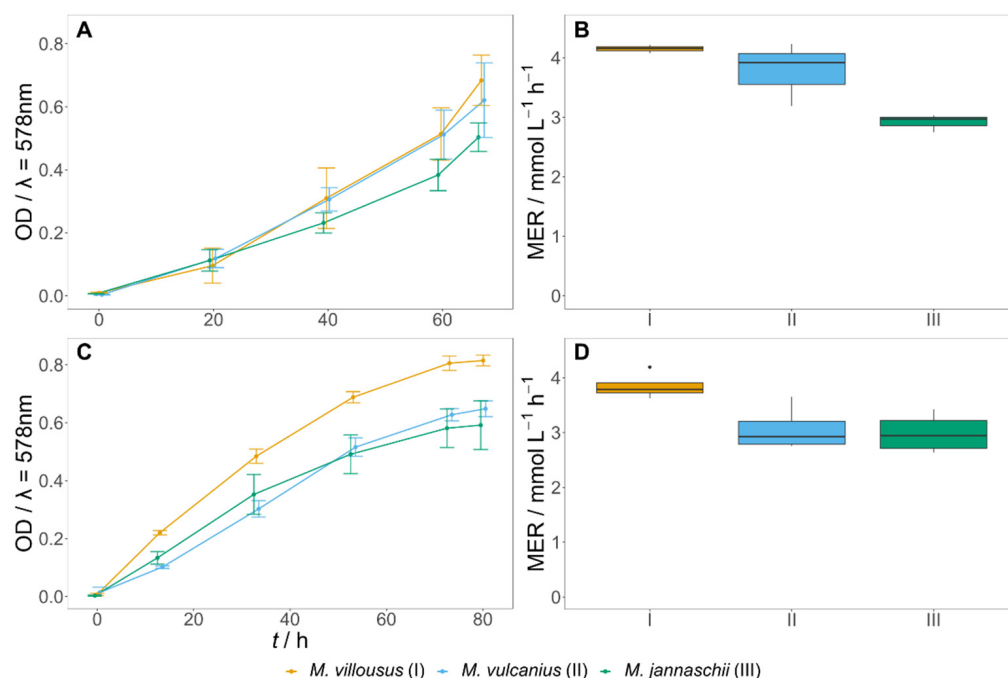
## 2.7. Analytical Procedures

OD of the cultures was measured via a spectrophotometer at  $\lambda = 578$  nm (Specord 200 Plus, Analytik Jena, Jena, Germany). The headspace gas composition before and after inoculation in pure cultures was determined via the gas headspace pressure difference [18,47,49]. Gas evolution and uptake rates were calculated according to methods described in refs. [47,50,51]. Samples that were withdrawn for gas chromatography (GC) analysis did not undergo the sampling procedure. The headspace gas composition in co-culture experiments was analysed via GC, and the evolution and uptake rates were calculated [52]. Some of the negative controls revealed “air contamination” and were removed from the calculations of the results. To maintain the correct atmosphere, OD was measured after completion of the GC run and as such is only an estimate of the true OD.

## 3. Results

### 3.1. Growth Kinetics of Methanogens in Defined Medium

Growth and gas conversion by the methanogens *M. villosus*, *M. vulcanius*, and *M. jannaschii* were analysed in defined versions of media A and B on  $\text{H}_2:\text{CO}_2$  (4:1), by removing complex components. Removal of the trace elements from the media hindered growth. *M. villosus* showed a higher methane evolution rate (MER) than the other two methanogens in medium A and B (Figure 1).



**Figure 1.** Growth kinetics and MER of *M. villosus*, *M. vulcanius*, and *M. jannaschii*. (A,B) grown in medium A; (C,D) grown in medium B. Both media were without yeast extract and vitamins. Error bars in the line graphs show the standard deviation. All experiments are N = 1, n = 3. However, N = 2, n = 3 for *M. villosus* using medium B.

*M. marburgensis* and *M. thermotrophicus* were grown on CO, H<sub>2</sub>:CO (3:1) and H<sub>2</sub>:CO<sub>2</sub> (4:1) [53]. The analysis showed that *M. marburgensis* and *M. thermotrophicus*, when grown on H<sub>2</sub>:CO<sub>2</sub> (4:1), had a high turnover, and furthermore, experiments on H<sub>2</sub>:CO resulted in poor CH<sub>4</sub> conversion. No growth was observed on pure CO (see Supplementary Materials, Figure S1, Table S5). Due to these findings, *M. marburgensis* and *M. thermotrophicus* were excluded from the co-culture experiments.

### 3.2. *T. onnurineus* Grown on CO

*T. onnurineus* was grown individually in a pure culture in media A and B. Results indicated that the organism reached higher OD<sub>578</sub> when grown on medium A as well as achieved a higher gas conversion than in media B. Omission of vitamins from medium B showed no difference regarding the H<sub>2</sub> evolution rate (HER) (see Supplementary Materials, Table S6, Figure S2).

### 3.3. Artificial Archaeal Co-Culture Engineering

Conversion of CO to CH<sub>4</sub> and CO<sub>2</sub> was performed with a co-culture consisting of *T. onnurineus* together with either *M. villosus*, *M. jannaschii*, or *M. vulcanius*. After pre-growth of the methanogens for 13 h, the cultures were inoculated with *T. onnurineus*. Growth and gas rates were analysed for all three co-cultures in media A and B (Tables 1 and 2, Figure 2). Co-cultures in medium A had relatively similar MERs ranging from 1.4 to 1.6 mmol L<sup>-1</sup> h<sup>-1</sup>, whereas in medium B, the co-culture consisting of *M. villosus* and *T. onnurineus* achieved MERs between 1.6 and 2.0 mmol L<sup>-1</sup> h<sup>-1</sup>. In general, the measured mean gas evolution and uptake rates were either equal or slightly higher in medium B. The higher CO uptake rate (COUR) and CO<sub>2</sub> evolution rate (CER) in medium B indicated that *T. onnurineus* performed better under this condition. It is likely that the H<sub>2</sub> uptake rate (HUR) of the methanogens positively influenced the COUR of *T. onnurineus* by creating favourable thermodynamic conditions [34].

**Table 1.** Mean gas evolution and uptake rates of the co-cultures cultivated in medium A on 100% CO<sup>1</sup>.

Co-Culture	MER/mmol L <sup>-1</sup> h <sup>-1</sup>	HUR/mmol L <sup>-1</sup> h <sup>-1</sup>	CUR/mmol L <sup>-1</sup> h <sup>-1</sup>	COUR/mmol L <sup>-1</sup> h <sup>-1</sup>	CER/mmol L <sup>-1</sup> h <sup>-1</sup>
<i>M. villosus</i> + <i>T. onnurineus</i>	1.4 ± 0.4	6.4 ± 1.5	1.4 ± 0.4	6.4 ± 1.5	5.0 ± 1.1
<i>M. vulcanius</i> + <i>T. onnurineus</i>	1.6 ± 0.3	7.0 ± 1.3	1.6 ± 0.3	7.0 ± 1.3	5.4 ± 0.9
<i>M. jannaschii</i> + <i>T. onnurineus</i>	1.5 ± 0.4	6.5 ± 1.5	1.5 ± 0.3	6.5 ± 1.5	5.0 ± 1.2

<sup>1</sup> Measurements were taken after a 7 h incubation period. Data collected at indicated timepoints in Figure 2 A. (N = 1, n = 6). Values are shown with standard deviation.

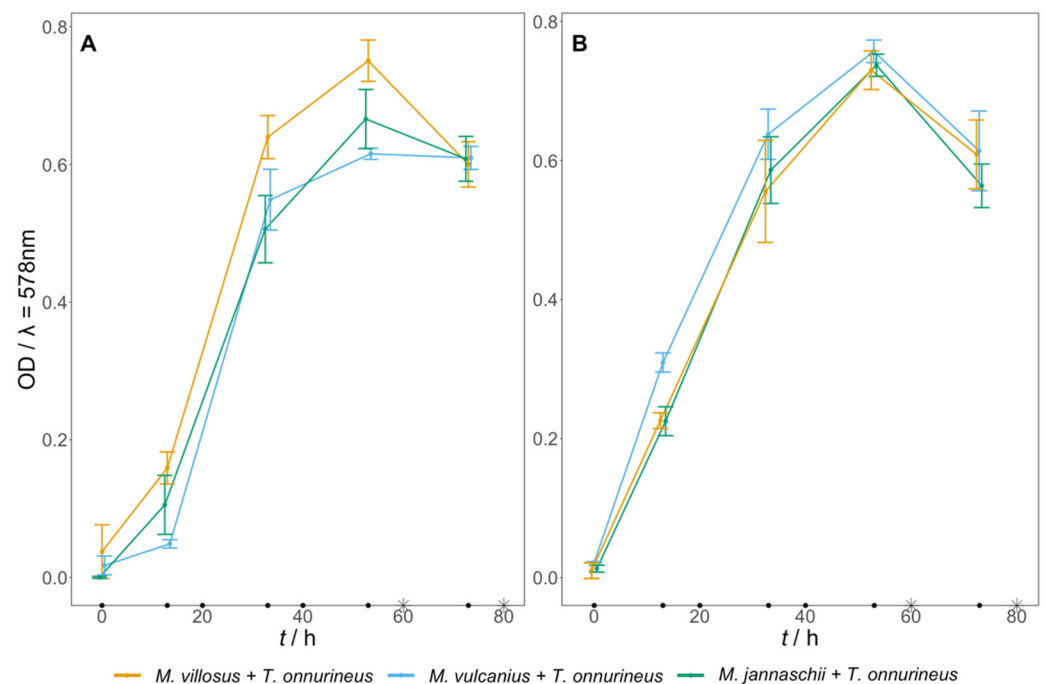
**Table 2.** Mean gas evolution and uptake rates of the co-cultures cultivated in medium B on 100% CO<sup>1</sup>.

Co-Culture	MER/mmol L <sup>-1</sup> h <sup>-1</sup>	HUR/mmol L <sup>-1</sup> h <sup>-1</sup>	CUR/mmol L <sup>-1</sup> h <sup>-1</sup>	COUR/mmol L <sup>-1</sup> h <sup>-1</sup>	CER/mmol L <sup>-1</sup> h <sup>-1</sup>
<i>M. villosus</i> + <i>T. onnurineus</i>	2.0 ± 0.3	8.3 ± 1.3	2.1 ± 0.3	8.4 ± 1.3	6.3 ± 0.9
<i>M. vulcanius</i> + <i>T. onnurineus</i>	1.6 ± 0.5	10.3 ± 0.2	2.6 ± 0.3	11.3 ± 0.7	8.7 ± 0.5
<i>M. jannaschii</i> + <i>T. onnurineus</i>	1.8 ± 0.4	9.0 ± 1.5	1.9 ± 0.5	9.1 ± 1.6	7.2 ± 1.2

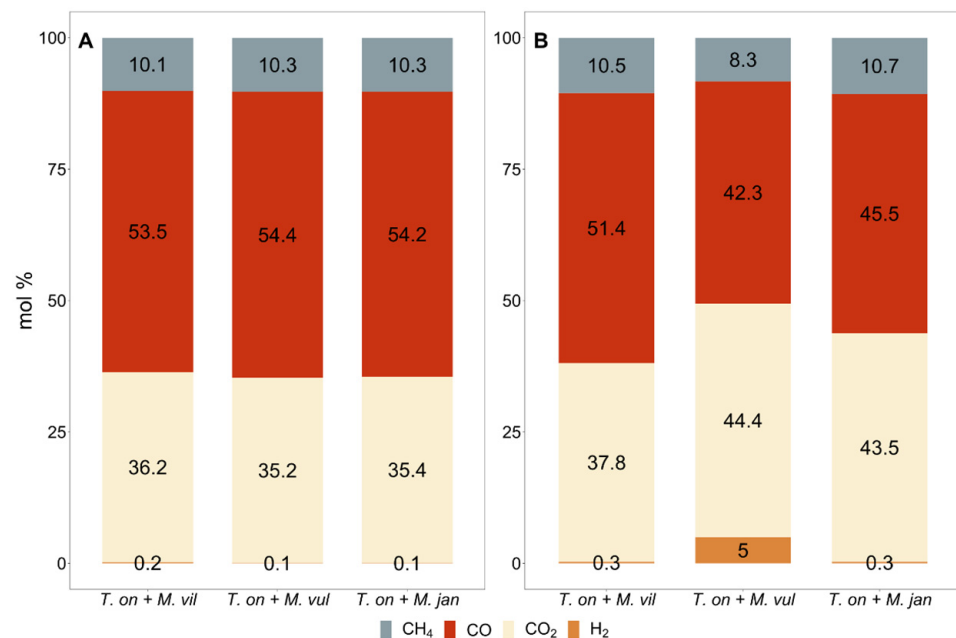
<sup>1</sup> Measurements were taken after a 7 h incubation period. Data collected at indicated timepoints in Figure 2 B. (N = 1, n = 6). Values are shown with standard deviation.

The results suggested that the co-culture with *M. vulcanius* was less efficient in medium B, as it had a higher CO<sub>2</sub> uptake rate (CUR) and HUR, compared to medium A, but not a higher MER. This agrees with the results obtained from pure-culture experiments, where medium B led to a slightly lower MER of *M. vulcanius* compared to the other methanogens.

Comparison of the MERs between the pure and the co-cultures suggested that, on average, a lower MER was measured in the co-cultures (Tables 1 and 2, Figure 1). A likely reason for this was that they were dependent on the conversion of CO to CO<sub>2</sub> and H<sub>2</sub> by *T. onnurineus*. Figure 3 shows that the CH<sub>4</sub> production and growth occurred at the highest capacity, as the H<sub>2</sub> content in most cultures was below 1 mol%, except for one case, suggesting it was fully converted. As such, the rate-limiting step in CH<sub>4</sub> production by the methanogens in the co-culture was the availability of H<sub>2</sub>.



**Figure 2.** Growth kinetics of either *M. villosus*, *M. jannaschii*, or *M. vulcanius* with *T. onnurineus*. After the first 13 h, the medium was inoculated with *T. onnurineus* and the gas phase was exchanged from  $H_2:CO_2$  to  $CO$ . The error bars show the standard deviation. Closed black circles on the  $x$ -axis mark the re-pressurising of the headspace with  $CO$ . The asterisks on the  $x$ -axis indicate the sampling points for GC analysis. (A) Growth in medium A; (B) growth in medium B.  $N = 1$ ,  $n = 6$ .



**Figure 3.** Relative mean molar gas composition in the co-cultures headspace after a 7 h incubation period on  $CO$ . Measurements were taken at the timepoints indicated in Figure 2. (A) Co-culture cultivated in medium A; (B) co-culture cultivated in medium B.  $N = 1$ ,  $n = 6$ .

To circumvent  $H_2$  limitation in the co-culture experiments, two strategies were employed. First, to create a functional culture with a high  $H_2$  production rate in advance of the methanogen being added, an inoculation scheme was tested, where *T. onnurineus* was initially grown 13 h on  $CO$ , prior to addition of said methanogen. Second, a different gas

composition, H<sub>2</sub>:CO (3:1) instead of pure CO, was used to provide additional H<sub>2</sub> available in the atmosphere. In addition, an experiment with a gas composition resembling that of industrial waste or syngases was performed [21]. The co-cultures were exposed to an artificial syngas (see Section 2.1) that could arise by industrial processes (Table 3). As *T. onnurineus* grown with *M. villosus* in medium B was considered the best co-culture, this pair was used. However, it should be noted that these were closed batch experiments and that the productivities are dependent on the conversion kinetics and on the tested time interval.

**Table 3.** Mean gas evolution rates of co-cultures in medium B under different gas compositions and inoculation orders <sup>1</sup>.

Co-Culture	Gas	MER/mmol L <sup>-1</sup> h <sup>-1</sup>	CER/mmol L <sup>-1</sup> h <sup>-1</sup>
<i>M. villosus</i> + <i>T. onnurineus</i>	CO	2.0 ± 0.3	6.3 ± 0.9
<i>T. onnurineus</i> + <i>M. villosus</i>	CO	1.1 ± 0.1	3.7 ± 1.0
<i>M. villosus</i> + <i>T. onnurineus</i>	H <sub>2</sub> :CO	1.0 ± 0.4	0.0 ± 0.0
<i>T. onnurineus</i> + <i>M. villosus</i>	H <sub>2</sub> :CO	1.0 ± 0.3	0.0 ± 0.0
<i>M. villosus</i> + <i>T. onnurineus</i>	Art. syngas	1.5 ± 0.5	0.9 ± 0.6
<i>T. onnurineus</i> + <i>M. villosus</i>	Art. syngas	0.9 ± 0.3	NA

<sup>1</sup> Measurements were taken after a 7 h incubation period (N = 1, n = 6). Values are shown with standard deviation.

In experiments with pure CO, the MER was twice as high when *M. villosus* was added first. The average H<sub>2</sub> content turned out to remain below 0.3 mol% (see Supplementary Materials, Table S7). When gassing with H<sub>2</sub>:CO, interestingly, both inoculation schemes showed a decreasing performance over time, as revealed by a MER, which was only half of what was achieved when pure CO was used (Table 3). However, the measured CO<sub>2</sub> levels were below 0.1 mol% in both cases (see Supplementary Materials, Table S7). This could have been caused by the presence of H<sub>2</sub> in the H<sub>2</sub>:CO, as the additional application of H<sub>2</sub> within the gas negatively affected growth and performance of *T. onnurineus*, which in turn most likely hindered the MER. The reduced CER by *T. onnurineus* may have been caused by the lower partial pressure of CO in the serum bottle headspace.

In the experiment where the artificial syngas mix was used and where *M. villosus* was pre-grown, the MER was 1.5 ± 0.5 mmol L<sup>-1</sup> h<sup>-1</sup>. The average CH<sub>4</sub> mol% increased by about 10% to 24.8 mol%. This increase was similar to what was obtained when using pure CO, although the MER decreased as the experiment progressed. We did not observe a negative impact on the MER during co-culture experiments when elemental sulphur was added.

#### 4. Discussion

This study is a new brick in the emerging research field of Archaea Biotechnology [54] and artificial microbial ecosystem design and engineering [55]. We investigated the conversion of one-carbon substrates (CO, H<sub>2</sub>:CO, and CO-rich waste gases) by the artificially designed co-cultures of either *M. villosus*, *M. jannaschii*, or *M. vulcanius* together with *T. onnurineus*. Our results showed fast and reliable gas conversion, with a reduction in pure CO to about 50 mol% and simultaneous production of ~10 mol% CH<sub>4</sub> within 7 h. The most efficient conversion of the artificial syngas was performed by the co-culture *M. villosus* with *T. onnurineus*, inoculated in this order. This culture showed a CO reduction of 7%, starting from 37.3 mol% and an increase in CH<sub>4</sub> by ~10 mol% within 7 h. This proved the ability of the co-cultures to convert a variety of different CO-containing gas compositions with a lower proportion of CO.

A study with a similar experimental setup reported an ~6% CH<sub>4</sub> increase after 22 h [35]. We obtained 10% increase in 7 h. This suggests that the established co-culture (*T. onnurineus*/*M. villosus*) is of higher catalytic power. Nonetheless, most up-to-date published co-cultures were tested in different setups than the one reported in this study, making a direct comparison of evolution and uptake rates rather difficult [26,30,34]. Establishing different co-cultures in a bioreactor setup will, thus, be of great importance to fully understand their growth and production kinetics.

Pure-culture closed batch experiments of the methanogens in a defined medium on H<sub>2</sub>:CO<sub>2</sub> showed a higher MER ( $4.2 \pm 0.1 \text{ mmol L}^{-1} \text{ h}^{-1}$ ) than the co-cultures ( $2.0 \pm 0.3 \text{ mmol L}^{-1} \text{ h}^{-1}$ ) (Figure 1, Table 3). Therefore, the potential for achieving a higher MER in co-cultures is possible if the necessary gas supply can be performed, and the inhibitory concentration of CO would not be surpassed [56]. Although the main limitation of the co-culture grown on pure CO was the availability of H<sub>2</sub> for methanogenesis and, hence, the conversions of CO to H<sub>2</sub> and CO<sub>2</sub> by *T. onnurineus* (Figure 3 and Supplementary Materials, Table S7). The addition of H<sub>2</sub> to the gas phase did not provide an increase in the MER. Rather, it led to a limitation of CO<sub>2</sub> availability (Supplementary Materials, Table S7), most likely due to the reduced performance of *T. onnurineus* under the lower CO partial pressure. Consequently, application of the artificial syngas led to an increase in MER, as biomethanation seems to be neither limited by CO<sub>2</sub> nor H<sub>2</sub> availability. Nonetheless, it did not reach the same values as in pure CO (Table 3). This can be explained by the concentration reduction in CO, CO<sub>2</sub>, and H<sub>2</sub> in syngas by the other initially present gases, reducing substrate availability.

A change in the cultivation method to a bioreactor setup with higher pressure, agitation, and a constant gassing, resulting in having a higher gas solubility and higher gas transfer rate to the liquid phase, might increase the conversion of CO by *T. onnurineus* and the potential of the co-culture [37,39,48]. However, the ratio of the gas in the liquid phase has to be considered carefully, as high agitation might also lead to an excessive CO availability for the methanogens [34]. As recently more and more genetic tools for archaea become available, an overexpression of the carbon monoxide dehydrogenase could also be a solution to debottleneck CO conversion by *T. onnurineus* [39,57].

Unfortunately, *T. onnurineus* is still dependent on a complex medium containing yeast extract, which limits the potential industrial applicability. However, co-cultivation could be used to gain advantages or improve growth of both microorganisms through improving their syntrophic relationships [34]. Finding a suitable defined medium for *T. onnurineus* or replacing it by a different organism that can catalyse the WGS from CO in minimal conditions is one suggested avenue of research. *Carboxydocella thermautotrophica* or *Carboxydocella sporoproducens* would fall into the same pH and temperature conditions as the herein employed methanogens [35].

A direct conversion of CO to CH<sub>4</sub> by a single organism such as *M. marburgensis* or *M. thermautotrophicus* is likely not the most suitable biotechnological approach, as the inhibitory concentration of CO for these methanogens is very low [31,34]. The artificially created archaeal co-cultures consisting of one of the hyperthermophilic methanogenic archaea *M. villosus*, *M. jannaschii*, and *M. vulcanius* together with *T. onnurineus*, as performed in this study, are highly efficient and reliable for biomethanation. By adaptation to a minimal medium and by performing targeted bioprocess development, artificial archaeal co-cultures could be of environmental, economic, and industrial value in renewable energy production and storage.

## 5. Conclusions

This contribution is another step in the rapidly developing research field of Archaea Biotechnology. Furthermore, it is a proof of principle for the design and engineering of artificial microbial co-cultures. Additionally, it marks a cornerstone in the use of artificial archaeal co-cultures for the biomethanation of syngas. This design of artificial archaeal co-cultures represents a novelty in the field of biomethanation, due the unique selection of



organisms and their hyperthermophilic growth conditions. The created co-cultures convert a variety of different CO-containing gases, including syngas, to CH<sub>4</sub>. As the WGSR might still be the limiting factor, finding the best organism for conversion of H<sub>2</sub>O:CO to H<sub>2</sub>:CO<sub>2</sub> will be of future relevance to enhance the kinetics of the artificial co-culture. Apart from the choice of the archaea, the inoculation sequence of the strains and medium development are crucial factors for a successful design. These factors will be important in engineering the next steps for scaling up the bioprocess of artificial archaeal co-cultures. Inferring from our results, hyperthermophilic and anaerobic archaea are of great biotechnological relevance, as they act as highly efficient H<sub>2</sub> and CH<sub>4</sub> cell factories in artificial co-culture.

**Supplementary Materials:** The following are available online at <https://www.mdpi.com/article/10.3390/fermentation7040276/s1>, Table S1: Chemical composition of medium A, Table S2: Chemical composition of medium B, Table S3: 141 trace element solution modified from DSMZ, Table S4: Holden's trace element solution 2, Table S5: The physiological maximal and mean values of CH<sub>4</sub> production and growth kinetics of *M. marburgensis* and *M. thermautotrophicus*, Table S6: HER of *T. onnurineus* after 7 h of incubation, Table S7: Relative mean molar gas composition of the co-culture's headspace after a 7 h incubation period, Figure S1: Growth of *M. marburgensis* and *M. thermautotrophicus* in defined medium, Figure S2: Growth of *T. onnurineus* at 1 barg CO.

**Author Contributions:** Conceptualization, A.Z., T.S. and S.K.-M.R.R.; methodology, B.R., I.K., M.V. and S.K.-M.R.R.; validation, A.Z., B.R. and S.K.-M.R.R.; formal analysis, A.Z.; investigation, A.Z., B.R., T.S., M.S. and C.P.; resources, M.V. and S.K.-M.R.R.; data curation, A.Z. and B.R.; writing—original draft preparation, A.Z., B.R. and S.K.-M.R.R.; writing—review and editing, A.Z., B.R., I.K., M.V. and S.K.-M.R.R.; visualization, A.Z.; supervision, S.K.-M.R.R.; project administration, M.V. and S.K.-M.R.R.; funding acquisition, M.V. and S.K.-M.R.R. All authors have read and agreed to the published version of the manuscript.

**Funding:** Greatly acknowledged is the Österreichische Forschungsförderungsgesellschaft (FFG) for funding the project BioHyMe (grant no. 853615). The BMBWF is acknowledged for supporting the research with the WTZ project CZ 08/2020. Open access funding by the University of Vienna.

**Institutional Review Board Statement:** Not applicable.

**Informed Consent Statement:** Not applicable.

**Data Availability Statement:** The datasets used and/or analysed during the current study are available from the corresponding author on reasonable request.

**Acknowledgments:** S.K.-M.R.R. greatly acknowledges Sung Gyun Kang (Korea Institute of Ocean Science and Technology (KIOST), Ansan, Republic of Korea) for providing *T. onnurineus* NA1. We want to thank Angus Hilts for comments on and proofreading of the manuscript.

**Conflicts of Interest:** B.R. and S.K.-M.R.R. declare competing interests due to their employment in the Arkeon GmbH. All other authors declare no competing interest.

## Abbreviations

CO <sub>2</sub>	Carbon dioxide
CH <sub>4</sub>	Methane
CO	Carbon monoxide
H <sub>2</sub>	Molecular hydrogen
WGSR	Water gas shift reaction
DSMZ	Deutsche Sammlung von Mikroorganismen und Zellkulturen
OD	Optical density
GC	Gas chromatography
MER	Methane evolution rate
HER	Molecular hydrogen evolution rate
COUR	Carbon monoxide uptake rate
CER	Carbon dioxide evolution rate
HUR	Molecular hydrogen uptake rate
CUR	Carbon dioxide uptake rate

## References

- EEA (European Environment Agency). *Primary Energy Consumption by Fuel in the EU-27*; EEA: København, Denmark, 2020; Volume 28.
- EEA (European Environment Agency). *National Emissions Reported to the UNFCCC and to the EU Greenhouse Gas Monitoring Mechanism*; EEA: København, Denmark, 2019; Available online: <https://www.eea.europa.eu/data-and-maps/data/national-emissions-reported-to-the-unfccc-and-to-the-eu-greenhouse-gas-monitoring-mechanism-14> (accessed on 10 November 2021).
- Sterner, M.; Specht, M. Power-to-Gas and Power-to-X—The History and Results of Developing a New Storage Concept. *Energies* **2021**, *14*, 6594. [CrossRef]
- Götz, M.; Lefebvre, J.; Mörs, F.; McDaniel Koch, A.; Graf, F.; Bajohr, S.; Reimert, R.; Kolb, T. Renewable Power-to-Gas: A Technological and Economic Review. *Renew. Energy* **2016**, *85*, 1371–1390. [CrossRef]
- Rönsch, S.; Schneider, J.; Matthischke, S.; Schlüter, M.; Götz, M.; Lefebvre, J.; Prabhakaran, P.; Bajohr, S. Review on Methanation – From Fundamentals to Current Projects. *Fuel* **2016**, *166*, 276–296. [CrossRef]
- Eyl-Mazzega, M.-A.; Mathieu, C.; Boesgaard, K.; Daniel-Gromke, J.; Denysenko, V.; Liebetrau, J.; Cornot-Gandolphe, S. *Biogas and Bio-Methane in Europe: Lessons from Denmark, Germany and Italy*; Études de l’Ifri; French Institute of International Relations (IFRI): Paris, France, 2019; ISBN 979-10-373-0025-6.
- Rittmann, S.K.-M.; Seifert, A.H.; Bernacchi, S. Kinetics, Multivariate Statistical Modelling, and Physiology of CO<sub>2</sub>-Based Biological Methane Production. *Appl. Energy* **2018**, *216*, 751–760. [CrossRef]
- Mauerhofer, L.-M.; Zwirtmayr, S.; Pappenreiter, P.; Bernacchi, S.; Seifert, A.H.; Reischl, B.; Schmider, T.; Taubner, R.-S.; Paulik, C.; Rittmann, S.K.-M.R. Hyperthermophilic Methanogenic Archaea Act as High-Pressure CH<sub>4</sub> Cell Factories. *Commun. Biol.* **2021**, *4*, 289. [CrossRef]
- Mauerhofer, L.-M.; Reischl, B.; Schmider, T.; Schupp, B.; Nagy, K.; Pappenreiter, P.; Zwirtmayr, S.; Schuster, B.; Bernacchi, S.; Seifert, A.H.; et al. Physiology and Methane Productivity of Methanobacterium Thermaggregans. *Appl. Microbiol. Biotechnol.* **2018**, *102*, 7643–7656. [CrossRef] [PubMed]
- Abdel Azim, A.; Pruckner, C.; Kolar, P.; Taubner, R.-S.; Fino, D.; Saracco, G.; Sousa, F.L.; Rittmann, S.K.-M.R. The Physiology of Trace Elements in Biological Methane Production. *Bioresour. Technol.* **2017**, *241*, 775–786. [CrossRef]
- Seifert, A.H.; Rittmann, S.; Herwig, C. Analysis of Process Related Factors to Increase Volumetric Productivity and Quality of Biomethane with Methanothermobacter Marburgensis. *Appl. Energy* **2014**, *132*, 155–162. [CrossRef]
- Seifert, A.H.; Rittmann, S.; Bernacchi, S.; Herwig, C. Method for Assessing the Impact of Emission Gasses on Physiology and Productivity in Biological Methanogenesis. *Bioresour. Technol.* **2013**, *136*, 747–751. [CrossRef]
- Burkhardt, M.; Jordan, I.; Heinrich, S.; Behrens, J.; Ziesche, A.; Busch, G. Long Term and Demand-Oriented Biocatalytic Synthesis of Highly Concentrated Methane in a Trickle Bed Reactor. *Appl. Energy* **2019**, *240*, 818–826. [CrossRef]
- Burkhardt, M.; Koschack, T.; Busch, G. Biocatalytic Methanation of Hydrogen and Carbon Dioxide in an Anaerobic Three-Phase System. *Bioresour. Technol.* **2015**, *178*, 330–333. [CrossRef] [PubMed]
- Jensen, M.B.; Strübing, D.; de Jonge, N.; Nielsen, J.L.; Ottosen, L.D.M.; Koch, K.; Kofoed, M.V.W. Stick or Leave—Pushing Methanogens to Biofilm Formation for Ex Situ Biomethanation. *Bioresour. Technol.* **2019**, *291*, 121784. [CrossRef]
- Nock, W.J.; Serna-Maza, A.; Heaven, S.; Banks, C.J. Evaluation of Microporous Hollow Fibre Membranes for Mass Transfer of H<sub>2</sub> into Anaerobic Digesters for Biomethanation. *J. Chem. Technol. Biotechnol.* **2019**, *94*, 2693–2701. [CrossRef]
- Tao, B.; Alessi, A.M.; Zhang, Y.; Chong, J.P.J.; Heaven, S.; Banks, C.J. Simultaneous Biomethanisation of Endogenous and Imported CO<sub>2</sub> in Organically Loaded Anaerobic Digesters. *Appl. Energy* **2019**, *247*, 670–681. [CrossRef]
- Rittmann, S.K.-M.; Seifert, A.; Herwig, C. Essential Prerequisites for Successful Bioprocess Development of Biological CH<sub>4</sub> Production from CO<sub>2</sub> and H<sub>2</sub>. *Crit. Rev. Biotechnol.* **2015**, *35*, 141–151. [CrossRef] [PubMed]
- Rittmann, S.K.-M.R.; Seifert, A.H.; Krajete, A. Biomethanisierung—ein Prozess zur Ermöglichung der Energiewende? *BIOspektrum* **2014**, *20*, 816–817. [CrossRef]
- Rittmann, S.K.-M.R. A Critical Assessment of Microbiological Biogas to Biomethane Upgrading Systems. In *Biogas Science and Technology*; Guebitz, G.M., Bauer, A., Bochmann, G., Gronauer, A., Weiss, S., Eds.; Advances in Biochemical Engineering/Biotechnology; Springer International Publishing: Cham, Switzerland, 2015; pp. 117–135. ISBN 978-3-319-21993-6.
- Van der Stricht, W.; De Maré, C.; Plattner, T.; Fleischanderl, A.; Haselgriber, M.; Nair, P.; Wolf, C. *Sustainable Production of Low Carbon, Renewable Fuels by Fermenting Industrial Process Gasses from the Iron and Steel Industry*; ArcelorMittal, Primetals Technologies, LanzaTech: Gent, Belgium, 2017.
- Safari, F.; Tavasoli, A.; Ataei, A.; Choi, J.-K. Hydrogen and Syngas Production from Gasification of Lignocellulosic Biomass in Supercritical Water Media. *Int. J. Recycl. Org. Waste Agric.* **2015**, *4*, 121–125. [CrossRef]
- Dürre, P.; Eikmanns, B.J. C1-Carbon Sources for Chemical and Fuel Production by Microbial Gas Fermentation. *Curr. Opin. Biotechnol.* **2015**, *35*, 63–72. [CrossRef]
- de Medeiros, E.M.; Noorman, H.; Maciel Filho, R.; Posada, J.A. Multi-Objective Sustainability Optimization of Biomass Residues to Ethanol via Gasification and Syngas Fermentation: Trade-Offs between Profitability, Energy Efficiency, and Carbon Emissions. *Fermentation* **2021**, *7*, 201. [CrossRef]
- Phillips, J.R.; Huhnke, R.L.; Atiyeh, H.K. Syngas Fermentation: A Microbial Conversion Process of Gaseous Substrates to Various Products. *Fermentation* **2017**, *3*, 28. [CrossRef]

26. Westman, S.Y.; Chandolias, K.; Taherzadeh, M.J. Syngas Biomethanation in a Semi-Continuous Reverse Membrane Bioreactor (RMBR). *Fermentation* **2016**, *2*, 8. [[CrossRef](#)]
27. Devarapalli, M.; Lewis, R.S.; Atiyeh, H.K. Continuous Ethanol Production from Synthesis Gas by *Clostridium Ragsdalei* in a Trickle-Bed Reactor. *Fermentation* **2017**, *3*, 23. [[CrossRef](#)]
28. Rittmann, S.K.-M.; Lee, H.S.; Lim, J.K.; Kim, T.W.; Lee, J.-H.; Kang, S.G. One-Carbon Substrate-Based Biohydrogen Production: Microbes, Mechanism, and Productivity. *Biotechnol. Adv.* **2015**, *33*, 165–177. [[CrossRef](#)] [[PubMed](#)]
29. Thauer, R.K. Citric-Acid Cycle, 50 Years on: Modifications and an Alternative Pathway in Anaerobic Bacteria. *Eur. J. Biochem.* **1988**, *176*, 497–508. [[CrossRef](#)]
30. Klasson, K.; Cowger, J.; Ko, C.; Vega, J.; Clausen, E.; Gaddy, J. Methane Production from Synthesis Gas Using a Mixed Culture Of *R. Rubrum* M. *Barkeri*, and *M. Formicicum*. *Appl. Biochem. Biotechnol.* **1990**, *24*, 317–328. [[CrossRef](#)]
31. Daniels, L.; Fuchs, G.; Thauer, R.; Zeikus, J. Carbon Monoxide Oxidation by Methanogenic Bacteria. *J. Bacteriol.* **1977**, *132*, 118–126. [[CrossRef](#)]
32. O'Brien, J.M.; Wolkin, R.; Moench, T.; Morgan, J.; Zeikus, J. Association of Hydrogen Metabolism with Unitrophic or Mixotrophic Growth of *Methanosarcina Barkeri* on Carbon Monoxide. *J. Bacteriol.* **1984**, *158*, 373–375. [[CrossRef](#)]
33. Diender, M.; Pereira, R.; Wessels, H.J.; Stams, A.J.; Sousa, D.Z. Proteomic Analysis of the Hydrogen and Carbon Monoxide Metabolism of *Methanothermobacter Marburgensis*. *Front. Microbiol.* **2016**, *7*, 1049. [[CrossRef](#)]
34. Diender, M.; Uhl, P.S.; Bitter, J.H.; Stams, A.J.; Sousa, D.Z. High Rate Biomethanation of Carbon Monoxide-Rich Gases via a Thermophilic Synthetic Culture. *ACS Sustain. Chem. Eng.* **2018**, *6*, 2169–2176. [[CrossRef](#)]
35. Kohlmayer, M.; Robert, H.; Raimund, B.; Wolfgang, M. Simultaneous CO<sub>2</sub> and CO methanation using microbes. *Microbiology* **2018**. [[CrossRef](#)]
36. Schmider, T. Ecophysiology and Methane Productivity of Carboxydrotrophy-Based Archaeal Co-Cultures. Master's Thesis, University of Vienna, Vienna, Austria, 2018.
37. Kim, M.-S.; Fitriana, H.N.; Kim, T.W.; Kang, S.G.; Jeon, S.G.; Chung, S.H.; Park, G.W.; Na, J.-G. Enhancement of the Hydrogen Productivity in Microbial Water Gas Shift Reaction by *Thermococcus Onnurineus* NA1 Using a Pressurized Bioreactor. *Int. J. Hydrog. Energy* **2017**, *42*, 27593–27599. [[CrossRef](#)]
38. Lee, S.H.; Kim, M.-S.; Lee, J.-H.; Kim, T.W.; Bae, S.S.; Lee, S.-M.; Jung, H.C.; Yang, T.-J.; Choi, A.R.; Cho, Y.-J.; et al. Adaptive Engineering of a Hyperthermophilic Archaeon on CO and Discovering the Underlying Mechanism by Multi-Omics Analysis. *Sci. Rep.* **2016**, *6*, 22896. [[CrossRef](#)]
39. Kim, M.-S.; Bae, S.S.; Kim, Y.J.; Kim, T.W.; Lim, J.K.; Lee, S.H.; Choi, A.R.; Jeon, J.H.; Lee, J.-H.; Lee, H.S.; et al. CO-Dependent H<sub>2</sub> Production by Genetically Engineered *Thermococcus Onnurineus* NA1. *Appl. Environ. Microbiol.* **2013**, *79*, 2048–2053. [[CrossRef](#)] [[PubMed](#)]
40. Bae, S.S.; Kim, T.W.; Lee, H.S.; Kwon, K.K.; Kim, Y.J.; Kim, M.-S.; Lee, J.-H.; Kang, S.G. H<sub>2</sub> Production from CO, Formate or Starch Using the Hyperthermophilic Archaeon, *Thermococcus onnurineus*. *Biotechnol. Lett.* **2012**, *34*, 75–79. [[CrossRef](#)] [[PubMed](#)]
41. Bae, S.-S.; Kim, Y.-J.; Yang, S.-H.; Lim, J.-K.; Jeon, J.-H.; Lee, H.-S.; Kang, S.-G.; Kim, S.; Lee, J. *Thermococcus onnurineus* Sp. Nov., a Hyperthermophilic Archaeon Isolated from a Deep-Sea Hydrothermal Vent Area at the PACMANUS Field. *J. Microbiol. Biotechnol.* **2006**, *16*, 1826.
42. Bellack, A.; Huber, H.; Rachel, R.; Wanner, G.; Wirth, R. *Methanocaldococcus villosus* Sp. Nov., a Heavily Flagellated Archaeon That Adheres to Surfaces and Forms Cell–Cell Contacts. *Int. J. Syst. Evol. Microbiol.* **2011**, *61*, 1239–1245. [[CrossRef](#)] [[PubMed](#)]
43. Jeanthon, C.; l'Haridon, S.; Reysenbach, A.-L.; Corre, E.; Vernet, M.; Messner, P.; Sleytr, U.; Prieur, D. *Methanococcus vulcanius* Sp. Nov., a Novel Hyperthermophilic Methanogen Isolated from East Pacific Rise, and Identification of *Methanococcus* Sp. DSM 4213Tas *Methanococcus fervens* Sp. Nov. *Int. J. Syst. Evol. Microbiol.* **1999**, *49*, 583–589. [[CrossRef](#)]
44. Jones, W.; Leigh, J.; Mayer, F.; Woese, C.; Wolfe, R. *Methanococcus jannaschii* Sp. Nov., an Extremely Thermophilic Methanogen from a Submarine Hydrothermal Vent. *Arch. Microbiol.* **1983**, *136*, 254–261. [[CrossRef](#)]
45. Diender, M.; Stams, A.J.; Sousa, D.Z. Pathways and Bioenergetics of Anaerobic Carbon Monoxide Fermentation. *Front. Microbiol.* **2015**, *6*, 1275. [[CrossRef](#)]
46. Balch, W.E.; Wolfe, R. New Approach to the Cultivation of Methanogenic Bacteria: 2-Mercaptoethanesulfonic Acid (HS-CoM)-Dependent Growth of *Methanobacterium Ruminantium* in a Pressurized Atmosphere. *Appl. Environ. Microbiol.* **1976**, *32*, 781–791. [[CrossRef](#)]
47. Taubner, R.-S.; Rittmann, S.K.-M. Method for Indirect Quantification of CH<sub>4</sub> Production via H<sub>2</sub>O Production Using Hydrogenotrophic Methanogens. *Front. Microbiol.* **2016**, *7*, 532. [[CrossRef](#)]
48. Rittmann, S.K.-M.; Herwig, C. A Comprehensive and Quantitative Review of Dark Fermentative Biohydrogen Production. *Microb. Cell Factories* **2012**, *11*, 115. [[CrossRef](#)] [[PubMed](#)]
49. Pappenreiter, P.A.; Zwirtmayr, S.; Mauerhofer, L.-M.; Rittmann, S.K.-M.R.; Paulik, C. Development of a Simultaneous Bioreactor System for Characterization of Gas Production Kinetics of Methanogenic Archaea at High Pressure. *Eng. Life Sci.* **2019**, *19*, 537–544. [[CrossRef](#)] [[PubMed](#)]
50. Rittmann, S.K.-M.; Seifert, A.; Herwig, C. Quantitative Analysis of Media Dilution Rate Effects on *Methanothermobacter Marburgensis* Grown in Continuous Culture on H<sub>2</sub> and CO<sub>2</sub>. *Biomass Bioenergy* **2012**, *36*, 293–301. [[CrossRef](#)]
51. Bernacchi, S.; Rittmann, S.K.-M.; Seifert, A.H.; Krajete, A.; Herwig, C. Experimental Methods for Screening Parameters Influencing the Growth to Product Yield (Y (x/CH<sub>4</sub>)) of a Biological Methane Production (BMP) Process Performed with *Methanothermobacter Marburgensis*. *AIMS Bioeng.* **2014**, *1*, 72–86. [[CrossRef](#)]
52. Reischl, B.; Ergal, I.; Rittmann, S.K.-M. Biohydrogen Production Characteristics of *Desulfurococcus Amylolyticus* DSM 16532. *Int. J. Hydrog. Energy* **2018**, *43*, 8747–8753. [[CrossRef](#)]

- 
53. Pruckner, C. Evolutionary and Physiological Aspects of Potentially Carboxydophilic Archaea. Master's Thesis, University of Vienna, Vienna, Austria, 2019.
  54. Pfeifer, K.; Ergal, I.; Koller, M.; Basen, M.; Schuster, B.; Rittmann, S.K.-M.R. Archaea Biotechnology. *Biotechnol. Adv.* **2021**, *47*, 107668. [[CrossRef](#)]
  55. Ergal, I.; Bochmann, G.; Fuchs, W.; Rittmann, S.K.-M.R. Design and Engineering of Artificial Microbial Consortia for Biohydrogen Production. *Curr. Opin. Biotechnol.* **2022**, *73*, 74–80. [[CrossRef](#)]
  56. Guiot, S.R.; Cimpoaia, R.; Carayon, G. Potential of Wastewater-Treating Anaerobic Granules for Biomethanation of Synthesis Gas. *Environ. Sci. Technol.* **2011**, *45*, 2006–2012. [[CrossRef](#)]
  57. Straub, C.T.; Counts, J.A.; Nguyen, D.M.N.; Wu, C.-H.; Zeldes, B.M.; Crosby, J.R.; Conway, J.M.; Otten, J.K.; Lipscomb, G.L.; Schut, G.J.; et al. Biotechnology of Extremely Thermophilic Archaea. *FEMS Microbiol. Rev.* **2018**, *42*, 543–578. [[CrossRef](#)]

# ANNEX 7

Pages 137 to 147

---

Fuchs W., Steger F., Reich J., Ribitsch D., Rittmann S.K.-M.R., Bochmann G.

**A Simple and Straightforward Method for Activity Measurement of Carbonic  
Anhydrases**

Catalysts (2021) 11(7):819

10.3390/catal11070819

---

## Article

# A Simple and Straightforward Method for Activity Measurement of Carbonic Anhydrases

Werner Fuchs <sup>1,\*</sup>, Franziska Steger <sup>1</sup> , Johanna Reich <sup>1</sup>, Doris Ribitsch <sup>2</sup>, Simon K.-M. R. Rittmann <sup>3</sup>  and Günther Bochmann <sup>1</sup> 

<sup>1</sup> Institute of Environmental Biotechnology, Department for Agrobiotechnology, University of Natural Resources and Life Sciences Vienna, Konrad Lorenz Str. 20, 3430 Tulln, Austria; franziska.steger@boku.ac.at (F.S.); johanna.reich@boku.ac.at (J.R.); guenther.bochmann@boku.ac.at (G.B.)  
<sup>2</sup> ACIB-Austrian Centre of Industrial Biotechnology, Krenngasse 37, 8010 Graz, Austria; doris.ribitsch@acib.at  
<sup>3</sup> Archaea Physiology & Biotechnology Group, Department of Functional and Evolutionary Ecology, University of Vienna, Althanstraße 14, 1090 Vienna, Austria; simon.rittmann@univie.ac.at  
 \* Correspondence: werner.fuchs@boku.ac.at; Tel.: +43-1-47654-97423

**Abstract:** Carbonic anhydrase (CA) is an enzyme of high interest due to its high implications relative to the medical and environmental sectors. In the current paper, an enzyme assay for the determination of CA activity is proposed and it is characterized by its simplicity and high practicability. It permits the straightforward comparison of CAs performance in physiological conditions. The methodology and the theoretical background of the evaluation method are explained in detail. Moreover, the presumed advantages over alternative assays are discussed. The assay has proven to be particularly useful for the screening of CA activity with respect to their application in CO<sub>2</sub>, capturing processes for further utilization or storage.

**Keywords:** carbonic anhydrase; activity assay; enzyme kinetics; modeling



**Citation:** Fuchs, W.; Steger, F.; Reich, J.; Ribitsch, D.; Rittmann, S.K.-M.R.; Bochmann, G. A Simple and Straightforward Method for Activity Measurement of Carbonic Anhydrases. *Catalysts* **2021**, *11*, 819. <https://doi.org/10.3390/catal11070819>

Academic Editors: Maria Elena Russo and Giuseppe Olivieri

Received: 9 June 2021

Accepted: 2 July 2021

Published: 6 July 2021

**Publisher's Note:** MDPI stays neutral with regard to jurisdictional claims in published maps and institutional affiliations.



**Copyright:** © 2021 by the authors. Licensee MDPI, Basel, Switzerland. This article is an open access article distributed under the terms and conditions of the Creative Commons Attribution (CC BY) license (<https://creativecommons.org/licenses/by/4.0/>).

## 1. Introduction

Carbonic anhydrases (CAs; EC 4.2.1.1) are a group of metalloenzymes that catalyze the inter-conversion of carbon dioxide and water into the bicarbonate ion and a proton. First isolated in 1933, CAs have been found to be abundant in algae, bacteria, archaea, plants and animal tissues [1,2]. Six different and evolutionarily unrelated classes have been identified, namely  $\alpha$ ,  $\beta$ ,  $\gamma$ ,  $\delta$ ,  $\zeta$  and  $\eta$  [3]. Despite their structural differences, all CAs utilize the same catalytic mechanism involving a central metal (mostly zinc) atom [4].

Due to their importance in the medical sector, CAs are thoroughly studied enzymes. CAs play a crucial role in numerous physiological processes, such as respiration, pH and CO<sub>2</sub> homeostasis, secretion, gluconeogenesis, or ureagenesis. In addition to the established role of CA inhibitors such as diuretics and antiglaucoma drugs, it has been made apparent that such inhibitors could have potential as novel anticancer and anti-infective drugs [5]. More recently, CAs have become the focus of environmental research. Climate change mitigation scenarios desire technologies that can be immediately implemented. These include carbon capture, utilization and storage [6]. In this context, CAs have raised high interest as enzymatic accelerators while proposing significant enhancement of the CO<sub>2</sub> capturing process in the aqueous phase [7,8].

A wide range of methods have been developed for the measurement of CA activity [9]. However, two of them are most widely applied. These are the Wilbur-Anderson assay and a colorimetric method, which is the so-called p-nitrophenol assay [10]. The Wilbur-Anderson assay makes use of the pH decrease caused by the reaction. One unit is defined as a pH drop from 8.3 to 6.3 per minute at 0 °C within a 20 mmol·L<sup>−1</sup> Tris-HCl buffer solution saturated with CO<sub>2</sub> [11]. However, the assay suffers certain drawbacks. It is conducted at non-physiological temperature conditions (0–3 °C) in order to increase CO<sub>2</sub>



solubility to provide sufficient substrate concentration. It is obvious that a comparison at or near zero temperature does not necessarily reproduce the activity at 'natural' conditions. Moreover, the unit is empirical and provides little information on enzyme kinetics. The p-nitrophenol assay utilizes another feature of CAs: In addition to its natural reaction, i.e., CO<sub>2</sub> hydration, CAs also exhibit certain carboxylic esterase activity. The release of nitrophenol, which is a chromophore with two characteristic adsorption peaks, through the hydrolysis of p-nitrophenol acetate is followed by spectrophotometric measurement [12]. This easily performable test is a valuable tool allowing the rapid comparison of CA activities. Nonetheless, the employment of an alternative substrate renders correct predictions of the actual CO<sub>2</sub> conversion capacity tricky.

More precise methods are available that provide highly accurate results. Frequently stopped-flow devices in combination with absorbance or fluorescence spectroscopy have been used to study the kinetics of CAs. Moreover, radioactive labelling with <sup>13</sup>C or <sup>18</sup>O and sophisticated analytical tools such as mass spectrometry or NMR have been employed [13]. There is no doubt that the application of such high end methods is well justified to address specific scientific questions, e.g., the measurement of undisturbed enzyme activity and its physiological effects in animal or plant tissues. However, the analytical effort and/or the required instrumentation increases significantly. On the other hand, the simple tests also have their merits, in particular, with the focus relative to technical applications such as the mentioned carbon sequestration processes.

Here, we report on a simple procedure and evaluation method that allows rapid estimation of enzyme activity. Background and method development are explained in detail and data interpretation in terms of kinetic constants are discussed.

## 2. Results

The presented assay is a modification of the Wilbur-Anderson protocol and the only analytical instrument employed is a pH meter with data recording. In order to allow adequate monitoring at higher temperatures by considering the associated enhanced enzyme activities, the time span necessary for a certain pH drop needs to be extended. For this purpose, the buffer concentration of the solution was raised from 20 to 100 mM. The buffer partially adsorbs the protons produced by the enzymatic conversion. In return, more CO<sub>2</sub> is also required for the overall reaction. Regarding the limited solubility of CO<sub>2</sub>, it has to be continuously delivered by means of gas sparging instead of providing a specific amount at the beginning of the test.

The development and evaluation of the method are based on the considerations and assumptions presented in the following. In some equations, amounts (in mol) are addressed whereas concentrations (in mol·L<sup>−1</sup>) are required for other equations describing equilibrium constants or kinetic reactions. However, taking a hypothetical reaction volume of 1 L allows the one-to-one interconversion of the two units.

### 2.1. Dependency of Bicarbonate Concentration on pH

The first step was to calculate the relation between measured pH and bicarbonate derived from conversion of CO<sub>2</sub>. The apparent pK<sub>a</sub> of carbonic acid, 6.35 at 25 °C, indicates a relatively weak acid being only slightly dissociated. However, it is well known that during the aqueous phase carbonic acid is in equilibrium with dissolved or aquatic CO<sub>2</sub> (CO<sub>2</sub>(a)). Both species can hardly be distinguished and the above-named value is actually comprised of two equilibria: interconversion of CO<sub>2</sub>(a)/H<sub>2</sub>CO<sub>3</sub> and the true pK<sub>a</sub>. In fact, carbonic acid is a relatively strong acid. The exact pK<sub>a</sub> value cannot be determined but it lies between 3.4 and 3.9 at room temperature 20 °C < T < 25 °C and at zero ionic strength [14]. The pH range observed in the investigated test system, i.e., ≥6.4 is at least 2.5 units higher. Based on the given definition of the pK<sub>a</sub>, Equation (1) can be developed.

$$[\text{H}_2\text{CO}_3] / [\text{HCO}_3^-] = 10^{(\text{pH} - \text{pK}_a)} \leq 0.00316 \quad (1)$$

Equation (1) shows that even at pH 6.4 less than 3.2‰, carbonic acid is present in the protonated form. It can therefore be simplified that the amount of CO<sub>2</sub> dissolved during the aquatic phase that undergoes further conversion corresponds to the HCO<sub>3</sub><sup>−</sup> ions present in the solution and an equivalent number of released protons. These protons either interact with the TRIS buffer system and/or causes a change of pH.

$$x = a + b \quad (2)$$

X is the total protons released that is equivalent to bicarbonate ions [HCO<sub>3</sub><sup>−</sup>].

a denotes the H<sup>+</sup> consumed by the buffer components.

b denotes the H<sup>+</sup> resulting in a change of pH.

Equation (3) describes the dissociation equilibrium of the TRIS buffer at the initial conditions.

$$K_a = [\text{TRIS}]_i \times [\text{H}^+] / [\text{TRISH}^+]_i \quad (3)$$

K<sub>a</sub> denotes the acid constant of TRIS.

Index 'i' indicates initial the concentration values at the beginning of the test.

At a given time, the new equilibrium concentrations are described as follows.

$$[\text{TRIS}] = [\text{TRIS}]_i - a \quad (4)$$

$$[\text{TRISH}^+] = [\text{TRISH}^+]_i + a \quad (5)$$

Considering that the proton concentration at the beginning is very low, 10<sup>−8.2</sup>, and is almost immediately outweighed by the protons released from H<sub>2</sub>CO<sub>3</sub> dissociation, it can be simplified that the absolute proton concentration is equal to b. This simplification is a standard approach also used in pH calculations of weak acids or puffer systems described in the following.

$$B \gg [\text{H}^+]_i \rightarrow [\text{H}^+] \approx b \quad (6)$$

Substituting Equations (4) and (5) into Equation (6) yields the following.

$$K_a = ([\text{TRIS}]_i - a) \times b / ([\text{TRISH}^+]_i + a) \quad (7)$$

Solving the set of Equations (2) and (7) for [HCO<sub>3</sub><sup>−</sup>] as a function of [H<sup>+</sup>] provides the following.

$$[\text{HCO}_3^-] = (-[\text{TRISH}^+]_i \times K_a + (K_a + [\text{TRIS}]_i) \times [\text{H}^+] + [\text{H}^+]^2) / (K_a + [\text{H}^+]) \quad (8)$$

With pK<sub>a</sub> = 8.1 (at 25 °C [15,16]) and a total buffer molarity of 0.1, the initial concentrations of the two buffer species at the start of pH (8.2) are the following: [TRIS]<sub>i</sub> = 0.056 and [TRISH<sup>+</sup>]<sub>i</sub> = 0.044. Inserting these values yields Equation (9), which allows the calculation of the bicarbonate concentration dependent on the measured pH as described as follows.

$$[\text{HCO}_3^-] = (-3.495 \times 10^{-10} + 0.056 \times [\text{H}^+] + [\text{H}^+]^2) / (7.943 \times 10^{-9} + [\text{H}^+]) \quad (9)$$

Using pH data, the gained bicarbonate concentration can be plotted versus time.

In order to prove that the resulting simplifications does not produce any significant errors, a more comprehensive calculation was performed. This included two more equations covering the ion dissociation of water and the initial proton concentration, described as follows.

$$x = a + b - r \quad (10)$$

$$[\text{H}^+] = b + [\text{H}^+]_i - r \quad (11)$$

The value, r, denotes the re-association of H<sup>+</sup> and OH<sup>−</sup> to maintain the ion-product of water (=10<sup>−14</sup>).

Recalculated data almost completely matched the data obtained before. It was therefore concluded that the simpler Equation (9) is sufficiently accurate for the proposed method.

## 2.2. Correlation between Bicarbonate and Enzyme Reactivity

The second step is the correlation of the bicarbonate concentration to the activity of the CA considering the CO<sub>2</sub> transfer to the aquatic phase. In contrast to the buffer reaction above, the steps discussed in what follows are rate limiting. Consequently, the timely change of concentrations and not the concentrations at equilibrium needs to be addressed. Firstly, the time course of CO<sub>2</sub> in the liquid phase was regarded. The course of gas transfer to liquid is described by the well-known differential Equation (12). Therein, the transfer rate correlates to the difference between the saturation concentration of CO<sub>2</sub> in the liquid phase ( $C_{\text{sat}}$ , which depends on the Henry constant) and the actual concentration at a given time multiplied by the mass transfer rate from gas to liquid  $k_1$  [17]. The latter is specific for a given set-up, which implying parameters such as gas flow rate, bubble size or mixing conditions, etc., while the saturation concentration can be calculated from the Henry coefficient or may otherwise be obtained from respective tables.

$$\partial \text{CO}_2(\text{a})' / \partial t = k_1 \times (C_{\text{sat}} - [\text{CO}_2(\text{a})]) \quad (12)$$

Solving this differential equation with a dissolved CO<sub>2</sub> concentration of zero at time zero results in Equation (13).

$$[\text{CO}_2(\text{a})]' = C_{\text{sat}} \times (1 - e^{-k_1 \times t}) \quad (13)$$

$C_{\text{sat}}$  denotes the saturation concentration of CO<sub>2</sub>(a).

This function describes the increasing form of an exponential decay and is generally valid for gas transfer reactions, e.g., for oxygenation. However, in the current case it is necessary to include the further reaction of dissolved CO<sub>2</sub> into bicarbonate and a proton. Following the law of mass action, both the forward and the backward reactions have to be taken into account. Therefore, Equation (12) needs to be extended by the following term.

$$\partial \text{CO}_2(\text{a})'' / \partial t = -k_2 \times [\text{CO}_2(\text{a})] + k_{-2} [\text{H}^+] \times [\text{HCO}_3^-] \quad (14)$$

$k_2$  is the rate constant of CO<sub>2</sub> conversion and  $k_{-2}$  is the rate constant of the back-reaction in the reverse direction. Combination of Equations (13) and (14) provides the timely change of CO<sub>2</sub> in the liquid phase. However, using Equation (9) to solve the complete differential equation is mathematically complex. Again, a simplification was employed: In the beginning, the back-reaction is very small due to the low concentrations of bicarbonate multiplied by the low concentration of protons. Therefore, the second part of the term can be neglected, which resulting in the following equation.

$$\partial [\text{CO}_2(\text{a})] / \partial t = k_1 \times (C_{\text{sat}} - [\text{CO}_2(\text{a})]) - k_2 \times [\text{CO}_2(\text{a})] \quad (15)$$

Rearrangement results in the following equation.

$$\partial [\text{CO}_2(\text{a})] / \partial t = (k_1 + k_2) \times (C_{\text{sat}} \times k_1 / (k_1 + k_2) - \text{CO}_2(\text{a})) \quad (16)$$

Integration of Equation (16) results in the same type of exponential function as Equation (12), however, with modified parameters.

$$[\text{CO}_2(\text{a})] = k_1 / (k_1 + k_2) \times C_{\text{sat}} \times (1 - e^{-(k_1 + k_2) \times t}) \quad (17)$$

Equation (17) describes the course of CO<sub>2</sub> concentration as long as the back reaction of bicarbonate is small. With this equation in mind, the use of a CO<sub>2</sub> sensitive electrode is another interesting option for following enzyme activity as it has been investigated by

Botrè and Botrè [18]. However, this alternative was not tested here. In the current case, further development of the relationship between  $\text{CO}_2(\text{a})$  and  $\text{HCO}_3^-$  concentration was worked out. In Equation (12), this context has already been addressed. Evidently, any  $\text{CO}_2$  converted occurs in the form of bicarbonate. Again, disregarding the backreaction due to the distance to the equilibrium concentrations, Equation (18) and, subsequently, Equation (19) can be developed.

$$\partial[\text{HCO}_3^-] / \partial t = [\text{CO}_2(\text{a})] \times k_2 \quad (18)$$

$$\partial[\text{HCO}_3^-] / \partial t = k_1 \times k_2 / (k_1 + k_2) \times C_{\text{sat}} \times (1 - e^{-(k_1 + k_2) \times t}) \quad (19)$$

In solving the differential equation with the initial condition, the concentration of zero at time zero yields Equation (20).

$$[\text{HCO}_3^-] = k_1 \times k_2 / (k_1 + k_2)^2 \times C_{\text{sat}} \times e^{-(k_1 + k_2) \times t} + k_1 \times k_2 / (k_1 + k_2) \times C_{\text{sat}} \times t - k_1 \times k_2 / (k_1 + k_2)^2 \quad (20)$$

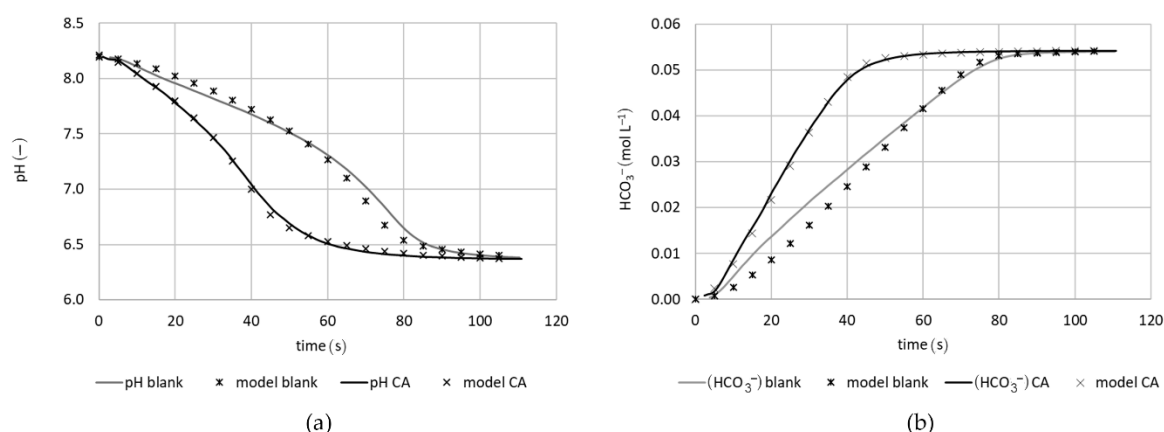
### 2.3. Elaboration of the Rate Constant of Enzymatic Turnover

It might be possible to utilize a curve-fitting program and to investigate the individual constants. Nevertheless, an easier solution was sought here. The exponential term in the beginning of Equation (19) is another e-function. With a negative exponent, it gradually progresses towards zero and the  $\text{HCO}_3^-$  concentration becomes a straight line. The slope (m) of the graph is described as follows.

$$m = k_1 \times k_2 / (k_1 + k_2) \times C_{\text{sat}} \quad (21)$$

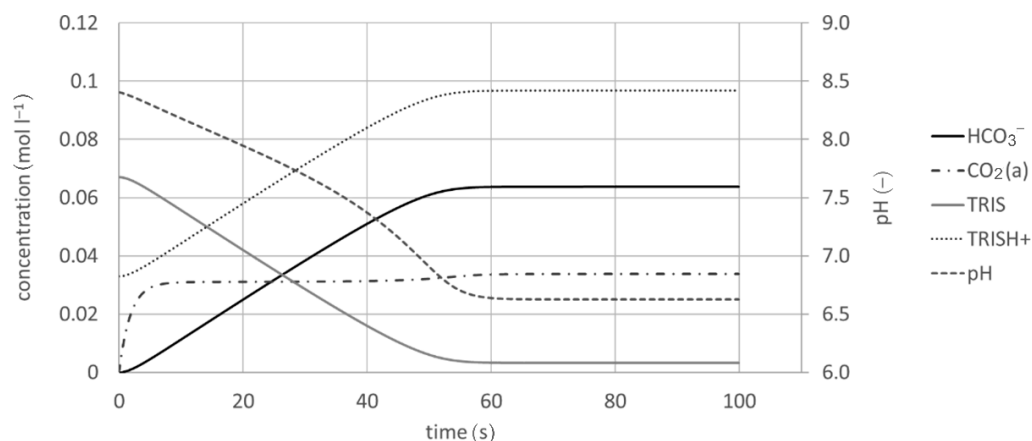
The value of m can be directly taken from the plot of the bicarbonate concentration. Using the blank experiment,  $k_1$  can be elaborated from the rearranged Equation (21) employing literature data for  $C_{\text{sat}}$  and  $k_2$ .  $C_{\text{sat}}$  is  $0.0343 \text{ mol.L}^{-1}$  at  $25^\circ \text{C}$  and 1 atm pressure (calculated from the Henry coefficient provided by [19]). Regarding the second parameter, it must be noted that the actual situation is more complex and that  $k_2$  is not a constant value. The reason is that there are two chemical reactions involved in the  $\text{CO}_2/\text{HCO}_3^-$  equilibrium:  $\text{CO}_2 + \text{H}_2\text{O} \rightleftharpoons \text{HCO}_3^- + \text{H}^+$  and  $\text{CO}_2 + \text{OH}^- \rightleftharpoons \text{HCO}_3^-$ . According to Schulz et al. [20] the rate constant at  $25^\circ \text{C}$  can be calculated by combining the two individual reaction constants:  $k_2 = k_{2,1} + k_{2,2} \times [\text{OH}^-]$  with  $k_{2,1} = 3.71 \times 10^{-2} \text{ s}^{-1}$  and  $k_{2,2} = 2.24 \times 10^3 \text{ L.mol}^{-1} \text{ s}^{-1}$ . Despite these explanations, we presume that the assumption of a fixed  $k_2$  is acceptable for the for the current purpose and keeping in mind all the other simplifications already made. In the given pH measurement range ( $\sim 8\text{--}6.5$ ), a  $k_2$  value for the uncatalyzed reaction of  $3.8 \times 10^{-2}$  is considered a reasonable approximation. According to these provisions, the estimated value for  $k_1$  is  $0.051 \text{ s}^{-1}$  for the specific set-up.

Modeling was employed to crosscheck the general validity of the described methodical approach. Firstly, model parameters were adjusted to fit the data for the blank experiment. Literature values or approximated values as listed in Table 1 (see Section 3. Materials and Methods) were applied. In a subsequent step, the  $\text{CO}_2$  transfer rate,  $k_1$ , was adjusted to best possibly fit the observed data. Figure 1 shows an overlay of the predicated course and actually measured pH values (a) as well as the predicted and calculated  $\text{HCO}_3^-$  concentration (b) for two experiments with or without the addition of CA, respectively. Despite certain deviations, in particular, for the blank experiment, the model reproduces the data observed for the CA catalyzed reaction and the hydration of  $\text{CO}_2$  dominates quite well. It should be noted that the final applied  $C_{\text{sat}}$  value was higher than initially considered. The locally higher dynamic pressure at the surface of the sparging device is a probable explanation for that.



**Figure 1.** Overlay of measured and predicted values for the blank experiment and the standard enzyme (0.25 mg L<sup>-1</sup>): (a) pH measured (solid line) versus model (x); (b)  $\text{HCO}_3^-$  concentration calculated from Equation (9) (solid line) versus model (x).

An example of model predictions depicting an entire view of all involved chemical species is provided in Figure 2. Again, the practically linear increase in  $\text{HCO}_3^-$  concentration is demonstrated.



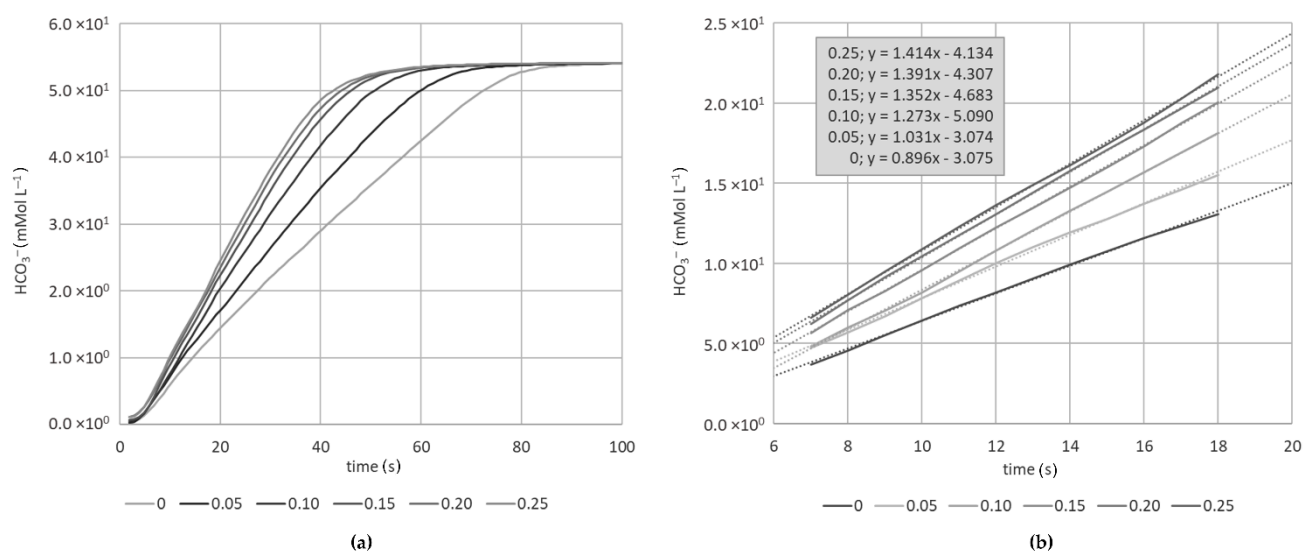
**Figure 2.** Example of model predictions. Course of the individual chemical species illustrating the linear increase in  $\text{HCO}_3^-$  over a certain time period.

Knowing the slope of the graph and the elaboration of  $k_1$  and  $C_{\text{sat}}$  from the blank experiment allows the theoretical calculation of the catalyzed rate constant  $k_2$  in each test. However, it has to be considered that the provision of the exact values for the individual constants is complex. The difficulties related to  $k_2$  were already mentioned. Moreover,  $C_{\text{sat}}$  is not only related to temperature and pressure but has also significant dependency on salinity or, more accurately, on the concentration and nature of the individual ions present in aquatic phase [21]. Even the  $\text{pK}_a$  of the Tris buffer is only valid in highly diluted solutions and has to be slightly corrected for ionic strength [22]. Finally, the last simplification made above which disregards the back reaction has some limitations. The back reaction sets in before the bicarbonate concentration reaches its highest inclination and, consequently, the maximum slope is slightly underestimated.

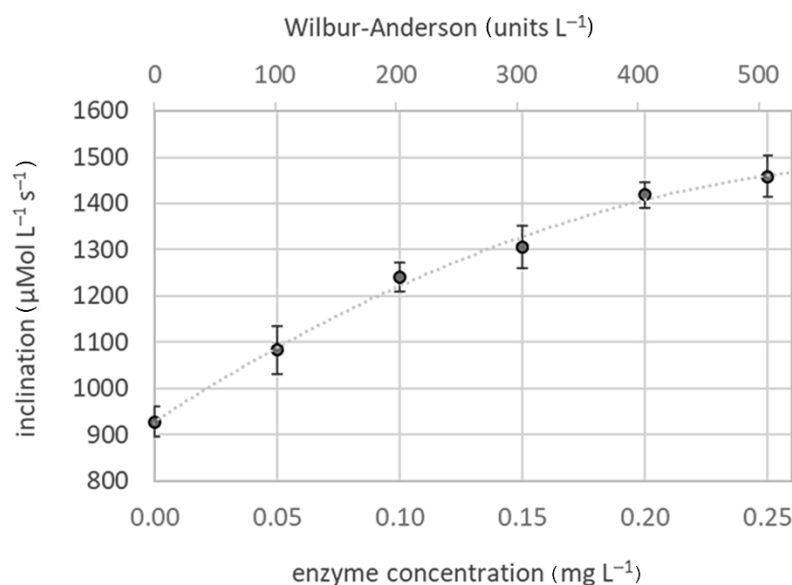
To summarize, there are certain imprecisions regarding the accuracy of the underlying parameters, as discussed previously. Nevertheless, the developed theory allows the reasonable estimation of the  $k_2$  of the catalyzed reaction, which permits good judgement of the practical potential of a certain enzyme.

#### 2.4. Calibration with a Standard Enzyme and Overall Assessment

For practical purposes, it was more straightforward and convenient to calibrate the test system with a standard enzyme of known activity. For this purpose, different concentrations of CA from bovine erythrocytes were subjected to the test. The corresponding calculations using pH data and Equation (9)  $\text{HCO}_3^-$  concentrations are provided in Figure 3a. Figure 3b demonstrates data evaluation through the determination of the slope of the graph. Even if it might be hard to precisely define the linear range, the inclination within any reasonable time frame of reasonable linearity can be taken as calibration values. The final elaborated calibration curve presenting the applied enzyme amounts (primary x-axis) or the corresponding Wilbur-Andersen units (secondary x-axis) versus the slope of  $\text{HCO}_3^-$  is presented in Figure 4.



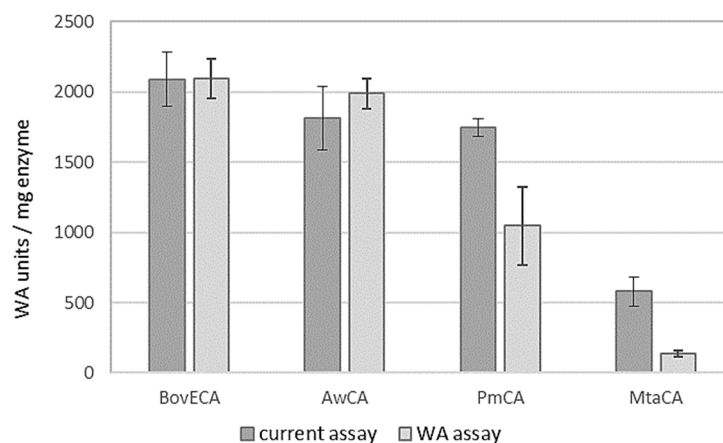
**Figure 3.** (a) Calculated course of  $\text{HCO}_3^-$  concentration from pH data utilizing Equation (9) at different enzyme concentrations (0 to 0.25  $\text{mg L}^{-1}$ ) and (b) data evaluation through the calculation of the incline by the corresponding linear trendlines.



**Figure 4.** Calibration curve using bovine CA: enzyme concentration/units versus inclination of the  $\text{HCO}_3^-$  graph. Wilbur-Anderson units were calculated from the measured activity of the standard enzyme.



A comparison of the standard enzyme and three further CAs is presented in Figure 5. Despite an obvious correlation between the two assays, the figure also illustrates that the general assessment of the potential of different enzymes does not provide the same picture. This underlines our hesitations regarding the validity of data obtained by the WA assay conducted at 0–4 °C due to the difference in temperature sensitivity of CAs.



**Figure 5.** Comparison of results obtained by the WA assay and the current method using the standard enzyme (CA from bovine erythrocytes) and three additional recombinant CAs.

A certain disadvantage of the proposed method is that the pH is not constant throughout the test. Although the buffer provides a certain stabilization effect, pH still drops in the course of the enzyme reaction. Accordingly, enzyme activity is not a distinct value at fixed conditions but an average value over a certain pH range. However, it has to be emphasized that this disadvantage is shared with the other commonly applied test, which is the Wilbur-Anderson assay. It is, of course, possible to combine the presented method with a titration approach to maintain the pH at a fixed set-point. A corresponding attempt has been already suggested by Magid and Turbeck [23]. However, this would imply an exchange of simplicity for higher accuracy and this would give up the biggest asset of the proposed test system. Despite certain shortcomings and keeping in mind the downsides of other CA assays, we particularly acknowledge the high practicability of the test. In our lab, we found the proposed assay extremely helpful for the purpose of a quick routine method to straightforwardly crosscheck or compare the CO<sub>2</sub> conversion efficiency of different CAs.

**Table 1.** Types of reaction, rate laws and constants used for modeling the timely behavior of chemical species.

Name	Rate Law	Reaction	Rate Constants <sup>1</sup>	
CO <sub>2</sub> transfer gas to liquid	Gas–liquid transfer according to Equation (11)	CO <sub>2</sub> (g) → CO <sub>2</sub> (a)	$k_1 = 5.1 \times 10^{-2} \text{ (s}^{-1}\text{)}^2$	$C_{\text{sat}} = 3.43 \times 10^{-2} \text{ (mol L}^{-1}\text{)}$
H <sub>2</sub> O dissociation	Mass action reversible	$\text{H}_2\text{O} \rightleftharpoons \text{H}^+ + \text{OH}^-$	$k_{\text{H}_2\text{O}_d} = 2.53 \times 10^{-5} \text{ (s}^{-1}\text{)}^*$	$k_{\text{H}_2\text{O}_a} = 1.4 \times 10^{11} \text{ (L} \cdot \text{mol}^{-1} \text{ s}^{-1}\text{)}^3$
CO <sub>2</sub> hydration	Mass action reversible	$\text{CO}_2 + \text{H}_2\text{O} \rightleftharpoons \text{H}^+ + \text{HCO}_3^-$	$k_{2_d} = 3.8 \times 10^{-2} \text{ (s}^{-1}\text{)}^4$	$k_{2_a} = 8.51 \times 10^4 \text{ (L} \cdot \text{mol}^{-1} \text{ s}^{-1}\text{)}^*$
TRIS buffer dissociation	Mass action reversible	$\text{TRISH}^+ \rightleftharpoons \text{TRIS} + \text{H}^+$	$k_{\text{TRIS}_d} = 7.94 \times 10^1 \text{ (s}^{-1}\text{)}^*$	$k_{\text{TRIS}_a} = 1.0 \times 10^{10} \text{ (L} \cdot \text{mol}^{-1} \text{ s}^{-1}\text{)}^5$

<sup>1</sup> For reversible mass action, the dissociation (index \_d) and association rates (index \_a) are provided. <sup>2</sup> Estimated value for the given setup from Equation (21) and the blank experiment. <sup>3</sup> [24]. <sup>4</sup> Approximated value for the uncatalyzed reaction (see text). <sup>5</sup> Estimated from data upon dissociation of amines provided in [25]. \* Calculated from the constant of the counter reaction and the dissociation constant at 25 °C.

### 3. Materials and Methods

#### 3.1. Setup

Titration was performed in a 100 mL glass beaker enclosed by a temperature-controlled vessel to maintain 25 °C. Recording of the pH course was conducted with an automatic titration device (Titrino 702, pH electrode: LL-Viscotrode and Software TiNet 2.5 (2003), Metrohm, Herisau, Switzerland). All solutions were maintained at 25 °C prior to use. Gas sparging was conducted with bottled CO<sub>2</sub> (purity 99.5%, Messer, Gumpoldskirchen, Austria). In order to assure that enzymatic conversion is the rate-limiting step, CO<sub>2</sub> has to be delivered much faster than its consumption due to CA activity. Therefore, a stainless-steel aerator made of sintered metal (cylindric porous frit product no. 84026, outer diameter 5.8 mm, length 22 mm, Reichelt Chemie Technik, Heidelberg, Germany,) was employed in order to achieve fine bubble distribution. In addition, a high flow rate (200 mL min<sup>−1</sup>) fixed by a mass flow controller (EL-Flow Select, Bronckhorst, Ruurlo, The Netherlands) was applied. Figure 6 illustrates the setup.

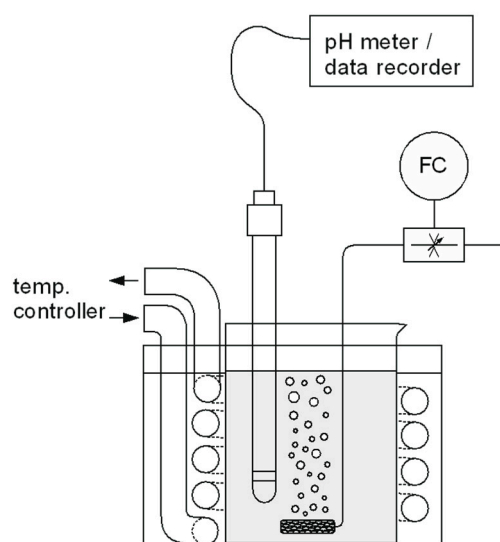


Figure 6. Experimental setup.

Tris buffer (0.1 mol·L<sup>−1</sup>) was made from Tris-base (Tris(hydroxymethyl)aminomethane, ultrapure grade ≥ 99.9%, Sigma-Aldrich, Vienna, Austria) adjusted to pH 8.2 at 25 °C with 6 mol·L<sup>−1</sup> H<sub>2</sub>SO<sub>4</sub> [14]. The measurement procedure was as follows. A 40 mL buffer was poured into the vessel. After a quick check of the appropriate temperature and pH, 0.1 mL enzyme solution was added and, at same time, gasification as well as pH recording began. Due to the intensive mixing through the rising bubbles, no additional stirring was necessary. The experiment ended when a final stable pH below 6.5 was achieved.

#### 3.2. Tested Enzymes

The utilized standard enzyme was CA from bovine erythrocytes (product no. C2624, Sigma-Aldrich, Vienna, Austria). The specific activity given by the provider was ≥3500 Wilbur-Anderson units.mg protein<sup>−1</sup>; however, our own measurements only showed an activity of 2090 (+/−115) Wilbur-Anderson units per mg. The following concentrations were applied: Enzyme stock of 0.1, 0.08, 0.06, 0.04 and 0.02 mg/mL (in 0.1 M Tris buffer) resulting in a final concentration in the test of 0.25, 0.2, 0.15, 0.1 and 0.05 mg L<sup>−1</sup>, respectively.

Three more microbial CAs derived from *Persephonella marina* EX-H1, *Methanobacterium thermoautotrophicum* and *Acetobacterium woodii* DSM 1030 were used for the evaluation of the method. CAs were obtained through the heterologous expression of the respective genes in *E. coli*. Detailed information on their preparation as well as the potential for CO<sub>2</sub> capturing will be provided in an upcoming publication.

### 3.3. Mathematical and Modeling Tools

Calculations were made or confirmed using the free online computing engine WolframAlpha available under <https://www.wolframalpha.com/> (accessed on 11 January 2021). In order to verify the validity of the approach and to crosscheck the impact of simplifications, modeling of the timely behavior of the individual chemical species was made utilizing the program COPASI (version 4.29, Build 228), which is a free software application for the simulation and analysis of biochemical networks available under <http://copasi.org/> (accessed on 10 February 2021). The simple model contained 4 reactions describing the rate of change of the involved chemical species. The types of reaction, rate laws and used constants are listed in Table 1. The software computes the timely development of the concentrations through iterative calculations for a given time interval.

## 4. Conclusions

In an era of growing concern relative to the record CO<sub>2</sub> levels in the atmosphere, the development of CO<sub>2</sub> capturing technologies is of high interest. On the path to full scale application, enzymatic enhancement is one of the options to improve efficiency of this approach. The CA activity assay proposed in the current paper resembles a simple method for judging enzyme activity requiring minimal analytical equipment. The continuous recording allows an accurate determination of conversion rates based on a larger set of data points compared to the Wilbur-Anderson assay. In contrast to this alternative routine method, activity is measured at an appropriate temperature and the gained values can be interpreted as thermodynamic constants. This allows easy and rapid comparison of CA activity. There are certainly assays of higher accuracy which, however, go hand in hand with elevated analytical effort. The introduced method is considered particularly useful for the screening of different CAs in environmental applications.

**Author Contributions:** Conceptualization, G.B. and S.K.-M.R.R.; methodology, F.S., J.R. and D.R.; data calculation and modeling, W.F., writing—original draft preparation, W.F. All authors have read and agreed to the published version of the manuscript.

**Funding:** The presented method was developed in the course of two research projects conducted at the institute. We kindly thank the Austrian Research promotion Agency (FFG) for funding of CarbonATE (FFG project no. 869728) and PTLiquid (FFG project no. 865091).

**Data Availability Statement:** The data presented in this study are available on request from the corresponding author. Detailed information on preparation and testing of the recombinant CAs listed in Section 3.2 will be provided in an upcoming paper.

**Conflicts of Interest:** The authors declare no conflict of interest and the funders had no role in the design of the study; in the collection, analyses or interpretation of data; in the writing of the manuscript or in the decision to publish the results.

## References

1. Smith, K.S.; Ferry, J.G. Prokaryotic carbonic anhydrases. *FEMS Microbiol. Rev.* **2000**, *24*, 335–366. [\[CrossRef\]](#)
2. Tripp, B.C.; Smith, K.; Ferry, J.G. Carbonic anhydrase: New insights for an ancient enzyme. *J. Biol. Chem.* **2001**, *276*, 48615–48618. [\[CrossRef\]](#)
3. Supuran, C.T. Structure and function of carbonic anhydrases. *Biochem. J.* **2016**, *473*, 2023–2032. [\[CrossRef\]](#) [\[PubMed\]](#)
4. Angeli, A.; Carta, F.; Supuran, C. Carbonic Anhydrases: Versatile and Useful Biocatalysts in Chemistry and Biochemistry. *Catalysts* **2020**, *10*, 1008. [\[CrossRef\]](#)
5. Supuran, C.T. Carbonic anhydrases: Novel therapeutic applications for inhibitors and activators. *Nat. Rev. Drug Discov.* **2008**, *7*, 168–181. [\[CrossRef\]](#) [\[PubMed\]](#)
6. Orr, F.M.J. Carbon Capture, Utilization, and Storage: An Update. *SPE J.* **2018**, *23*, 2444–2455. [\[CrossRef\]](#)
7. Boone, C.D.; Gill, S.; Habibzadegan, A.; McKenna, R. Carbonic Anhydrase: An Efficient Enzyme with Possible Global Implications. *Int. J. Chem. Eng.* **2013**, *2013*, 1–6. [\[CrossRef\]](#)
8. Sharma, T.; Sharma, S.; Kamyab, H.; Kumar, A. Energizing the CO<sub>2</sub> utilization by chemo-enzymatic approaches and potentiality of carbonic anhydrases: A review. *J. Clean. Prod.* **2020**, *247*, 119138. [\[CrossRef\]](#)
9. Forster, R.E. Methods for the Measurement of Carbonic Anhydrase Activity. In *The Carbonic Anhydrases*; Springer: Berlin/Heidelberg, Germany, 1991; pp. 79–98.

10. Effendi, S.S.W.; Ng, I.-S. The prospective and potential of carbonic anhydrase for carbon dioxide sequestration: A critical review. *Process. Biochem.* **2019**, *87*, 55–65. [CrossRef]
11. Wilbur, K.M.; Anderson, N.G. Electrometric and Colorimetric Determination of Carbonic Anhydrase. *J. Biol. Chem.* **1948**, *176*, 147–154. [CrossRef]
12. Verpoorte, J.A.; Mehta, S.; Edsall, J.T. Esterase Activities of Human Carbonic Anhydrases B and C. *J. Biol. Chem.* **1967**, *242*, 4221–4229. [CrossRef]
13. Zhao, P.; Geyer, R.; Boron, W.F. A Novel Stopped-Flow Assay for Quantitating Carbonic-Anhydrase Activity and Assessing Red-Blood-Cell Hemolysis. *Front. Physiol.* **2017**, *8*, 169. [CrossRef] [PubMed]
14. Pines, D.; Ditzkovich, J.; Mukra, T.; Miller, Y.; Kiefer, P.M.; Daschakraborty, S.; Hynes, J.T.; Pines, E. How Acidic Is Carbonic Acid? *J. Phys. Chem. B* **2016**, *120*, 2440–2451. [CrossRef] [PubMed]
15. Goldberg, R.N.; Kishore, N.; Lennen, R.M. Thermodynamic Quantities for the Ionization Reactions of Buffers. *J. Phys. Chem. Ref. Data* **2002**, *31*, 231–370. [CrossRef]
16. Sigma-Aldrich, Tris(hydroxymethyl)aminomethane; Tris, Sigma Technical Bulletin No. 106B. Available online: <https://www.sigmaaldrich.com/deepweb/assets/sigmaaldrich/product/documents/301/225/106bbul.pdf> (accessed on 26 May 2021).
17. Holmén, K.; Liss, P. Models for air-water gas transfer: An experimental investigation. *Tellus B Chem. Phys. Meteorol.* **1984**, *36*, 92–100. [CrossRef]
18. Botrè, C.; Botrè, F. Determination of carbonic anhydrase activity by a pCO<sub>2</sub> sensor. *Anal. Biochem.* **1990**, *185*, 254–264. [CrossRef]
19. NIST. *Chemistry WebBook, NIST Standard Reference Database Number 69*; Linstrom, P.J., Mallard, W.G., Eds.; National Institute of Standards and Technology: Gaithersburg, MD, USA, 2018. [CrossRef]
20. Schulz, K.; Riebesell, U.; Rost, B.; Thoms, S.; Zeebe, R. Determination of the rate constants for the carbon dioxide to bicarbonate inter-conversion in pH-buffered seawater systems. *Mar. Chem.* **2006**, *100*, 53–65. [CrossRef]
21. Weiss, R. Carbon dioxide in water and seawater: The solubility of a non-ideal gas. *Mar. Chem.* **1974**, *2*, 203–215. [CrossRef]
22. Clancy, M.J. The formulation of buffers and media for enzyme histochemistry. *J. Mol. Histol.* **1987**, *19*, 27–34. [CrossRef]
23. Magid, E.; Turbeck, B. The rates of the spontaneous hydration of CO<sub>2</sub> and the reciprocal reaction in neutral aqueous solutions between 0° and 38°. *Biochim. Biophys. Acta (BBA) Gen. Subj.* **1968**, *165*, 515–524. [CrossRef]
24. Stillinger, F.H. Proton Transfer Reactions and Kinetics in Water. In *Theoretical Chemistry*; Elsevier: Amsterdam, The Netherlands, 1978; Volume 3, pp. 177–234.
25. Eigen, M. Proton Transfer, Acid-Base Catalysis, and Enzymatic Hydrolysis. Part I: Elementary Processes. *Angew. Chem. Int. Ed.* **1964**, *3*, 1–19. [CrossRef]

# ANNEX 8

Pages 149 to 161

---

Pende N., Sogues A., Megrian D., Sartori-Rupp A., England P., Palabikyan H.,  
Rittmann S.K.-M.R., Graña M., Wehenkel A.M., Alzari P.M., Gribaldo S.

**SepF is the FtsZ-anchor in Archaea: conservation and divergence of an ancestral cell  
division system**

Nature Communications (2021) 12(1):3214

10.1038/s41467-021-23099-8

---

## ARTICLE


<https://doi.org/10.1038/s41467-021-23099-8>

OPEN

# SepF is the FtsZ anchor in archaea, with features of an ancestral cell division system

Nika Pende<sup>1,8</sup>, Adrià Sogues<sup>2,8</sup>, Daniela Megrian<sup>1,3</sup>, Anna Sartori-Rupp<sup>4</sup>, Patrick England<sup>5</sup>, Hayk Palabikyan<sup>6</sup>, Simon K.-M. R. Rittmann<sup>6</sup>, Martín Graña<sup>7</sup>, Anne Marie Wehenkel<sup>2</sup>✉, Pedro M. Alzari<sup>2</sup> & Simonetta Gribaldo<sup>1</sup>✉

Most archaea divide by binary fission using an FtsZ-based system similar to that of bacteria, but they lack many of the divisome components described in model bacterial organisms. Notably, among the multiple factors that tether FtsZ to the membrane during bacterial cell constriction, archaea only possess SepF-like homologs. Here, we combine structural, cellular, and evolutionary analyses to demonstrate that SepF is the FtsZ anchor in the human-associated archaeon *Methanobrevibacter smithii*. 3D super-resolution microscopy and quantitative analysis of immunolabeled cells show that SepF transiently co-localizes with FtsZ at the septum and possibly primes the future division plane. *M. smithii* SepF binds to membranes and to FtsZ, inducing filament bundling. High-resolution crystal structures of archaeal SepF alone and in complex with the FtsZ C-terminal domain (FtsZ<sub>CTD</sub>) reveal that SepF forms a dimer with a homodimerization interface driving a binding mode that is different from that previously reported in bacteria. Phylogenetic analyses of SepF and FtsZ from bacteria and archaea indicate that the two proteins may date back to the Last Universal Common Ancestor (LUCA), and we speculate that the archaeal mode of SepF/FtsZ interaction might reflect an ancestral feature. Our results provide insights into the mechanisms of archaeal cell division and pave the way for a better understanding of the processes underlying the divide between the two prokaryotic domains.

<sup>1</sup> Evolutionary Biology of the Microbial Cell Unit, CNRS UMR2001, Department of Microbiology, Institut Pasteur, Paris, France. <sup>2</sup> Structural Microbiology Unit, Institut Pasteur, CNRS UMR 3528, Université de Paris, Paris, France. <sup>3</sup> École Doctorale Complexité du vivant, Sorbonne University, Paris, France. <sup>4</sup> Ultrastructural Bioluminescence Unit, Institut Pasteur, Paris, France. <sup>5</sup> Plate-forme de biophysique moléculaire, C2RT-Institut Pasteur, CNRS, UMR 3528, Paris, France. <sup>6</sup> Archaea Physiology & Biotechnology Group, Department of Functional and Evolutionary Ecology, University of Vienna, Wien, Austria. <sup>7</sup> Bioinformatics Unit, Institut Pasteur of Montevideo, Montevideo, Uruguay. <sup>8</sup> These authors contributed equally: Nika Pende, Adrià Sogues. ✉email: [anne-marie.wehenkel@pasteur.fr](mailto:anne-marie.wehenkel@pasteur.fr); [simonetta.gribaldo@pasteur.fr](mailto:simonetta.gribaldo@pasteur.fr)



Traditionally viewed as inhabitants of extreme environments, the Archaea are now fully recognized as ubiquitous prokaryotes of great ecological and evolutionary importance<sup>1–3</sup>. Additionally, the human “archaeome”—whose research is still in its infancy—is receiving growing attention, as an imbalance of archaeal methanogens has been linked to various pathologies such as Inflammatory Bowel Disease, multiple sclerosis, anorexia and colorectal cancer<sup>4</sup>. Despite this potential clinical relevance, knowledge on the process of cytokinesis and the involved actors is still very partial in Archaea with respect to Bacteria. While some Archaea (Crenarchaeota) divide by using homologs of the eukaryotic ESCRT system<sup>5,6</sup>, most archaeal genomes possess one or two homologs of FtsZ (FtsZ1 and FtsZ2)<sup>7</sup>, and some also other tubulin-like proteins such as the CetZ family<sup>8,9</sup>. The role of FtsZ during cytokinesis has been shown in a few model archaeal organisms<sup>10–13</sup>, such as *Haloferax volcanii* where FtsZ1 localization at the mid-cell constriction site provided the first cytological evidence of an archaeal FtsZ role in cell division<sup>13</sup>. A more recent study showed that *H. volcanii* FtsZ1 and FtsZ2 co-localize at midcell as a dynamic division ring, with FtsZ1 involved in stabilization of the FtsZ2 ring and in cell shape, while FtsZ2 is involved in cell constriction<sup>10</sup>.

Only few homologs of the bacterial division machinery that interact with FtsZ have been identified in Archaea, such as the positive and negative FtsZ regulators SepF and MinD, respectively<sup>7,14,15</sup>. SepF was originally identified as a component of the *Bacillus subtilis* divisome required for correct septal morphology and that interacts with the C-terminal domain of FtsZ (FtsZ<sub>CTD</sub>)<sup>16,17</sup>. In *B. subtilis*, SepF is non-essential and has an overlapping role with FtsA, as overexpression of SepF can rescue an FtsA depletion strain<sup>16,17</sup>. In contrast, in other bacterial lineages where FtsA is absent, such as most *Actinobacteria* and *Cyanobacteria*, SepF is an essential component of the early divisome, orchestrating Z-ring assembly and participating in membrane remodeling<sup>18–21</sup>. The first crystal structure of a bacterial SepF-FtsZ complex was only recently obtained from the *Actinobacterium Corynebacterium glutamicum*<sup>21</sup>. It showed that SepF forms a functional dimer that is required for FtsZ binding<sup>21</sup>. *C. glutamicum* SepF binds to the FtsZ<sub>CTD</sub> through a conserved pocket and interacts with residues at the  $\alpha$ -helical interface of the functional dimer<sup>21</sup>.

An early analysis of the distribution of cell division proteins in Archaea revealed that SepF is present in almost all FtsZ-containing taxa, which led to the suggestion that it could act as the main FtsZ anchor<sup>7</sup>. The structures of two archaeal SepF-like proteins have been reported<sup>22</sup>, but their biological function has not been studied.

Here we provide experimental evidence for a functional role of archaeal SepF in cytokinesis through interaction with FtsZ by using as model *Methanobrevibacter smithii*, the most abundant species of archaeal methanogens in the human microbiome<sup>4</sup>. *M. smithii* contains only one copy of FtsZ1 (*MsFtsZ*) and one copy of SepF (*MsSepF*) and is therefore an interesting model with respect to the more complex Haloarchaea which have two FtsZ copies in addition to up to six tubulin-like proteins of the CetZ family<sup>8</sup>. As no genetic tools are currently available for *M. smithii*, we used an integrative study combining cell imaging, protein biochemistry and structural analysis. We demonstrate that SepF co-localizes with FtsZ to midcell during cell constriction and binds to membranes. Structural and biochemical analysis shows that SepF also forms a functional dimer which binds the FtsZ<sub>CTD</sub> via a pocket that is partially conserved with Bacteria, but with a markedly different interaction pattern occurring through the  $\beta$ – $\beta$  interface. Finally, we complement these results by a thorough evolutionary analysis of SepF and FtsZ in Bacteria and Archaea. This reveals that SepF and FtsZ were already present in the Last Universal Common Ancestor, and that the Archaea might have

retained features of an ancestral minimal cytokinesis machinery, while Bacteria diverged substantially, likely to accommodate the emergence of a rigid cell wall and the complex divisome.

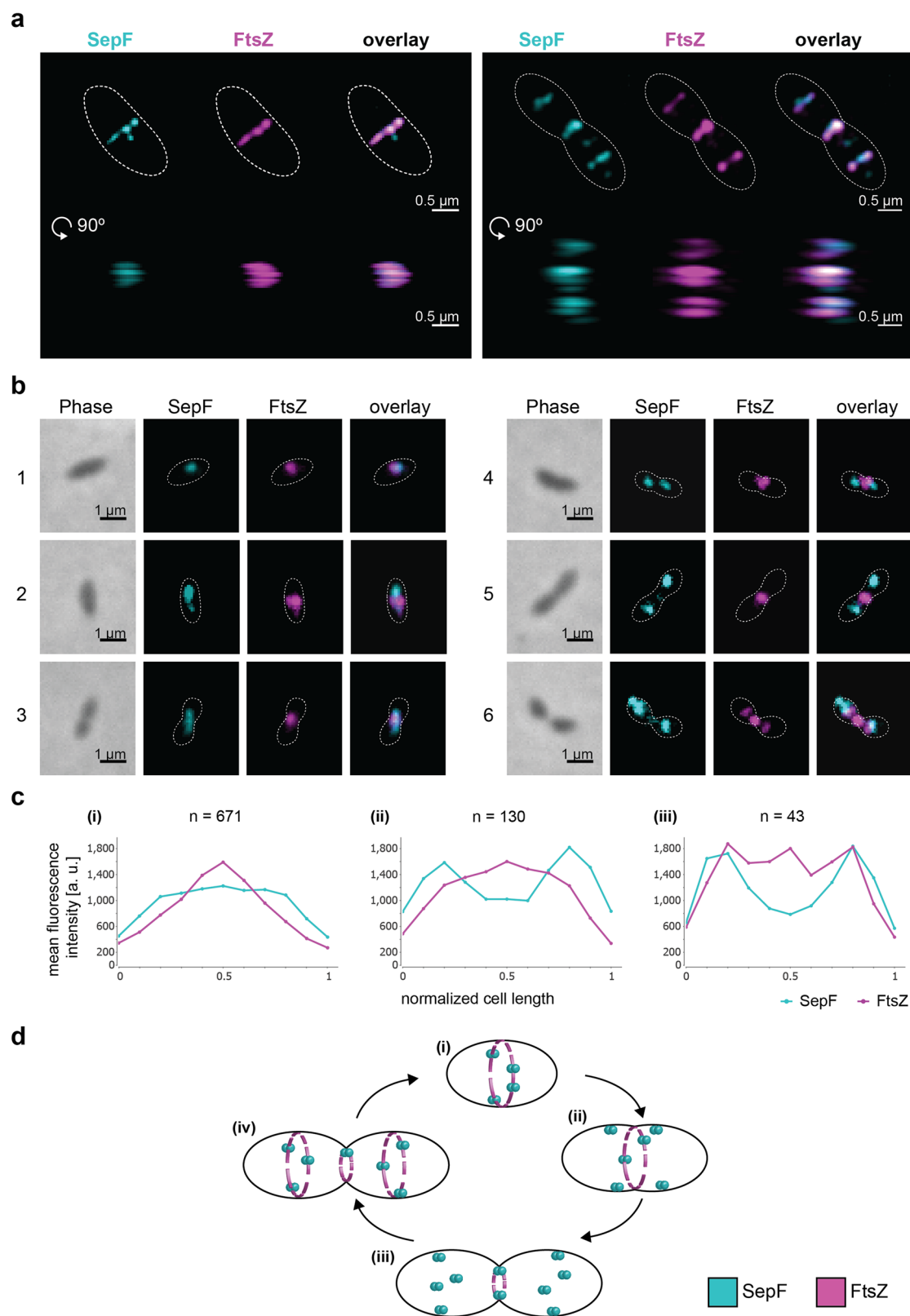
## Results

**SepF transiently co-localizes with FtsZ during the *M. smithii* cell cycle.** To investigate the function of *MsSepF* and its potential interaction with *MsFtsZ*, we studied the localization pattern of these two proteins during the *M. smithii* cell cycle by immunolabelling, using specific anti-*MsFtsZ* and anti-*MsSepF* antibodies (Methods, Fig. 1). The cell wall of *M. smithii* (as well as all Methanobacteriales and the sister order Methanopyrales) consists of pseudo-peptidoglycan (pPG)<sup>23,24</sup>. The archaeal pPG oligosaccharide backbone is composed of L-N-acetylglucosamine with a  $\beta$ –1,3 linkage to N-acetylglucosamine and the stem peptide is made of only L-amino acids<sup>23</sup>. These structural differences compared to bacterial PG make these archaea resistant to most lysozymes and proteases<sup>23</sup>. Therefore, we developed a new protocol for immunolabelling where cells are pre-treated with the phage endoisopeptidase *PeiW*<sup>25,26</sup> which specifically permeabilizes the pPG cell wall (Methods). Using Western Blot analysis, we quantified FtsZ and SepF levels and showed that the FtsZ/SepF molar ratio is about six during exponential growth (Supplementary Fig. 1). To study the intracellular localization of *MsFtsZ* and *MsSepF*, we performed co-immunolabelling with anti-*MsSepF* and anti-*MsFtsZ* antibodies and imaged the cells by 3-dimensional (3D) super-resolution microscopy (Methods, Fig. 1a). In the ovococoidal *M. smithii* cells, *MsFtsZ* forms a patchy ring-like structure at mid-cell and *MsSepF* largely overlaps with it (Fig. 1a, left panel, Supplementary Movie 1). At a later stage of division, a smaller FtsZ ring corresponds with the almost completed cell constriction and two new rings appear in the future daughter cells, defining the new septation planes, with SepF forming discontinuous arcs largely overlapping with FtsZ (Fig. 1a right panel, Supplementary Movie 2).

We then performed quantitative analysis with several hundreds of co-immunolabeled *M. smithii* cells imaged by conventional epifluorescence microscopy (Methods, Fig. 2b and c). Our results show that in cells exhibiting very slight or no constriction, *MsSepF* and *MsFtsZ* co-localize at the future septation plane (Fig. 1b, cell 1; 2c(i); Supplementary Fig. 2). In cells that start to constrict, *MsFtsZ* is present at the septation plane and *MsSepF* is found slightly lateral of the Z-ring (Fig. 2b, cells 2–3; 2c(i); Supplementary Fig. 2). At a later stage, two distinct fluorescent *MsSepF* foci can be seen further away from the single *MsFtsZ* focus, suggesting that SepF moves to the future division planes of the prospective daughter cells before FtsZ (Fig. 2b, cells 4–5; 2c(ii); Supplementary Fig. 2). Finally, in strongly constricted cells, FtsZ appears in the prospective daughter cells overlapping with the SepF signal, but it is also still present in the current septation plane, where only a weak SepF signal can be detected (Fig. 2b, cell 6; 2c(iii)).

From these results, we propose a model for FtsZ and SepF localization during the *M. smithii* cell cycle (Fig. 1d): (i) in non-constricting cells, both proteins co-localize at the septation plane; (ii and iii) as constriction starts and proceeds, SepF primes the future septation plane in the prospective daughter cells by progressively moving there before FtsZ; (iv) in cells that have almost completed constriction, FtsZ and SepF co-localize at the prospective septation plane of the daughter cells.

***MsSepF* binds to membranes and to the FtsZ<sub>CTD</sub> inducing filament bundling.** *MsSepF* is composed of 149 amino acids and presents the same conserved domain organization as previously described for bacterial SepF proteins<sup>21,22</sup> consisting of an N-terminal amphipathic helix representing the putative membrane-



binding domain (residues 1-12) connected through a flexible linker to a putative C-terminal FtsZ-binding core (residues 54 to 149, Fig. 2a, Supplementary Fig. 3). We show that the membrane-binding domain of *MsSepF* interacts with small unilamellar vesicles (SUVs) with an affinity of  $43 \pm 0.2 \mu\text{M}$  (Methods, Supplementary Fig. 4a), a value in the same range as that reported for *C. glutamicum*<sup>21</sup>. Moreover, thermal shift assays show an

important increase of the melting temperature of *MsSepF*<sub>core</sub> (from 70.6 to 82.3 °C) upon addition of *MsFtsZ*<sub>CTD</sub>. Supplementary Fig. 5a), indicating a direct interaction between the two proteins. The apparent *K*<sub>d</sub> value for this interaction is  $84.0 \pm 8.5 \mu\text{M}$  as determined by surfaces plasmon resonance (SPR) (Supplementary Fig. 5b), a value in the same range as the one described for *C. glutamicum*<sup>21</sup>.

**Fig. 1 SepF co-localizes with FtsZ during the *M. smithii* cell cycle.** *M. smithii* cells were permeabilized with PeiW and immunostained with anti-MsSepF and anti-MsFtsZ antibodies. **a** 3D Structured Illumination Microscopy (SIM) maximum projections of a non-constricting *M. smithii* cell (left panel) and a constricting cell (right panel) stained with anti-MsSepF (cyan) and anti-MsFtsZ antibodies (magenta). Front views of single channels and the overlay are depicted (above) as well as the side view shifted by 90° (below). White dotted lines represent the cell outlines and scale bars are 0.5 μm. **b** Phase contrast (Phase) and corresponding epifluorescence images of representative co-labeled *M. smithii* cells (SepF in cyan, FtsZ in magenta and an overlay of both). Cells are arranged from non-constricting to constricting from 1 to 6. White dotted lines represent the cell outlines deduced from the corresponding phase contrast images and the scale bars are 1 μm. **c** Mean fluorescence intensity plots of cells grouped into three classes according to the detected FtsZ fluorescent maxima (0–1, 2 or 3 maxima detected) with the corresponding SepF (cyan) and FtsZ (magenta) mean fluorescence intensity [a. u.] of each group plotted against the normalized cell length [0–1]. **d** Schematic view of SepF (cyan) and FtsZ (magenta) localization pattern during the life cycle of *M. smithii*. (i) In non-constricting cells, both proteins co-localize at the septation plane. (ii) and (iii) SepF progressively moves to the future division plane prior FtsZ. (iv) As constriction is almost completed, FtsZ and SepF co-localize at the prospective septation plane of the daughter cells. The data shown here are representative for experiments performed in triplicate.

Table 1 Crystallographic data.		
	MsSepF <sub>c</sub>	MsSepF <sub>c</sub> + FtsZ <sub>CTD</sub>
<b>Data collection</b>		
Space group	P 3 <sub>1</sub> 2 1	P 6 <sub>1</sub> 2 2
Cell dimensions		
a, b, c (Å)	53.05, 53.05, 53.91	64.85, 64.85, 107.92
α, β, γ (°)	90, 90, 120	90, 90, 120
Resolution (Å)*	45.95–1.4 (1.42–1.4)	38.91 – 2.7 (2.83 – 2.7)
R <sub>sym</sub>	0.056 (1.029)	0.076 (0.702)
I/σ(I)	27.1 (3.4)	15.4 (2.7)
Completeness (%)	99.9 (100)	95.7 (96.3)
Redundancy	19.6 (19.9)	5.5 (5.7)
CC ½	0.999 (0.921)	0.999 (0.918)
<b>Refinement</b>		
Resolution (Å)	1.4	2.7
Number of reflections	17673	3806
R-work/R-free	0.182 / 0.216	0.229 / 0.255
Number of atoms		
protein	684	746
ligands/ions	8	—
water	57	—
B-factors (Å <sup>2</sup> )		
protein	25.47	61.5
ligands/ions	25.49	—
water	37.47	—
RMS deviations		
Bond length (Å)	0.009	0.008
Bond angles (°)	1.057	1.02
<b>PDB code</b>	<b>7AL1</b>	<b>7AL2</b>

\* Values in parenthesis refer to the highest recorded resolution shell.

As shown for *C. glutamicum* SepF (CgSepF)<sup>21</sup>, or *B. subtilis*<sup>20</sup>, MsSepF is also able to remodel SUVs, as observed by negative stain EM (Fig. 2b(i)), and this remodeling was reversed upon addition of the FtsZ<sub>CTD</sub>, giving rise to smaller, more regular lipid vesicles (Fig. 2b(ii)), the control of SUVs alone is shown in Supplementary Fig. 4c). Moreover, we confirmed that the MsSepF<sub>core</sub>, which is lacking the MTS and linker domains does not polymerize in the presence of SUVs (Supplementary Fig. 4b). Additionally, MsSepF<sub>core</sub> is capable of inducing bundling of FtsZ protofilaments, giving rise to longer and straighter filaments than FtsZ-GTP alone (Fig. 2c and d). Taken together, these results strongly suggest conservation of common functional features between archaeal and bacterial SepF.

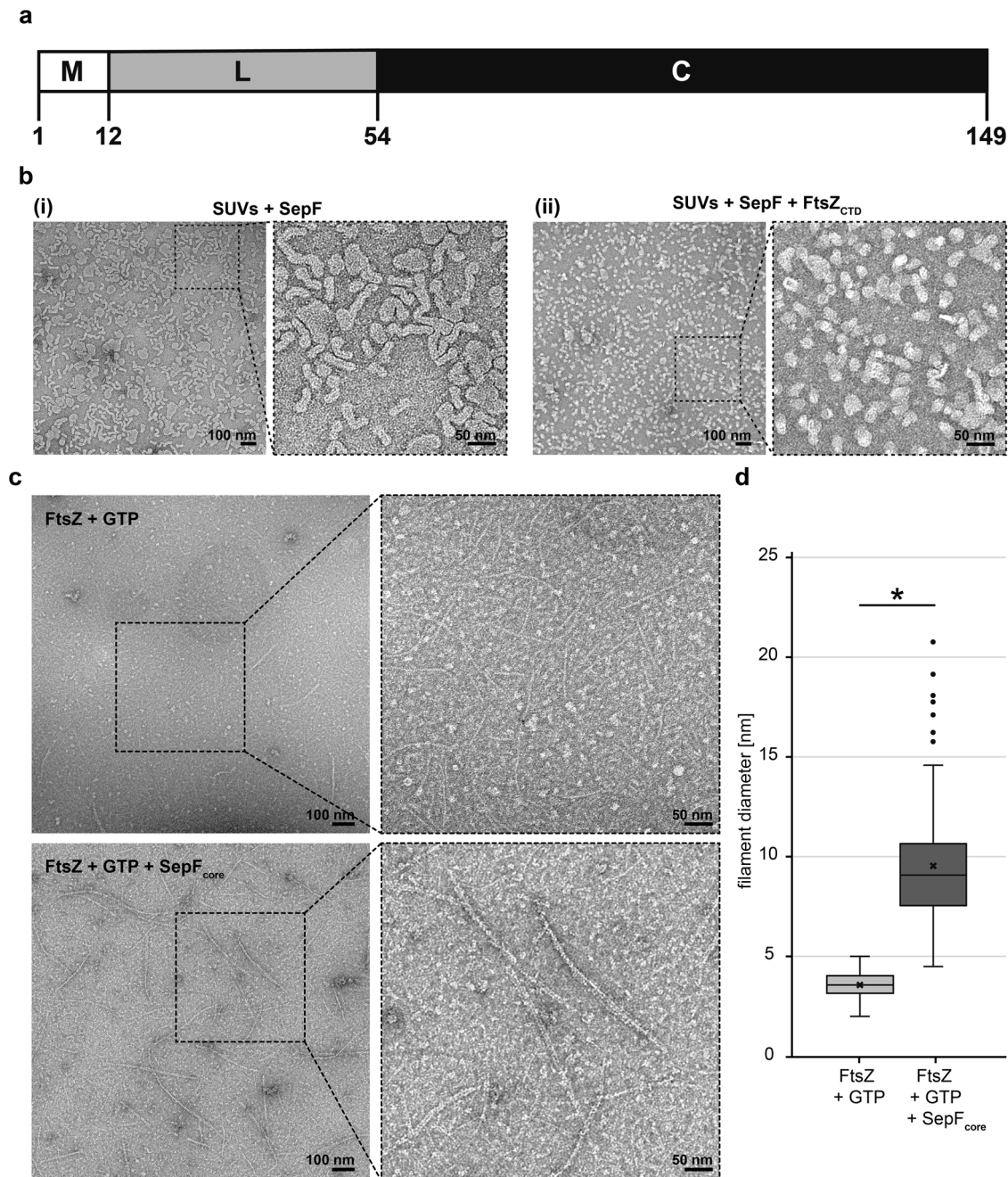
**High-resolution crystal structures of MsSepF<sub>core</sub> alone and in complex with the FtsZ<sub>CTD</sub>, reveal specific archaeal features.** We determined the crystal structure of MsSepF<sub>core</sub>, at 1.4 Å resolution

(Fig. 3a, Table 1). The protein is a dimer in solution (Supplementary Fig. 6), with each protomer consisting of a 5-stranded β-sheet flanked by 2 α-helices (Fig. 3a). In addition, a helical turn insertion (η1), between strand β2 and helix α2, is conserved in archaeal sequences but is absent in bacterial homologs (Supplementary Fig. 7). The overall dimer organization of MsSepF<sub>core</sub> matches that previously described for the structures of archaeal SepF-like proteins from *Archaeoglobus fulgidus* and *Pyrococcus furiosus*<sup>22</sup> (Supplementary Fig. 8), with the dimer interface (~1200 Å<sup>2</sup>) formed by the exposed faces of the two central β-sheets, in which the last strand (β5) forms part of the opposing β-sheet (Fig. 3a). Despite their quite similar monomeric structure, the dimeric arrangement of archaeal SepF differs from that observed for the functional dimer in CgSepF, where the dimer interface is formed by a 4 α-helical bundle (Fig. 3b). Interestingly, both interfaces—formed by the α-helices or the β-sheets—have been simultaneously observed in crystals of *Bacillus subtilis* SepF, generating linear polymers of tightly packed SepF dimers<sup>22</sup>.

To further characterize the interaction between SepF and FtsZ, we crystallized MsSepF<sub>core</sub> in complex with the FtsZ<sub>CTD</sub> peptide and determined the structure of the complex at 2.7 Å resolution (Table 1). The bound peptide is well-defined in the electron density for 10 out of 13 residues (Supplementary Fig. 9) and adopts an extended conformation within a pronounced groove of the SepF monomer (Fig. 4a). The association is mediated by both hydrophobic and electrostatic interactions (Fig. 4b and Supplementary Fig. 10), the latter including 3 intermolecular ion pairs (FtsZ Asp 370 – SepF Arg 130, Asp 371 – Lys 115 and Asp 374 – Arg 118) and seven additional hydrogen bonds. Three of these H bonds are made by backbone atoms of the FtsZ<sub>CTD</sub> peptide with the strand β3, partially extending the β-sheet (Supplementary Fig. 11a). The archaeal-specific η1 insertion (residues 97–102) promotes the formation of a wider binding pocket compared to bacterial SepF (Fig. 4c) and is involved in a network of hydrogen bonding interactions that contributes to stabilize the FtsZ-SepF complex (Supplementary Fig. 11b).

The residues defining the binding pocket are highly conserved in archaeal SepF homologs (Supplementary Fig. 12), suggesting a similar FtsZ-binding mode. Furthermore, despite their evolutionary distance and sequence divergence, the structures of bacterial and archaeal SepF-FtsZ complexes share a partially conserved mode of interaction for the N-terminal part of the FtsZ<sub>CTD</sub> (residues LDDFI in MsSepF and DLDV in CgSepF), which binds to a similar groove formed between α2 and β3 in the SepF monomer (Fig. 4c). However, the binding modes of the C-terminal half of FtsZ<sub>CTD</sub> are markedly different between Archaea and Bacteria. In fact, in *C. glutamicum* this region interacts with residues from the two monomers of the SepF functional dimer at the α-helical interface (Fig. 4c, right panel), while in *M. smithii* it largely binds to only one monomer of the functional dimer



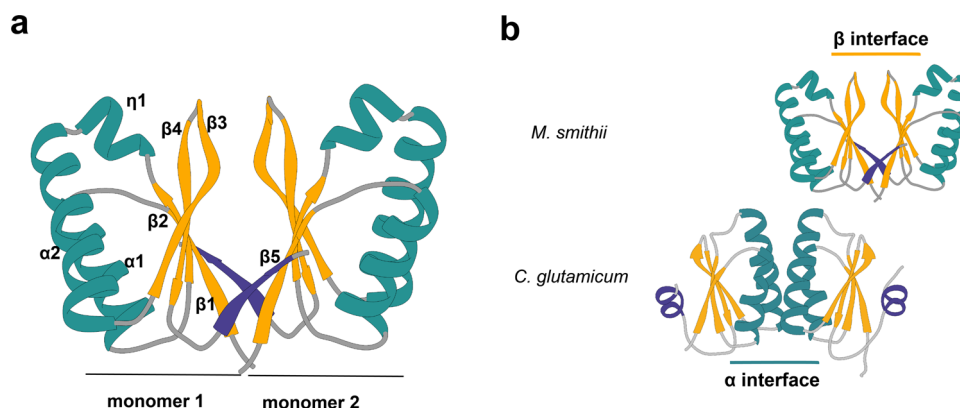


**Fig. 2 MsSepF binds to membranes and to FtsZ<sub>CTD</sub> inducing filament bundling.** **a** Domain organization of SepF from *M. smithii* with an N-terminal amphipathic helix (M), flexible linker (L) and putative C-terminal FtsZ-binding core (C). **b** Negative stain electron microscope images of SUVs ( $100 \mu\text{mol L}^{-1}$ ) and MsSepF ( $50 \mu\text{mol L}^{-1}$ ) with (i) or without (ii) FtsZ<sub>CTD</sub> ( $100 \mu\text{mol L}^{-1}$ ). **c** Negative stain electron microscope images of FtsZ ( $30 \mu\text{mol L}^{-1}$ ) and GTP ( $3 \text{ mmol L}^{-1}$ ) with (upper panel) or without (lower panel) MsSepF<sub>core</sub> ( $20 \mu\text{mol L}^{-1}$ ). **b** and **c** Panels show original image with an enlarged inlet that is marked by black dotted square next to it. Scale bars are 100 nm (original images) and 50 nm (inlets). These experiments were performed two times. **d** Boxplots showing filament diameter measurements [nm] for FtsZ + GTP ( $n=130$ ) and FtsZ + GTP + SepF<sub>core</sub> ( $n=130$ ). Box is the inter quartile range, where the lower edge is 25<sup>th</sup> percentile and the upper edge the 75<sup>th</sup> percentile. Whiskers show the range between the lowest value and the highest value. Line inside each box indicates the median and x indicates the mean. Black circles are outliers. A 2-sample t-test was conducted, the result was found to be  $-23.8032$  and the test resulted in a critical t-value of  $t(\alpha)$  of  $1.9692$  for an alpha of  $0.025$ . A significant difference of the diameter was found at a 5% level of significance, because the  $H_0$  was rejected, as the modulus of the critical value was  $> \alpha/2$ . (\*) indicates that means of diameter are significantly different.

(Fig. 4c, left panel), enlarging the monomer-peptide interface surface ( $600 \text{ \AA}^2$ ) with respect to that observed in *C. glutamicum* ( $390 \text{ \AA}^2$ ). In *M. smithii*, only the terminal residue of FtsZ<sub>CTD</sub> (Phe377) binds to a surface hydrophobic pocket in the second SepF monomer at the  $\beta$ -sheet dimer interface. Phe377 does not seem conserved in other archaeal SepF homologs except for those

phylogenetically close to *M. smithii*. Therefore, the hydrophobic interaction via the FtsZ<sub>CTD</sub> terminal residue is likely specific to these taxa.

Archaeal SepF homologs are expected to bind both FtsZ1 and FtsZ2 isoforms, as the conservation pattern of the CTDs from these two isoforms, centered around a nearly invariant GID motif



**Fig. 3 Structural characterization of MsSepF<sub>core</sub>.** **a** Crystal structure of the MsSepF dimer composed of two identical monomers, color-coded according to secondary structure (helices, green; strands, yellow). Each protomer consists of a 5-stranded  $\beta$ -sheet flanked by 2  $\alpha$ -helices and a helical turn ( $\eta_1$ ). In each protomer, the C-terminal strand  $\beta_5$  (in purple) forms part of the opposing  $\beta$ -sheet. **b** Comparison of functional SepF dimer interfaces in Bacteria and Archaea, as defined by the complexes with FtsZ. The  $\alpha$  interface has only been found in the crystal structures of bacterial SepF dimers such as those of *C. glutamicum* (PDB 6SCP, shown in the figure) and *B. subtilis* (PDB 3ZIH), whereas the  $\beta$  interface has been found in all Archaeal structures (e.g. *Archaeoglobus fulgidus* (PDB: 3ZIE), *Pyrococcus furiosus* (PDB: 3ZIG), see also Supplementary Fig. 8). The C-terminal secondary structure element of the crystal structures ( $\beta_5$  in *M. smithii* and  $\alpha_3$  in *C. glutamicum*) are depicted in purple.

(Fig. 4d, left panel), are very similar to each other. In contrast, the archaeal motif is clearly different from that of the bacterial FtsZ<sub>CTD</sub> (Fig. 4d, right panel). In particular, it is interesting to note that the bifurcation pointing the FtsZ<sub>CTD</sub> towards the  $\beta$  interface in Archaea is found between the highly conserved isoleucine and aspartate residues of the GID motif (Fig. 4c and d, left panel), further strengthening the argument that this dimer interface was selected early on in archaeal evolution. In contrast, the almost universally conserved proline residue in bacterial FtsZ<sub>CTD</sub> is at the bifurcation pointing towards the alpha interface in bacteria (Fig. 4c and d, right panel). Therefore, the different FtsZ-binding modes of MsSepF and CgSepF are driven by their specific self-association (dimerization) modes.

**Distribution and phylogeny of SepF and FtsZ indicates an ancient origin prior to the divergence between Bacteria and Archaea.** The specificities of archaeal SepF/FtsZ interaction with respect to those observed in Bacteria are intriguing and may lie in an ancient and fundamental divergence in cell division between the two prokaryotic domains. We therefore sought to investigate when these two proteins emerged and how they evolved in the two prokaryotic domains.

We updated the distribution of FtsZ1, FtsZ2 and SepF homologs, as well as the presence of the ESCRT-like system in the large number of archaeal genomes that have recently become available<sup>1–3,7,27</sup> (Methods, Fig. 5a, Supplementary Data 1). Most Archaea have one SepF homolog which systematically co-occurs with one or two copies of FtsZ (FtsZ1 and FtsZ2), while it is absent from the genomes that do not have FtsZ homologs. Interestingly, while the genes coding for FtsZ and SepF frequently exist in close proximity in bacterial genomes, this is rarely the case in Archaea, where they co-occur only in a few members of the DPANN superphylum, while they localize with different genes in the other Archaea (*ftsZ1* mostly with components of the translation machinery, *ftsZ2* frequently with *parD*, and *sepF* displaying a more variable genomic context) (Supplementary Fig. 13). Methanopyri are the only Archaea to possess an FtsA-like homolog along with SepF, which likely originated via horizontal gene transfer from bacteria, and whose function is unknown.

In contrast with the wide distribution of SepF in Archaea, its presence in Bacteria is much more scattered, being found mostly in a few phyla belonging to the Terrabacteria clade

(Cyanobacteria and related uncultured candidate phyla, Actinobacteria, Firmicutes, Armatimonadetes, Abtidibacteriota, and the uncultured candidate phylum Eremiobacteraeota), frequently together with FtsA, as opposed to the Gracilicutes (including *Escherichia coli*) which have FtsA only (Fig. 5b and Supplementary Data 2).

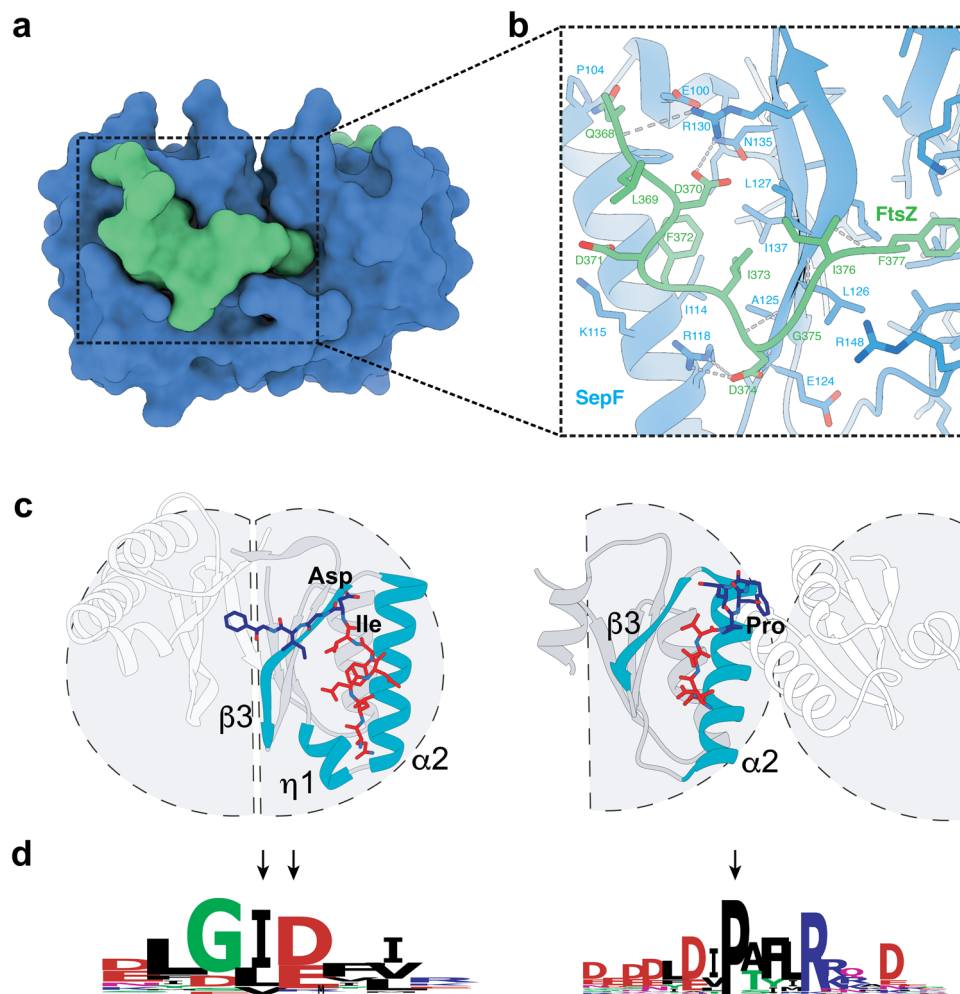
The phylogeny of SepF clearly shows a separation of archaeal and bacterial homologs and—although not fully resolved due to the small number of informative positions—an overall topology consistent with vertical inheritance, i.e., monophyly of major phyla and relationships roughly congruent with the reference bacterial and archaeal phylogeny (Supplementary Fig. 14). A similar evolutionary history can be inferred from FtsZ, which shows a clear separation among archaeal and bacterial homologs (Supplementary Fig. 15), and suggests an ancient gene duplication in Archaea giving rise to FtsZ1 and FtsZ2 paralogues, consistent with recent reports<sup>10</sup>. These results strongly suggest that SepF and FtsZ emerged before the divergence of Archaea and Bacteria, likely being part of the division machinery in the Last Universal Common Ancestor (LUCA) and subsequently co-evolved in the two prokaryotic domains. However, while SepF was largely retained in the Archaea, it was lost massively during bacterial diversification, possibly after the emergence of FtsA whose phylogeny shows an early origin in Bacteria (Supplementary Fig. 16).

## Discussion

Cell division is one of the most ancient and fundamental processes of life. Yet, Bacteria and Archaea present profound differences in the way they divide, illustrated by the fact that the majority of components of the bacterial divisome are absent in Archaea. Moreover, in contrast to the well-studied FtsA, the function of SepF has been analyzed in a few bacteria so far<sup>16,17,19–22,28</sup>, and only one crystal structure in complex with FtsZ is currently available from *C. glutamicum*<sup>21</sup>.

Here, we report the first experimental evidence that archaeal SepF also acts as the FtsZ membrane anchor during cytokinesis. By applying our newly developed immunolabelling protocol for archaeal methanogens with a cell wall made of pPG and 3D super resolution microscopy, we show that the only copy of FtsZ in *M. smithii* forms a ring-like structure and co-localizes at mid cell with SepF. A very recent study in *H. volcanii* suggests that FtsZ1 goes first to the division plane followed by SepF that then recruits





**Fig. 4 The SepF-FtsZ<sub>CTD</sub> complex.** **a** Surface representation of the crystal structure of FtsZ<sub>CTD</sub> (green) bound to MsSepF<sub>core</sub> (blue). **b** Detailed protein-protein interactions within the binding pocket. The side-chains of contact residues ( $d < 5 \text{ \AA}$ ) are shown in stick representation and hydrogen bonds are represented by gray dotted lines. **c** Cartoon representations of the different functional dimers of archaeal MsSepF (left panel) and bacterial CgSepF (right panel) bound to FtsZ<sub>CTD</sub> (for clarity, only one of the two bound peptides is shown in stick representation). The N-terminal half of FtsZ<sub>CTD</sub> (in red) binds to a similar groove of the SepF monomer formed between secondary structure elements  $\alpha 2$ ,  $\beta 3$  and  $\eta 1$  (only in MsSepF), shown in turquoise. Highly conserved positions in archaeal and bacterial FtsZ<sub>CTD</sub> are labeled. **d** Sequence conservation logo of archaeal (left) and bacterial (right) FtsZ<sub>CTD</sub> sequences. The arrows indicate the highly conserved residues across Archaea or Bacteria that are labeled in panel **c**.

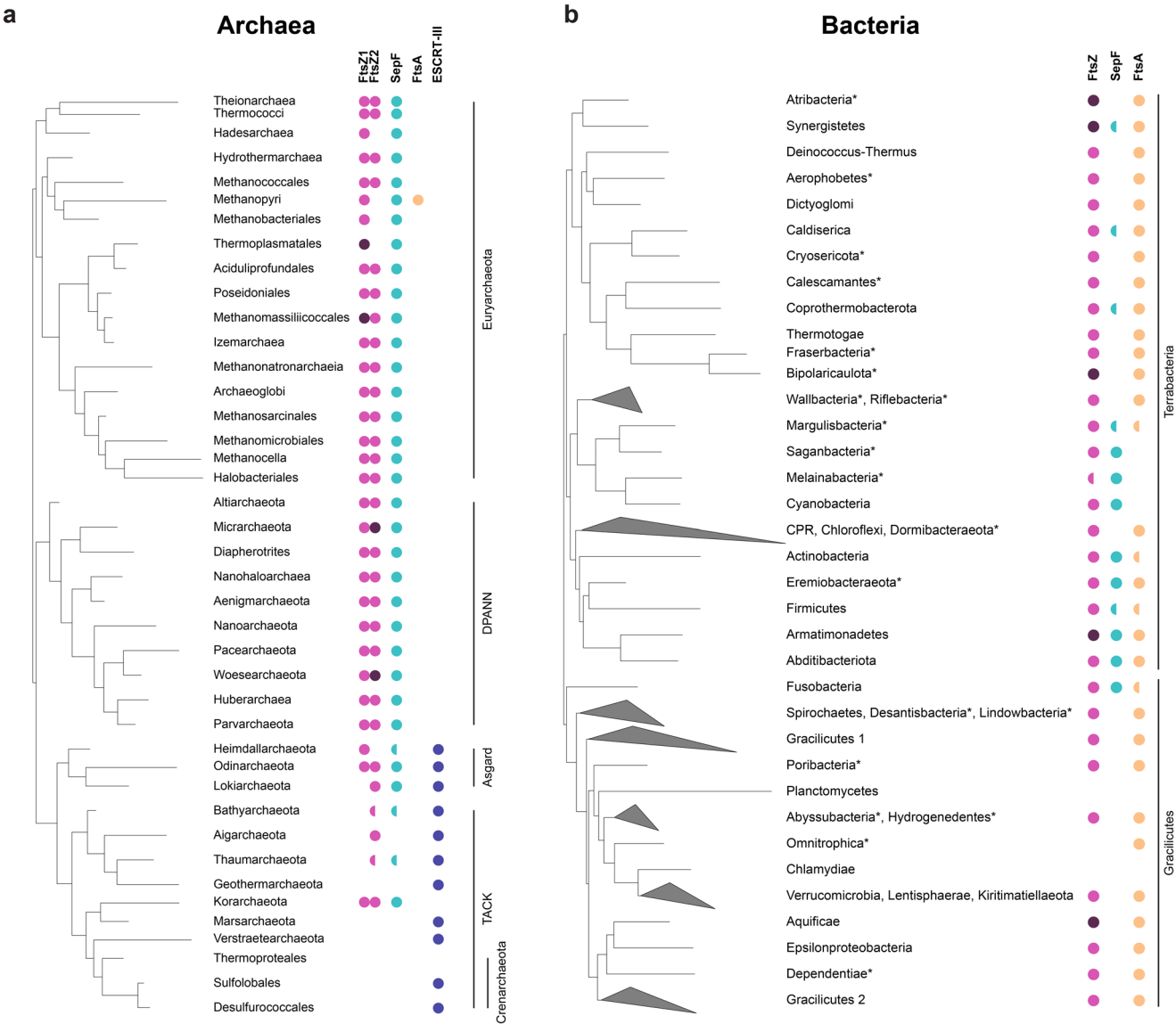
and anchors FtsZ2 to the septum<sup>29</sup>. In *M. smithii* SepF seems to localize to the future division site before FtsZ (Fig. 1d). This is in contrast to what was observed in the ovococoid bacterium *Streptococcus pneumoniae*, where SepF and FtsZ initially colocalize at the septum, but then FtsZ only relocates to the new division sites<sup>30</sup>. However, *S. pneumoniae* also possess the essential alternative Z-ring tether FtsA<sup>30</sup> as well as MapZ, a transmembrane protein that forms a ring-like structure, marks the division site before FtsZ and positions the Z-ring<sup>31</sup>. *M. smithii* SepF may also have a role similar to bacterial MapZ in priming the division site and placing FtsZ. However, unlike MapZ, archaeal SepF is fully cytoplasmic. This would mean that an additional partner may exist in *M. smithii* to help position SepF at mid-cell, but this will need further investigations.

Our results show that SepF-mediated anchoring of FtsZ to the membrane for cytokinesis dates back to billions of years ago, prior to the divergence between Archaea and Bacteria. In agreement with this hypothesis, the crystal structures of the SepF-FtsZ<sub>CTD</sub> complexes from Bacteria<sup>21</sup> and Archaea (this work) reveal a partially conserved FtsZ-binding pocket in monomeric SepF that might reflect a common ancestral feature. However, the

crystallographic studies as well as the consensus motifs of archaeal and bacterial FtsZ<sub>CTD</sub> (Fig. 4d) reveal clearly distinctive characteristics, notably at the level of the dimer interface and FtsZ binding. Such major divergence may be linked to fundamental differences in cell envelope and division in the two prokaryotic domains which are worth discussing.

The overall structure of the SepF monomer is very similar in all available archaeal and bacterial crystal structures, and in all cases the functional unit is a dimer. But a notable difference is the wider and deeper binding cleft of the FtsZ binding pocket in MsSepF formed between  $\alpha 2$  and  $\beta 3$  through the archaeal-specific conserved  $\eta 1$  insertion. This results in a more important interaction of the FtsZ<sub>CTD</sub> with the SepF monomer in Archaea than in Bacteria (Fig. 4c) and could point towards an ancestral binding mode where a single monomer of SepF might have been sufficient for FtsZ binding. Interestingly, the functional dimer (as defined by its complex with FtsZ) strikingly differs between MsSepF, where it is formed via a  $\beta$ - $\beta$  interface, and CgSepF, where it is formed via an  $\alpha$ - $\alpha$  interface (Figs. 3b and 4c). Importantly, a bacterial-like  $\alpha$ - $\alpha$  interface is not possible in archaeal SepF because a crucial glycine residue (Gly114 in CgSepF) buried at the





**Fig. 5** SepF is widely present in Archaea and co-occurs with FtsZ. **a** Distribution of FtsZ1, FtsZ2, SepF, FtsA and ESCRT-III (CdvB) homologs on a schematic reference phylogeny of the Archaea. FtsZ1 and FtsZ2 homologs are present in most archaeal lineages (magenta), and frequently in two or more copies each (dark magenta). Semicircles indicate that the corresponding protein could not be identified in all the taxa of the corresponding clade and may be either due to true absences or partial genomes. The presence of SepF (turquoise) correlates to that of FtsZ in the majority of taxa. A FtsA homolog was only identified in Methanopyri (orange). Homologs of ESCRT-III (CdvB and homologs) (purple) are only present in the Asgard superphylum and in most representatives of the TACK superphylum, except for Korarchaeota and Thermoproteales. For full data see Supplementary Data 1. **b** Distribution of FtsZ, SepF and FtsA homologs on a schematic reference phylogeny of Bacteria. FtsZ (magenta) is present in most bacterial phyla, with the exception of some phyla within the PVC superphylum (Planctomycetes, Omnitrophica and Chlamydiae), which are known to have specific FtsZ-less cytokinesis. Both SepF and FtsA are also absent in Planctomycetes and Chlamydiae. Two copies of FtsZ can be identified in Atribacteria, Synergistetes, Biopolaricaulota, Armatimonadetes and Aquificae (dark magenta). SepF is present in some phyla (Synergistetes, Caldiseica, Coprothermobacterota, Margulisbacteria, Melainabacteria, Cyanobacteria, Actinobacteria, Eremiobacteraeota, Firmicutes, Armatimonadetes, Abditibacteriota and Fusobacteria), most belonging to the Terrabacteria. In contrast, all Gracilicutes except Fusobacteria, and the remaining Terrabacteria phyla have only FtsA, while Cyanobacteria, Melainabacteria and Saganbacteria have only SepF. Finally, some members of Synergistetes, Caldiseica, Coprothermobacterota, Margulisbacteria, Actinobacteria, Eremiobacteraeota, Firmicutes, Armatimonadetes, Abditibacteriota and Fusobacteria have both FtsA and SepF. Semicircles indicate that the corresponding protein could not be identified in all the analyzed taxa in the lineage displayed. \* indicates uncultured Candidate phyla for which many genomes are incomplete. These phyla were not included in phylogenetic reconstructions. For full data see Supplementary Data 2.

center of the bacterial interface is substituted by charged residues with longer side chains (Lys, Glu, Asp) in archaeal sequences (Supplementary Fig. 10), precluding such interaction to occur. Interestingly, the crystal structure of *B. subtilis* SepF has shown that it can form both bacterial-like  $\alpha$ - $\alpha$  and archaeal-like  $\beta$ - $\beta$  interfaces<sup>22</sup>. The presence of these two self-interacting interfaces has suggested a simple mechanism for *B. subtilis* SepF, where FtsZ

binding occurs through the  $\alpha$ - $\alpha$  interface and polymerization through the  $\beta$ - $\beta$  interface<sup>22</sup>, a mechanism which would therefore be absent in Archaea. However, the only other available bacterial SepF structure (CgSepF) revealed that a C-terminal helix  $\alpha$ 3 interacts with the  $\beta$ -sheet of SepF and would therefore preclude formation of a  $\beta$ - $\beta$  interface<sup>21</sup>. Remarkably, helix  $\alpha$ 3 is predicted to be conserved in most bacterial sequences including *B. subtilis*,

but not in Archaea (Supplementary Fig. 7). This observation may suggest that the  $\beta$ - $\beta$  interface observed in the crystal structure of *B. subtilis* SepF is not involved in bacterial SepF polymerization and might rather be a vestigial feature of the ancestral archaeal-like SepF. Alternatively, by interacting with other cell division partners, the amphipathic helix  $\alpha$ 3 may be involved in regulating bacterial SepF polymerization through formation of a  $\beta$ - $\beta$  interface, a possibility that will require further study.

In Bacteria, SepF polymerization has been associated with membrane remodeling<sup>21,22</sup>. Here, we show that MsSepF is also able to tubulate liposome surfaces, although it remains to be determined whether this requires polymerization. In fact, we (and others<sup>29</sup>) did not obtain conclusive experimental evidence that MsSepF polymerizes, and the three available archaeal SepF structures provide no hints about a possible mechanism.

The fundamental divergence between SepF/FtsZ interaction in *M. smithii* and *C. glutamicum* correlates well with the profound differences in the cell envelope structure of Archaea with respect to Bacteria, the former being much more variable and generally lacking a peptidoglycan cell wall<sup>24</sup>. In contrast, the emergence of a rigid cell wall made of peptidoglycan occurred very early in bacterial evolution and likely drove the emergence of the associated complex multi-protein divisome machinery to provide additional mechanical force. Our results suggest that FtsA has also an early origin in Bacteria (Supplementary Fig. 16) and may have provided an alternative tether in addition to SepF, eventually replacing it completely during bacterial diversification. This phenomenon could be linked with the fact that FtsA is a highly dynamic ATP-dependent protein that might therefore have allowed to couple cell division with the energy status of the cell.

The evolution of cytokinesis in Archaea seems to have been less constrained and more dynamic, with (1) the early presence of two FtsZ paralogues and their subsequent independent losses<sup>1,7</sup>, (2) the appearance of a multitude of FtsZ-like protein families in some lineages such as Haloarchaea<sup>8,32</sup>, and (3) eventually the emergence of the ESCRT-like system and its takeover of cytokinesis in the archaeal lineages closest to the origin of eukaryotes<sup>1,7</sup>. The emergence of a cell wall made of pPG in *M. smithii* and all *Methanobacteriales* and the related *Methanopyrales* is more recent than in Bacteria and is very likely an evolutionary convergence. It will be interesting to investigate if it led to a peculiar SepF/FtsZ interaction by obtaining additional structural data in other wall-less archaeal lineages. Indeed, a single amino acid (Phe377) in FtsZ specifically interacts with the second protomer in the SepF dimer (Fig. 4). This position is only conserved in *M. smithii* related taxa and perhaps provides extra mechanical strength to drive invagination of their thick pPG cell wall.

Finally, our results strongly suggest that a SepF/FtsZ system was already present in the LUCA, unequivocally defining it as a cellular entity. LUCA may not have possessed a complex envelope, and cell division could have been mainly achieved by a minimal system where SepF converted the dynamic energy of FtsZ into mechanical force to achieve membrane constriction<sup>33,34</sup>. Several pieces of evidence suggest that the LUCA only contained a rather basic plasma membrane with the absence of a cell wall<sup>35,36</sup>, thus, a membrane-interacting protein bound to a dynamic cytoskeleton element could have represented enough to promote cell division. Therefore, a plausible evolutionary scenario could be that SepF and FtsZ represent the minimal ancestral cell division apparatus in the LUCA, possibly together with a few auxiliary proteins. Given the large conservation of the SepF/FtsZ system in Archaea with respect to Bacteria, combined with its peculiar features, it is tempting to speculate that it may have retained ancestral features dating back to the LUCA.

In conclusion, our results pave the way for future studies to understand cell division in different archaeal models, in particular

gut-associated methanogens with a cell wall made of pPG. FtsZ/SepF interaction represents only part of the story and many questions remain to be answered, such as how the Z-ring is positioned in Archaea, and which other proteins are part of the archaeal divisome. The answers to these questions will allow to reveal fundamental features of contemporary archaeal cell biology, while at the same time dwelling into the most ancient evolutionary past.

## Methods

**Bacterial and archaeal strains and growth conditions.** All bacterial and archaeal strains used in this study are listed in Supplementary table 1. *Escherichia coli* DH5 $\alpha$  or Top10 were used for cloning and were grown in Luria-Bertani (LB) broth or agar plates at 37 °C supplemented with 50  $\mu$ g mL<sup>-1</sup> kanamycin or 100  $\mu$ g mL<sup>-1</sup> ampicillin when required. For protein production, *E. coli* BL21 (DE3) was grown in LB or 2YT broth supplemented with 50  $\mu$ g mL<sup>-1</sup> kanamycin or 100  $\mu$ g mL<sup>-1</sup> ampicillin at the appropriate temperature for protein expression.

*Methanothermobacter wolfeii* DSM 2970 and *Methanobrevibacter smithii* strain DSM 861 were obtained from the Deutsche Sammlung von Mikroorganismen und Zellkulturen (DSMZ; Braunschweig, Germany). *M. wolfeii* and *M. smithii* were grown approximately two to three weeks in 100 mL serum bottles (clear glass bottle, Supelco) in chemically defined media under strict anaerobic conditions. The gas phase used for both strains was 80 Vol.-% H<sub>2</sub> in CO<sub>2</sub> at 2.0 bar. *M. wolfeii* was grown at 60 °C and *M. smithii* at 37 °C, both shaking at 180 rpm.

**Methanogen media.** *M. wolfeii* was grown in *Methanothermobacter marburgensis* medium as described in<sup>37</sup>. *M. smithii* was grown in adapted DSMZ 141 Methanogen medium that contained 0.17 g KCl, 2 g MgCl<sub>2</sub>·6H<sub>2</sub>O, 0.125 g NH<sub>4</sub>Cl, 0.053 g CaCl<sub>2</sub>, 0.055 g KH<sub>2</sub>PO<sub>4</sub>, 0.84 g MgSO<sub>4</sub>, 3 g NaCl, 0.5 g Na-acetate, 1 g yeast extract, 5 mL of trace element solution, 1 mL of FeII(NH<sub>4</sub>)<sub>2</sub>(SO<sub>4</sub>)<sub>2</sub>·6H<sub>2</sub>O solution, 50  $\mu$ L of Na-resazurin solution (0.7 mg mL<sup>-1</sup>), and was filled up with 480 mL of ddH<sub>2</sub>O. The medium was brought to boil and was boiled for 5 min. After the temperature descended to 50 °C, 5 mL of vitamin solution, 2.5 g NaHCO<sub>3</sub>, 0.25g L-Cystein-HCl and 0.1 g Na<sub>2</sub>S·H<sub>2</sub>O were added. The pH was adjusted to 7 with HCl and the medium was filled up with ddH<sub>2</sub>O to a final volume of 500 mL. The medium was flushed with CO<sub>2</sub> and transferred with a glass syringe into 100 mL serum bottles. 50 mL of the medium were aliquoted into serum bottles and sealed with blue rubber stoppers (pretreated by boiling ten times for 30 min in fresh ddH<sub>2</sub>O; 20 mm, Bellco) and open-top aluminum caps (9.5 mm opening, Merck Group). The sealed serum bottles containing the medium were autoclaved for 20 min at 120 °C. Composition of trace element solution was: 1.5 g Nitrilotriacetic acid, 3g MgSO<sub>4</sub>·7H<sub>2</sub>O, 0.585 g MnCl<sub>4</sub>·4H<sub>2</sub>O, 1 g NaCl, 0.1 g FeSO<sub>4</sub>·7H<sub>2</sub>O, 0.18 g CoSO<sub>4</sub>·7H<sub>2</sub>O, 0.1 g CaCl<sub>2</sub>·2H<sub>2</sub>O, 0.18 g ZnSO<sub>4</sub>·7H<sub>2</sub>O, 0.006 g CuSO<sub>4</sub>, 0.02 g KAl(SO<sub>4</sub>)<sub>2</sub>·12H<sub>2</sub>O, 0.01 g H<sub>3</sub>BO<sub>3</sub>, 0.01 g Na<sub>2</sub>MoO<sub>4</sub>·2H<sub>2</sub>O, 0.03 g NiCl<sub>2</sub>·6H<sub>2</sub>O, 0.3 mg Na<sub>2</sub>SeO<sub>3</sub>·5H<sub>2</sub>O, 0.4 mg Na<sub>2</sub>WO<sub>4</sub>·2H<sub>2</sub>O. First nitrilotriacetic acid was dissolved and pH was adjusted to 6.5 with KOH. Then minerals were added, medium was filled up with ddH<sub>2</sub>O to a final volume of 1000 mL and pH was adjusted to 7.0 with KOH. Composition of Vitamin solution was: 2 mg Biotin, 2 mg Folic acid, 10 mg Pyridoxine-HCl, 5 mg Thiamine-HCl, 5 mg Riboflavin, 5 mg Nicotinic acid, 5 mg D-Ca-pantothenate, 0.1 mg Vitamin B<sub>12</sub>, 5 mg p-Aminobenzoic acid, 5 mg Lipoic acid and filled up with ddH<sub>2</sub>O to a final volume of 1000 mL.

## Cloning of *M. wolfeii* *PeiW* for recombinant protein production in *E. coli*.

Genomic DNA from *M. wolfeii* was obtained by extracting with a phenol-chloroform extraction procedure. The gene encoding for *PeiW* (*psiM100p36*) was amplified by PCR<sup>38</sup> and the sequence of amplified *peiW* was verified by Sanger sequencing (Eurofins Genomics, Ebersberg, Germany). The insert and the Novagen vector pET-15b (Merck Group, Darmstadt, Germany) were digested with *NdeI* (NEB, Ipswich, MA, USA) and *XhoI* (NEB, Ipswich, MA, USA) and ligation of digested *peiW* and pET-15b with Quick ligase™ (NEB, Ipswich, MA, USA) generated the plasmid pET-15b-*peiW*, which was transformed into *E. coli* Top10. The successful transformation was confirmed by a colony PCR and by Sanger sequencing (Eurofins Genomics, Ebersberg, Germany). Plasmid DNA was obtained by extracting with a Miniprep Kit (Pure Yield™, Promega, Madison, WI, USA), and pET-15b-*peiW* was transformed into *E. coli* DE3 BL21-AI (Life technologies, Van Allen Way Carlsbad, CA, USA). All plasmids and primers used in this study are listed in Supplementary table 1 and Supplementary table 2 respectively.

**Protein expression and purification of *PeiW*.** The expression of recombinant *PeiW* was induced at OD<sub>600</sub> = 0.6 by the addition of 0.2 % (w/v) L-arabinose and 1 mmol L<sup>-1</sup> IPTG to LB medium (100  $\mu$ g mL<sup>-1</sup> ampicillin). Cell cultures (3 × 250 mL) were harvested after 3 h of incubation by a centrifugation of 15 min at 3170 × g at 4 °C. To verify the expression of recombinant *PeiW* cell pellets were resuspended to a concentration of 0.01 optical density unit (ODU)  $\mu$ L<sup>-1</sup> in 5x Laemmli buffer and 1  $\mu$ L DTT (1 mol L<sup>-1</sup>) and lysed 5 min at 95 °C and 1050 rpm. Crude extracts were centrifuged 30 min at 16,100 × g at 4 °C and supernatant was loaded on two 12.5 % (w/v) polyacrylamide gels. The gel was stained with Coomassie Brilliant Blue (50% (v/v)

ddH<sub>2</sub>O, 40 % (v/v) ethanol (ethanol absolute), 10 % (v/v) 100 Vol.-% acetic acid, 0.1 % (w/v) R-250 Brilliant Blue).

For protein purification frozen cell pellets were resuspended in Ni-NTA lysis buffer (50 mmol L<sup>-1</sup> NaH<sub>2</sub>PO<sub>4</sub>, 300 mmol L<sup>-1</sup> NaCl, 10 mmol L<sup>-1</sup> imidazole, at pH 8) at 4 °C and lysed by sonication. The lysate was centrifuged for 20 min at 16.9x g at 4 °C. The cleared lysate was incubated for 2 h at 4 °C with Ni-NTA agarose resin (Invitrogen) under slight agitation. The lysate with the beads was passed through a gravity flow chromatography column (Econo-Pac chromatography columns, Biorad). The column was washed with four column volumes of washing buffer (50 mmol L<sup>-1</sup> NaH<sub>2</sub>PO<sub>4</sub>, 300 mmol L<sup>-1</sup> NaCl, 20 mmol L<sup>-1</sup> imidazole, at pH 8). His-tagged proteins were eluted with 3 × 1 mL elution buffer (50 mmol L<sup>-1</sup> NaH<sub>2</sub>PO<sub>4</sub>, 300 mmol L<sup>-1</sup> NaCl, 250 mmol L<sup>-1</sup> imidazole, pH = 8) and fractions were collected separately. The fractions containing the protein of interest were loaded on a PD-midi Trap G25 column (GE Health Care) and eluted with 1.5 mL of 50 mmol L<sup>-1</sup> Hepes buffer (at pH 7) for buffer exchange.

### Cloning of *M. smithii* SepF and FtsZ for recombinant protein production in *E. coli*.

Genomic DNA from *M. smithii* was obtained by resuspending a pellet of densely grown culture in ddH<sub>2</sub>O and boiling it for 5 min at 99 °C. Subsequently, 1 µL of archaeal suspension was used as template in each 50 µL PCR reaction to amplify the genes encoding for *M. smithii* ftsz (MSM\_RS03130), sepF full length (SepF, MSM\_RS02010) as well as only the core region of sepF (SepF<sub>core</sub>) comprising amino acids from 54 to 149. The products of the right size were cloned in to the pT7 vector containing an N-terminal 6xHis-SUMO tag by Gibson assembly. The constructs were transformed into chemically competent DH5α *E. coli* cells. The successful transformation was confirmed by a colony PCR and by Sanger sequencing (Eurofins Genomics, France).

**Protein expression and purification.** Protein expression and purification was carried out as previously describes in<sup>21</sup>. In brief, N-terminal 6xHis-SUMO-tagged SepF and SepF<sub>core</sub> from *M. smithii* were expressed in *E. coli* BL21 (DE3). After 4 h at 37 °C cells were grown for 24 h at 20 °C in 2YT complemented auto-induction medium<sup>39</sup> containing 50 µg mL<sup>-1</sup> kanamycin. Cell pellets were resuspended in 50 mL lysis buffer (50 mmol L<sup>-1</sup> Hepes pH8, 300 mmol L<sup>-1</sup> NaCl, 5 % (v/v) glycerol, 1 mmol L<sup>-1</sup> MgCl<sub>2</sub>, benzonase, lysozyme, 0.25 mmol L<sup>-1</sup> TCEP, EDTA-free protease inhibitor cocktails (ROCHE)) at 4 °C and lysed by sonication. The lysate was centrifuged for 30 min at 30,000x g at 4 °C and loaded onto a Ni-NTA affinity chromatography column (HisTrap FF crude, GE Healthcare). His-tagged proteins were eluted with a linear gradient of buffer B (50 mmol L<sup>-1</sup> Hepes at pH 8, 300 mmol L<sup>-1</sup> NaCl, 5 % (v/v) glycerol, 1 mol L<sup>-1</sup> imidazole). The eluted protein of interest was dialyzed at 4 °C overnight in SEC buffer (50 mmol L<sup>-1</sup> Hepes at pH 8, 150 mmol L<sup>-1</sup> NaCl, 5 % (v/v) glycerol) in the presence of the SUMO protease (ratio used, 1:100). The cleaved protein was concentrated and loaded onto a Superdex 75 16/60 size exclusion (SEC) column (GE Healthcare) pre-equilibrated at 4 °C in 50 mmol L<sup>-1</sup> Hepes at pH 8, 150 mmol L<sup>-1</sup> NaCl, 5 % (v/v) glycerol. The purified protein was concentrated, aliquoted, flash frozen in liquid nitrogen and stored at -80 °C.

N-terminal 6xHis-SUMO-tagged *M. smithii* FtsZ was produced and purified as described above, except induction was performed at 37 °C, KCl was used instead of NaCl in all the buffers and a TALON FF crude column (GE Healthcare) was used for affinity chromatography.

**Thermal shift assay.** Tests were performed using 96 well plate and 20 µL of reaction volume per well. A total of 3 µg of MsSepF<sub>core</sub> was used per assay in a buffer containing 150 mmol L<sup>-1</sup> NaCl, 25 mmol L<sup>-1</sup> Hepes at pH 8 and 5 % (v/v) glycerol. When used, FtsZ<sub>CTD</sub> peptide (NEDQLDDFIDGIF purchased from Genosphere) was added to a final concentration of 1 mmol L<sup>-1</sup>. Next, 0.6 µL of 50X Sypro Orange solution (Invitrogen) was added to each well and samples were heated from 25 to 95 °C in 1 °C steps of 1 min each in a CFX96 Touch™ Real-Time PCR Detection System (BioRad). Excitation/emission filters of 492 and 516 nm were used to monitor the fluorescence increase resulting from binding of the Sypro Orange to exposed hydrophobic regions of the unfolding MsSepF<sub>core</sub>. The midpoint of the protein unfolding transition was defined as the melting temperature (T<sub>m</sub>).

**Surface plasmon resonance (SPR) assay.** SPR experiments were performed on a Biacore T200 instrument (Cytiva) equilibrated at 25 °C in Biacore Buffer buffer (150 mmol L<sup>-1</sup> NaCl, 25 mmol L<sup>-1</sup> Hepes pH8). For the MsSepF<sub>core</sub> covalent immobilization, two flowcells of a CM5 sensorchip (Cytiva) were covalently functionalized using NHS/EDC amine coupling chemistry. The carboxymethylated dextran surface was first activated by flowing a mixture of NHS (50 mmol L<sup>-1</sup>) and EDC (200 mmol L<sup>-1</sup>) for 10 min at 5 µL min<sup>-1</sup>. MsSepF<sub>core</sub> (diluted in 10 mmol L<sup>-1</sup> acetate pH4) was then injected on one flowcell for 20 min at 6 µg mL<sup>-1</sup> and on another for 30 min at 30 µg mL<sup>-1</sup>. Both surfaces were then de-activated by injecting ethanolamine 1 mol L<sup>-1</sup> for 10 min. The final densities of MsSepF<sub>core</sub> were respectively 3200 RU and 5000 RU (1RU~1 pg/mm<sup>2</sup>). For Real-time monitoring of the interaction between the FtsZ<sub>CTD</sub> peptide and MsSepF<sub>core</sub>, 9 concentrations of the FtsZ<sub>CTD</sub> peptide (ranging from 3.9 to 1000 nmol L<sup>-1</sup>) were flowed in triplicate for 30 s at 20 µL min<sup>-1</sup> over the two covalently-immobilized

MsSepF<sub>core</sub> surfaces. The dissociation of the peptide/MsSepF<sub>core</sub> complexes was then monitored for 240 s by flowing buffer over the two flowcells. The dissociation equilibrium constant of the interaction (K<sub>d</sub>) was determined by analyzing the concentration-dependence of the steady-state SPR signals (Req) using the following equation: Req = R<sub>max</sub> × C/K<sub>d</sub> + C (where C is the FtsZ<sub>CTD</sub> peptide concentration and R<sub>max</sub> the SPR response at saturating peptide concentration).

**Crystallization.** Crystallization screens were set up for MsSepF<sub>core</sub> apo form and in complex with FtsZ<sub>CTD</sub> (molar ratio 1:5) using the sitting-drop vapor diffusion method at 18 °C in a Mosquito nanoliter-dispensing crystallization robot (TTP Labtech, Melbourn, UK) as detailed in<sup>40</sup>. Optimal crystals of MsSepF<sub>core</sub> (14 mg mL<sup>-1</sup>) appeared after 5 days in a buffer containing 0.1 mol L<sup>-1</sup> TRIS at pH 8.5 and 30 % (w/v) PEG 10 K. The complex MsSepF<sub>core</sub>-FtsZ<sub>CTD</sub> crystallized in a buffer containing 0.2 mol L<sup>-1</sup> (NH<sub>4</sub>)<sub>2</sub>SO<sub>4</sub> and 30 % (w/v) PEG 8 K after 1 week using MsSepF<sub>core</sub> at 14 mg mL<sup>-1</sup> and FtsZ<sub>CTD</sub> at 6 mg mL<sup>-1</sup>. Crystals were cryo-protected in the crystallization buffer containing 33 % (v/v) glycerol.

**Data collection, structure determination and refinement.** X-ray diffraction data were collected at 100 K using beamlines Proxima-1 and Proxima-2 at the Soleil synchrotron (GIF-sur-YVETTE, France). Both data sets were processed using XDS<sup>41</sup> and AIMLESS from the CCP4 suite<sup>42</sup>. The crystal structures were solved by molecular replacement using Phaser<sup>43</sup> and a single monomer of the PDB 3ZIE as a search model. All structures were refined through several cycles of manual building with COOT<sup>44</sup> and reciprocal space refinement with BUSTER<sup>45</sup>. Both final models exhibit a good stereochemistry, with no Ramachandran outliers. The Table 1 shows the crystallographic statistics. Structural figures were generated using Chimera<sup>46</sup>. Atomic coordinates and structure factors can be found in the protein data bank under the accession codes 7AL1 and 7AL2.

**Small unilamellar vesicles (SUVs) preparation.** SUVs were prepared as previously describes in<sup>21</sup>. In brief, reverse phase evaporation was used. A 10 mmol L<sup>-1</sup> lipids chloroform solution was prepared and chloroform was removed by evaporation under vacuum conditions. The dried phospholipid film was resuspended in a mixture of diethyl ether and 25 mmol L<sup>-1</sup> Hepes buffer at pH 7.4 and remaining diethyl ether was eliminated by reverse phase evaporation. Finally, SUVs were obtained by sonication during 30 min at 4 °C.

**Lipid peptide interaction (tryptophan fluorescence emission titration).** To estimate the partition coefficient (K<sub>x</sub>) between SUVs and SepF a similar protocol as described in<sup>21</sup> was used. In brief, we used the synthetic peptide WMGFTDALKRSLGF (purchased from Genosphere), which contains the SepF<sub>M</sub> sequence of *M. smithii* with an extra W residue at the N-terminal. K<sub>x</sub> is defined as the ratio of peptide concentration in the lipid and in the buffer phases. K<sub>x</sub> can be expressed by the following equation:

$$K_x = \frac{P_L / (P_L + [L])}{P_W / (P_W + [W])}$$

in which P<sub>W</sub> represent the concentration of soluble peptide (in aqueous phase) and P<sub>L</sub> the peptide concentration bound to lipid membranes (lipidic phase). [L] refers to the lipid concentration and [W] refers to the water concentration. K<sub>x</sub> is directly related to the apparent dissociation constant as K<sub>x</sub> \* K<sub>d</sub> = [W] with K<sub>d</sub> \* P<sub>L</sub> = P<sub>W</sub> × [L]. The Kaleidagraph software was used to fit the K<sub>x</sub> to the experimental data.

We used a FP-8200 (Jasco, Tokyo, Japan) spectrophotometer equipped with a thermostatic Peltier ETC-272T at 25 °C. Experiments were performed in a high precision cell cuvette made of Quartz with a light Path of 10 × 4 mm (Hellma, France). A bandwidth of 5 nm was used for emission and excitation. 1 µmol L<sup>-1</sup> of peptide was used in Titration buffer (100 mmol L<sup>-1</sup> KCl and 25 mmol L<sup>-1</sup> Hepes at pH 7.4). We measured the fluorescence emission between 300 and 400 nm at a scan rate of 125 nm min<sup>-1</sup> with an excitation wavelength of 280 nm. The obtained spectra were corrected by blank subtraction (SUV light scattering in titration buffer). Next, the maximum wavelength value (λ<sub>max</sub>) was calculated to measure the partition coefficient (K<sub>x</sub>).

**SepF polymerization assay.** Purified MsSepF and MsSepF<sub>core</sub> were precleared at 25,000 g for 15 min at 4 °C. To follow the polymerization of MsSepF in the presence of lipids, we used MsSepF or MsSepF<sub>core</sub> plus SUVs at a final concentration of 50 µmol L<sup>-1</sup> each in SepF polymerization buffer containing 100 mmol L<sup>-1</sup> KCl, 10 mmol L<sup>-1</sup> MgCl<sub>2</sub> and 25 mmol L<sup>-1</sup> Pipes at pH 6.9. The mixture was placed into a quartz cuvette with a light path of 10 mm. Data acquisition started immediately using an UV-Visible Spectrophotometer (Thermo scientific Evolution 220) during 600 s at 25 °C using 400 nm for excitation and emission and spectra with slits widths of 1 nm. Measurements were taken every 15 s during 600 s and keeping a constant temperature of 25 °C.

**Electron microscopy.** For negative stain sample preparations, incubations were performed at room temperature. SUVs (100 µmol L<sup>-1</sup>) alone or in the presence of SepF (50 µmol L<sup>-1</sup>) with or without FtsZ<sub>CTD</sub> (100 µmol L<sup>-1</sup>) were incubated in a buffer containing 100 mmol L<sup>-1</sup> KCl, 10 mmol L<sup>-1</sup> MgCl<sub>2</sub> and 25 mmol L<sup>-1</sup> Pipes



at pH 6.9 for 10 min. In order to visualize FtsZ filaments, FtsZ ( $30 \mu\text{mol L}^{-1}$ ) was incubated with or without SepF<sub>core</sub> ( $20 \mu\text{mol L}^{-1}$ ) in polymerization buffer ( $2 \text{ mol L}^{-1}$  KCl,  $50 \text{ mmol L}^{-1}$  Hepes at pH 7.4 and  $10 \text{ mmol L}^{-1}$  MgCl<sub>2</sub>) supplemented with freshly prepared  $0.6 \text{ mol L}^{-1}$  Trimethylamine N-oxide (TMAO) and  $3 \text{ mmol L}^{-1}$  GTP. Reactions were incubated for 10 min before applied onto the grid.

For all samples, 400 mesh carbon coated grids (Electron Microscopy Sciences; CF 400-Cu) were glow-discharged on an ELMO system for 30 sec at 2 mA.  $5 \mu\text{L}$  of sample was applied onto the grid and incubated for 30 s, the sample was blotted, washed in three drops of buffer ( $100 \text{ mmol L}^{-1}$  KCl,  $10 \text{ mmol L}^{-1}$  MgCl<sub>2</sub> and  $25 \text{ mmol L}^{-1}$  Pipes at pH 6.9) and then stained with 2% (w/v) uranyl acetate. Images were recorded on a Gatan UltraScan4000 CCD camera (Gatan) on a Tecnai T12 BioTWINLaB6 electron microscope operating at a voltage of 120 kV.

**Statistical analysis of FtsZ filament diameter.** Electron microscopy images of negatively stained FtsZ filaments (FtsZ + GTP) and FtsZ bundles (FtsZ + GTP + SepF<sub>core</sub>) were analyzed using the public domain program Fiji (ImageJ) Version 2.0.0-rc-68/1.52i. The diameter of each 130 FtsZ filaments and FtsZ bundles was measured in several images each and the data were extracted into Microsoft Excel 2016. Boxplots were created by using Microsoft Excel 2016 with the Real Statistics Resource Pack for Excel 2016 (<http://www.real-statistics.com>). Each data set for diameter of FtsZ filaments and FtsZ bundles was tested for normal distribution using the Kolmogorov-Smirnov test (KS-test). The KS-statistic was 0.9798 ( $p = 5.5\text{E}-0111$ ) for FtsZ filaments and 1.0000 ( $p = 1.3\text{E}-0115$ ) for FtsZ bundles. For a level of significance of 5%, critical values of 0.1178 and 0.1178 were obtained, respectively. Hence, the data are normal distributed in both cases, because the null hypothesis ( $H_0$ ) was not rejected, as the critical values are  $>\alpha$ . A 2-sample  $t$ -test was conducted to test whether the means of the diameter of FtsZ filaments and FtsZ bundles are significantly different. The result for the  $t$ -statistic was found to be  $-23.8032$ . The 2-sample  $t$ -test resulted in a critical  $t$ -value of  $t(\alpha/2)$  of 1.9692 for an alpha of 0.025.  $\alpha/2$  is to be used for a two sample two tailed test. Thus, a significant difference of the diameter was found at a 5% level of significance, because the  $H_0$  was rejected, as the modulus of the critical value was  $> \alpha/2$ . The statistical analysis was performed using DataLab version 4.0 (Epina GmbH, Pressbaum, Austria).

**Western blots and SepF and FtsZ quantification.** Purified MsSepF<sub>core</sub> protein was used to raise antibodies in guinea pig (Covalab). Two peptides (CEN-AENGLEKLKSAADT and CGESDSGDRALESVHE) in equimolar amounts were used to raise antibodies in rabbit against *M. smithii* FtsZ (Genosphere Biotech). To prepare cell extracts, archaeal cell pellets were resuspended in PBS buffer ( $137 \text{ mmol L}^{-1}$  NaCl,  $10 \text{ mmol L}^{-1}$  Na<sub>2</sub>HPO<sub>4</sub>,  $1.8 \text{ mmol L}^{-1}$  KH<sub>2</sub>PO<sub>4</sub>,  $2.7 \text{ mmol L}^{-1}$  KCl, at pH 7.4) together with LDS sample buffer (Invitrogen) and  $100 \text{ mmol L}^{-1}$  DTT, and disrupted at RT with  $0.1 \text{ mm}$  glass beads and using the MP FastPrep-24™ 5 G homogenizer. In order to test the expression of the proteins and quantify the amount of SepF and FtsZ in cells, crude extracts and purified recombinant SepF and FtsZ in serial dilution were loaded on a 4–12% (w/v) Bis-Tris PAGE gel (Invitrogen). The amounts of crude extract were  $120 \mu\text{g}$  for FtsZ and  $290 \mu\text{g}$  for SepF. Purified FtsZ protein was serially diluted from  $100 \text{ ng}$  to  $6.25 \text{ ng}$ , and purified SepF protein from  $6.25 \text{ ng}$  to  $0.1 \text{ ng}$ . After separation of proteins on SDS-PAGE gel, they were electro-transferred onto a  $0.2 \mu\text{m}$  Nitrocellulose membrane. Membranes were blocked with 5% (w/v) skimmed milk for 45 min at room temperature (RT). Membranes were incubated with either an anti-MsSepF antibody or an anti-MsFtsZ antibody, both at 1:500 dilution for 1 h at RT. After washing in TBS-Tween buffer ( $10 \text{ mmol L}^{-1}$  Tris-HCl at pH 8;  $150 \text{ mmol L}^{-1}$  NaCl; Tween 20 0.05% (v/v)), the membranes were incubated with an anti-rabbit horseradish peroxidase-linked antibody for FtsZ and an anti-guinea pig horseradish peroxidase-linked antibody for SepF (Invitrogen), both at 1:5000 dilution for 45 min. The membranes were washed and revealed with HRP substrate (Immobilon Forte, Millipore) and imaged using the ChemiDoc MP Imaging System (Biorad). Quantification of the bands was performed using the software Image Lab (Biorad) and the band volume was plotted against the ng loaded in order to obtain a strand curve. All uncropped blots are shown in Supplementary Fig. 1.

**Immunostaining.** Cells of *M. smithii* grown to early exponential phase were harvested by 5 min of centrifugation at  $3.5 \times g$  (all centrifugation steps were performed at  $3.5 \times g$ ). Pellets were washed in PBS buffer, pelleted, fix with 100% ice cold methanol and stored at  $-20^\circ\text{C}$ . Cells were rehydrated and washed in  $50 \text{ mmol L}^{-1}$  HEPES buffer at pH 7 for 10 min at RT, followed by permeabilization of the archaeal pPG by incubation for 10 min with  $3.5 \mu\text{g}$  of purified 6xHis-PeiW in  $50 \text{ mmol L}^{-1}$  HEPES buffer containing  $1 \text{ mmol L}^{-1}$  DTT at  $71^\circ\text{C}$ . After the incubation, cells were allowed to cool on ice for 2 min. Cells were pelleted and washed one time in  $50 \text{ mmol L}^{-1}$  HEPES buffer and two times in PBS-T (PBS buffer with Tween 20 at 0.1% (v/v)). Blocking was carried out for 1 h in PBS-T containing 2% (w/v) bovine serum albumin (blocking solution) at RT. Cells were incubated with a 1:200 dilution of rabbit polyclonal anti-MsFtsZ peptide antibody and 1:200 dilution of guinea pig polyclonal anti-MsSepF antibody overnight at  $4^\circ\text{C}$  in blocking solution. Upon incubation with primary antibody samples were pelleted and washed three times in PBS-T, and incubated with a 1:500 dilution of secondary Alexa555-conjugated anti-rabbit for FtsZ and Alexa488-conjugated anti-

guinea pig for SepF (Invitrogen) in blocking solution for 1 h at RT. Unbound secondary antibody was removed by three washing steps in PBS-T. Finally, cells were resuspended in few  $\mu\text{L}$  of PBS and slides were prepared either for super resolution microscopy or epifluorescence microscopy (see below).

**Three-dimensional structured illumination microscopy (3D SIM) imaging and analysis.** Archaeal cell suspensions were applied on high precision coverslips (No. 1.5H, Sigma-Aldrich) coated with 0.01% (w/v) of Poly-L-Lysin. After letting the cells attach onto the surface of the coverslip for 10 min, residual liquid was removed,  $8 \mu\text{L}$  of antifade mounting medium (Vectashield) were applied and the coverslip was sealed to a slide. SIM was performed on a Zeiss LSM 780 Elyra PS1 microscope (Carl Zeiss, Germany) using C Plan-Apochromat  $63\times/1.4$  oil objective with a 1.518 refractive index oil (Carl Zeiss, Germany). The samples were excited with laser at 488 nm and 561 nm and the emission was detected through emission filter BP 495–575 + LP 750 and BP 570–650 + LP 750, respectively. The fluorescence signal was detected on an EMCCD Andor Ixon 887 1 K camera. Raw images are composed of fifteen images per plane per channel (five phases, three angles), and acquired with a Z-distance of  $0.10 \mu\text{m}$ . Acquisition parameters were adapted from one image to one other to optimize the signal to noise ratio. SIM images were processed with ZEN software (Carl Zeiss, Germany) and then corrected for chromatic aberration using  $100 \text{ nm}$  TetraSpeck microspheres (ThermoFisher Scientific) embedded in the same mounting media as the sample. The Fiji plugin SIMcheck was used to analyze the quality of the acquisition and the processing in order to exclude imaging artifacts<sup>47</sup>. The analysis was performed on the whole field of view imaged and results of the SIMcheck are shown in Supplementary table 3. For further image analysis of SIM image z stacks we used Fiji (ImageJ) Version 2.0.0-rc-68/1.52i. Namely, we assigned a color to the fluorescent channel, stacks were fused to a single image (z projection, maximum intensity), stacks were rotated  $90^\circ$  (resliced) prior z projection for the side view, and movies were created via 3D projection. Regions of interest were cut out and, for uniformity, placed on a black squared background. Figures were compiled using Adobe Illustrator 2020 (Adobe Systems Inc. USA).

**Morphometric and fluorescence measurements.**  $2 \mu\text{L}$  of immunolabelled *M. smithii* cells solution together with  $1 \mu\text{L}$  of Vectashield (Vector Labs) were applied to an 1% (w/v) agarose covered microscopy slide and imaged using a Zeiss Axioplan 2 microscope equipped with an Axiocam 503 mono camera (Carl Zeiss, Germany). Epifluorescence images were acquired using the ZEN lite software (Carl Zeiss, Germany) and processed using Fiji (ImageJ) Version 2.0.0-rc-68/1.52i in combination with plugin MicrobeJ Version 5.13.1. The cell outlines were traced and cell length, width, fluorescence intensity along the cell length and presence of fluorescent maxima were measured automatically. Automatic cell recognition was manually double-checked. For the mean fluorescence intensity plots cells were automatically grouped into four classes according to the detected FtsZ (0–3 fluorescent maxima detected; the data of 0 and 1 fluorescent maxima detected were pooled) and the corresponding FtsZ and SepF mean fluorescence intensity of each group was plotted against the normalized cell length. For the plots showing the relative position of detected maxima, cells were automatically grouped into four classes for SepF (1–4 fluorescent maxima detected) and three for FtsZ (1–3 fluorescent maxima detected). Both, fluorescence intensity and relative position of detected maxima plots were created in MicrobeJ, representative cells were chosen from bigger fields of few and their brightness and contrast were adapted in Fiji. Figures were compiled using and Illustrator 2020 (Adobe Systems Inc. USA).

**Sequence analysis.** The C-terminal domain was defined as the conserved regions flanking the 'GID' motif in Archaea and the 'PAFLR' motif in Bacteria. Noisy columns in the alignments were removed for clarity. Once defined, the C-terminal was realigned with MAFFT using the L-INS-i algorithm<sup>48</sup> and columns with  $>70\%$  gaps removed with trimAL<sup>49</sup>. WebLogos<sup>50</sup> correspond to alignments of 181 bacterial FtsZ, 117 FtsZ1 and 111 FtsZ2 from Archaea. The low number of well annotated FtsZ2 sequences made us further reduce redundancy of the bacterial dataset, for comparative purposes.

For structure-based SepF alignment, representative sequences from Bacteria and Archaea were manually chosen and aligned using T-Coffee<sup>51</sup>. Graphical representation was made using ENDscript server<sup>52</sup> and manually edited. For secondary structure prediction, sequences were aligned using MAFFT with the L-INS-i algorithm<sup>48</sup> and secondary structures were detected using Ali2D<sup>53</sup>. Figures were compiled using Illustrator 2020 (Adobe Systems Inc. USA).

**Distribution, phylogeny, and synteny analysis.** A customized local genome database was compiled for 362 Bacteria and 150 Archaea representative of all major phyla in NCBI (as of January 2020). The presence of FtsZ, FtsA, SepF and ESCRT-III (CdvB) homologs was assessed by performing HMM-based homology searches using custom made HMM models and the HMMER package<sup>54,55</sup> (default parameters). Separate searches were carried out with archaeal and bacterial queries and absences were checked with TBLASTN<sup>56</sup> or individual HMMER searches against all available taxa in NCBI corresponding to those phyla. Results were mapped onto the bacterial and archaeal reference phylogenies using iTOL<sup>57</sup>. The schematic reference phylogeny of Bacteria and Archaea is based on phylogenies constructed

by using a concatenation of RNA polymerase subunits B, B' and IF-2 in the case of Bacteria and of phyloSift markers (41 markers as in<sup>1</sup>) for the Archaea.

For phylogenetic analysis, FtsZ, FtsA and SepF homologs were aligned using MAFFT (L-INS-i algorithm)<sup>58</sup>. Columns with excess gaps (>80% for FtsA/SepF, >70% for FtsZ) were removed with trimAl<sup>49</sup>. Maximum likelihood trees were generated using IQ-TREE v1.6.7.2<sup>59</sup>, using the SH-aLRT branch test ('-alrt 1000' option) and the ultrafast bootstrap approximation<sup>60</sup> (option '-bb 1000') for branch supports. Exchangeability matrices and overall evolutionary models for each alignment were determined using ModelFinder<sup>61</sup>, with heterogeneity rates modeled with the gamma distribution (four rate categories, G4), or free-rate models (+R5 to +R9, depending on the protein). For the analysis of bacteria a subset of 190 taxa was used.

To carry out synteny analysis, for each archaeal genome, ten genes upstream and downstream *ftsZ1* and *ftsZ2* and *sepF* were extracted and the corresponding proteins were subjected to all-vs-all pairwise comparisons using BLASTP v2.6.0<sup>56</sup> with default parameters. From the output of the BLASTP search, protein families were assembled with SILX v1.2.951<sup>62</sup> with default parameters. HMM profiles were created for the families containing members of three or more archaeal lineages using the HMMER package<sup>55</sup>. The families were annotated manually by using BLASTP v2.6.0<sup>56</sup> and the Conserved Domain Database from NCBI<sup>63</sup>. MacSyFinder<sup>64</sup> was then used to identify, in each archaeal taxon, clusters containing at least three genes with a separation no greater than five other genes.

**Reporting summary.** Further information on research design is available in the Nature Research Reporting Summary linked to this article.

## Data availability

The crystallographic data is available from the Protein Data Bank ([www.rcsb.org](http://www.rcsb.org)), under the accession numbers 7AL1 and 7AL2 (PDB code, <https://doi.org/10.2210/pdb7AL1/pdb>; <https://doi.org/10.2210/pdb7AL2/pdb>). The data used for phylogenetic analysis and alignments is found here: <https://data.mendeley.com/datasets/pz8893jzgk/draft?as=5a5da375-729f-44b3-83a2-ca2adf6675d6>. All other data are available from the corresponding authors upon reasonable request. Source data are provided with this paper.

Received: 3 December 2020; Accepted: 15 April 2021;

Published online: 04 June 2021

## References

- Adam, P. S., Borrel, G., Brochier-Armanet, C. & Gribaldo, S. The growing tree of Archaea: new perspectives on their diversity, evolution and ecology. *ISME J.* **11**, 2407–2425 (2017).
- Spang, A., Caceres, E. F. & Ettema, T. J. G. Genomic exploration of the diversity, ecology, and evolution of the archaeal domain of life. *Science* **357**, eaaf3883 (2017).
- Baker, B. J. et al. Diversity, ecology and evolution of Archaea. *Nat. Microbiol.* **5**, 887–900 (2020).
- Borrel, G., Brugère, J. F., Gribaldo, S., Schmitz, R. A. & Moissl-Eichinger, C. The host-associated archaeome. *Nat. Rev. Microbiol.* 1–15 <https://doi.org/10.1038/s41579-020-0407-y> (2020).
- Samson, R. Y., Obita, T., Freund, S. M., Williams, R. L. & Bell, S. D. A role for the ESCRT system in cell division in archaea. *Science* **322**, 1710–1713 (2008).
- Lindås, A.-C., Karlsson, E. A., Lindgren, M. T., Ettema, T. J. G. & Bernander, R. A unique cell division machinery in the Archaea. *Proc. Natl Acad. Sci. USA* **105**, 18942–18946 (2008).
- Makarova, K. S., Yutin, N., Bell, S. D. & Koonin, E. V. Evolution of diverse cell division and vesicle formation systems in Archaea. *Nat. Publ. Gr.* **8**, 731 (2010).
- Duggin, I. G. et al. CetZ tubulin-like proteins control archaeal cell shape. *Nature* **519**, 362–365 (2015).
- Makarova, K. S. & Koonin, E. V. Two new families of the FtsZ-tubulin protein superfamily implicated in membrane remodeling in diverse bacteria and archaea. *Biol. Direct* **5**, 33 (2010).
- Liao, Y., Ithurbide, S., Löwe, J. & Duggin, I. G. Two FtsZ proteins orchestrate archaeal cell division through distinct functions in ring assembly and constriction. <https://doi.org/10.1101/2020.06.04.133736> (2020).
- Walsh, J. C. et al. Division plane placement in pleomorphic archaea is dynamically coupled to cell shape. *Mol. Microbiol.* **112**, 785–799 (2019).
- Poplawski, A., Gullbrand, B. & Bernander, R. The *ftsZ* gene of *Haloferax mediterranei*: Sequence, conserved gene order, and visualization of the FtsZ ring. *Gene* **242**, 357–367 (2000).
- Wang, X. & Lutkenhaus, J. FtsZ ring: the eubacterial division apparatus conserved in archaeobacteria. *Mol. Microbiol.* **21**, 313–320 (1996).
- Gérard, E., Labedan, B. & Forterre, P. Isolation of a minD-like gene in the hyperthermophilic archaeon *pyrococcus* AL585, and phylogenetic characterization of related proteins in the three domains of life. *Gene* **222**, 99–106 (1998).
- Nussbaum, P. et al. An oscillating MinD protein determines the cellular positioning of the motility machinery in archaea. <https://doi.org/10.1101/2020.04.03.021790> (2020).
- Hamoen, L. W., Meile, J. C., De Jong, W., Noirot, P. & Errington, J. SepF, a novel FtsZ-interacting protein required for a late step in cell division. *Mol. Microbiol.* **59**, 989–999 (2006).
- Ishikawa, S., Kawai, Y., Hiramatsu, K., Kuwano, M. & Ogasawara, N. A new FtsZ-interacting protein, YlmF, complements the activity of FtsA during progression of cell division in *Bacillus subtilis*. *Mol. Microbiol.* **60**, 1364–1380 (2006).
- Marbouty, M., Saguez, C., Cassier-Chauvat, C. & Chauvat, F. Characterization of the FtsZ-interacting septal proteins SepF and Ftn6 in the spherical-celled cyanobacterium *Synechocystis* strain PCC 6803. *J. Bacteriol.* **191**, 6178–6185 (2009).
- Gola, S., Munder, T., Casonato, S., Manganelli, R. & Vicente, M. The essential role of SepF in mycobacterial division. *Mol. Microbiol.* **97**, 560–576 (2015).
- Schlimpert, S. et al. Two dynamin-like proteins stabilize FtsZ rings during *Streptomyces* sporulation. *Proc. Natl Acad. Sci. USA* **114**, E6176–E6183 (2017).
- Sogues, A. et al. Essential dynamic interdependence of FtsZ and SepF for Z-ring and septum formation in *Corynebacterium glutamicum*. *Nat. Commun.* **11**, 1641 (2020).
- Duman, R. et al. Structural and genetic analyses reveal the protein SepF as a new membrane anchor for the Z ring. *Proc. Natl Acad. Sci. USA* **110**, E4601–E4610 (2013).
- König, H., Hartmann, E. & Kärcher, U. Pathways and principles of the biosynthesis of methanobacterial cell wall polymers. *Syst. Appl. Microbiol.* **16**, 510–517 (1993).
- Albers, S. V. & Meyer, B. H. The archaeal cell envelope. *Nat. Rev. Microbiol.* **9**, 414–426 (2011).
- Kok, J., Visweswaran, G. R. R. & Dijkstra, B. W. Two major archaeal pseudomurein endoisopeptidases: PeiW and PeiP. *Archaea* **2010**, 480492 (2010).
- Luo, Y., Pfister, P., Leisinger, T. & Wasserfallen, A. The genome of archaeal prophage  $\psi$ M100 encodes the lytic enzyme responsible for autolysis of *Methanothermobacter wolfeii*. *J. Bacteriol.* **183**, 5788–5792 (2001).
- Samson, R. Y., Dobro, M. J., Jensen, G. J. & Bell, S. D. The structure, function and roles of the archaeal ESCRT apparatus. *Subcell. Biochem* **84**, 357–377 (2017).
- Mura, A. et al. Roles of the essential protein FtsA in cell growth and division in *Streptococcus pneumoniae*. *J. Bacteriol.* **199**, 608–624 (2017).
- Nußbaum, P., Gerstner, M., Dingethal, M., Erb, C. & Albers, S.-V. The archaeal protein SepF is essential for cell division in *Haloferax volcanii*. *Nat Commun.* (in press).
- Mura, A. et al. Roles of the essential protein FtsA in cell growth and division in *Streptococcus pneumoniae*. *J. Bacteriol.* **199**, 608–624 (2017).
- Fleurie, A. et al. MapZ marks the division sites and positions FtsZ rings in *Streptococcus pneumoniae*. *Nature* **516**, 259–262 (2014).
- Aylett, C. H. S. & Duggin, I. G. The tubulin superfamily in archaea. *Subcell. Biochem* **84**, 393–417 (2017).
- Miyagishima, S.-Y., Nakamura, M., Uzuka, A. & Era, A. FtsZ-less prokaryotic cell division as well as FtsZ- and dynamin-less chloroplast and non-photosynthetic plastid division. *Front. Plant Sci.* **15**, 459 <https://doi.org/10.3389/fpls.2014.00459> (2014).
- Leaver, M., Domínguez-Cuevas, P., Coxhead, J. M., Daniel, R. A. & Errington, J. Life without a wall or division machine in *Bacillus subtilis*. *Nature* **457**, 849–853 (2009).
- Koonin, E. V. & Mulkidjanian, A. Y. Evolution of cell division: from shear mechanics to complex molecular machineries. *Cell* **152**, 942–944 (2013).
- Tocheva, E. I., Ortega, D. R. & Jensen, G. J. Sporulation, bacterial cell envelopes and the origin of life. *Nature* <https://doi.org/10.1038/nrmicro.2016.85> (2016).
- Taubner, R.-S. & Rittmann, S. K.-M. R. Method for indirect quantification of CH<sub>4</sub> production via H<sub>2</sub>O production using hydrogenotrophic methanogens. *Front. Microbiol.* **7**, 532 (2016).
- Nakamura, K. et al. Application of pseudomurein endoisopeptidase to fluorescence in situ hybridization of methanogens within the family Methanobacteriaceae. *Appl. Environ. Microbiol.* **72**, 6907–6913 (2006).
- Studier, F. W. Protein production by auto-induction in high density shaking cultures. *Protein Expr. Purif.* **41**, 207–234 (2005).
- Weber, P. et al. High-throughput crystallization pipeline at the crystallography core facility of the institut pasteur. *Molecules* **24**, 4451 (2019).
- Kabsch, W. et al. XDS. *Acta Crystallogr. Sect. D. Biol. Crystallogr.* **66**, 125–132 (2010).

42. Winn, M. D. et al. Overview of the CCP4 suite and current developments. *Acta Crystallogr. Sect. D: Biol. Crystallogr.* **67**, 235–242 (2011).
43. McCoy, A. J. et al. Phaser crystallographic software. *J. Appl. Crystallogr.* **40**, 658–674 (2007).
44. Emsley, P. & Cowtan, K. Coot: model-building tools for molecular graphics. *Acta Crystallogr. Sect. D: Biol. Crystallogr.* **60**, 2126–2132 (2004).
45. Smart, O. S. et al. Exploiting structure similarity in refinement: automated NCS and target-structure restraints in BUSTER. *Acta Crystallogr. Sect. D: Biol. Crystallogr.* **68**, 368–380 (2012).
46. Pettersen, E. F. et al. UCSF Chimera - a visualization system for exploratory research and analysis. *J. Comput. Chem.* **25**, 1605–1612 (2004).
47. Ball, G. et al. SIMcheck: a toolbox for successful super-resolution structured illumination microscopy. *Sci. Rep.* **5**, 1–12 (2015).
48. Katoh, K., Kuma, K., Toh, H. & Miyata, T. MAFFT version 5: improvement in accuracy of multiple sequence alignment. *Nucleic Acids Res.* **33**, 511–8 (2005).
49. Capella-Gutiérrez, S., Silla-Martínez, J. M. & Gabaldón, T. trimAl: a tool for automated alignment trimming in large-scale phylogenetic analyses. *Bioinformatics* **25**, 1972–1973 (2009).
50. Crooks, G. E., Hon, G., Chandonia, J. M. & Brenner, S. E. WebLogo: a sequence logo generator. *Genome Res.* **14**, 1188–1190 (2004).
51. Notredame, C., Higgins, D. G. & Heringa, J. T-coffee: A novel method for fast and accurate multiple sequence alignment. *J. Mol. Biol.* **302**, 205–217 (2000).
52. Robert, X. & Gouet, P. Deciphering key features in protein structures with the new ENDscript server. *Nucleic Acids Res.* **42**, W320–W324 (2014).
53. Zimmermann, L. et al. A completely reimplemented MPI bioinformatics toolkit with a new HHpred server at its core. *J. Mol. Biol.* **430**, 2237–2243 (2018).
54. Johnson, L. S., Eddy, S. R. & Portugaly, E. Hidden Markov model speed heuristic and iterative HMM search procedure. *BMC Bioinformatics* **11**, 431 (2010).
55. Eddy, S. R. Profile hidden Markov models. *Bioinformatics* **14**, 755–763 (1998).
56. Altschul, S. F. et al. Gapped BLAST and PSI-BLAST: a new generation of protein database search programs. *Nucleic Acids Res.* **25**, 3389–3402 (1997).
57. Letunic, I. & Bork, P. Interactive Tree of Life (iTOL) v4: recent updates and new developments. *Nucleic Acids Res.* **47**, (2019).
58. Katoh, K. & Standley, D. M. MAFFT multiple sequence alignment software version 7: Improvements in performance and usability. *Mol. Biol. Evol.* **30**, 772–780 (2013).
59. Nguyen, L.-T., Schmidt, H. A., von Haeseler, A. & Minh, B. Q. IQ-TREE: a fast and effective stochastic algorithm for estimating maximum-likelihood phylogenies. *Mol. Biol. Evol.* **32**, 268–74 (2015).
60. Minh, B. Q., Nguyen, M. A. T. & Von Haeseler, A. Ultrafast approximation for phylogenetic bootstrap. *Mol. Biol. Evol.* **30**, 1188–1195 (2013).
61. Kalyaanamoorthy, S., Minh, B. Q., Wong, T. K. F., Von Haeseler, A. & Jermini, L. S. ModelFinder: Fast model selection for accurate phylogenetic estimates. *Nat. Methods* **14**, 587–589 (2017).
62. Miele, V., Penel, S. & Duret, L. Ultra-fast sequence clustering from similarity networks with SiLiX. *BMC Bioinforma.* **12**, 116 (2011).
63. Lu, S. et al. CDD/SPARCLE: The conserved domain database in 2020. *Nucleic Acids Res.* **48**, D265–D268 (2020).
64. Abby, S. S., Néron, B., Ménager, H., Touchon, M. & Rocha, E. P. C. MacSyFinder: a program to mine genomes for molecular systems with an application to CRISPR-Cas systems. *PLoS One* **9**, e110726 (2014).

## Acknowledgements

This work was partially supported by grants from the Institut Pasteur (Paris), the CNRS (France) and the Agence Nationale de la Recherche (PhoCellDiv, ANR-18-CE11-0017-01 and ArchEvol, ANR-16-CE02-0005-01). N.P. is supported by a Pasteur-Roux Post-doctoral Fellowship from the Institut Pasteur (Paris). A.S. and D.M. are part of the Pasteur - Paris University (PPU) International PhD Program, funded by the European

Union's Horizon 2020 research and innovation program under the Marie Skłodowska-Curie grant agreement No 665807. M.G. thanks support from Programa de Desarrollo de las Ciencias Básicas (PEDECIBA) and Agencia Nacional de Investigación e Innovación (ANII), Uruguay. We thank A. Chenal for help with the lipid interaction studies. We gratefully acknowledge the core facilities at the Institut Pasteur C2RT, A. Haouz, P. Weber, C. Pissis (PFC). We thank the staff of the synchrotron SOLEIL for assistance and support in using beamlines PX1 and PX2. We thank A. Salle for help with the 3D SIM. We gratefully acknowledge the UTechS Photonic BioImaging (Imagopole), C2RT, Institut Pasteur (Paris, France) as well as the France-BioImaging infrastructure network supported by the French National Research Agency (ANR-10-INSB-04; Investments for the Future), and the Région Ile-de-France (program Domaine d'Intérêt Majeur-Malinf) for the use of the Zeiss LSM 780 Elyra PS1 microscope. We acknowledge technical assistance by Barbara Reischl.

## Author contributions

N.P. performed immunolabelling, epifluorescence microscope and 3D SIM imaging and image analysis. N.P. and A.S. conducted the protein biochemistry and purification for structural and biophysical studies. N.P. and A.S. carried out the biochemical and biophysical studies of protein-protein interactions. A.S. carried out binding studies of lipid membrane-protein interactions. D.M. and M.G. performed sequence and phylogenetic analyses. H.P. and S.K.-M.R.R. carried out PeiW purification and provided material. A.S. and P.M.A. carried out the crystallogenesis and crystallographic studies. A.M.W. and A.S.R. performed the negative stain EM studies. P.E. performed the SPR assay. N.P. and S.K.-M.R.R. performed statistical analysis. N.P., A.S. and D.M. made the figures. A.M.W., P.M.A. and S.G. supervised the work. N.P., A.S., A.M.W., P.M.A. and S.G. wrote the manuscript. All authors edited the final version of the manuscript.

## Competing interests

The authors declare no competing interests.

## Additional information

**Supplementary information** The online version contains supplementary material available at <https://doi.org/10.1038/s41467-021-23099-8>.

**Correspondence** and requests for materials should be addressed to A.M.W. or S.G.

**Peer review information** *Nature Communications* thanks the anonymous reviewers for their contribution to the peer review of this work. Peer reviewer reports are available.

**Reprints and permission information** is available at <http://www.nature.com/reprints>

**Publisher's note** Springer Nature remains neutral with regard to jurisdictional claims in published maps and institutional affiliations.



**Open Access** This article is licensed under a Creative Commons Attribution 4.0 International License, which permits use, sharing, adaptation, distribution and reproduction in any medium or format, as long as you give appropriate credit to the original author(s) and the source, provide a link to the Creative Commons license, and indicate if changes were made. The images or other third party material in this article are included in the article's Creative Commons license, unless indicated otherwise in a credit line to the material. If material is not included in the article's Creative Commons license and your intended use is not permitted by statutory regulation or exceeds the permitted use, you will need to obtain permission directly from the copyright holder. To view a copy of this license, visit <http://creativecommons.org/licenses/by/4.0/>.

© The Author(s) 2021



# ANNEX 9

Pages 163 to 174

---

Mauerhofer L.-M., Zwirtmayr S., Pappenreiter P., Bernacchi S., Seifert A. H., Reischl B.,  
Schmider T., Taubner R.-S., Paulik C., Rittmann S.K.-M.R.

**Hyperthermophilic methanogenic archaea act as high-pressure CH<sub>4</sub> cell factories**

Communications Biology (2021) 4(1):289

10.1038/s42003-021-01828-5

---

## Hyperthermophilic methanogenic archaea act as high-pressure CH<sub>4</sub> cell factories

Lisa-Maria Mauerhofer<sup>1</sup>, Sara Zwirtmayr<sup>2</sup>, Patricia Pappenreiter<sup>2</sup>, Sébastien Bernacchi<sup>3</sup>, Arne H. Seifert<sup>3</sup>, Barbara Reischl<sup>1,3</sup>, Tilman Schmider<sup>1</sup>, Ruth-Sophie Taubner<sup>1,2</sup>, Christian Paulik<sup>2</sup> & Simon K.-M. R. Rittmann<sup>1</sup>✉

Bioprocesses converting carbon dioxide with molecular hydrogen to methane (CH<sub>4</sub>) are currently being developed to enable a transition to a renewable energy production system. In this study, we present a comprehensive physiological and biotechnological examination of 80 methanogenic archaea (methanogens) quantifying growth and CH<sub>4</sub> production kinetics at hyperbaric pressures up to 50 bar with regard to media, macro-, and micro-nutrient supply, specific genomic features, and cell envelope architecture. Our analysis aimed to systematically prioritize high-pressure and high-performance methanogens. We found that the hyperthermophilic methanococci *Methanoterris igneus* and *Methanocaldococcus jannaschii* are high-pressure CH<sub>4</sub> cell factories. Furthermore, our analysis revealed that high-performance methanogens are covered with an S-layer, and that they harbour the amino acid motif Tyr<sup>α444</sup> Gly<sup>α445</sup> Tyr<sup>α446</sup> in the alpha subunit of the methyl-coenzyme M reductase. Thus, high-pressure biological CH<sub>4</sub> production in pure culture could provide a purposeful route for the transition to a carbon-neutral bioenergy sector.

<sup>1</sup>Archaea Physiology & Biotechnology Group, Department Functional and Evolutionary Ecology, Universität Wien, Wien, Austria. <sup>2</sup>Institute for Chemical Technology of Organic Materials, Johannes Kepler Universität Linz, Linz, Austria. <sup>3</sup>Krajete GmbH, Linz, Austria. ✉email: [simon.rittmann@univie.ac.at](mailto:simon.rittmann@univie.ac.at)

Methane ( $\text{CH}_4$ ) is an energy carrier of worldwide importance. It can be produced through biogenic, thermogenic, and pyrogenic processes<sup>1</sup>. Most biogenic  $\text{CH}_4$  is emitted by methanogenic archaea (methanogens)<sup>2</sup>, with minor amounts originating from cyanobacteria<sup>3</sup> and marine microorganisms<sup>4</sup>. Methanogens are a phylogenetically diverse group of microorganisms, which can be found in various anoxic environments<sup>5</sup>. Among other substrates, methanogens convert short chain organic acids and one-carbon compounds to  $\text{CH}_4$  through their energy and carbon metabolism<sup>2,5,6</sup>. Their metabolic capability is important for anaerobic organic matter degradation in environments with low concentrations of sulfate, nitrate, manganese, or iron<sup>5</sup>. Moreover, methanogens are of biotechnological relevance due to their ability to produce isoprenoid-containing lipids<sup>7,8</sup> or polyphosphate<sup>9</sup>, and were recently described to excrete proteinogenic amino acids<sup>8</sup>. Methanogens are central to biofuels production, as they can be employed as autocatalysts for carbon dioxide ( $\text{CO}_2$ ) and molecular hydrogen ( $\text{H}_2$ ) conversion in the  $\text{CO}_2$ -based biological  $\text{CH}_4$  production ( $\text{CO}_2$ -BMP) process.

The  $\text{CO}_2$ -BMP process can be employed in multiple applications such as biogas upgrading, power-to-gas applications, decentralized energy production, and for the conversion of  $\text{H}_2/\text{CO}_2$  of process flue gasses in waste to value concepts from, e.g., ethanol, petroleum, steel, and chemical industries<sup>10</sup>. There are two main approaches for  $\text{CO}_2$ -BMP<sup>11</sup>: ex situ biomethanation using pure cultures<sup>12,13</sup> or enriched mixed cultures<sup>14–16</sup>, and in situ biomethanation<sup>17,18</sup>. In situ biomethanation is examined for upgrading the  $\text{CH}_4$  content of biogas by adding  $\text{H}_2$  to anaerobic digesters. Ex situ pure culture biomethanation exhibits high volumetric  $\text{CH}_4$  productivity and offers a straightforward bioprocess control by utilizing biochemically and biotechnologically well-characterized microorganisms in pure culture<sup>12</sup>. Among the most studied organisms in this regard is *Methanothermobacter marburgensis*<sup>12,19</sup>, exhibiting several advantageous traits such as flexibility with regard to substrate gas impurities<sup>10</sup> and high  $\text{CH}_4$  productivity<sup>20</sup>. In addition, *M. marburgensis* can be used for  $\text{CO}_2$ -BMP when short-term transitions in the order of minutes are demanded between stand-by to full load biomethanation. Furthermore, downtime periods above 500 h did not reduce  $\text{CH}_4$  productivity after a process restart<sup>21</sup>.

Compared to  $\text{CO}_2$ -BMP, chemical methanation or the “Sabatier reaction” should not be operated intermittently due to various catalytic constraints<sup>22</sup> and the fast bulk-like oxidation of the nickel catalyst in the  $\text{CO}_2$  atmosphere<sup>23</sup>. Furthermore, activity loss of the chemical catalyst after a certain lifespan necessitates the exchange of the catalyst and the carrier material leading to periodic downtimes in production. Thus, applying methanogens, which are autocatalysts, offers numerous advantages compared to a chemically catalyzed  $\text{CO}_2$  methanation. The lower power demand and the stable selectivity observed in  $\text{CO}_2$ -BMP compared to chemical methanation<sup>22</sup> strongly suggest that  $\text{CO}_2$ -BMP is a viable biotechnological alternative to chemical methanation. However, the autocatalytic characteristics of methanogens require further investigation.

The  $\text{CO}_2$ -BMP bioprocess can be operated as a gas transfer limited process<sup>12</sup> when a proper feeding strategy is applied<sup>24</sup>. In this case, the kinetic limiting step is the mass transfer of  $\text{H}_2$  to the liquid phase. In biochemical engineering, gas to liquid mass transfer can be enhanced by several technical measures<sup>20</sup>. Besides reactor geometry and agitation, which influence the specific mass transfer coefficient ( $k_{\text{La}}$ ), pressure increases the solubility of  $\text{H}_2$  in the liquid phase. The influence of pressure on substrate uptake, growth, and production kinetics of methanogens is therefore an important parameter in  $\text{CO}_2$ -BMP. Some experiments with *Methanocaldococcus jannaschii* have already been performed at high pressure in order to investigate transcription profiles<sup>25</sup> or

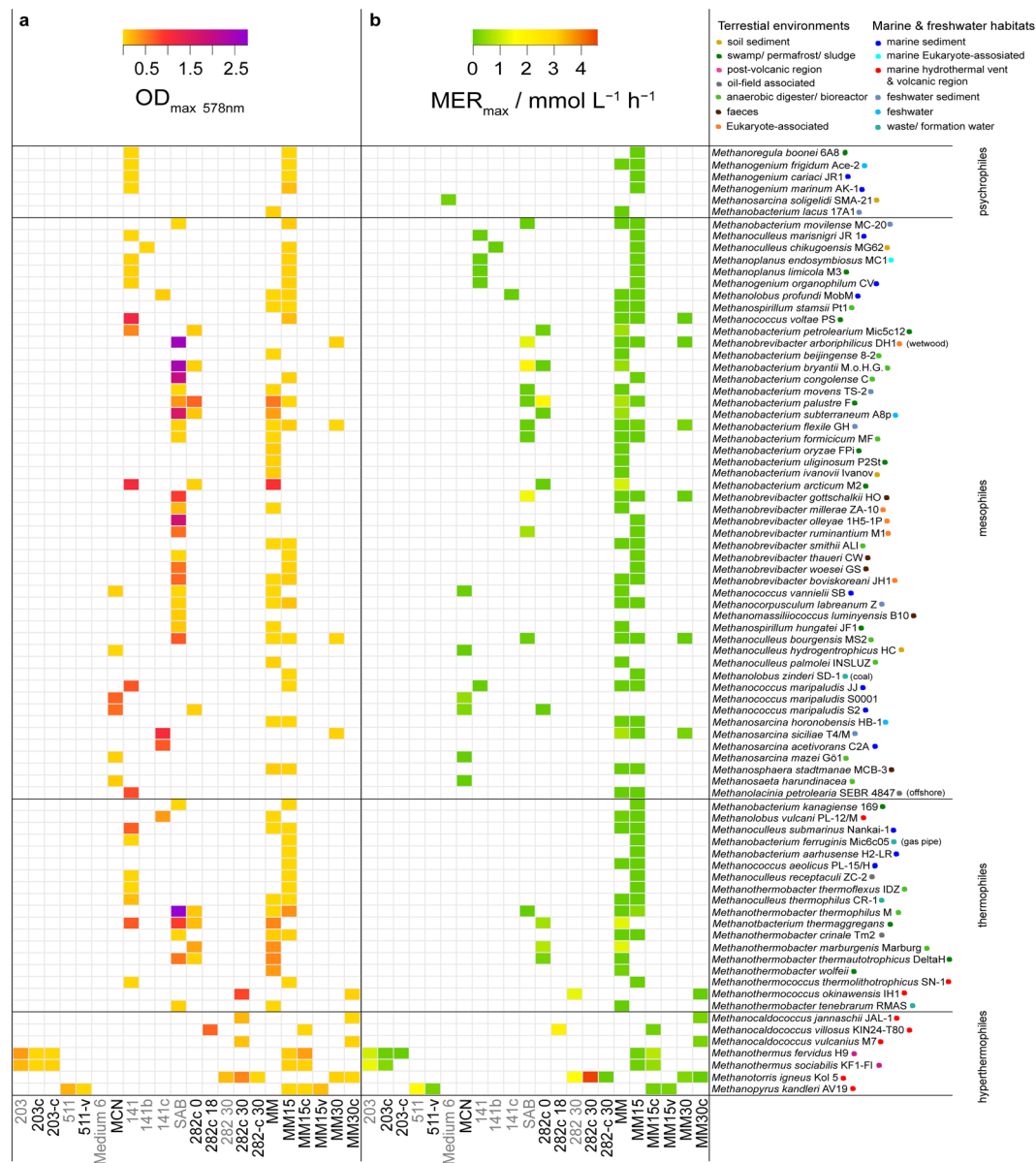
growth and  $\text{CH}_4$  production<sup>26</sup>. The effect of pressure on  $\text{CH}_4$  production has also been examined in bioreactors<sup>20,27</sup>, while media for cultivation of methanogens have been developed and their growth assessed<sup>28–31</sup>. However, a systematic biotechnological survey with regard to nutritional demands of methanogens across different temperature regimes in the same cultivation conditions and at different pressure levels has not yet been the focus of any study.

On the way to develop a high-pressure pure culture  $\text{CH}_4$  production bioprocess, we systematically and quantitatively investigated the productivity of methanogens at pressures up to 50 bar. Growth, conversion, and  $\text{CH}_4$  productivity were first examined in order to identify cell factories with the highest  $\text{CH}_4$  productivity among 80 methanogens, in a range of different media (in terms of composition and medium amendments) and in conditions ranging from psychrophilic to hyperthermophilic. Secondly, the 14 prioritized fastest growing and with the highest productivity methanogens were investigated using a high frequency gassing (HFG) experiment and by using 10 bar  $\text{H}_2/\text{CO}_2$  to  $\text{CH}_4$  conversion experiments. Among these 14 methanogens, four strains were chosen for the third step, consisting of 50 bar  $\text{H}_2/\text{CO}_2$  to  $\text{CH}_4$  conversion experiments. Finally, we analyzed these results in the context of their natural habitat, temperature optima, specific genomic features, and their cell envelope architecture.

## Results

**High-throughput screening revealed high-performance methanogens.** In order to investigate essential macro- and micro-nutrient growth medium amendments of methanogens in the context of their physiology and  $\text{CH}_4$  productivity in a systematic and quantitative physiological approach, a multivariate high-throughput screening of 80 methanogens on various media and medium amendments was performed (Fig. 1 and Supplementary Figs. S1 and S2). This multivariate high-throughput screening was conducted on 22 complex and defined media in order to characterize methanogens from psychrophilic, mesophilic, thermophilic, and hyperthermophilic temperature groups with regard to maximum biomass and  $\text{CH}_4$  production kinetics in a closed batch setting, with initially 2 bar  $\text{H}_2/\text{CO}_2$  (4:1) in the headspace. Maximum optical density ( $\text{OD}_{\text{max}}$ ), maximum substrate conversion ( $\text{turnover}_{\text{max}}$ ), and maximum volumetric  $\text{CH}_4$  evolution rate ( $\text{MER}_{\text{max}}$ ) were selected as experimental output variables. To elucidate if the chosen methanogens showed a homogenous or heterogenous growth pattern which would indicate a balanced or unbalanced biomass increase<sup>32</sup>, respectively, the biomass increase rate (“Material and Methods”, Eq. (1)) was used for comparing growth kinetics.

All tested psychrophilic methanogens grew to an  $\text{OD}_{\text{max}}$  of below 0.2, showed  $\text{turnover}_{\text{max}}$  lower than 40%, and exhibited a very low  $\text{MER}_{\text{max}}$  of only up to  $0.1 \text{ mmol L}^{-1} \text{ h}^{-1}$  on complex or defined media. Mesophilic methanogens grew heterogeneously when cultivated on complex and/or defined media. Biomass growth to an  $\text{OD}_{\text{max}}$  beyond 1.0, a  $\text{turnover}_{\text{max}}$  over 70%, and a  $\text{MER}_{\text{max}}$  higher than  $1.0 \text{ mmol L}^{-1} \text{ h}^{-1}$  at cultivation temperatures between 35 and 37 °C on complex media were measured. Growth of moderate thermophilic methanogens between 40 and 45 °C resulted in an  $\text{OD}_{\text{max}}$  between 0.3 and 0.7 on complex media, while on defined media only an  $\text{OD}_{\text{max}}$  of 0.003–0.025 was obtained. Growth of thermophilic methanogens (60–65 °C) resulted in an  $\text{OD}_{\text{max}}$  range from 0.4 to 0.8, a  $\text{turnover}_{\text{max}}$  between 75 and 96% and a  $\text{MER}_{\text{max}}$  beyond  $1.0 \text{ mmol L}^{-1} \text{ h}^{-1}$ . Hyperthermophilic growth between 80 and 98 °C resulted in an  $\text{OD}_{\text{max}}$  between 0.2 and 0.7, a  $\text{turnover}_{\text{max}}$  from 83 to 97% and a  $\text{MER}_{\text{max}}$  ranging from 1.0 to  $4.6 \text{ mmol L}^{-1} \text{ h}^{-1}$  (Fig. 1 and Supplementary Fig. S2). Most methanogens showed a



**Fig. 1 Biomass and CH<sub>4</sub> production kinetics of the multivariate prescreen of 80 methanogens in defined and complex media.** Experiments were performed in closed batch cultivation systems at 2 bar (120 mL flasks, 50 mL medium). On the y-axis, methanogens were arranged as groups according to their temperature optimum in psychrophiles, mesophiles, thermophiles, or hyperthermophiles. Methanogens are listed with ascending strain-specific temperature optimum from top to bottom. Coloured points next to the strain designation on the y-axis indicate the isolation site of the tested methanogen (terrestrial habitats: golden brown—soil sediment, dark green—swamp/permafrost/sludge, pink—post-volcanic region, gray—oil-field associated, light green—anaerobic digester/bioreactor, brown—feces, orange—eukaryote-associated; marine and freshwater environments: bright blue—marine sediment, turquoise—marine eukaryote-associated, red—marine hydrothermal vent and volcanic region, gray blue—freshwater sediment, sky blue—freshwater, green blue—waste/formation water). In total, 22 defined and complex media were tested, but not every strain was cultivated on every medium. Defined and complex media are shown on the x-axis in black and gray fonts, respectively. For each closed batch cultivation, three biological replicates (in some cases, two biological replicates) plus one negative control were used. **a** The maximum absorption is shown as OD<sub>max</sub> at 578 nm, and **b** the maximum volumetric CH<sub>4</sub> production rate is shown as MER<sub>max</sub> / mmol L<sup>-1</sup> h<sup>-1</sup>.

homogenous growth pattern and a biomass increase rate below 10 (Supplementary Fig. S1). Interestingly, mesophilic methanogens grown on SAB (complex medium) showed a biomass increase rate between 10 and 40 (Supplementary Fig. S1).

**Correlating nutritional demands, growth, and CH<sub>4</sub> productivity.** In order to correlate nutritional demands to associated growth, substrate conversion, and productivity, a standardized principal component analysis (PCA) and subsequent k-means

cluster analysis was performed. The cluster analysis was performed for OD<sub>max</sub>, turnover<sub>max</sub>, MER<sub>max</sub>, and the combination of those variables together with the concentrations of sulfate and/or sulfur, ammonium, phosphate, and cysteine in the respective media. These data were then linked to strain-specific information such as taxonomy and cultivation temperature. Further, medium-associated parameters were used for interpretation, such as the applied medium with the corresponding trace element solution (TES), and the addition of vitamin solution (VS), cysteine, and yeast/peptone to the medium. The clustering approach then

enabled the grouping of the mentioned variables and parameters into clusters.

High OD values were achieved on complex medium with VS, cysteine, and yeast extract/peptone (Supplementary Data 1, Table S1 and Supplementary Fig. S3). Mesophilic strains *Methanococcus* spp., *Methanobacterium* spp., and thermophilic methanogens belonging to the genera *Methanothermobacter* and *Methanobacterium* grew on defined media without vitamins and cysteine (MM medium, Fig. 1 and Supplementary Data 1, Table S1). At least 50% reduction of OD<sub>max</sub> was observed with strains that grew best on MM medium when cultivated on 282c 0 medium (rich-TE and cysteine addition), except for *Methanobacterium palustre*. This strain showed similar growth on MM and 282c 0 medium indicated by an OD<sub>max</sub> of 0.53 and 0.66. *M. palustre* also showed higher CH<sub>4</sub> production kinetics on 282c 0 medium compared to MM medium, indicated by a turnover<sub>max</sub> up to 93% and a 2.6-fold higher MER<sub>max</sub> of 1.9 mmol L<sup>-1</sup> h<sup>-1</sup> in 282c 0 medium (Fig. 1 and Supplementary Data 1, Table S2). Methanogens that require supplements (VS or cysteine) in the media, like *Methanopyri* or *Methanococci*, reached OD<sub>max</sub> values between 0.2 and 0.8.

The highest turnover was achieved by methanogens grown in defined media. *Methanococci* and *Methanobacteria* showed a turnover<sub>max</sub> between 90 and 98% on medium 203 and 282-based media (Supplementary Data 1, Table S3, and Supplementary Fig. S4). A turnover<sub>max</sub> between 80 and 90% was achieved on media MM, MCN, SAB, and 511. The highest turnover<sub>max</sub> values (90–98%) were obtained in a medium with 30 times lower phosphate concentration and five times lower ammonium concentration compared to the media used in the turnover<sub>max</sub> range 80–90% (Supplementary Data 1, Table S3, and Supplementary Fig. S4), which might indicate that phosphate and ammonium concentrations in the medium need optimization.

*Methanococci*, *Methanobacteria*, and *Methanopyri* were found to be highly productive in a closed batch cultivation mode at 2 bar, indicated by a MER<sub>max</sub> range from 1.1 to 4.6 mmol L<sup>-1</sup> h<sup>-1</sup> (Supplementary Data 1, Table S4, and Supplementary Fig. S5). These methanogens grew on 282, MM-based media, 511, SAB, and 203 media. The highest MER<sub>max</sub> values of 2.1 and 4.6 mmol L<sup>-1</sup> h<sup>-1</sup> were achieved by *Methanococci* on 282-based media without yeast/peptone and the addition of cysteine (cluster 1, Supplementary Data 1, Table S4, and Supplementary Fig. S5). The highest MER<sub>max</sub> of 4.61 mmol L<sup>-1</sup> h<sup>-1</sup> was measured for *Methanotorris igneus*. *Methanococci* showed the highest turnover<sub>max</sub> and MER<sub>max</sub> values (Supplementary Figs. S4–S6, Supplementary Data 1, and Table S5), assuming that growth and CH<sub>4</sub> productivity is positively influenced by sulfate, sulfur, and cysteine.

On defined medium without cysteine (MM-based and MCN medium), mesophilic methanogens from the order *Methanobacteria*, *Methanomicrobia*, and *Methanococci* (with the exception of *Methanothermobacter fervidus*) reached a MER<sub>max</sub> range of 0.5 to 1.0 mmol L<sup>-1</sup> h<sup>-1</sup> (Supplementary Data 1 and Table S4). Strains isolated from hyperthermophilic environments (Fig. 1) like *Methanocaldococcaceae* and *Methanopyraceae* required cysteine or vitamins in the medium to exhibit high MERs (282-based and 511 media). They showed growth to an OD<sub>max</sub> < 0.03, and a turnover<sub>max</sub> and MER<sub>max</sub> reduction of 90% and 95%, respectively, when cysteine or vitamins were excluded from the media (282-c 30, 511-v, Fig. 1). Attempts to restore the MER of *Methanocaldococcus* spp., *Methanothermococcus* sp., *Methanothermobacter* sp., and *Methanopyrus* sp. on MM medium at their optimum salt concentration through the addition of cysteine or vitamins after they had been grown in media without these compounds did not recover their CH<sub>4</sub> productivity, except for *M. fervidus*. This organism showed an OD<sub>max</sub> of 0.34 on 203 and MM15c medium. However, the productivity of *M. fervidus* on medium MM15c was

decreased compared to 203 medium, indicated by a MER<sub>max</sub> of 0.9 and 1.1 mmol L<sup>-1</sup> h<sup>-1</sup> (Fig. 1, Supplementary Data 1, and Table S1).

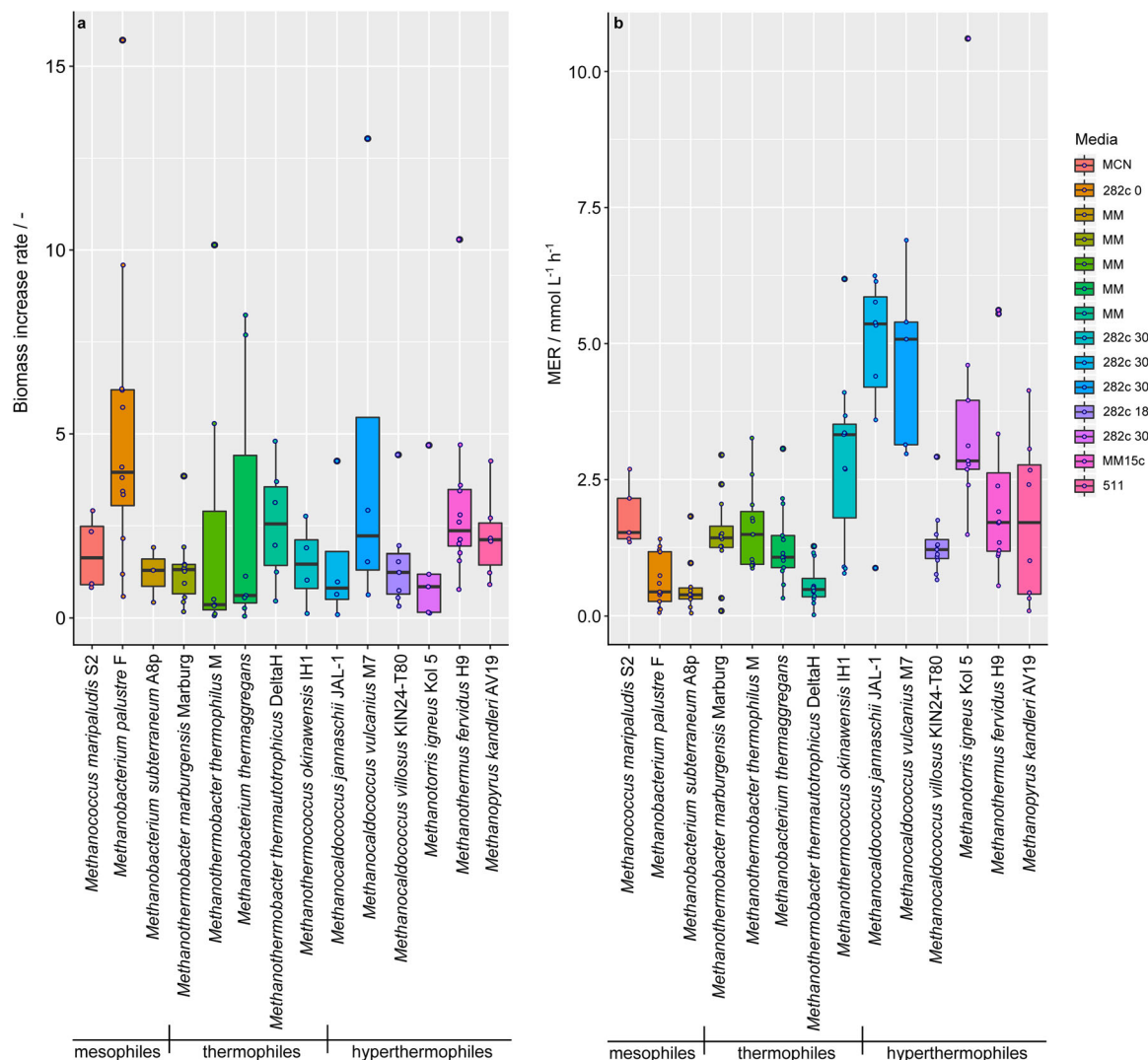
From this comprehensive multivariate, quantitative analysis of growth and CH<sub>4</sub> production kinetics, we prioritized *Methanobacterium* spp. and *Methanococcus* sp. (mesophilic), *Methanothermobacter* spp., *Methanobacterium* sp., and *Methanothermococcus* sp. (thermophilic), and *Methanocaldococcus* spp., *Methanothermobacter* sp., and *Methanopyrus* sp. (hyperthermophilic) for the subsequent 10 bar H<sub>2</sub>/CO<sub>2</sub> conversion experiments. These methanogens were selected due to their ability to grow fast on defined media (cluster 1 and 3 in Supplementary Data 1, Table S2, and Supplementary Fig. S3), and their successful reactivation after dormancy (Supplementary Table S1). Prioritized high-performance methanogens showed a turnover<sub>max</sub> > 70% (cluster 1, 2, and 4 in Supplementary Data 1, Table S3, and Supplementary Fig. S4) and 90% of the strains exhibited a MER<sub>max</sub> > 1 mmol L<sup>-1</sup> h<sup>-1</sup> (cluster 1, 3, and 4 in Supplementary Data 1, Table S4, and Supplementary Fig. S5).

**Identification of high-performance methanogens.** The multivariate quantitative comparative investigation resulted in the prioritization of 14 fast converting and/or fast growing autotrophic hydrogenotrophic methanogens (Fig. 2). Prioritized methanogens belong to Class I methanogens<sup>26</sup>. In a closed batch cultivation system, gas-utilizing methanogens experience extreme gas-limiting conditions, as the substrate (gas in the headspace of the cultivation vessel) is converted at a decreasing rate<sup>27</sup>. To reduce the effect of gas-limiting conditions for fast converting methanogens during closed batch cultivation, HFG experiments were conducted. During HFG experiments the headspace of the serum bottle was replenished with H<sub>2</sub>/CO<sub>2</sub> before turnover<sub>max</sub> was reached. Thus, we found that the mesophilic methanogen *Methanococcus maripaludis* and the hyperthermophilic methanogens *M. jannaschii* and *Methanocaldococcus vulcanius* showed a turnover rate > 5 h<sup>-1</sup> (Supplementary Fig. S7). Furthermore, HFG experiments enabled a quantitative and comparative analysis of MERs and biomass increase rates among prioritized methanogens (Fig. 2).

The biomass increase rates of *M. palustre*, *Methanothermobacter thermophilus*, *Methanobacterium thermaggregans*, and *M. vulcanius* varied, indicating a heterogeneous growth pattern (Fig. 2a). Based on the position of the median in the boxplot figures (Fig. 2a), we could observe that *M. thermophilus* and *M. thermaggregans* have a longer lag phase compared to the other tested methanogens. All other strains showed little variation regarding the biomass increase rates, indicating that these strains had a homogenous growth pattern under the tested conditions (Fig. 2a). *M. vulcanius* and *M. jannaschii* showed a MER median value > 5 mmol L<sup>-1</sup> h<sup>-1</sup>, which is 1.5-fold the amount compared to *Methanothermococcus okinawensis* and twice the amount of *M. igneus* as well as approximately four times higher compared to the other tested methanogens (Fig. 2b).

**Methanogens with a surface protein layer are CH<sub>4</sub> cell factories.** The highest MERs were observed for hyperthermophilic methanogens that grow within a temperature range of 80–85 °C on defined medium 282c 30 and known to possess a surface protein layer (S-layer)<sup>33,34</sup>. These S-layer proteins harbor the InterPro domains IPR022651 S\_layer\_C, IPR006454 S\_layer\_MJ, and IPR022650 S\_layer\_N (Supplementary Data 2). Furthermore, *M. fervidus* is covered with an S-layer protein (slgA in a p6 lattice pattern)<sup>35</sup>. The slgA consists of six InterPro features, IPR006633 Carb-bd\_sugar\_hydrolysis-dom, IPR007742 NosD-dom, IPR022441 Para\_beta\_helix\_rpt-2, IPR006626 PbH1,





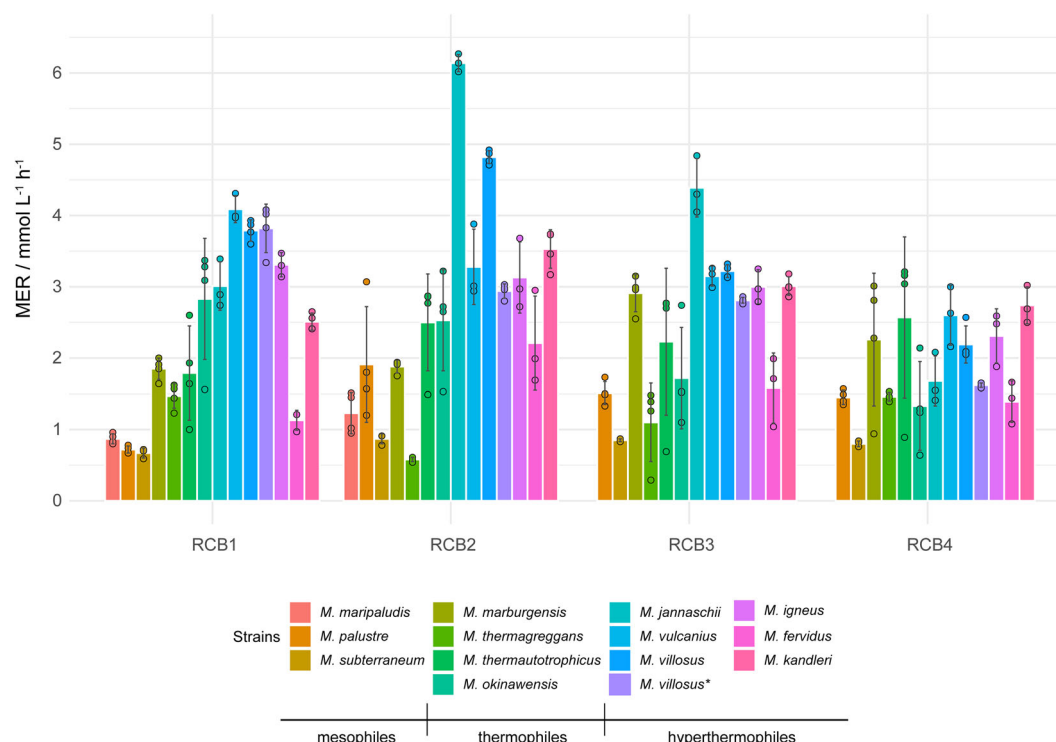
**Fig. 2 Results of high frequency gassing (HFG) experiments of prioritized methanogens at 2 bar in defined medium.** All experiments were performed in quadruplicates including a negative control. **a** The biomass increase rate/- and **b** The MER / mmol L<sup>-1</sup> h<sup>-1</sup>. Boxplots are used for data visualization. In both subfigures, three temperature blocks are distinguished and highlighted from left to right. Left block: mesophilic methanogens grown at 37 °C (*Methanococcus maripaludis* S2, *Methanobacterium palustre* F, *Methanobacterium subterraneum* A8p); middle block: five thermophilic strains grown at 65 °C (*Methanothermobacter marburgensis* Marburg, *Methanothermobacter thermophilus* M, *Methanobacterium thermaggregans*, *Methanothermobacter thermautotrophicus* DeltaH, *Methanothermococcus okinawensis* IH1); right block: six hyperthermophilic methanogens (*Methanocaldococcus jannaschii* JAL-1 (80 °C), *Methanocaldococcus vulcanius* M7 (80 °C), *Methanocaldococcus villosus* KIN24-T80 (80 °C), *Methanotortrix igneus* Kol 5 (85 °C), *Methanothermobacter fervidus* H9 (80 °C), *Methanopyrus kandleri* AV19 (98 °C)).

IPR012334 Pectin\_lyas\_fold, IPR011050 Pectin\_lyase\_fold/virulence as well as the Pfam motif PF05048 NosD. The same motifs can be found in the genomes of *M. marburgensis* and *M. thermautotrophicus* (Supplementary Data 2). This might be an indication for the presence of S-layers on the cell envelop of *M. marburgensis* and *M. thermautotrophicus*. However, up to now S-layers were never described for these organisms, and the function of these homologous proteins would therefore require characterization. Furthermore, the IPR032812, IPR013783 Ig-like\_fold, and IPR032812 SbsA\_Ig features can be found in the genome of *M. marburgensis*, with the later Ig-like domain present in the S-layer protein SbsA. While *M. thermautotrophicus* does not harbor an IPR032812 SbsA\_Ig feature, it encodes an IPR013783 Ig-like\_fold feature, a motif which was also detected in *M. vulcanius* and *M. villosus*. *M. kandleri* was shown earlier to possess a S-layer<sup>36</sup>, although no S-layer related motifs or domains could be found in our in silico analysis (Supplementary Data 2), but the

IPR011330 Glyco\_hydro/deAcase\_b/a-brl and IPR002509 NODB\_dom features were detected.

**High-performance methanogens harbor a specific MCRA amino acid motif.** A subsequent bioinformatic examination of the key enzyme for methanogenesis, methyl-coenzyme M reductase (MCR), and especially the alpha subunit of the MCR (MCRA) revealed that all highly productive prioritized methanogens harbor the Tyr<sup>a444</sup> Gly<sup>a445</sup> Tyr<sup>a446</sup> amino acid motif and belong to the Class I methanogens (Supplementary Fig. S8). Borrel et al. showed that Tyr<sup>a444</sup> is substituted to phenylalanine in some *Methanocella* spp., *Methanoregula* spp., *Methanocorpusculum* spp., and *Methanosarcina* spp.<sup>37</sup>. We found that Tyr<sup>a444</sup> to Phe<sup>a444</sup> is specific to Class II methanogens, except to *Methanomicrococcus blatticola* and *Methanolinea tarda* (Supplementary Fig. S8). In Class I methanogens, Tyr<sup>a444</sup> anchors the coenzyme





**Fig. 3 Results of high-pressure RCB cultivations of prioritized methanogens in the simultaneous bioreactor system (SBRs) at 10 bar.** All experiments were performed in quadruplicates in the SBRs system at a gassing ratio of  $H_2/CO_2$  (4:1)<sup>35</sup>. Mean and standard deviation are shown. The principle of the cultivation was to repressurize each of the bioreactors to 10 bar after full headspace gas conversion. RCB1, RCB2, RCB3, and RCB4 indicate results from individual and successive closed batch headspace gas conversions. MER /  $mmol L^{-1} h^{-1}$  is shown. The left block indicates mesophilic methanogens grown at 37 °C (*Methanococcus maripaludis* S2, *Methanobacterium palustre* F, *Methanobacterium subterraneum* A8p); the middle block shows the thermophilic methanogens grown at 65 °C (*Methanothermobacter marburgensis* Marburg, *Methanobacterium thermaggregans*, *Methanothermobacter thermautotrophicus* DeltaH, *Methanothermobacter okinawensis* IH1); and the right block shows hyperthermophilic methanogens (*Methanocaldococcus jannaschii* JAL-1 (80 °C), *Methanocaldococcus vulcanius* M7 (80 °C), *Methanocaldococcus villosus* KIN24-T80 (80 °C), *Methanocaldococcus villosus* KIN24-T80\*-grown on 282c 18\_E medium (80 °C), *Methanoterris igneus* Kol 5 (85 °C), *Methanothermobacter fervidus* H9 (80 °C), *Methanopyrus kandleri* AV19 (98 °C)).

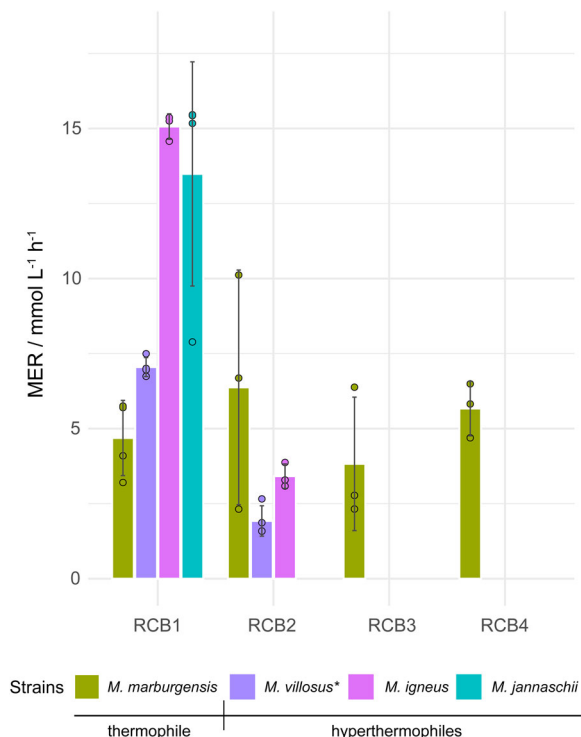
M together with two other amino acid residues in the catalytic center of the MCR<sup>38</sup>. Additionally, Tyr<sup>a446</sup> is predominately exchanged to phenylalanine in *Methanosarcinaceae*, *Methanosarcina* spp.<sup>37</sup>, *Methanohalophilus* spp., *Methanohalobium* sp., *Methanococcoides* spp., *Methanobrevibacter* spp., and *Methanomethylovorans* sp.. Moreover, we found an amino acid exchange from Tyr<sup>a446</sup> to Phe<sup>a446</sup> in some *Methanobrevibacter* spp..

***M. igneus* and *M. jannaschii* are high-pressure  $CH_4$  cell factories.** High-pressure cultivation of methanogens offers an opportunity to improve the gas transfer rate of substrate gases into the liquid phase. In order to investigate the gas conversion kinetics and the barotolerance of applied methanogens, high-pressure experiments were designed to examine the MER<sub>max</sub> and conversion kinetics, including the turnover rate and the maximum conversion rate ( $k_{min}/bar h^{-1}$ ) at a hyperbaric pressure of 10 and 50 bar in the simultaneous bioreactor system (SBRs)<sup>39</sup>.

Four subsequent repetitive closed batch (RCB) experiments were performed by flushing and replenishing the SBRs headspace after reaching turnover<sub>max</sub> (Supplementary Figs. S9 and S10). After adaptation to hyperbaric conditions in RCB1, ten of the 14 prioritized methanogens achieved MER<sub>max</sub> and turnover rates in RCB2 (Fig. 3 and Supplementary Fig. S10). The MERs of *M. jannaschii* indicated a putative liquid limitation already in RCB2. Seven methanogens showed similar MERs and turnover rates in RCB3 and RCB4, probably as a result of limitation of the liquid substrates. Half of the tested strains showed an enhanced MER, when comparing 2 bar HFG and 10 bar RCB experiments (Figs. 2

and 3). In general, a fivefold higher pressure lead to an average MER increase of  $2.2 \pm 0.9 mmol L^{-1} h^{-1}$ . Some methanogens showed an average MER fold decrease of  $0.6 \pm 0.1 mmol L^{-1} h^{-1}$ , which might indicate a pressure sensitivity or could have been due to a potentially low pH present at hyperbaric conditions, since higher pressure in the cultivation vessel results in a higher soluble  $CO_2$ , which lowers the pH<sup>40</sup>.

The highest MERs of  $6.14 \pm 0.12 mmol L^{-1} h^{-1}$  and  $4.39 \pm 0.41 mmol L^{-1} h^{-1}$  were achieved by *M. jannaschii* in RCB2 and RCB3, respectively, even without growth medium optimization. Besides MER and turnover rate, the parameter  $k_{min}$  (Supplementary Fig. S11), derived from the maximum negative slope of the pressure curves (Supplementary Fig. S9), indicates the time point of MER<sub>max</sub>.  $k_{min}$  was therefore used to unambiguously identify the most productive strains and prioritize them for the subsequent 50 bar cultivations. These strains were *M. jannaschii*, *M. igneus*, *M. villosus* (using 282c 18\_E medium), and *M. marburgensis*. The  $CO_2$ -BMP model organism *M. marburgensis* was successfully cultivated at 50 bar without facing liquid limitations (Fig. 4). *M. thermaggregans*, which is a high  $CH_4$  productivity strain in fed-batch cultivation mode<sup>13</sup>, did not grow at 50 bar (Supplementary Fig. S12) and *M. villosus* and *M. igneus* showed a decrease of MER and turnover rate directly in RCB2 (Fig. 4 and Supplementary Fig. S13), indicating a liquid limitation or sensitivity toward low pH, putatively caused by hyperbaric cultivation conditions. *M. jannaschii* did not fully convert  $H_2/CO_2$  in RCB2 (Supplementary Fig. S12). Therefore, the medium for *Methanocaldococcus* spp. requires improvement, which should be based on a spectrophotometric analysis of quantities and quality of trace element



**Fig. 4 Results of RCB cultivations of thermophilic and hyperthermophilic methanogens in the SBRS at 50 bar.** The RCB cultivations were performed in quadruplicates with four runs RCB1, RCB2, RCB3, and RCB4. Mean and standard deviation of MER / mmol L<sup>-1</sup> h<sup>-1</sup> is shown. Thermophile: *Methanothermobacter marburgensis* Marburg (65 °C, MM medium); hyperthermophiles: *Methanocaldococcus villosus* KIN24-T80\* (80 °C, 282c18\_E medium), *Methanoterris igneus* Kol 5 (85 °C, 282c 30 medium), and *Methanocaldococcus jannaschii* JAL-1 (80 °C, 282c 30 medium).

species and basal medium ingredients consumed during medium development<sup>41,42</sup>. Although the *Methanocaldococcus* medium needs further improvement, *M. villosus* and *M. igneus* did not show a lag phase at 50 bar. However, *M. villosus* directly started to convert H<sub>2</sub>/CO<sub>2</sub> exponentially from the beginning of the experiment, compared to *M. igneus*, which showed linear, thus liquid-limited or low pH-retarded growth, directly from the onset of the cultivation (Supplementary Fig. S12). *M. igneus* comprised a threefold higher MER and *M. villosus* comprised a twofold higher  $k_{min}$  compared to *M. marburgensis* at 50 bar, when comparing the performance during RCB1 (Fig. 4 and Supplementary Fig. S11). *M. igneus* exhibited the highest MER of  $15.1 \pm 0.4$  mmol L<sup>-1</sup> h<sup>-1</sup> and turnover rate of  $4.8 \pm 0.2$  h<sup>-1</sup> in the 50 bar cultivation experiments (Fig. 4 and Supplementary Fig. S13), however we quantified a lower  $k_{min}$  for *M. villosus* than for *M. igneus*. Furthermore, *M. igneus* and *M. jannaschii* exhibited the highest MER<sub>max</sub> (Supplementary Fig. S14). These results show that a nutrient limitation occurred and/or insufficient catalytically active biomass was present, meaning that CH<sub>4</sub> production was operated at  $q_{CH_4,max}$ <sup>12,20,30</sup>. The fold increase of gaseous substrate in the media was found not to be proportional with the CH<sub>4</sub> productivity of the methanogens. The 25-fold higher gaseous substrate presence in the media, compared to a 2 bar cultivation, lead to an average MER increase of  $2.92 \pm 0.43$  mmol L<sup>-1</sup> h<sup>-1</sup>. The time until full conversion of H<sub>2</sub>/CO<sub>2</sub> at 50 bar was on average increased compared to 10 bar RCBs, by 2.5-fold (*M. marburgensis*,  $67.79 \pm 6.24$  h), 2-fold (*M. villosus*, 43.21 h), and 5 h (*M. jannaschii*, 23.61 h). In contrast, *M. igneus* was 2 h (18.72 h) faster to reach full conversion under 50 bar RCBs compared to 10 bar RCBs.

## Discussion

Pure culture CO<sub>2</sub>-BMP is regarded as a key technology combining chemical energy storage, CO<sub>2</sub> utilization and biofuel production. Within CO<sub>2</sub>-BMP, methanogens are employed as autotrophic CH<sub>4</sub> cell factories. Thus, we aimed to identify and characterize the highest performing CH<sub>4</sub> cell factories. This up to now unprecedented quantitative comparative physiological, bioinformatic, and biotechnological analysis provides a comprehensive view on growth and CH<sub>4</sub> production kinetics, essential nutritional components and barotolerance of 80 methanogens. The quantitative analysis of axenic methanogenic cultures enabled the identification of high performing cell factories for CH<sub>4</sub> production (high  $q_{CH_4}$ ) with a high maximum specific growth rate ( $\mu_{max}$ ), straightforward cultivation methods (in terms of sterility, media demand, reproducibility), and tolerance to hyperbaric cultivation conditions.

Psychrophilic methanogens reached a rather low OD<sub>max</sub> < 0.2 in this study. This could be explained by the fact that psychrophilic microbes have in general a slower metabolism or a longer doubling time compared to microorganisms that grow at higher temperatures<sup>43–45</sup>. The heterogeneous growth pattern of mesophilic methanogens on complex and defined media could be explained by their ecological and phylogenetic heterogeneity. Although high biomass concentrations are often linked to growth on complex medium, highest productive methanogens do not necessarily require complex medium to reach a high OD. The highest CH<sub>4</sub> productivities were achieved by Methanococci, and especially by *Methanocaldococcus* spp. and *Methanoterris* sp. which exhibited higher conversions and CH<sub>4</sub> production kinetics (Fig. 2 and Supplementary Fig. S7) than thermophilic methanogens belonging to Methanobacteria.

Methanococci were shown to possess a faster metabolism, indicated by higher CH<sub>4</sub> production kinetics, possibly due to the usage of [NiFeSe]-hydrogenases for H<sub>2</sub> oxidation. Instead of using [NiFe]-hydrogenases for the oxidation of H<sub>2</sub> as *Methanothermobacter* spp. (F<sub>420</sub>-reducing hydrogenase Frh and F<sub>420</sub>-nonreducing hydrogenase Mvh), *Methanococcus* spp. and *Methanocaldococcus* spp. use [NiFeSe]-hydrogenases (F<sub>420</sub>-reducing hydrogenase Fru and F<sub>420</sub>-nonreducing hydrogenase Vhu) that display much higher catalytic activities<sup>46,47</sup>. Additionally, *Methanocaldococcus* spp. do not harbor selenium-free hydrogenases<sup>46,48,49</sup>. The catalytic activity of [NiFeSe]-hydrogenases is greatly increased compared to [NiFe]-hydrogenases. Vhu of *M. voltae* showed a catalytic activity of 43,540 U mg<sup>-1</sup><sup>147</sup>, whereas Mvh of *M. marburgensis* indicated a catalytic activity of 1600 U mg<sup>-1</sup><sup>150</sup>.

Our results reveal that methanogens, which showed the highest turnover rates and MERs, were covered with an S-layer. S-layer proteins can be positively or negatively charged, and it has been shown that charged S-layers enhance diffusion through the membrane<sup>51</sup>. The cell envelope of *M. kandleri* is known to be covered with an S-layer<sup>36</sup>, although no S-layer motif was found during our UniProtKB search. Therefore, one could hypothesize that the S-layer proteins present on *M. kandleri* are characteristic for this phylogenetic group. Furthermore, our bioinformatic analysis of MCRA revealed that all highly productive prioritized methanogens harbor the Tyr<sup>a444</sup> Gly<sup>a445</sup> Tyr<sup>a446</sup> amino acid motif and belong to Class I methanogens (Supplementary Fig. S8).

Among the amino acids, especially cysteine is a required media supplement for certain methanogens (Supplementary Table S2). Compared to the prioritized Methanobacteria, hyperthermophilic Methanococci have a necessity of cysteine in the cultivation media, although Class I methanogens (Methanobacteriales, Methanococcales, and Methanopyrales) use primarily sulfide and not cysteine as sulfur source, such as Class II methanogens<sup>52</sup>. The

cysteine requirement of hyperthermophilic Methanococci in the medium could be linked to the usage of cysteine via cysteine desulphidase (CDD) for  $\text{H}_2\text{S}$ ,  $\text{NH}_4^+$ ,  $\text{H}^+$ , and pyruvate production<sup>53</sup>, the production of cysteine via the t-RNA dependent pathway (SepRS/SepCysS)<sup>54,55</sup>, and absence of cysteine desulphurase (CSD)<sup>52,53,55</sup> (Supplementary Table S2). Besides that, CDD seems to be associated with the sulfur transfer for Fe-S cluster biosynthesis<sup>55–57</sup>. In case of *M. fervidus*, where CSD was found to be expressed and CDD had not been (Supplementary Table S2), cysteine might have a key function in tolerating elevated temperatures<sup>58</sup>.

Besides the nutritional demand of methanogens regarding cysteine, the TES that is used in a medium plays an important role in the biocatalytic activity. The trace element composition of a medium should mimic the heavy metal composition and respective concentrations present at the isolation spot, but might need to be optimized for meeting a biotechnological purpose. Based on our findings during the multivariate comparative analyses, methanogens that were cultivated on a medium with a rich-TES composition (TES1, TES2, TES4, and TES5) require additional cysteine or vitamins in the growth medium. Growth on a defined medium including a minimal/optimized TES (TES3), without cysteine or vitamins, was just possible for certain groups of methanogens, such as some Methanobacteria and *M. maripaludis* (cluster 3 in Supplementary Data 1, Table S1, and Supplementary Fig. S6). Vice versa, strains that grow best on media with a rich-TES composition, cysteine or vitamin addition indicated poor growth and  $\text{CH}_4$  productivity on a medium with a minimal TES (TES3, MM medium), even with cysteine and/or vitamins also added. This leads to the conclusion that the combination of a rich TES and the addition of cysteine and/or vitamins is essential for the tested hyperthermophilic methanogens to exhibit high MERs.

We obtained the highest conversion and  $\text{CH}_4$  production kinetics under hyperthermophilic and hyperbaric conditions.  $\text{H}_2$  solubility at hyperbaric pressure of 10 or 50 bar leads to a 5- or 25-times higher substrate availability in the medium, compared to a cultivation at 2 bar. Therefore, adaptations to hyperbaric conditions, liquid limitation, and the suitability of the cultivation medium for high-pressure bioreactor cultivations can be studied if the experimental set-up is designed accordingly<sup>12,20,24,30</sup>. Instead of achieving a 5- and 25-fold productivity increase at 10 and 50 bar RCB experiments, an average of two- and threefold productivity increase was achieved, respectively. This might be due to cell envelope characteristics of the investigated methanogens and/or corresponding low pH<sup>40</sup>, lipid composition, limitation of conversion kinetics by a liquid nutrient, or not enough available catalytically active biomass (biomass limitation) to instantly convert the additionally available gas, which could also be a result from a liquid limitation or natural borders if the culture is growing at  $\mu_{\text{max}}$ .

The  $\text{CH}_4$  productivity pattern between RCB1 and RCB2 at 10 and 50 bar (Fig. 3 and *M. marburgensis* in Fig. 4) could be an adaptation response to hyperbaric cultivation conditions. However, the tested thermophilic and hyperthermophilic Methanococci have a different core lipid composition (archaeol, macrocyclic archaeol, and tetraether lipids) than Methanobacteria (archaeol and tetraether lipids). Strains from both orders increase the percentage of tetraethers under challenging growth conditions (Supplementary Table S3). *M. jannaschii* decreases archaeol and increases the percentage of tetraether lipids with increasing temperature<sup>59</sup>, or temperature and pressure<sup>60</sup>, while *M. marburgensis* increases tetraether lipids (GDGT-0), when growing with detergents<sup>61</sup>. Moreover, *M. okinawensis* increases tetraether lipids (GMGT-0, GMGT-0', and GDGT-0) and decreases archaeol upon addition of high amounts of inhibitors, such as

ammonium chloride and/or methanol, except for formaldehyde, which leads to an increase of archaeol<sup>7,8</sup>.

At 10 bar, putative liquid limitation or biomass limitation occurred during RCB3 and RCB4 (*M. marburgensis*, *M. thermotrophicus*, *M. jannaschii*, *M. vulcanius*, *M. villosus*, *M. igneus*, and *M. kandleri*) (Fig. 3 and Supplementary Fig. S9). However, at 50 bar putative liquid limitations arose right after RCB1 for *Methanocaldococcus* spp. and during RCB3 for *M. marburgensis*. Our findings indicate that just *M. marburgensis* is growing on a well-optimized medium (MM medium)<sup>30</sup>. The growth media (282c 18 or 282c 30) for *Methanocaldococcus* spp. would need to be adapted for hyperbaric applications. Although 282-based media were not yet designed for cultivations at 50 bar, the time for full conversion of  $\text{H}_2/\text{CO}_2$  was not affected in the cases of *M. igneus* and *M. jannaschii*, which did not show any retardation in  $\text{CH}_4$  production during 50 bar cultivations. Perhaps these strains could be tested at higher pressure conditions, such as *M. okinawensis*, which showed  $\text{CH}_4$  production up to 90 bar<sup>40</sup>. *Methanocaldococcus* spp. exhibited higher specific growth rates than *M. marburgensis* (Supplementary Data 1 and Table S1), and thus liquid limitation occurs faster. Besides that, the metabolism of *M. marburgensis* is slower compared to *Methanocaldococcus* spp., indicated by the lower  $k_{\text{min}}$  values of *Methanocaldococcus* spp. (Supplementary Fig. S11). Therefore, the liquid limitation in our setup might not have had a strong effect.

This study on high-pressure biological  $\text{CH}_4$  production in pure culture is a cornerstone of the emerging research and development field of Archaea Biotechnology<sup>19</sup>. The systematic assessment indicated that the high-performance strains belong to Class I methanogens. Hyperthermophilic Methanococci are high-pressure  $\text{CH}_4$  production cell factories and the addition of cysteine and a rich TES in the media are essential for efficient growth of these Methanococci. Therefore, we propose to perform bioprocess development utilizing *M. igneus* and *M. jannaschii* to develop these organisms into high-pressure  $\text{CH}_4$  cell factories. Moreover, methanogens that exhibited the highest turnover rates and MERs are covered with S-layers, and the amino acid motif Tyr<sup>α444</sup> Gly<sup>α445</sup> Tyr<sup>α446</sup> in the alpha subunit of MCR is present in all high-performance methanogens. This analysis sets the foundation for a future high-pressure bioprocess optimization endeavor with the identified hyperthermophilic  $\text{CH}_4$  cell factories. The autotrophic activity of hyperthermophilic, autotrophic, hydrogenotrophic methanogens could therefore be employed for balancing the power grid system (energy storage) or to biologically depressurize  $\text{H}_2$  and/or  $\text{CO}_2$  containing emission flue gasses to  $\text{CH}_4$  via the  $\text{CO}_2$ -BMP process. High-pressure biological  $\text{CH}_4$  production in pure culture could provide a purposeful route for the transition to an independent carbon-free or low-carbon energy bioeconomy.

## Methods

**Strains.** All screening experiments including HFG (closed batch up to 2 bar) were performed with the methanogenic archaeal strains listed in Fig. 1. Methanogens were obtained from the Deutsche Sammlung für Mikroorganismen und Zellkulturen GmbH (DSMZ) (Braunschweig, Germany). High-pressure experiments were performed with selected strains in the SRBR in closed batch mode at 10 and 50 bar (Figs. 3 and 4).

**Chemicals.**  $\text{CO}_2$  (99.995 Vol.-%),  $\text{H}_2$  (99.999 Vol.-%), and  $\text{H}_2/\text{CO}_2$  (80 Vol.-%  $\text{H}_2$  in  $\text{CO}_2$ ) were obtained from Air Liquide (Air Liquide GmbH, Schwechat, Austria). The  $\text{H}_2/\text{CO}_2$  mixture (80 Vol.-%  $\text{H}_2$  and Vol.-%  $\text{CO}_2$ ) for high-pressure cultivations was obtained from Linde Gas (Linde Gas GmbH, Wels, Austria). All other chemicals were of highest available grade.

**Media.** Considering the nutritional requirements of the screened strains, several media were used to cultivate methanogenic archaeal strains, as they are SAB medium<sup>28</sup>, McN medium<sup>31</sup>, Medium 6<sup>29</sup>, DSMZ medium (141, 141b, 141c, 282,



203, 511), *Methanothermobacter marburgensis* medium (MM)<sup>30</sup> and MM medium with 15 or 30 g of NaCl (MM15, MM30). Some media were modified to test specific nutritional requirements (203c, 203-c, 511-v, 282c 0, 282c 18, 282c 18\_E, 282c 30, 282-c 30, MM15c, MM15v, MM30c). The addition of “c” to the medium designation indicates the presence of cysteine in the medium, whereas “-c or -v” indicates the omission of cysteine or vitamins, respectively; the succeeding numbers refer to the amount of NaCl provided to the medium. Every media or solution was prepared with ultrapure H<sub>2</sub>O Milli-Q<sup>®</sup> if not stated differently. To ensure growth in a respective medium and exclude any stimulative effects of medium contained in the inoculum, methanogens were grown in two passages or two times washed with fresh medium. Before inoculation on minimal medium, inocula were washed by centrifugation following by the removal of the supernatant, adding 1 mL of minimal medium and resuspending the pellet, centrifugation (10 min, 13,000 rpm), discarding the supernatant and resuspending the pellet in 1 mL of minimal medium. The exact media compositions are listed in Supplementary Information.

**Multivariate analysis of cultivation conditions.** Growth and CH<sub>4</sub> productivity of 80 methanogenic archaea were screened in closed batch cultivation mode up to 2 bar relative to atmospheric pressure, 2 barg, in an anaerobic atmosphere consisting out of 80% H<sub>2</sub> in CO<sub>2</sub> (4:1). For simplicity, all pressure assignments are described as 2, 10, or 50 bar relative pressure. The optimal growth temperatures of the tested methanogens range from 15 to 98 °C. The tested methanogens are classified as psychrophiles including psychrotolerant methanogens (15–30 °C), mesophiles (30–37 °C), thermophiles (40–70 °C), and hyperthermophiles (80–98 °C). Methanogenic strains were grown in 120 mL serum bottles (crimp neck vial, VWR International, Pennsylvania, USA) in a chemically defined media (see “Media” section). After autoclaving, media filled bottles (autoclave Systec VX-120, Systec GmbH, Linden, Germany), inoculation was performed inside an anaerobic chamber (Coy Laboratory Products, Grass Lake, USA). Thereafter, bottles were pressurized with a H<sub>2</sub>/CO<sub>2</sub> gas mixture (80% H<sub>2</sub> in CO<sub>2</sub>) at 2 bar as previously described<sup>62</sup>. A sterile gaseous substrate supply requires the usage of sterile syringe filters (w/0.2 µm cellulose, 514-0061, VWR International, USA) and disposable hypodermic needles (Gr 14, 0.60 × 30 mm, 23 G × 1 1/4”, RX129.1, Braun, Germany). The gas phase was flushed by an insertion of a second needle at regular intervals for 2–4 s. After pressurizing, bottles were incubated in water baths (orbital shaking, water bath 1083, GFL Gesellschaft für Labortechnik mbH, Germany) or air incubators (100 rpm, Labwit incubators, Labwit Scientific Pty. Ltd, Australia) according to the optimal growth temperature of the respective cultivated strains. Bottles were taken out of the incubator and cooled down or heated up to room temperature. Thereafter, pressure and OD<sub>578 nm</sub> measurements (liquid samples of 0.7 mL were taken) were performed to monitor the cultivation. After the measurements, bottles were flushed, repressurized, and incubated again at microbial-specific cultivation temperatures.

**High frequency gassing experiments.** The experimental set-up of HFG followed the procedure described above, except for the gassing frequency, which was increased to twice a day. In total 14 strains, three mesophilic methanogens grown at 37 °C (*M. maripaludis* S2, *M. palustre* F, *Methanobacterium subterraneum* A8p), five thermophilic methanogenic archaea cultivated at 65 °C (*M. marburgensis* Marburg, *M. thermophilus* M, *M. thermaggregans*, *M. thermautotrophicus* DeltaH, *M. okinawensis* IH1), and six hyperthermophilic methanogens (*M. jannaschii* JAL-1 (80 °C), *M. vulcanius* M7 (80 °C), *M. villosus* KIN24-T80 (80 °C), *M. igneus* Kol 5 (80 °C), *M. fervidus* H9 (80 °C), *M. kandleri* AV19 (98 °C)) were selected for HFG.

**Dormancy study.** Before methanogens reached the stationary growth phase, they were put into dormancy state in a 4 °C room or in a –80 °C freezer (Thermo Scientific™ TSU™ Series –86 °C Upright Ultra-Low Temperature Freezers, Thermo Fisher Scientific, USA). For the –80 °C dormancy study, cryostocks were used (800 µL culture and 200 µL 50% (v/v) glycerol). After dormancy at 4 or –80 °C, strains were inoculated into fresh medium. In case of strains that were kept at 4 °C, an aliquot of 1 mL was used as inoculum. The 1 mL –80 °C cryostocks were thawed and used as inoculum after removing the glycerol by centrifugation (10 min, 13,000 rpm). The respective dormancy periods are listed in Supplementary Table S1.

**Analysis of growth and productivity.** During all 2 bar screening experiments including HFG, growth and CH<sub>4</sub> formation was examined by OD and pressure measurements. Growth was monitored via offline OD measurements at 578 nm (OD<sub>578 nm</sub>) by using a spectrophotometer (DU800, Beckman Coulter, California, USA). Before every OD<sub>578 nm</sub> measurement, the sample was vortexed (Vortex Mixer MX-S, Biologix Group Limited, China). In total, 0.7 mL of the culture was sampled at regular intervals for OD<sub>578 nm</sub> determinations. CH<sub>4</sub> production capacity was investigated through headspace pressure measurements of serum bottles in regular intervals using a digital manometer (LEO1-Ei, –1/3 bar relative, Keller, Germany)<sup>27</sup>. Produced CH<sub>4</sub> was replaced by discontinuous gassing with H<sub>2</sub>/CO<sub>2</sub> in regular intervals.

**Data analysis.** Two heatmaps are shown in Fig. 1, illustrating max. growth via OD<sub>max</sub>, by measuring at 578 nm, and max. volumetric CH<sub>4</sub> productivity,

depicted as MER<sub>max</sub> / mmol L<sup>–1</sup> h<sup>–1</sup>. The heatmaps showing turnover<sub>max</sub> / % (Supplementary Fig. S2) and biomass increase rate (Supplementary Fig. S1) can be found in Supplementary Information. The biomass increase rate depicts the average value of all biomass increase rates of a specific strain during the cultivation and is calculated according to Eq. (1). Figure 2 shows two boxplots, max. volumetric CH<sub>4</sub> productivity as MER / mmol L<sup>–1</sup> h<sup>–1</sup> and the biomass increase rate. The corresponding boxplot illustrating the turnover rate / h<sup>–1</sup> is shown in the Supplementary file (Supplementary Fig. S7). All data points were included into the boxplots. The heatmaps and the boxplots were generated using Rstudio Version 1.1.463 – © 2009–2018 RStudio, Inc. The R package ggplot2<sup>63</sup> was used. The graphical design was refined using Illustrator CS6 (Adobe Systems Inc., USA).

$$\frac{OD_{\max} \cdot \mu}{OD \cdot \mu_{\text{average}}} \quad (1)$$

**Correlation between nutritional demand and productivity.** To correlate the nutritional demand of methanogens with their associate growth, substrate conversion, and productivity on respective media, a standardized principal components analysis (PCA) followed by a k-means clustering was performed. Clustering was performed on OD<sub>max</sub>, turnover<sub>max</sub>, MER<sub>max</sub>, and the combination of those with medium-associated components such as salt, sulfate, sulfur, ammonium, phosphate, and cysteine concentrations. This analysis was then linked to medium-based information (trace elements solution, VS, the addition of yeast, peptone, or cysteine) and strain-specific characteristics like taxonomy and cultivation temperature. After collecting the data, missing values got imputed via PCA imputation using the R package missMDA<sup>64</sup>, followed by a normalization of the data using the stats package<sup>65</sup>. Thereafter the PCA (stats<sup>65</sup>) was performed, followed by the k-means clustering (stats<sup>65</sup>) using the first two components. The within cluster sum of squares accounted 85.5% for OD<sub>max</sub>, 93.2% for MER<sub>max</sub>, 91.8% for turnover<sub>max</sub>, and 86.3% for the combination of these variables. The following R packages were applied during the analysis: R packages ggplot2<sup>66</sup>, missMDA<sup>64</sup>, FactoMineR<sup>63,66,67</sup>, and stats<sup>65</sup>. The biplots were generated using Rstudio Version 1.1.463 – © 2009–2018 RStudio, Inc. The graphical design was refined using Illustrator CS6 (Adobe Systems Inc., USA).

**Cell envelope and S-layer composition of prioritized methanogens.** Cell envelop structures including core lipid composition and putative S-layer presence on prioritized methanogens were investigated via literature research. Furthermore, a bioinformatic screen on the UniProt Knowledgebase (UniProtKB)<sup>68</sup> regarding the presence of S-layer on tested methanogenic strains was conducted. The combination of strain-specific designation and “S-layer protein, glycoprotein, or glyco protein” were used as query terms. Additional information about protein family classification (Interpro) and functional regions/domain of the protein are indicated via Pfam<sup>69</sup>.

**Amino acid conservation of curtail interacting partners within methyl-coenzyme M reductase I, subunit alpha.** Protein sequences were obtained using the protein–protein BLAST (blastp)<sup>70,71</sup>. The Reference Sequence (RefSeq) collection was used as sequence database for the blastp (version January 2020). MCR I, subunit alpha from *Methanothermobacter marburgensis* Marburg (GenBank: ADL59127.1) was used as a query. The default algorithm parameters were chosen (scoring matrix BLOSUM62) besides the max. target sequences which was increased to 500. Protein sequences from methanogens that were investigated during this study and were not obtained through blastp were afterwards added to the blastp sequences. Missing protein sequences were downloaded from UniProtKB<sup>68</sup>. Thereafter, protein sequences were aligned with the multiple sequence alignment tool Clustal Omega<sup>72</sup> applying the default settings. The download of amino acid sequences and the following analysis was performed in February 2020. The alignment was illustrated using Jalview version 2.10.5<sup>73</sup>. The graphical design was refined with Illustrator CS6 (Adobe Systems Inc., USA).

**High-pressure SRBS cultivation of methanogens.** An experimental design was developed to examine H<sub>2</sub>/CO<sub>2</sub> conversion kinetics through online pressure measurements and to identify the most productive methanogens at a hyperbaric relative pressure of 10 and 50 bar. Further, possible liquid limitations and kinetic stability of CH<sub>4</sub> production of prioritized methanogens at 10 bar was examined. The SRBS consisted of four identical cultivation vessels (160 mL), suitable for investigation of microbial activity at pressures up to 50 bar and temperatures up to 145 °C<sup>39</sup>. All pressure assignments are given in bar and described as relative pressure (10 and 50 bar relative to atmospheric pressure). Pressure within the bioreactors (R1, R2, R3, and R4) was accurately measured with online pressure sensors (Pressure Transducers and Transmitters, Type: PTDVB0601B1C2, Parker, Cleveland, USA). Before bioreactors were pressurized, the gas inlet line pressure was set to 10 or 50 bar of H<sub>2</sub>/CO<sub>2</sub> with an analogous manometer (WIKA Messgerätevertrieb Ursula Wiegand GmbH & Co. KG, Vienna, Austria, 0–60 bar)<sup>39</sup>. Thus, pressure was checked online and offline during the pressurization step. During the experiments, pressure was monitored with the online pressure sensing tool. The pressure sensor and the manometer were calibrated before installation. The accuracy of the heating jacket was also tested beforehand. The fact that each

experiment was performed in quadruplicates, strengthens the validity of the results. Some high-pressure experiments could not be investigated with all four bioreactors due to technical or biological failure. Since this was a screening approach, high-performance methanogens were further investigated and their growth and CH<sub>4</sub> production kinetics were then analyzed in detail.

**SBRS inoculation procedure.** After cleaning and autoclaving the SBRS, an anaerobic environment in each bioreactor vessel was established, followed by setting the cultivation temperature, respectively, to the strain's optimal growth temperature based on DSMZ data. Before combining medium, supplements, and culture in a vial (100 mL crimp neck vial, Macherey-Nagel GmbH & Co. KG, Germany), the culture was reactivated for 10 min via flushing with 1 bar H<sub>2</sub>/CO<sub>2</sub>. Based on the used medium, supplement solutions like NaHCO<sub>3</sub>, 0.5 mol L<sup>-1</sup> Na<sub>2</sub>S, L-Cysteine-HCl-H<sub>2</sub>O, and vitamins (Wolf's VS, see medium 141) were added to the medium right before inoculation. The inoculum (medium, supplements, and culture) was transferred into the bioreactor<sup>39</sup>. Thereafter an appropriate incubation pressure (10 or 50 bar, depending on the experiment) was adjusted. The RCB set-up included three repressurization steps either at 10 or 50 bar, respectively. After a total gas conversion, a gas sample from each bioreactor was taken for gas composition analysis via gas chromatography. Full conversion is achieved if 2 bar (10 bar) or 10 bar (50 bar), i.e. one-fifth of the initial pressure, of residual gas in the bioreactors R1, R2, R3, and R4 is present, respectively, to production of CH<sub>4</sub> (4 H<sub>2</sub> + CO<sub>2</sub> → CH<sub>4</sub> + 2 H<sub>2</sub>O) to avoid a driving force limitation. Before repressurization, the residual pressure was released. The following strains were investigated for 10 bar RCB: mesophiles 37 °C: *M. maripaludis* S2 (MCN medium), *M. palustre* F (282c 0 medium), *M. subterraneum* A8p (MM medium); thermophiles 65 °C: *M. marburgensis* Marburg (MM medium), *M. thermophilus* M (was not tested), *M. thermaggregans* (MM medium), *M. thermautotrophicus* DeltaH (MM medium), *M. okinawensis* IH1 (282c 30 medium); hyperthermophiles 80 °C: *M. jannaschii* JAL-1 (282c 30 medium), *M. vulcanius* M7 (282c 30 medium), *M. villosus* KIN24-T80 (282c 18 and 282c 18\_E medium), *M. fervidus* H9 (MMc15 medium); hyperthermophiles 85 and 98 °C: *M. igneus* Kol 5 (282c 30 medium), *M. kandleri* AV19 (511 medium). *M. maripaludis*: in RCB1, R2 was leaking at the beginning and fixed after taking note of the leakage. After 80 h in RCB3 no growth was observed, thus RCB3 was stopped. *M. subterraneum*: R2 was not functional during all RCB runs. After recognizing the leakage on the following day, the pressure decreased to 3.3 bar. Subsequently R2 bioreactor was repressurized and RCB2 was started. R2 in RCB3 was again leaking. The problem was fixed before starting RCB4. *M. thermautotrophicus*: the pressure curve of R1 in RCB3 (100 h) did not follow the trend of the others, thus it is was not shown and not repressurized in RCB4. R1 was not working for cultivations of *M. jannaschii*, *M. vulcanius*, and *M. igneus*. *M. fervidus*: the performance of R1 was not comparable to the others in RCB1 and therefore not repressurized for following RCB runs. *M. kandleri*: after RCB3, R1 was not working properly and therefore not repressurized.

The following strains were investigated in 50 bar RCBs: *M. marburgensis* Marburg, *M. thermaggregans*, *M. villosus* KIN24-T80\*, *M. igneus* Kol 5, and *M. jannaschii* JAL-1. After RCB2 cultivations of *M. villosus* KIN24-T80\*, *M. igneus* Kol 5, and *M. jannaschii* JAL-1 the experiments were stopped due to much lower CH<sub>4</sub> productivity compared to RCB1. *M. thermaggregans*: after 120 h of cultivation no growth was detected, thus RCB1 was stopped.

#### Analysis of biomass, CH<sub>4</sub> productivity, and head space gas composition (SBRS)

During all RCB runs at 10 and 50 bar, growth and CH<sub>4</sub> formation were examined with offline cell dry weight analysis, online pressure measurements, and offline headspace gas determinations. Growth was determined via offline cell dry weight analysis by using a centrifuge (tabletop centrifuge Heraeus Megafuge 1.0 R, Thermo Electron Corporation, Massachusetts, USA) to pellet the harvested biomass. Biomass was centrifuged for 15 min at 3500 rpm, followed by drying the wet biomass at 105 °C overnight (Heraeus drying cabinet model T 5050, Heraeus, Hanau, Germany). Pressure drop, which corresponds to CH<sub>4</sub> production, was monitored by online pressure sensors. After total gas conversion, gas samples were taken via headspace vials (10 mL headspace vial, Schmidling Labor + Service GmbH, Switzerland) which were crimped with crimp caps (crimp cap with bore hole, Carl Roth, Germany) and vacuumed for 5 min before usage. The CH<sub>4</sub> off-gas concentration (CH<sub>4</sub> / Vol.-%) in the gas samples are analyzed with a gas chromatograph (Trace GC Ultra 2000, Thermo Fisher Scientific Inc., US) equipped with a thermal conductivity detector. Chromatographic separation was executed on a Carboxen-1000 packed column (10 m, 3/8"). Helium used as carrier gas with a constant pressure of 2.35 bar and a split flow of 90/10. A representative gas sample with a volume of 1 mL was injected. Following GC parameters were chosen for the analysis: inlet heater 150 °C, detector 200 °C, oven initial temperature 35 °C hold for 5 min, temperature raising rate of 20 °C min<sup>-1</sup> to 225 °C (hold for 10 min) at final temperature.

**Data analysis of SBRS 10 and 50 bar cultivations.** To elucidate the CH<sub>4</sub> production kinetics from cultivated methanogenic strains, the following variables were calculated: methane evolution rate calculated with GC data MER<sub>GC</sub> / mmol L<sup>-1</sup> h<sup>-1</sup> or pressure data MER<sub>pressure</sub> / mmol L<sup>-1</sup> h<sup>-1</sup>, carbon uptake rate CUR / mmol L<sup>-1</sup> h<sup>-1</sup>, hydrogen uptake rate HUR / mmol L<sup>-1</sup> h<sup>-1</sup>, maximum conversion rate *k*<sub>min</sub> / bar h<sup>-1</sup>.

MER was calculated either by using CH<sub>4</sub> concentration obtained from GC measurements or through the integration of the recorded curve for the online pressure probe in every bioreactor. Data collection was performed by a data acquisition unit (USB-2019, ICP DAS-EUROPE GmbH, Germany) and recorded via LabVIEW (National Instruments, Austin, USA). During cultivation the record interval was set to 5 min. All calculations were performed by using the program Origin 2019 (Originlab Corporation, USA). After selecting a proper record interval (30 min) for data analysis, the CH<sub>4</sub> production kinetics (MER, turnover rate, *k*<sub>min</sub>) were calculated, while neglecting biomass formation<sup>39,62</sup>. These MER values were used to determine the respective point in time where MER reached its maximum (MER<sub>max</sub>). *k*<sub>min</sub> indicates the highest slope in the curve, which reflects the point of highest turnover, showing the time point of MER<sub>max</sub>. MER<sub>total</sub> indicates the MER value over the total experimental time including all data points. MER values got smoothed and plotted over time. To determine the lag and the stationary phase during cultivation and neglect these data points, an integration over the obtained curve was performed. The integration start (*x*<sub>start</sub>) and end (*x*<sub>end</sub>) points of the curves were identified as follows: *x*<sub>start</sub> and *x*<sub>end</sub> are intersection points, which were elucidated by shifting the *x*-axis to low points of the curve (minimum *x* = 0.1). The difference of these points reflects the time period Δ*t* of microbial growth phases. MER<sub>global</sub> was determined by dividing the calculated area by Δ*t*<sup>33</sup>. Finally, the program Origin indicated the associated pressure data for the *x*<sub>start</sub> and *x*<sub>end</sub> values. The associated pressure data were subsequently used for calculating of MER<sub>GC</sub>, MER<sub>pressure</sub>, CUR, HUR, and *k*<sub>min</sub>. The barplots were generated using Rstudio Version 1.1.463 – © 2009-2018 RStudio, Inc.. The R package ggplot2 was used<sup>66</sup>. The graphical design was refined using Illustrator CS6 (Adobe Systems Inc., California, USA).

**Statistics and reproducibility.** All information on statistics and reproducibility of the experiments is provided in the respective "Materials and methods" sections or in the Supplementary Information, Supplementary Data 1 and Data 2. The 2 bar multivariate screening experiments were performed with 80 methanogens with an ranging optimal growth temperature between 15 and 98 °C. The tested methanogens are classified as psychrophiles including psychrotolerant methanogens (15–30 °C), mesophiles (30–37 °C), thermophiles (40–70 °C), and hyperthermophiles (80–98 °C). The multivariate screening was followed by the HFG experiments, which were performed with 14 methanogens. For each closed batch cultivation (multivariate screening or HFG), three biological replicates (in some cases, two biological replicates) plus one negative control were used. Thereafter, 10 and 50 bar hyperbaric cultivations were performed. The 10 bar RCB cultivations were investigated with 13 methanogens. Followed by 50 bar RCB cultivations with four methanogens. Hyperbaric cultivations were performed in quadruplicates. In some cases, just three bioreactors were used, due to a non-functionality of one of the bioreactors of the SBRS.

**Reporting summary.** Further information on research design is available in the Nature Research Reporting Summary linked to this article.

#### Data availability

All relevant data are available from the corresponding author upon request.

Received: 23 August 2020; Accepted: 10 February 2021;

Published online: 05 March 2021

#### References

- Kirschke, S. et al. Three decades of global methane sources and sinks. *Nat. Geosci.* **6**, 813–823 (2013).
- Lyu, Z. & Whitman, W. B. Transplanting the pathway engineering toolbox to methanogens. *Curr. Opin. Biotechnol.* **59**, 46–54 (2019).
- Bižić, M. et al. Aquatic and terrestrial cyanobacteria produce methane. *Sci. Adv.* **6**, eaax5343 (2020).
- Repeta, D. J. et al. Marine methane paradox explained by bacterial degradation of dissolved organic matter. *Nat. Geosci.* **9**, 884–887 (2016).
- Thauer, R. K., Kaster, A.-K., Seedorf, H., Buckel, W. & Hedderich, R. Methanogenic archaea: ecologically relevant differences in energy conservation. *Nat. Rev. Micro* **6**, 579–591 (2008).
- Abdel Azim, A., Rittmann, S. K.-M. R., Fino, D. & Bochmann, G. The physiological effect of heavy metals and volatile fatty acids on *Methanococcus maripaludis* S2. *Biotechnol. Biofuels* **11**, 301 (2018).
- Baumann, L. M. F. et al. Intact polar lipid and core lipid inventory of the hydrothermal vent methanogens *Methanocaldococcus villosus* and *Methanothermococcus okinawensis*. *Org. Geochem.* **126**, 33–42 (2018).
- Taubner, R.-S. et al. Membrane lipid composition and amino acid excretion patterns of *Methanothermococcus okinawensis* GROWN in the presence of inhibitors detected in the enceladian plume. *Life* **9**, 85 (2019).
- Wang, L. et al. Bioinformatics analysis of metabolism pathways of archaeal energy reserves. *Sci. Rep.* **9**, 1034 (2019).

10. Seifert, A. H., Rittmann, S., Bernacchi, S. & Herwig, C. Method for assessing the impact of emission gasses on physiology and productivity in biological methanogenesis. *Bioresour. Technol.* **136**, 747–751 (2013).
11. Rittmann, S. K.-M. R. A critical assessment of microbiological biogas to biomethane upgrading systems. In *Biogas Science and Technology* (eds Guebitz, G. M., Bauer, A., Bochmann, G., Gronauer, A. & Weiss, S.) 117–135 (Springer International Publishing, 2015).
12. Rittmann, S. K.-M. R., Seifert, A. H. & Bernacchi, S. Kinetics, multivariate statistical modelling, and physiology of CO<sub>2</sub>-based biological methane production. *Appl. Energy* **216**, 751–760 (2018).
13. Mauerhofer, L.-M. et al. Physiology and methane productivity of *Methanobacterium thermaggregans*. *Appl. Microbiol. Biotechnol.* **102**, 7643–7656 (2018).
14. Strübing, D., Huber, B., Leubhn, M., Drewes, J. E. & Koch, K. High performance biological methanation in a thermophilic anaerobic trickle bed reactor. *Bioresour. Technol.* **245**, 1176–1183 (2017).
15. Jensen, M. B. et al. Stick or leave—pushing methanogens to biofilm formation for ex situ biomethanation. *Bioresour. Technol.* **291**, 121784 (2019).
16. Rachbauer, L., Voith, G., Bochmann, G. & Fuchs, W. Biological biogas upgrading capacity of a hydrogenotrophic community in a trickle-bed reactor. *Appl. Energy* **180**, 483–490 (2016).
17. Nock, W. J., Serna-Maza, A., Heaven, S. & Banks, C. J. Evaluation of microporous hollow fibre membranes for mass transfer of H<sub>2</sub> into anaerobic digesters for biomethanization. *J. Chem. Technol. Biotechnol.* **94**, 2693–2701 (2019).
18. Tao, B. et al. Simultaneous biomethanisation of endogenous and imported CO<sub>2</sub> in organically loaded anaerobic digesters. *Appl. Energy* **247**, 670–681 (2019).
19. Pfeifer, K. et al. Archaea biotechnology. *Biotechnol. Adv.* **47**, 107668 (2021).
20. Seifert, A. H., Rittmann, S. & Herwig, C. Analysis of process related factors to increase volumetric productivity and quality of biomethane with *Methanothermobacter marburgensis*. *Appl. Energy* **132**, 155–162 (2014).
21. Graf, F., Götz, M., Wonneberger, A.-M., & Köppel, W. Techno-ökonomische Studie zur biologischen Methanisierung bei PtG-Konzepten. (2014).
22. Rönsch, S. et al. Review on methanation—from fundamentals to current projects. *Fuel* **166**, 276–296 (2016).
23. Mutz, B., Carvalho, H. W. P., Mangold, S., Kleist, W. & Grunwaldt, J.-D. Methanation of CO<sub>2</sub>: structural response of a Ni-based catalyst under fluctuating reaction conditions unraveled by operando spectroscopy. *J. Catal.* **327**, 48–53 (2015).
24. Bernacchi, S., Krajete, A., Seifert, A. H., Herwig, C. & Rittmann, S. Experimental methods for screening parameters influencing the growth to product yield (Y(x/CH<sub>4</sub>)) of a biological methane production (BMP) process performed with *Methanothermobacter marburgensis*. *AIMS Bioeng.* **1**, 72–87 (2014).
25. Boonyaratanakornkit, B., Córdova, J., Park, C. B. & Clark, D. S. Pressure affects transcription profiles of *Methanocaldococcus jannaschii* despite the absence of barophilic growth under gas-transfer limitation. *Environ. Microbiol.* **8**, 2031–2035 (2006).
26. Miller, J. F., Shah, N. N., Nelson, C. M., Ludlow, J. M. & Clark, D. S. Pressure and temperature effects on growth and methane production of the extreme thermophile *Methanococcus jannaschii*. *Appl. Environ. Microbiol.* **54**, 3039–3042 (1988).
27. Nishimura, N., Kitaura, S., Mimura, A. & Takahara, Y. Cultivation of thermophilic methanogen KN-15 on H<sub>2</sub>-CO<sub>2</sub> under pressurized conditions. *J. Fermentation Bioeng.* **73**, 477–480 (1992).
28. Khelaifa, S., Raoult, D. & Drancourt, M. A versatile medium for cultivating methanogenic archaea. *PLoS ONE* **8**, e61563 (2013).
29. Wagner, M., Amann, R., Lemmer, H. & Schleifer, K. H. Probing activated sludge with oligonucleotides specific for proteobacteria: Inadequacy of culture-dependent methods for describing microbial community structure. *Appl. Environ. Microbiol.* **59**, 1520–1525 (1993).
30. Rittmann, S., Seifert, A. & Herwig, C. Quantitative analysis of media dilution rate effects on *Methanothermobacter marburgensis* grown in continuous culture on H<sub>2</sub> and CO<sub>2</sub>. *Biomass Bioeng.* **36**, 293–301 (2012).
31. Whitman, W. B., Shieh, J., Sohn, S., Caras, D. S. & Premachandran, U. Isolation and characterization of 22 mesophilic methanococci. *Syst. Appl. Microbiol.* **7**, 235–240 (1986).
32. Mauerhofer, L.-M. et al. Methods for quantification of growth and productivity in anaerobic microbiology and biotechnology. *Folia Microbiol.* **64**, 321–360 (2019).
33. Akca, E. et al. Genes and derived amino acid sequences of S-layer proteins from mesophilic, thermophilic, and extremely thermophilic methanococci. *Extremophiles* **6**, 351–358 (2002).
34. Bellack, A., Huber, H., Rachel, R., Wanner, G. & Wirth, R. *Methanocaldococcus villosus* sp. nov., a heavily flagellated archaeon that adheres to surfaces and forms cell-cell contacts. *Int. J. Syst. Evol. Microbiol.* **61**, 1239–1245 (2011).
35. Bröckl, G. et al. Analysis and nucleotide sequence of the genes encoding the surface-layer glycoproteins of the hyperthermophilic methanogens *Methanothermobacter fervidus* and *Methanothermobacter sociabilis*. *Eur. J. Biochem.* **199**, 147–152 (1991).
36. König, H., Rachel, R. & Claus, H. Proteinaceous surface layers of Archaea: ultrastructure and biochemistry. In *Archaea* (ed. Cavicchioli, R.) 315–340 (American Society of Microbiology, 2007).
37. Borrel, G. et al. Wide diversity of methane and short-chain alkane metabolisms in uncultured archaea. *Nat. Microbiol.* **4**, 603–613 (2019).
38. Ermler, U., Grabarse, W., Shima, S., Goubeaud, M. & Thauer, R. K. Crystal structure of methyl-coenzyme M reductase: the key enzyme of biological methane formation. *Science* **278**, 1457–1462 (1997).
39. Pappenreiter, P. A., Zwirtmayr, S., Mauerhofer, L.-M., Rittmann, S. K.-M. R. & Paulik, C. Development of a simultaneous bioreactor system for characterization of gas production kinetics of methanogenic archaea at high pressure. *Eng. Life Sci.* **19**, 537–544 (2019).
40. Taubner, R.-S. et al. Biological methane production under putative Enceladus-like conditions. *Nat. Commun.* **9**, 748 (2018).
41. Blazevic, A. et al. Biotransformation of Scheelite CaWO<sub>4</sub> by the Extreme Thermophilic Metallosphaera sedula: Tungsten-Microbial Interface. *Front. Microbiol.* **10**, 1492 (2019).
42. Nischkauer, W., Vanhaecke, F., Bernacchi, S., Herwig, C. & Limbeck, A. Radial line-scans as representative sampling strategy in dried-droplet laser ablation of liquid samples deposited on pre-cut filter paper disks. *Spectrochimica Acta Part B At. Spectrosc.* **101**, 123–129 (2014).
43. Ingraham, J. L. & Bailey, G. F. Comparative study of effect of temperature on metabolism of psychrophilic and mesophilic bacteria. *J. Bacteriol.* **77**, 609 (1959).
44. Price, P. B. & Sowers, T. Temperature dependence of metabolic rates for microbial growth, maintenance, and survival. *Proc. Natl Acad. Sci. USA* **101**, 4631 (2004).
45. Schulte, P. M. The effects of temperature on aerobic metabolism: towards a mechanistic understanding of the responses of ectotherms to a changing environment. *J. Exp. Biol.* **218**, 1856 (2015).
46. Baltazar, C. S. A. et al. Nickel-iron-selenium hydrogenases—an overview. *Eur. J. Inorg. Chem.* **2011**, 948–962 (2011).
47. Sorgenfrei, O., Linder, D., Karas, M. & Klein, A. A novel very small subunit of a selenium containing [NiFe] hydrogenase of *Methanococcus voltae* is posttranslationally processed by cleavage at a defined position. *Eur. J. Biochem.* **213**, 1355–1358 (1993).
48. Rother, M., Resch, A., Wilting, R. & Böck, A. Selenoprotein synthesis in archaea. *Biofactors* **14**, 75–83 (2001).
49. Zhang, Y. & Gladyshev, V. N. General trends in trace element utilization revealed by comparative genomic analyses of Co, Cu, Mo, Ni, and Se. *J. Biol. Chem.* **285**, 3393–3405 (2010).
50. Stojanovic, A., Mander, G. J., Duin, E. C. & Hedderich, R. Physiological role of the F420-non-reducing hydrogenase (Mvh) from *Methanothermobacter marburgensis*. *Arch. Microbiol.* **180**, 194–203 (2003).
51. Li, P.-N. et al. Nutrient transport suggests an evolutionary basis for charged archaeal surface layer proteins. *ISME J.* **12**, 2389–2402 (2018).
52. Liu, Y., Sieprawska-Lupa, M., Whitman, W. B. & White, R. H. Cysteine Is Not the Sulfur Source for Iron-Sulfur Cluster and Methionine Biosynthesis in the Methanogenic Archaeon *Methanococcus maripaludis*. *J. Biol. Chem.* **285**, 31923–31929 (2010).
53. Tchong, S.-I., Xu, H. & White, R. H. l-Cysteine desulfidase: an [4Fe-4S] enzyme isolated from *Methanocaldococcus jannaschii* that catalyzes the breakdown of l-Cysteine into pyruvate, ammonia, and sulfide. *Biochemistry* **44**, 1659–1670 (2005).
54. Liu, Y., Beer, L. L. & Whitman, W. B. Methanogens: a window into ancient sulfur metabolism. *Trends Microbiol.* **20**, 251–258 (2012).
55. Hidesse, R., Inoue, T., Imanaka, T. & Fujiwara, S. Cysteine desulfurase plays an important role in environmental adaptation of the hyperthermophilic archaeon *Thermococcus kodakarensis*. *Mol. Microbiol.* **93**, 331–345 (2014).
56. Whitman, W. B., Ankwarda, E. & Wolfe, R. S. Nutrition and carbon metabolism of *Methanococcus voltae*. *J. Bacteriol.* **149**, 852 (1982).
57. Whitman, W. B., Bowen, T. L. & Boone, D. R. The methanogenic bacteria. In *The Prokaryotes: Volume 3: Archaea. Bacteria: Firmicutes, Actinomycetes* (eds Dworkin, M., Falkow, S., Rosenberg, E., Schleifer, K.-H. & Stackebrandt, E.) 165–207 (Springer, 2006).
58. Horne, A. J. & Lessner, D. J. Assessment of the oxidant tolerance of *Methanosarcina acetivorans*. *FEMS Microbiol. Lett.* **343**, 13–19 (2013).
59. Sprott, G. D., Meloche, M. & Richards, J. C. Proportions of diether, macrocyclic diether, and tetraether lipids in *Methanococcus jannaschii* grown at different temperatures. *J. Bacteriol.* **173**, 3907 (1991).
60. Kaneshiro, S. M. & Clark, D. S. Pressure effects on the composition and thermal behavior of lipids from the deep-sea thermophile *Methanococcus jannaschii*. *J. Bacteriol.* **177**, 3668 (1995).
61. Gräther, O. W., Arigoni, D. & Jaun, B. Zur Struktur und Biosynthese der Tetraetherlipide der Archaea. (1994).



62. Taubner, R. S. & Rittmann, S. K. M. R. Method for indirect quantification of CH<sub>4</sub> production via H<sub>2</sub>O production using hydrogenotrophic methanogens. *Front. Microbiol.* **7**, 532 (2016).
63. Galili, T. dendextend: an R package for visualizing, adjusting and comparing trees of hierarchical clustering. *Bioinformatics* **31**, 3718–3720 (2015).
64. Josse, J. & Husson, F. missMDA: a package for handling missing values in multivariate data analysis. *J. Stat. Softw.* **70**, 1–31 (2016).
65. R Core Team. R: A Language and Environment for Statistical Computing (R Foundation for Statistical Computing, 2019).
66. Wickham, H. *ggplot2: Elegant Graphics for Data Analysis* (Springer, 2016).
67. Lê, S., Josse, J. & Husson, F. FactoMineR: an R Package for multivariate analysis. *J. Stat. Softw.* **25**, 1–18 (2008).
68. The UniProt Consortium UniProt: a worldwide hub of protein knowledge. *Nucleic Acids Res.* **47**, D506–D515 (2018).
69. El-Gebali, S. et al. The Pfam protein families database in 2019. *Nucleic Acids Res.* **47**, D427–D432 (2019).
70. States, D. J. & Gish, W. QGB: combined use of sequence similarity and codon bias for coding region identification. *J. Computational Biol.* **1**, 39–50 (1994).
71. Altschul, S. F. et al. Gapped BLAST and PSI-BLAST: a new generation of protein database search programs. *Nucleic Acids Res.* **25**, 3389–3402 (1997).
72. Madeira, F. et al. The EMBL-EBI search and sequence analysis tools APIs in 2019. *Nucleic Acids Res.* **47**, W636–W641 (2019).
73. Waterhouse, A. M., Procter, J. B., Martin, D. M. A., Clamp, M. & Barton, G. J. Jalview Version 2—a multiple sequence alignment editor and analysis workbench. *Bioinformatics* **25**, 1189–1191 (2009).

## Acknowledgements

Maria Wolfgruber is acknowledged for assisting with high-pressure experiments. Dr. Lydia M.F. Baumann is acknowledged for helpful discussions. Dr. Melina Kerou is acknowledged for proofreading the manuscript. Greatly acknowledged is the Österreichische Forschungsförderungsgesellschaft (FFG) for funding the projects BioHyMe (grant 853615), Bioraffinerie (grant 854156), and NitroFix (grant 859293). Open access funding by the University of Vienna.

## Author contributions

L.-M.M.: writing paper draft, writing paper review and editing, closed batch cultivations, high-pressure cultivations, bioinformatic analysis, data analysis, preparation of figures. S.Z.: high-pressure cultivations, data analysis. P.P.: high-pressure cultivations, data ana-

lysis. S.B.: design of experiments, writing paper review and editing. A.H.S.: design of experiments, writing paper review and editing. B.R.: closed batch cultivations. T.S.: closed batch cultivations. R.-S.T.: closed batch cultivations, writing paper review and editing. C.P.: supervision of high-pressure experiments, supervision of data analysis, writing paper review and editing, funding acquisition. S.K.-M.R.R. closed batch cultivations, supervision of closed batch experiments, supervision of data analysis, supervision of bioinformatic analyses, writing paper draft, writing paper review and editing, funding acquisitions.

## Competing interests

S.B. and A.H.S. declare to have competing financial interests due to their employment in the Krajete GmbH. All other authors declare no competing interests.

## Additional information

**Supplementary information** The online version contains supplementary material available at <https://doi.org/10.1038/s42003-021-01828-5>.

**Correspondence** and requests for materials should be addressed to S.K.-M.R.R.

**Reprints and permission information** is available at <http://www.nature.com/reprints>

**Publisher's note** Springer Nature remains neutral with regard to jurisdictional claims in published maps and institutional affiliations.



**Open Access** This article is licensed under a Creative Commons Attribution 4.0 International License, which permits use, sharing, adaptation, distribution and reproduction in any medium or format, as long as you give appropriate credit to the original author(s) and the source, provide a link to the Creative Commons license, and indicate if changes were made. The images or other third party material in this article are included in the article's Creative Commons license, unless indicated otherwise in a credit line to the material. If material is not included in the article's Creative Commons license and your intended use is not permitted by statutory regulation or exceeds the permitted use, you will need to obtain permission directly from the copyright holder. To view a copy of this license, visit <http://creativecommons.org/licenses/by/4.0/>.

© The Author(s) 2021

# ANNEX 10

Pages 176 to 195

---

Ergal I., Reischl B., Hasibar B., Manoharan L., Zipperle A., Bochmann G., Fuchs W., Rittmann S.K.-M.R.

**Formate utilization by the Crenarchaeon *Desulfurococcus amylolyticus***

Microorganisms (2020) 8(3):454

10.3390/microorganisms8030454

---



## Article

# Formate Utilization by the Crenarchaeon *Desulfurococcus amylolyticus*

Ipek Ergal <sup>1</sup>, Barbara Reischl <sup>1</sup>, Benedikt Hasibar <sup>2</sup> , Lokeshwaran Manoharan <sup>1</sup> , Aaron Zipperle <sup>1</sup> , Günther Bochmann <sup>2</sup>, Werner Fuchs <sup>2</sup> and Simon K.-M. R. Rittmann <sup>1,\*</sup>

<sup>1</sup> Archaea Physiology & Biotechnology Group, Department of Functional and Evolutionary Ecology, Universität Wien, 1090 Wien, Austria; ipek.ergal@univie.ac.at (I.E.); barbara.reischl@univie.ac.at (B.R.); Lokeshwaran.Manoharan@nbs.se (L.M.); aaronzipperle@gmail.com (A.Z.)

<sup>2</sup> Department IFA Tulln, Institute for Environmental Biotechnology, University of Natural Resources and Life Sciences, 1180 Wien, Austria; benedikt.kleibel@boku.ac.at (B.H.); guenther.bochmann@boku.ac.at (G.B.); werner.fuchs@boku.ac.at (W.F.)

\* Correspondence: simon.rittmann@univie.ac.at; Tel.: +43-4277-76513; Fax: +43-4277-876513

Received: 9 February 2020; Accepted: 20 March 2020; Published: 23 March 2020



**Abstract:** Formate is one of the key compounds of the microbial carbon and/or energy metabolism. It owes a significant contribution to various anaerobic syntrophic associations, and may become one of the energy storage compounds of modern energy biotechnology. Microbial growth on formate was demonstrated for different bacteria and archaea, but not yet for species of the archaeal phylum Crenarchaeota. Here, we show that *Desulfurococcus amylolyticus* DSM 16532, an anaerobic and hyperthermophilic Crenarchaeon, metabolises formate without the production of molecular hydrogen. Growth, substrate uptake, and production kinetics on formate, glucose, and glucose/formate mixtures exhibited similar specific growth rates and similar final cell densities. A whole cell conversion experiment on formate revealed that *D. amylolyticus* converts formate into carbon dioxide, acetate, citrate, and ethanol. Using bioinformatic analysis, we examined whether one of the currently known and postulated formate utilisation pathways could be operative in *D. amylolyticus*. This analysis indicated the possibility that *D. amylolyticus* uses formaldehyde producing enzymes for the assimilation of formate. Therefore, we propose that formate might be assimilated into biomass through formaldehyde dehydrogenase and the oxidative pentose phosphate pathway. These findings shed new light on the metabolic versatility of the archaeal phylum Crenarchaeota.

**Keywords:** Archaea; Crenarchaeota; anaerobe; microbial physiology; metabolism; one-carbon; formaldehyde

## 1. Introduction

Formic acid, a monocarboxylic acid, is one of the simplest organic compounds. It is a colourless liquid with a pungent odour [1]. The freezing and the boiling points of formate are 8.3 and 100.7 °C, respectively. The carbon of formic acid is a poor electrophile. This characteristic makes formic acid a strong acid ( $pK_a = 3.75$ ), e.g., compared to acetic acid ( $pK_a = 4.75$ ) [2]. The salt of formic acid is formate. Formate can be produced using various routes such as the electrochemical reduction of  $CO_2$  [3–7], photo-reduction of  $CO_2$  [8], hydrogenation of  $CO_2$  [9,10], selective oxidation of biomass [11,12], partial oxidation of natural gas [13], and hydration of syngas (e.g., carbon monoxide) [14]. In 1670, John Wray had already isolated formate from ants [15], and later it was named after “formicidae”, the ant family. Formate has numerous functions in biological systems, such as serving as an irritant in the sprayed venom of some ant species [16], as antibacterial substance [17], and it is used for food preservation, as cosmetic additive, or as pesticide [18]. Moreover, it can be used as a non-flammable liquid fuel [19],

an energy storage compound [20,21], and as a feedstock for cultivation of microorganisms [22]. Hence, biological production and utilization of formate is of ecological and biotechnological significance.

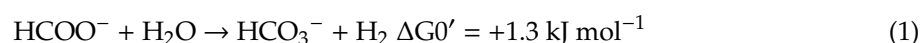
Metabolisation of formate can occur during acetogenesis [23], methanogenesis [24], and molecular hydrogen (H<sub>2</sub>) production [25]. Moreover, formate can provide cells with both a carbon source and reducing power. It delivers a significant contribution to anaerobic syntrophic associations, as formate is transferred as redox currency between the organisms [26]. According to a search using the PubChem Substance and Compound Databases [27], there are 189 biological systems that include formate as a reaction component. This shows the significance of formate in functioning of biological systems. Therefore, formate assimilation pathways and studying how microorganisms with different physiologies can convert formate into specific metabolites are increasingly attracting attention.

One possible way to biologically produce formate is the reduction of CO<sub>2</sub> by H<sub>2</sub> through the hydrogen-dependent CO<sub>2</sub> reductase (HDCR). The HDCR was first isolated and characterized in *Acetobacterium woodii* [28]. It consists of four subunits: a putative formate dehydrogenase (FdhF1/2), a Fe–Fe hydrogenase (HydA), and two small electron transfer subunits [28,29]. The HDCR operates the direction of the catalysis depends on the substrate concentration [28].

Another option to biologically produce formate is through pyruvate cleavage by pyruvate formate lyase (PFL) (30). PFL is an oxygen sensitive, ubiquitous enzyme that supports increased ATP yield during fermentation of, e.g., glucose [14]. PFL plays a central role in many organisms providing formate and acetyl-coenzyme A (CoA) via the conversion of pyruvate and CoA. The activation of PFL occurs with an enzyme referred to as PFL-activating enzyme (PFL-AE). The activation of PFL involves an abstraction of hydrogen through PFL-AE, which belongs to the radical S-adenosyl-methionine (SAM) super-family [30,31]. To understand the assimilation of formate and how it can support microbial growth, the reverse PFL reaction was studied in vivo in *Escherichia coli*. [32]. PFL-dependent co-assimilation of acetate and formate was demonstrated with *E. coli* mutant strains. It was concluded that PFL could support growth on formate as the carbon source.

Oxidation of formate can be catalysed by some microorganisms such as Burkholderiaceae [33], Clostridiaceae [34,35], and Enterobacteriaceae [36–44]. The oxidation of formate is performed to avoid cellular toxification through intracellular formate accumulation [45]. In *E. coli*, formate is able to disturb the membrane potential and allows the hydrogen ion (H<sup>+</sup>) to enter the cell from the medium [45,46]. At certain concentrations, this leads to a collapse of the pH gradient across the cytoplasmic membrane, referred to as uncoupling, that consequently ceases the metabolism [47]. Hence, detoxification mechanisms were developed to avoid uncoupling at high concentrations of formate. In *E. coli*, formate is disproportionated into H<sub>2</sub>/CO<sub>2</sub> by the formate hydrogen lyase (FHL) complex. There, Fdh along with hydrogenase-3 (Hyd-3) which is encoded by *hyc* operon, can form the FHL complex [48].

Even though the oxidation of formate can occur as a result of detoxification mechanism, formate cannot be metabolised by members of Burkholderiaceae, Clostridiaceae, and Enterobacteriaceae, as this reaction is not energetically sufficient to support growth. Under anoxic conditions, the stoichiometry of formate conversion is given below (Equation (1)):



Until the discovery of the hyperthermophilic archaeon *Thermococcus onnurineus* NA1 [49,50], it was assumed that the reaction is only thermodynamically possible when a methanogenic or sulphate-reducing partner is present to remove H<sub>2</sub>, which is one of the end products of syntrophic formate oxidation [51–54]. *T. onnurineus* is able to oxidise formate into H<sub>2</sub>/CO<sub>2</sub>, and coupling this reaction to chemiosmotic ATP synthesis [25,55]. The metabolic pathway responsible for formate oxidation in *T. onnurineus* was characterised by using proteomics [56]. It was found that formate oxidation proceeds via a membrane-bound enzyme system, comprised of Fdh, and a membrane-bound hydrogenase (Mfh), a sodium-proton (Na<sup>+</sup>/H<sup>+</sup>) antiporter (Mnh) and a Na<sup>+</sup>-dependent ATP synthase [57]. Furthermore, it was revealed that several copies of hydrogenase gene clusters

(*fdh-mfh-mnh*) are present in *T. onnurineus*. The hydrogenase genes in *fdh2-mfh2-mnh2* were upregulated more than 2-fold when formate was provided as sole energy source to *T. onnurineus*, which is an indication of the importance of the hydrogenase genes in the *fdh2-mfh2-mnh2* gene cluster for growth coupled to formate oxidation and H<sub>2</sub> production [25].

Recently, a novel synthetic formate-fixing pathway was proposed, which is involved in the acetyl-CoA exchange to formyl-CoA and formate reduction to formaldehyde [58]. Formaldehyde can be integrated into the central carbon metabolism much easier than direct formate utilization, since it is a highly reactive compound [59]. However, the reduction potential of formate to formaldehyde is quite low under standard biochemical conditions [ $-650\text{ mV} \leq E^{\circ'} \leq -450\text{ mV}$  ( $6 \leq \text{pH} \leq 8$ ;  $0 \leq I \leq 0.25\text{ mol L}^{-1}$ )] [60]. Hence, the activation of formate requires an electron donor such as universal electron carrier NAD(P)H ( $-370\text{ mV} \leq E' \leq -280\text{ mV}$ ) [58]. One of the formate-fixing reactions is catalysed through the formaldehyde dehydrogenase (FoDH) enzyme, which directly converts formate to formaldehyde using NADH as a cofactor [61,62]. Investigating formate assimilation in other organisms could contribute to the identification of new formate-fixation pathways and its enzymes.

*Desulfurococcus amylolyticus* DSM 16532 [63] is an anaerobic, hyperthermophilic Crenarchaeon able to grow on a broad range of polymers and sugars [63,64]. Recently, physiological variables, such as the specific growth rate ( $\mu$ ), were determined for *D. amylolyticus* grown on fructose or glucose in chemically defined medium [65]. A metabolic reconstruction revealed that *D. amylolyticus* contains all glucose metabolism-related genes and harbours several genes for H<sub>2</sub> production, such as pyruvate ferredoxin oxidoreductase, glyceraldehyde-3-phosphate ferredoxin oxidoreductase, and two membrane-bound hydrogenases [64,65]. As growth on formate coupled to H<sub>2</sub> production by hyperthermophilic Archaea could be an opportunity in biotechnology [66,67], we investigated whether *D. amylolyticus* could be used for this purpose.

In this work, we examined the substrate uptake, growth, and production kinetics of *D. amylolyticus* grown on formate, glucose, and a mixture of glucose/formate in closed batch cultivation mode. The intention was to physiologically characterise the organism with respect to  $\mu$ , cell-specific H<sub>2</sub> and CO<sub>2</sub> productivities, and maximum cell concentration. After this, the mass balance analysis of substrate uptake and product formation kinetics was performed in whole cell conversion experiments. Finally, we investigated and compared the metabolic capacity for formate utilization of *D. amylolyticus* to other formate metabolising microorganisms on the genomic level with the goal of revealing possible formate assimilation pathways.

## 2. Material and Methods

### 2.1. Chemicals

The standard test gas utilized in gas chromatography (GC) comprised the following composition: 0.01 Vol.-% CH<sub>4</sub>; 0.08 Vol.-% CO<sub>2</sub> in N<sub>2</sub> (Messer GmbH, Wien, Austria). All other chemicals were of highest grade available. H<sub>2</sub>, CO<sub>2</sub>, N<sub>2</sub>, 20 Vol.-% CO<sub>2</sub> in N<sub>2</sub>, and CO were of test gas quality (Air Liquide, Schwechat, Austria).

### 2.2. Microorganism and Medium Composition

*Desulfurococcus amylolyticus* DSM 16532 [63,68] was purchased from the Deutsche Sammlung von Mikroorganismen und Zellkulturen GmbH (DSMZ). The medium was prepared as previously described [64,65]. A modified DSMZ medium, No. 395, without yeast extract, powdered sulphur and glucose was prepared when only formic acid containing medium was used for growth of *D. amylolyticus*. The medium contained (per L): 0.33 g of NH<sub>4</sub>Cl; 0.33 g of KH<sub>2</sub>PO<sub>4</sub>; 0.33 g of KCl; 0.44 g of CaCl<sub>2</sub>·2H<sub>2</sub>O; 0.70 g of MgCl<sub>2</sub>·6H<sub>2</sub>O; 0.50 g of NaCl; 0.80 g of NaHCO<sub>3</sub>; 0.50 g of Na<sub>2</sub>S·9H<sub>2</sub>O; 1 mL of trace elements SL-10; and 10 mL of vitamin solution as previously described [64,65].



### 2.3. Closed Batch Cultivations

Closed batch cultivations were conducted in two different sets of experiments. The first set of experiments were designed as “end-point experiments” where growth was monitored at each time-point, whereas substrate uptake and production measurements were only performed at end of the experiment. The second set of experiments were designed as “time-point experiments” where substrate uptake, growth and production kinetics were observed and measured at each time-point during the experiment.

Cultures of *D. amylolyticus* were grown anaerobically at  $0.2\text{--}0.3 \cdot 10^5$  Pa in a 100 Vol.-%  $\text{N}_2$  atmosphere in a closed batch set-up as previously described [64,65]. Concentrations of carbon sources were adjusted to the same carbon concentration ( $\text{C}\cdot\text{mmol L}^{-1}$ ). For end-point experiments the following carbon sources were individually tested: formic acid and glucose at  $116.6 \text{ C}\cdot\text{mmol L}^{-1}$ , respectively. Formic acid at a concentration of  $50 \text{ C}\cdot\text{mmol L}^{-1}$ , and glucose at a concentration of  $66.6 \text{ C}\cdot\text{mmol L}^{-1}$  (total  $116.6 \text{ C}\cdot\text{mmol L}^{-1}$ ) were added for the co-substrate experiment. Additionally, glucose and formic acid were tested as carbon sources at  $66.6$  and  $50 \text{ C}\cdot\text{mmol L}^{-1}$ , respectively, to assess the difference in substrate uptake, growth and production kinetics between the co-substrate and single substrate experiment.

The pre-culture for inoculation was obtained from a formic acid pre-grown *D. amylolyticus* culture. All experiments were performed in quadruplicates together with a negative (un-inoculated) control and reproduced twice. Moreover, we performed an additional positive–negative (inoculated on medium without formic acid) control to observe growth kinetics on medium containing just vitamins and trace elements, without formic acid (Supplementary Figure S1). Pressure measurements of the serum bottle headspace were performed with a digital manometer (LEO1-Ei,  $-1\text{--}3\text{bar}$  rel, Keller, Germany) and the measurements were performed before samples were taken for microscope analysis. For time-point experiments, formic acid was used as the carbon source at concentration of  $100 \text{ C}\cdot\text{mmol L}^{-1}$ . For each time-point, identical sets of serum bottles (quadruplicates) were prepared and inoculated. They were not manipulated until the destructive gas chromatography (GC) measurement (see below in GC section).

### 2.4. Whole Cell Conversion Experiments

*D. amylolyticus* was pre-grown on formic acid and harvested by centrifugation (Eppendorf Centrifuge 5415R, Eppendorf, Hamburg, Germany) for 20 min and  $15,700 \text{ g}$ . The supernatant was removed and the resulting pellet was washed with the respective medium. After the washing step, the cells were resuspended in buffer containing (per L):  $\text{NH}_4\text{Cl}$  0.33 g;  $\text{KH}_2\text{PO}_4$  0.33 g;  $\text{KCl}$  0.33 g;  $\text{CaCl}_2 \cdot 2\text{H}_2\text{O}$  0.44 g;  $\text{MgCl}_2 \cdot 6 \text{H}_2\text{O}$  0.70 g;  $\text{NaCl}$  0.50 g;  $\text{NaHCO}_3$  0.80 g. Serum bottles of 120 mL were supplemented with formic acid (concentration of 20, 50, and  $100 \text{ C}\cdot\text{mmol L}^{-1}$ ). Cultures ( $1 \cdot 10^8 \text{ cells mL}^{-1}$ ) were incubated for 5 and 12 h, respectively and GC analyses were immediately conducted afterwards. All experiments were performed in triplicates together with a negative (un-inoculated) control.

### 2.5. Cell Counting

*D. amylolyticus* cells were counted using a Nikon Eclipse 50i microscope (Nikon, Amsterdam, Netherlands) at each sampling point. The samples for cell count were taken from each individual closed batch run using syringes (Soft-Ject, Henke Sass Wolf, Tuttlingen, Germany) and hypodermic needles (Sterican size 14, B. Braun, Melsungen, Germany). An amount of  $10 \mu\text{L}$  of sample was applied onto a Neubauer improved cell counting chamber (Superior Marienfeld, Lauda-Königshofen, Germany) with a grid depth of 0.1 mm.

## 2.6. Gas Chromatography

Time-point and end-point GC measurements were performed from serum bottles that remained without any manipulation after inoculation, except incubation in air bath until the GC measurement was performed. To analyse the gas composition inside the serum bottles from end-point and time-point experiments, destructive sampling was employed. The gas compositions were analysed using a GC (7890A GC System, Agilent Technologies, Santa Clara, CA, USA) with a 19808 Shin Carbon ST Micropacked Column (Restek GmbH, Bad Homburg, Germany) and provided with a gas injection and control unit (Joint Analytical System GmbH, Moers, Germany) as described earlier [64].

## 2.7. Formic Acid Analysis

The Formic Acid Assay Kit (Megazyme Inc., Bray, Ireland) was used for measurements of formic acid concentrations in samples which were previously diluted to the linear range of the assay kit to yield a formic acid concentration of 0.004–0.200 g L<sup>-1</sup>. The microplate (Crystal Clear, Greiner Bio One) assay was applied according to manufacturer's instructions: a 255 µL reaction volume.

## 2.8. HPLC

The determination of sugars, volatile fatty acids (VFAs), organic acids, and alcohols were performed with high performance liquid chromatography (HPLC) system (Agilent 1100), consisting of a G1310A isocratic pump, a G1313A ALS autosampler, a Transgenomic ICSep ICE-ION-300 column, a G1316A column thermostat set at 45 °C, a G1362A RID refractive index detector, measuring at 45 °C (all modules were from Agilent 1100 (Agilent Technologies, CA, USA)). The measurement was performed with 0.005 mol L<sup>-1</sup> H<sub>2</sub>SO<sub>4</sub> as solvent, with a flow rate of 0.325 mL min<sup>-1</sup> and a pressure of 48–49 bar. The injection volume was 40 µL.

## 2.9. Data Analysis

For the quantitative analysis, the maximum specific growth rate ( $\mu_{\max}$  [h<sup>-1</sup>]) and mean specific growth rate ( $\mu_{\text{mean}}$  [h<sup>-1</sup>]) were calculated as follows:  $N = N^0 \cdot e^{\mu t}$  with  $N$ , cell number [cells mL<sup>-1</sup>];  $N^0$ , initial cell number [cells mL<sup>-1</sup>];  $t$ , time [h] and  $e$ , Euler number. According to the delta cell counts in between sample points,  $\mu$  was assessed. The CO<sub>2</sub> evolution rate (CER [mmol L<sup>-1</sup> h<sup>-1</sup>] (C-molar)), the cell specific CO<sub>2</sub> productivity ( $q_{\text{CO}_2}$ , cell [mmol cell<sup>-1</sup> h<sup>-1</sup>] (C-molar)) [67] was calculated from the end point gas composition of the non-manipulated serum bottles. The ash content and elementary composition of *D. amylolyticus* were presumed to relate to published results [69]. The elementary composition was used for the calculation of the mean molar weight, Carbon balance (C-balance) and the degree of reduction (DoR) balance of the corresponding biomass. DoR denotes the number of electrons an atom can donate, summed up for all the atoms of a molecule, or biomass elementary composition, divided by the number of carbon atoms in the molecule/biomass elementary composition. Yields of by-products were determined after HPLC measurement. The values were normalized according to zero (time-point zero) control and negative values (if there were any) were assumed as zero.

## 2.10. Gibbs Free Energy Calculations

Standard Gibbs free energy change ( $\Delta G^{\circ}$ ) is used to describe whether a certain chemical reaction can be utilized for microbial energy conservation. However, the underlying thermodynamic calculations are usually standardized to 25 °C and 1 bar pressure. For thermophilic bioprocesses the physiological conditions differ significantly and, consequently, values have to be adapted, as especially temperature has a huge impact on thermodynamics [70]. In the present study, *D. amylolyticus* was cultivated at 80 °C. The recalculation method applied in the current study is based on previously published results [70], which provide standard state thermodynamic properties at temperatures up to 200 °C for a wide variety of anaerobic metabolic reactions. Moreover, they discuss the thermodynamic framework in detail and the application of the revised Helgeson Kirkham Flowers (HKF) equation of state to obtain

standard molal Gibbs free energies of formation ( $G_f^0$ ) at elevated temperatures and pressures for individual aqueous compounds. With one important exemption, the values for  $G_f^0$  are taken from this paper. Unfortunately, the named study does not include data for formaldehyde, which were therefore obtained from another publication [71], and recalculated as specified. Finally, the Gibbs values for the overall reaction at standard concentrations (1 mol L<sup>-1</sup>) and pH of 7 ( $\Delta G^0$ ) were calculated as previously described [70].

### 2.11. Genome Analysis

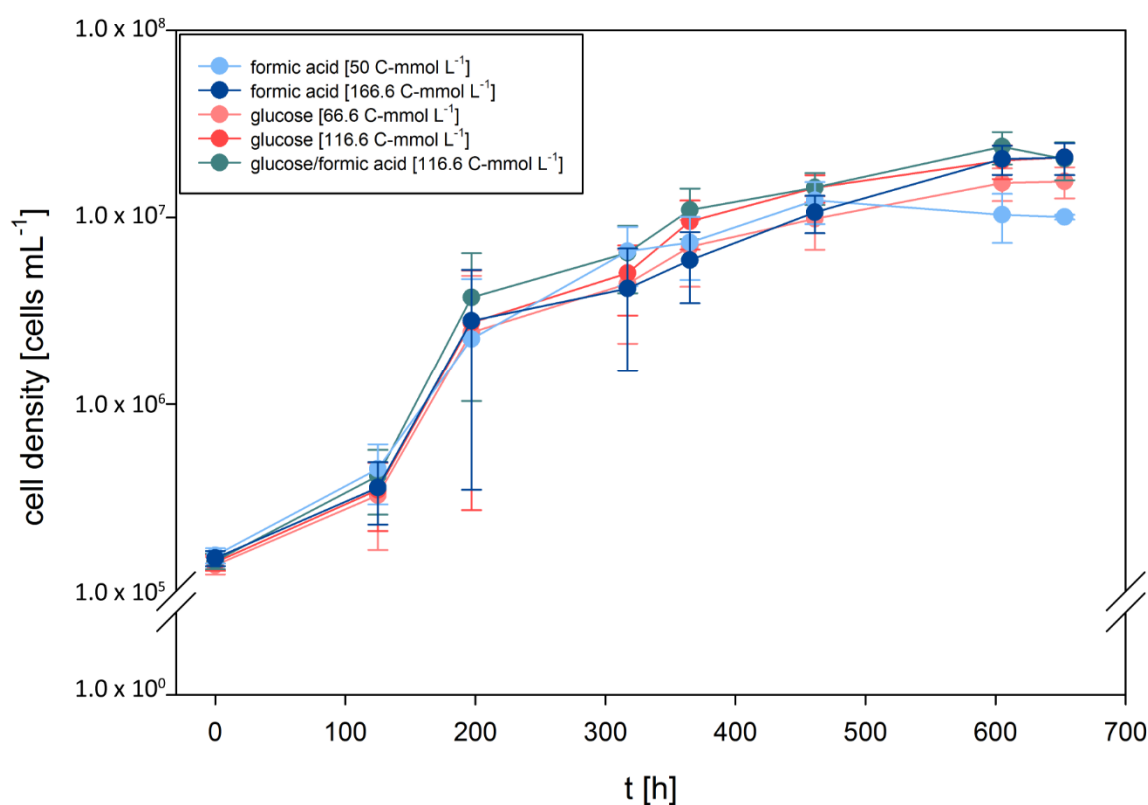
To investigate the formate metabolism of *D. amylolyticus*, the protein sequences from the whole genome of organisms where formate related pathways were previously described like *T. onnurineus* (Ton\_GCF\_000018365.1\_ASM1836v1), *Pyrococcus furiosus* (Pfu\_GCF\_000007305.1\_ASM730v1), *E. coli* K-12 (Eco\_GCF\_000750555.1\_ASM75055v1), *Methanosarcina barkeri* (Mba\_GCF\_000195895.1\_ASM19589v1), *Thermoanaerobacter kivui* (Tki\_GCF\_000763575.1\_ASM76357v1) and *A. woodii* (Awo\_GCF\_000247605.1\_ASM24760v1) were obtained from the NCBI RefSeq [72] database. Homologous proteins involved in formate-related metabolism of *D. amylolyticus* were identified by using Basic Local Alignment Search Tool (BLAST) [73] against the manually sorted proteins from characterised enzymes (Supplementary Table S1) with E-values and local identity cutoffs of  $<10^{-10}$  and  $>25\%$ , respectively. Orthologous genes (genome level) were obtained by pair-wise all versus all BLAST of the aforementioned organisms using the "OrthoFinder" tool [74]. Furthermore, the orthologous gene (gene in a different species that evolved from a common ancestral gene by speciation) groups (ortho-groups) containing the characterised enzymes related to formate-related metabolism were retrieved. After sorting the proteins of interest, enzyme complexes were identified by using bidirectional BLAST. Results for query coverage, E-value, and identity can be found in Supplementary Table S2 and Supplementary Table S3. In addition, the Pfam domains [75] of all the proteins in *D. amylolyticus* were also predicted for a further look into the domains of enzymes related to the formate metabolism.

## 3. Results

### 3.1. *D. amylolyticus* Grows on Formate

Recently, we investigated growth characteristics of *D. amylolyticus* on cellulose, fructose, arabinose, glucose, lactose, maltose, starch, and sucrose. Moreover, we partially re-annotated the genome and metabolically reconstructed the central carbon metabolism [65]. According to the metabolic reconstruction of *D. amylolyticus*, it seemed to be possible that the organism could grow through metabolisation of formate. To elucidate the growth kinetics of *D. amylolyticus* on formate and to be able to compare them to glucose and formate–glucose mixtures, end-point experiments were designed to analyse growth kinetics in defined medium with each of the substrates at the same concentration (166.6 C-mmol L<sup>-1</sup>). Additionally, formate and glucose were tested at concentrations of 50 and 66.6 C-mmol L<sup>-1</sup>, respectively, to be able to examine the growth kinetics at lower substrate concentrations. The results of the growth characteristics are shown in Figure 1. Clearly, *D. amylolyticus* did not grow on a medium where formic acid was omitted (Supplementary Figure S1). The lag time lasted approximately 125 h, until growth of *D. amylolyticus* on each of the substrates commenced. The key physiological variables are presented in Table 1. The organism grew almost equally well on all substrates tested and at all concentrations. Astonishingly, the organism grew on formate as the sole energy source with a  $\mu_{\max}$  of 0.032 h<sup>-1</sup>. A slightly higher  $\mu_{\max}$  of 0.035 and 0.036 h<sup>-1</sup> was only obtained on glucose and formate/glucose, respectively. The differences in  $\mu_{\max}$  might be explained by slightly different concentrations and hyperbolic relationship between  $\mu$  and the substrate concentration [76,77]. In a previous study, we showed that *D. amylolyticus* comprises a  $\mu_{\max}$  of 0.059 h<sup>-1</sup> at a concentration of 166.5 C-mmol L<sup>-1</sup> glucose [65]. In our previous studies [64,65], growth of *D. amylolyticus* resulted in low cell densities only, a characteristic shared with many other hyperthermophilic microorganisms [78].

The growth of *D. amylolyticus* on glucose was accompanied by lactate, acetate, and formate production, whereas growth on formate resulted in production of acetate, citrate, and ethanol (Table 2).



**Figure 1.** Growth curves of *D. amylolyticus* on formate, glucose, and glucose/formate at different concentrations. A slightly higher  $\mu$  could be obtained when glucose/formate was used as substrate. All the substrate concentrations are given as C-mmol L<sup>-1</sup>. A negative (un-inoculated) control and positive-negative (inoculated into medium where formic acid was omitted) control were performed in each set and no growth was observed.

**Table 1.** Growth characteristics of *D. amylolyticus*.

Compound and Concentration	$\mu_{\max}$ [h <sup>-1</sup> ]	$\mu_{\text{mean}}$ [h <sup>-1</sup> ]	Final Cell Concentration [cells per mL]
Glucose [66.6 C-mmol L <sup>-1</sup> ]	0.033	0.011	$1.55 \cdot 10^7$
Glucose [116.6 C-mmol L <sup>-1</sup> ]	0.035	0.012	$2.09 \cdot 10^7$
Formic acid [50 C-mmol L <sup>-1</sup> ]	0.032	0.010	$1.24 \cdot 10^7$
Formic acid [116.6 C-mmol L <sup>-1</sup> ]	0.032	0.011	$2.08 \cdot 10^7$
Glucose/Formic acid [66 and 50 C-mmol L <sup>-1</sup> ]	0.036	0.012	$2.38 \cdot 10^7$

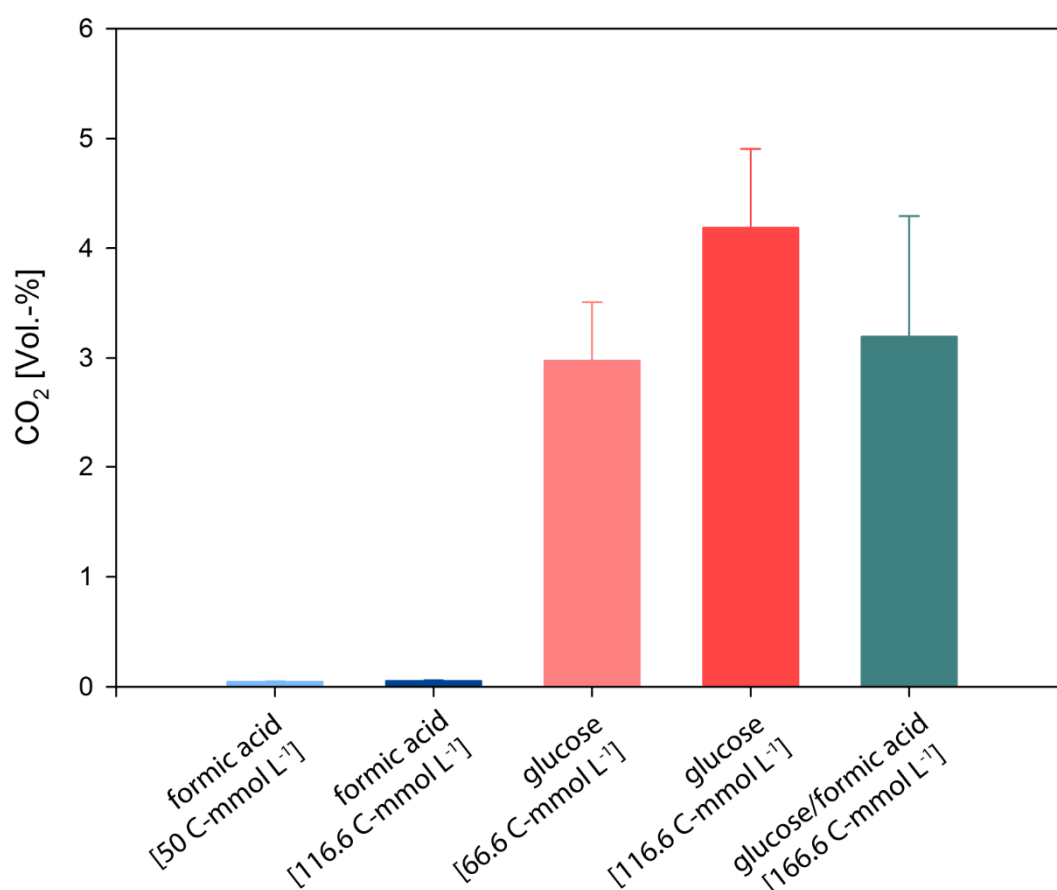
**Table 2.** Productivity and yields of *D. amylolyticus* from glucose or formic acid metabolism during closed batch end-point experiments.

Compound and Concentration	CER [mmol L <sup>-1</sup> h <sup>-1</sup> ] (C-Molar)	qCO <sub>2</sub> [pmol h <sup>-1</sup> g <sup>-1</sup> ] (C-Molar)	Y(CO <sub>2</sub> /s) [C-mol/ C-mol] *	Y(Lact/s) [C-mol/ C-mol] *	Y(Ac/s) [C-mol/ C-mol] *	Y(Form/s) [C-mol/ C-mol] *	Y(Glu/s) [C-mol/ C-mol] *	Y(Buty/s) [C-mol/ C-mol] *	Y(Citr/s) [C-mol/ C-mol] *	Y(Eth/s) [C-mol/ C-mol] *	Y(x/s) [C-mol/ C-mol]	C-Balance <sup>+</sup>	DoR-Balance <sup>#</sup>
Glucose [66.6 C-mmol L <sup>-1</sup> ]	3.34·10 <sup>-5</sup>	2.41·10 <sup>-3</sup>	2.64·10 <sup>-2</sup>	2.96·10 <sup>-1</sup>	5.64·10 <sup>-1</sup>	6.14·10 <sup>-2</sup>					1.29·10 <sup>-4</sup>	94.80%	89.08%
Glucose [116.6 C-mmol L <sup>-1</sup> ]	4.04·10 <sup>-5</sup>	2.59·10 <sup>-3</sup>	4.43·10 <sup>-1</sup>	2.48·10 <sup>-1</sup>	5.89·10 <sup>-1</sup>	8.10·10 <sup>-2</sup>					2.42·10 <sup>-3</sup>	136.12%	87.82%
Formic acid [50 C-mmol L <sup>-1</sup> ]	1.20·10 <sup>-6</sup>	1.16·10 <sup>-2</sup>	7.20·10 <sup>-4</sup>		1.45·10 <sup>-1</sup>		8.69·10 <sup>-3</sup>	2.15·10 <sup>-4</sup>	5.59·10 <sup>-2</sup>	5.17·10 <sup>-1</sup>	6.34·10 <sup>-5</sup>	72.79%	194.37%
Formic acid [116.6 C-mmol L <sup>-1</sup> ]	3.48·10 <sup>-6</sup>	2.23·10 <sup>-4</sup>	5.02·10 <sup>-4</sup>		6.21·10 <sup>-1</sup>		5.12·10 <sup>-2</sup>		1.02·10 <sup>-2</sup>	1.59·10 <sup>-2</sup>	3.18·10 <sup>-5</sup>	69.84%	140.65%

\* Y; Yield of product (CO<sub>2</sub>, lactate, acetate, formate, glucose, butyrate, citrate, ethanol, biomass) per substrate (s) consumed. <sup>+</sup> Carbon balance. <sup>#</sup> Degree of reduction balance.



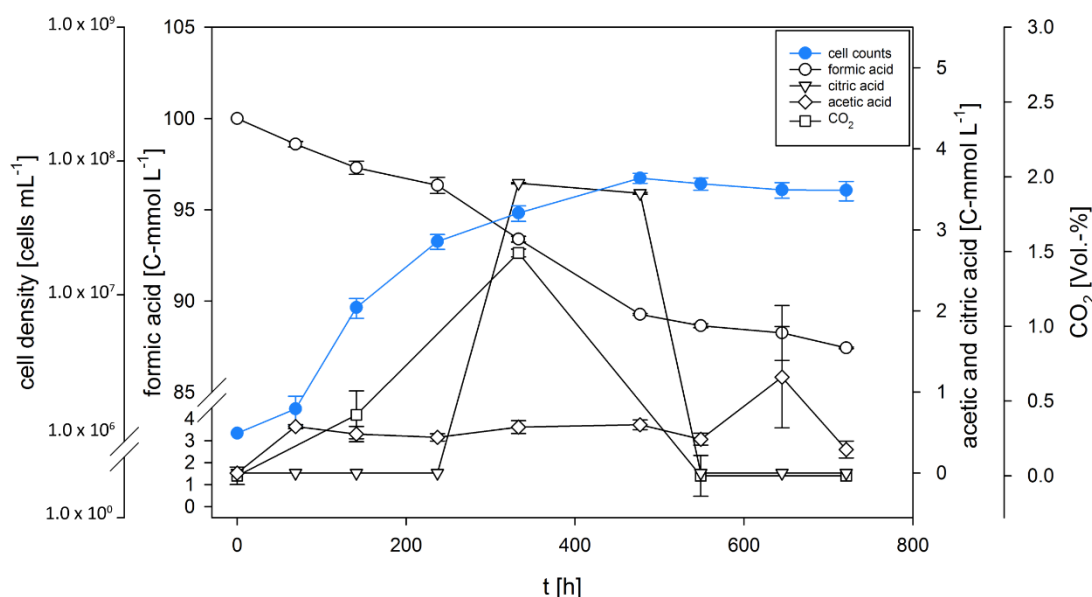
Following this, we examined the gaseous product formation spectrum from all quadruplicate closed batch experiments on formate, glucose, and formate/glucose. CO<sub>2</sub> was the only gas detectable in all growth experiments. The CO<sub>2</sub> concentrations are shown in Figure 2, and an overview of CO<sub>2</sub> productivities are presented in Table 2. In cultures which were grown on formate, the cumulative CO<sub>2</sub> levels were in the ppm range. However, during growth on glucose or formate/glucose, the cumulative CO<sub>2</sub> values were more than one order of magnitude higher. H<sub>2</sub> could not be detected in any growth experiment, which is in contradiction to experiments in bioreactors [64], but in agreement to our previous closed batch experiments [65]. This indicates that *D. amylolyticus* did not use the electrons from formate or glucose to balance homeostasis by producing H<sub>2</sub>. However, instead it could be possible that the electrons were used to balance anaplerotic reactions, which indicates that during formate metabolization, CO<sub>2</sub> was assimilated into biomass through some of the several annotated CO<sub>2</sub>-fixing enzymes [65]. However, up to now it is not clear if the ATP for the CO<sub>2</sub> fixation is retrieved from substrate level phosphorylation via glycolysis or from chemiosmotic ATP production or the pseudo-TCA cycle.



**Figure 2.** End point gas composition of *D. amylolyticus* grown at different concentrations of formate, glucose, and glucose/formate at the end of the cultivation. The results indicate that the CO<sub>2</sub> production is very low in the cultures grown on formate compared to cultures grown on glucose or glucose/formate. All the substrate concentrations are given as C-mmol L<sup>-1</sup>.

During the time-point experiments (Figure 3), the observed growth kinetics showed a similar trend as in the end-point experiments (Figure 1). Production and consumption of citrate and CO<sub>2</sub> are shown in Figure 3 and an overview of CO<sub>2</sub> productivities and mass balances are presented in Table 3. The results of the closed batch time-point experiment indicate that CO<sub>2</sub>-fixation occurs. Hence, during the first 300 h, CO<sub>2</sub> was produced and subsequently consumed within the next 200 h of the experiment. We have previously shown that *D. amylolyticus* harbours several genes, which might be involved in

CO<sub>2</sub> fixation [65], and the results presented in this study suggest the possibility that CO<sub>2</sub> might be fixed through enzymes of the reductive citric acid cycle, as citric acid is one of the produced metabolites and consumed compounds.



**Figure 3.** Growth, substrate uptake, and production kinetics of *D. amylolyticus* on 100 C-mmol L<sup>-1</sup> formate. The results indicate that CO<sub>2</sub> and citric acid were produced and consumed completely during the cultivation and only after the consumption of CO<sub>2</sub> and citric acid, acetic acid was produced.

### 3.2. *D. amylolyticus* Converts Formate to CO<sub>2</sub>, Acetate, Citrate, and Ethanol

To investigate the metabolism on formate in more detail, whole cell conversion experiments were performed. A whole cell conversion experiment has unique advantages, such as minimising side reactions and avoiding biomass production [79–81]. Therefore, we performed experiments with high cell densities (1·10<sup>8</sup> cells mL<sup>-1</sup>) using *D. amylolyticus* at formate concentrations of 20, 50, and 100 C-mmol L<sup>-1</sup> in buffer. This experiment revealed astonishing findings. A summary of the obtained physiological variables is shown in Table 4. The highest formate uptake rate of 20.7 C-mmol L<sup>-1</sup> was observed when *D. amylolyticus* was incubated at a concentration of 100 C-mmol L<sup>-1</sup> formate. After 5 h of incubation, the production of small amounts of butyrate was detected in 50 and 100 C-mmol L<sup>-1</sup> formate, and citrate, as well as ethanol, was only detected in one of the other. After 12 h of incubation, ethanol and low amounts of citrate were detected at all tested formate concentrations, but acetate was only detected at 100 C-mmol L<sup>-1</sup> formate. The detection of citrate production during growing conditions and during the whole cell conversion experiment (compare Tables 2 and 4) might indicate that the citric acid cycle was involved during formate assimilation. However, in our previous study, a canonical citric acid cycle or a reverse citric acid cycle could not be observed in the genome of *D. amylolyticus* [65].

**Table 3.** Productivities and yields of *D. amylolyticus* grown on formic acid during time-point experiments.

Time [h]	CER [mmol L <sup>-1</sup> h <sup>-1</sup> ] (C-Molar)	qCO <sub>2</sub> [pmol h <sup>-1</sup> g <sup>-1</sup> ] (C-Molar)	Y <sub>(CO2/s)</sub> [C-mol/C-mol] *	Y <sub>(Ac/s)</sub> [C-mol/C-mol] *	Y <sub>(Citr/s)</sub> [C-mol/C-mol] *	Y <sub>(x/s)</sub> [C-mol/C-mol] *	C-Balance +	DoR-Balance #
69				4.09·10 <sup>-1</sup>		1.05·10 <sup>-5</sup>	40.93%	81.87%
141	2.12·10 <sup>-5</sup>	2.65·10 <sup>-6</sup>	2.32·10 <sup>-3</sup>	3.73·10 <sup>-1</sup>		6.57·10 <sup>-5</sup>	37.55%	74.67%
237				4.57·10 <sup>-1</sup>		2.75·10 <sup>-4</sup>	45.75%	91.53%
333	5.35·10 <sup>-5</sup>	1.31·10 <sup>-6</sup>	6.04·10 <sup>-3</sup>	1.93·10 <sup>-1</sup>	1.21·10 <sup>0</sup>	1.46·10 <sup>-4</sup>	141.12%	220.45%
477				1.44·10 <sup>-1</sup>	8.36·10 <sup>-1</sup>	1.91·10 <sup>-4</sup>	98.05%	154.30%
549	NA §	NA§	1.82·10 <sup>-3</sup>	6.74·10 <sup>-1</sup>		1.15·10 <sup>-3</sup>	66.53%	134.93%
645				3.03·10 <sup>0</sup>		1.65·10 <sup>-3</sup>	302.83%	90.15%
721	NA §	NA§	3.53·10 <sup>-3</sup>	3.54·10 <sup>-1</sup>		7.76·10 <sup>-4</sup>	34.11%	70.77%

\* Y; Yield of product (CO<sub>2</sub>, acetate, citrate, biomass) per substrate (s) consumed. + Carbon balance. # Degree of reduction balance. § NA; Not available.

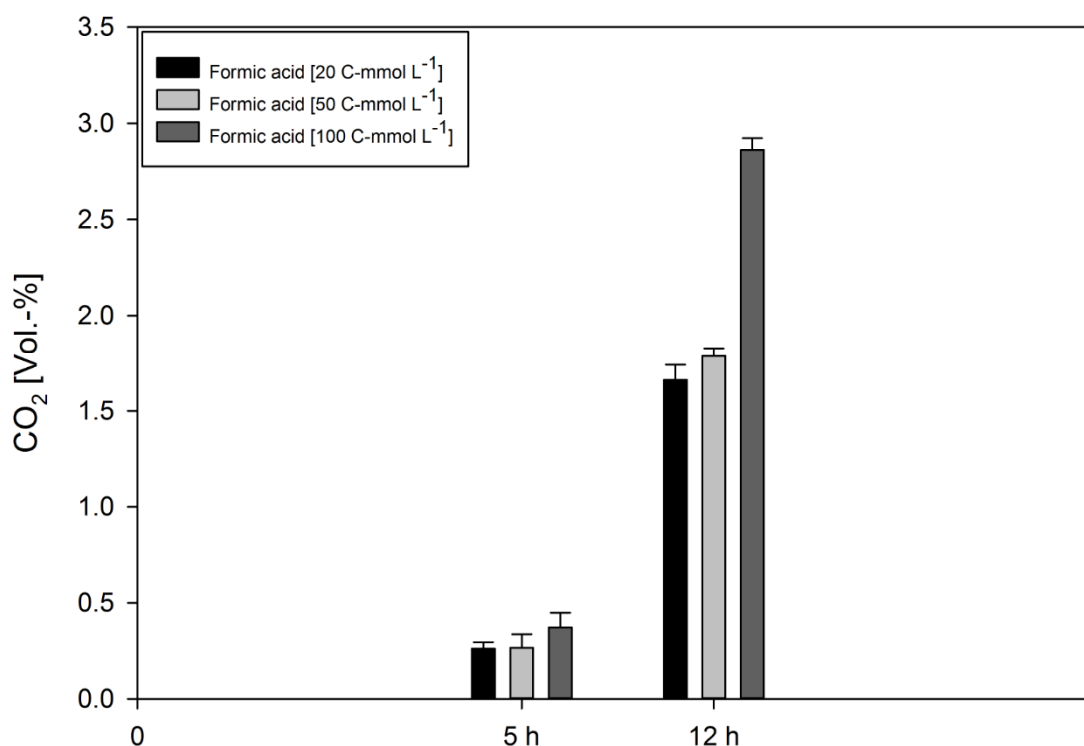
**Table 4.** Physiological key variables of *D. amylolyticus* obtained from whole cell conversion experiments on formic acid.

Time [h]	Concentration [C-mmol L <sup>-1</sup> ]	Formic acid Consumption [%]	CER [mmol L <sup>-1</sup> h <sup>-1</sup> ] (C-Molar)	qCO <sub>2</sub> [mmol h <sup>-1</sup> g <sup>-1</sup> ] (C-Molar)	Y <sub>(CO2/s)</sub> * [C-mol/C-mol]	Y <sub>(Ac/s)</sub> * [C-mol/C-mol]	Y <sub>(Buty/s)</sub> * [C-mol/C-mol]	Y <sub>(Citr/s)</sub> * [C-mol/C-mol]	Y <sub>(Eth/s)</sub> * [C-mol/C-mol]
5	100	1.42	2.50·10 <sup>-5</sup>	1.60·10 <sup>-15</sup>	8.78·10 <sup>-5</sup>		3.41·10 <sup>-3</sup>		5.72·10 <sup>-2</sup>
5	50	0.71	1.79·10 <sup>-5</sup>	1.14·10 <sup>-15</sup>	2.53·10 <sup>-4</sup>		1.97·10 <sup>-3</sup>	2.95·10 <sup>-2</sup>	
5	20	0.08	1.76·10 <sup>-5</sup>	1.13·10 <sup>-15</sup>	5.41·10 <sup>-3</sup>				
12	100	41.05	1.93·10 <sup>-4</sup>	1.23·10 <sup>-14</sup>	5.63·10 <sup>-5</sup>	3.06·10 <sup>-1</sup>		1.43·10 <sup>-4</sup>	4.63·10 <sup>-4</sup>
12	50	9.35	1.20·10 <sup>-4</sup>	7.71·10 <sup>-15</sup>	3.09·10 <sup>-4</sup>			7.72·10 <sup>-3</sup>	2.81·10 <sup>-2</sup>
12	20	9.36	1.12·10 <sup>-4</sup>	7.17·10 <sup>-15</sup>	7.18·10 <sup>-5</sup>			1.92·10 <sup>-4</sup>	1.26·10 <sup>-2</sup>

\* Y; Yield of product (CO<sub>2</sub>, acetate, butyrate, citrate, ethanol, biomass) per substrate (s) consumed.

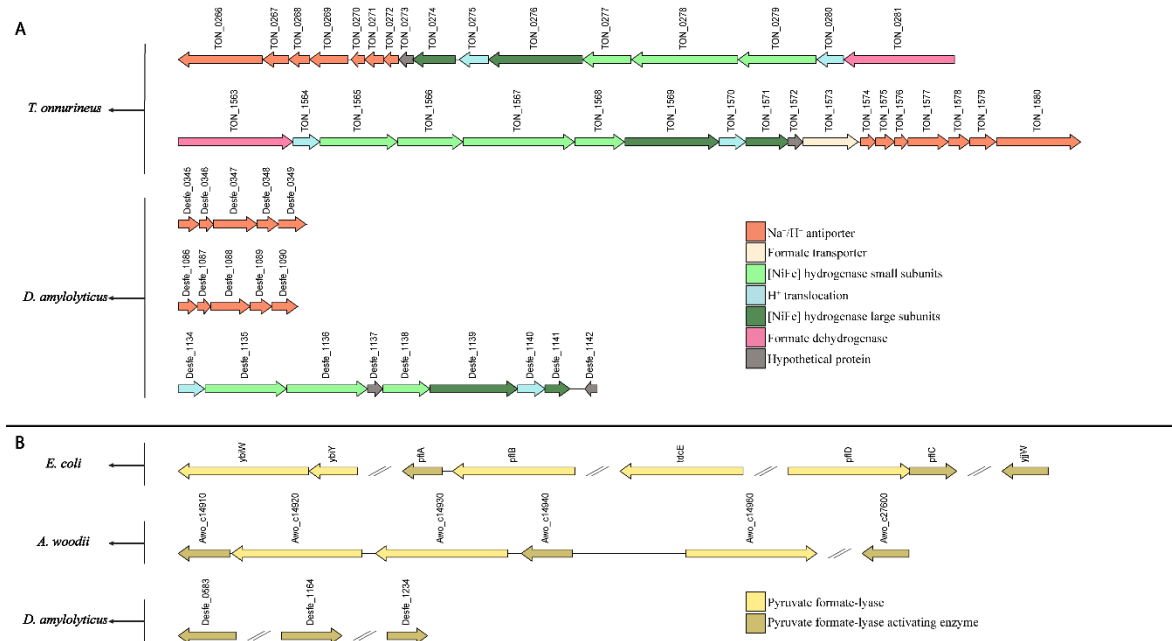
Gas production analyses indicated CO<sub>2</sub> production, but again no H<sub>2</sub> was detected. Interestingly, the qCO<sub>2</sub> values detected at any formate concentration were much lower compared to the growth experiments (compare Tables 2 and 4). However, this finding is in strong contrast to the growth experiments, as the final CO<sub>2</sub> concentrations during formate metabolism were much higher (compare Figure 2 to Figure 4). These observations suggest that the metabolism of *D. amylolyticus* was retarded during the whole cell conversion experiment and that the released CO<sub>2</sub> could not be assimilated into biomass. The results of the whole cell conversion experiments revealed that the CO<sub>2</sub>, citrate, acetate, and ethanol play key roles in the functioning of the formate metabolism of *D. amylolyticus*.

Based on the obtained metabolite excretion profile, we examined the bioenergetics of formate conversion. The results are shown in Supplementary Table S4.  $\Delta G^{0'}$  and  $\Delta G^{0'}$ /formate at 25 °C and 80 °C for the anaerobic production of formaldehyde + CO<sub>2</sub>, H<sub>2</sub> + CO<sub>2</sub>, ethanol + CO<sub>2</sub>, acetate + CO<sub>2</sub> and acetate + ethanol + CO<sub>2</sub> from formate.  $\Delta G^{0'}$ /formate is given to compare the calculated values based on 1 mol of used formate. Negative values of  $\Delta G^{0'}$  show that a reaction is thermodynamically favourable under the given conditions. The formation of formaldehyde + CO<sub>2</sub> from formate is thermodynamically not favourable. Nevertheless, this does not exclude the proposed formaldehyde pathway, as formaldehyde is not an end product. When formaldehyde is converted into other substances after formation, for example for the assimilation into biomass, the complete reaction has to be considered. Ethanol and acetate were found to be the main end products in whole cell conversion with formate as only carbon source. The results show, that these reactions are thermodynamically favourable under the given conditions. The formation of acetate and ethanol out of formate provides small amounts of energy, consistent with the slow growth of *D. amylolyticus*. As the results show, temperature has little influence on  $\Delta G^{0'}$  for these reactions in the range of 25 to 80 °C.



**Figure 4.** Headspace gas composition of *D. amylolyticus*, from experiments performed in triplicates, at the end points of the whole cell conversion experiment. The experiment was designed and performed to be able to measure the cumulative gas accumulation in the serum bottle headspace. Despite the application of high cell density in the whole cell conversion experiment no H<sub>2</sub> accumulation was detected.

To understand the formate metabolism of *D. amylolyticus*, we retrieved the amino acid sequences of characterized enzyme complexes, which are known to be involved in different formate utilization pathways: PFL, HDCR, Fdh, and FoDH. We then used the protein sequences of the formate utilization pathway-related enzyme complexes from selected microorganisms (*T. onnurineus*, *P. furious*, *E. coli*, *M. barkeri*, *T. kivui*, and *A. woodii*), to identify their homologous proteins in the genomes of *D. amylolyticus*. Based on these analyses, formate-related pathways were predicted in *D. amylolyticus*. Furthermore, we examined if the genetic arrangement of these sequences resembled the one for *D. amylolyticus*. The results of this analysis are shown in Figure 5.



**Figure 5.** Comparison of genetic organization of (A) the fdh complex subunits in *T. onnurineus*, and (B) the pyruvate formate lyase (PFL) complex subunits in *E. coli* and *A. woodii* to the genetic organisation in *D. amylolyticus*.

The protein subunits of the HDCR complex of *A. woodii* are one of the microbial formate assimilation mechanisms. According to our ortho-group analysis, only the electron transfer subunits (Awo\_c08200, Awo\_c08230, Awo\_c08250) of *A. woodii* belong to the same ortho-group as *D. amylolyticus* (Desfe\_1134), which indicates that both may have the same function. On the other hand, FdhF1/2 and HydA proteins were located in different ortho-groups and were not identified in the genome of *D. amylolyticus*.

We then hypothesised whether *D. amylolyticus* possesses the genes of PFL and PFL-AE [30]. While, the Desfe\_1164 sequence of *D. amylolyticus* showed similarities with *pflA* of *E. coli* [32], Desfe\_0583 resembled TON\_0415 of *T. onnurineus* and Awo\_c27600 sequence of *A. woodii*, which are annotated as PFL-AE [28]. A comparison of sequences of PFL and PFL-AE proteins from *A. woodii* with *D. amylolyticus* revealed that the alignment is significant concerning E-value and identity (Figure 5, Supplementary Table S1). The PFL (or formate C-acetyltransferase) (EC 2.3.1.54) present in *E. coli* and *A. woodii* could not be detected in *D. amylolyticus*. Even though the similar PFL systems were not detected in *D. amylolyticus*, our analysis revealed that the genome harbours a high number of radical SAM proteins (Desfe\_0007, Desfe\_0149, Desfe\_0201, Desfe\_0288, Desfe\_0298, Desfe\_0313, Desfe\_0363, Desfe\_0369, Desfe\_0376, Desfe\_0576, Desfe\_0583, Desfe\_0693, Desfe\_0860, Desfe\_1164, Desfe\_0130, Desfe\_0177, Desfe\_1197, Desfe\_1234) [31]. This might indicate that the PFL function is supported by another radical SAM protein, which is not similar to the PFL of *E. coli* or *A. woodii*. This finding is also not surprising considering that very few archaea possess PFL [82,83]. However, *D. amylolyticus*



possesses PFL-AE genes (Desfe\_0583, Desfe\_1164, and Desfe\_1234), and it was recently shown that the PFL-AE homolog in *T. onnurineus* NA1 is strongly upregulated during growth on formate [56].

We then investigated the *D. amylolyticus* genome with respect to the hydrogenase gene clusters of *T. onnurineus* to identify possible orthologous proteins. Our sequence alignment showed that *D. amylolyticus* possesses one multimeric membrane bound hydrogenase subcluster (*mfh*) Desfe\_1135-1141), and two  $H^+/Na^+$  antiporters (*mnh*) (Desfe\_0344-0350 and Desfe\_1085-1091) that are similar to subcluster *mfh2* and *mnh1-mnh2* of *T. onnurineus*. Regarding the *fdh* subcluster, which contains *fdh* and electron transfer genes, we were able to identify only the electron transfer gene (Desfe\_1134) in *D. amylolyticus*. Additionally, all protein sequences of *fdh* subcluster belonging to molybdopterin Pfam family of proteins were downloaded for all species from Pfam, including the aforementioned strains, and compared them with the *D. amylolyticus* genome. Unfortunately, we couldn't detect any *fdh* genes in *D. amylolyticus* (Figure 5, Table S1). However, the auxiliary proteins involved in hydrogenase maturation (Desfe\_0501, Desfe\_0337, Desfe\_0339), which were found to be homologous to hydrogenase maturation proteins of *T. onnurineus* (*Hyc I*; TON\_0263, *Hyp F*; TON\_0287, *Hyp E*; TON\_0286), were identified in the genome of *D. amylolyticus*. Several studies conducted with *E. coli* and *T. onnurineus* resulted in the identification of known auxiliary proteins involved in hydrogenase maturation [28,56,84]. These studies showed that the expression of the *hyc* operon, which contains hydrogenase maturation genes, was upregulated in formate grown cells. This could indicate that the auxiliary proteins of *D. amylolyticus* (Desfe\_0501, Desfe\_0337, Desfe\_0339) might also have an important role in formate metabolism in *D. amylolyticus*.

Furthermore, we examined whether the necessary genes to generate ATP in *T. onnurineus* can be identified in the genome of *D. amylolyticus*. In *T. onnurineus*, a hydrogenase is coupled to an  $H^+$  antiporter involved in the formation of a  $Na^+$  gradient, which can be used for ATP generation [25,57]. Despite the fact that *D. amylolyticus* might possess an orthologous membrane bound hydrogenase, which is coupled to a  $H^+$  antiporter in *T. onnurineus*, the *fdh* subcluster genes could not be detected in the genome. This analysis also supports the experimental observations that *D. amylolyticus* did not produce any  $H_2$  from formate. However, it must be noted that *D. amylolyticus* produced ppm amounts of  $H_2$  from cellulose and glucose during batch fermentation in bioreactors [64] and in previously published closed batch cultivations [63]. On the other hand,  $H_2$  was not detectable during our recent closed batch experiments [65]. Hence, such an ATP synthesis system in *D. amylolyticus* remains to be detected.

The gluconeogenesis and pentose phosphate (PP) pathway enzymes of *T. onnurineus* were already investigated during formate utilisation. It was shown that the glyceraldehyde-3-phosphate dehydrogenase (TON\_0639), 2-phosphoglycerate kinase, (TON\_0742), fructose biphosphatase (TON\_1497), ribose-5-phosphate isomerase (TON\_0168), adenine phosphoribosyl transferase (TON\_0120), AMP phosphorylase homolog DeoA (TON\_1062), and 3-hexulose-6-phosphate synthase/6-phospho-3-hexuloisomerase (HPS/PHI) (TON\_0336) were upregulated during growth on formate in *T. onnurineus* [56]. It was also demonstrated that gluconeogenesis and the PP pathway products, such as ribose-5-phosphate and NADPH were favoured when formate was used as a substrate [56].

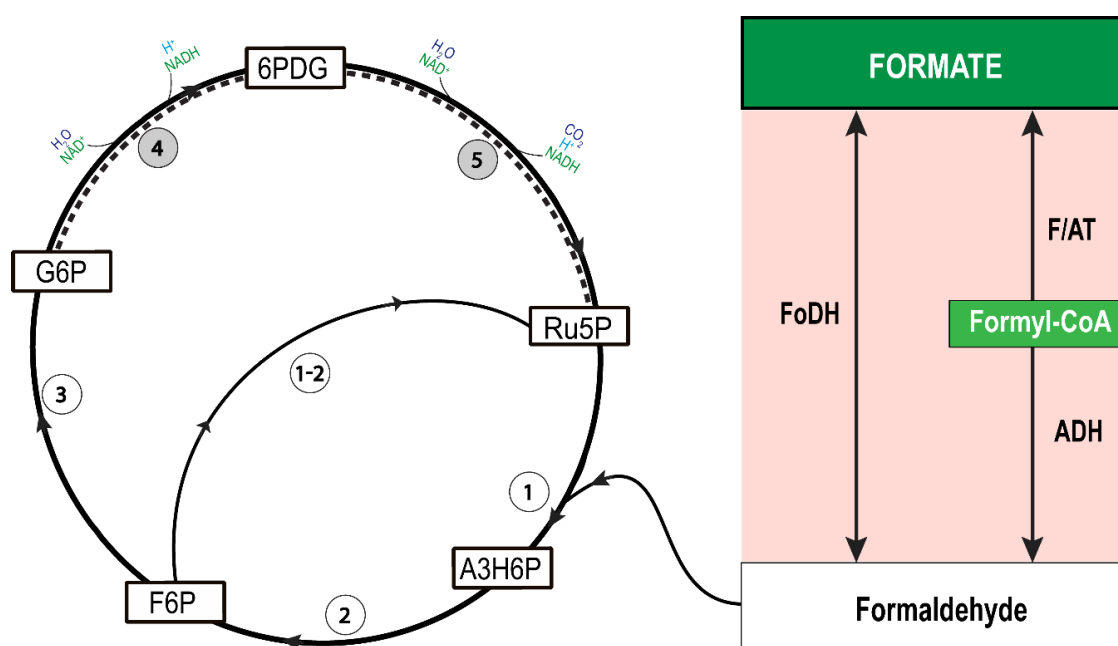
The genome of *D. amylolyticus* encodes for several NADH generating genes, however, according to the results of this study, formate oxidation is not coupled to  $H_2$  evolution and PFL encoding genes are missing in the genome of *D. amylolyticus*.

#### 4. Discussion

Based on the above analysis, we hypothesise that the organism might operate the central metabolism with formaldehyde rather than formate. Therefore, we propose that two formate-metabolising reactions might occur in *D. amylolyticus*. First, the reduction of formate with coenzyme A (CoA) to formyl-CoA, which might be catalysed by acetyl-CoA synthetase, and furthermore, the

conversion of formaldehyde with the support of an acetylating acetaldehyde dehydrogenase [58]. Second, the direct conversion of formate to formaldehyde through NADH via FoDH [61].

Our analysis showed that *D. amylolyticus* harbours the following proteins: Desfe\_0278, Desfe\_0067, and Desfe\_0019-Desfe\_1240 for the enzymes formyl/acetyl transferase (F/AT) [3.1.2.10], (catalyses the reaction: formate  $\rightleftharpoons$  formyl-CoA), acylating acetaldehyde dehydrogenase (ADH) [1.2.1.10] (catalyses formyl-CoA  $\rightleftharpoons$  formaldehyde), and glutathione-independent formaldehyde dehydrogenase [1.2.1.46] (catalyses formaldehyde + NAD<sup>+</sup> + H<sub>2</sub>O  $\rightleftharpoons$  Formate + NADH + H<sup>+</sup>), respectively (Supplementary Table S1). The generated formaldehyde can be assimilated with the oxidative PP pathway (OPPP) which is an efficient route for the assimilation of one-carbon compounds into the central carbon metabolism [85–87]. OPPP enzymes catalyse the oxidation of glucose-6-phosphate (G6P) to ribulose-5-phosphate (Ru5P), which was recently shown in halophilic archaea [88]. However, the genes encoding some of the OPPP enzymes, glucose-6-phosphate dehydrogenase and 6-phosphogluconate dehydrogenase are missing in the genome of *D. amylolyticus*. In several Archaea, it has been shown that the conventional PP pathway is incomplete [89]. Moreover, it has been confirmed through biochemical and genome analyses of Archaea that ribulose monophosphate pathway (RuMP) substitutes for the incomplete PP pathway [90]. The generated formaldehyde can be assimilated with inclusion of the synthesis of Ru5P from fructose 6-phosphate (F6P) through the reverse reaction of formaldehyde fixation by HPS/PHI via the RuMP (Figure 6).



**Figure 6.** Schematic illustration of the proposed route for formate assimilation in *D. amylolyticus*. The first part of the cycle is formaldehyde production from formate, which might be catalysed by formaldehyde dehydrogenase (FoDH), or formyl/acetyl transferase (F/AT) and aldehyde dehydrogenase (ADH). The second part of the cycle represents formaldehyde assimilation and ribulose 5-phosphate (Ru5P) regeneration via ribulose monophosphate pathway (RuMP) and oxidative pentose phosphate pathway (OPPP). Formaldehyde could be fixed by Ru5P to form D-arabino-3-hexulose-6-phosphate (A3H6P) by 3-hexulose-6-phosphate synthase (HPS) (1) and then isomerized to fructose 6-phosphate (F6P) by 6-phospho-3-hexuloisomerase (PHI) (2). In the genome of *D. amylolyticus*, only gene was found for an HPS-PHI-fused bifunctional enzyme (1-2). F6P is further isomerized to glucose-6-phosphate (G6P) by glucose-6-phosphate isomerase (3). Later, G6P is oxidized to Ru5P by glucose-6-phosphate dehydrogenase (4) and 6-phosphogluconate dehydrogenase (5).

The RuMP provided metabolic precursors for the anabolism. The key enzymes are HPS (Desfe\_0079), catalysing the reaction from formaldehyde to arabino-3-hexulose-6-phosphate and

PHI (Desfe\_0297), which catalyses the isomerization of arabino-3-hexulose-6-phosphate to fructose 6-phosphate (F6P). Further, F6P can be metabolised and generate Ru5P by the bifunctional activity of HPS/PHI (Supplementary Table S1). The required energy can be substituted by the assimilation of CO<sub>2</sub> together with ribulose 1,5 bis-phosphate to 3-phosphoglycerate via the activity of RuBisCO [91]. The produced 3-phosphoglycerate could be used for ATP production via glycolysis, while ATP and CO<sub>2</sub> production can occur via incomplete/pseudo TCA cycle [56]. However, our hypothesis would need to be validated through the combined approach of transcriptomics and proteomics—an endeavour of importance and of high dignity—considering the fastidious growth characteristics of this fascinating organism.

## 5. Conclusions

Through a combined approach of in silico analyses and physiological experiments, we could show that *D. amylolyticus* has the ability to metabolise formate as carbon and energy substrate. *D. amylolyticus* grew at similar  $\mu$  on formate and glucose, which suggests that this organism faces inherent growth limitations, independent of the supplied carbon and energy substrate concentration. Supported by our experiments and analyses, we propose that the identified homologs of formaldehyde dehydrogenase genes are the only currently-known possibility allowing the metabolisation of formate. Therefore, we would like to raise the possibility that *D. amylolyticus* uses FoDH as a formate assimilation mechanism to produce formaldehyde, and that formaldehyde is subsequently assimilated into biomass through the RuMP. We consequently demonstrate that the CO<sub>2</sub> released during growth on formate is efficiently assimilated into biomass. Our findings shed new light on the metabolic versatility of the archaeal phylum Crenarchaeota and offers insight into a putative new C1 assimilation pathway in prokaryotes.

**Supplementary Materials:** The following are available online at <http://www.mdpi.com/2076-2607/8/3/454/s1>, **Supplementary Figure S1:** Growth curves of *D. amylolyticus* in a medium with the addition of formic acid compared to a medium where formic acid was omitted (positive–negative control). Clearly *D. amylolyticus* does not grow on a medium where formic acid is not supplied. **Supplementary Table S1:** Manually sorted homologous proteins from characterized enzymes involved in formate-related metabolism of *D. amylolyticus*. **Supplementary Table S2:** Identification of enzyme complexes of *D. amylolyticus* by using bidirectional BLAST. **Supplementary Table S3:** List of orthologous genes of *D. amylolyticus*, *T. onnurineus*, *P. furiosus*, *E. coli*, *M. barkeri*, *T. kivui* and *A. woodii* based on pair-wise all versus all BLAST using the “OrthoFinder” tool. **Supplementary Table S4:** Gibbs values of expected intermediates and metabolic end products from formate metabolisation by *D. amylolyticus* at 25 °C and 80 °C.

**Author Contributions:** Conceptualization, I.E. and S.K.-M.R.R.; methodology, I.E., B.R., B.H. and A.Z.; software, L.M.; validation, I.E., W.F. and S.K.-M.R.R.; formal analysis, S.K.-M.R.R.; investigation, I.E. and S.K.-M.R.R.; resources, G.B., W.F. and S.K.-M.R.R.; data curation, I.E.; writing—original draft preparation, I.E. and S.K.-M.R.R.; writing—review and editing, I.E., G.B., W.F. and S.K.-M.R.R.; visualization, I.E.; supervision, S.K.-M.R.R.; project administration, G.B. and S.K.-M.R.R.; funding acquisition, G.B., W.F. and S.K.-M.R.R. All authors have read and agreed to the published version of the manuscript.

**Funding:** The Austrian Research Promotion Agency (Forschungsförderungsgesellschaft (FFG)) is gratefully acknowledged supporting this research in the frame of the projects H2.AT (grant 853618) and NitroFix (grant 859293).

**Acknowledgments:** We thank Christian Pruckner for his help with bioinformatic analyses. We thank Melina Kerou for proofreading the manuscript. Open access funding by the University of Vienna.

**Conflicts of Interest:** The authors declare no conflict of interest.

## References

1. Gibson, H.W. Chemistry of formic acid and its simple derivatives. *Chem. Rev.* **1969**, *69*, 673–692. [CrossRef]
2. Guillory, J.K. Dissociation Constants of Organic Acids and Bases. *J. Med. Chem.* **2009**, *52*, 5560. [CrossRef]
3. Agarwal, A.S.; Zhai, Y.; Hill, D.; Sridhar, N. The Electrochemical Reduction of Carbon Dioxide to Formate/Formic Acid: Engineering and Economic Feasibility. *ChemSusChem* **2011**, *4*, 1301–1310. [CrossRef]
4. Kopljär, D.; Inan, A.; Vindayer, P.; Wagner, N.; Klemm, E. Electrochemical reduction of CO<sub>2</sub> to formate at high current density using gas diffusion electrodes. *J. Appl. Electrochem.* **2014**, *44*, 1107–1116. [CrossRef]
5. Wang, Q.; Dong, H.; Yu, H. Fabrication of a novel tin gas diffusion electrode for electrochemical reduction of carbon dioxide to formic acid. *RSC Adv.* **2014**, *4*, 59970–59976. [CrossRef]

6. Lu, X.; Leung, D.Y.C.; Wang, H.; Leung, M.K.H.; Xuan, J. Electrochemical Reduction of Carbon Dioxide to Formic Acid. *ChemElectroChem* **2014**, *1*, 836–849. [[CrossRef](#)]
7. Taheri, A.; Berben, L.A. Making C–H bonds with CO<sub>2</sub>: Production of formate by molecular electrocatalysts. *ChemComm* **2016**, *52*, 1768–1777. [[CrossRef](#)]
8. Albert, J.; Wölfel, R.; Bösmann, A.; Wasserscheid, P. Selective oxidation of complex, water-insoluble biomass to formic acid using additives as reaction accelerators. *Energy Environ. Sci.* **2012**, *5*, 7956–7962. [[CrossRef](#)]
9. Sorokin, A.B.; Kudrik, E.V.; Alvarez, L.X.; Afanasiev, P.; Millet, J.M.M.; Bouchu, D. Oxidation of methane and ethylene in water at ambient conditions. *Catal. Today* **2010**, *157*, 149–154. [[CrossRef](#)]
10. Shukla, R.S.; Bhatt, S.D.; Thorat, R.B.; Jasra, R.V. A novel effective hydration of carbon monoxide in liquid phase by a water-soluble ruthenium complex catalyst at moderate pressures in aqueous medium. *Appl. Catal. A Gen.* **2005**, *294*, 111–118. [[CrossRef](#)]
11. Li, H.; Opgenorth, P.H.; Wernick, D.G.; Rogers, S.; Wu, T.-Y.; Higashide, W.; Malati, P.; Huo, Y.-X.; Cho, K.M.; Liao, J.C. Integrated Electromicrobial Conversion of CO<sub>2</sub> to Higher Alcohols. *Science* **2012**, *335*, 1596. [[CrossRef](#)]
12. Kanehisa, M. KEGG: Kyoto Encyclopedia of Genes and Genomes. *Nucleic Acids Res.* **2000**, *28*, 27–30. [[CrossRef](#)]
13. Christensen, K.E.; MacKenzie, R.E. Chapter 14 Mitochondrial Methylenetetrahydrofolate Dehydrogenase, Methenyltetrahydrofolate Cyclohydrolase, and Formyltetrahydrofolate Synthetases. In *Vitam Horm*; Elsevier: Amsterdam, The Netherlands, 2008; Volume 79, pp. 393–410.
14. Stairs, C.W.; Roger, A.J.; Hampl, V. Eukaryotic Pyruvate Formate Lyase and Its Activating Enzyme Were Acquired Laterally from a Firmicute. *Mol. Biol. Evol.* **2011**, *28*, 2087–2099. [[CrossRef](#)]
15. Wray, J. Extract of a Letter, Written by Mr. John Wray to the Publisher Concerning some uncommon observations and experiments made with an acid juice to be found in ants. *Philos. Trans.* **1670**, 2063–2066.
16. LeBrun, E.G.; Jones, N.T.; Gilbert, L.E. Chemical Warfare Among Invaders: A Detoxification Interaction Facilitates an Ant Invasion. *Science* **2014**, *343*, 1014–1017. [[CrossRef](#)]
17. Thompson, J.L.; Hinton, M. Antibacterial activity of formic and propionic acids in the diet of hens on salmonellas in the crop. *Br. Poult. Sci.* **1997**, *38*, 59–65. [[CrossRef](#)]
18. Hietala, J.; Vuori, A.; Johnsson, P.; Pollari, I.; Reutemann, W.; Kieczka, H. Formic Acid. In *Ullmann's Encyclopedia of Industrial Chemistry*; Wiley-VCH Verlag GmbH & Co. KGaA: Weinheim, Germany, 2016; pp. 1–22.
19. Zhou, W.; Lee, J.Y. Particle Size Effects in Pd-Catalyzed Electrooxidation of Formic Acid. *J. Phys. Chem.* **2008**, *112*, 3789–3793. [[CrossRef](#)]
20. Enthaler, S.; von Langermann, J.; Schmidt, T. Carbon dioxide and formic acid—The couple for environmental-friendly hydrogen storage? *Energy Environ. Sci.* **2010**, *3*, 1207. [[CrossRef](#)]
21. Grasemann, M.; Laurenczy, G. Formic acid as a hydrogen source—Recent developments and future trends. *Energy Environ. Sci.* **2012**, *5*, 8171. [[CrossRef](#)]
22. Yishai, O.; Lindner, S.N.; Gonzalez de la Cruz, J.; Tenenboim, H.; Bar-Even, A. The formate bio-economy. *Curr. Opin. Chem. Biol.* **2016**, *35*, 1–9. [[CrossRef](#)]
23. Drake, H.L.; Küsel, K.; Matthies, C. Acetogenic Prokaryotes. In *The Prokaryotes*; Rosenberg, E., DeLong, E.F., Lory, S., Stackebrandt, E., Thompson, F., Eds.; Springer: Berlin/Heidelberg, Germany, 2013; pp. 3–60.
24. Thauer, R.K.; Kaster, A.-K.; Seedorf, H.; Buckel, W.; Hedderich, R. Methanogenic archaea: Ecologically relevant differences in energy conservation. *Nat. Rev. Microbiol.* **2008**, *6*, 579–591. [[CrossRef](#)]
25. Kim, Y.J.; Lee, H.S.; Kim, E.S.; Bae, S.S.; Lim, J.K.; Matsumi, R.; Lebedinsky, A.V.; Sokolova, T.G.; Kozhevnikova, D.A.; Cha, S.-S.; et al. Formate-driven growth coupled with H<sub>2</sub> production. *Nature* **2010**, *467*, 352–355. [[CrossRef](#)] [[PubMed](#)]
26. Dolfig, J.; Jiang, B.; Henstra, A.M.; Stams, A.J.M.; Plugge, C.M. Syntrophic Growth on Formate: A New Microbial Niche in Anoxic Environments. *Appl. Environ. Microbiol.* **2008**, *74*, 6126–6131. [[CrossRef](#)] [[PubMed](#)]
27. Kim, S.; Thiessen, P.A.; Bolton, E.E.; Chen, J.; Fu, G.; Gindulyte, A.; Han, L.; He, J.; He, S.; Shoemaker, B.A.; et al. PubChem Substance and Compound databases. *Nucleic Acids Res.* **2016**, *44*, D1202–D1213. [[CrossRef](#)]
28. Schuchmann, K.; Müller, V. Direct and Reversible Hydrogenation of CO<sub>2</sub> to Formate by a Bacterial Carbon Dioxide Reductase. *Science* **2013**, *342*, 1382–1385. [[CrossRef](#)]
29. Poehlein, A.; Schmidt, S.; Kaster, A.-K.; Goenrich, M.; Vollmers, J.; Thürmer, A.; Bertsch, J.; Schuchmann, K.; Voigt, B.; Hecker, M.; et al. An Ancient Pathway Combining Carbon Dioxide Fixation with the Generation and Utilization of a Sodium Ion Gradient for ATP Synthesis. *PLoS ONE* **2012**, *7*, e33439. [[CrossRef](#)]



30. Crain, A.V.; Broderick, J.B. Pyruvate Formate-lyase and Its Activation by Pyruvate Formate-lyase Activating Enzyme. *J. Biol. Chem.* **2014**, *289*, 5723–5729. [[CrossRef](#)]
31. Broderick, J.B.; Duffus, B.R.; Duschene, K.S.; Shepard, E.M. Radical S-Adenosylmethionine Enzymes. *Chem. Rev.* **2014**, *114*, 4229–4317. [[CrossRef](#)]
32. Zelbuch, L.; Lindner, S.N.; Zegman, Y.; Vainberg Slutskin, I.; Antonovsky, N.; Gleizer, S.; Milo, R.; Bar-Even, A. Pyruvate Formate-Lyase Enables Efficient Growth of *Escherichia coli* on Acetate and Formate. *Biochemistry* **2016**, *55*, 2423–2426. [[CrossRef](#)]
33. Klibanov, A.M.; Alberti, B.N.; Zale, S.E. Enzymatic synthesis of formic acid from H<sub>2</sub> and CO<sub>2</sub> and production of hydrogen from formic acid. *Biotechnol. Bioeng.* **1982**, *24*, 25–36. [[CrossRef](#)]
34. Lu, Y.; Zhang, C.; Zhao, H.; Xing, X.-H. Improvement of Hydrogen Productivity by Introduction of NADH Regeneration Pathway in *Clostridium paraputrificum*. *Appl. Biochem. Biotechnol.* **2012**, *167*, 732–742. [[CrossRef](#)] [[PubMed](#)]
35. Matsumoto, M.; Nishimura, Y. Hydrogen production by fermentation using acetic acid and lactic acid. *J. Biosci. Bioeng.* **2007**, *103*, 236–241. [[CrossRef](#)]
36. Bakonyi, P.; Nemestóthy, N.; Lövitusz, É.; Bélafi-Bakó, K. Application of Plackett–Burman experimental design to optimize biohydrogen fermentation by *E. coli* (XL1-BLUE). *Int. J. Hydrogen Energy* **2011**, *36*, 13949–13954. [[CrossRef](#)]
37. Hill, S.; Viollet, S.; Smith, A.T.; Anthony, C. Roles for enteric Formate Utilization by the Crenarchaeo d-type cytochrome oxidase in N<sub>2</sub> fixation and microaerobiosis. *J. Bacteriol.* **1990**, *172*, 2071–2078. [[CrossRef](#)] [[PubMed](#)]
38. Maeda, T.; Sanchez-Torres, V.; Wood, T.K. Metabolic engineering to enhance bacterial hydrogen production. *Microb. Biotechnol.* **2008**, *1*, 30–39. [[CrossRef](#)]
39. Pakes, W.C.C.; Jollyman, W.H. XL.—The bacterial decomposition of formic acid into carbon dioxide and hydrogen. *J. Chem. Soc. Trans.* **1901**, *79*, 386–391. [[CrossRef](#)]
40. Seol, E.; Kim, S.; Raj, S.M.; Park, S. Comparison of hydrogen-production capability of four different Enterobacteriaceae strains under growing and non-growing conditions. *Int. J. Hydrogen Energy* **2008**, *33*, 5169–5175. [[CrossRef](#)]
41. Seol, E.; Manimaran, A.; Jang, Y.; Kim, S.; Oh, Y.-K.; Park, S. Sustained hydrogen production from formate using immobilized recombinant *Escherichia coli* SH5. *Int. J. Hydrogen Energy* **2011**, *36*, 8681–8686. [[CrossRef](#)]
42. Shin, J.-H.; Yoon, J.H.; Lee, S.H.; Park, T.H. Hydrogen production from formic acid in pH-stat fed-batch operation for direct supply to fuel cell. *Bioresour. Technol.* **2010**, *101*, S53–S58. [[CrossRef](#)]
43. Yoshida, A.; Nishimura, T.; Kawaguchi, H.; Inui, M.; Yukawa, H. Enhanced Hydrogen Production from Formic Acid by Formate Hydrogen Lyase-Overexpressing *Escherichia coli* Strains. *Appl. Environ. Microbiol.* **2005**, *71*, 6762–6768. [[CrossRef](#)]
44. Yoshida, A.; Nishimura, T.; Kawaguchi, H.; Inui, M.; Yukawa, H. Efficient induction of formate hydrogen lyase of aerobically grown *Escherichia coli* in a three-step biohydrogen production process. *Appl. Microbiol. Biotechnol.* **2007**, *74*, 754–760. [[CrossRef](#)]
45. Bagramyan, K.; Mnatsakanyan, N.; Poladian, A.; Vassilian, A.; Trchounian, A. The roles of hydrogenases 3 and 4, and the F<sub>0</sub>F<sub>1</sub>-ATPase, in H<sub>2</sub> production by *Escherichia coli* at alkaline and acidic pH. *FEBS Lett.* **2002**, *516*, 172–178. [[CrossRef](#)]
46. Jones, D.T.; Woods, D.R. Acetone-butanol fermentation revisited. *Microbiol. Rev.* **1986**, *50*, 484–524. [[CrossRef](#)]
47. Herrero, A.A.; Gomez, R.F.; Snedecor, B.; Tolman, C.J.; Roberts, M.F. Growth inhibition of *Clostridium thermocellum* by carboxylic acids: A mechanism based on uncoupling by weak acids. *Appl. Microbiol. Biotechnol.* **1985**, *22*, 53–62. [[CrossRef](#)]
48. Bagramyan, K.; Trchounian, A. Structural and functional features of formate hydrogen lyase, an enzyme of mixed-acid fermentation from *Escherichia coli*. *Biochemistry* **2003**, *68*, 1159–1170. [[CrossRef](#)]
49. Lim, J.K.; Bae, S.S.; Kim, T.W.; Lee, J.-H.; Lee, H.S.; Kang, S.G. Thermodynamics of Formate-Oxidizing Metabolism and Implications for H<sub>2</sub> Production. *Appl. Environ. Microbiol.* **2012**, *78*, 7393–7397. [[CrossRef](#)]
50. Lee, J.; Seol, E.; Kaur, G.; Oh, Y.-K.; Park, S. Hydrogen production from C1 compounds by a novel marine hyperthermophilic archaeon *Thermococcus onnurineus* NA1. *Int. J. Hydrogen Energy* **2012**, *37*, 11113–11121. [[CrossRef](#)]
51. Jackson, B.E.; McInerney, M.J. Anaerobic microbial metabolism can proceed close to thermodynamic limits. *Nature* **2002**, *415*, 454–456. [[CrossRef](#)]



52. Mayer, F.; Müller, V. Adaptations of anaerobic archaea to life under extreme energy limitation. *FEMS Microbiol. Rev.* **2014**, *38*, 449–472. [\[CrossRef\]](#)
53. Schink, B. Energetics of syntrophic cooperation in methanogenic degradation. *Microbiol. Mol. Biol. Rev.* **1997**, *61*, 262–280. [\[CrossRef\]](#)
54. Stams, A.J.M.; Plugge, C.M. Electron transfer in syntrophic communities of anaerobic bacteria and archaea. *Nat. Rev. Microbiol.* **2009**, *7*, 568–577. [\[CrossRef\]](#)
55. Lee, H.S.; Kang, S.G.; Bae, S.S.; Lim, J.K.; Cho, Y.; Kim, Y.J.; Jeon, J.H.; Cha, S.-S.; Kwon, K.K.; Kim, H.-T.; et al. The Complete Genome Sequence of *Thermococcus onnurineus* NA1 Reveals a Mixed Heterotrophic and Carboxydutrophic Metabolism. *J. Bacteriol.* **2008**, *190*, 7491–7499. [\[CrossRef\]](#)
56. Moon, Y.-J.; Kwon, J.; Yun, S.-H.; Lim, H.L.; Kim, M.-S.; Kang, S.G.; Lee, J.-H.; Choi, J.-S.; Kim, S.I.; Chung, Y.-H. Proteome Analyses of Hydrogen-producing Hyperthermophilic Archaeon *Thermococcus onnurineus* NA1 in Different One-carbon Substrate Culture Conditions. *Mol. Cell. Proteomics* **2012**, *11*, M111.015420. [\[CrossRef\]](#)
57. Lim, J.K.; Mayer, F.; Kang, S.G.; Muller, V. Energy conservation by oxidation of formate to carbon dioxide and hydrogen via a sodium ion current in a hyperthermophilic archaeon. *Proc. Natl. Acad. Sci. USA* **2014**, *111*, 11497–11502. [\[CrossRef\]](#)
58. Bar-Even, A. Formate Assimilation: The Metabolic Architecture of Natural and Synthetic Pathways. *Biochemistry* **2016**, *55*, 3851–3863. [\[CrossRef\]](#)
59. Heim, L.E.; Konnerth, H.; Prechtel, M.H.G. Future perspectives for formaldehyde: Pathways for reductive synthesis and energy storage. *Green Chem.* **2017**, *19*, 2347–2355. [\[CrossRef\]](#)
60. Flamholz, A.; Noor, E.; Bar-Even, A.; Milo, R. eQuilibrator—The biochemical thermodynamics calculator. *Nucleic Acids Res.* **2012**, *40*, D770–D775. [\[CrossRef\]](#)
61. Ogushi, S.; Ando, M.; Tsuru, D. Formaldehyde dehydrogenase from *Pseudomonas putida*: A zinc metalloenzyme. *J. Biochem.* **1984**, *96*, 1587–1591. [\[CrossRef\]](#)
62. Yoshimoto, M.; Yamashita, T.; Kinoshita, S. Thermal stabilization of formaldehyde dehydrogenase by encapsulation in liposomes with nicotinamide adenine dinucleotide. *Enzyme Microb. Technol.* **2011**, *49*, 209–214. [\[CrossRef\]](#)
63. Perevalova, A.A. *Desulfurococcus fermentans* sp. nov., a novel hyperthermophilic archaeon from a Kamchatka hot spring, and emended description of the genus *Desulfurococcus*. *Int. J. Syst. Evol. Microbiol.* **2005**, *55*, 995–999. [\[CrossRef\]](#)
64. Reischl, B.; Ergal, I.; Rittmann, S.K.-M.R. Biohydrogen production characteristics of *Desulfurococcus amylolyticus* DSM 16532. *Int. J. Hydrogen Energy* **2018**, *43*, 8747–8753. [\[CrossRef\]](#)
65. Reischl, B.; Ergal, I.; Rittmann, S.K.-M.R. Metabolic reconstruction and experimental verification of glucose utilization in *Desulfurococcus amylolyticus* DSM 16532. *Folia Microbiol.* **2018**, *63*, 713–723. [\[CrossRef\]](#)
66. Rittmann, S.K.-M.R.; Lee, H.S.; Lim, J.K.; Kim, T.W.; Lee, J.-H.; Kang, S.G. One-carbon substrate-based biohydrogen production: Microbes, mechanism, and productivity. *Biotechnol. Adv.* **2015**, *33*, 165–177. [\[CrossRef\]](#) [\[PubMed\]](#)
67. Ergal, I.; Fuchs, W.; Hasibar, B.; Thallinger, B.; Bochmann, G.; Rittmann, S.K.-M.R. The physiology and biotechnology of dark fermentative biohydrogen production. *Biotechnol. Adv.* **2018**, *36*, 2165–2186. [\[CrossRef\]](#) [\[PubMed\]](#)
68. Kublanov, I.V.; Bidzhieva, S.K.; Perevalova, A.A.; Lebedinsky, A.V.; Mukhopadhyay, B.; Bonch-Osmolovskaya, E.A. Reclassification of *Desulfurococcus mobilis* as a synonym of *Desulfurococcus mucosus*, *Desulfurococcus fermentans* and *Desulfurococcus kamchatkensis* as synonyms of *Desulfurococcus amylolyticus*, and emendation of the *D. mucosus* and *D. amylolyticus* species descriptions. *Int. J. Syst. Evol. Microbiol.* **2016**, *66*, 514–517.
69. Erickson, L.E. Biomass elemental composition and energy content. *Biotechnol. Bioeng.* **1980**, *22*, 451–456. [\[CrossRef\]](#)
70. Amend, J.P.; Shock, E.L. Energetics of overall metabolic reactions of thermophilic and hyperthermophilic Archaea and bacteria. *FEMS Microbiol. Rev.* **2001**, *25*, 175–243. [\[CrossRef\]](#)
71. Schulte, M.D.; Shock, E.L. Aldehydes in hydrothermal solution: Standard partial molal thermodynamic properties and relative stabilities at high temperatures and pressures. *Geochim. Cosmochim. Acta* **1993**, *57*, 3835–3846. [\[CrossRef\]](#)
72. Pruitt, K.D.; Tatusova, T.; Brown, G.R.; Maglott, D.R. NCBI Reference Sequences (RefSeq): Current status, new features and genome annotation policy. *Nucleic Acids Res.* **2012**, *40*, D130–D135. [\[CrossRef\]](#)

73. Altschul, S. Gapped BLAST and PSI-BLAST: A new generation of protein database search programs. *Nucleic Acids Res.* **1997**, *25*, 3389–3402. [\[CrossRef\]](#)
74. Emms, D.M.; Kelly, S. OrthoFinder: Solving fundamental biases in whole genome comparisons dramatically improves orthogroup inference accuracy. *Genome Biol.* **2015**, *16*. [\[CrossRef\]](#)
75. Bateman, A. The Pfam protein families database. *Nucleic Acids Res.* **2004**, *32*, 138–141. [\[CrossRef\]](#)
76. Monod, J. *Recherches Sur la Croissance Des Cultures Bactériennes*; Hermann: Paris, France, 1941.
77. Gaudy, A.F.; Obayashi, A.; Gaudy, E.T. Control of growth rate by initial substrate concentration at values below maximum rate. *Appl. Microbiol.* **1971**, *22*, 1041–1047. [\[CrossRef\]](#)
78. Robb, F.T.; Shukla, H.D.; Clark, D.S. 10 Heat Shock Proteins in Hyperthermophiles. In *Methods in Microbiology*; Elsevier: Amsterdam, The Netherlands, 2006; Volume 35, pp. 233–252.
79. Schäfer, T.; Schönheit, P. Pyruvate metabolism of the hyperthermophilic archaeobacterium *Pyrococcus furiosus*: Acetate formation from acetyl-CoA and ATP synthesis are catalyzed by an acetyl-CoA synthetase (ADP forming). *Arch. Microbiol.* **1991**, *155*, 366–377. [\[CrossRef\]](#)
80. Hansen, T.; Schönheit, P. Purification and properties of the first-identified, archaeal, ATP-dependent 6-phosphofructokinase, an extremely thermophilic non-allosteric enzyme, from the hyperthermophile *Desulfurococcus amylolyticus*. *Arch. Microbiol.* **2000**, *173*, 103–109. [\[CrossRef\]](#)
81. Lin, B.; Tao, Y. Whole-cell biocatalysts by design. *Microb. Cell Fact.* **2017**, *16*, 106. [\[CrossRef\]](#)
82. Fukui, T. Complete genome sequence of the hyperthermophilic archaeon *Thermococcus kodakaraensis* KOD1 and comparison with *Pyrococcus* genomes. *Genome Res.* **2005**, *15*, 352–363. [\[CrossRef\]](#)
83. Mardanov, A.V.; Ravin, N.V.; Svetlitchnyi, V.A.; Beletsky, A.V.; Miroshnichenko, M.L.; Bonch-Osmolovskaya, E.A.; Skryabin, K.G. Metabolic Versatility and Indigenous Origin of the Archaeon *Thermococcus sibiricus*, Isolated from a Siberian Oil Reservoir, as Revealed by Genome Analysis. *Appl. Environ. Microbiol.* **2009**, *75*, 4580–4588. [\[CrossRef\]](#)
84. Rossmann, R.; Sawers, G.; Böck, A. Mechanism of regulation of the formate-hydrogenlyase pathway by oxygen, nitrate, and pH: Definition of the formate regulon. *Mol. Microbiol.* **1991**, *5*, 2807–2814. [\[CrossRef\]](#)
85. Goldberg, I.; Rock, J.S.; Ben-Bassat, A.; Mateles, R.I. Bacterial yields on methanol, methylamine, formaldehyde, and formate. *Biotechnol. Bioeng.* **1976**, *18*, 1657–1668. [\[CrossRef\]](#)
86. Bar-Even, A.; Noor, E.; Flamholz, A.; Milo, R. Design and analysis of metabolic pathways supporting formatotrophic growth for electricity-dependent cultivation of microbes. *Biochim. Biophys. Acta Bioenerg.* **2013**, *1827*, 1039–1047. [\[CrossRef\]](#)
87. He, H.; Edlich-Muth, C.; Lindner, S.N.; Bar-Even, A. Ribulose Monophosphate Shunt Provides Nearly All Biomass and Energy Required for Growth of *E. coli*. *ACS Synth. Biol.* **2018**, *7*, 1601–1611. [\[CrossRef\]](#)
88. Pickl, A.; Schönheit, P. The oxidative pentose phosphate pathway in the haloarchaeon *Haloferax volcanii* involves a novel type of glucose-6-phosphate dehydrogenase—The archaeal Zwischenferment. *FEBS Lett.* **2015**, *589*, 1105–1111. [\[CrossRef\]](#)
89. Sato, T.; Imanaka, H.; Rashid, N.; Fukui, T.; Atomi, H.; Imanaka, T. Genetic Evidence Identifying the True Gluconeogenic Fructose-1,6-Bisphosphatase in *Thermococcus kodakaraensis* and Other Hyperthermophiles. *J. Bacteriol.* **2004**, *186*, 5799–5807. [\[CrossRef\]](#)
90. Orita, I.; Yurimoto, H.; Hirai, R.; Kawarabayashi, Y.; Sakai, Y.; Kato, N. The Archaeon *Pyrococcus horikoshii* Possesses a Bifunctional Enzyme for Formaldehyde Fixation via the Ribulose Monophosphate Pathway. *J. Bacteriol.* **2005**, *187*, 3636–3642. [\[CrossRef\]](#)
91. Yoshida, S.; Inui, M.; Yukawa, H.; Kanao, T.; Tomizawa, K.; Atomi, H.; Imanaka, T. Phototrophic growth of a Rubisco-deficient mesophilic purple nonsulfur bacterium harboring a Type III Rubisco from a hyperthermophilic archaeon. *J. Biotechnol.* **2006**, *124*, 532–544. [\[CrossRef\]](#)



# ANNEX 11

Pages 197 to 205

---

Mooshammer M., Alves R.J.E., Bayer B., Melcher M., Stieglmeier M., Jochum L.,  
Rittmann S.K.-M.R., Watzka M., Schleper C., Herndl G., Wanek W.

**Nitrogen isotope fractionation during archaeal ammonia oxidation: coupled estimates  
from measurements of residual ammonium and accumulated nitrite**

Frontiers in Microbiology (2020) 11:1710

10.3389/fmicb.2020.01710

---



# Nitrogen Isotope Fractionation During Archaeal Ammonia Oxidation: Coupled Estimates From Measurements of Residual Ammonium and Accumulated Nitrite

Maria Mooshammer<sup>1†</sup>, Ricardo J. E. Alves<sup>2†</sup>, Barbara Bayer<sup>2†</sup>, Michael Melcher<sup>2</sup>, Michaela Stieglmeier<sup>2</sup>, Lara Jochum<sup>3</sup>, Simon K.-M. R. Rittmann<sup>2</sup>, Margarete Watzka<sup>1</sup>, Christa Schleper<sup>2</sup>, Gerhard J. Herndl<sup>2,4</sup> and Wolfgang Wanek<sup>1\*</sup>

## OPEN ACCESS

### Edited by:

Laura E. Lehtovirta-Morley,  
University of East Anglia,  
United Kingdom

### Reviewed by:

Soo-Je Park,  
Jeju National University, South Korea  
Anne E. Taylor,  
Oregon State University,  
United States  
Karen L. Casciotti,  
Stanford University, United States

### \*Correspondence:

Wolfgang Wanek  
wolfgang.wanek@univie.ac.at

### † Present address:

Maria Mooshammer,  
Department of Environmental  
Science, Policy, and Management,  
University of California, Berkeley,  
Berkeley, CA, United States  
Ricardo J. E. Alves,  
Lawrence Berkeley National  
Laboratory, Climate and Ecosystem  
Sciences Division, Earth  
and Environmental Sciences,  
Berkeley, CA, United States  
Barbara Bayer,  
Department of Ecology, Evolution  
and Marine Biology, University  
of California, Santa Barbara,  
Santa Barbara, CA, United States

### Specialty section:

This article was submitted to  
Microbial Physiology and Metabolism,  
a section of the journal  
Frontiers in Microbiology

Received: 18 February 2020

Accepted: 29 June 2020

Published: 28 July 2020

<sup>1</sup> Centre for Microbiology and Environmental Systems Science, University of Vienna, Vienna, Austria, <sup>2</sup> Department of Functional and Evolutionary Ecology, University of Vienna, Vienna, Austria, <sup>3</sup> LMU – Max von Pettenkofer Institute for Hygiene and Medical Microbiology, Ludwig Maximilian University of Munich, Munich, Germany, <sup>4</sup> Department of Marine Microbiology and Biogeochemistry, Royal Netherlands Institute for Sea Research (NIOZ), Utrecht University, Utrecht, Netherlands

The naturally occurring nitrogen (N) isotopes, <sup>15</sup>N and <sup>14</sup>N, exhibit different reaction rates during many microbial N transformation processes, which results in N isotope fractionation. Such isotope effects are critical parameters for interpreting natural stable isotope abundances as proxies for biological process rates in the environment across scales. The kinetic isotope effect of ammonia oxidation (AO) to nitrite (NO<sub>2</sub><sup>−</sup>), performed by ammonia-oxidizing archaea (AOA) and ammonia-oxidizing bacteria (AOB), is generally ascribed to the enzyme ammonia monooxygenase (AMO), which catalyzes the first step in this process. However, the kinetic isotope effect of AMO, or ε<sub>AMO</sub>, has been typically determined based on isotope kinetics during product formation (cumulative product, NO<sub>2</sub><sup>−</sup>) alone, which may have overestimated ε<sub>AMO</sub> due to possible accumulation of chemical intermediates and alternative sinks of ammonia/ammonium (NH<sub>3</sub>/NH<sub>4</sub><sup>+</sup>). Here, we analyzed <sup>15</sup>N isotope fractionation during archaeal ammonia oxidation based on both isotopic changes in residual substrate (RS, NH<sub>4</sub><sup>+</sup>) and cumulative product (CP, NO<sub>2</sub><sup>−</sup>) pools in pure cultures of the soil strain *Nitrososphaera viennensis* EN76 and in highly enriched cultures of the marine strain *Nitrosopumilus adriaticus* NF5, under non-limiting substrate conditions. We obtained ε<sub>AMO</sub> values of 31.9–33.1‰ for both strains based on RS (δ<sup>15</sup>NH<sub>4</sub><sup>+</sup>) and showed that estimates based on CP (δ<sup>15</sup>NO<sub>2</sub><sup>−</sup>) give larger isotope fractionation factors by 6–8‰. Complementary analyses showed that, at the end of the growth period, microbial biomass was <sup>15</sup>N-enriched (10.1‰), whereas nitrous oxide (N<sub>2</sub>O) was highly <sup>15</sup>N depleted (−38.1‰) relative to the initial substrate. Although we did not determine the isotope effect of NH<sub>4</sub><sup>+</sup> assimilation (biomass formation) and N<sub>2</sub>O production by AOA, our results nevertheless show that the discrepancy between ε<sub>AMO</sub> estimates based on RS and CP might have derived from the incorporation of <sup>15</sup>N-enriched residual NH<sub>4</sub><sup>+</sup> after AMO reaction into microbial biomass and that N<sub>2</sub>O production did not affect isotope fractionation estimates significantly.

**Keywords:** ammonia oxidation, nitrification, nitrous oxide, stable isotope fractionation, Thaumarchaeota

## INTRODUCTION

Knowledge of natural  $^{15}\text{N}$  abundances and of nitrogen (N) isotope fractionation effects associated with key microbial N transformation processes has contributed greatly to our understanding of the marine N cycle (Casciotti and Buchwald, 2012; Buchwald and Casciotti, 2013) and of terrestrial gaseous N emissions (Houlton and Bai, 2009), namely atmospheric  $\text{N}_2\text{O}$  sources and sinks (Yoshida and Toyoda, 2000), and biological N fixation (Vitousek et al., 2013). The oxidation of  $\text{NH}_4^+$  to  $\text{NO}_2^-$ —the first and rate-limiting step in nitrification—is a central process in the marine and terrestrial N cycles, as well as the major driver of a large N isotope effect that leads to formation of  $^{15}\text{N}$ -depleted products such as  $\text{NO}$ ,  $\text{N}_2\text{O}$ ,  $\text{NO}_2^-$ , and  $\text{NO}_3^-$ , while residual  $\text{NH}_4^+$  becomes  $^{15}\text{N}$ -enriched during that process (Mariotti et al., 1981; Sigman and Casciotti, 2001). A detailed understanding of N isotope effects of the range of N transformation processes is thus critical for adequate biological interpretation of natural  $^{15}\text{N}$  isotope patterns in the environment (Casciotti, 2016).

Besides the recently discovered comammox bacteria (Daims et al., 2015; van Kessel et al., 2015), ammonia oxidation is catalyzed by both ammonia-oxidizing archaea (AOA) and ammonia-oxidizing bacteria (AOB), with different relative contributions across ecosystems and environmental conditions (Prosser and Nicol, 2012; Prosser et al., 2019). On a cellular level, ammonia oxidation is a multi-step process that comprises different enzymatic reactions and chemical equilibrium processes, which can all contribute to the N isotope fractionation effects inferred from extracellular N pools (Casciotti et al., 2003; Santoro and Casciotti, 2011). The isotopic fractionation effect ( $\epsilon$ ) of ammonia oxidizers has been typically inferred based on changes in  $\delta^{15}\text{N}$  of the cumulative product (CP)  $\text{NO}_2^-$  ( $\epsilon_{\text{CP}}$ ), and attributed to the initial enzymatic step catalyzed by the ammonia monooxygenase (AMO) enzyme, defined as  $\epsilon_{\text{AMO}}$ . However,  $\epsilon_{\text{CP}}$  estimates reflect the combined fractionation effects of the isotope equilibrium between  $\text{NH}_4^+$  and  $\text{NH}_3$  [ $\text{NH}_3$ , the proposed substrate for ammonia oxidation, is depleted in  $^{15}\text{N}$  relative to  $\text{NH}_4^+$  (Hermes et al., 1985)], the AMO-catalyzed reaction, and accumulation of several intermediates derived from subsequent enzymatic processes (Casciotti et al., 2003). For instance,  $\epsilon_{\text{CP}}$  estimates may be affected by the accumulation of essential intermediates, such as hydroxylamine ( $\text{NH}_2\text{OH}$ ) and by the production of gaseous N by-products (nitric oxide,  $\text{NO}$ ; and nitrous oxide,  $\text{N}_2\text{O}$ ), which may represent further  $^{15}\text{N}$  fractionation steps. Consequently, this could result in a difference of kinetic isotope effect estimates derived from residual substrate (RS) and CP (Casciotti et al., 2003). Not only could these “leakage” processes alter CP-based estimates of  $\epsilon_{\text{AMO}}$ , but their different contributions to ammonia utilization and to  $\epsilon_{\text{CP}}$  may also underlie the large differences observed in  $\epsilon_{\text{AMO}}$  between ammonia-oxidizing organisms (Mariotti et al., 1981; Yoshida, 1988; Casciotti et al., 2003; Santoro and Casciotti, 2011).

Estimates of isotope effects based on the change in  $\delta^{15}\text{N}$  ( $\epsilon_{\text{RS}}$ ) can circumvent many of the expected biases associated with  $\epsilon_{\text{CP}}$ , as they are not affected by the multiple subsequent

equilibria, enzymatic transformations, and intermediate N pools, as discussed but not quantified previously (Casciotti et al., 2003; Santoro and Casciotti, 2011). However, to our knowledge, only one study has determined the isotope fractionation factors based on concurrent measurements of changes in isotopic composition of RS and CP of ammonia oxidation, namely in cultures of the AOB *Nitrosomonas europaea* (Mariotti et al., 1981). This study found no difference between  $\epsilon_{\text{RS}}$  and  $\epsilon_{\text{CP}}$ , suggesting that ammonia oxidation can be effectively regarded as a “one-step process,” where the AMO-catalyzed reaction constitutes the rate-limiting and sole isotope fractionation step. On the other hand, AOB and AOA seem to harbor fundamentally distinct ammonia oxidation pathways and exhibit different yields of gaseous N compounds per mole of  $\text{NH}_4^+$  consumed (Walker et al., 2010; Kozłowski et al., 2016). Importantly, the enzyme hydroxylamine dehydrogenase (HAO), which performs the second step in ammonia oxidation of AOB, has not been identified in AOA, and thus it remains unclear how  $\text{NH}_2\text{OH}$  is converted to  $\text{NO}_2^-$  in AOA (Walker et al., 2010; Kerou et al., 2016). Moreover, a recent study has provided evidence that the bacterial HAO oxidizes  $\text{NH}_2\text{OH}$  to  $\text{NO}$  rather than to  $\text{NO}_2^-$ , as generally assumed, with the latter resulting from non-enzymatic oxidation of  $\text{NO}$  by oxygen (Caranto and Lancaster, 2017). Previous studies have shown that  $\text{NO}$  is also an essential intermediate in ammonia oxidation by AOA, as their growth and activity is highly sensitive to exposure to an  $\text{NO}$  scavenger (Shen et al., 2013; Kozłowski et al., 2016).

Here, we tested whether the kinetic isotope effect of archaeal ammonia oxidation based on CP ( $\delta^{15}\text{N}$ ) alone might be biased, by comparing the isotope fractionation factors inferred from both RS and CP pools. For this, we determined the kinetic isotope effects during growth of two phylogenetically and ecologically distinct AOA: the axenic strain *Nitrososphaera viennensis* EN76 (Stieglmeier et al., 2014a), isolated from soil, and the highly enriched marine strain *Nitrosopumilus adriaticus* NF5 (Bayer et al., 2016). This is also the first study of  $^{15}\text{N}$  isotope fractionation of ammonia oxidation by an AOA strain in pure culture. All previous studies of kinetic isotope effects of AOA have been performed with enrichment cultures with varying degrees of enrichment (Santoro and Casciotti, 2011; Nishizawa et al., 2016) and bacterial contaminants that may have contributed to the variation in isotope effects through consumption of and inputs to the same N pools.

## MATERIALS AND METHODS

Pure cultures of *N. viennensis* EN76 were cultivated in freshwater medium and incubated at  $37^\circ\text{C}$ , as described by Tourna et al. (2011). In a first experiment, quadruplicate cultures were supplemented with 1 mM  $\text{NH}_4^+$  and 0.1 mM pyruvate; in a second experiment, quadruplicate cultures were supplemented with 2 mM  $\text{NH}_4^+$  and 0.5 mM pyruvate to generate higher cell biomass and sufficient  $\text{N}_2\text{O}$  concentrations for isotopic analysis, in order to determine their potential effect on  $\epsilon_{\text{AMO}}$ . Quadruplicate enrichment



cultures of *N. adriaticus* NF5 were cultivated in Synthetic Crenarchaeota Medium (SCM) at 30°C as described by Bayer et al. (2016). The medium was supplemented with 1 mM  $\text{NH}_4^+$  and 5% (v/v) autoclaved seawater, which was sterile-filtered (0.22  $\mu\text{m}$  GTTP, Millipore). Kanamycin at a final concentration of 100  $\mu\text{g ml}^{-1}$  was used to inhibit bacterial contaminants. At the time of the experiment (January 2013), the enrichment level of strain NF5 was  $\sim 95\%$ , as it contained a heterotrophic non-nitrifying/non-denitrifying contaminant of the alphaproteobacterial species *Oceanicaulis alexandrii* (Bayer et al., 2019).

Ammonia-oxidizing archaea growth was monitored by measuring nitrite production using the Griess method (Hood-Nowotny et al., 2010), coupled to  $\text{NH}_4^+$  consumption determined using the Berthelot method for *N. viennensis* cultures (Hood-Nowotny et al., 2010) and the o-Phthalaldehyde (OPA) method for *N. adriaticus* cultures (Goyal et al., 1988).  $\delta^{15}\text{NH}_4^+$  was quantified by microdiffusion (Sørensen and Jensen, 1991) with subsequent analysis on a continuous-flow isotope ratio mass spectrometer consisting of an elemental analyzer (EA1110, CE Instruments) coupled via a ConFlo III interface (Finnigan MAT, Thermo Fisher Scientific) to the isotope ratio mass spectrometer (IRMS; DeltaPLUS, Finnigan MAT, Thermo Fisher Scientific).  $\delta^{15}\text{NO}_2^-$  was determined based on the reduction of  $\text{NO}_2^-$  to  $\text{N}_2\text{O}$  by azide under acidified conditions (Lachouani et al., 2010). Concentrations and isotopic ratios of  $\text{N}_2\text{O}$  were determined using a purge-and-trap GC/IRMS system (PreCon - GasBench II headspace analyzer, Delta Advantage V IRMS; Thermo Fischer Scientific, Vienna, Austria). For  $\text{NH}_4^+$  and  $\text{NO}_2^-$  isotope measurements, we included blanks, concentration standards, and isotope standards varying in natural  $^{15}\text{N}$  abundance together with the samples through the full microdiffusion and azide procedures to allow corrections for blank contribution, incomplete reaction, and procedural isotope fractionation (Lachouani et al., 2010). Nitrogen content and  $\delta^{15}\text{N}$  signature of AOA biomass were determined by EA-IRMS as described above.  $\delta^{15}\text{N}$  signatures [‰ vs. AIR] were calculated relative to the ratio R ( $^{15}\text{N}:^{14}\text{N}$ ) of the atmospheric  $\text{N}_2$  standard (AIR), as  $\delta^{15}\text{N} = (R_{\text{sample}}/R_{\text{standard}} - 1) \times 1000$ .

Isotope fractionation factors ( $\epsilon$ ) were calculated based on the Rayleigh closed system isotope fractionation, based on changes in the isotopic compositions of RS (i.e.,  $\text{NH}_4^+$ ) and CP (i.e.,  $\text{NO}_2^-$ ) (Mariotti et al., 1981):

$$10^3 \ln \frac{10^{-3}\delta_{\text{RS}} + 1}{10^{-3}\delta_{\text{S0}} + 1} = \epsilon \ln(f) \quad (1)$$

$$\delta_{\text{CP}} - \delta_{\text{S0}} = -\epsilon f \frac{\ln(f)}{(1-f)}, \quad (2)$$

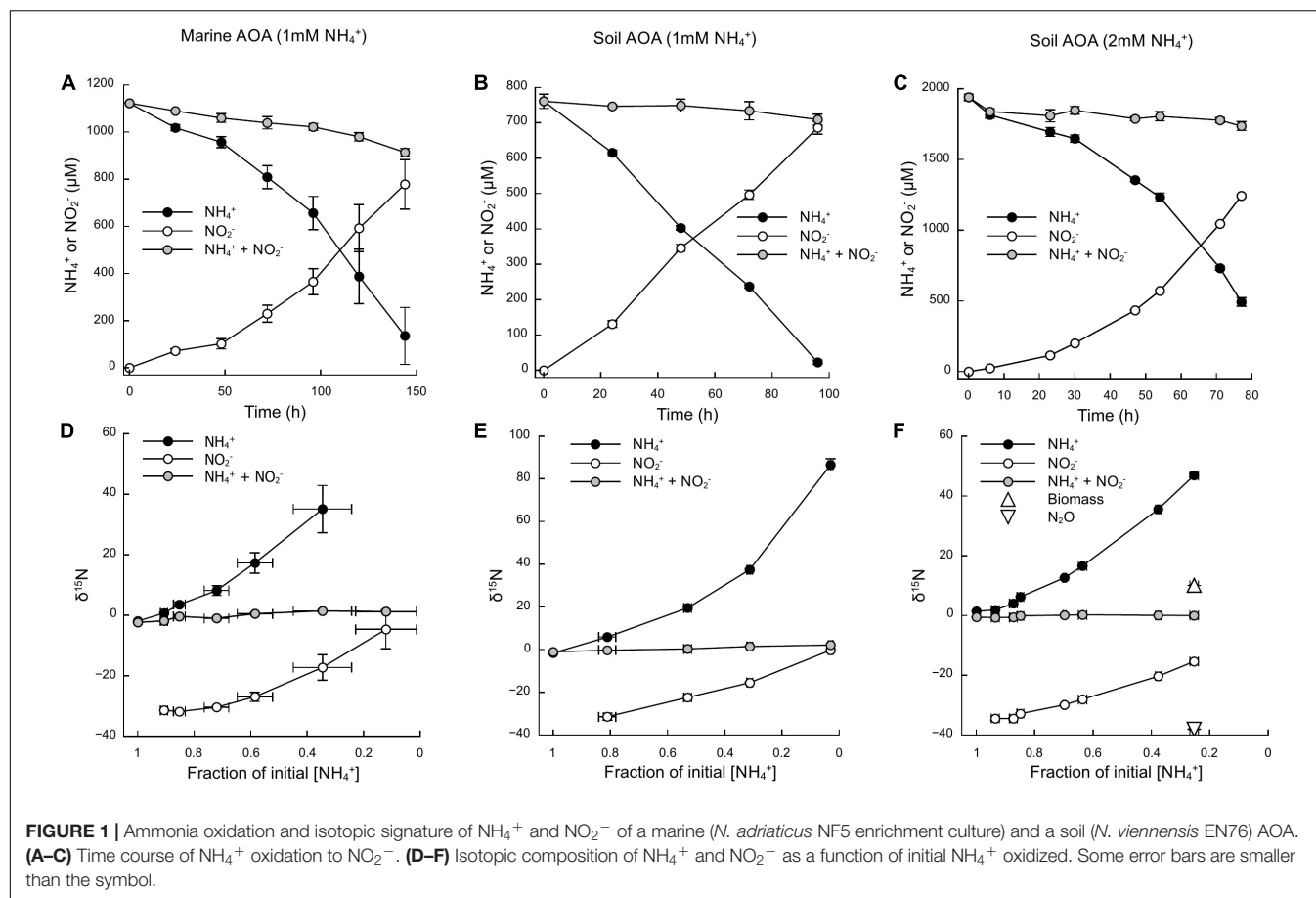
where  $\delta_{\text{S0}}$  is  $\delta^{15}\text{N}$  of initial  $\text{NH}_4^+$ ,  $\delta_{\text{RS}}$  is  $\delta^{15}\text{NH}_4^+$ ,  $\delta_{\text{CP}}$  is  $\delta^{15}\text{NO}_2^-$  and  $f$  is the fraction of the initial  $[\text{NH}_4^+]$  remaining in the culture. Plots of  $10^3 \frac{10^{-3}\delta_{\text{RS}} + 1}{10^{-3}\delta_{\text{S0}} + 1}$  versus  $\ln(f)$  and of  $\delta_{\text{CP}} - \delta_{\text{S0}}$  versus  $f \frac{\ln(f)}{(1-f)}$  yield linear relations, with the slope representing the kinetic isotope effect based on the isotopic change in

substrate ( $\epsilon_{\text{RS}}$ ) and product ( $\epsilon_{\text{AP}}$ ), respectively. Uncertainties of  $\epsilon$  are expressed as standard error of the slope. Differences in isotope fractionation effects between cultures were assessed by testing significant differences between their regression plots, using R (R Development Core Team, 2012).

## RESULTS AND DISCUSSION

Based on the oxidation of  $\text{NH}_3/\text{NH}_4^+$  to  $\text{NO}_2^-$ —a typical proxy for ammonia oxidizer growth, as it strongly correlates with growth rates (Stieglmeier et al., 2014a; Bayer et al., 2016)—all cultures showed growth curves typical for batch cultures of AOA, reaching stationary phase after 7 days for *N. adriaticus*, and after 3–4 days for *N. viennensis* cultures (Figures 1A–C). Nitrogen isotope fractionation was reflected in both the substrate (i.e.,  $\text{NH}_4^+$ ) and the product (i.e.,  $\text{NO}_2^-$ ) of ammonia oxidation, and followed typical Rayleigh isotope fractionation kinetics for closed systems (Figures 1D–F):  $\text{NH}_4^+$  became increasingly  $^{15}\text{N}$ -enriched with the fraction of  $\text{NH}_4^+$  oxidized, while  $\text{NO}_2^-$  was strongly  $^{15}\text{N}$ -depleted after correction for  $\text{NO}_2^-$  deriving from the inoculum. With an increasing fraction of  $\text{NH}_4^+$  oxidized,  $\delta^{15}\text{NO}_2^-$  converged toward the isotopic signature of the initial  $\text{NH}_4^+$ . Both *N. adriaticus* and *N. viennensis* (including cultures grown on 1 and 2 mM  $\text{NH}_4^+$ ) exhibited  $^{15}\text{N}$  isotope fractionation factors based on substrate ( $\epsilon_{\text{RS}}$ ) between 31.9 and 33.1‰, and based on product ( $\epsilon_{\text{CP}}$ ) between 37.7 and 49.1‰ (Figures 2A–F). We found no significant difference between the isotope fractionation factors of the different AOA cultures studied here based on  $\delta^{15}\text{N}$  evolution of the substrate ( $\epsilon_{\text{RS}}$ ; comparison of slopes,  $df = 2$ ,  $F = 0.519$ ,  $p = 0.598$ ) or the product ( $\epsilon_{\text{CP}}$ ; comparison of slopes,  $df = 2$ ,  $F = 2.380$ ,  $p = 0.102$ ). The N isotope fractionation factors based on  $\delta^{15}\text{NO}_2^-$  ( $\epsilon_{\text{CP}}$ ) were larger than those based on  $\delta^{15}\text{NH}_4^+$  ( $\epsilon_{\text{RS}}$ ) by 8.0, 5.8, and 5.9‰ for *N. adriaticus*, and for *N. viennensis* grown on 1 mM or 2 mM  $\text{NH}_4^+$ , respectively.

Nitrogen isotope fractionation has been studied in several AOB strains, but only in three marine and one thermophilic AOA enrichment cultures. These AOA enrichment cultures showed average N isotope fractionation factors between 22 and 25‰ at low substrate concentrations, and up to 32.0‰ at higher ammonium concentrations (Santoro and Casciotti, 2011; Nishizawa et al., 2016, measured via the isotopic composition of the product nitrite; see Table 1). These estimates are in the same range as the reported average isotope effects for different AOB strains, i.e., 14–38‰ (Delwiche and Steyn, 1970; Mariotti et al., 1981; Casciotti et al., 2003).  $^{15}\text{N}$  isotope fractionation factors of *N. viennensis* and *N. adriaticus* are in the upper range, or higher, than those previously reported for AOA, which might be due to the higher ammonia concentrations applied in our study (1–2 mM in our study vs. 200  $\mu\text{M}$  in Nishizawa et al., 2016; 10–75  $\mu\text{M}$  in Santoro and Casciotti, 2011). Previous studies have indicated that higher initial ammonia concentrations lead to more stable



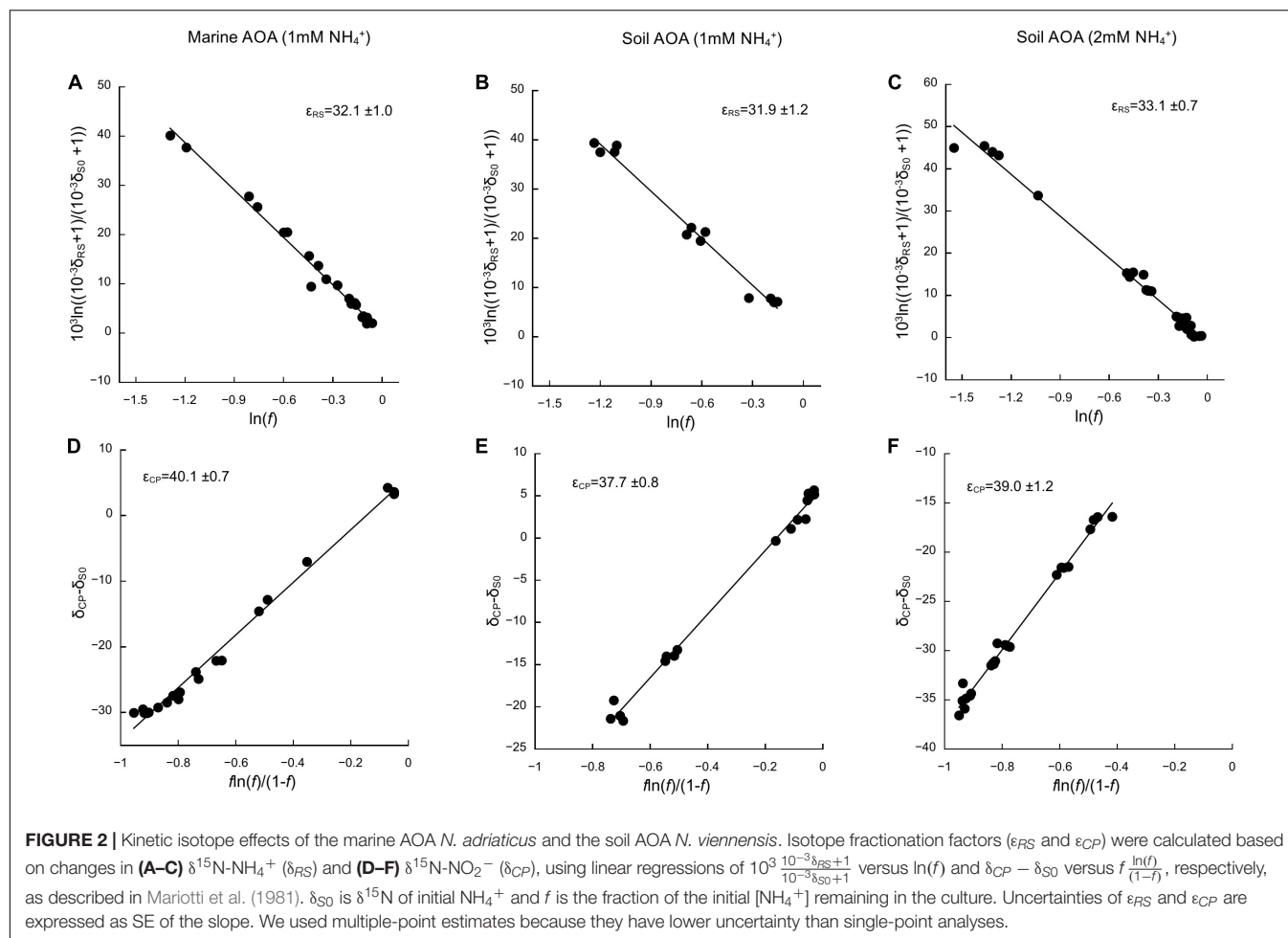
**FIGURE 1 |** Ammonia oxidation and isotopic signature of NH<sub>4</sub><sup>+</sup> and NO<sub>2</sub><sup>-</sup> of a marine (*N. adriaticus* NF5 enrichment culture) and a soil (*N. viennensis* EN76) AOA. (A–C) Time course of NH<sub>4</sub><sup>+</sup> oxidation to NO<sub>2</sub><sup>-</sup>. (D–F) Isotopic composition of NH<sub>4</sub><sup>+</sup> and NO<sub>2</sub><sup>-</sup> as a function of initial NH<sub>4</sub><sup>+</sup> oxidized. Some error bars are smaller than the symbol.

and higher <sup>15</sup>N isotope fractionation (Casciotti et al., 2003; Santoro and Casciotti, 2011).

We also measured  $\epsilon_{AMO}$  based on changes in  $\delta^{15}\text{NH}_4^+$  (i.e., the residual substrate) to both circumvent and assess potential biases associated with estimates based on  $\delta^{15}\text{NO}_2^-$  (i.e., the cumulative product). It should be noted, however, that different apparent isotope effects in whole cells may also be observed in the NH<sub>4</sub><sup>+</sup> pool, despite constant AMO enzyme-level isotope effects, depending, for example, on the balance between ammonia oxidation rates and ammonia diffusion across the S-layer (i.e., outermost cell envelope component in AOA) (Casciotti et al., 2003; Li et al., 2018). Published models of AOA and AOB metabolism favor the hypothesis of a (pseudo-)periplasmic location of the ammonia oxidation process (Arp and Stein, 2003; Walker et al., 2010; Simon and Klotz, 2013). However, AOA and AOB harbor very distinct NH<sub>3</sub>/NH<sub>4</sub><sup>+</sup> transport systems (Offre et al., 2014), whose role in ammonia oxidation and contribution to observed differences in <sup>15</sup>N isotope fractionation remain unclear (Arp and Stein, 2003). At low ammonia concentrations, ammonia oxidation rates are expected to become limited by NH<sub>4</sub><sup>+</sup> transport/NH<sub>3</sub> diffusion, resulting in the convergence of the isotope effect toward that of NH<sub>4</sub><sup>+</sup>/NH<sub>3</sub> equilibrium (if NH<sub>3</sub> is mainly taken up by the cells) or NH<sub>4</sub><sup>+</sup>/NH<sub>3</sub> transport. The NH<sub>4</sub><sup>+</sup>/NH<sub>3</sub> equilibrium isotope effect has been estimated to

be 19.2‰ in aqueous solution (Hermes et al., 1985), whereas secondary active ammonium (AMT) transporters, which are highly expressed in AOA (Carini et al., 2017), have been shown to exert isotope fractionation of around 13–15‰, due to deprotonation of NH<sub>4</sub><sup>+</sup> during transport (Ariz et al., 2018). It is unlikely that ammonia oxidation has been limited by NH<sub>3</sub> availability in our study, because of the high substrate concentrations used, which are well above the *K<sub>m</sub>* of the AMO of *N. viennensis* (5.4 μM NH<sub>3</sub> + NH<sub>4</sub><sup>+</sup>; Kits et al., 2017) and that of the marine strain *Nitrosopumilus maritimus* strain SCM1 (0.13 μM NH<sub>3</sub> + NH<sub>4</sub><sup>+</sup>; Martens-Habben et al., 2009), which is closely related to *N. adriaticus*. Furthermore, Nishizawa et al. (2016) estimated that, when NH<sub>3</sub> concentrations in the pseudo-periplasm are lower than in the medium under laboratory conditions, cell-specific NH<sub>3</sub> diffusion rates into the pseudo-periplasm are higher than cell-specific ammonia oxidation rates. It has also been proposed that the charged S-layer proteins of AOA enhance the diffusion of charged solutes, such as NH<sub>4</sub><sup>+</sup>, which concentrates NH<sub>4</sub><sup>+</sup> in the pseudo-periplasmic space near the active site of the AMO (Li et al., 2018), where then the equilibrium reaction between NH<sub>4</sub><sup>+</sup> and NH<sub>3</sub> is relatively fast and considered not to be rate-limiting.

Even if ammonia oxidation was not limited by periplasmic NH<sub>3</sub> availability, the apparent isotope effect of the AMO can



also be underestimated due to concurrent  $\text{NH}_4^+$  assimilation, which has a smaller isotope effect. This process would alter observed  $\epsilon_{RS}$  estimates in proportion to the amount of  $\text{NH}_4^+$  assimilated and the isotope effect for  $\text{NH}_4^+$  assimilation (4–27‰; Hoch et al., 1992). Therefore, we also measured  $\delta^{15}\text{N}$  of the cell biomass at the end of incubation of *N. viennensis* grown on 2 mM  $\text{NH}_4^+$  (Figures 1F, 3). Although it is impossible to infer directly the contribution of N assimilation to  $\epsilon_{RS}$  from just one end-point measurement, we propose that N assimilation substantially contributed to the decrease of  $\epsilon_{RS}$  relative to  $\epsilon_{CP}$  in our study, as biomass was  $^{15}\text{N}$ -enriched by ~10‰ compared to initial  $\text{NH}_4^+$ . Biomass N represented 3.1% ( $\pm 0.3$  SE) of ammonia oxidized by *N. viennensis* grown on 2 mM  $\text{NH}_4^+$ . Although dissolved inorganic N (DIN) concentrations (sum of  $[\text{NH}_4^+]$  and  $[\text{NO}_2^-]$ ) were relatively constant over the course of ammonia oxidation, we recovered only 81.9% ( $\pm 1.5$  SE) of the initial DIN by the end of incubation of *N. adriaticus*, and 94.7% ( $\pm 3.4$  SE) and 90.7% ( $\pm 1.1$  SE) of *N. viennensis* grown on 1 mM  $\text{NH}_4^+$  or 2 mM  $\text{NH}_4^+$ , respectively. In *N. adriaticus* cultures, assimilation of N by contaminant bacteria likely did not contribute substantially to the lower  $\epsilon_{RS}$  relative to  $\epsilon_{CP}$ , due to the high enrichment level of the culture (95%) at the time

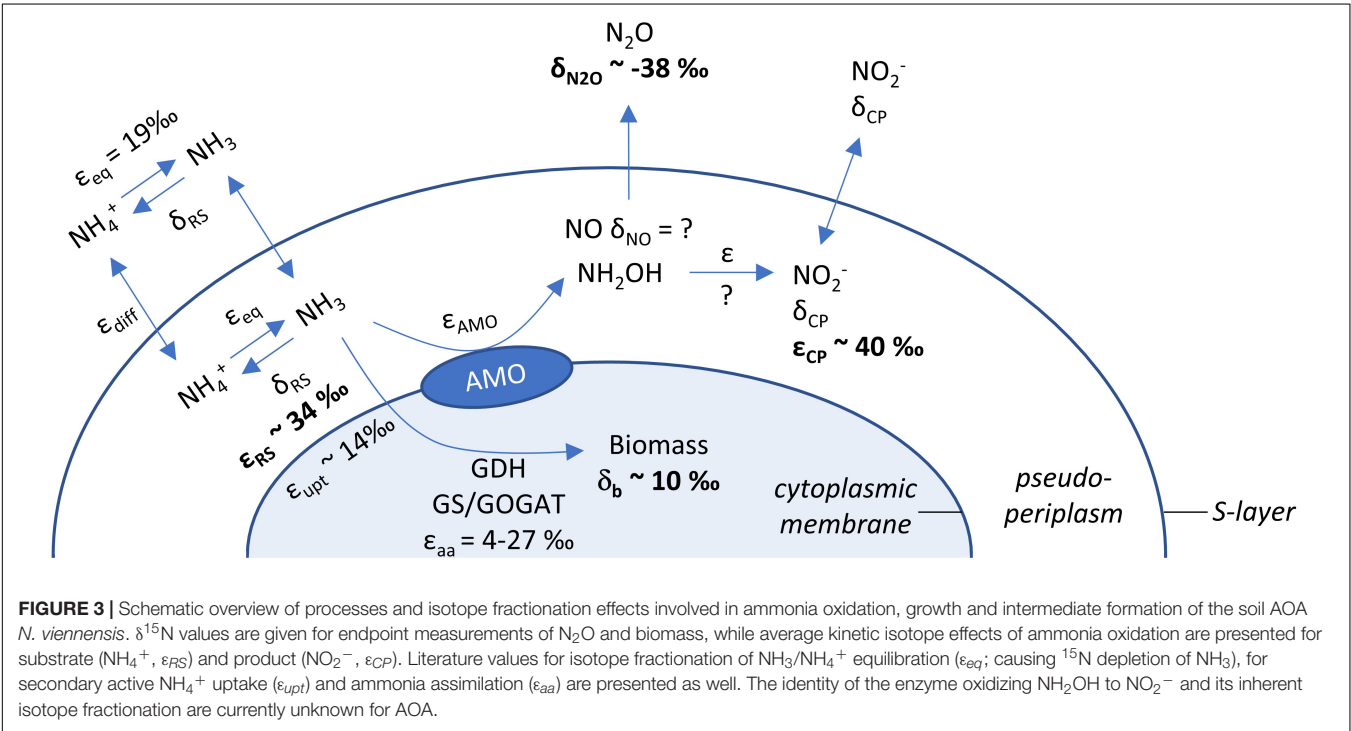
of the experiment, and the fact that  $\epsilon_{RS}$  of *N. adriaticus* was similar to that of *N. viennensis* in pure culture. In addition, the  $^{15}\text{N}$ -enrichment of *N. viennensis*' biomass shows that AMO preferentially, and primarily, reacts on pseudo-periplasmic  $\text{NH}_3$ , causing  $^{15}\text{N}$ -enrichment of the residual ammonia, which is subsequently assimilated into biomass. We thus propose that under substrate replete conditions, the observed isotope effects of  $\epsilon_{RS}$  of 31.9–33.1‰ primarily reflect the kinetic isotope effect of the AMO-catalyzed reaction, modified by the  $\text{NH}_4^+/\text{NH}_3$  equilibrium isotope effect (19.2‰; Hermes et al., 1985) and decreased by the contribution of the lower kinetic isotope effect of  $\text{NH}_4^+$  assimilation for anabolic purposes (4–27‰; Hoch et al., 1992). Moreover, it should be noted that some ammonia oxidizers use distinct pathways of  $\text{NH}_4^+$  assimilation, even among just AOA, which may contribute to different kinetic isotope effects. For instance, some members of the AOA genus *Candidatus Nitrosocosmicus* appear to assimilate  $\text{NH}_4^+$  via glutamate synthase (GOGAT), whereas all other known AOA use the glutamate dehydrogenase (GDH) pathway (Alves et al., 2019).

Despite these potential isotope fractionation effects on the RS level, a higher  $\epsilon_{CP}$  relative to  $\epsilon_{RS}$  may also result from accumulation of metabolic intermediates, allowing for at least

**TABLE 1 |** Compilation of published kinetic isotope effects of AOA and AOB.

Source	AOA/AOB	Strain	Initial [NH <sub>4</sub> <sup>+</sup> ] (mM)	Other conditions	ε <sub>RS</sub>		ε <sub>CP</sub>	
					Mean	SD	Mean	SD
This study	AOA	<i>Nitrosopumilus adriaticus</i> NF5	1		32.1	1.0	40.1	0.7
	AOA	<i>Nitrososphaera viennensis</i> EN76	1		31.9	1.2	37.7	0.8
	AOA	<i>Nitrososphaera viennensis</i> EN76	2		33.1	0.7	39.0	1.2
Santoro and Casciotti (2011)	AOA	Marine AOA enrichment CN25†	0.01–0.075				22	5
		Marine AOA enrichment CN75					21	10
		Marine AOA enrichment CN150					22	5
Nishizawa et al. (2016)	AOA	<i>Candidatus Nitrosocaldus</i> sp.	0.2				22.0	5.0
		<i>Candidatus Nitrosocaldus</i> sp.	14				24.7	2.1
Mariotti et al. (1981)	AOB	<i>Nitrosomonas europaea</i>	4.7–25		34.7	2.5	31.9	6.4
Delwiche and Steyn (1970)	AOB	<i>Nitrosomonas europaea</i>					26.0	5.6
Yoshida (1988)	AOB	<i>Nitrosomonas europaea</i>	38	pO <sub>2</sub> low			24.6	
	AOB	<i>Nitrosomonas europaea</i>	38	pO <sub>2</sub> medium			29.0	
	AOB	<i>Nitrosomonas europaea</i>	38	pO <sub>2</sub> high			32.0	
Casciotti et al. (2003)	AOB	<i>Nitrosomonas marina</i>	2				14.2	3.6
		<i>Nitrosomonas</i> sp. C-113a	2				19.1	1.2
		<i>Nitrospira tenuis</i>	1				24.6	1.4
		<i>Nitrosomonas eutropha</i>	1				32.8	1.7
		<i>Nitrosomonas europaea</i>	1				38.2	1.6
Casciotti et al. (2010)	AOB	<i>Nitrosomonas</i> sp. C-113a	0.005–0.05				30–46	
	AOB	<i>Nitrosococcus oceani</i>	0.005–0.05				30–46	
	AOB	<i>Nitrospira briensis</i>	0.005–0.05				30–46	

† Currently designated as *Candidatus Nitrosopelagicus brevis* CN25 (Santoro et al., 2015).





**TABLE 2** | Nitrogen pools for *N. viennensis* culture grown on 2 mM  $\text{NH}_4^+$ .

	N pool ( $\mu\text{M}$ )	$\delta^{15}\text{N}$ of N pool (‰)	Percent of missing N pool	Percent of ammonia oxidized
Missing	204.4 ( $\pm 25.2$ )	-7.6 ( $\pm 5.2$ )		
Biomass	38.8 ( $\pm 3.4$ )	10.1 ( $\pm 0.1$ )	22.8 ( $\pm 4.1$ )	3.1 ( $\pm 0.3$ )
$\text{N}_2\text{O}$ -N	6.5 ( $\pm 0.2$ )	-38.1 ( $\pm 0.3$ )	3.5 ( $\pm 0.4$ )	0.5 ( $\pm 0.1$ )
Unaccounted	139.2 ( $\pm 27.1$ )	-18.5 ( $\pm 1.7$ )	73.7 ( $\pm 4.5$ )	

The missing N pool is N that was not present at  $\text{NH}_4^+$  and  $\text{NO}_2^-$  at the last sampling time point when biomass and  $\text{N}_2\text{O}$  was collected for isotope analysis. We used a mass balance approach to calculate  $\delta^{15}\text{N}$  of the missing and unaccounted N pool. Standard errors are given in parentheses.

a second  $^{15}\text{N}$  isotope fractionation step to be observed. First, accumulation of  $\text{NH}_2\text{OH}$ , or any other intermediate, has not been observed in AOA cells, and the coupled activities of AMO and hydroxylamine oxidoreductase (yet unknown in AOA) are assumed to maintain  $\text{NH}_2\text{OH}$  at low steady-state concentrations. Therefore, isotope effects associated with  $\text{NH}_2\text{OH}$  oxidation should have a limited impact on  $\delta^{15}\text{NO}_2^-$ . Second, any process that adds an additional isotope fractionation step, either prior, or subsequent, to  $\text{NO}_2^-$  formation, such as the production of the gases  $\text{NO}$  and  $\text{N}_2\text{O}$ , may result in an under- or overestimation of the kinetic isotope fractionation factor. The effect of  $\text{N}_2\text{O}$  and  $\text{NO}$  production on  $\delta^{15}\text{NO}_2^-$  will depend on their formation pathways, and respective isotope effects and by-product yields. In the *N. viennensis* culture grown on 2 mM  $\text{NH}_4^+$ , we measured cumulative  $\text{N}_2\text{O}$  at the end of the incubation, which represented 0.5% ( $\pm 0.01$  SE) of the  $\text{NH}_4^+$  oxidized, or 3.5% ( $\pm 0.4$  SE) of the “missing” N pool.  $\text{N}_2\text{O}$  yields of AOA are generally low. For example, *N. viennensis* has been shown to produce  $\text{N}_2\text{O}$  at rates of about 0.1% of those of ammonia oxidation when grown on 1 mM  $\text{NH}_4^+/\text{NH}_3$  (Stieglmeier et al., 2014b), whereas the marine AOA *N. maritimus* SCM1 produces even less (0.002–0.03%; Löscher et al., 2012). Here, the cumulative  $\text{N}_2\text{O}$  of the *N. viennensis* culture had a  $\delta^{15}\text{N}$  of -38.1‰ ( $\pm 0.3$  SE) (Figures 1F, 3), which was more  $^{15}\text{N}$ -depleted than previously observed for AOA enrichment cultures. AOA have been shown to produce  $\text{N}_2\text{O}$  with  $\delta^{15}\text{N}$  signatures ranging between -35 and -13‰ in soil enrichment cultures and -9‰ in marine enrichment cultures (Santoro et al., 2011; Jung et al., 2014), while  $\text{N}_2\text{O}$  produced by AOB tends to have lower  $\delta^{15}\text{N}$ , ranging between -66‰ (*Nitrosomonas europaea*; Yoshida, 1988) and -10‰ (*Nitrosomonas marina*; Frame and Casciotti, 2010). Furthermore, by-products that are more  $^{15}\text{N}$ -depleted than the main product of ammonia oxidation (i.e.,  $\text{NO}_2^-$ ) would decrease the apparent kinetic isotope effect of AMO ( $\epsilon_{\text{CP}}$ ), instead of increasing it. Using an isotopic mass balance approach, we calculated that the missing N pool (i.e., the  $\text{NH}_4^+$  taken up which was not oxidized to  $\text{NO}_2^-$ ), would need to have a  $\delta^{15}\text{N}$  of -18.5‰ ( $\pm 1.7$  SE) in order to account for the difference in isotope fractionation between  $\epsilon_{\text{RS}}$  and  $\epsilon_{\text{CP}}$  (Table 2). Therefore, the  $\delta^{15}\text{N}_2\text{O}$  signature of -38.1‰ cannot explain the observed large isotope fractionation based on  $\delta^{15}\text{NO}_2^-$ , since

the  $\text{N}_2\text{O}$  produced would need to be a larger contributor to the “missing” N pool, as well as to be  $^{15}\text{N}$ -enriched relative to  $\text{NO}_2^-$ .

Nitric oxide is an important intermediate in the ammonia oxidation pathway, particularly in that of AOA. Unlike in AOB,  $\text{NO}$  is a necessary co-reactant for the oxidation of  $\text{NH}_2\text{OH}$  to  $\text{NO}_2^-$  in AOA, despite being produced in relatively small amounts (Kozłowski et al., 2016). Although the  $\delta^{15}\text{N}$  signature of  $\text{NO}$  produced by AOA has not yet been determined, Yoshida (1988) found that  $\text{NO}$  produced during nitrification by *N. europaea* had a  $\delta^{15}\text{N}$  between 0 and +20‰. The production of such  $^{15}\text{N}$ -enriched  $\text{NO}$  could significantly contribute to the observed overestimation of  $\epsilon_{\text{CP}}$  in AOA.

## CONCLUSION

In conclusion, our results show that, under non-limiting substrate conditions, the  $\epsilon_{\text{AMO}}$  of two phylogenetically and ecologically distinct AOA strains was 31.9–33.1‰ based on  $\delta^{15}\text{NH}_4^+$ , whereas the more commonly estimated  $\epsilon_{\text{AMO}}$  based on  $\delta^{15}\text{NO}_2^-$  was higher (37.7–40.1‰). Thus,  $\text{NH}_4^+$  assimilation, but not  $\text{N}_2\text{O}$  production, significantly affected the isotope fractionation factor of AMO estimated for *N. viennensis* (Figure 3). Although the potential role of  $\text{NO}$  in this context remains to be tested, isotopic analysis of this molecule is difficult and therefore future measurements of  $\epsilon_{\text{AMO}}$  may rely on coupled estimates from  $\delta^{15}\text{NH}_4^+$  and  $\delta^{15}\text{NO}_2^-$ .

## DATA AVAILABILITY STATEMENT

The raw data supporting the conclusion of this article have been deposited at DRYAD (doi: 10.5061/dryad.0gb5mkkz1).

## AUTHOR CONTRIBUTIONS

WW designed the study. MMo, RA, BB, MMe, MS, LJ, SR, and MW performed the experiments. MMo, RA, BB, MS, and LJ analyzed the data. GH and CS provided the resources and strains. MMo, RA, and WW wrote the manuscript with contributions from all co-authors.

## FUNDING

This study was funded by the Austrian Science Fund (FWF; project P28037-B22). Open access funding was provided by University of Vienna.

## ACKNOWLEDGMENTS

We thank the students of the course “Stable Isotopes in Ecology” of the years 2012–2014 at the University of Vienna, who contributed to the sample analyses and discussion of the data.



## REFERENCES

- Alves, R. J. E., Kerou, M., Zappe, A., Bittner, R., Abby, S. S., Schmidt, H., et al. (2019). Ammonia oxidation by the arctic terrestrial thaumarchaeote *Ca. Nitrosocosmicus arcticus* is stimulated by increasing temperatures. *Front. Microbiol.* 10:1571. doi: 10.3389/fmicb.2019.01571
- Ariz, I., Boeckstaens, M., Gouveia, C., Martins, A. P., Sanz-Luque, E., Fernández, E., et al. (2018). Nitrogen isotope signature evidences ammonium deprotonation as a common transport mechanism for the AMT-Mep-Rh protein superfamily. *Sci. Adv.* 4:eaar3599. doi: 10.1126/sciadv.aar3599
- Arp, D. J., and Stein, L. Y. (2003). Metabolism of inorganic N compounds by ammonia-oxidizing bacteria. *Crit. Rev. Biochem. Mol. Biol.* 38, 471–495. doi: 10.1080/10409230390267446
- Bayer, B., Pelikan, C., Bittner, M. J., Reinthaler, T., Könneke, M., Herndl, G. J., et al. (2019). Proteomic response of three marine ammonia-oxidizing archaea to hydrogen peroxide and their metabolic interactions with a heterotrophic alphaproteobacterium. *mSystems* 4:e00181-19. doi: 10.1128/mSystems.00181-19
- Bayer, B., Vojvoda, J., Offre, P., Alves, R. J. E., Elisabeth, N. H., Garcia, J. A. L., et al. (2016). Physiological and genomic characterization of two novel marine thaumarchaeal strains indicates niche differentiation. *ISME J.* 10, 1051–1063. doi: 10.1038/ismej.2015.200
- Buchwald, C., and Casciotti, K. L. (2013). Isotopic ratios of nitrite as tracers of the sources and age of oceanic nitrite. *Nat. Geosci.* 6, 308–313. doi: 10.1038/ngeo1745
- Caranto, J. D., and Lancaster, K. M. (2017). Nitric oxide is an obligate bacterial nitrification intermediate produced by hydroxylamine oxidoreductase. *Proc. Natl. Acad. Sci. U.S.A.* 114, 8217–8222. doi: 10.1073/pnas.1704504114
- Carini, P., Dupont, C., and Santoro, A. E. (2017). Correlated expression of archaeal ammonia oxidation machinery across disparate environmental and culture conditions. *BioRxiv* [Preprint]. doi: 10.1101/175141
- Casciotti, K. L. (2016). Nitrogen and oxygen isotopic studies of the marine nitrogen cycle. *Ann. Rev. Mar. Sci.* 8, 379–407. doi: 10.1146/annurev-marine-010213-135052
- Casciotti, K. L., and Buchwald, C. (2012). Insights on the marine microbial nitrogen cycle from isotopic approaches to nitrification. *Front. Microbiol.* 3:356. doi: 10.3389/fmicb.2012.00356
- Casciotti, K. L., McIlvin, M., and Buchwald, C. (2010). Oxygen isotopic exchange and fractionation during bacterial ammonia oxidation. *Limnol. Oceanogr.* 55, 753–762. doi: 10.4319/lo.2010.55.2.0753
- Casciotti, K. L., Sigman, D. M., and Ward, B. B. (2003). Linking diversity and stable isotope fractionation in ammonia-oxidizing bacteria. *Geomicrobiol. J.* 20, 335–353. doi: 10.1080/01490450303895
- Daims, H., Lebedeva, E. V., Pjevac, P., Han, P., Herbold, C., Albertsen, M., et al. (2015). Complete nitrification by *Nitrospira* bacteria. *Nature* 528:504. doi: 10.1038/nature16461
- Delwiche, C. C., and Steyn, P. L. (1970). Nitrogen isotope fractionation in soils and microbial reactions. *Environ. Sci. Technol.* 4, 929–935. doi: 10.1021/es60046a004
- Frame, C. H., and Casciotti, K. L. (2010). Biogeochemical controls and isotopic signatures of nitrous oxide production by a marine ammonia-oxidizing bacterium. *Biogeosciences* 7, 2695–2709. doi: 10.5194/bg-7-2695-2010
- Goyal, S. S., Rains, D. W., and Huffaker, R. C. (1988). Determination of ammonium ion by fluorometry or spectrophotometry after on-line derivatization with o-phthalaldehyde. *Anal. Chem.* 60, 175–179. doi: 10.1021/ac00153a016
- Hermes, J. D., Weiss, P. M., and Cleland, W. W. (1985). Use of nitrogen-15 and deuterium isotope effects to determine the chemical mechanism of phenylalanine ammonia-lyase. *Biochemistry* 24, 2959–2967. doi: 10.1021/bi00333a023
- Hoch, M. P., Fogel, M. L., and Kirchman, D. L. (1992). Isotope fractionation associated with ammonium uptake by a marine bacterium. *Limnol. Oceanogr.* 37, 1447–1459. doi: 10.4319/lo.1992.37.7.1447
- Hood-Nowotny, R., Umana, N. H.-N., Inselbacher, E., Oswald, L., Lachouani, P., and Wanek, W. (2010). Alternative methods for measuring inorganic, organic, and total dissolved nitrogen in soil. *Soil Sci. Soc. Am. J.* 74:1018. doi: 10.2136/sssaj2009.0389
- Houlton, B. Z., and Bai, E. (2009). Imprint of denitrifying bacteria on the global terrestrial biosphere. *Proc. Natl. Acad. Sci. U.S.A.* 106, 21713–21716. doi: 10.1073/pnas.0912111106
- Jung, M.-Y., Well, R., Min, D., Giesemann, A., Park, S.-J., Kim, J.-G., et al. (2014). Isotopic signatures of N<sub>2</sub>O produced by ammonia-oxidizing archaea from soils. *ISME J.* 8, 1115–1125. doi: 10.1038/ismej.2013.205
- Kerou, M., Offre, P., Villedor, L., Abby, S. S., Melcher, M., Nagler, M., et al. (2016). Proteomics and comparative genomics of *Nitrososphaera viennensis* reveal the core genome and adaptations of archaeal ammonia oxidizers. *Proc. Natl. Acad. Sci. U.S.A.* 113, E7937–E7946. doi: 10.1073/pnas.1601212113
- Kits, K. D., Sedlacek, C. J., Lebedeva, E. V., Han, P., Bulaev, A., Pjevac, P., et al. (2017). Kinetic analysis of a complete nitrifier reveals an oligotrophic lifestyle. *Nature* 549:269. doi: 10.1038/nature23679
- Kozłowski, J. A., Stieglmeier, M., Schleper, C., Klotz, M. G., and Stein, L. Y. (2016). Pathways and key intermediates required for obligate aerobic ammonia-dependent chemolithotrophy in bacteria and Thaumarchaeota. *ISME J.* 10, 1836–1845. doi: 10.1038/ismej.2016.2
- Lachouani, P., Frank, A. H., and Wanek, W. (2010). A suite of sensitive chemical methods to determine the  $\delta^{15}\text{N}$  of ammonium, nitrate and total dissolved N in soil extracts. *Rapid Commun. Mass Spectrom.* 24, 3615–3623. doi: 10.1002/rcm.4798
- Li, P.-N., Herrmann, J., Tolar, B. B., Poitevin, F., Ramdasi, R., Bargar, J. R., et al. (2018). Nutrient transport suggests an evolutionary basis for charged archaeal surface layer proteins. *ISME J.* 12, 2389–2402. doi: 10.1038/s41396-018-0191-0
- Löscher, C. R., Kock, A., Koenneke, M., LaRoche, J., Bange, H. W., and Schmitz, R. A. (2012). Production of oceanic nitrous oxide by ammonia-oxidizing archaea. *Biogeosciences* 9, 2419–2429. doi: 10.5194/bg-9-2419-2012
- Mariotti, A., Germon, J. C., Hubert, P., Kaiser, P., Letolle, R., Tardieu, A., et al. (1981). Experimental determination of nitrogen kinetic isotope fractionation: some principles; illustration for the denitrification and nitrification processes. *Plant Soil* 62, 413–430. doi: 10.1007/bf02374138
- Martens-Habben, W., Berube, P. M., Urakawa, H., José, R., and Stahl, D. A. (2009). Ammonia oxidation kinetics determine niche separation of nitrifying Archaea and Bacteria. *Nature* 461:976. doi: 10.1038/nature08465
- Nishizawa, M., Sakai, S., Konno, U., Nakahara, N., Takaki, Y., Saito, Y., et al. (2016). Nitrogen and oxygen isotope effects of ammonia oxidation by thermophilic Thaumarchaeota from a geothermal water stream. *Appl. Environ. Microbiol.* 82, 4492–4504. doi: 10.1128/aem.00250-16
- Offre, P., Kerou, M., Spang, A., and Schleper, C. (2014). Variability of the transporter gene complement in ammonia-oxidizing archaea. *Trends Microbiol.* 22, 665–675. doi: 10.1016/j.tim.2014.07.007
- Prosser, J. I., Hink, L., Gubry-Rangin, C., and Nicol, G. W. (2019). Nitrous oxide production by ammonia oxidisers: physiological diversity, niche differentiation and potential mitigation strategies. *Glob. Chang. Biol.* 26, 103–118. doi: 10.1111/gcb.14877
- Prosser, J. I., and Nicol, G. W. (2012). Archaeal and bacterial ammonia-oxidisers in soil: the quest for niche specialisation and differentiation. *Trends Microbiol.* 20, 523–531. doi: 10.1016/j.TIM.2012.08.001
- R Development Core Team (2012). *R: A Language and Environment for Statistical Computing*. Vienna: R Foundation for Statistical Computing.
- Santoro, A. E., Buchwald, C., McIlvin, M. R., and Casciotti, K. L. (2011). Isotopic signature of N<sub>2</sub>O produced by marine ammonia-oxidizing archaea. *Science* 333, 1282–1285. doi: 10.1126/science.1208239
- Santoro, A. E., and Casciotti, K. L. (2011). Enrichment and characterization of ammonia-oxidizing archaea from the open ocean: phylogeny, physiology and stable isotope fractionation. *ISME J.* 5:1796. doi: 10.1038/ismej.2011.58
- Santoro, A. E., Dupont, C. L., Richter, R. A., Craig, M. T., Carini, P., McIlvin, M. R., et al. (2015). Genomic and proteomic characterization of “*Candidatus Nitrosopelagicus brevis*”: an ammonia-oxidizing archaeon from the open ocean. *Proc. Natl. Acad. Sci. U.S.A.* 112, 1173–1178. doi: 10.1073/pnas.1416223112
- Shen, T., Stieglmeier, M., Dai, J., Urich, T., and Schleper, C. (2013). Responses of the terrestrial ammonia-oxidizing archaeon *Ca. Nitrososphaera viennensis* and the ammonia-oxidizing bacterium *Nitrososphaera multiformis* to nitrification inhibitors. *FEMS Microbiol. Lett.* 344, 121–129. doi: 10.1111/1574-6968.12164
- Sigman, D. M., and Casciotti, K. L. (2001). “Nitrogen isotopes in the ocean,” in *Encyclopedia of Ocean Sciences*, ed. J. H. Steele (Cambridge, MA: Academic Press), 1884–1894. doi: 10.1006/rwos.2001.0172
- Simon, J., and Klotz, M. G. (2013). Diversity and evolution of bioenergetic systems involved in microbial nitrogen compound transformations. *Biochim. Biophys. Acta Bioenerget.* 1827, 114–135. doi: 10.1016/j.bbabi.2012.07.005
- Sørensen, P., and Jensen, E. S. (1991). Sequential diffusion of ammonium and nitrate from soil extracts to a polytetrafluoroethylene trap for <sup>15</sup>N

- determination. *Anal. Chim. Acta* 252, 201–203. doi: 10.1016/0003-2670(91)87215-s
- Stieglmeier, M., Klingl, A., Alves, R. J. E., Rittmann, S. K.-M. R., Melcher, M., Leisch, N., et al. (2014a). *Nitrososphaera viennensis* gen. nov., sp. nov., an aerobic and mesophilic, ammonia-oxidizing archaeon from soil and a member of the archaeal phylum Thaumarchaeota. *Int. J. Syst. Evol. Microbiol.* 64, 2738–2752. doi: 10.1099/ijs.0.063172-0
- Stieglmeier, M., Mooshammer, M., Kitzler, B., Wanek, W., Zechmeister-Boltenstern, S., Richter, A., et al. (2014b). Aerobic nitrous oxide production through N-nitrosating hybrid formation in ammonia-oxidizing archaea. *ISME J.* 8, 1135–1146. doi: 10.1038/ismej.2013.220
- Tourna, M., Stieglmeier, M., Spang, A., Könneke, M., Schintlmeister, A., Urich, T., et al. (2011). *Nitrososphaera viennensis*, an ammonia oxidizing archaeon from soil. *Proc. Natl. Acad. Sci. U.S.A.* 108, 8420–8425. doi: 10.1073/pnas.1013488108
- van Kessel, M. A. H. J., Speth, D. R., Albertsen, M., Nielsen, P. H., den Camp, H. J. M. O., Kartal, B., et al. (2015). Complete nitrification by a single microorganism. *Nature* 528, 555–559. doi: 10.1038/nature16459
- Vitousek, P. M., Menge, D. N. L., Reed, S. C., and Cleveland, C. C. (2013). Biological nitrogen fixation: rates, patterns and ecological controls in terrestrial ecosystems. *Philos. Trans. R. Soc. B Biol. Sci.* 368:20130119. doi: 10.1098/rstb.2013.0119
- Walker, C. B., De La Torre, J. R., Klotz, M. G., Urakawa, H., Pinel, N., Arp, D. J., et al. (2010). *Nitrosopumilus maritimus* genome reveals unique mechanisms for nitrification and autotrophy in globally distributed marine crenarchaea. *Proc. Natl. Acad. Sci. U.S.A.* 107, 8818–8823. doi: 10.1073/pnas.0913533107
- Yoshida, N. (1988). <sup>15</sup>N-depleted N<sub>2</sub>O as a product of nitrification. *Nature* 335:528. doi: 10.1038/335528a0
- Yoshida, N., and Toyoda, S. (2000). Constraining the atmospheric N<sub>2</sub>O budget from intramolecular site preference in N<sub>2</sub>O isotopomers. *Nature* 405, 330–334. doi: 10.1038/35012558

**Conflict of Interest:** The authors declare that the research was conducted in the absence of any commercial or financial relationships that could be construed as a potential conflict of interest.

**Citation:** Mooshammer M, Alves RJE, Bayer B, Melcher M, Stieglmeier M, Jochum L, Rittmann SK-MR, Watzka M, Schleper C, Herndl GJ and Wanek W (2020) Nitrogen Isotope Fractionation During Archaeal Ammonia Oxidation: Coupled Estimates From Measurements of Residual Ammonium and Accumulated Nitrite. *Front. Microbiol.* 11:1710. doi: 10.3389/fmicb.2020.01710

Copyright © 2020 Mooshammer, Alves, Bayer, Melcher, Stieglmeier, Jochum, Rittmann, Watzka, Schleper, Herndl and Wanek. This is an open-access article distributed under the terms of the Creative Commons Attribution License (CC BY). The use, distribution or reproduction in other forums is permitted, provided the original author(s) and the copyright owner(s) are credited and that the original publication in this journal is cited, in accordance with accepted academic practice. No use, distribution or reproduction is permitted which does not comply with these terms.

# ANNEX 12

Pages 207 to 217

---

Milojevic T., Kölbl D., Ferrière L., Albu M., Kish A., Flemming R. L., Rupert A. N.,  
Koeberl C., Blazevic A., Zebec Z., Rittmann S.K.-M.R., Schleper C., Pignitter M., Somoza V.,  
Schimak M. P.

**Exploring the microbial biotransformation of extraterrestrial material on nanometer  
scale**

Scientific Reports (2019) 9:18028

10.1038/s41598-019-54482-7

---

OPEN

# Exploring the microbial biotransformation of extraterrestrial material on nanometer scale

Tetyana Milojevic<sup>1\*</sup>, Denise Kölbl<sup>1</sup>, Ludovic Ferrière<sup>2</sup>, Mihaela Albu<sup>3</sup>, Adrienne Kish<sup>4</sup>, Roberta L. Flemming<sup>5</sup>, Christian Koeberl<sup>2,9</sup>, Amir Blazevic<sup>1</sup>, Ziga Zebec<sup>1,6</sup>, Simon K.-M. R. Rittmann<sup>6</sup>, Christa Schleper<sup>6</sup>, Marc Pignitter<sup>7</sup>, Veronika Somoza<sup>7</sup>, Mario P. Schimak<sup>8</sup> & Alexandra N. Rupert<sup>5</sup>

Exploration of microbial-meteorite redox interactions highlights the possibility of bioprocessing of extraterrestrial metal resources and reveals specific microbial fingerprints left on extraterrestrial material. In the present study, we provide our observations on a microbial-meteorite nanoscale interface of the metal respiring thermoacidophile *Metallosphaera sedula*. *M. sedula* colonizes the stony meteorite Northwest Africa 1172 (NWA 1172; an H5 ordinary chondrite) and releases free soluble metals, with Ni ions as the most solubilized. We show the redox route of Ni ions, originating from the metallic Ni<sup>0</sup> of the meteorite grains and leading to released soluble Ni<sup>2+</sup>. Nanoscale resolution ultrastructural studies of meteorite grown *M. sedula* coupled to electron energy loss spectroscopy (EELS) points to the redox processing of Fe-bearing meteorite material. Our investigations validate the ability of *M. sedula* to perform the biotransformation of meteorite minerals, unravel microbial fingerprints left on meteorite material, and provide the next step towards an understanding of meteorite biogeochemistry. Our findings will serve in defining mineralogical and morphological criteria for the identification of metal-containing microfossils.

The ability of chemolithotrophic microorganisms to catalyze redox transformations of metals is an exquisite tool for energy transduction between a mineral body and a living entity. The different types of meteorites from diverse parental bodies (asteroids, Moon, or Mars) represent exceptional metal-bearing substrates that have experienced an exposure to multiple extreme conditions during their interstellar or interplanetary travel. During their journey in space, these meteoroids are constantly exposed to vacuum, radiation, and extreme temperature fluctuations. While microbial-mineral interfaces have been extensively investigated and microbial-mediated processing of metal-bearing terrestrial minerals has been abundantly harnessed, exploitation of meteorite resources requires detailed investigations of microbe-extraterrestrial mineral interactions. The study of meteorite-associated physiology of chemolithotrophic microbes is of a special focus due to implications for assessing the potential of extraterrestrial materials as a source of accessible nutrients and energy on the early Earth. Meteorites may have delivered a variety of essential compounds facilitating the evolution of life, as we know it on Earth<sup>1–3</sup>. Moreover, assessing the biogenicity based on extraterrestrial materials provides a valuable source of information for exploring the putative extraterrestrial bioinorganic chemistry that potentially might have occurred in the Solar System.

<sup>1</sup>Extremophiles/Space Biochemistry Group, Department of Biophysical Chemistry, University of Vienna, Althanstrasse 14, A-1090, Vienna, Austria. <sup>2</sup>Natural History Museum, Burgring 7, A-1010, Vienna, Austria. <sup>3</sup>Graz Centre for Electron Microscopy, Graz, Austria. <sup>4</sup>Unité Molécules de Communication et Adaptation des Microorganismes (MCAM), Muséum National d'Histoire Naturelle, CNRS, 57 rue Cuvier, 75005, Paris, France. <sup>5</sup>Department of Earth Sciences, Western University, London, UK. <sup>6</sup>Archaea Biology and Ecogenomics Division, Department of Ecogenomics and Systems Biology, University of Vienna, Althanstraße 14, A-1090, Vienna, Austria. <sup>7</sup>Department of Physiological Chemistry, Faculty of Chemistry, University of Vienna, Althanstraße 14, 1090, Vienna, Austria. <sup>8</sup>Max Planck Institute for Marine Microbiology, Celsiusstrasse 1, D-28359, Bremen, Germany. <sup>9</sup>Department of Lithospheric Research, University of Vienna, Althanstrasse 14, A-1090, Vienna, Austria. \*email: [tetyana.milojevic@univie.ac.at](mailto:tetyana.milojevic@univie.ac.at)

Given that returned extraterrestrial mineralogical samples are to date inaccessible, meteorites are “space probes” available on Earth. The compositional variety of meteorites is very broad; over 400 minerals have been found in meteorites, predominantly troilite, olivine, pyroxene, feldspar, phyllosilicates, magnetite, kamacite, and taenite. The primitive (chondritic) classes of meteorites are the most abundant, with iron and nickel as the dominant ferrous metals<sup>4</sup>. Troilite [FeS] and FeNi alloys [Fe1-xNi] as meteoritic components can be potentially used as electron donors by iron and sulfur oxidizing organisms. Several laboratory experiments on meteorites have been performed, demonstrating that some iron-oxidizing bacteria (e.g., *Leptospirillum ferrooxidans*, *Acidithiobacillus ferrooxidans*) could propagate on metal-bearing meteorite materials and use them as energy sources<sup>5,6</sup>. Recently, an *in situ* assessment of the microbial communities, which colonize stony meteorites, has been published, aiming to reveal metal-cycling microorganisms naturally contaminating astromaterials rich in FeNi-alloys and FeS<sup>7</sup>. The extreme thermoacidophile *Metallosphaera sedula* is a metallophilic archaeon that lives in hot acidic conditions (73 °C and pH 2) and uses various metal-containing ores to run its respiratory electron transport chain<sup>8–10</sup>. Previously, we have shown that this metal mobilizing archaeon can grow on Martian regolith simulants, actively colonizing these artificial extraterrestrial materials, releasing free soluble metals into the leachate solution and leaving specific spectral fingerprints<sup>11</sup>. In the present work, we explore the physiology and metal-microbial interface of *M. sedula*, living on and interacting with a real extraterrestrial material, H5 ordinary chondrite Northwest Africa 1172 (NWA 1172), Supplementary Fig. 1)<sup>12</sup>. Specific chemical analysis of the meteorite-microbial interface at nm-scale spatial resolution allowed us to trace the trafficking of meteorite inorganic constituents into a microbial cell and to investigate iron redox behavior. Combining several analytical spectroscopy techniques with transmission electron microscopy (TEM) analysis, we provide a set of biogeochemical fingerprints left upon *M. sedula* growth on the NWA 1172 meteorite.

## Results and Discussion

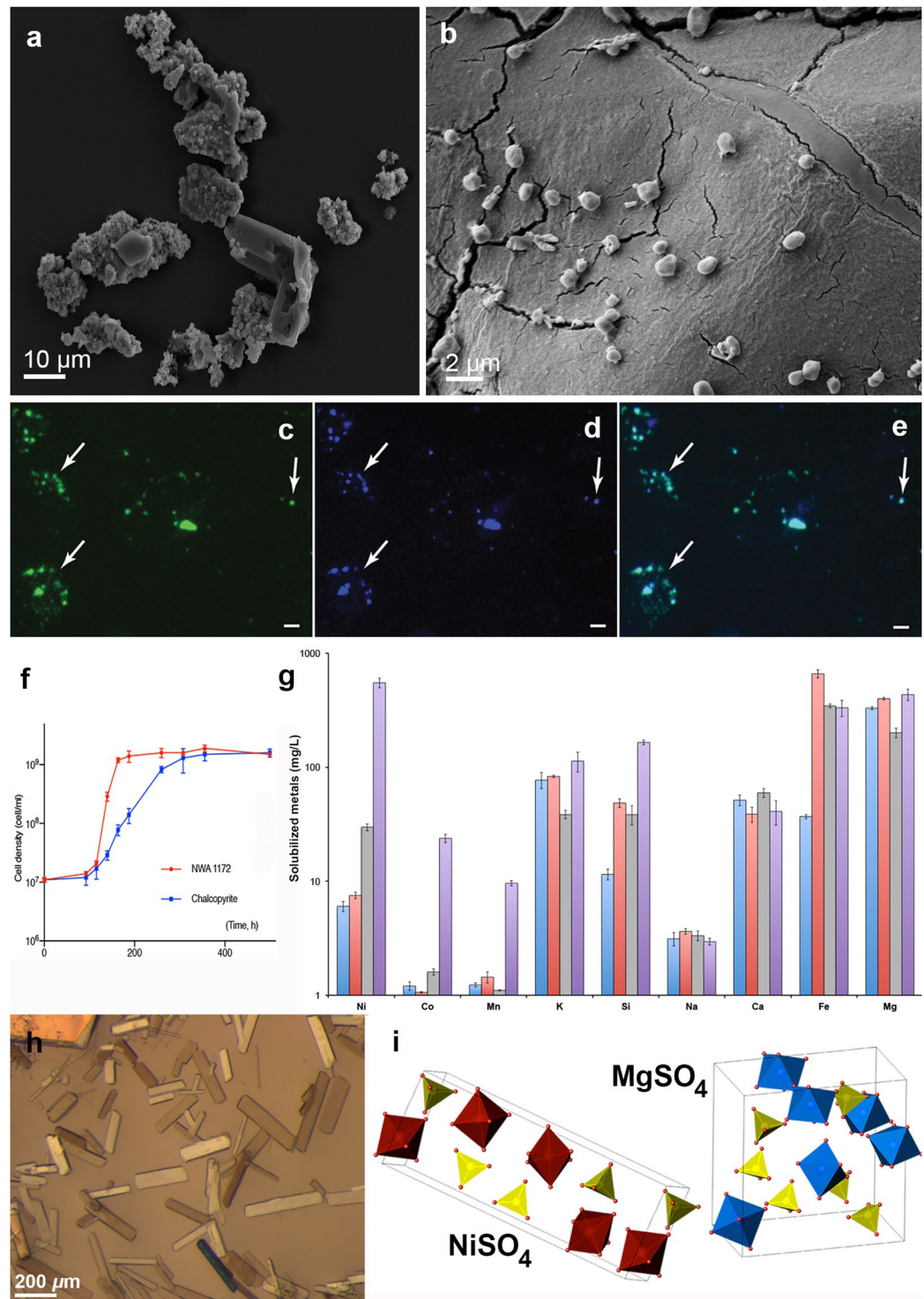
**Chemolithotrophic growth of *M. sedula* on NWA 1172.** *M. sedula* was capable of autotrophic growth on stony meteorite NWA 1172, utilizing metals trapped within it as the sole energy source. Scanning electron microscopy (SEM) investigations (Fig. 1a,b and Supplementary Fig. 2) and multi-labeled fluorescence *in situ* hybridization (MiL-FISH) with an *M. sedula*-specific ribosomal RNA-targeted probe (Fig. 1c–e, Supplementary Fig. 3, and Supplementary Table 1) indicate an active colonization of the meteorite material by *M. sedula*. As reported earlier, the round to slightly irregular coccoid cells of *M. sedula* possess pilus-like structures and can be motile when grown on the metal ore<sup>9</sup>. When grown in the presence of NWA 1172, cells of *M. sedula* were characterized by intensive vivid motility (Supplementary Movie 1). In comparison to chalcopyrite, *M. sedula* had a superior growth rate on the stony meteorite (Fig. 1f). Grown in the presence of chalcopyrite, cells of *M. sedula* displayed motility as well (Supplementary Movie 2). Meteorite-grown *M. sedula* reached stationary phase at 163 h (maximum density  $18.5 \pm 2 \times 10^8$  cells/mL, a mean generation time of 8 h), while chalcopyrite-grown cells were still in exponential phase at that time point, and reached the stationary phase after 300 h (maximum density  $15.1 \pm 5 \times 10^8$  cells/mL, a mean generation time of 21.4 h) (Fig. 1f). This difference reflects the beneficial contribution of NWA 1172 as the sole electron donor suggesting its preferential nature as energy source for *M. sedula*. NWA 1172 is a chondrite meteorite with relatively high iron abundance<sup>12</sup> and a wide range of other metal elements (Supplementary Fig. 1). Those might be used by *M. sedula* as an energy source to satisfy its bioenergetic needs and as specific metabolic/enzymatic cofactors, providing more optimal constitutive and/or structural elements for enzymatic machinery. In addition, copper sulfides, such as chalcopyrite, dictate certain inevitable issues in respect with metal mobilizing due to their refractory characteristics. Hence, the porosity of NWA 1172 (typically of a few percent<sup>13</sup>) might also reflect the superior growth rate of *M. sedula* over refractory and densely packed chalcopyrite.

As a result of tight biogeochemical interactions, by means of its metal oxidizing machinery<sup>14–16</sup>, *M. sedula* released free soluble metals (Ni, Si, Co, Mn, and K) into the cultivation medium (Fig. 1g). Ni and Si were predominantly released, reaching 0.55 and 0.17 g/L, respectively, with lesser contributions from Co, Mn, and K ions (Fig. 1g). Dehydration-crystallization and X-ray diffraction experiments (Supplementary Fig. 4) revealed the chemical speciation of the released Ni: nickel sulfate hexahydrate<sup>17</sup> in the tetragonal space group  $P 4_1 2_1 2$  ( $a = 6.8 \text{ \AA}$ ,  $b = 6.8 \text{ \AA}$ ,  $c = 18.29999$ ,  $\alpha = \beta = \gamma = 90^\circ$ ) and magnesium sulfate heptahydrate<sup>18</sup> in the orthorhombic space group  $P 2_1 2_1 2_1$  ( $a = 11.868 \text{ \AA}$ ,  $b = 11.996 \text{ \AA}$ ,  $c = 6.857 \text{ \AA}$ ,  $\alpha = \beta = \gamma = 90^\circ$ ), suggesting +2 oxidation state of extracted Ni ions and the occurrence of nickel sulfate in the leachate solution (Fig. 1i).

**Nanoanalytical spectroscopy of meteorite-microbial interface.** Observations of ultra-thin sections of *M. sedula* cells grown on NWA 1172 revealed round-shaped, irregular cocci with a diameter around 1  $\mu\text{m}$  (Fig. 2). These irregular coccoid morphologies were characterized by the presence of electron-dense dark areas along the cell envelope and extensive dark accumulations in the cytosol (Fig. 2). Elemental ultrastructural analysis of *M. sedula* grown on NWA 1172 was performed to investigate metal acquisition patterns of this archaeon, i.e., enabling us to verify the content and localization of metals in *M. sedula* (Fig. 2). The following observations were made using energy-dispersive X-ray spectroscopy (EDS) analysis performed in scanning transmission electron microscopy (STEM) mode: (1) the elemental maps show abundant C, O, N, S, Cu, P, Fe, Al, Co, and K content of *M. sedula* cells; (2) Cu, K, Cl, Fe, Al, and P signals were localized both on the cell surface and intracellularly; (3) C, O, and N were evenly distributed giving strong intracellular signals which likely arose from organic content (e.g., proteins and carbohydrates) present in *M. sedula* cells; (4) Si accumulations produced strong intracellular signals, which correspond to the dark electron dense areas of the TEM image (intracellular deposits); and (5) Co and K were evenly represented inside the cell; (Fig. 2, Supplementary Fig. 5).

The pronounced membrane-bound signal of Cu reflects the great diversity and active content of multi-copper oxidases widely distributed in *M. sedula* branched respiratory chains within a diverse number of terminal oxidases<sup>10,14–16</sup>. Apart from these multi-copper oxidases involved in iron and sulfur oxidative respiration network,





**Figure 1.** Biotransformation of the chondrite meteorite NWA 1172 by *M. sedula*. (a) Scanning electron microscopy (SEM) image of fragments of the chondrite meteorite NWA 1172 bioprocessed by *M. sedula*. (b) SEM image showing *M. sedula* cells colonizing the surface of the meteorite particles. (c–e) Multi-Labeled-Fluorescence *in situ* Hybridization (MiL-FISH) of *M. sedula* cells grown on NWA 1172 as the sole energy sources: (c) MiL-FISH images of cells (green) after hybridization with the specific oligonucleotide probe targeting *M. sedula*; (d) DAPI staining of the same field (blue); (e) Overlaid epifluorescence image, showing overlap of the specific oligonucleotide probe targeting *M. sedula* with DAPI signals. Arrows indicate cells of *M. sedula*. Scale bar, 2  $\mu\text{m}$ . (f) Growth curves of autotrophic cultures of *M. sedula* cultivated at 73 °C on NWA 1172 (red) and chalcopyrite (blue). Legends represent the corresponding type of energy source. (g) Inductively coupled plasma-optical emission spectrometry (ICP-OES) analysis of released metal ions in the supernatant of *M. sedula* cultures grown on NWA 1172 as the sole energy source. Samples were taken at “0” time point (red), from late exponentially growing cultures of *M. sedula* (purple), and from corresponding abiotic controls (blue).

and grey, respectively). **(h)** Single crystals of nickel sulfate hexahydrate and magnesium sulfate heptahydrate were obtained after recrystallization of the crystalline material ( $\alpha$ ) shown in Supplementary Fig. 4. **(i)** Atomic structures of  $\text{NiSO}_4 \times 6 \text{H}_2\text{O}$  and  $\text{MgSO}_4 \times 7 \text{H}_2\text{O}$  from crystals in **(h)** as investigated with single crystal X-ray diffraction, with the unit cell for each structure represented. Crystal water has been removed for clarity. Legend:  $\text{Ni}(\text{H}_2\text{O})_6$ , red octahedra;  $\text{Mg}(\text{H}_2\text{O})_6$ , blue octahedra;  $\text{SO}_4^{2-}$ , yellow tetrahedra. Points and error bars show the mean and error-represented standard deviation, respectively, of  $n = 3$  biological replicates. If not visible, error bars are smaller than symbols.

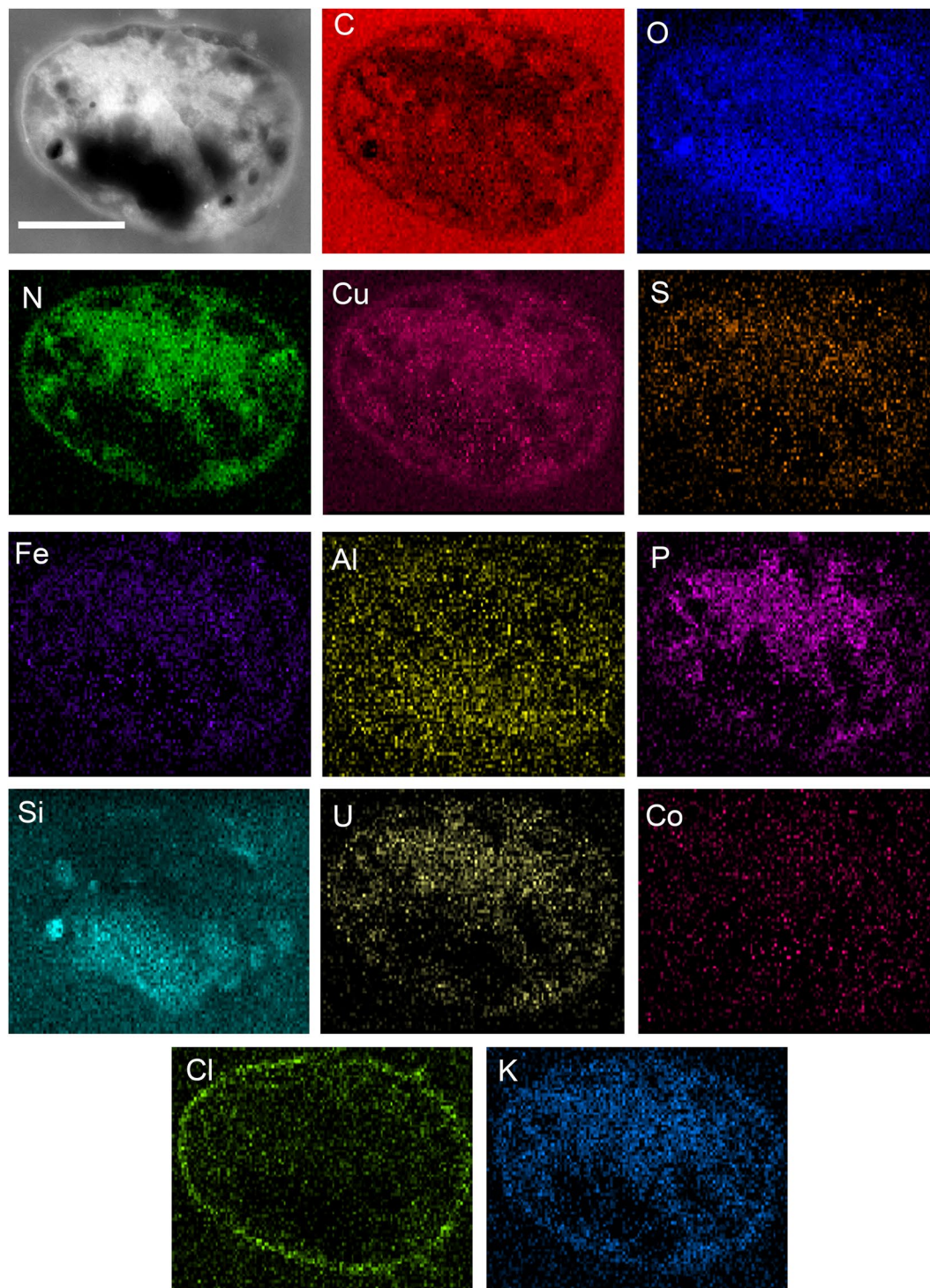
membrane-associated specific Cu-transporters might also implement in Cu binding observed in Fig. 2 (Cu map). An efficient Cu transportation and sequestration system was described in *M. sedula*<sup>19,20</sup>. Incorporation of Fe and S may naturally speak on the account that these elements are potentially used as energy sources in oxidation process coupled to electron breathing (Fig. 2, Fe and S maps). Intracellular Si accumulations in form of bulk deposits comprise 5.9% of the overall elemental content, and suggest the beginning of silicification of *M. sedula* during growth on meteorite material (Fig. 2, Si map and Supplementary Table 2). Silicification processes have been shown for various microbial systems, including *in situ* studies in modern silicifying hydrothermal systems<sup>21</sup> and laboratory investigations of artificial microbial silicification<sup>22–24</sup>, highlighting the potential of silica matrices for the morphological preservation of putative microfossils.

TEM analysis revealed the presence of extracellular vesicle-like morphologies (encapsulated round-shaped particles with an average diameter of 200 nm; Supplementary Fig. 6a). The monolayers of *M. sedula* vesicles have been shown to catalyze iron oxidation and solubilization of mineralized copper from chalcopyrite under the energy-limited lithoautotrophic conditions<sup>25</sup>. Apart from metal transformation, synthesis and secretion of membrane vesicles might serve as a general mechanism of extracellular metal sequestration by binding with chelating agents, e.g., proteins, and enzymatic detoxification of the metal to a less toxic form. The observed vesicles, formed during the growth of *M. sedula*, may be capable of mineral oxidation, contributing to metal biotransformation and potentially metal immobilization from NWA 1172. Our EDS analysis performed in STEM mode showed that these carbonaceous and oxygenated vesicles harbor Si, Ni, Cu, Fe, Cl, and Al (Supplementary Fig. 6a), which reflects their ability to immobilize metals from the meteorite material.

Notably, TEM observations of cross-sections of *M. sedula* cells revealed the coexistence of cells in different stages of biomineralization: cells with not fully mineralized cell envelope (Fig. 2) and at more advanced steps of mineral formation as heavily encrusted mineralized cell remnants (Fig. 3 and Supplementary Figs. 7, 8). Elemental ultrastructural analysis of heavily encrusted cell remnants showed that the crust layer of variable thickness (up to 250 nm) was composed of Fe, Cu, Si, Al, Ni, S, C, N, O, and P (Supplementary Table 3). Further comparative electron energy loss spectra (EELS) analysis uncovered the spatial distribution and fine structure of iron species in heavily encrusted cell remains and on the cell surface of *M. sedula* (Fig. 3, bottom panel). The EELS measurements, acquired locally (point analysis with a beam diameter of 1 Å) in STEM mode, demonstrate that the cell surface of *M. sedula* is bearing a mixed valence iron distribution with dominant  $\text{Fe}^{2+}$  species (dotted line at Fig. 3, bottom panel).  $\text{Fe}^{2+}$  detected on the cell surface (Fe  $L_{3-}$ -edge at ~708 eV, Fig. 3, bottom panel) may primarily originate due to the leaching of  $\text{Fe}^{2+}$  from the meteorite. This spectrum also shows the minor presence of  $\text{Fe}^{3+}$  species (a shoulder of Fe  $L_{3-}$ -edge at ~710 eV) which can be explained by extracellular  $\text{Fe}^{2+}$  oxidation performed by a membrane bound iron oxidizing machinery of *M. sedula*, which is encoded by genes of the *fox* cluster<sup>10,14–16</sup>. A microbially replenished  $\text{Fe}^{3+}$  supply (in addition to abiotic  $\text{Fe}^{3+}$ ) ensures further meteorite oxidation as well as access to metals for the cells. The  $\text{Fe}^{3+}$  species detected on the cell surface of *M. sedula* can effectively function as an oxidizing agent for meteorite at the cell-meteorite interface. In addition to the direct *M. sedula* mediated biooxidation of metals, the involvement of abiotic factors may facilitate the process of metals mobilization from NWA 1172, representing an indirect mechanism of metal solubilization. Abiotic oxidizing attack of  $\text{Fe}^{3+}$  on the solid mineral enables the mobilization of metals from the solid matrix<sup>26</sup>, suggesting that both direct and indirect mechanisms contribute to the dissolution of metals mediated by *M. sedula*. The Fe  $L_{2,3}$  edges from heavily encrusted cell remnants show the predominant presence of  $\text{Fe}^{3+}$  species (solid line at Fig. 3, bottom panel, Fe  $L_{3-}$ -edge at ~710 eV), which can be explained by accomplished  $\text{Fe}^{2+}$  oxidation followed by cell encrustation and entombment in the mineralized form of a mixture of different amorphous iron oxides/hydroxides with the predominant form of  $\text{Fe}^{3+}$ . Similar cell surface encrustation, but with tungsten crystalline nanolayers, we have previously shown for *M. sedula* grown on tungsten-bearing terrestrial materials<sup>27,28</sup>. In the case of our study with NWA 1172, TEM observations show that the encrusted cell remnants and iron bearing accumulations on the cell surface of *M. sedula* have an amorphous structure. Consequently, further studies were directed at spectral and mineralogical analysis of the meteorite surface after the exposure to *M. sedula*.

**Mineralogical and geochemical analyses of microbial fingerprints left on NWA 1172.** Investigations of the biologically mediated alteration of the meteorite surface by cultivation of *M. sedula* with slab fragments of NWA 1172 indicated the presence of globular iron-rich aggregates (with a size ranging from <0.5 to 2 µm for single globules) along with areas of crystalline iron oxides as a specific microbial alteration left upon *M. sedula* growth (Fig. 4a,b,d). Similar types of globular iron-rich aggregates were observed on the surface of the meteorite abiotically exposed to *M. sedula* medium at 73 °C, illustrating that they are the result of abiotic, i.e., chemically induced rusting processes (Fig. 4c). EDS analysis of these globular aggregates in chemically changed and biologically altered meteorite surfaces showed that they are dominated by Fe and P with a variable amount of S and Si (Fig. 4e). However, the iron oxides (as determined using EDS), which appear as branched porous network represented on Fig. 4b,d,f, occurred only along the meteorite surface exposed to *M. sedula*, suggesting that it is solely of biogenic origin. In a few previously published studies, iron meteorites and carbonaceous chondrite

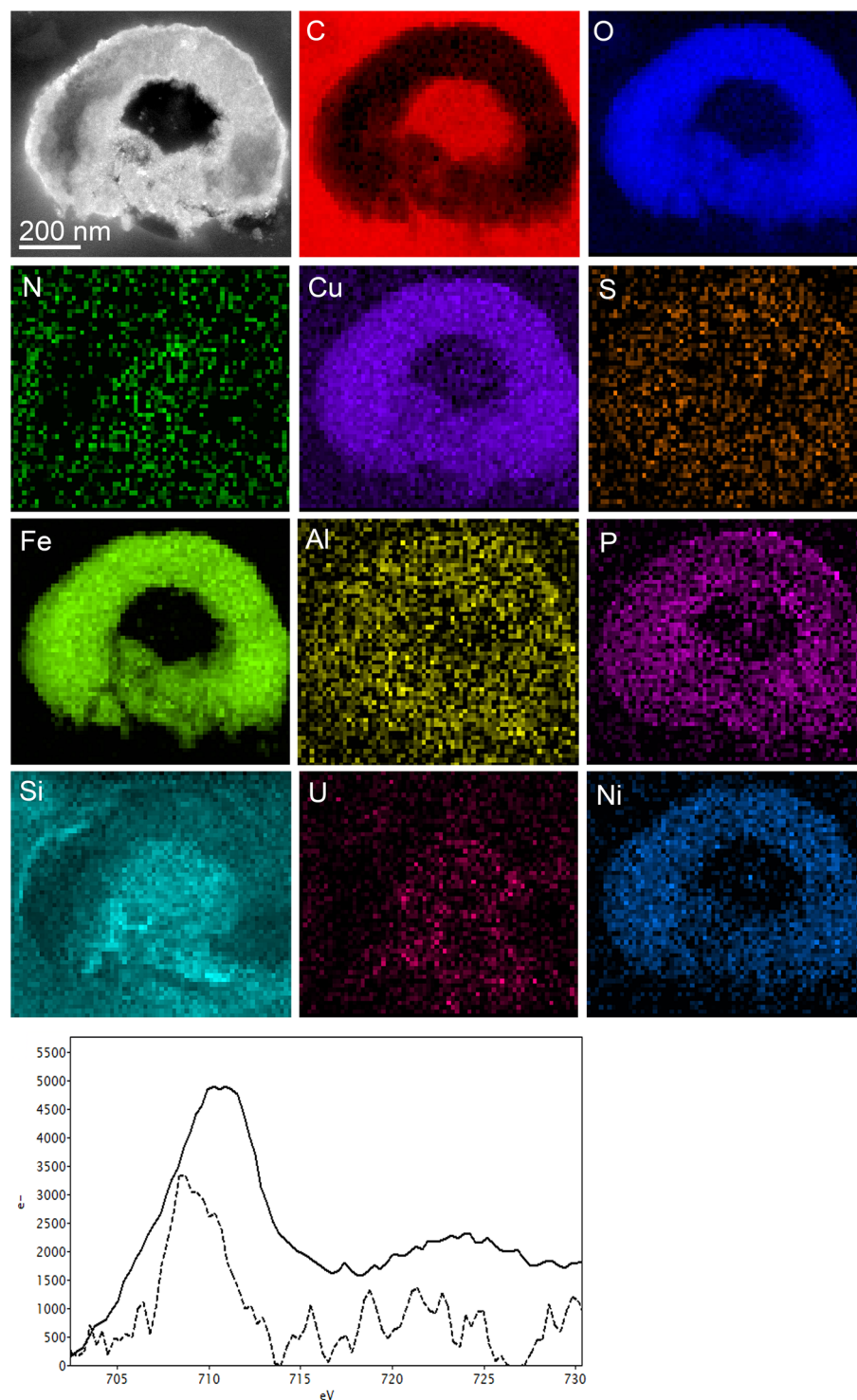




**Figure 2.** Elemental ultrastructural analysis of *M. sedula* grown on NWA 1172. The annular dark field (ADF) scanning transmission electron microscopy (STEM) image of a cell of *M. sedula* used for the EDS spectrum image acquisition and corresponding extracted carbon (C), oxygen (O), nitrogen (N), copper (Cu), sulfur (S), potassium (K), chlorine (Cl), iron (Fe), aluminum (Al), phosphorus (P), cobalt (Co), silicon (Si), and uranium (U) elemental maps. Scale bar, 0.5  $\mu\text{m}$ .

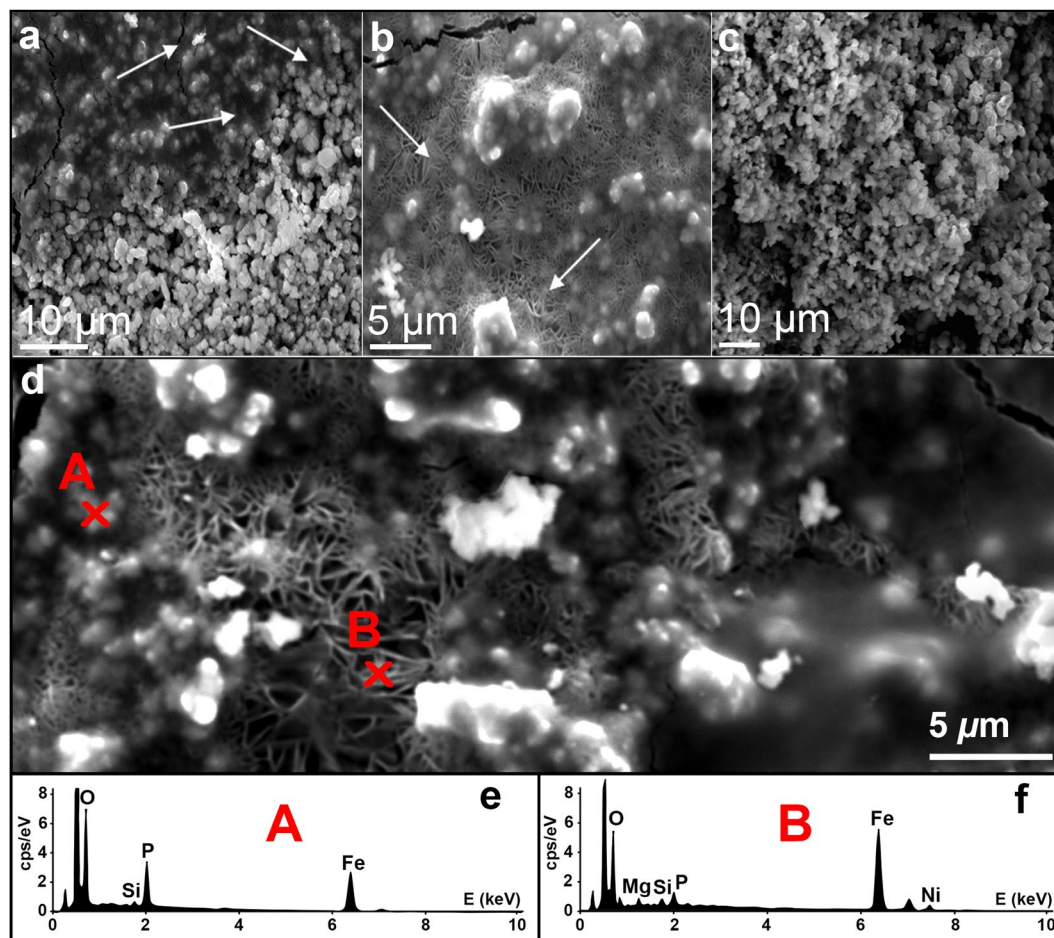
meteorites provided metal components as suitable energy substrates to maintain the bacterial growth and chemolithotrophic metabolism<sup>5,6</sup>. Similar near-spherical Fe-, P-, and S-containing aggregates along with needle-like crystals of iron oxides were observed during iron meteorite weathering by the iron-oxidizing acidophilic bacteria *A. ferrooxidans*<sup>5</sup>.

Micro X-ray diffraction ( $\mu\text{XRD}$ ) data were acquired on a bioprocessed NWA 1172 slab fragment after the cultivation with *M. sedula*, and the following secondary oxides/alteration minerals were characterized: goethite,



**Figure 3.** Elemental ultrastructural analysis of *M. sedula* empty envelopes encrusted during growth on NWA 1172 and corresponding Fe  $L_{2,3}$ -edge core electron energy loss (EEL) spectra. The high angular annular dark field (HAADF) scanning transmission electron microscopy (STEM) image of a heavily encrusted cell remnants of *M. sedula* used for the EDS spectrum image acquisition and corresponding carbon (C), copper (Cu), phosphorus (P), iron (Fe) oxygen (O), nickel (Ni), sulfur (S), and nitrogen (N) elemental maps. Corresponding Fe  $L_{2,3}$ -edge core electron energy loss (EEL) spectra acquired from the S-layer of *M. sedula* cells depicted in Supplementary Fig. 8a (shown as dotted line) and from the crust in Supplementary Fig. 8c (shown as solid line) are provided at the bottom panel.



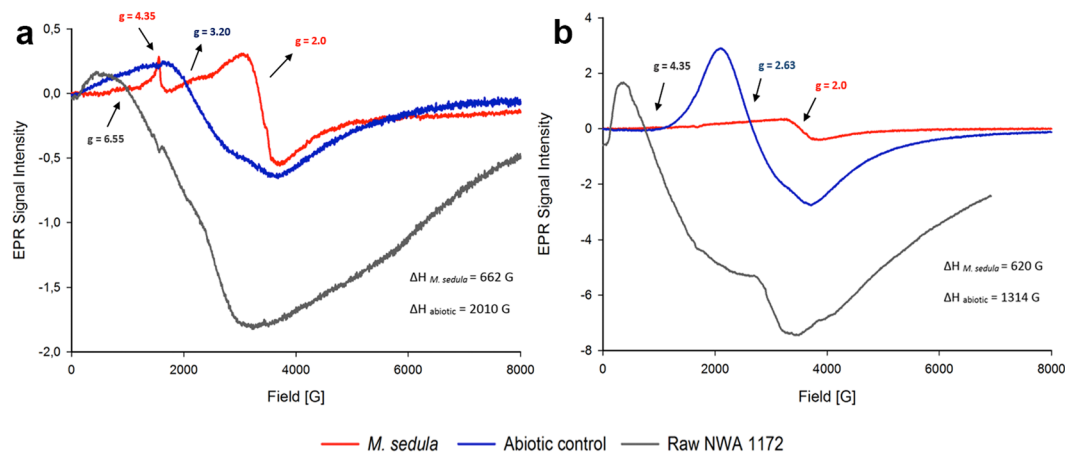


**Figure 4.** Alteration of the surface of the chondrite meteorite NWA 1172 slabs mediated by *M. sedula*. (a) Secondary electron (SE) image of a NWA 1172 slab cultivated with *M. sedula* at 73 °C. (b) Magnified SE image of a NWA 1172 slab cultivated with *M. sedula* at 73 °C. (c) SE image of abiotically exposed slab of NWA 1172 to the cultivation medium at 73 °C. (d) Magnified area of SE image of NWA 1172 slab cultivated with *M. sedula* at 73 °C. (e) EDS spectra of globular structures (marked with red A) that form iron oxides aggregates, containing mainly Fe and P. (f) EDS spectra of branched network of crystalline iron oxides (marked with red b). Arrows indicate the areas where crystalline iron oxides occur.

lepidocrocite, ferrihydrite, hematite, and maghemite (*i.e.*, similar work conducted on an unprocessed meteorite slab shows that none of these minerals were originally present in the meteorite) (Supplementary Fig. 9). The most-abundant primary minerals in ordinary chondrites are olivine and enstatite (+/– plagioclase). These primary minerals are visible on every pattern in  $\mu$ XRD analysis performed in this study, as X-rays penetrate through the surface layer with microbial alterations. Occasionally, primary kamacite, troilite, and magnetite were also detected. Our  $\mu$ XRD measurements are in agreement with previously reported biogenic crystalline ferric iron (oxy)hydroxides, such as goethite and lepidocrocite for the iron oxidizing acidophile *Acidithiobacillus ferrooxidans* during iron meteorite weathering<sup>5</sup> and closely related species *Sulfolobus acidocaldarius*, the only other member of the *Sulfolobales* for which such measurements are available<sup>29</sup>.

Electron Paramagnetic Resonance (EPR) measurements were performed to (1) identify paramagnetic species in NWA 1172 and to (2) investigate the impact of *M. sedula* on NWA 1172 with a possible effect on the oxidation state of paramagnetic species. Measurements were performed at 90 K (Fig. 5a) and 273 K (Fig. 5b) to increase the chance for unambiguous iron detection. Iron oxides are the predominant component (51%) of the chondrite NWA 1172 (Supplementary Fig. 1) and iron mixed paramagnetic  $\text{Fe}^{3+}$  species in high and low spin states in biogenic samples were identified via EPR. Accumulation of  $\text{Fe}^{3+}$  in the biogenic sample at 90 K (Fig. 5a, red line) was observed and might be the consequence of extensive  $\text{Fe}^{2+}$  oxidation of the minerals mediated by *M. sedula*. After cultivation with *M. sedula*, the biogenic sample shows a prominent sharp high spin  $\text{Fe}^{3+}$  signal with a g-value of 4.35 and a low spin  $\text{Fe}^{3+}$  signal at g-value 2 (Fig. 5a). Compared to the raw meteorite material, the appearance of a prominent high spin  $\text{Fe}^{3+}$  signal (a sharp peak with a g-value of 4.35) along with a low spin  $\text{Fe}^{3+}$  signal at g-value 2 in the biogenic sample may indicate an increase in  $\text{Fe}^{3+}$  species due to biooxidative activity of *M. sedula*. These characteristic sharp high spin and low spin  $\text{Fe}^{3+}$  signals are not represented in abiotically treated NWA 1172 (Fig. 5). The abiotic spectrum is characterized by a signal with a shifted g-value 3.20 and broad linewidth





**Figure 5.** Electron Paramagnetic Resonance (EPR) spectra of raw NWA 1172 (gray line), NWA 1172 bioprocessed by *M. sedula* (red line) and NWA 1172 after the treatment with cultivation medium, but without *M. sedula* (abiotic control, blue line). (a) Spectra recorded at 90 K with assigned linewidth ( $\Delta H$ ) and g-values. (b) Spectra recorded at 273 K.

( $\Delta H = 2010$  G), which might refer to multiple ionic mixtures. Interestingly, the spectral features of abiotically treated NWA 1172 closely resemble those of abiotically treated Martian regolith simulant S-MRS<sup>11</sup>. This abiotic peak at g-value 3.20 is not detectable anymore in biogenic samples of NWA 1172 (Fig. 5a, red curve) and S-MRS<sup>11</sup>. While the distinct high spin  $\text{Fe}^{3+}$  signal is not detectable in the biogenic sample when measured at 273 K (Fig. 5b), the low spin  $\text{Fe}^{3+}$  signal at g-value 2 appears after the cultivation showing us the presence of mineral transforming iron-oxidizing microorganisms.

## Conclusions

Our investigations provide the further step towards extending our knowledge of meteorite biogeochemistry. Heterogeneous iron species  $\text{Fe}^{2+}/\text{Fe}^{3+}$  with dominant  $\text{Fe}^{2+}$  are represented on the cell surface, indicating active Fe redox processing at the cell surface of *M. sedula* and suggesting Fe oxidative solubilization of meteorite material. *M. sedula* releases free solubilized metals (Fig. 1g) and is capable of intracellular and cell surface incorporation of metals when grown on meteorite material (Figs. 2, 3, and 4). Meteorite biotransformation mediated by *M. sedula* leads to nickel solubilization (Fig. 1g–i) with the formation of nickel sulfate ( $\text{NiSO}_4$ )-bearing material (Fig. 1h,i). Such nickel enrichment/ $\text{NiSO}_4$  deposition can be considered as a metabolic signature resulted from microbial leaching activity of meteorite minerals. The heavily metal encrusted cell remnants described in the present study and its fine structural details may constitute relevant biosignatures to be looked for in the geological record, if they are not destructed during diagenetic or metamorphic processes and are intact during different stages of fossilization. Our nanoanalytical spectroscopy investigations of heavily mineralized *M. sedula* cells grown on the NWA 1172 meteorite revealed the enrichment of Cu, Fe, O, and Si in the amorphous crust with a mixture of P, Ni, S and Al, which may likely correspond to the amorphous product  $\text{Cu}_x\text{Fe}_y\text{O}_z(\text{SPNiAl})-\text{SiO}_2$  formed on the late biomineralization stages of cells encrustation. Our work provides a deeper insight into the biologically-mediated processing of extraterrestrial material and implications for natural samples, representing a special interest for space exploration missions.

## Methods

**Cultivation of *M. sedula*.** *M. sedula* (DSMZ 5348) cultures were grown aerobically in DSMZ88 *Sulfolobus* medium containing 1.3 g  $(\text{NH}_4)_2\text{SO}_4$ , 0.28 g  $\text{KH}_2\text{PO}_4$ , 0.25 g  $\text{MgSO}_4 \cdot 7 \text{H}_2\text{O}$ , 0.07 g  $\text{CaCl}_2 \cdot 2 \text{H}_2\text{O}$ , and 0.02 g  $\text{FeCl}_3 \cdot 6 \text{H}_2\text{O}$  dissolved in 1 L of water. After autoclaving, Allen's trace elements solution was added to 1 L media resulting in 1.80 mg  $\text{MnCl}_2 \cdot 4 \text{H}_2\text{O}$ , 4.50 mg  $\text{Na}_2\text{B}_4\text{O}_7 \cdot 10 \text{H}_2\text{O}$ , 0.22 mg  $\text{ZnSO}_4 \cdot 7 \text{H}_2\text{O}$ , 0.05 mg  $\text{CuCl}_2 \cdot 2 \text{H}_2\text{O}$ , 0.03 mg  $\text{Na}_2\text{MoO}_4 \cdot 2 \text{H}_2\text{O}$ , 0.03 mg  $\text{VSO}_4 \cdot 2 \text{H}_2\text{O}$ , and 0.01 mg  $\text{CoSO}_4$  final concentration. The pH was adjusted to 2.0 with 10 N  $\text{H}_2\text{SO}_4$ .

Cultivation of *M. sedula* was performed as described before<sup>11</sup> in 1 L glassblower modified Schott-bottle bioreactors (Duran DWK Life Sciences GmbH, Wertheim/Main, Germany), equipped with a thermocouple connected to a heating and magnetic stirring plate (IKA RCT Standard/IKA C-MAG HS10, Lab Logistics Group GmbH, Meckenheim, Germany) for temperature and agitation control. The bioreactors were equipped with three 10 mL graduated glass pipettes, permitting carbon dioxide and air gassing (with the gas flow of  $9 \text{ mL min}^{-1}$ , adjusted to five bubbles  $\text{s}^{-1}$  by using 8 mm valves (Serto, Frauenfeld, Switzerland)) and sampling of culture, respectively. The graduated pipettes used for gassing were connected by silicon tubing to sterile  $0.2 \mu\text{m}$  filters (Millex-FG Vent filter unit, Millipore, Billerica, USA). The graduated pipettes used for sampling were equipped with a Luer-lock system in order to permit sampling with sterile syringes (Soft-Ject, Henke Sass Wolf, Tuttlingen, Germany). The offgas was forced to exit via a water-cooled condenser (Ochs GmbH, Bovenden, Germany). For the cultivations of *M. sedula* at 73 °C the temperature inside the bioreactors was controlled by electronic thermocouple via the heating and magnetic stirring plates. For chemolithoautotrophic growth cultures were supplemented with 10 g/liter either chalcopyrite (provided by E. Libowitzky from the mineral collection of the Department of Mineralogy

and Crystallography, University of Vienna) or NWA 1172 meteorite (provided by the NHM, Vienna). The minerals were ground and temperature sterilized at 180 °C in a heating chamber for a minimum of 24 hours prior to autoclavation at 121 °C for 20 min. When intact, rectangular slabs of NWA 1172 were used for fermentation, the aforementioned two steps sterilization procedure was applied, too. Abiotic controls consisting of culture media supplemented with sterilized NWA 1172 without *M. sedula* cells were included in the experiments. Growth of cells was monitored by phase contrast/epifluorescence microscopy and metal release; doubling times (in h) during exponential phase growth were calculated from the slopes of the growth curves based on time required for 2-fold increase of cell number. For the visualization of cells wiggling on solid particles they were stained by a modified “DAPI” (4'-6'- Diamidino-2-phenylindole) procedure<sup>30</sup>, observed and recorded with ProgRes® MF cool camera (Jenoptik) mounted on Nikon eclipse 50i microscope, equipped with F36–500 Bandpass Filterset (ex, 377/50 nm; em, 447/60 nm).

**Multi-labelled-Fluorescence *in Situ* Hybridization (MiL-FISH).** *M. sedula* cells were fixed in 2% paraformaldehyde (PFA) at room temperature for 1 hour, washed three times in distilled water, centrifuged at 10,000 rpm and stored in 50:50, ethanol:PBS (phosphate buffer saline). A 16 S rRNA phylotype specific probe for *M. sedula* was designed with the software package ARB<sup>31</sup> and labeled with 4x Atto488 via Click chemistry (biomers.net GmbH, Ulm, Germany) (Supplementary Table 1). Fixed cells were mounted on 10 well Diagnostica glass slides (Thermo Fisher Scientific Inc. Waltham, USA) and MiL-FISH conducted directly on them after Kölbl *et al.*<sup>11</sup>. Cells were hybridized with 30% formamide for 16 hours. For experimental positive controls *Gramella forsetii* strain KT0803 was hybridized with a 4x labelled general bacterial probe EUB338. Positive control for the specificity of the phylotype specific probe *M. sedula* 174 was given by including *M. sedula* DSM5348 in all experiments. After hybridization slides were washed for 15 minutes at 48 °C (14 to 900 mM NaCl, 20 mM Tris-HCl [pH 8], 5 mM EDTA [pH 8], and 0.01% SDS) at a stringency adjusted to the formamide concentration used. Cells were counterstained by incubation for 10 min with 10 mg ml<sup>-1</sup> DAPI followed by rinsing in distilled water 3 times before CitiFluor (CitiFluor Ltd., London, England) mounting medium was applied to slides with a coverslip. Fluorescence images were taken with an AxioCam Mrm camera mounted on an Axioscope2 epifluorescence microscope (Carl Zeiss AG, Oberkochen, Germany) equipped with F36-525 Alexa 488 (ex, 472/30 nm; em, 520/35 nm) filter cube. Images were recorded with the PC-based AxioVision (release 4.6.3 SP1) imaging software.

**Metal analysis.** To determine the extracellular concentrations of metal ions mobilized from the sulfide ores and from NWA 1172, culture samples were clarified by centrifugation. Samples of the resulting supernatants were filtered (0.44 µm pore size) and analyzed by inductively coupled plasma-optical emission spectrometer (ICP-OES) Perkin Elmer Optima 5300 DV. All reported values are averages from triplicate samples.

**Dehydration/Crystallization experiments.** Cultures of *M. sedula* autotrophically grown on meteorite were harvested at early stationary phase, spread evenly on glass plates, and dehydrated within 60 days under oxic conditions at room temperature (Ø 7 cm, VWR International). Abiotic controls consisting of uninoculated culture media were included in all the experiments. Dehydration of cultures by slow evaporation led to the formation of a crystalline and an amorphous phase. The crystalline phase was isolated and recrystallized in aqueous solution. Single crystals were mounted on loops and investigated using a Bruker D8 Venture, equipped with multilayer monochromator, INCOATEC microfocus sealed tube ( $\lambda$  (MoK $\alpha$ ) = 0.71073 Å) and CMOS Photon Detector.

**Preparation and characterization of NWA 1172 meteorite samples.** A partially fusion crusted NWA 1172 meteorite sample with fresh broken surfaces was selected for the current study (Supplementary Fig. 1). This sample was selected because it represents a very pristine example of an H5 type ordinary chondrite. Even if it is not an observed fall meteorite, it is classified as W0, thus corresponding to the least weathered (or more pristine) type of meteorite (*i.e.*, with no visible oxidation of metal or troilite; see, *e.g.*, Wlotzka, 1993)<sup>32</sup>. The classification as W0 was further confirmed during our preliminary optical microscope observations (*i.e.*, thin sections of this meteorite).

After cutting off the fusion crusted parts of the sample, rectangular slabs with dimensions of about 40 × 23 × 10 mm and about 30 g each were prepared (the rest of the sample was used for the preparation of polished thin sections and for the experiments with crushed material). One of the two large surfaces of all the prepared slabs was then polished, the other five faces staying “raw” (*i.e.*, cut surfaces).

After completion of the experiments, the slabs were withdrawn from 1 L glassblower modified Schott-bottle bioreactors and characterized with SEM. SEM characterization was conducted at the Natural History Museum (Vienna, Austria) using a JEOL JSM 6610-LV with the operating conditions of 15 kV accelerating voltage and 0.1 nA beam current.

**Scanning electron microscopy.** Cells of *M. sedula* harvested at stationary phase were prepared for electron microscopy by fixing in a solution of 1 vol.% glutaraldehyde in Na-Cacodylate buffer. Samples were dehydrated in a graded series of ethanol solutions and dried chemically using Hexamethyldisilazan (HMDS). Fixed samples were mounted on aluminum stubs, sputter-coated with Au, and examined at the University of Vienna with a Zeiss Supra 55 VP scanning electron microscope operated at 5 kV.

**Transmission electron microscopy.** Cells of *M. sedula* harvested at stationary phase were primary fixed at 4 °C in a 1 M Na-Cacodylate buffer containing 2.5% glutaraldehyde. After primary fixation cells were post-fixed for 2 h in 1% OsO<sub>4</sub>. Cells were washed three times (2 × 0.1 M Na-cacodylate, 1x dH<sub>2</sub>O) and subsequently dehydrated by a gradual ethanol series (30%, 50%, 70%, 90%, abs.), each step with an incubation time of 30 minutes. Cells were spun down after each dehydration step for another 30 minutes and resuspended for the following ethanol treatment. Samples were embedded in Spurr Low Viscosity Resin (Electron Microscopy Sciences, United

States) and polymerized at 60 °C for a minimum of 48 h. Semi- and ultrathin sectioning were performed via a Reichert-Jung Ultracut E ultramicrotome, 50–70 nm ultrathin sections were deposited on formvar/carbon-coated 200 mesh copper grids (Agar Scientific, UK).

High resolution STEM investigations were performed at the Graz Centre for Electron Microscopy (FELMI-ZFE, Graz), on a probe corrected FEI Titan G2 60–300 (S/TEM) microscope with an X-FEG Schottky field-emission electron source operated at 60 and 300 kV (current of 150 pA, beam diameter of 1 Å). The microscope is equipped with a FEI Super-X detector (Chemi-STEM technology), consisting of four separate silicon drift detectors and a Dual EELS - Gatan Imaging Filter (GIF) Quantum. High Angular Annular Dark Field (HAADF) and Annular Dark Field (ADF) detectors were used to acquire micrographs. Scanning transmission electron microscopy (STEM) and analytical spectroscopy by using electron energy loss (EELS) and dispersive X-ray (EDS) Spectrum Images were carried out for different areas of *M. sedula* cells. For each area, elemental maps were extracted from EELS and EDS spectrum images. Further, EELS and EDS spectra from representative areas on the cell surface and inside the cells have been acquired/extracted. The images and spectra were processed with Gatan's Digital Micrograph being corrected for dark current and gain variations. Element quantification for EDS spectra was performed by using the k-factor method<sup>33,34</sup>.

**Micro X-ray diffraction analysis.** Data were collected on a Bruker D8 Discover at the University of Western Ontario (London, Ontario, Canada), having  $\theta$ - $\theta$  geometry, operating at 35 kV, and 45 mA with a radiation source of CoK $\alpha$  (1.79026 Å), and a Göbel mirror with a 300  $\mu$ m pinhole collimator. A HI-STAR detector with General Area Detector Diffraction System (GADDS; Bruker-AXS 2010) software was used<sup>35</sup>.

**Electron Paramagnetic Resonance spectroscopy.** The Electron Paramagnetic Resonance (EPR) spectra were recorded as described earlier (11) at the University of Vienna on an X-Band Bruker Elexsys-II E500 CW-EPR spectrometer (Bruker Biospin GmbH, Rheinstetten, Germany) at  $90 \pm 1$  and  $293 \pm 1$  K using a high sensitivity cavity (SHQE1119). Solid state EPR measurements were performed setting microwave frequency to 9 GHz, modulation frequency to 100 kHz, center field to 6000 G, sweep width to 12000 G, sweep time to 335.5 s, modulation amplitude to 20.37 G, microwave power to 15 mW, conversion time to 81.92 ms, and resolution to 4096 points. The samples were put in EPR quartz tubes (Wilma-LabGlass, Vineland, NJ, United States) and scanned three times, of which the average was used for analysis. The spectrum of an empty control tube was subtracted from all sample spectra. All spectra were analyzed with the Bruker Xepir software.

Received: 9 August 2019; Accepted: 15 November 2019;

Published online: 02 December 2019

## References

- Pasek, M. A., Harnmeijer, J. P., Buick, R., Gull, M. & Atlas, Z. Evidence for reactive reduced phosphorus species in the early Archean ocean. *Proc. Natl. Acad. Sci. USA* **110**, 10089–10094 (2013).
- Pasek, M. A. & Lauretta, D. S. Aqueous corrosion of phosphide minerals from iron meteorites: a highly reactive source of prebiotic phosphorus on the surface of the early Earth. *Astrobiology* **5**, 515–535 (2005).
- Pasek, M. A. & Lauretta, D. S. Extraterrestrial flux of potentially prebiotic C, N, and P to the early Earth. *Orig. Life Evol. Biosph.* **38**, 5–21 (2008).
- Scott, E. R. D. & Krot, A. N. Chondrites and their components. In *Meteorites, comets, and planets*, edited by Davis A. M. Treatise on Geochemistry, vol. 1. pp. 143–200 (2003).
- González-Toril, E., Martínez-Frías, J., Gómez, J. M., Rull, F. & Amils, R. Iron meteorites can support the growth of acidophilic chemolithoautotrophic microorganisms. *Astrobiology* **5**, 406–414 (2005).
- Gronstal, A. *et al.* Laboratory experiments on the weathering of iron meteorites and carbonaceous chondrites by iron-oxidizing bacteria. *Meteorit. Planet. Sci.* **44**, 233–247 (2009).
- Tait, A. W., Gagen, E. J., Wilson, S. A., Tomkins, A. G. & Southam, G. Microbial Populations of Stony Meteorites: Substrate Controls on First Colonizers. *Front. Microbiol.* **8**, 1227 (2017).
- Mukherjee, A., Wheaton, G. H., Blum, P. H. & Kelly, R. M. Uranium extremophily is an adaptive, rather than intrinsic, feature for extremely thermoacidophilic *Metallosphaera* species. *Proc. Natl. Acad. Sci. USA* **109**, 16702–16707 (2012).
- Huber, G., Spinnler, C., Gambacorta, A. & Stetter, K. O. *Metallosphaera sedula* gen. and sp. nov. represents a new genus of aerobic, metal-mobilizing, thermoacidophilic archaeobacteria. *Syst. Appl. Microbiol.* **12**, 38–47 (1989).
- Auernik, K. S. & Kelly, R. M. Impact of molecular hydrogen on chalcopyrite bioleaching by the extremely thermoacidophilic archaeon *Metallosphaera sedula*. *Appl. Environ. Microbiol.* **76**, 2668–2672 (2010).
- Kölbl, D. *et al.* Exploring fingerprints of the extreme thermoacidophile *Metallosphaera sedula* grown on synthetic martian regolith materials as the sole energy sources. *Front. Microbiol.* **8**, 1918 (2017).
- Russell, S., Zipfel, J., Grossman, J. & Grady, M. The Meteoritical Bulletin No. 86. *Meteorit. Planet. Sci.* **37**, 157–184 (2002).
- Consolmagno, G. J., Britt, D. T. & Macke, R. J. The significance of meteorite density and porosity. *Chemie der Erde - Geochemistry* **68**, 1–29 (2008).
- Auernik, K. S., Maezato, Y., Blum, P. H. & Kelly, R. M. The genome sequence of the metal-mobilizing, extremely thermoacidophilic archaeon *Metallosphaera sedula* provides insights into bioleaching-associated metabolism. *Appl. Environ. Microbiol.* **74**, 682–692 (2008).
- Auernik, K. S. & Kelly, R. M. Physiological versatility of the extremely thermoacidophilic archaeon *Metallosphaera sedula* supported by transcriptomic analysis of heterotrophic, autotrophic, and mixotrophic growth. *Appl. Environ. Microbiol.* **76**, 931–935 (2010).
- Auernik, K. S. & Kelly, R. M. Identification of components of electron transport chains in the extremely thermoacidophilic crenarchaeon *Metallosphaera sedula* through iron and sulfur compound oxidation transcriptomes. *Appl. Environ. Microbiol.* **74**, 7723–7732 (2008).
- Beevers, C. A. & Lipson, H. The Crystal Structure of Nickel Sulphate Hexahydrate, NiSO<sub>4</sub> · 6H<sub>2</sub>O. *Z. Kristallogr. - Cryst. Mater.* **1**–6, 123–135 (1932).
- Baur, W. On the crystal chemistry of salt hydrates. IV. The refinement of the crystal structure of MgSO<sub>4</sub> · 7H<sub>2</sub>O (epsomite). *Acta Cryst.* **17**, 1361–1369 (1964).
- Maezato, Y., Johnson, T., McCarthy, S., Dana, K. & Blum, P. Metal resistance and lithoautotrophy in the extreme thermoacidophile *Metallosphaera sedula*. *J. Bacteriol.* **194**, 6856–6863 (2012).

20. McCarthy, S. *et al.* Role of an archaeal PitA transporter in the copper and arsenic resistance of *Metallosphaera sedula*, an extreme thermoacidophile. *J. Bacteriol.* **196**, 3562–3570 (2014).
21. Reysenbach, A. L. & Cady, S. L. Microbiology of ancient and modern hydrothermal systems. *Trends Microbiol.* **9**, 79–86 (2001).
22. Orange, F. *et al.* Experimental fossilization of the Thermophilic Gram-positive Bacterium *Geobacillus* SP7A: A Long Duration Preservation Study. *Geomicrobiol. J.* **31**, 578–589 (2014).
23. Oggerin, M. *et al.* Specific jarosite biomineralization by *Purpureocillium lilacinum*, an acidophilic fungi isolated from Río Tinto. *Environ. Microbiol.* **8**, 2228–2237 (2013).
24. Gaboyer, F. *et al.* Mineralization and Preservation of an extremotolerant Bacterium Isolated from an Early Mars Analog Environment. *Sci. Rep.* **7**, 8775 (2017).
25. Johnson, T. B. *et al.* Secretion and fusion of biogeochemically active archaeal membrane vesicles. *Geobiology*. **16**, 659–673 (2018).
26. Wheaton, G. H. *et al.* Extremely thermoacidophilic *Metallosphaera* species mediate mobilization and oxidation of vanadium and molybdenum oxides. *Appl. Environ. Microbiol.* **85**, e02805–18 (2019).
27. Blazejic, A. *et al.* Biotransformation of scheelite  $\text{CaWO}_4$  by the extreme thermoacidophile *Metallosphaera sedula*: tungsten-microbial interface. *Front. Microbiol.* **10**, 1492 (2019).
28. Milojevic, T. *et al.* Nanoscale tungsten-microbial interface of the metal immobilizing thermoacidophilic archaeon *Metallosphaera sedula* cultivated with tungsten polyoxometalate. *Front. Microbiol.* **10**, 1267 (2019).
29. Kish, A. *et al.* Preservation of archaeal surface layer structure during mineralization. *Sci. Rep.* **25**, 26152 (2016).
30. Huber, H., Huber, G. & Stetter, K. O. A modified DAPI fluorescence staining procedure suitable for the visualization of lithotrophic bacteria. *Syst. Appl. Microbiol.* **6**, 105–106 (1985).
31. Ludwig, W. ARB: a software environment for sequence data. *Nucleic Acids Res.* **32**, 1363–1371 (2004).
32. Wlotzka, F. A weathering scale for the ordinary chondrites. *Meteoritics* **28**, 460–460 (1993).
33. Albu, M. *et al.* Self-organized Sr leads to solid state twinning in nano-scaled eutectic Si phase. *Sci. Rep.* **6**, 31635 (2016).
34. Goldstein, J. I., Williams, D. B. & Cliff, G. Quantification of energy dispersive spectra, in: Joy, D. C., Romig, A. D. & Goldstein, J. L. (Eds.), *Principles of Analytical Electron Microscopy*, Plenum Press, New York, 1986, pp. 155–217.
35. Flemming, R. L. Micro X-ray diffraction ( $\mu\text{XRD}$ ): A versatile technique for characterization of Earth and planetary materials. *Can. J. Earth Sci.* **44**, 1333–1346 (2007).

## Acknowledgements

We thank F. Brandstätter for fruitful discussions and G. Batic (both at the Natural History Museum Vienna, Austria) for the preparation of the meteorite slabs and sections that were used for this study. We also acknowledge T. Hofmann and W. Obermaier (University of Vienna, Department of Environmental Geosciences), D. Gruber and I. Lichtscheidl-Schultz (University of Vienna, Core Facility Cell Imaging and Ultrastructure Research), R. Moeller (German Aerospace Center (DLR), Cologne), and S. Pierdzig (CRB Analyse Service GmbH, Germany) for fruitful discussions and help with ICP-OES, EM, and XRF analysis. Electron microscopy assistance of S. Puchegger (University of Vienna, Physics Faculty Center for Nano Structure Research) is greatly appreciated. We wish to thank H. Huber (University of Regensburg) for providing the *M. sedula* DSM5348 strain, P. Yilmaz (MPI for Marine Mikrobiologie, Bremen) for ARB 16S rRNA probe design, E. Libowitzky (Department of Mineralogy and Crystallography, University of Vienna) for providing sulfide ores, and R. M. Kelly (North Carolina State University) for his inspiring life time research with *M. sedula*. The authors gratefully acknowledge Chakib Djediat (Muséum National d'Histoire Naturelle, Paris) for the help during the TEM sample preparation. This paper is dedicated to the memory of Christian Anger (1965–2009), an Austrian meteorite collector, from which the meteorite used for this study originates. This work was supported by the Austrian Science Fund (FWF) through an Elise-Richter Research fellowship V333 “Iron and Sulfur-oxidizing Machinery of the bioleaching Archaeon *Metallosphaera sedula*” to T.M.

## Author contributions

T.M., D.K., M.A., A.K., L.F., A.B., M.P., Z.Z., S.K.M.R.R., and M.P.S. performed experiments; all authors provided editorial input. T.M. led, conceived, and designed the project, analyzed the data, interpreted experiments, and wrote the manuscript.

## Competing interests

The authors declare no competing interests.

## Additional information

**Supplementary information** is available for this paper at <https://doi.org/10.1038/s41598-019-54482-7>.

**Correspondence** and requests for materials should be addressed to T.M.

**Reprints and permissions information** is available at [www.nature.com/reprints](http://www.nature.com/reprints).

**Publisher's note** Springer Nature remains neutral with regard to jurisdictional claims in published maps and institutional affiliations.



**Open Access** This article is licensed under a Creative Commons Attribution 4.0 International License, which permits use, sharing, adaptation, distribution and reproduction in any medium or format, as long as you give appropriate credit to the original author(s) and the source, provide a link to the Creative Commons license, and indicate if changes were made. The images or other third party material in this article are included in the article's Creative Commons license, unless indicated otherwise in a credit line to the material. If material is not included in the article's Creative Commons license and your intended use is not permitted by statutory regulation or exceeds the permitted use, you will need to obtain permission directly from the copyright holder. To view a copy of this license, visit <http://creativecommons.org/licenses/by/4.0/>.

© The Author(s) 2019



**Mag. Mag. Dr. techn.**

**Simon K.-M. R. Rittmann Privatdoz. Bakk.**

Archaea Physiology & Biotechnology Group

1090 Wien, Austria

Tel.: +43 1 4277 76513

Email.: [simon.rittmann@univie.ac.at](mailto:simon.rittmann@univie.ac.at)

Homepage: <https://archaea.univie.ac.at/research/simon-rittmann-lab/>



Date of Birth: January 26, 1978

Place of Birth: Freilassing, Germany

Nationality: German

Sex: Male

---

## **Specialisation      Microbiology and Biotechnology**

### **Work Experience**

Since 01/2017	PI and Head of the Archaea Physiology & Biotechnology Group, Department of Functional and Evolutionary Ecology, University of Vienna, Vienna, Austria
02/2024 to 01/2025	Chief Scientist and Co-founder, Arkeon GmbH, Tulln a.d. Donau, Austria
07/2023 to 01/2024	Chief Technology Officer (CTO), Chief Scientist and Co-founder, Arkeon GmbH, Tulln a.d. Donau, Austria
08/2022 to 09/2022	Post Doc (visiting scientist), Department of Experimental Biology, Faculty of Science, Masarykova univerzita, Brno, Czech Republic
07/2021 to 06/2023	Chief Scientific Officer (CSO) and Co-founder, Arkeon GmbH, Tulln a.d. Donau, Austria
01/2014 to 12/2016	“Universitätsassistent”, Post Doc, University of Vienna, Department of Ecogenomics and Systems Biology, University of Vienna, Vienna, Austria
11/2012 to 12/2013	Post Doc, Krajete GmbH, Linz, Austria
10/2009 to 12/2012	PhD student, Department of Chemical Engineering, Vienna University of Technology, Vienna, Austria
02/2007 to 04/2009	Research Assistant, Intercell AG, Department of Molecular Microbiology, Vienna, Austria



01/2006 to 11/2006      Research Assistant, Institute of Applied Microbiology, University of Natural Resources and Life Sciences, Vienna, Austria

05/2003 to 04/2004      Project co-worker, Institute of Genetics and General Biology, Faculty of Natural Sciences, University of Salzburg, Austria

## Education

07/2020      **Habilitation**  
*Venia docendi* in Microbiology and Biotechnology at the University of Vienna, Austria

04/2013      **Graduation: Dr. techn.**  
Doktor der Technischen Wissenschaften, Vienna University of Technology, Austria

10/2009 to 12/2012      **Doctorate**  
“Bioprocess development and quantitative analysis of biomethane production and dark fermentative biohydrogen production”, Department of Chemical Engineering, Faculty of Chemistry, Vienna University of Technology, Austria

03/2009      **Graduation with honours: MSc**  
Magister der Biologie, University of Salzburg, Austria

01/2008 to 01/2009      **Diploma Study**  
“Overview on fermentative microorganisms capable of biohydrogen production - a putative comprehensive survey of literature”, Department of Molecular Biology, Faculty of Natural Sciences, University of Salzburg, Austria

02/2006      **Graduation with honours: MSc**  
Magister der Biologie, University of Salzburg, Austria

09/2004 to 10/2005      **Diploma Study**  
“Identification of 14-3-3 isoforms in *Lilium longiflorum* pollen”, Department of Molecular Biology, Faculty of Natural Sciences, University of Salzburg, Austria

03/2005 to 02/2006      **University Studies**  
Magisterstudium: Botanik/Pflanzenbiologie, University of Salzburg, Austria

04/2003 to 03/2009      **University Studies**  
Magisterstudium: Genetik/Biotechnologie, University of Salzburg, Austria

03/2003      **Graduation: Bachelor**

Bakkalaureus der Biologie, University of Salzburg, Austria

10/1999 to 03/2003	<b>University Studies</b> Bakkalaureatstudium: Genetik/Molekularbiologie, University of Salzburg, Austria
09/1997 to 10/1999	<b>Military Service</b> Education as Officer in the German Forces, Specialisation: Gebirgsjäger (mountain soldier), in Bad Reichenhall, Berchtesgaden, and Mittenwald, Germany
07/1997	<b>Matura</b> Rudolf-Steiner Schule, Salzburg, Austria

## Scientific experience

### *Projects – Principal investigator (PI)*

- 1.) Archaeal CO<sub>2</sub>-fixation pathways  
Duration: 01.01.2024-31.12.2028  
Funding agency: FFG via ACIB GmbH
- 2.) Process engineering and modelling  
Duration: 01.05.2024-30.04.2027  
Funding agency: FFG via ACIB GmbH
- 3.) Bioleaching with archaea  
Duration: 15.05.2023-28.02.2025  
Funding agency: Montanuniversität Leoben
- 4.) Analysis of Microbial Community Composition of Plastic Surface Biofilms  
Duration: 01.03.2021-30.10.2021  
Funding agency: Direct industrial funding by Borealis AG
- 5.) Analyse der Biozönose während der mikrobiellen Umsetzung von Kohlenmonoxid zu Methan  
Duration: 01.10.2020-30.09.2021  
Funding agency: FFG
- 6.) Artificial microbial consortium for food waste utilization  
Duration: 01.01.2020-31.12.2022  
Funding agency: Austrian Agency for International Cooperation in Education and Research (OeAD GmbH)
- 7.) Analysen für PTLiquid  
Duration: 27.06.2019-26.05.2021  
Funding agency: University of Natural Resources and Life Sciences (BOKU)
- 8.) BioHyMe: Entwicklung eines Hochdruckproduktionsverfahrens für die gekoppelte biologische Wasserstoff- und Methanproduktion  
Duration: 01.05.2016-30.07.2019  
Funding agency: FFG

- 9.) H2.AT: Extremophile mikrobielle Zellfabriken zur hocheffizienten Produktion von Biowasserstoff  
Duration: 01.04.2016-31.03.2019  
Funding agency: FFG
- 10.) Produktion von methanogener Biomasse  
Duration: 27.08.2015-31.12.2015  
Funding agency: Direct industrial funding by Krajete GmbH
- 11.) Studie zur Umsetzung von Kohlenmonoxid aus synthetischem Pyrolysegas als neue Kohlenstoff- und Energiequelle für die Methanogenese  
Duration: 01.06.2015-31.10.2015  
Funding agency: FFG

***Projects – Co-PI, National collaborator, or Host***

- 1.) Cell Division Dynamics in cell-walled Archaea  
*Host of Dr. Nika Pende*  
Duration: 01.09.2022-31.08.2025  
Funding agency: FWF
- 2.) FlaeXmethan: Flexible acide ex-situ Methanisierung von Biogas mit erneuerbarem Wasserstoff  
*Co-PI*  
Duration: 01.10.2021-31.03.2023  
Funding agency: FFG
- 3.) Geomicrobiology of the cryptocrystalline Kraubath magnesite deposit and the relevance of methanogenic archaea  
*National collaborator and host of Dr. Jennifer Zwicker*  
Duration: 01.10.2020-30.09.2023  
Funding agency: FWF
- 4.) NitroFix: Prototypenentwicklung zur mikrobiologischen Stickstofffixierung  
*Co-PI*  
Duration: 01.09.2017-30.04.2022  
Funding agency: FFG
- 5.) Model system mimicking the cell envelope of archaea  
*National collaborator*  
Duration: 01.10.2016-31.01.2022  
Funding agency: FWF
- 6.) Entwicklung mikrobiologischer Bioraffineriekonzepte  
*Co-PI*  
Duration: 01.05.2016-28.02.2019  
Funding agency: FFG

### ***Publications (peer-reviewed)***

- 1) Klein M., Hilts A.S., Fennessy R.T., Trattnig N., Stehrer-Polášek T., Rittmann S.K.-M.R., Fink C. (2025) Markerless mutagenesis enables isoleucine biosynthesis solely from threonine in *Methanothermobacter marburgensis*, **Microbiology Spectrum**, revision submitted
- 2) Hofmann W., Orthofer M., Salas Wallach N., Ruddyard A., Ungerank M., Paulik C., Rittmann S.K.-M.R. (2025) Method for automated high performance closed batch cultivation of gas-utilizing methanogens, **AMB Express**, accepted for publication
- 3) Reischl B., Schupp B., Palabikyan H., Steger-Mähnert B., Fink C., Rittmann S.K.-M.R. (2025) Quantitative analysis of amino acid excretion by *Methanothermobacter marburgensis* under N<sub>2</sub>-fixing conditions, **Scientific Reports**, 15:3755
- 4) Bychkova S., Bychkov M., Dordević D., Rittmann S.K.-M.R., Vítězová M., Kushkevych I. (2024) The impact of 3-sulfo-taurolithocholic acid on atpase activity in patients' colorectal cancer and normal colon tissues, and its hepatic effects in rodents, **Frontiers in Veterinary Science** 11:1480122
- 5) Kushkevych I., Procházka V., Vítězová M., Dordević D., Abd El-Salam M., Rittmann S.K.-M.R. (2024) Anoxygenic photosynthesis with emphasis on green sulfur bacteria and a perspective for hydrogen sulfide detoxification of anoxic environments, **Frontiers in Microbiology** 15:1417714
- 6) Lyu Z., Rotaru A.-E., Pimentel M., Zhang C., Rittmann S.K.-M.R., Ferry J.G. (2024) Editorial: Cross-boundary significance of methanogens – the methane moment and beyond: Preface, **Frontiers in Microbiology** 15:1434586
- 7) Kushkevych I., Martínková K., Mráková L., Giudici F., Baldi S., Novak D., Gajdács M., Vítězová M., Dordević D., Amedei A., Rittmann S.K.-M.R., (2024) Molecular detection of microbial communities in patients with ulcerative colitis and molecular mechanisms of their association with bowel diseases, **Microbial Cell** 11(1):79-89
- 8) Bychkova S., Bychkov M., Dordević D., Vítězová M., Rittmann S.K.-M.R., Kushkevych I. (2024) Bafilomycin A1 molecular effect on ATPase activity of subcellular fraction of human colorectal cancer and rat liver, **International Journal of Molecular Sciences** 25(3):1567
- 9) Salas E., Gorfer M., Bandian D., Eichorst S.A., Schmidt H., Horak J., Rittmann S.K.-M.R., Schleper C., Reischl B., Pribasnić T., Jansa J., Kaiser C., Wanek W. (2024) Reevaluation and novel insights into amino sugar and neutral sugar necromass biomarkers in archaea, bacteria, fungi, and plants **Science of the Total Environment** 906:167463

- 10) Kushkevych I., Dordević D., Alberfkani M.I., Gajdács M., Ostorházi E Vítězová M., Rittmann S.K.-M.R. (2023) NADH and NADPH peroxidases as antioxidant defense mechanisms in intestinal sulfate-reducing bacteria (2023) **Scientific Reports** 13(1):13992
- 11) Fuchs W., Rachbauer L., Rittmann S.K.-M.R., Bochmann G., Ribitsch D., Steger F. (2023) Eight up-coming biotech tools to combat climate crisis, **Microorganisms** 11(6):1514
- 12) Taubner R.-S., Baumann L.M.F., Steiner M., Pfeifer K., Reischl B., Korynt K., Bauersachs T., Mähnert B., Clifford E.L., Peckmann J., Schuster B., Birgel D., Rittmann S.K.-M.R. (2023) Lipidomics and comparative metabolite excretion analysis of methanogenic archaea reveal organism-specific adaptations to varying temperature and substrate concentration, **mSystems** 8(2):e01159-22
- 13) Melcher M., Hodgskiss L. H., Mardini M. A., Schleper C., Rittmann S.K.-M.R., (2023) Analysis of biomass productivity and physiology of *Nitrososphaera viennensis* grown in continuous culture, **Frontiers in Microbiology** 14:1076342
- 14) Rodrigues-Oliveira T., Wollweber F., Ponce-Toledo R.I., Xu J., Rittmann S.K.-M.R., Klingl A., Pilhofer M., Schleper C. (2023) Complex cytoskeleton and cell architecture in an Asgard archaeon, **Nature** 613:332–339
- 15) Lyu Z., Rotaru A.-E., Pimentel M., Zhang C., Rittmann S.K.-M.R. (2022) Editorial: The Methane Moment – Cross-boundary significance of methanogens: Preface, **Frontiers in Microbiology** 13:1055494
- 16) Palabikyan H., Ruddyard A., Pomper L., Novak D., Reischl B., Rittmann S.K.-M.R. (2022) Scale-up of biomass production by *Methanococcus maripaludis*, **Frontiers in Microbiology** 13:1031131
- 17) Koller M., Rittmann S.K.-M.R. (2022) Haloarchaea as emerging big players in future polyhydroxyalkanoate bioproduction: Review of trends and perspectives, **Current Research in Biotechnology** 4:377-391
- 18) Pfeifer K., Ehmoser E.-K., Rittmann S.K.-M.R., Schleper C., Pum D., Sleytr U.B., Schuster B. (2022) Isolation and characterization of cell envelope fragments comprising archaeal S-layer proteins, **Nanomaterials** 12(14):2502
- 19) Donadu M.G., Ferrari M., Mazzarello V., Zanetti S., Kushkevych I., Rittmann S.K.-M.R., Stájer A., Baráth Z., Szabó D., Urbán E., Gajdács M. (2022) No correlation between biofilm forming-capacity and antibiotic resistance in environmental *Staphylococcus* spp.: in vitro results, **Pathogens** 11(4):471
- 20) Baumann L.M.F., Taubner R.-S., Oláh K., Rohrweber A.-C., Schuster B., Birgel D., Rittmann S.K.-M.R. (2022) Quantitative analysis of core lipid



production in *Methanothermobacter marburgensis* at different scales, **Bioengineering** 9(4):169

- 21) Steger F., Ergal Ī, Daubek A., Loibl N., Rachbauer L., Fuchs W., Rittmann S.K.-M.R., Bochmann G. (2022) Trickle-bed bioreactors for acetogenic H<sub>2</sub>/CO<sub>2</sub> conversion, **Frontiers in Energy Research** 10:842284
- 22) Ergal Ī, Zech E., Hanišáková N., Kushkevych I., Fuchs W., Vítěz T., Vítězová M., Bochmann G., Rittmann S.K.-M.R. (2022) Scale-up of dark fermentative biohydrogen production by artificial microbial co-cultures, **Applied Microbiology** 2(1):215
- 23) Hanišáková N., Vítězová M., Rittmann S.K.-M.R. (2022) The historical development of cultivation techniques for methanogens and other strict anaerobes and their application in modern microbiology, **Microorganisms** 10(2):412
- 24) Steger F., Reich J., Fuchs W., Rittmann S.K.-M.R., Gübitz G.M., Ribitsch D., Bochmann G. (2022) Comparison of carbonic anhydrases for CO<sub>2</sub> sequestration, **International Journal of Molecular Sciences** 23(2):957
- 25) Ergal Ī, Bochmann G., Fuchs W., Rittmann S.K.-M.R. (2022) Design and engineering of artificial microbial consortia for biohydrogen production, **Current Opinion in Biotechnology**, 73:74-80
- 26) Zipperle A., Reischl B., Schmider T., Stadlbauer M., Kushkevych I., Pruckner C., Vítězová M., Rittmann S.K.-M.R. (2021) Biomethanation of carbon monoxide by artificial archaeal co-cultures, **Fermentation** 7(4):276
- 27) Kushkevych I., Kovářová A., Dordević D., Gaine J.J., Kollar P., Vítězová M., Rittmann S.K.-M.R. (2021) Distribution of sulfate-reducing bacteria in the environment: cryopreservation techniques and their potential storage application, **Processes** 9(10):1843
- 28) Fuchs W., Steger F., Reich J., Ribitsch D., Rittmann S.K.-M.R., Bochmann G. (2021) A Simple and Straightforward Method for Activity Measurement of Carbonic Anhydrases, **Catalysts** 11:819
- 29) Kushkevych I., Procházka J., Gajdács M., Rittmann S.K.-M.R., Vítězová M. (2021) Molecular Physiology of Anaerobic Phototrophic Purple and Green Sulfur Bacteria, **International Journal of Molecular Sciences** 22(12):6398
- 30) Pende N., Sogues A., Megrian D., Sartori-Rupp A., England P., Palabikyan H., Rittmann S.K.-M.R., Graña M., Wehenkel A.M., Alzari P.M., Gribaldo S. (2021) SepF is the FtsZ-anchor in Archaea: conservation and divergence of an ancestral cell division system, **Nature Communications** 12:3214

- 31) Kushkevych I., Bosáková V., Vítězová M., Rittmann S.K.-M.R. (2021) Anoxygenic Photosynthesis in Photolithotrophic Sulfur Bacteria and Their Role in Detoxication of Hydrogen Sulfide, **Antioxidants** 10(6):829
- 32) Kushkevych I., Hýžová B., Vítězová M., Rittmann S.K.-M.R. (2021) Microscopic methods for identification of sulfate-reducing bacteria from various habitats, **International Journal of Molecular Sciences** 22(8):4007
- 33) Mauerhofer L.-M., Zwirtmayr S., Pappenreiter P., Bernacchi S., Seifert A. H., Reischl B., Schmider T., Taubner R.-S., Paulik C., Rittmann S.K.-M.R. (2021) Hyperthermophilic methanogenic archaea act as high-pressure CH<sub>4</sub> cell factories, **Communications Biology** 4:289
- 34) Pfeifer K., Ergal Ī., Koller M., Basen M., Schuster B., Rittmann S.K.-M.R. (2021) Archaea Biotechnology, **Biotechnology Advances** 47:107668
- 35) Kushkevych I., Abdulina D., Dordević D., Rozehnalová M., Vítězová M., Černý M., Svoboda P., Rittmann S.K.-M.R. (2021) Basic bioelements content in anaerobic intestinal sulfate-reducing bacteria, **Applied Sciences** 11(3):1152
- 36) Kushkevych I., Martínková K., Vítězová M., Rittmann S.K.-M.R. (2021) Intestinal microbiota and perspectives of the use of meta-analysis for comparison of ulcerative colitis studies, **Journal of Clinical Medicine** 10(3):462
- 37) Kushkevych I., Dordević D., Vítězová M., Rittmann S.K.-M.R. (2021) Environmental impact of sulfate-reducing bacteria, their role in intestinal bowel diseases, and possible control by bacteriophages, **Applied Sciences** 11(2):735
- 38) Hasibar B., Ergal Ī., Moser S., Bochmann G., Rittmann S.K.-M.R., Fuchs W. (2020) Increasing biohydrogen production with the use of a co-culture inside a microbial electrolysis cell, **Biochemical Engineering Journal** 164:107802
- 39) Ergal Ī., Gräf O., Hasibar B., Steiner M., Vukotić S., Bochmann G., Fuchs W., Rittmann S.K.-M.R. (2020) Biohydrogen production beyond the Thauer limit by precision design of artificial microbial consortia, **Communications Biology** 3:443
- 40) Mooshammer M., Alves R.J.E., Bayer B., Melcher M., Stieglmeier M., Jochum L., Rittmann S.K.-M.R., Watzka M., Schleper C., Herndl G., Wanek W. (2020) Nitrogen isotope fractionation during archaeal ammonia oxidation: coupled estimates from measurements of residual ammonium and accumulated nitrite, **Frontiers in Microbiology** 11:1710
- 41) Kushkevych I., Coufalová M., Vítězová M., Rittmann S.K.-M.R. (2020) Sulfate-reducing bacteria of the oral cavity and their relation with periodontitis – recent Advances, **Journal of Clinical Medicine** 9(8):2347

- 42) Kushkevych I., Castro Sangrador J., Dordević D., Rozehnalová M., Černý M., Fafula R., Vítězová M., Rittmann S.K.-M.R. (2020) Evaluation of physiological parameters of intestinal sulfate-reducing bacteria isolated from patients suffering from IBD and healthy people, **Journal of Clinical Medicine** 9(6):1920
- 43) Kushkevych I., Abdulina D., Kováč J., Dordević D., Vítězová M., Iutynska G., Rittmann S.K.-M.R. (2020) Adenosine-5'-phosphosulfate- and sulfite reductases activities of sulfate-reducing bacteria from various environments, **Biomolecules** 10(6):921
- 44) Ergal Ī., Reischl B., Hasibar B., Manoharan L., Zipperle A., Bochmann G., Fuchs W., Rittmann S.K.-M.R. (2020) Formate utilization by the Crenarchaeon *Desulfurococcus amylolyticus*, **Microorganisms** 8(3):454
- 45) Hasibar B., Ergal Ī., Dias S.A., Bochmann G., Rittmann S.K.-M.R., Fuchs W. (2020) Competing acetate consumption and production inside a microbial electrolysis cell, **Journal of Environmental Chemical Engineering** 8(4):103847
- 46) Jebbar M., Hickman-Lewis K., Cavalazzi B., Taubner R.-S., Rittmann S.K.-M.R., Antunes A. (2020) Microbial diversity and biosignatures: an icy moons perspective, **Space Science Reviews** 216(1):10
- 47) Milojevic T., Kölbl D., Ferrière L., Albu M., Kish A., Flemming R. L., Rupert A. N., Koeberl C., Blazevic A., Zebec Z., Rittmann S.K.-M.R., Schleper C., Pignitter M., Somoza V., Schimak M. P. (2019) Exploring the microbial biotransformation of extraterrestrial material on nanometer scale, **Scientific Reports** 9:18028
- 48) Taubner R.-S., Baumann L.M.F., Bauersachs T., Clifford E.L., Mähnert B., Reischl B., Seifert R., Peckmann J., Rittmann S.K.-M.R., Birgel D. (2019) Membrane lipid composition and amino acid excretion patterns of *Methanothermococcus okinawensis* grown in the presence of inhibitors detected in the Enceladian plume, **Life** 9:85
- 49) Blazevic A., Albu M., Mitsche S., Rittmann S.K.-M.R., Habler G., Milojevic T. (2019) Tungsten encrustation of the extreme thermoacidophile *Metallosphaera sedula* during the biotransformation of scheelite CaWO<sub>4</sub>, **Frontiers in Microbiology** 10(1492):1-11
- 50) Pappenreiter P.A., Zwirtmayr S., Mauerhofer L.-M., Rittmann S.K.-M.R., Paulik C. (2019) Development of a simultaneous bioreactor system for characterization of gas production kinetics of methanogenic archaea at high pressure, **Engineering in Life Sciences** 19:537–544
- 51) Mauerhofer L.-M., Pappenreiter P., Paulik C., Bernacchi S., Seifert A.H., Rittmann S.K.-M.R. (2019) Methods for quantification of growth and

productivity in anaerobic microbiology and biotechnology, **Folia Microbiologica** 64(3):321-360

- 52) Ergal Ī., Fuchs W., Hasibar B., Thallinger B., Bochmann G., Rittmann S.K.-M.R. (2018) The physiology and biotechnology of dark fermentative biohydrogen production, **Biotechnology Advances** 36(8):2165-2186
- 53) Baumann L.M.F., Taubner R.-S., Bauersachs T., Steiner M., Schleper C., Peckmann J., Rittmann S.K.-M.R., Birgel D. (2018) Intact polar lipid and core lipid inventory of the hydrothermal vent methanogens *Methanocaldococcus villosus* and *Methanothermococcus okinawensis*, **Organic Geochemistry** 126:33-42
- 54) Abdel Azim A., Rittmann S.K.-M.R., Fino D., Bochmann G. (2018) The physiological effect of heavy metals and volatile fatty acids on *Methanococcus maripaludis* S2, **Biotechnology for Biofuels** 11(301):1-16
- 55) Mauerhofer L.-M., Reischl B., Schmider T., Schupp B., Nagy K., Pappenreiter P., Zwirtmayr S., Schuster B., Bernacchi S., Seifert A. H., Paulik C., Rittmann S.K.-M.R. (2018) Physiology and methane productivity of *Methanobacterium thermaggregans*, **Applied Microbiology and Biotechnology** 102(17):7643-7656
- 56) Reischl B., Ergal Ī., Rittmann S.K.-M.R. (2018) Metabolic reconstruction and experimental verification of glucose utilization in *Desulfurococcus amylolyticus* DSM 16532, **Folia Microbiologica** 63(6):713-723
- 57) Reischl B., Ergal Ī., Rittmann S.K.-M.R. (2018) Biohydrogen production characteristics of *Desulfurococcus amylolyticus* DSM 16532, **International Journal of Hydrogen Energy** 43(18):8747-8753
- 58) Zwicker J., Birgel D., Bach W., Richoz S., Smrzka D., Grasemann B., Gier S., Schleper C., Rittmann S.K.-M.R., Koşun E. Peckmann, J. (2018) Evidence for *in situ* archaeal methanogenesis within peridotite veins at the onshore Chimaera seeps, Turkey, **Chemical Geology** 483:567-580
- 59) Pende N., Wang J., Weber P. M., Verheul J., Kuru E., Rittmann S.K.-M.R., Leisch N., Vischer N., Brun Y., van Nieuwenhze M.S., den Blaauwen T. Bulgheresi S. (2018) Host-polarized cell growth in animal symbionts, **Current Biology** 28(7):1039-1051
- 60) Rittmann S.K.-M.R., Seifert A.H., Bernacchi S. (2018) Kinetics, multivariate statistical modelling, and physiology of CO<sub>2</sub>-based biological methane production, **Applied Energy**, 216:751-760
- 61) Taubner R.-S., Pappenreiter P., Zwicker J., Smrzka D., Pruckner C., Kolar P. Bernacchi S., Seifert A.H., Krajete A., Bach W., Peckmann J., Paulik C., Firneis M.G., Schleper C., Rittmann S.K.-M.R. (2018) Biological methane

production under putative Enceladus-like conditions, **Nature Communications** 9:748

- 62) Abdel Azim A., Pruckner C., Kolar P., Taubner R.-S., Fino D., Saracco G., de Sousa F.L., Rittmann S.K.-M.R. (2017) The physiology of trace elements in biological methane production, **Bioresource Technology** 241:775-786
- 63) Taubner R.-S., Rittmann, S.K.-M.R. (2016) Method for indirect quantification of CH<sub>4</sub> production via H<sub>2</sub>O production using hydrogenotrophic methanogens, **Frontiers in Microbiology** 7(532):1-11
- 64) Taubner R.-S., Schleper C., Firneis M.G., Rittmann, S.K.-M.R. (2015) Assessing the Ecophysiology of Methanogens in the Context of Recent Astrobiological and Planetological Studies, **Life** 5(4): 1652-1686
- 65) Rittmann S., Seifert A., Herwig C. (2015) Essential prerequisites for successful bioprocess development of biological CH<sub>4</sub> production from CO<sub>2</sub> and H<sub>2</sub>, **Critical Reviews in Biotechnology** 35(2):141-151
- 66) Rittmann S.K.-M.R., Lee H.S., Lim J.K., Kim T.W., Kang, S.G. (2015) One-carbon substrate-based biohydrogen production: Microbes, mechanism, and productivity, **Biotechnology Advances** 33:165-177
- 67) Bernacchi S., Rittmann S., Seifert A.H., Krajete A., Herwig C. (2014) Experimental methods for screening parameters influencing the growth to product yield ( $Y_{(x/CH_4)}$ ) for a biological methane production (BMP) process performed with *Methanothermobacter marburgensis*, **AIMS Bioengineering** 1(2):72-87
- 68) Stieglmeier M., Klingl A., Alves R.E., Rittmann S.K.-M.R., Melcher M., Leisch N., Schleper C. (2014) *Nitrososphaera viennensis* sp. nov., an aerobic and mesophilic ammonia oxidizing archaeon from soil and member of the novel archaeal phylum Thaumarchaeota, **International Journal of Systematic and Evolutionary Microbiology**, 64: 2738–2752
- 69) Seifert A., Rittmann S., Herwig C. (2014) Analysis of process related factors to increase volumetric productivity and quality of biomethane with *Methanothermobacter marburgensis*, **Applied Energy**, 132:155-162
- 70) Rittmann S., Holubar P. (2014) Rapid extraction of total RNA from anaerobic sludge biocoenosis, **Folia Microbiologica**, 59:127-132
- 71) Martinez-Porqueraz E., Rittmann S., Herwig C. (2013) Analysis of H<sub>2</sub> to CO<sub>2</sub> yield and physiological key parameters of *Enterobacter aerogenes* and *Caldicellulosiruptor saccharolyticus*, **International Journal of Hydrogen Energy**, 38:10245-10251



- 72) Seifert A., Rittmann S., Bernacchi S., Herwig C. (2013) Method for assessing the impact of industrial flue gasses on CH<sub>4</sub> production with *Methanothermobacter marburgensis*, **Bioresource Technology**, 136:747-751
- 73) Spadiut O., Rittmann S., Dietzsch C., Herwig C. (2013) Dynamic process conditions in bioprocess development, **Engineering in Life Sciences**, 13:88-101
- 74) Rittmann S., Herwig C. (2012) A comprehensive and quantitative review of dark fermentative biohydrogen production, **Microbial Cell Factories**, 11:115
- 75) Martinez-Porqueras E., Rittmann S., Herwig C. (2012) Biofuels and CO<sub>2</sub> neutrality: an opportunity, **Biofuels**, 3(4):413-426
- 76) Rittmann S., Seifert A., Herwig C. (2012) Quantitative analysis of media dilution rate effects on *Methanothermobacter marburgensis* grown in continuous culture on H<sub>2</sub> and CO<sub>2</sub>, **Biomass and Bioenergy**, 36:293-301
- 77) Pertl H., Rittmann S., Schulze W., Obermeyer G. (2011) Identification of lily pollen 14-3-3 isoforms and their subcellular and time-dependent expression profile, **Biological Chemistry**, 392(3):249-62

### ***Book chapters***

- 78) Jebbar M., Hickman-Lewis K., Cavalazzi B., Taubner R.-S., Rittmann S.K.-M.R., Antunes A. (2021) Microbial diversity and biosignatures: an icy moons perspective, In: Coustenis A., Rodrigo R., Spohn T., Hand K.P., Hayes A., Ollson-Francis K., Postberg F., Sotin C., Raulin F., Walter N., L'Harridon J.; Ocean Worlds, ISBN: 978-94-024-2069-2, Series: **Space Science Series of ISSI** p:253-299
- 79) Rittmann S.K.-M.R. (2015) A critical assessment of microbiological biogas to biomethane upgrading systems, In: Gübitz G. M., Bauer A., Bochmann G., Gronauer A., Weiss S.; Biogas Science and Technology, ISBN: 978-3-319-21992-9, Series: **Advances in Biochemical Engineering/Biotechnology** 151:117-135

### ***eBook***

- 80) Lyu Z., Rotaru, A.-E., Pimentel, M., Zhang, C., Rittmann, S.K.-M.R., 2024. The methane moment – Cross-boundary significance of methanogens. Frontiers Media SA, Lausanne.

### ***Conference proceedings***

Donadu M.G., Ferrari M., Mazzarello V., Zanetti S., Kushkevych I, Rittmann S.K.-M.R., Stájer A., Ónodi B., Baráth Z., Urbán E., Gajdács M. (2022) Is There a relationship between biofilm forming-capacity and antibiotic resistance in *Staphylococcus* spp.? In vitro results, Medical Sciences Forum 12(1):29, <https://doi.org/10.3390/eca2022-12734>

Zwirmayr S., Mauerhofer L.-M., Bernacchi S., Seifert A.H., Rittmann S.K.-M.R., Paulik C. (2020) Biologische Methanproduktion mit Archaea-Stämmen unter Hochdruckbedingungen, Chemie Ingenieur Technik 92(9):1200, <https://doi.org/10.1002/cite.202055420>

Bochmann G., Fuchs W., Rittmann S.K.-M.R. (2019) Book of Abstracts – Workshop on Gas in Biotechnology, ISBN: 978-3-900932-60-2

Taubner R.-S., Pappenreiter P., Zwicker J., Smrzka D., Pruckner C., Kolar P. Bernacchi S., Seifert A.H., Krajete A., Bach W., Peckmann J., Paulik C., Firneis M.G., Schleper C., Rittmann S.K.-M.R. (2018) Simulating putative Enceladus-like conditions: The possibility of biological methane production on Saturn's icy moon, Origins: From the Protosun to the First Steps of Life Proceedings IAU Symposium No. 345, <https://doi.org/10.1017/S1743921319001789>

Rittmann S., Legat A., Fendrihan S., Stan-Lotter H. (2004) Viability and Morphology of *Halobacterium* Species following Desiccation – Implications for Contamination on Mars, Proceedings of the Third European Workshop on Exo-Astrobiology, ESA SP-545:275-276, ISBN: 92-9092-856-5

Leuko S., Weidler G., Rittmann S., Stan-Lotter H. (2003) LIVE/DEAD kit: a powerful tool to detect haloarcheal survival (and life?) in unknown environmental samples, Proceedings of the Third European Workshop on Exo-Astrobiology, ESA SP-545:231-232, ISBN: 92-9092-856-5

Stan-Lotter H., Legat A., Gruber C., Fendrihan S., Radax C., Pfaffenhüemer M., Leuko S., Weidler G., Rittmann S. (2003) Haloarchaeal survival over geological times and the detection of extraterrestrial halite – implication for the search of life on Mars, Proceedings of the Third European Workshop on Exo-Astrobiology, ESA SP-545:63-66, ISBN: 92-9092-856-5

Radax C., Pfaffenhüemer M., Wieland H., Rittmann S., Leuko S., Weidler G., Gruber C., Stan-Lotter H. (2002) Microbes in Rock Salt: How to find out what is in there, Proceedings of the Second European Workshop on Exo-Astrobiology, ESA SP-518:485-486, ISBN: 92-9092-828-X

### ***Other publications***

Rittmann S.K.-M.R., Pfeifer K., Palabikyan H., Ergal İ., Schuster B. (2021) Archaea in der Biotechnologie, BIOSpektrum 27:96-98

Taubner R.-S., Rittmann S.K.-M.R., Bach W. (2018) Methan auf Enceladus könnte teilweise biologischen Ursprungs sein, Spektrum der Wissenschaft – Sterne und Weltraum 9:16-17

Krajete A., Seifert A., Bernacchi S., Sibilla F., Rittmann S. (2016) Krajete® process for CO<sub>2</sub> valorization, Pan Europeans Networks, Science & Technology, 18:38-39, March

Rittmann S.K.-M.R., Seifert A.H., Krajete A. (2014) Biomethanisierung – ein Prozess zur Ermöglichung der Energiewende? BIOSpektrum, 20(7):816-817. DOI: 10.1007/s12268-014

### ***Blog posts***

Weinhandl K., Rittmann S.K.-M.R. Back to the roots – Archaea save the world, 8<sup>th</sup> of May 2023: <https://acib.at/back-to-the-roots-archaea-save-the-world/>

### ***Patents***

Rittmann, S.K.-M.R., Schupp B., Reischl B., Taubner, R.-S., Palabikyan H., Ergal Í., Fennessy R. (2023) Method for fermentatively producing norvaline, **WO2023247743A1**

Rittmann, S.K.-M.R., Schupp B., Reischl B., Taubner, R.-S., Palabikyan H., Ergal Í., Fennessy R. (2023) Method for producing amino acids in a bioreactor, **WO2023247742A1**

Rittmann, S.K.-M.R., Schupp B., Reischl B., Taubner, R.-S., Palabikyan H., Ergal Í., Fennessy R. (2023) Method for producing amino acids in a bioreactor with methanogenic microorganisms, **WO2023247741A1**

Rittmann, S.K.-M.R., Schupp B., Reischl B., Taubner, R.-S., Palabikyan H., Ergal Í., Fennessy R. (2023) Method for producing amino acids with methanogenic microorganisms in a bioreactor, **WO2023247740A1**

Krajete A., Herwig C., Rittmann S., Seifert A., Bernacchi S. (2014) Method and system for producing methane using methanogenic microorganisms and applying specific nitrogen concentrations in the liquid phase, **WO2014128300A1**

Krajete A., Herwig C., Rittmann S., Seifert A. (2014) Method and system for producing methane using high gas feed rates, **WO2014009026A1**

Herwig C., Rittmann S., Lorantfy B., Jazini M., Henssen G., Pohl W. (2013)  
Method for the reduction of total organic carbon in hypersaline water,  
**WO2013124375A3**

### *Invited lectures*

1. Rittmann S.K.-M.R., Conversion of CO<sub>2</sub> by methanogenic archaea for amino acid production, **CHASE Expert Days**, 19-20<sup>th</sup> of November 2024, Vienna, Austria
2. Rittmann S.K.-M.R., Amino acid production by methanogenic archaea, **International Conference on Geo-Omics of Archaea**, 8-10<sup>th</sup> of November 2024, Shenzhen, China
3. Rittmann S.K.-M.R., Biomethanation of H<sub>2</sub>/CO<sub>2</sub>, **OMV Group**, 30<sup>th</sup> of October 2024, Vienna, Austria
4. Rittmann S.K.-M.R., Synthetic biology of archaea for biotechnological applications, **Seminar Series on Geo-Omics of Archaea**, 30<sup>th</sup> of September 2024, Broadcasted via Zoom and Koushare in China, >3320 participants (online)
5. Rittmann S.K.-M.R., CO<sub>2</sub>-fixation by a thermophilic archaeon for proteinogenic amino acid production, **Keynote Lecture, 14<sup>th</sup> International Congress on Extremophiles**, 22<sup>nd</sup>-26<sup>th</sup> of September 2024, Loutraki, Greece
6. Rittmann S.K.-M.R., Synthetic Biology and Gasfermentation of Archaea, **Engineering Biology Workshop at the The Carbon Recycling Network – Fourth Annual Conference**, 25<sup>th</sup>-27<sup>th</sup> of March 2024, Shrigley Hall, Nr Macclesfield, Cheshire, United Kingdom
7. Rittmann S.K.-M.R., CO<sub>2</sub>-fixation for proteinogenic amino acid production, **Bioprocessing Days 2024**, 26<sup>th</sup>-28<sup>th</sup> of February 2024, Westfälische Hochschule, Recklinghausen, Germany
8. Rittmann S.K.-M.R., Innovative Herstellung von Aminosäuren aus H<sub>2</sub> und CO<sub>2</sub>, **Plattform Grüne Chemie – Zukunft: Chemie**, 19<sup>th</sup> of October 2023, Bundesministerium für Klimaschutz, Vienna, Austria
9. Rittmann S.K.-M.R., Conversion of CO<sub>2</sub> into food ingredients, **2<sup>nd</sup> BBNet Conference: “Green Futures” What’s next for biorefineries?**, 22<sup>nd</sup>-24<sup>th</sup> of March 2023, Harrogate, United Kingdom
10. Rittmann S.K.-M.R., Archaea in gas fermentation bioprocesses, **Technische Universität Hamburg**, 20<sup>th</sup> of December 2022, Hamburg, Germany

11. Rittmann S.K.-M.R., Purpose building the next generation of protein ingredients from CO<sub>2</sub>, **European Summit of Industrial Biotechnology (ESIB)**, 14<sup>th</sup>-16<sup>th</sup> of November 2022, Graz, Austria
12. Rittmann S.K.-M.R., Conversion of CO<sub>2</sub> into food ingredients, **Österreichischen Chemischen Gesellschaft Mini Symposien 2022**, 19<sup>th</sup> of September 2022, Vienna, Austria
13. Rittmann S.K.-M.R., Methane cell factories, **Keynote Lecture, Webinar series on biological carbon capture and utilization**, 11.05.2021, Vienna, Austria (online)
14. Rittmann S.K.-M.R., Biomethanation: Research and Development, **Workshop Biomethane – timely solutions for successful implementation and use**, 15.04.2021, Vienna, Austria (online)
15. Rittmann S.K.-M.R., The physiology of archaea with relevance to biotechnology, **Masarykova Universita**, 11.03.2021, Brno, Czech Republic (online)
16. Rittmann S.K.-M.R., The physiology of anaerobic archaea with relevance to ecology and biotechnology, **Universität Regensburg**, 17.12.2020, Regensburg, Germany (online)
17. Rittmann S.K.-M.R., Highlights from ten years of pure culture biological CH<sub>4</sub> production from H<sub>2</sub>/CO<sub>2</sub>, **UFZ Energy Days 2019**, Helmholtz Zentrum für Umweltforschung, 8.10.-9.10.2019, Leipzig, Germany
18. Rittmann S.K.-M.R., Archaea and bioleaching of scheelite, **Wolfram Bergbau und Hütten AG**, 17.05.2019, St. Martin i.S., Austria
19. Rittmann S.K.-M.R., Advances in Archaea Biotechnology – pure culture biological methane production from H<sub>2</sub> and CO<sub>2</sub>, **Technische Universität Bergakademie Freiberg**, 07.05.2019, Freiberg, Germany
20. Rittmann S.K.-M.R., Utilization of formate by the Crenarchaeon *Desulfurococcus amylolyticus* DSM 16532, **Universität Leipzig**, 08.04.2019, Leipzig, Germany
21. Rittmann S.K.-M.R., The physiology and biotechnology of pure culture biological methane production from H<sub>2</sub> and CO<sub>2</sub>, **AD Network Research Colloquium “Beyond Biogas”**, 23.01.2019-25.01.2019, Manchester, United Kingdom
22. Rittmann S.K.-M.R., Biological methane production under putative Enceladus-like conditions, **Keynote Lecture, GEOBONN 2018**, 02.09.2018-06.09.2018, Bonn, Germany



23. Rittmann S.K.-M.R., The physiology of methanogens with respect to biotechnological applications, **Goethe-University Frankfurt**, 10.07.2018, Frankfurt am Main, Germany
24. Rittmann S.K.-M.R., Modelling biological methane production from continuous culture experiments, **Masarykova Universita**, 18.06.2018, Brno, Czech Republic
25. Rittmann S.K.-M.R., Novel insights into the physiology and biotechnology of methanogens, **2<sup>nd</sup> European C1 Meeting**, 17.05.2018-18.05.2018, Nijmegen, The Netherlands
26. Rittmann S.K.-M.R., Biological methane production under putative Enceladus-like conditions, **Christian-Albrechts Universität zu Kiel**, 22.21.2018, Kiel, Germany
27. Rittmann S.K.-M.R., Novel insights into the physiology and biotechnology of CO<sub>2</sub> to CH<sub>4</sub> conversion, **Johannes Kepler Universität Linz**, 09.05.2017, Linz, Austria
28. Rittmann S.K.-M.R., Modeling, qualitative and quantitative assessment of biological CH<sub>4</sub> production (BMP) from H<sub>2</sub> and CO<sub>2</sub>, **Politecnico di Torino**, 20.07.2016, Torino, Italy
29. Rittmann S.K.-M.R., Archaea Biotechnology – Biomethanation of H<sub>2</sub> and CO<sub>2</sub> to CH<sub>4</sub>, **Nanotech ITALY**, 25.11.2015-27.11.15, Bologna, Italy
30. Rittmann S.K.-M.R., Bernacchi S., Seifert A., Krajete A., Neueste Entwicklungen im Bereich der Biologischen Methanisierung, **Fachforum Biologische Methanisierung**, 11.11.2015, Regensburg, Germany
31. Rittmann S.K.-M.R., Taubner R.-S., Schleper C., Progress in Archaea Biotechnology – biohydrogen and biomethane production, Institute of Microbiology, 26.03.2015, **University of Innsbruck**, Innsbruck, Austria
32. Bernacchi S., Seifert A., Krajete A., Rittmann S.K.-M.R., Anwendungen der Methanogenese zur Biogasveredelung und Stromspeicherung, **Biogas 13**, 04.12.13-05.12.13, St. Pölten, Austria

### ***Panel discussions***

1. Rittmann S.K.-M.R., Nitschinger H., Manafi A., Stamenov M., Moderation: Haimberger C., **Gründer:innen Panel, 1.Portfolio Day (AWS)**, Connect Day 2023, WKÖ, 31<sup>st</sup> of May 2023, Vienna, Austria, >15 participants (live)
2. Rittmann S.K.-M.R., Dokalik-Jonak E., Stifftinger E., Groß Amelie, Moderation: Jovicevic D., **Entrepreneurship Night of the University of Vienna**, 6<sup>th</sup> of March 2023, Vienna, Austria, >400 participants (live)

3. Rittmann S.K.-M.R., Jakl T., Guisasola A., Schwab, H., CO<sub>2</sub>, the future feedstock for biobased processes, **European Summit of Industrial Biotechnology (ESIB)**, 14<sup>th</sup>-16<sup>th</sup> of November 2022, Graz, Austria; >50 participants (live)
4. Rittmann S.K.-M.R., Schwarz, J.P., Halbwidl I., Moderation: Fauma G., **u:talk "Green Technology & Entrepreneurship"** 25.04.2022, University of Vienna, Vienna, Austria; >40 participants (live)
5. Rittmann S.K.-M.R., Bach B., Vogel T., Moderation: Stanzl E., **Kaiserschild Lectures "Wieviel Zukunft steckt in grünem Wasserstoff?"** 21.04.2022, University of Vienna, Vienna, Austria; >200 participants (live and online)

### *Oral presentations*

1. Salas E., Gorfer M., Bandian D., Eichorst S.A., Schmidt H., Horak J., Rittmann S.K.-M.R., Schleper C., Reischl B., Pribasnig T., Jansa J., Kaiser C., Wanek W. (2024) Quantifying amino acid and amino sugar biomarkers in a single approach to estimate necromass from soil archaea, bacteria, fungi, and plants, **European Geosciences Union General Assembly (EGU)**, Vienna, Austria & Online | 14–19 April 2024.
2. Hofmann W., Orthofer M., Ungerank M., Rittmann S.K.-M.R. Method for rapid screening of cultivation parameters for identification of methane cell factories, **First Central European Power-to-Gas Conference: Regional perspectives of power-to-methane and carbon capture technologies** 12.12-13.12.22, Budapest, Hungary
3. Rodrigues-Oliveira T., Wollweber F., Ponce-Toledo R.I., Xu J., de Sousa M.F., Rittmann S.K.-M.R., Klingl A., Pilhofer M., Schleper C., Complex cytoskeleton and cell architecture in an Asgard archaeon, **Molecular Biology of Archaea 2022**, Frankfurt, Germany, 1.8.-4.8.2022
4. Hanišáková N., Vítězová M., Rittmann S.K.-M.R., The microorganisms as the possible solution of degradation high-lipid food waste, **The annual conference of the Association of General and Applied Microbiology**, Düsseldorf, Germany and Online, 21.-23.02.2022, ISBN 978-3-948023-22-5.
5. Pende N., Sogues A., Megrian D., Palabikyan H., Sartori-Rupp A., Rittmann S.K.-M.R., Graña M., Wehenkel A.M., Alzari P.M., Gribaldo S. (2021) SepF is the FtsZ-anchor in Archaea: conservation and divergence of an ancestral cell division system, talk 28<sup>th</sup> of July 2021, **Archaea Online 2021 (AOL2021)**, virtual meeting from 26<sup>th</sup> to 30<sup>th</sup> of July 2021
6. Marzynski M., Neubauer M., Fuchs W., Schulze S, Deutsch M. Ergal Í, Steger F., Rachbauer L., Rittmann S.K.-M.R., Bochmann G., Drosch B., Operation of

a continuous anaerobic trickle-bed reactor for microbial acetate production, **Webinar series on biological carbon capture and utilization**, 18.05.2021, Vienna, Austria (online)

7. Steger F., Reich J., Fuchs W., Ribitsch D., Rittmann S.K.-M.R., Bochmann G., Characterization of three different carbonic anhydrases for CO<sub>2</sub> sequestration, **Webinar series on biological carbon capture and utilization**, 04.05.2021, Vienna, Austria (online)
8. Zwirmayr S., Pappenreiter P., Mauerhofer L.-M., Rittmann S.K.-M.R., Paulik C., High throughput screening of methanogens under high pressure, **12<sup>th</sup> European Congress on Chemical Engineering/5<sup>th</sup> European Congress on Applied Biotechnology**, September 15-19, 2019, Florence, Italy
9. Mauerhofer L.-M., Reischl B., Schmieder T., Schupp B., Nagy K., Pappenreiter P., Zwirmayr S., Schuster B., Bernacchi S., Seifert A. H., Paulik C., Rittmann S.K.-M.R., H<sub>2</sub>/CO<sub>2</sub> fed-batch cultivation of *Methanobacterium thermaggregans*, **Workshop on Gas in Biotechnology**, January 28-29, 2019, Vienna, Austria
10. Abdel Azim A., Rittmann S.K.-M.R., Fino D., Bochmann G. The physiology of methanogens in the presence of inorganic and organic compounds, **Workshop on Gas in Biotechnology**, January 28-29, 2019, Vienna, Austria
11. Ergal I., Fuchs W., Hasibar B., Bochmann G., Rittmann S.K.-M.R., The physiology of dark fermentative biohydrogen production, **Workshop on Gas in Biotechnology**, January 28-29, 2019, Vienna, Austria
12. Hasibar B., Ergal I., Bochmann G., Rittmann S.K.-M.R., Fuchs W., Competing acetate consumption and production inside a microbial electrolysis cell, **Workshop on Gas in Biotechnology**, January 28-29, 2019, Vienna, Austria
13. Rittmann S.K.-M.R., Reischl B., Ergal I., Utilization of formate by the Crenarchaeon *Desulfurococcus amylolyticus* DSM 16532, **Workshop on Gas in Biotechnology**, January 28-29, 2019, Vienna, Austria
14. Taubner R.-S., Baumann L.M.F., Steiner M., Firneis M.G., Schleper C., Peckmann J., Birgel D., Rittmann S.K.-M.R., Lipid Pattern of *Methanothermococcus okinawensis* under Varying Enceladus-like Conditions, **18<sup>th</sup> European Astrobiology Conference (EANA 2018)**, September 24 – 28, 2018, Berlin, Germany
15. Taubner R.-S., Pappenreiter P., Zwicker J., Smrzka D., Pruckner C., Kolar P., Bernacchi S., Seifert A.H., Krajete A., Bach W., Peckmann J., Paulik C., Firneis, M.G., Schleper C., Rittmann S.K.-M.R., Simulating putative Enceladus-like conditions: The possibility of biological methane production on Saturn's icy moon, **30<sup>th</sup> IAU General Assembly, Symposium 345**:

**Origins: From the Protosun to the First Steps of Life**, August 20 – 31, 2018, Vienna, Austria

16. Taubner R.-S., Pappenreiter P., Zwicker J., Smrzka D., Pruckner C., Kolar P., Bernacchi S., Seifert A. H., Krajete A., Bach W., Peckmann J., Paulik C., Firneis M. G., Schleper C., Rittmann S.K.-M.R., 2018, Biological methane production under putative Enceladus-like conditions; **Workshop ExoOceans: Space Exploration of the Outer Solar System Icy Moons Oceans at the International Space Science Institute**, June 18-22, Bern, Switzerland
17. Taubner R.-S., Baumann L.M.F., Birgel D., Firneis, M.G., Schleper C., Rittmann S.K.-M.R., Lipid pattern of *Methanothermococcus okinawensis* under varying Enceladus-like conditions, **Astrobiology 2017: A research meeting by Interantional Astronautical Federation**, Coyhaique, Chile
18. Rittmann S.K.-M.R., Reischl B., Ergal Ī., The physiology and metabolism of *Desulfurococcus amylolyticus*, **14<sup>th</sup> International Meeting on Thermophiles**, 27<sup>th</sup> of August to 1<sup>st</sup> of September 2017, Skukuza, South Africa
19. Mauerhofer L.-M., Pappenreiter P., Reischl B., Schmieder T., Schupp B., Bernacchi S., Seifert A. H., Krajete A., Paulik C., Rittmann S.K.-M.R., Novel insights into the physiology and productivity of a H<sub>2</sub>/CO<sub>2</sub> converting methanogen, **7<sup>th</sup> International Conference on Biological Air Pollution and Control**, 19<sup>th</sup> of July to 21<sup>st</sup> of July 2017, La Coruna, Spain
20. Ergal Ī., Kleibel B., Thallinger B., Fuchs W., Bochmann G., Rittmann S.K.-M.R., Quantitative and Qualitative Assessment of Pure Culture Dark Fermentative Biohydrogen Production, **7<sup>th</sup> International Conference on Biological Air Pollution and Control**, 19<sup>th</sup> of July to 21<sup>st</sup> of July 2017, La Coruna, Spain
21. Thallinger B., Hasibar B., Ergal Ī, Fuchs W., Rittmann S.K.-M.R. Bochmann G., Visualisation of structured mixed species biofilms for biohydrogen production, **7<sup>th</sup> International Conference on Biological Air Pollution and Control**, 19<sup>th</sup> of July to 21<sup>st</sup> of July 2017, La Coruna, Spain
22. Baumann L.M.F., Taubner R.-S., Birgel D., Schleper C., Peckmann J., Rittmann S.K.-M.R., Variable growth conditions induce changes in the membrane lipid compositions of *Methanothermococcus okinawensis* and *Methanocaldococcus villosus*, **Frontiers in Geology – Tracing back the fossil record of archaea**, 7<sup>th</sup>-8<sup>th</sup> of July 2017, Göttingen, Germany
23. Rittmann S.K.-M.R., Abdel Azim A., Taubner R.-S., Pappenreiter P., Mauerhofer L.-M., Reischl B., Paulik C., Novel insights into the physiology and biotechnology of CO<sub>2</sub> to CH<sub>4</sub> conversion, **10<sup>th</sup> International Symposium on Anaerobic Microbiology (ISAM 10)**, 11.07.2017-14.07.2017, Liblice, Czech Republic

24. Taubner R.-S., Pappenreiter P., Pruckner C., Zwiscker J., Smrzka D., Firneis M. G., Paulik C., Schleper C., Rittmann S.K.-M.R., Testing the habitability of Saturn's icy moon Enceladus in an Interdisciplinary attempt; **12<sup>th</sup> Rencontres du Vietnam**, 11<sup>th</sup>-16<sup>th</sup> of December 2016, Quy Nhon, Vietnam
25. Ergal I., Fuchs W., Bochmann G., Rittmann S.K.-M.R., Quantitative assessment of pure culture dark fermentative biohydrogen production, **Workshop on ABE Production and H<sub>2</sub>/CO<sub>2</sub> Fermentation**, 10<sup>th</sup>-11<sup>th</sup> of November 2016, University of Natural Resources, Vienna, Austria
26. Rittmann S.K.-M.R., Seifert A. H., Bernacchi S., Modelling, qualitative and quantitative analysis of pure-culture biological methane production (BMP) from H<sub>2</sub> and CO<sub>2</sub>, **Workshop on ABE Production and H<sub>2</sub>/CO<sub>2</sub> Fermentation**, 10<sup>th</sup>-11<sup>th</sup> of November 2016, University of Natural Resources, Vienna, Austria
27. Abdel Azim A., Pruckner C., Kolar P., Fino D., Saracco G., Rittmann S.K.-M.R., H<sub>2</sub>/CO<sub>2</sub> (fed-batch) fermentation for biological production of CH<sub>4</sub> by (pure culture of) hydrogenotrophic archaea, **Workshop on ABE Production and H<sub>2</sub>/CO<sub>2</sub> Fermentation**, 10<sup>th</sup>-11<sup>th</sup> of November 2016, University of Natural Resources, Vienna, Austria
28. Pappenreiter P., Taubner R.-S., Seifert A.H., Bernacchi S., Paulik C., Schleper C., Firneis M.G., Rittmann S.K.-M.R., Testing the habitability of Enceladus with *Methanothermococcus okinawensis*, **Workshop on ABE Production and H<sub>2</sub>/CO<sub>2</sub> Fermentation**, 10<sup>th</sup>-11<sup>th</sup> of November 2016, University of Natural Resources, Vienna, Austria
29. Taubner R.-S., Rittmann S.K.-M.R., A new method for indirect quantification of methane production via water production using hydrogenotrophic methanogens, **Workshop on ABE Production and H<sub>2</sub>/CO<sub>2</sub> Fermentation**, 10<sup>th</sup>-11<sup>th</sup> of November 2016, University of Natural Resources, Vienna, Austria
30. Mauerhofer L.-M., Reischl B., Schmieder T., Schupp B., Pappenreiter P., Bernacchi S., Seifert A. H., Krajete A., Paulik C., Rittmann S.K.-M.R., Development of a high-pressure process to couple biological hydrogen and methane production, **Workshop on ABE Production and H<sub>2</sub>/CO<sub>2</sub> Fermentation**, 10<sup>th</sup>-11<sup>th</sup> of November 2016, University of Natural Resources, Vienna, Austria
31. Taubner R.-S., Pappenreiter P., Pruckner C., Zwiscker J., Smrzka D., Firneis M. G., Paulik C., Schleper C., Rittmann S.K.-M.R., An interdisciplinary approach: On the habitability of Saturn's icy moon Enceladus, **Astrobiology Seminar of the University of Stockholm**, 28<sup>th</sup> of September 2016, Stockholm, Sweden
32. Taubner R.-S., Pappenreiter P., Pruckner C., Zwiscker J., Smrzka D., Firneis M. G., Paulik C., Schleper C., Rittmann S.K.-M.R., Testing the habitability of

Saturn's icy moon Enceladus; **16<sup>th</sup> European Astrobiology Conference**, Athens, Greece, September 27–30.

33. Taubner R.-S., Firneis M. G., Schleper C., Rittmann S.K.-M.R., Cultivation of methanogens in Enceladus-like conditions, **Science Day of the Faculty of Life Sciences of the University of Vienna**, 1<sup>st</sup> of July 2016, Wien, Austria
34. Kutlucinar K., Kleiner F., Zebec Z., Rittmann S., Schleper C., Ferrière L. Milojevic T., Acquiring the microbial-mineral interface of *Metallosphaera sedula* grown on stony meteorite. **15<sup>th</sup> European Astrobiology Conference** (EANA 15), ESTEC, 6<sup>th</sup>-9<sup>th</sup> of October 2015, Noordwijk, Netherlands
35. Taubner R.-S., Rittmann S.K.-M.R., A new method for quantification of methane production of hydrogenotrophic methanogens; **15<sup>th</sup> European Astrobiology Conference**, (EANA 15), ESTEC, 6<sup>th</sup>-9<sup>th</sup> of October 2015 Noordwijk, Netherlands
36. Taubner R.-S., Rittmann S.K.-M.R., Method for determination of methane production via water production using hydrogenotrophic methanogens; 9<sup>th</sup> **International Symposium on Anaerobic Microbiology** (ISAM 9) 25.06.15-27.06.15, Portorož, Slovenia, ISBN: 978-961-6204-71-2
37. Zebec Z., Rittmann S., Schleper C., Milojevic T., Meteorite-associated growth physiology of the iron oxidizing extremophile *Metallosphaera sedula*. **European Geosciences Union General Assembly**, Vienna, Austria, 12–17 April
38. Bernacchi S., Rittmann S., Krajete A., Seifert A., Applications of Methanogenesis for CO<sub>2</sub> Utilization and Intermittent Power Storage, 2<sup>nd</sup> **Conference on Carbon Dioxide as Feedstock for Chemistry and Polymers**, 08.10.2013, Essen, Germany
39. Bernacchi S., Seifert A., Rittmann S., Krajete A., Benefits of biological methanation, **DBI-Fachforum Energiespeicher – Pilotprojekte**, 18.09.2013, Berlin, Germany
40. Rittmann S., Seifert A., Krajete A., Bioprocess development for thermophilic biological methane production from H<sub>2</sub> and CO<sub>2</sub>, **12<sup>th</sup> International Meeting on Thermophiles**, 08.09.13-13.09.13, Regensburg, Germany
41. Bernacchi S., Seifert A., Rittmann S., Krajete A., Biological methanogenesis for intermittent power storage, **2. Forum Power to Gas – Integration von Biogasanlagen & Biologische Methanisierung**, 10.09.2013, Regensburg, Germany
42. Rittmann S., Seifert A., Bernacchi S., Prerequisites for pure culture biological methane production – a case study with *Methanothermobacter marburgensis*, **8<sup>th</sup> International Symposium on Anaerobic Microbiology** (ISAM 8), 12.06.2013-15.06.2013, Innsbruck, Austria, ISBN:978-3-902936-03-5



43. Seifert A., Rittmann S., Herwig C., Influence of gas/liquid mass transfer on the volumetric production rate and product quality during biological methanogenesis, **ProcessNet-Jahrestagung**, 10.09.2012 - 13.09.2012, Karlsruhe, Germany
44. Seifert A., Bernacchi S., Rittmann S. Herwig C. Krajete A., Archaea Mikroorganismen zur biologischen Stromspeicherung, **Deutscher Verein des Gas- und Wasserfaches**, 28.8.2012 Essen, Germany
45. Seifert A., Bernacchi S., Rittmann S., Herwig C., Krajete A., Archaea Microorganisms for Biological Power Storage, Karlsruhe, **2. VDI-Fachkonferenz: Stationäre Energiespeicher für Erneuerbare Energien**, 20.06.2012 – 21.06.2012, Karlsruhe, Germany

### ***Open access data***

Pfeifer K., Ergal I., Rittmann S.K.-M.R. (2020) Archaea Biotechnology: Supplementary Material, <https://doi.org/10.25365/phaidra.165>

Taubner R.-S. Rittmann S.K.-M.R. (2023) Lipidomics and comparative metabolite excretion analysis of methanogenic archaea reveal organism-specific adaptations to varying temperature and substrate concentration: data, <https://doi.org/10.25365/phaidra.380>

Reischl B., Rittmann S.K.-M.R. (2024) Quantitative analysis of amino acid excretion by *Methanothermobacter marburgensis* under N<sub>2</sub>-fixing conditions: data 1, <https://doi.org/10.25365/phaidra.515>

Reischl B., Rittmann S.K.-M.R. (2024) Quantitative analysis of amino acid excretion by *Methanothermobacter marburgensis* under N<sub>2</sub>-fixing conditions: data 2, <https://doi.org/10.25365/phaidra.516>

Hofmann W., Salas Wallach N., Rittmann S.K.-M.R. (2024) The Gas and Pressure Controller (GPC): a device for automated closed batch cultivations and assessment of cultivation parameters of gas-converting microbial cell factories: data, <https://doi.org/10.25365/phaidra.519>

Salas Wallach N., Hofmann W., Rittmann S.K.-M.R. (2024) The Gas and Pressure Controller (GPC): a device for automated closed batch cultivations and assessment of cultivation parameters of gas-converting microbial cell factories: code, <https://doi.org/10.25365/phaidra.518>

### ***Radio, TV, and youtube broadcasts***

**NHK-BS Premium: Cosmic Front Next**  
2.8.2018

Fernsehbeitrag  
Hiroshi Niitsuma (Redakteur)  
Simon K.-M.R. Rittmann (Interview partner)

**Alleine im All?** Mayrs Magazin – Wissen für alle  
3.12.2021  
Fernsehbeitrag: Österreichischer Rundfunk (ORF 2)  
Robert Pfannhauser (Redakteur)  
Simon K.-M.R. Rittmann (Interview partner)

**Kaiserschild Lecture 2022: Wieviel Zukunft steckt in grünem Wasserstoff?**  
21.4.2022  
<https://www.youtube.com/watch?v=5AUlMJBrAro>  
Eva Stanzl (Panel discussion chair)  
Simon K.-M.R. Rittmann (Panel discussion partner)

**Nahrung aus Luft:** Mayrs Magazin – Wissen für alle  
13.5.2022  
Fernsehbeitrag: Österreichischer Rundfunk (ORF 2)  
Robert Pfannhauser (Redakteur)  
Simon K.-M.R. Rittmann (Interview partner)

**BBC Arabic News: Arkeon**  
28.11.2022  
<https://www.youtube.com/watch?v=XWB8EtjKlm4>  
Ali Oudjana (Reporter)  
Simon K.-M.R. Rittmann (Interview partner)

**Ö1 Radiokolleg:** Series *Lexikon of Chemical Elements* – Methan, das unterschätzte Treibhausgas  
22.02.2023  
<https://oe1.orf.at/artikel/701266/Methan>  
Radiobeitrag: Österreichischer Rundfunk (Ö1)  
Monika Halkort (Reporterin)  
Simon K.-M.R. Rittmann (Interview partner)

**PhD Career Stories:** #124 – Simon Rittmann Innovating on Two Fronts: Founding a Company while Thriving in Academia  
<https://www.youtube.com/watch?v=2IYkDjiWHfU>  
<https://phdcareerstories.com/pub/srittmann/release/1>  
14.07.2023  
Tina Persson (Redakteurin)

Simon K.-M-R. Rittmann (Interview partner)

5<sup>th</sup> **Entrepreneurship Night**: Arkeon – Aminosäuren aus CO<sub>2</sub>

<https://www.youtube.com/watch?v=O1fpmXMuUE0>

8.5.2024

Petra Schiefer (Redakteurin)

Simon K.-M-R. Rittmann (Interview partner)

**Geo-Omics Seminar Series 2024**: Synthetic biology of archaea for biotechnological applications

<https://www.koushare.com/live/details/37557>

30.9.2024

Prof. Dr. Chunlun Zhang (Organisator)

Simon K.-M-R. Rittmann (Vortragender)

### ***Poster presentations***

1. Hilts A. S., Casini I., Fink C., Rittmann S.K-M.R. (2024) Towards holistic metabolic engineering of *Methanothermobacter marburgensis* using a combination of in silico methods, European Summit of Industrial Biotechnology, 12<sup>th</sup>–14<sup>th</sup> of November 2024, Graz, Austria (Poster Award)
2. King A. Y., Krause N., Viehboeck T., Bulgheresi S., Rittmann S.K-M.R., Pende N. (2024) Ploidy and Chromosome Configuration in Human Gut-Associated *Methanobrevibacter smithii* European Summit of Industrial Biotechnology, 12<sup>th</sup>–14<sup>th</sup> of November 2024, Graz, Austria
3. Hofmann W., Orthofer M., Salas Wallach N., Ruddyard A., Ungerank M., Paulik C., Rittmann S.K-M.R. (2024) The Gas and Pressure Controller (GPC): a device for automated closed batch cultivations and assessment of cultivation parameters of gas-converting microbial cell factories, European Summit of Industrial Biotechnology, 12<sup>th</sup>–14<sup>th</sup> of November 2024, Graz, Austria
4. Hilts A. S., Casini I., Fink C., Rittmann S.K-M.R. (2024) Current in silico modeling techniques for engineering the archaeon *Methanothermobacter marburgensis*, 16<sup>th</sup> ÖGMBT Annual Meeting, 17<sup>th</sup>–19<sup>th</sup> of September 2024, Graz, Austria
5. Hilts A. S., Casini I., Fink C., Rittmann S.K-M.R. (2024) Expanding metabolic modelling of *Methanothermobacter marburgensis* with the current in silico techniques, Molecular Biology of Archaea, 25<sup>th</sup> to 27<sup>th</sup> of June 2024, Paris, France
6. Fink C., Klein M., Hilts A., Fennessy R., Rittmann S.K-M.R. (2024) Carbon Recycling The Arkeon Way: We Turn CO<sub>2</sub> Into Functional, Climate Positive

7. Weiss S., Reischl B., Kugler C., Eder M., Schleper C., Rittmann S.K.-M.R., Sami H., Ogris M. (2023) Methanogenic archaea: from cancer homing to proliferation in solid tumors, Tumor Heterogeneity, Plasticity and Therapy (THPT) (2<sup>nd</sup> edition), October 3<sup>rd</sup> – 4<sup>th</sup>, Leuven, Belgium
8. Palabikyan H., Taubner R.-S., Rittmann S.K.-M.R. (2023) Application of methanogenic archaea as cell factories for life support systems in space, BEACON 2023, May 8<sup>th</sup> – 12<sup>th</sup>, Fuencaliente de La Palma, Spain
9. Orthofer M., Hofmann W., Paulik C., Rittmann S.K.-M.R., Ungerank M., Voithofer P., Höckner J. (2022) Demonstration of a biological sensor to determine hydrogen mass transfer in biological methanation using methanogenic archaea, 19<sup>th</sup> Austrian Chemistry Days, September 20<sup>th</sup> – 22<sup>nd</sup>, Vienna, Austria
10. Donadu M.G., Ferrari M., Mazzarello V., Zanetti S., Kushkevych I., Rittmann S.K.-M.R., Stájer A., Baráth Z., Szabó D., Urbán E., Gajdács M. (2022) Is there a relationship between biofilm forming-capacity and antibiotic resistance in *Staphylococcus* spp.? In vitro results, The 2<sup>nd</sup> International Electronic Conference on Antibiotics — Drugs for Superbugs: Antibiotic Discovery, Modes of Action And Mechanisms of Resistance, Part of the International Electronic Conference on Antibiotics series, 15-30 June 2022, online
11. Zwiirtmayr S., Mauerhofer L.-M., Bernacchi S., Seifert A.H., Rittmann S.K.-M.R., Paulik C. (2020) Biologische Methanproduktion mit Archaea-Stämmen unter Hochdruckbedingungen, 34. DECHEMA Jahrestagung der Biotechnologen 2020, September 21<sup>st</sup> -24<sup>th</sup>, 2020, Aachen, Germany
12. Pende N., Taib N., Megrian D., Rittmann S.K.-M.R., Bulgheresi S., Gribaldo S., Bacteria and methanogenic archaea share homologs of proteins involved in cell wall synthesis, EMBO Workshop: Bacterial Cell Division: Closing the gap, June 9-12, Lund, Sweden
13. Pende N., Taib N., Megrian D., Rittmann S.K.-M.R., Bulgheresi S., Gribaldo S., A phylogenomic investigation of archaeal pseudomurein synthesis genes, Cell Biology of Prokaryotes, April 7-11, Bad Staffelstein, Germany
14. Taubner R.-S., Pappenreiter P., Zwicker J., Smrzka D., Pruckner C., Kolar P., Bernacchi S., Seifert A.H., Krajete A., Bach W., Peckmann J., Paulik C., Firneis, M.G., Schleper C., Rittmann S.K.-M.R., Potential biological methane production in the Solar System: Saturn's icy moon Enceladus as a promising target, Workshop on Gas in Biotechnology, January 28-29, 2019, Vienna, Austria

15. Taubner R.-S., Pappenreiter P., Zwicker J., Smrzka D., Pruckner C., Kolar P., Bernacchi S., Seifert A.H., Krajete A., Bach W., Peckmann J., Paulik C., Firneis, M.G., Schleper C., Rittmann S.K.-M.R., Biological Methane Production under putative Enceladus-like conditions, MBoA6 Workshop: Molecular Biology of Archaea: from mechanisms to ecology, September 3-5, 2018, Vienna, Austria
16. Zwartmayr S., Pappenreiter P., Mauerhofer L.-M. Rittmann S.K.-M.R., Paulik C., Screening of methanogens in a Simultaneous Bioreactor System (SBRS) with multiple determination under high pressure conditions, MBoA6 Workshop: Molecular Biology of Archaea: from mechanisms to ecology, September 3-5, 2018, Vienna, Austria
17. Pende N., Rittmann S.K.-M.R., Bulgheresi S., Gribaldo S., A phylogenomic investigation of archaeal pseudomurein synthesis genes, MBoA6 Workshop: Molecular Biology of Archaea: from mechanisms to ecology, September 3-5, 2018, Vienna, Austria
18. Pappenreiter P., Paulik C., Mauerhofer L.-M., Rittmann S.K.-M.R., Bernacchi S., Seifert A., Experimental methods for investigations of biomethanation processes at elevated operating pressures, 10<sup>th</sup> World Congress on Chemical Engineering (WCCE), 1<sup>st</sup>-5<sup>th</sup> of October 2017, Barcelona, Spain
19. Zwicker J., Smrzka D., Taubner R.-S., Bach W., Rittmann S.K.-M.R., Schleper C., Peckmann J., Low-temperature serpentinization reactions can explain molecular hydrogen production on Saturn's moon Enceladus: implications for potential microbial life, European Planetary Science Congress, 17<sup>th</sup>-22<sup>nd</sup> of September 2017, Riga, Latvia
20. Zwartmayr S., Pappenreiter P., Mauerhofer L.-M., Bernacchi S., Seifert A.H., Krajete A., Rittmann S.K.-M.R., Paulik C., Development of a Simultaneous Bioreactor System (SBRS) for high throughput screening and characterization of methanogens at high pressure, 17<sup>th</sup> Austrian Chemistry Days, 25<sup>th</sup>-28<sup>th</sup> of September 2017, Salzburg, Austria
21. Taubner R.-S., Abdel Azim A., Rittmann S.K.-M.R., Trace Elements of methanogens in an astrobiological context, 17<sup>th</sup> Astrobiology Conference, 14<sup>th</sup>-17<sup>th</sup> of August 2017, Aarhus, Denmark
22. Smrzka D., Zwicker J., Taubner R.-S., Bach W., Rittmann S.K.-M.R., Schleper C., Peckmann J., Molecular hydrogen production during low-temperature serpentinization: A modeling study with implications for potential microbial life on Saturn's moon Enceladus, Goldschmidt 2017, 13<sup>th</sup>-18<sup>th</sup> of August, Paris, France
23. Zwicker J., Birgel D., Bach W., Richoz S., Gier S., Smrzka D., Neubeck A., Ivarsson M., Schleper C., Rittmann S.K.-M.R., Grasemann B., Peckmann J.,

Archaeal methanogenesis at the onshore serpentinite-hosted Chimaera seeps, Turkey, Goldschmidt 2017, 13<sup>th</sup>-18<sup>th</sup> of August, Paris, France

24. Rittmann S.K.-M.R., Reischl B., Ergal İ., The physiology and metabolism of *Desulfurococcus amylolyticus*, Gordon Research Conference Archaea: Ecology, Metabolism & Molecular Biology July 23<sup>rd</sup>-28<sup>th</sup> of July 2017, Waterville Valley, United States of America
25. Rohrweber A.-C., Thiele M., Baumann LM.F., Rittmann S.K.-M.R., Taubner R.-S., Peckmann J., Schleper C., Birgel C., Culturing conditions impact the lipid biomarker composition of the (hyper)thermophilic hydrogenotrophic methanogens *Methanothermococcus okinawensis* and *Methanocaldococcus villosus*, Frontiers in Geology – Tracing back the fossil record of archaea, 7<sup>th</sup>-8<sup>th</sup> of July 2017, Göttingen, Germany
26. Abdel Azim A., Pruckner C., Kolar P., Taubner R.-S., Fino D., Saracco G., Sousa F.L., Rittmann S.K.-M.R., 2017, CO<sub>2</sub> bioconversion: trace elements utilization in biological methane production (BMP), 7<sup>th</sup> International Conference on Biological Air Pollution and Control 19<sup>th</sup>-21<sup>st</sup> of July 2017, La Coruna, Spain
27. Ergal İ., Reischl B., Rittmann S.K.-M.R., The physiology and metabolism of *Desulfurococcus amylolyticus*, 10<sup>th</sup> International Symposium on Anaerobic Microbiology (ISAM 10), 11<sup>th</sup>-14<sup>th</sup> of June 2017, Liblice, Czech Republic
28. Zwicker J., Birgel D., Bach W., Richoz S., Gier S., Smrzka D., Neubeck A., Ivarsson M., Schleper C., Rittmann S.K.-M.R., Grasemann B., Peckmann J., Archaeal methanogenesis at the onshore serpentinite-hosted Chimaera seeps, Turkey, Abstracts of the European Geosciences Union General Assembly 8<sup>th</sup>-13<sup>th</sup> of April 2017, Vienna, Austria
29. Zwicker J., Smrzka D., Taubner R.-S., Bach W., Rittmann S.K.-M.R., Schleper C., Peckmann J., Modeling low-temperature serpentinization reactions to estimate molecular hydrogen production with implications for potential microbial life on Saturn's moon Enceladus, Abstracts of the European Geosciences Union General Assembly 8<sup>th</sup>-13<sup>th</sup> of April 2017, Vienna, Austria
30. Taubner R.-S., Rittmann S.K.-M.R., Leitner J. J., Firneis M. G., Schleper C., 2016, Habitability beyond the snow line: The potential of Icy moons to serve as a habitat for life-as-we-know-it, Abstracts of the Astrophysics of Planetary Habitability Conference, 8<sup>th</sup>-12<sup>th</sup> of February 2016, Vienna, Austria
31. Taubner R.-S., Rittmann S.K.-M.R., Leitner J. J., Schleper C., Firneis M. G., Hitzemberger R., 2014, Assessing the feasibility to cultivate methanogens under Enceladus-like conditions reservoir; Poster presented at the “Summer course on Exoplanets”, 24<sup>th</sup> of September to the 2<sup>nd</sup> of October 2015, La Palma, Spain



32. Taubner R.-S., Schleper C., Firneis M. G., Rittmann S.K.-M.R., 2015, Methanogens in the Solar System; Abstracts of the European Geosciences Union General Assembly 2015, Vol. 17, EGU2015-13520, 12–17 of April, Vienna, Austria
33. Taubner R.-S., Rittmann S.K.-M.R., Leitner J. J., Schleper C., Firneis M. G., Hitzemberger R., 2014, Assessing the feasibility to cultivate methanogens under Enceladus-like conditions reservoir; 14<sup>th</sup> European Astrobiology Conference (EANA 2014), 13–16 October 2014, Edinburgh, United Kingdom
34. Rittmann S., Zebec Z., Bittner R., Kutlucinar K., Schleper C., Milojevic T., 2015, Meteorite supplementation of the iron-oxidizing archaeon *Metallosphaera sedula* expands the boundaries of thermophilic life. Habitability in the Universe: From the Early Earth to Exoplanets, Porto, Portugal, 22-27 March, 2015.
35. Zebec Z., Rittmann S., Kerou M., Schleper C., Milojevic T. "Iron-oxidising thermoacidophilic archaeon *Metallosphaera sedula*: insights into astrobiological application“, 14<sup>th</sup> European Astrobiology Conference (EANA 2014), 13–16 October 2014, Edinburgh, United Kingdom
36. Seifert A., Rittmann S., Herwig. C., "Biomethane Production from Gaseous Substrates Using Methanogenesis", 19<sup>th</sup> Biomass Conference and Exhibition, 06-10 June 2011, Berlin, Germany
37. Rittmann S., Seifert A., Sautaux C., Denk K., Martinez Porqueraz E., Herwig, C. "Quantitative Bioprocess Development for the Production of Biofuels and Cocurrent CO<sub>2</sub> Fixation", 1<sup>st</sup> Bioscience Technologies Day, 15<sup>th</sup> of November 2010, Vienna University of Technology, Vienna, Austria
38. Rittmann S., Pertl H., Obermeyer G. "Molecular identification of 14-3-3 isoforms of lily pollen and their possible role in activation of the plasma membrane H<sup>+</sup>ATPase", International Botanical Congress (IBC), 17-23 July 2005, Vienna, Austria
39. Rittmann S., Legat A., Fendrihan S., Stan-Lotter H., "Viability and Morphology of *Halobacterium* Species following Desiccation - Implications for Contamination on Mars", 3<sup>rd</sup> European Workshop on Exo-Astrobiology“, November 18-20 2003, Madrid, Spain
40. Radax C., Pfaffenhuemer M., Wieland H., Rittmann S., Leuko S., Weidler G., Gruber C., Stan-Lotter H. "Microbes in Rock Salt: How to find out what is in there", 2<sup>nd</sup> European Workshop on Exo-Astrobiology, September 16-23 2002, Graz, Austria

### ***Supervision of PhD students***

01/2022 ongoing	<u>Angus Hilt</u> s, MSc BSc, Title: Metabolic networks in <i>Methanothermobacter marburgensis</i> for cell factory development Supervisor: Dr. Simon K.-M. R. Rittmann, Privatdoz.
11/2021 ongoing	<u>Walter Hofmann</u> , MSc BSc, Title: Physiological and biotechnological characteristics of archaea for methane and bioplastic production Supervisor: Dr. Simon K.-M. R. Rittmann, Privatdoz.
03/2021 ongoing	<u>Barbara Reischl</u> , MSc BSc, Title: Physiological and biotechnological aspects of amino acid production by methanogenic archaea Supervisor: Dr. Simon K.-M. R. Rittmann, Privatdoz.
03/2020 ongoing	<u>Hayk Palabikyan</u> , MSc BSc: Converting carbon dioxide into bioplastics by anaerobic autotrophic methanogenic archaea Supervisor: Dr. Simon K.-M. R. Rittmann, Privatdoz.
05/2015 to 11/2020	<u>Lisa-Maria Mauerhofer</u> , MSc BSc, Title: Comparative Physiology of methanogenic archaea with respect to biotechnological applications Supervisor: Dr. Simon K.-M. R. Rittmann, Privatdoz.
05/2015 to 09/2020	<u>Ipek Ergal</u> , MSc BSc, Title: Physiology and biotechnology of artificial microbial H <sub>2</sub> production ecosystems Supervisor: Dr. Simon K.-M. R. Rittmann, Privatdoz.

### ***Co-supervision of PhD students***

03/2013 to 09/2018	<u>Ruth-Sophie Taubner</u> , MSc BSc, Title: An interdisciplinary approach: on the habitability of Enceladus' potential subsurface water reservoir Supervisors: Prof. Dr. Christa Schleper and Prof. Dr. Maria Firneis
01/2015 01/2018	<u>Annalisa Abdel Azim</u> , MSc BSc, Title: From CO <sub>2</sub> to CH <sub>4</sub> via biological methanogenesis Supervisor: Prof. Dr. Deborah Fino

### ***Supervision of master students***

01/2024 to ongoing	<u>Selina Madlmayr</u> , BSc, Title: t.b.d.
04/2024 to ongoing	<u>Nicolas Salas Wallach</u> , BSc, Title: Physiological and biotechnological examination of methanogenic archaea for CO <sub>2</sub> conversion
04/2024 to ongoing	<u>Andrew Y. King</u> , BSc, Title: DNA segregation and ploidy in methanogenic archaea

06/2021 to 09/2022	<u>Lara Pomper</u> , BSc, Title: Scale-up of biomass production with <i>Methanococcus maripaludis</i> and biochemical characterization of carbon storage pathway enzymes of <i>Nitrososphaera viennensis</i>
05/2021 to 04/2022	<u>Michael Stadlbauer</u> , BSc, Title: A cumulative work on different aspects of biological methanogenesis
03/2020 to 02/2022	<u>Elisa Zech</u> , BSc, Title: Dark fermentative biohydrogen production in artificial co-culture
09/2020 to 11/2021	<u>Walter Hofmann</u> , BSc, Title: Purification and characterization of carbon storage pathway proteins from <i>Nitrososphaera viennensis</i>
01/2020 to 07/2021	<u>Aquilla Ruddyard</u> , BSc, Title: Experimental strategy for rapid <i>Methanococcus maripaludis</i> biomass production in fed-batch cultivation mode
09/2018 to 08/2020	<u>Oliver Gräf</u> , BSc, Title: Ecology and biotechnology of biohydrogen producing <i>Enterobacter aerogenes</i> and <i>Clostridium acetobutylicum</i> in mono-culture and co-culture
11/2017 to 03/2020	<u>Benjamin Schupp</u> , BSc, Title: Nitrogen fixation in methanogens
09/2018 to 01/2020	<u>Hayk Palabikyan</u> , BSc, Title: Heterologous expression of genes encoding for the carbon storage metabolism of <i>Nitrososphaera viennensis</i> in <i>Methanococcus maripaludis</i>
09/2017 to 01/2020	<u>Michael Steiner</u> , BSc, Title: Ecological and biotechnological aspects of mono and multispecies hydrogen production systems
03/2017 to 02/2019	<u>Christian Pruckner</u> , BSc, Title: Evolutionary and physiological aspects of potentially carboxydophilic Archaea
03/2017 to 12/2018	<u>Tilman Schmider</u> , BSc, Title: Ecophysiology and productivity of carboxydophilic-based artificial microbial ecosystems
10/2014 to 04/2015	<u>Barbara Reischl</u> , BSc, Title: Physiology, metabolism and biohydrogen production of <i>Desulfurococcus fermentans</i>

### ***Supervision of bachelor students***

01/2020 to 08/2020	<u>Sonja Vukotic</u> , Title: Growth quantification of <i>Geobacter sulfurreducens</i> DSM 12127
02/2020 to 07/2020	<u>Aaron Zipperle</u> , Title: Growth characteristics of <i>Desulfurococcus amylolyticus</i> DSM 16532

11/2015	<u>Lisa Fragner</u> , Title: Diversität methanogener Archaeen in und um Piran und Maribor (Slowenien)
07/2015 to 10/2015	<u>Christian Pruckner</u> , Title: Cultivation of <i>Methanothermobacter marburgensis</i> in an exponential feed-setup
10/2013 to 12/2013	<u>Katharina Schultz</u> , Title: Analysis of enrichment cultures from environmental samples, taken from fumaroles and hot springs at Ischia and Pozzuoli, Italy, for methanogenic archaea

## Awards

- 2023 *Frontiers in Microbiology – Outstanding article 2023* to Melcher M., Hodgskiss L. H., Mardini M. A., Schleper C., Rittmann S.K.-M.R. entitled “Analysis of biomass productivity and physiology of *Nitrososphaera viennensis* grown in continuous culture”.
- 2019 Rectorate program *Freiräume schaffen* has been awarded for frequently submitting to high risk – high gain national and international calls. The rectorate program has a value of 3,048 € and was doubled by the Dean of the Faculty of Life Sciences of the University of Vienna to 6,096 €.
- 2018 *Young Investigator Award of the University of Vienna* awarded by the Faculty of Life Sciences to honour young postdoctoral scientists publishing in the top journals of their field. The award has a value of 7,000 €.
- 2002 *European Space Agency (ESA) travel grant* to the International Astronautical Federation and the World Space Congress (IAF-WSC), October 10-19 2002, Houston, Texas, USA
- 2001 *European Space Agency (ESA) travel grant* to the 1<sup>st</sup> European Workshop on Exo-Astrobiology, Mai 21-23 2001, Frascati, Italy

## Community services

### *Opponent*

24<sup>th</sup> of April 2021      Thitiwut Vongkampang, Exploring strategies to improve volumetric hydrogen productivities of *Caldicellulosiruptor* species, Lund University, Faculty of Engineering, Sweden

### *Organisation of meetings*

01/2019      Organiser of the Workshop: “Gas in Biotechnology”, 28<sup>th</sup>-29<sup>th</sup> of January 2019, Vienna, Austria (56 participants)

09/2018      Co-organiser of the EMBO workshop: “Molecular Biology of Archaea: From mechanisms to ecology”, 3<sup>rd</sup>-5<sup>th</sup> of September 2018, Vienna, Austria (165 participants)

### *Session chairs*

2014      International scientific conference on Biogas Science, Vienna, Austria chairing two sessions (#16 and #27) on Gas Technology

### *Editorial roles*

Since 2022      Frontiers, Associate editor of *Frontiers in Microbiology*,  
Section: Archaea Biology

Since 2023      Elsevier, Executive editor of *Current Research in Biotechnology*

### *Reviewer and editor commitments*

<https://publons.com/author/827982/simon-k-m-r-rittmann#profile>

### *Scientific webpages, portals, and IDs*

Group page      <https://archaea.univie.ac.at/research/simon-rittmann-lab/>

Research Gate      [https://www.researchgate.net/profile/Simon\\_Rittmann](https://www.researchgate.net/profile/Simon_Rittmann)

Google Scholar      <https://scholar.google.at/citations?user=0sU9aSIAAA&hl=de>

Linked-In      <https://www.linkedin.com/in/simon-rittmann-286b53218/>

ORCID      <https://orcid.org/0000-0002-9746-3284>

ResearcherID      <http://www.researcherid.com/rid/D-6205-2013>



## **Additional experience**

### ***Language abilities***

<b><i>German:</i></b>	native speaker
<b><i>English:</i></b>	fluent
<b><i>Czech:</i></b>	very basic knowledge
<b><i>French:</i></b>	very basic knowledge
<b><i>Russian:</i></b>	very basic knowledge

### ***Computer skills***

Knowledge of Ubuntu, Apple, and Microsoft operating systems  
Knowledge of data calculation and word processing programs *i.e.*: MS Word, MS Excel, MS PowerPoint, Planner, and Evolution  
Knowledge of non-commercial and commercial bioinformatics software including MEGA, CLUSTAL, Vector NTI  
Knowledge of statistics software *i.e.* Datalab, R-Project, MODDE, Design-Expert

### ***Other***

Former Assistant Fire Protection Officer of the Department of Functional and Evolutionary Ecology